NUMERICAL MODELLING OF DEFLECTIONS OF REINFORCED CONCRETE FLAT SLABS UNDER SERVICE LOADS

Tahsin Reza Hossain

BSc Engg(Civil), MSc Engg(Civil)

July 1999

A thesis submitted for the degree of

Doctor of Philosophy of the University of London

and for the

Diploma of Membership of Imperial College

Department of Civil and Environmental Engineering

Imperial College of Science, Technology and Medicine

London SW7 2BU



BIBL
LONDON

Abstract

This thesis is principally concerned with the modelling of short- and long-term deflections of flat slabs. The main objective was to develop a simple but accurate numerical method of estimating deflections, utilising currently available moment-curvature or effective moment of inertia relationships which model the effects of cracking, creep, shrinkage and loss of tension stiffening. A finite-element (FE) method based on the effective-stiffness approach with secant-stiffness formulations has been developed to calculate deflections of reinforced concrete slabs under service loads. Several short-term models and the CEB-FIP Model Code 1990 (MC-90) long-term model are incorporated into an existing FE package. The performances of the short- and long-term models have been verified on the basis of existing experimental results. The ACI and MC-90 models are also extended for biaxial bending with a compressive force to model cracking, creep and shrinkage in columns and their efficiencies have been checked by comparing them with experimental results. A slab, in reality, experiences a non-uniform load throughout its construction and operational life, which needs to be considered for a realistic estimate of long-term slab deflections. A method based on the MC-90 model is proposed for calculating the deflection due to a time-varying load history. The method has been used to estimate deflections of the floors of the Cardington ECBP building and the comparison with field measurements to date is good. A series of parametric studies has been carried out to identify the influence of the relevant parameters and two simplified approaches are proposed to estimate long-term slab deflections due to a time-varying load history.

Acknowledgements

The work described in this thesis was carried out under the joint supervision of Dr. R. L. Vollum and Professor M. N. Pavlović of the Concrete Structures Section. The author would like to express his deepest gratitude to his supervisors for their invaluable guidance, strong support and constant encouragement during the course of this research work. Their kindness and patience are thankfully acknowledged.

Dr. D. Hitchings of Aeronautics Department of Imperial College, modified his finite-element package FE77 according to need of the work which is greatly acknowledged with thanks.

The author would also like to thank Dr. R. Moss of Building Research Establishment for giving him access to the results from European Concrete Building Project at Cardington. Thanks are also due to Mr. R. Whittle of Ove Arup and Partners for providing him the unpublished test results of the Taywood slab.

The author had been funded by the Commonwealth Scholarship Commission and is grateful to them. Bangladesh University of Engineering and Technology, of which the author is an employee, granted him the leave of absence to conduct this work, which is greatly acknowledged.

The author owes a tremendous amount to his parents, Mr. Masharraf Hossain and Mrs. Rokeya Sultana, whose sacrifices over the years have ensured a sound education and up-bringing. Their support has been instrumental in his achievements thus far.

The author is deeply indebted to his wife Jesmin for her constant love and affection. Her strong support and encouragement are highly appreciated.

Contents

Abstract 2

Acknowledgements 3

List of figures 12

List of tables 22

List of symbols 24

1 Introduction 27

1.1 Background 27

1.2 Scope and objectives of the research work 28

1.3 Outline of the thesis 28

2 Literature review: general background 31

2.1 Introduction 31

2.2 Uncertainty in slab design 31

2.3 Provision of different codes 32

2.3.1 BS 8110 32

2.3.2 CEB-FIP Model Code 1990 33

2.3.3 Eurocode 2 34

2.3.4 ACI code 36

2.3.5 Maximum permissible computed deflections 38

2.4 Long-term multipliers 38
2.5 Restraint cracking 39
2.6 Variability in field-measured deflection 40
2.7 Construction load 41
2.8 Biaxial bending and compression 43
2.9 Crack models 43
2.9.1 Assumptions 44
2.9.2 MC-90/EC2-91 model 44
2.9.3 Effective moment of inertia model 52
2.9.4 Gilbert model 53
2.10 Extension of MC-90 model to incorporate long-term effects 54
2.11 Concluding remarks 57

3 Review of FE models **59**
3.1 Introduction 59
3.2 Finite-element analysis 59
3.2.1 Effective-stiffness model 60
3.2.2 Layered model 62
3.2.3 3-D model 63
3.2.4 Discussion 63
3.2.5 Iteration Technique 64
3.3 Scanlon & Murray approach 65
3.4 Polak approach 67
3.5 Jofriet & McNeice approach 67
3.6 Favre *et al.* approach 71
3.7 Effective steel for different crack orientation 72
3.7.1 Jofriet & McNeice approach to calculate effective steel areas across cracks 73
3.7.2 Limitations of Jofriet & McNeice's approach 75
3.7.3 Other approaches for calculating effective steel 76
3.8 Concluding remarks 77

4 Incorporation of models in FE package and their performances 78

4.1 Introduction 78

4.2 Comparison with other methods 78

4.3 Incorporation of FE models 79

4.3.1 Sequences of analysis 80

4.3.2 Assumptions in the analysis of the slabs 82

4.4 Equivalent steel areas 83

4.4.1 Derivation of equivalent steel areas for bending of plate . . . 83

4.4.2 Suitability of the different sets of equations 86

4.5 Deflection comparison using different equations to calculate the effective steel 88

4.5.1 Short-term loading: McNeice slab 88

4.5.2 Short-term loading: Shukla & Mittal slabs 92

4.5.3 Long-term loading: Taywood slab 95

4.6 Proposed approach for calculating the effective steel 100

4.7 Incorporation of ACI and Gilbert's method 100

4.8 MC-90 method 102

4.8.1 Calculation for long-term deflection 103

4.8.2 Calculation for state 1 104

4.8.3 Calculation for state 2 105

4.8.4 Mean curvature 106

4.8.5 The modification factor 106

4.9 Formation of $[E]$ matrices 106

4.10 Effect of modifying the shear terms of the $[E]$ matrix 108

4.11 Selection of convergence procedure 109

4.12 Comparison with short-term experimental results 115

4.12.1 McNeice's two-way corner-supported slab 115

4.12.2 McNeice's one-way slab 118

4.12.3 Cement and Concrete Association beam 120

4.12.4 Jain & Kennedy's one-way slab 122

4.12.5 Elstner & Hognestad corner-supported slab 125

4.12.6 Zaghlool *et al.* column-supported slab 127
4.12.7 Shukla & Mittal two-way edge-supported slab 130
4.13 Comparison with long-term experimental results 132
4.13.1 Favre *et al.* slab 132
4.13.2 Ganeswaran & Rangan one-way slab 137
4.14 Concluding remarks 141

5 Performance of ACI and MC-90 models for biaxial bending and compression **142**

5.1 Introduction 142
5.2 Assumptions 143
5.3 Short-term analysis 143
5.3.1 Curvature in state 1 143
5.3.2 Curvature in state 2 144
5.3.3 Mean inertia by ACI equations 151
5.3.4 Mean curvature by MC-90 equations 152
5.4 Comparison with short-term experimental results 153
5.4.1 One-directional eccentricity: experiment by Sakai & Kakuta . 153
5.4.2 Two-directional eccentricity: analysis by Hsu & Mirza 156
5.4.3 Two-directional eccentricity: Experiment by Wang *et al.* . . 159
5.5 Long-term analysis 161
5.5.1 Calculation for long-term in state 1 161
5.5.2 Calculation for long-term in state 2 161
5.5.3 Mean curvature 162
5.6 FE analysis 162
5.6.1 Equivalent section 162
5.6.2 Numerical example 164
5.7 Zaghlool *et al.* slab 166
5.8 Parker & Bullman slab 168
5.9 Conclusions 174

6 Time-varying load history **175**

6.1 Introduction 175

6.2 Assumptions 176

6.3 Analysis method for time-varying load history 176

6.3.1 Instantaneous change in curvature due to load increment . . 177

6.3.2 Change in curvature with time under constant load 178

6.4 Analysis method for slab 179

6.5 Calculation for unloading and reloading 183

6.5.1 Instantaneous unloading 183

6.5.2 Long-term after unloading: creep recovery 186

6.5.3 Long-term after unloading: interpolation coefficient 188

6.6 Effect of subdivision of load step: slab 189

6.6.1 Statically determinate one-way slab 190

6.6.2 Statically indeterminate fixed-edge slab 193

6.7 Analysis method for column 196

6.8 Effect of subdivision of load step: column 198

6.8.1 Statically determinate cantilever 198

6.8.2 Statically indeterminate propped cantilever 201

6.9 Taywood slab 203

6.9.1 Selection of mesh 203

6.9.2 The effect of modelling a column for cracking, creep and shrinkage 206

6.9.3 The effect of redistribution of stresses in column and slab . . 209

6.9.4 The effect of creep recovery 213

6.9.5 The effect of the β_2 factor 216

6.10 Conclusions 220

7 Parametric study **222**

7.1 Introduction 222

7.1.1 Geometric parameters (including reinforcement) 222

7.1.2 Material properties 223

7.1.3 Construction factors 223
7.1.4 Service-life factors 224
7.2 Details of the slab used in parametric study 224
7.2.1 Loading and design 224
7.2.2 Material properties 225
7.2.3 Imposed load 226
7.3 Effect of geometric properties 227
7.3.1 Effect of slab thickness 227
7.3.2 Effect of providing more bottom steel than required 231
7.3.3 Effect of distribution of reinforcement 233
7.3.4 Effect of column dimensions 236
7.4 Effect of material properties 239
7.4.1 Effect of concrete strength 239
7.4.2 Effect of variation in tensile strength 242
7.4.3 Effect of variation in creep coefficient 245
7.4.4 Effect of variation in shrinkage strain 247
7.4.5 Effect of variation in modulus of elasticity of concrete 249
7.4.6 Varying material properties to extremes 251
7.5 Effect of construction load sequences and their timings 254
7.5.1 Adopting different construction sequences 254
7.5.2 Early creep and recovery 260
7.5.3 A simplified method to model construction loading 266
7.5.4 A single-step method to calculate long-term deflection 269
7.5.5 Effect of age at striking 272
7.6 Effect of service-life factors 276
7.6.1 Effect of magnitude of imposed load and application time . . 276
7.6.2 Effect of relative humidity 278
7.7 Conclusions 280
7.7.1 Geometric properties 280
7.7.2 Material properties 281
7.7.3 Construction parameters 282

7.7.4 Service-life parameters 282

8 Modelling of full scale testing: Cardington ECBP building 284

8.1 Introduction 284

8.2 Description of the ECBP building 286

8.2.1 Material properties 288

8.2.2 Loading 290

8.2.3 Deflection measurement 292

8.3 FE analysis 292

8.3.1 Assumptions 293

8.3.2 Mesh-sensitivity 293

8.3.3 Simplified loading history 294

8.3.4 Material properties used 295

8.4 Modelling of deflection with time 296

8.4.1 Deflection development: floor 3 297

8.4.2 Deflection development: floor 4 300

8.4.3 Deflection development: floor 6 302

8.5 Contribution of creep and shrinkage 304

8.6 Contribution of reinforcement 306

8.6.1 Reinforcement contribution: floor 3 308

8.6.2 Reinforcement contribution: floor 4 310

8.6.3 Reinforcement contribution: floor 6 312

8.7 Pattern load 314

8.7.1 Deflections of floor 3 314

8.7.2 Deflections of floor 4 317

8.7.3 Deflections of floor 6 319

8.8 Conclusions 321

9 Conclusions 323

9.1 Introduction 323

9.2 Summary of the work 324

9.2.1 Literature review 324

9.2.2 Modelling of cracking, creep and shrinkage 325
9.2.3 Modelling of time-varying load history 326
9.2.4 Parametric study 327
9.2.5 Modelling of Cardington slab 329
9.3 Recommendations for future work 330

A Effective steel **332**

B MC-90 creep coefficient and shrinkage strain **340**
B.1 Development of modulus of elasticity with time 340
B.2 Creep coefficient 341
B.3 Shrinkage 342

References **344**

List of Figures

2.1 Stress in a reinforced concrete member cracked due to an axial force; (a) cracking of a tie; (b) stress in reinforcement; (c) bond stress; (d) stress in concrete ($\sigma_c \leq f_{ct}$) 46

2.2 Axial forces versus mean strain in a member subjected to axial tension 48

2.3 A reinforced concrete member in flexure 49

2.4 Moment versus curvature in a reinforced concrete member in flexure 51

2.5 Gilbert's model 54

3.1 Effective-stiffness model 61

3.2 Layered model 62

3.3 3-D model 63

3.4 Effective steel area 73

4.1 Flow chart showing the sequences of calculation 81

4.2 Equivalent steel area 84

4.3 Details of corner-supported two-way slab tested by McNeice 89

4.4 Load versus deflection curves for the corner-supported McNeice slab using different equations to calculate effective steel: node 7 90

4.5 Load versus deflection curves for the corner-supported McNeice slab using different equations to calculate effective steel: node 69 90

4.6 Load versus deflection curves for the corner-supported McNeice slab using different equations to calculate effective steel: node 147 91

4.7 Load versus deflection curves for the corner-supported McNeice slab using different equations to calculate effective steel: node 157 91
4.8 Details of edge-supported two-way slabs tested by Shukla & Mittal . 93
4.9 Load versus deflection curves for the edge-supported Shukla & Mittal slab S-8 using different equations to calculate the effective steel . . . 93
4.10 Load versus deflection curves for the edge-supported Shukla & Mittal slab S-11 using different equations to calculate effective steel 94
4.11 Load versus deflection curves for the edge-supported Shukla & Mittal slab S-12 using different equations to calculate effective steel 94
4.12 Details of Taywood slab 96
4.13 Simplified load history for Taywood slab 97
4.14 Deflection versus time curves for column-supported Taywood slab using different equations to calculate the effective steel: node 1 97
4.15 Service load versus deflection curves (at 30 days) for the column-supported Taywood slab using different equations to calculate the effective steel: node 1 98
4.16 Deflection versus time curves for column-supported Taywood slab using different equations to calculate the effective steel: node 157 . . . 98
4.17 Service load versus deflection curves (at 30 days) for the column-supported Taywood slab using different equations to calculate the effective steel: node 157 99
4.18 Details of flat slab used in the selection of the convergence procedure 112
4.19 Different convergence approaches: node 35 112
4.20 Different convergence approaches: node 147 113
4.21 Different convergence approaches: node 169 113
4.22 Different convergence approaches: node 325 114
4.23 Load versus deflection curves for the corner-supported McNeice slab: node 7 116
4.24 Load versus deflection curves for the corner-supported McNeice slab: node 69 116

4.25 Load versus deflection curves for the corner-supported McNeice slab: node 147 117
4.26 Load versus deflection curves for the corner-supported McNeice slab: node 157 117
4.27 Details of simply supported one-way slab tested by McNeice 118
4.28 Load versus deflection curves for the simply supported one-way slab tested by McNeice 119
4.29 Details of simply supported beam tested by the Cement and Concrete Association 120
4.30 Load versus deflection curves for the beam tested by the Cement and Concrete Association 121
4.31 Details of simply supported one-way slab tested by Jain & Kennedy 123
4.32 Moment versus deflection curves for the simply supported one-way slab tested by Jain & Kennedy: taken from the ABAQUS manual . 124
4.33 Moment versus deflection curves for the simply supported one-way slab tested by Jain & Kennedy 124
4.34 Details of the corner-supported two-way slab tested by Elstner & Hognestad 126
4.35 Load versus deflection curves for the corner supported slab tested by Elstner & Hognestad 126
4.36 Details of the column-supported slab tested by Zaghlool *et al.* . . . 128
4.37 Load versus deflection curves for the column-supported slab tested by Zaghlool *et al.* 129
4.38 Variation of total central moment with load for the column-supported slab tested by Zaghlool *et al.* 129
4.39 Load versus deflection curves for the edge-supported Shukla & Mittal slab S-8 130
4.40 Load versus deflection curves for the edge-supported Shukla & Mittal slab S-11 131
4.41 Load versus deflection curves for the edge-supported Shukla & Mittal slab S-12 131

4.42 Details of one-way simply-supported slab tested by Favre *et al.* . . 133
4.43 Experimental and MC-90 creep coefficient for concrete for slabs CF4 and A1 134
4.44 Experimental and MC-90 shrinkage strain for concrete for slabs CF4 and A1 134
4.45 Moment-curvature relationship: Favre *et al.* slab A1 135
4.46 Moment-curvature relationship: Favre *et al.* slab CF4 135
4.47 Deflection versus time: Favre *et al.* slab A1 136
4.48 Deflection versus time: Favre *et al.* slab CF4 136
4.49 Details of one-way simply-supported slabs tested by Ganeswaran & Rangan 138
4.50 Experimental and MC-90 creep coefficient for concrete S/62 138
4.51 Experimental and MC-90 shrinkage strain for concrete S/62 139
4.52 Deflection versus time: Ganeswaran & Rangan slab S/62-0.63 139
4.53 Deflection versus time: Ganeswaran & Rangan slab S/62-0.80 140
4.54 Deflection versus time: Ganeswaran & Rangan slab S/62-0.98 140

5.1 Curvature in state 1 144
5.2 Curvature in state 2 145
5.3 Cross-section analysed in numerical example 149
5.4 Location of axial loads and neutral axis 150
5.5 Test specimen and loading method, experiment by Sakai & Kakuta . 154
5.6 Moment-curvature curves for steel percentage 0.932 (experiment by Sakai & Kakuta) 155
5.7 Moment-curvature curves for steel percentage 0.596 (experiment by Sakai & Kakuta) 155
5.8 Details of section with material properties, analysis by Hsu & Mirza 157
5.9 Moment-curvature curves: around x- or y-axis, analysis by Hsu & Mirza, ACI and MC-90 model 157
5.10 Moment-curvature curves: around x-axis, analysis by Hsu & Mirza, ACI and MC-90 model 158

5.11 Moment-curvature curves: around y-axis, analysis by Hsu & Mirza, ACI and MC-90 model 158
5.12 Details of column U-5 with material properties, tested by Wang *et al.* 159
5.13 Moment-curvature curves: around x-axis, experiment by Wang *et al.* 160
5.14 Moment-curvature curves: around y-axis, experiment by Wang *et al.* 160
5.15 Equivalent section for FE analysis 163
5.16 Column section and equivalent section 165
5.17 Effect of modelling column cracking on deflection: slab tested by Zaghlool *et al.* 167
5.18 Effect of modelling column cracking on central moment: slab tested by Zaghlool *et al.* 167
5.19 Test arrangement: slab tested by Parker & Bullman 169
5.20 Slab reinforcement: slab tested by Parker & Bullman 169
5.21 Load-deflection curves: Parker & Bullman slab 6a 170
5.22 Load-deflection curves: Parker & Bullman slab 6b 171
5.23 Load-deflection curves: Parker & Bullman slab 6c 171
5.24 Load-deflection curves: Parker & Bullman slab 6d 172
5.25 Load-deflection curves: Parker & Bullman slab 6e 172
5.26 Load-deflection curves: Parker & Bullman slab 6f 173

6.1 Time-varying load 177
6.2 Moment-curvature relationship proposed by Model Code 90 184
6.3 Moment-curvature relationship proposed by Rotilio 185
6.4 Principle of superposition of creep curvatures 186
6.5 Recoverable and irrecoverable creep components 187
6.6 Moment-curvature relationship: loading and unloading 188
6.7 FE mesh for the fixed-edge and one-way slab 191
6.8 One-way slab: node 1 deflection with time 192
6.9 One-way slab: node 17 deflection with time 192
6.10 Fixed-edge slab: node 1 deflection with time 194
6.11 Fixed-edge slab: node 17 deflection with time 194

6.12 Fixed-edge slab: node 79 deflection with time 195

6.13 X directional sway of top of the cantilever with time 199

6.14 Y directional sway of top of the cantilever with time 200

6.15 X directional sway of middle of the propped cantilever with time . . 201

6.16 Y directional sway of middle of the propped cantilever with time . . 202

6.17 Sensitivity analysis: mesh 1 204

6.18 Sensitivity analysis: mesh 2 205

6.19 Sensitivity analysis: mesh 3 205

6.20 Effect of modelling a column: deflection with time for the Taywood slab, node 1 207

6.21 Effect of modelling a column: service load-deflection (at 30 days) for the Taywood slab, node 1 207

6.22 Effect of modelling a column: deflection with time for the Taywood slab, node 157 208

6.23 Effect of modelling a column: service load-deflection (at 30 days) for the Taywood slab, node 157 208

6.24 Effect of redistribution of stresses: deflection with time for the Taywood slab, node 1 211

6.25 Effect of redistribution of stresses: service load-deflection (at 30 days) for the Taywood slab, node 1 211

6.26 Effect of redistribution of stresses: deflection with time for the Taywood slab, node 157 212

6.27 Effect of redistribution of stresses: service load-deflection (at 30 days) for the Taywood slab, node 157 212

6.28 Effect of creep recovery: deflection with time for the Taywood slab, node 1 214

6.29 Effect of creep recovery: service load-deflection (at 30 days) for the Taywood slab, node 1 214

6.30 Effect of creep recovery: deflection with time for the Taywood slab, node 157 215

6.31 Effect of creep recovery: service load-deflection (at 30 days) for the Taywood slab, node 157 215
6.32 Effect of the β_2 factor: deflection with time for the Taywood slab, node 1 218
6.33 Effect of the β_2 factor: service load-deflection (at 30 days) for the Taywood slab, node 1 218
6.34 Effect of the β_2 factor: deflection with time for the Taywood slab, node 157 219
6.35 Effect of the β_2 factor: service load-deflection (at 30 days) for the Taywood slab, node 157 219

7.1 Effect of slab thickness on elastic deflection 229
7.2 Effect of slab thickness on instant deflection 230
7.3 Effect of slab thickness on long-term deflection 230
7.4 Effect of providing more bottom steel than required for strength on instant deflection 232
7.5 Effect of providing more bottom steel than required for strength on long-term deflection 232
7.6 Effect of distribution of reinforcement on instant deflection 234
7.7 Effect of distribution of reinforcement on long-term deflection 235
7.8 Effect of column size on elastic deflection 237
7.9 Effect of column size on instantaneous deflection 238
7.10 Effect of column size on long-term deflection 238
7.11 Effect of concrete strength on elastic deflection 240
7.12 Effect of concrete strength on instantaneous deflection 241
7.13 Effect of concrete strength on long-term deflection 241
7.14 Effect of tensile strength on instant deflection 244
7.15 Effect of tensile strength on long-term deflection 244
7.16 Effect of creep coefficient on long-term deflection 246
7.17 Effect of shrinkage strain on long-term deflection 248
7.18 Effect of elasticity of concrete on instant deflection 250

7.19 Effect of elasticity of concrete on long-term deflection 250
7.20 Effect of varying material properties to extremes on instant deflection 253
7.21 Effect of varying material properties to extremes on long-term deflection 253
7.22 Different construction sequences 255
7.23 Effect of different construction sequences: mean f_{ct}, R =0.5 257
7.24 Effect of different construction sequences: mean f_{ct}, R =1.0 257
7.25 Effect of different construction sequences: low f_{ct}, R =0.5 258
7.26 Effect of different construction sequences: low f_{ct}, R =1.0 258
7.27 Effect of different construction sequences: high f_{ct}, R =0.5 259
7.28 Effect of different construction sequences: high f_{ct}, R =1.0 259
7.29 Creep recovery: superposition with different R factors 260
7.30 Effect of recovery factor, R: 3 shores method 261
7.31 Effect of recovery factor, R: 1 shore-2 reshores method 262
7.32 Effect of recovery factor, R: Cardington loading 262
7.33 Creep recovery: simplified load history 263
7.34 Creep recovery: different R factors 265
7.35 Simplified load history: different construction sequences 267
7.36 Effect of age at striking: β_2=1 and 0.5 for instant and long-term respectively (with no construction load) 274
7.37 Effect of age at striking: β_2=0.5 for both instant and long-term (with no construction load) 274
7.38 Influence of striking time: Cardington loading 275
7.39 Influence of striking time: Cardington loading, uncracked slab 275
7.40 Effect of magnitude of imposed load and their application time: Cardington loading 277
7.41 Effect of relative humidity on long-term deflection 279

8.1 Cardington building 285
8.2 Floor plan and deflection measurement grid 286

8.3 Comparison of creep and shrinkage properties: measured and MC-90 predictions for floor 3 288
8.4 Comparison of creep and shrinkage properties: measured and MC-90 predictions for floor 4 289
8.5 Comparison of creep and shrinkage properties: measured and MC-90 predictions for floor 6 289
8.6 Actual and simplified load histories of floors 3, 4 and 6. 291
8.7 FE mesh for Cardington floors 295
8.8 Deflection development with time: corner panel, floor 3 298
8.9 Deflection development with time: external panel, floor 3 299
8.10 Deflection development with time: internal panel, floor 3 299
8.11 Deflection development with time: corner panel, floor 4 300
8.12 Deflection development with time: external panel, floor 4 301
8.13 Deflection development with time: internal panel, floor 4 301
8.14 Deflection development with time: corner panel, floor 6 302
8.15 Deflection development with time: external panel, floor 6 303
8.16 Deflection development with time: internal panel, floor 6 303
8.17 Contribution of creep and shrinkage: corner panel, floor 3 304
8.18 Contribution of creep and shrinkage: external panel, floor 3 305
8.19 Contribution of creep and shrinkage: internal panel, floor 3 305
8.20 Comparison of measured deflections of different floors: corner panel . 306
8.21 Comparison of measured deflections of different floors: external panel 307
8.22 Comparison of measured deflections of different floors: internal panel 307
8.23 Contribution of reinforcement meshes: corner panel, floor 3 308
8.24 Contribution of reinforcement meshes: external panel, floor 3 309
8.25 Contribution of reinforcement meshes: internal panel, floor 3 309
8.26 Contribution of reinforcement meshes: corner panel, floor 4 310
8.27 Contribution of reinforcement meshes: external panel, floor 4 311
8.28 Contribution of reinforcement meshes: internal panel, floor 4 311
8.29 Contribution of reinforcement meshes: corner panel, floor 6 312
8.30 Contribution of reinforcement meshes: external panel, floor 6 313

8.31 Contribution of reinforcement meshes: internal panel, floor 6 313

8.32 Pattern load: corner panel, floor 3 315

8.33 Pattern load: external panel, floor 3 315

8.34 Pattern load: internal panel, floor 3 316

8.35 Pattern load: corner panel, floor 4 317

8.36 Pattern load: external panel, floor 4 318

8.37 Pattern load: internal panel, floor 4 318

8.38 Pattern load: corner panel, floor 6 319

8.39 Pattern load: external panel, floor 6 320

8.40 Pattern load: internal panel, floor 6 320

A.1 Isotropic mesh: A_{sx}=0.6% and A_{sy}=0.6% 334

A.2 Orthotropic mesh: A_{sx}=1.2% and A_{sy}=0.6% 335

A.3 Orthotropic mesh: A_{sx}=1.8% and A_{sy}=0.6% 336

A.4 Isotropic mesh: A_{sx}=0.6% and A_{sy}=0.6% 337

A.5 Orthotropic mesh: A_{sx}=1.2% and A_{sy}=0.6% 338

A.6 Orthotropic mesh: A_{sx}=1.8% and A_{sy}=0.6% 339

List of Tables

2.1 Basic ratios of span-to-effective depth, f_{yk}= 460 N/mm^2 34

2.2 Minimum thickness of flat slabs 37

2.3 Comparison of recommended design multipliers 39

4.1 Properties of Taywood slab 96

4.2 Effect of modifying the shear and torsional terms of the $[E]$ matrix . 109

5.1 Position and orientation of neutral axis and steel stresses for different load cases 150

5.2 Identification and properties of the Sakai & Kakuta specimens . . . 154

5.3 Geometric and material properties: Parker & Bullman slab 170

6.1 Mesh sensitivity: Taywood slab 204

7.1 Effect of slab thickness 227

7.2 Effect of providing more bottom steel than required 231

7.3 Effect of distribution of reinforcement 233

7.4 Effect of column size 236

7.5 Effect of concrete strength 240

7.6 Effect of tensile strength 242

7.7 Effect of loss of stiffness: using $\beta_2 = 0.5$ 243

7.8 Effect of creep coefficient 245

7.9 Effect of shrinkage strain 247

7.10 Effect of modulus of elasticity of concrete 249

7.11 Effect of varying material properties to extremes 252
7.12 Effect of construction sequences 256
7.13 Effect of recovery factor 261
7.14 Amount of creep recovery 264
7.15 Comparison between results from simplified load history and rigorous step analyses 268
7.16 Single-step load: selecting f_{ct-mod} 270
7.17 Single-step load: comparison with the results of simplified and rigorous step analyses 271
7.18 Effect of imposed load: comparison of material properties 277
7.19 Effect of relative humidity 278
7.20 Summary of parametric study: geometric properties 280
7.21 Summary of parametric study: material properties 281
7.22 Summary of parametric study: construction factors 283
7.23 Summary of parametric study: service-life factors 283

8.1 Details of concrete mix and reinforcement arrangements at each floor 287
8.2 Mesh-sensitivity: Cardington slab 294
8.3 Material properties used in FE analysis 297

List of symbols

The following notation is used in this thesis. Where more than one meaning has been assigned to a symbol, the correct definition will be evident from the context in which it is used. Those not define below are explained in the text.

c_n	Depth of neutral axis
d, t	Effective depth and thickness of section
e, e_x, e_y	Eccentricity and its component in x and y directions
f_c'	Concrete cylinder compressive strength
f_{ct}	Tensile strength of concrete
f_{cu}	Concrete cube compressive strength
f_r	Modulus of rupture of concrete
f_y	Yield strength of the reinforcing steel
k	Curvature reduction factor to take into account of the effect of reinforcement
l	Slab span
n	Modular ratio= E_s/E_c
r_c	Radius of gyration of concrete section
r_{nt}	Ratio of steel strains in principal directions= ϵ_n/ϵ_t
t_0	Time of application of first load step P_1
t_n	Time of application of load step P_{n+1}
A_{sx}, A_{sy}	Tensile reinforcement areas in x and y directions
A_{sn}, A_{st}	Tensile reinforcement areas in principal directions n and t

A_{sxp}, A_{syp}	Compressive reinforcement areas in x and y directions
A_{snp}, A_{stp}	Compressive reinforcement areas in principal directions n and t
$[E]$	Elasticity matrix in x-y directions
$[E']$	Elasticity matrix in principal directions
E_c	Modulus of elasticity of concrete
$\bar{E}_c$	Age-adjusted modulus of elasticity of concrete
E_s	Modulus of elasticity of steel
$E(i,j)$	(i,j)th element of $[E]$ matrix
EI_{eqx}, EI_{eqy}	Flexural rigidity of equivalent section around x and y directions
E_1	Elasticity of the brick element in the axial direction
E_2	Elasticity of the line elements on y axis in the axial direction
E_3	Elasticity of the line elements on x axis in the axial direction
G	Shear modulus
I_{cr}	Second moment of area of cracked (no tension in concrete) section
I_e	Effective second moment of area
I_g	Second moment of area of gross (without reinforcement) uncracked section
M	Bending moment at a section
M_{cr}	Cracking moment as defined by ACI
M_r	Cracking moment as defined by MC-90
$M_n(t_n)$	Moment due to load P_n at time t_n
$M_n(t_{n+1})$	Moment due to load P_n at time t_{n+1}
P_n	Load step sustained from time t_n to t_{n+1}
Z	Lever arms of section
α_n, α_t	Modification factors to include the effect of cracking, creep and shrinkage in the $[E']$ matrices
β_1	Takes into account the bond properties of bars
β_2	Takes into account the deterioration of tension stiffening for long-term and repeated loads
ϵ	Strain
ϵ_{cs}	Shrinkage strain

ζ	Interpolation coefficient to find the mean curvature from states 1 and 2 curvatures
θ	Angle of major principal direction with x axis
μ	$=A_{sy}/A_{sx}$
ν	Poisson's ratio
ρ	Tensile steel percentage
σ_1, σ_2	Stresses in the outer fibre of the section in principal directions
σ_c	Stress in concrete
σ_s	Stress in steel at moment M
σ_{sr}	Stress at steel at cracking moment M_{cr}
$\phi(t, t_0)$	Creep coefficient of concrete, i.e. ratio of creep strain to the instantaneous strain due to a stress applied at time t_0 and sustained to time t
χ	Aging coefficient
$\psi_1(t_0)$, $\psi_1(t)$	State 1 curvature at time t_0 and t
$\psi_2(t_0)$, $\psi_2(t)$	State 2 curvature at time t_0 and t
$\psi_m(t_0)$, $\psi_m(t)$	Mean curvature at time t_0 and t
ψ_{mx}, ψ_{my}	x and y component of mean curvature
$\psi_m^*(t_n)$	Mean curvature calculated using a single load step for moment $M_n(t_n)$ and all the incremental creep and shrinkage curvatures occurring up to t_n are added to it
$\psi_m^*(t_{n+1})$	Mean curvature calculated using a single load step for moment $M_n(t_{n+1})$ and all the incremental creep and shrinkage curvatures occurring up to t_{n+1} are added to it
$\psi_m^*(t_n^-)$	Mean curvature calculated using a single load step for moment $M_{n-1}(t_n^-)$
$\Delta\psi_1$	Change in state 1 curvature due to creep and shrinkage
$\Delta\psi_2$	Change in state 2 curvature due to creep and shrinkage
$\Delta\psi_m$	Change in mean curvature due to creep and shrinkage or due to load change

Chapter 1

Introduction

1.1 Background

Over the last three decades, much research has been carried out to model slab deflections under uniform loading using non-linear FE analysis. The realistic estimate of slab deflections at the serviceability limit state has become more important due to the increasing use of high strength materials in recent years. Different building codes provide a wide range of guidelines for selecting safe span-to-depth ratios that can be used without any deflection calculations. However, a survey (Reinforced Concrete Council, 1990) of flat slab structures, all designed in accordance with BS8110 (1985), found variations in span-to-depth ratio between 24 and 36. This indicates that there is considerable uncertainty within the design community over the best strategy to select the thickness of flat slabs. The RCC has produced a cost model (Reinforced Concrete Council, 1993) which suggests that reducing slab thicknesses could lead to overall potential savings of £50m to UK plc and additional equal or greater savings in the whole building cost due to reductions in the cost of cladding and foundations. To reduce the uncertainty in selection of thickness of flat slabs, there is clearly a need to develop improved methods for predicting deflections under service loads.

1.2 Scope and objectives of the research work

The objective of the research work is to develop a numerical model to predict deflections of flat slabs under service loads. In reality, a slab undergoes a time-varying load during its construction and operational life, which needs to be accounted for if long-term deflections are to be modelled realistically. To this end, the author has developed an FE-based numerical method that accounts for the full load history of a slab, including construction loads which often govern the level of cracking. However, the research work starts with developing the FE method for short- and long-term predictions of test results under uniform loading. This work is extended to model cracking, creep and shrinkage in columns. The author's method of predicting deflections for a time-varying load successfully models the deflection of the Cardington floors. An extensive parametric study is carried out to identify the influence of different geometrical, loading and material factors on slab deflections. Furthermore, two simplified methods are proposed for predicting long-term deflections due to a time-varying load.

1.3 Outline of the thesis

The thesis consists of 9 chapters and 2 appendices which are outlined in this section.

Chapter 1- General background to the research programme and summary of aims and objectives.

Chapter 2- This chapter points out the uncertainty in selection of slab thickness, gives different code provisions for span-to-depth ratios, code methods for calculating long-term deflections and the maximum permissible deflections. The variation of the different suggested multipliers is shown. Previous work on restraint shrinkage, construction load and biaxial bending with compression is discussed. Different crack models are explained along with the assumptions and mathematical formulations. Finally, the CEB-FIP model code (MC-90) method to calculate long-term curvatures is discussed.

Chapter 3- FE models for calculation of short- and long-term deflections are re-

viewed along with their assumptions, limitations and mathematical formulations.

Chapter 4- Here, the author develops an FE method that is based on the effective-stiffness approach with secant-stiffness formulations. Several short-term models- namely, ACI or Branson model, Gilbert model and MC-90 model- have been incorporated into an existing FE package. The MC-90 method has been used to model the long-term effects of creep and shrinkage. Equations have been proposed for determining the effective area of steel in the principal directions for cracked and uncracked sections. The procedure of modifying the elasticity matrices is described in detail. A convergence procedure to reach a stable solution is presented along with numerical results. Performances of short- and long-term models have been verified for some available experimental results.

Chapter 5- The MC-90 model for biaxial bending with a compressive force is also included in the package so that cracking, creep and shrinkage in columns can be simulated. An iterative method is used to determine the position and orientation of the neutral axis. The column is modelled with brick and line elements, the stiffnesses of which are adjusted to represent the cracked column under biaxial bending due to an eccentric load.

Chapter 6- A method based on the MC-90 model is proposed for calculating the deflection due to a time-varying load history. Moments and curvatures of all the elements are stored at the end of each load step. Incremental moments, and thereby incremental curvatures, are calculated for the next load step which are then added to the previous curvatures to find the curvature at the end of the step.

Chapter 7- A series of parametric studies has been carried out to identify the influence of relevant parameters. Two simplified approaches are proposed to estimate long-term slab deflections for a non-uniform load history.

Chapter 8- A full scale 7-storey building has been constructed at Cardington which presents a unique opportunity to measure deflections in a real building under known and controlled conditions. The model has been used to estimate deflections of the Cardington slab and the results are compared with the measurements from Cardington to date.

Chapter 9- Conclusions and recommendations for future work.

Appendix A- Different methods to calculate effective steel in the principal directions are compared.

Appendix B- MC-90 equations to calculate creep coefficient and shrinkage strain are presented.

Chapter 2

Literature review: general background

2.1 Introduction

Considerable uncertainty exists within the design community over the selection of thickness of flat slabs. Different building codes provide a wide range of guidelines to select safe span-to-depth ratios which can be used without any deflection calculations. Also there are simplified methods in codes to calculate short- and long-term deflections. A literature review was carried out which is presented in Chapter 2 and 3. Chapter 2 identifies the uncertainties in design, and describes different code provisions, maximum permissible deflection, simplified method of calculating long-term deflections using multipliers, effect of construction load etc. Different crack models and CEB-FIP Model Code 1990, MC-90 (1993) long-term model are also presented with assumption and formulations. Chapter 3 explains different finite element analyses and approaches used by several authors to incorporate cracking and long-term effects.

2.2 Uncertainty in slab design

The key problem faced by designers of reinforced concrete floors are, first, choosing a suitable floor system and, secondly, determining member depths which are usually governed by the need to restrict deflections under service loads. It is important to select an appropriate floor system because at least 80% of the cost of a reinforced

concrete frame lies in the cost of the slabs (concrete, reinforcement and form-work). The RCC has produced a cost model (Reinforced Concrete Council, 1993) which indicates that reducing slab thicknesses could lead to overall potential savings of £50m to UK plc and additional equal or greater savings in the whole building cost due to reductions in the cost of cladding and foundations. The scope for reducing slab thickness is highlighted by a survey of flat slab structures that was carried out by the RCC (1990). This found variations in span-to-depth ratio between 24 and 36 for spans in the range of 6m to 9.2m, with design imposed loads in the range of 5 to 6 kN/m^2. The slab with the largest span, the only one designed using a finite element analysis, had the largest span-to-depth ratio and contained the least reinforcement per square metre. The fact that all these slabs were designed in accordance with BS 8110 (1985) indicates that there is considerable uncertainty within the design community over the best strategy to select the thickness of flat slabs.

2.3 Provision of different codes

Design provisions for deflection and minimum thickness of concrete slabs are available in various codes, but the approaches differ considerably.

2.3.1 BS 8110

BS 8110 (1997) recommends that for flat slabs, the span-to-effective depth ratios for beams are multiplied by 0.9. The basic span-to-effective depth ratio for continuous beams with rectangular section is 26. The ratio should be adjusted for tension and compression reinforcement. The multiplication factor for tension reinforcement is:

$$= 0.55 + \frac{(477 - f_s)}{120\left(0.9 + \frac{M}{bd^2}\right)} \leq 2.0 \tag{2.1}$$

where M is the design ultimate moment at the centre of the span and design service stress, f_s in tension reinforcement may be estimated from:

$$f_s = \frac{5 f_y A_{s,req}}{8 A_{s,prov}} . \frac{1}{\beta_b} \tag{2.2}$$

where β_b is the ratio of moments at any section after and before redistribution. For a continuous beam, if the percentages of redistribution is not known but the design ultimate moment at mid-span is obviously the same as or greater than the elastic ultimate moment, the f_s can be taken as 5/8 f_y.

The multiplication factor for compression reinforcement is:

$$= 1.0 + \frac{\frac{100A'_{s,prov}}{bd}}{\left(3.0 + \frac{100A'_{s,prov}}{bd}\right)} \leq 1.5 \tag{2.3}$$

BS 8110 claims that in normal cases the deflections will not be excessive if the above span-to-effective depth ratio is used.

2.3.2 CEB-FIP Model Code 1990

The Model Code 1990 (MC-90) (1993) provides moment-curvature relationships for uncracked and cracked sections that are valid up to and beyond the yield moment. Moment-curvature relationships are discussed in detail in section 2.9.2. The code also proposes a simplified method based on a bilinear relationship between load and deflection to calculate long-term deflections excluding the effect of shrinkage:

$$a = (1 + \phi)a_c \quad \text{for } M_d < M_r \tag{2.4}$$

$$a = (h/d)^3 \eta (1 - 20\rho_{cm})a_c \quad \text{for } M_d > M_r \tag{2.5}$$

where

a_c= the elastic deflection calculated on the basis of the gross section neglecting reinforcement,

M_d= the bending moment at mid span of a beam or a slab,

h = nominal size of member,

d = effective depth of section,

ρ_{cm} = the geometric mean percentage of compressive reinforcement,

η= a correction factor which includes the effect of cracking and creep.

A detailed check on deflection may not be necessary if the span-to-depth ratio

of a reinforced concrete element does not exceed a critical value given by:

$$l/d \leq \frac{1}{\sqrt[3]{\delta\eta(l/a)_{\text{lim}}}} \tag{2.6}$$

where,

$\delta = a_c h^3/l^4$

$(l/a)_{\text{lim}}$= limiting value of span/deflection = 300.

For reinforced concrete flexural elements, without axial force, the following formula may be applied

$$l/d \leq \lambda = \lambda_0 k_T k_l (400/f_{yk}) \tag{2.7}$$

where,

λ_0 = constant, 21 and 30 for highly and lightly stressed concrete respectively. If the reinforcement ratio is known, λ_0 can be obtained by interpolation assuming lightly stressed values to correspond to $\rho = 0.5\%$ and highly stressed to $\rho = 1.5\%$.

$k_T = 1.0$ for flat slab,

$k_l = 7/l \leq 1$, with l in metre,

l= span in metre,

f_{yk}= yield strength of the reinforcing steel in MPa.

2.3.3 Eurocode 2

Minimum thickness

Eurocode 2, EC2 (1991) suggests that the deflections of flat slabs will normally be satisfactory if they are dimensioned in accordance with the span-to-effective depth ratios given in Table 2.1 which are adapted from Concise Eurocode (1993).

Structural system	Concrete condition (reinforcement percentage)		
	Highly stressed (≥ 1.5)	Lightly stressed (0.5)	Nominally reinforced (≤ 0.15)
Flat slab	18.3	26.1	35.7

Table 2.1 Basic ratios of span-to-effective depth, f_{yk}= 460 N/mm^2

For flat slabs, where the greater span exceeds 8.5 m, the ratio should be multiplied by 8.5/span; for steel of characteristic strength other than 460 N/mm^2, the value should be multiplied by $460/f_{yk}$; where more reinforcement is provided than is required for the ultimate limit state, the value may be multiplied by $A_{s,prov}/A_{s,req}$, provided that the resulting value is not greater than that for nominally reinforced concrete.

Short- and long-term deflections

EC2 also provides methods to calculate short- and long-term deflections. Two limiting conditions are assumed to exist for the deformation of concrete section: the uncracked state and fully cracked state. Members which are not expected to be loaded above the level which would cause the tensile strength of concrete to be exceeded anywhere within the member will be considered to be uncracked. Members which are expected to crack will behave in a manner intermediate between the uncracked and fully cracked conditions as follows:

$$\alpha = \zeta\alpha_2 + (1-\zeta)\alpha_1 \tag{2.8}$$

where

α is the parameter considered which may be strain, a curvature, a rotation or deflection.

α_1 and α_2 are, respectively, the value of the parameter calculated for the uncracked (state 1) and cracked (state2) conditions.

ζ is a distribution coefficient given by:

$$\zeta = 1 - \beta_1\beta_2\left(\frac{\sigma_{sr}}{\sigma_s}\right)^2 \tag{2.9}$$

β_1 is a coefficient which takes account of the bond properties of bars; β_1=1.0 for high bond bars and 0.5 for plain bars.

β_2 is a coefficient which takes account of the duration of the loading or of repeated loading; β_2=1.0 for a single short-term loading and 0.5 for sustained loads or many cycles of repeated loading.

σ_s is the stress in the tension steel calculated on the basis of a cracked section.

σ_{sr} is the stress in the tension steel calculated on the basis of a cracked section under the loading which will just cause cracking at the section being considered.

Creep may be allowed for by using an effective modulus of elasticity calculated from:

$$\bar{E}_c = \frac{E_{cm}}{(1+\phi)} \tag{2.10}$$

where ϕ is the creep coefficient.

Shrinkage curvature may be assessed by:

$$\psi_{cs} = \epsilon_{cs}\bar{n}\frac{S}{I} \tag{2.11}$$

where

ϵ_{cs} is the free shrinkage strain.

S is the first moment of area of the reinforcement about the centroid of the section.

I is the second moment of area of the section.

$\bar{n}$ is the effective modular ratio=$E_s/\bar{E}_c$.

The most rigorous method of assessing deflections using the above equations is to compute the curvatures at frequent sections along the member and then calculate the deflection by numerical integration. EC2 does not find this method justified due to the effort involved and recommends that it will be acceptable to compute deflection twice assuming the whole member to be in the uncracked and fully cracked states and then employ eq. 2.8 to calculate the deflection.

2.3.4 ACI code

Two methods are given in the ACI code (1989) for controlling deflections of one-way and two-way flexural systems. The deflection may be controlled indirectly by compliance with specified minimum thicknesses or directly by limiting computed deflections, both of these are described below.

Minimum thickness

ACI code provides a guideline for minimum total thickness for flat slabs which is presented in Table 2.2.

Yield Strength f_y, psi	Exterior panel without edge beam	Exterior panel with edge beam	Interior panel
40,000	$\frac{l_n}{33}$	$\frac{l_n}{36}$	$\frac{l_n}{36}$
60,000	$\frac{l_n}{30}$	$\frac{l_n}{33}$	$\frac{l_n}{33}$
75,000	$\frac{l_n}{28}$	$\frac{l_n}{31}$	$\frac{l_n}{31}$

Table 2.2 Minimum thickness of flat slabs

Short- and long-term deflections

Short-term deflection can be calculated on the basis of an effective moment of inertia given by Branson's equation (see eq. 2.37 later on). Additional long-term deflections resulting from creep and shrinkage of flexural members (normal weight or light-weight concrete) are determined by multiplying the immediate deflection by the factor as

$$\lambda = \frac{\xi}{1 + 50\rho'} \tag{2.12}$$

where

ρ' = compression reinforcement ratio at mid span for simple and continuous spans, and at support for cantilever.

ξ = time-dependent factor for sustained loads, the value of which varies from 1.0 to a maximum of 2.0 for a time spanning from 3 months to 5 years or more.

The ACI code presumes that the maximum long-term deflection is three times the short-term deflection for a member without compression reinforcement. According to Solanki (1996), both the ACI equations and MC-90 simplified equations lead to similar deflections for flat slabs.

2.3.5 Maximum permissible computed deflections

The deflection limits for different codes are as follows.

1. If roof or floor construction supporting or attached to non-structural elements are likely to be damaged by large deflections, the ACI code limits the incremental deflection to span/480. Incremental deflection includes part of the total deflection that occurs after attachment of non-structural elements i.e. sum of the long-term deflection due to all sustained loads and the immediate deflection due to any additional live load are to be considered. The MC-90, EC2 and BS 8110 limit deflection under similar condition to span/500.

2. If the roof or floor construction supports or is attached to non-structural elements that are unlikely to be damaged by large deflections, the ACI code limits total deflection to span/240. The MC-90, EC2 and BS 8110 limit this type of deflection to span/250.

Solanki (1996) pointed out that the slight differences in the allowable deflections is probably due to rounding values in Imperial versus SI units.

2.4 Long-term multipliers

Graham & Scanlon (1986) suggested that the long-term multiplier given in the ACI Building Code (i.e. λ in eq. 2.12) should be increased for two-way slab deflections. Sbarounis (1984b) suggested the following equation to calculate the multiplier :

$$\lambda_t = 1 + \lambda_c \frac{\phi_u}{2.35} + \lambda_{sh} \frac{\epsilon_{sh_u}}{800 * 10^{-6}} \tag{2.13}$$

Sbarounis used a value of 2.8 for the creep deflection multiplier λ_c and 1.2 for the shrinkage deflection multiplier λ_{sh}. These values are applicable for an ultimate creep coefficient of 2.35 and an ultimate shrinkage strain of $800 * 10^{-6}$ in/in. Multipliers can be obtained for other values using eq. 2.13. Multipliers for one month and one year are also prescribed in Sbarounis (1984b). Graham & Scanlon (1986) also adopted eq. 2.13 but replaced the ultimate shrinkage strain by $780 * 10^{-6}$ in/in, λ_c and λ_{sh} values were assumed to be 1.5 and 1.0, respectively, when the modulus

Source	Recommended design multipliers			
	Immediate	Creep	Shrinkage	Total
Graham & Scanlon (1986)				
with $f_r = 7.5\sqrt{f'_c}$	1.0	2.0	2.0	5
with $f_r = 4\sqrt{f'_c}$	1.0	1.5	1.0	3.5
ACI (1989) and CSA	1.0	Total=2.0		3.0
Sbarounis (1984b)	1.0	2.8	1.2	5.0
Branson (1977)	1.0	2.0	1.0	4.0

Table 2.3 Comparison of recommended design multipliers

of rupture, f_r, is assumed to be $4\sqrt{f'_c}$ psi ($0.33\sqrt{f'_c}$ MPa) but were both taken as 2.0 when $7.5\sqrt{f'_c}$ psi ($0.62\sqrt{f'_c}$ MPa) is used for f_r. Table 2.3 presents multipliers recommended by several authors to estimate long-term deflection from instantaneous deflection. As can be seen in Table 2.3, both Sbarounis (1984b) and Graham & Scanlon (1986) suggest that long-term deflections are 5 times the instantaneous deflection.

2.5 Restraint cracking

In an under-reinforced concrete slab, flexural stiffness, and consequently deflection, is significantly affected by the degree of cracking in the slab. Cracking arises from flexural tensile stresses due to transverse loads. In addition, a significant amount of cracking can be caused by tensile stresses resulting from restrained volume change, primarily shrinkage. The development of cracks in a given slab system depends on a large number of factors, including creep and shrinkage, the tensile strength of the concrete, the degree of restraint, as well as construction and service loads. Shrinkage begins to take place shortly after the concrete is placed. Tensile stresses that develop due to restraint of shrinkage, are reduced by the effects of creep. However, tensile stresses exceeding the tensile strength of concrete may be expected to occur in many cases. Thus, the deflection is affected by shrinkage in two ways. The first is a direct effect: shrinkage produces curvature which increases deflection. The

second effect is indirect: shrinkage-induced tensile stress may reduce the load at which cracking occurs and may be sufficient to cause cracking. Scanlon & Murray (1982) suggested that the effect of cracking due to restrained volume change could be incorporated in a plate-bending analysis by use of a reduced effective modulus of rupture. The numerical studies and comparison between calculated and field-measured deflections outlined in Tam & Scanlon (1986) indicated that a range of effective moduli of rupture (from $2\sqrt{f'_c}$ psi to $7.5\sqrt{f'_c}$ psi) would provide a good estimate of the range of deflections likely to be encountered for a given slab. A value of $4\sqrt{f'_c}$ psi ($0.33\sqrt{f'_c}$ MPa) is recommended for estimating the mean deflection in a series of papers [(Thompson & Scanlon, 1988), (Scanlon & Murray, 1982), (Tam & Scanlon, 1986)].

Ghali (1989) proposed an alternative method for taking account of the tensile stress induced by restrained shrinkage. He used the following equation to calculate the actual tensile stress induced at the tensile face of the slab due to restrained shrinkage:

$$(\Delta\sigma)_{cs} = \bar{E}_c \left[(\Delta\psi)_{cs} y - \epsilon_{cs} \left(1 - \frac{A_c}{\bar{A}} \right) \right] \tag{2.14}$$

The modulus of rupture is reduced by this amount. As a result, cracking occurs at a reduced bending moment.

2.6 Variability in field-measured deflection

Results of a survey of two-way flat slab deflections both during and after construction of a 28-storey office tower were presented by Jokinen & Scanlon (1987). A comparison was made between measured deflections and deflections computed using a finite-element program that includes the effect of cracking. Effects of time-dependent deformations were included in the calculations. The comparison between the measured and the calculated deflections illustrates the high variability in the measured values. The calculated deflections corresponding to moduli of rupture of $7.5\sqrt{f'_c}$ and $2\sqrt{f'_c}$ psi were closely related to the lower and upper ranges of measured deflections. Deflections calculated with a modulus of rupture equal to $4\sqrt{f'_c}$ psi were close to the mean values of measured deflection. The maximum deflection was cal-

culated on the basis of construction load and then scaled to the sustained load level. The scaled deflection was multiplied by a long-term multiplier as recommended by Graham & Scanlon (1986).

2.7 Construction load

Relatively high construction loads applied to young slabs with low tensile strengths and low elastic moduli will cause extensive flexural cracking and large initial deflection. The high applied stress/developed strength ratio may cause significant creep, generally non-recoverable, resulting in large long-term deflections. Construction loads on the lower slabs in the supporting assembly may often exceed the service loads regardless of the number of floors used to support the newly cast slabs unless appropriate construction methods are used. Sbarounis (1984a) suggested that, in fact, for certain combinations of design loads, slab thickness, and span the calculated overloads are close to the ultimate strength of the slabs.

Construction loads are evidently related to the method of re-propping adopted and the number of floors which are back-propped. The following three systems of back-propping are used:

1. In low-rise buildings, floors can be continuously propped back to ground in which case construction loads are zero.

2. The most recently cast slab is struck and is allowed to deflect under its self-weight before any reprops are installed. The reprops are initially only lightly tightened and, consequently, initially carry only a nominal load.

3. The most recently struck slab is not allowed to deflect under its self-weight when struck and the supporting props are, consequently, initially stressed.

Grundy & Kabaila (1963) developed a procedure for calculating the load ratio $w_{construction}/w_{dead}$ for each slab for propping system 3. They assumed linear elastic behaviour and infinitely rigid props. They found that the maximum load ratio was greater than 2 even if four levels of back-props were used. The maximum construction load is considerably reduced if system 2 is adopted with two or more levels of

back-propping. For example, the maximum load ratio is approximately 1.5 if two levels of back-props are used. Liu *et al.* (1988) developed a computer-based computational procedure using the same assumptions as Grundy & Kabaila (1963) for rapid calculations of construction loads imposed on slabs which can be extended to examine whether the slab loads are greater than the available strength at each step of construction in high-rise buildings. Liu *et al.* (1985) also developed a three-dimensional computer model which can be used to evaluate the effect of variations of the foundation rigidity, column axial stiffness, slab aspect ratio, and shore stiffness distribution on the value of the shore loads and slab moment: the authors proposed a modification coefficient that varies from 1.05 to 1.1 to conservatively correct the load ratio given by Grundy & Kabaila. However, Stivaros & Halvorsen (1992) suggested that, due to inherent shortcomings, Grundy & Kabaila's method underestimates the construction load and that 10 % correction coefficient is not adequate for all construction procedures. They developed a computer program based on the ACI equivalent frame concept and suggested that it be used on site to ensure safety. To show the importance of coordination between designer and contractor, an example is shown where a slab designed for low live load cannot possibly be constructed safely unless a column-mounted shoring system is used. Ambrose *et al.* (1994) reported that, over 25 years in the US, there have been more than 85 collapses of structures under construction which have been directly attributed to form-work failure. Even if the slab does not collapse, its serviceability may be severely impaired due to a faulty construction procedure. Gardner (1990) also emphasised the need for interdependence of contractor and designer to ensure long-term serviceability. In another paper, Gardner & Fu (1987) presented experimental results where long-term deflections were five to eight times the sustained-load short-term deflections for different construction-load sequences. They suggested that, in order to ensure adequate deflection behaviour, the slab designer must specify the construction schedule, including the number of forms and reshores and the concrete strength at stripping. El-Sheikh & Chen (1988) pointed out the increases in short- and long-term deflections due to faster construction rate and recommended use of high-strength concrete.

2.8 Biaxial bending and compression

In a series of papers, Brøndum-Nielsen presented a method of stress analysis for a cracked concrete section under combined biaxial bending and axial force. Brøndum-Nielsen (1980) showed a method of stress calculation of cracked arbitrary concrete section under service loads. Creep is accounted for by using an effective modulus of elasticity for the concrete and shrinkage is considered in terms of a force which can be obtained by multiplying the steel area with the shrinkage stress. It was suggested that the stress analysis can be used to study fatigue, buckling, deformation and crack width even though the tension-stiffening effect was not considered. Brøndum-Nielsen (1986a) extended the method for cracked reinforced or partially prestressed, arbitrary polygonal concrete sections with mixed reinforcement consisting of a combination of prestressed and non-prestressed reinforcement under axial load and biaxial bending. The method covers symmetrical and unsymmetrical cross-sections and cases with polygonal holes in the cross-section. A similar problem has been treated in Brøndum-Nielsen (1984) where analysis was limited to a special cross-section. The effects of creep, shrinkage and relaxation are considered for a symmetrical bending case without axial force (1986b) and with axial force (1986c). A simplified method was also presented in Brøndum-Nielsen (1987) for non-prestressed cross-sections without axial force where the active compression zone is triangular or trapezoidal. The method is quick but does not consider shrinkage.

Branson & Trost (1982) presented unified effective moment of inertia procedures for predicting the deflection and centroidal-axis location of partially cracked nonprestressed and prestressed (with or without nonprestressed tension steel) concrete members. The authors also compared these procedures with experimental results and concluded that the agreement ranged from reasonably satisfactory to quite good.

2.9 Crack models

Cracks occur in reinforced concrete structures when the tensile stress exceeds the strength of concrete in tension. The reduction in stiffness that results upon cracking must be considered in the calculation of displacements. The least stiff section in a

cracked member is at the location of the crack. Away from the crack, the concrete in the tension zone is capable of resisting some tensile stress and thus contributes to the stiffness of the member. Thus, the stiffness of a cracked member varies from a minimum value at the cracks to a maximum value midway between cracks. For the calculation of displacement, a mean value of flexibility for the member is used.

2.9.1 Assumptions

Consider a reinforced concrete member subjected to an axial force or a bending moment. The member is free from cracks if the stress in concrete has never exceeded its tensile strength. The reinforcement and the concrete undergo compatible strains. This condition is termed state 1.

Cracks occur when the tensile strength of the concrete is exceeded. At the location of a crack, the tensile stress is assumed to be resisted entirely by the reinforcement. The tensile zone is assumed to be fully cracked and this condition is referred to as state 2.

In a section between two successive cracks, the bond between the concrete and the reinforcing bars restrains the elongation of the steel and thus a part of the tensile force in the reinforcement at the crack is transmitted to the concrete situated between the cracks. In other words, concrete between the cracks contributes to the rigidity of the member through tension-stiffening. Due to this tension stiffening effect, the stress and strain in any section will be in an intermediate condition between states 1 and 2. The strain in the reinforcing bars varies from a maximum value at the cracks to a minimum value midway between the cracks. Different building codes propose alternative approximate methods to interpolate between state 1 and state 2.

2.9.2 MC-90/EC2-91 model

MC-90 (1993) and EC2-91 (1991) use almost the same type of equations to obtain a mean curvature. The background to their approach is described here.

Strain due to axial tension

A reinforced concrete member subjected to axial tension will be free from cracks when the value of N is lower than

$$N_r = f_{ct}(A_c + nA_s) = f_{ct}A_1 \tag{2.15}$$

where f_{ct} is the strength of concrete in tension; N_r is the value of the axial force that produces first cracking; A_c and A_s are the cross-sectional areas of concrete and steel and $n = E_s/E_c$, with E_s being the modulus of elasticity of steel and E_c the secant modulus of elasticity of concrete. A_1 is the area of a transformed section in state 1, composed of A_c plus nA_s.

Just before cracking, the section is in state 1; the stress in the concrete is f_{ct} and the stress in the steel is nf_{ct}. Immediately after cracking, the section at a crack is in state 2 and the stress in the steel is given by:

$$\sigma_{sr} = N_r/A_s \tag{2.16}$$

The first crack occurs at N_r. At the crack, the tensile stress in the concrete drops to zero and the total tension is resisted by the steel reinforcement (state 2). The sudden increase in stress in the steel leads to an incompatibility of strain in the steel and the adjacent concrete which results in widening of the crack.

Away from the crack, concrete, bonded to the reinforcement, tends to restrain the elongation and the bond stress τ transmits part of the tensile force from the bar to the surrounding concrete. At a certain distance s from the first crack, strain compatibility is recovered (state 1) and the tensile strength in concrete is again reached, causing a second crack. Figure 2.1 shows the variation of steel stress, bond stress and concrete stress over the length of a cracked member subjected to an axial force $N > N_r$. At a crack, the section is in state 2, the concrete stress is zero and the steel stress and strain for $N > N_r$

$$\sigma_{s2} = N/A_s \tag{2.17}$$

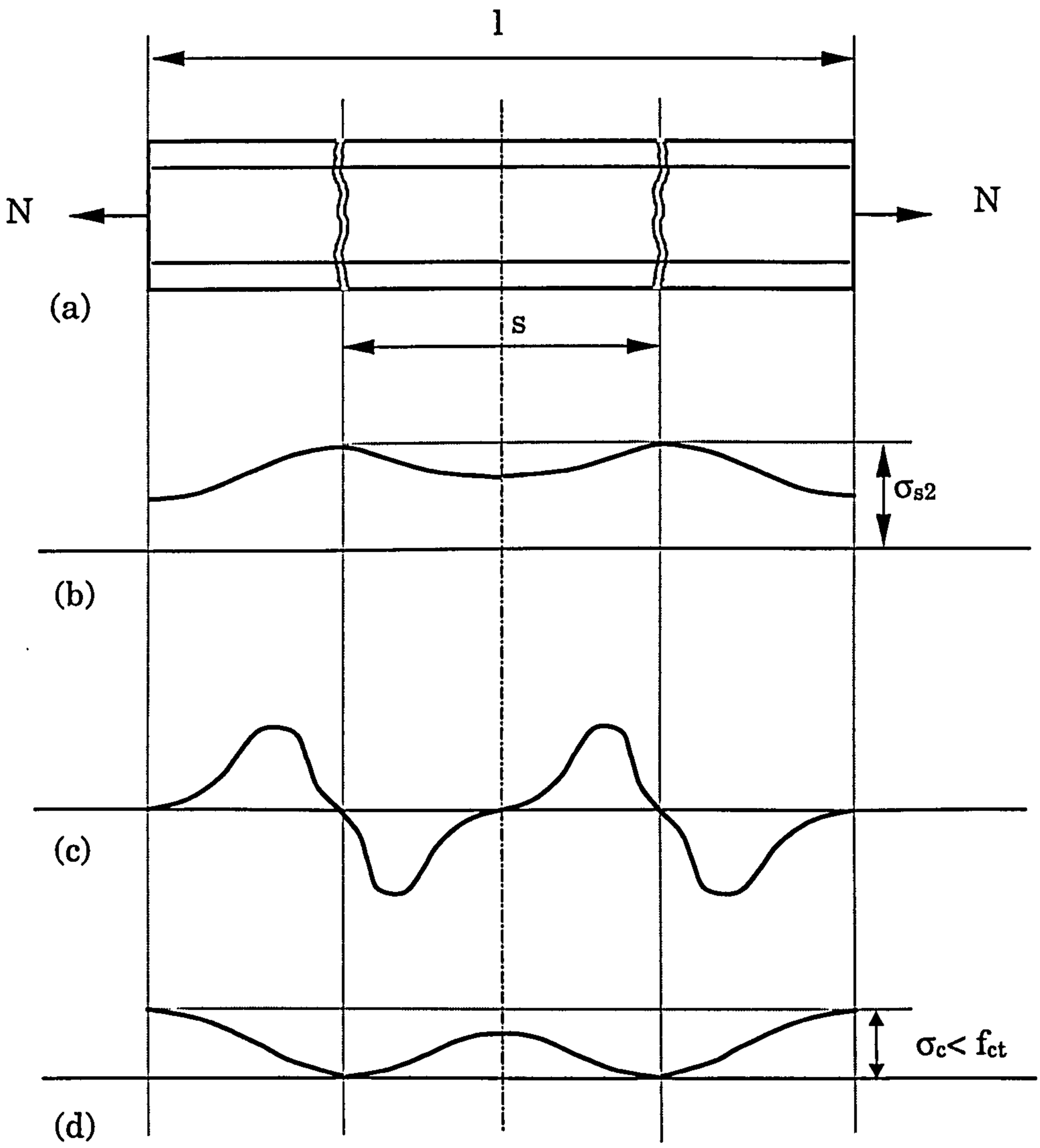


Figure 2.1 Stress in a reinforced concrete member cracked due to an axial force; (a) cracking of a tie; (b) stress in reinforcement; (c) bond stress; (d) stress in concrete ($\sigma_c \leq f_{ct}$): adapted from Ghali & Favre (1994)

$$\epsilon_{s2} = N/E_s A_s \tag{2.18}$$

Midway between consecutive cracks, the tensile stress in the concrete has some unknown value smaller than f_{ct} and the steel stress is smaller than σ_{s2}. Thus, the strain in the reinforcement varies along the length of the member; a mean value of the steel strain is

$$\epsilon_{sm} = \Delta l/l \tag{2.19}$$

where l is the original length of the member and Δl is the member extension. The symbol ϵ_{sm} represents an overall mean strain value for the cracked member. Obviously, ϵ_{sm} is smaller than ϵ_{s2} which is the steel strain at the cracked section. Let

$$\epsilon_{sm} = \epsilon_{s2} - \Delta\epsilon_s \tag{2.20}$$

$\Delta\epsilon_s$ is the reduction in steel strain caused by the participation of concrete in carrying the tensile stress between the cracks. Figure 2.2 shows the variation of the mean strain ϵ_{sm} with the applied load N; it follows a curve situated between the two straight lines representing ϵ_{s1} and ϵ_{s2}. Here, ϵ_{s1} is the hypothetical strain in the reinforcement, assuming that state 1 continues to apply when $N > N_r$. Thus,

$$\epsilon_{s1} = \epsilon_{c1} = \frac{N}{E_s(A_c + nA_s)} = \frac{N}{E_c A_1} \tag{2.21}$$

where A_1 is the area of the transformed section in state 1.

The value of $\Delta\epsilon_s$ represents the difference between the mean steel strain ϵ_{sm} and the steel strain in a fully cracked section. This difference has a maximum value, $\Delta\epsilon_{smax}$, at the start of cracking, when $N = N_r$. Based on experimental evidence, it is assumed that $\Delta\epsilon_s$ has a hyperbolic variation with σ_{s2} as follows:

$$\Delta\epsilon_s = \Delta\epsilon_{smax}\frac{\sigma_{sr}}{\sigma_{s2}} \tag{2.22}$$

From the geometry of the graph in Fig. 2.2, one obtains

$$\Delta\epsilon_{smax} = (\epsilon_{s2} - \epsilon_{s1})\frac{\sigma_{sr}}{\sigma_{s2}} \tag{2.23}$$

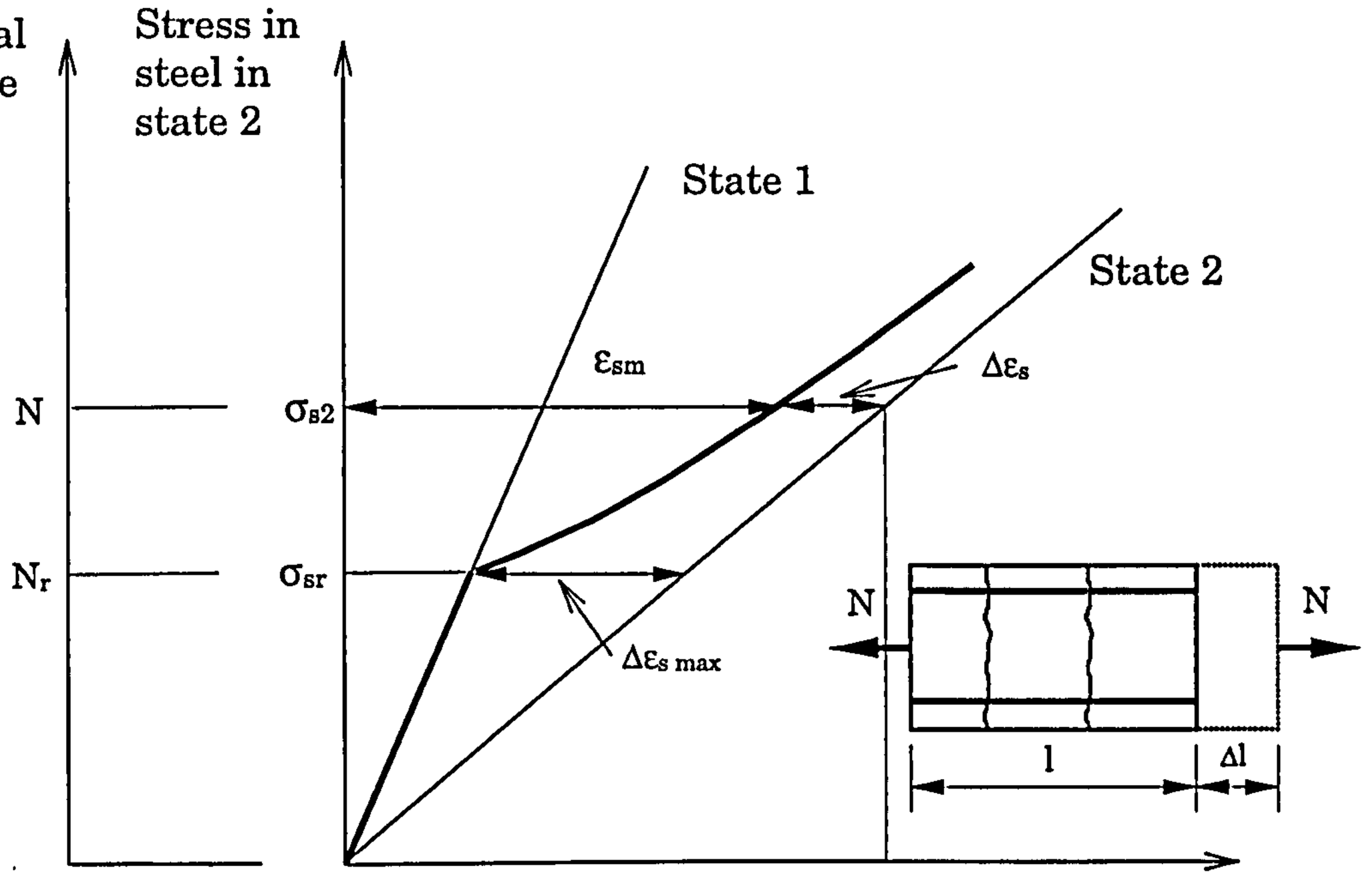


Figure 2.2 Axial forces versus mean strain in a member subjected to axial tension: adapted from Ghali & Favre (1994)

Substitution of eqs 2.22 and 2.23 into eq. 2.20 gives, for a cracked member, an overall strain value which is also the mean strain in the steel:

$$\epsilon_{sm} = (1 - \zeta)\epsilon_{s1} + \zeta\epsilon_{s2} \tag{2.24}$$

where ζ is a dimensionless coefficient, between 0 and 1, representing the extent of cracking. Thus, $\zeta = 0$ for an uncracked ($N < N_r$), and $0 < \zeta < 1$ for a fully cracked section. The value of ζ is given by:

$$\zeta = 1 - \left(\frac{\sigma_{sr}}{\sigma_{s2}}\right)^2, \text{ for } \sigma_{s2} > \sigma_{sr} \tag{2.25}$$

or

$$\zeta = 1 - \left(\frac{N_r}{N}\right)^2, \text{ for } N > N_r \tag{2.26}$$

In eq. 2.24, the mean strain in the steel is determined by interpolation between the steel strains ϵ_{s1} and ϵ_{s2} in states 1 and 2. The interpolation coefficient ζ depends upon the ratio of the steel stresses σ_{sr} and σ_{s2} in a fully cracked section when the

applied forces are N_r and N, respectively.

In order to take into account the bond properties of the reinforcing bars and the influence of duration of the application or the repetition of loading, the EC2-91 (1991) and MC-90 (1993) introduce the coefficients β_1 and β_2 into eq. 2.25 as follows:

$$\zeta = 1 - \beta_1\beta_2 \left(\frac{\sigma_{sr}}{\sigma_{s2}}\right)^2 \text{ (with } \sigma_{s2} \geq \sigma_{sr} \text{)} \tag{2.27}$$

where $\beta_1 = 1$ and 0.5 for high bond bars and for plain bars, respectively. According to EC2-91, $\beta_2 = 1$ and 0.5 for first loading and for loads applied in a sustained manner (or for a large number of load cycles), respectively. MC-90 utilises β_2 =0.8 for first loading.

Curvature due to bending

A reinforced concrete member subjected to a bending moment (Fig. 2.3) will be free from cracks when the bending moment is less than

$$M_r = W_1 f_{ct} \tag{2.28}$$

where M_r is the value of the bending moment that produces first cracking; W_1 is the section modulus in state 1. Thus, W_1 is calculated for the cross-section area of concrete plus n times the cross-section area of steel. f_{ct} is the tensile strength of concrete in flexure (modulus of rupture).

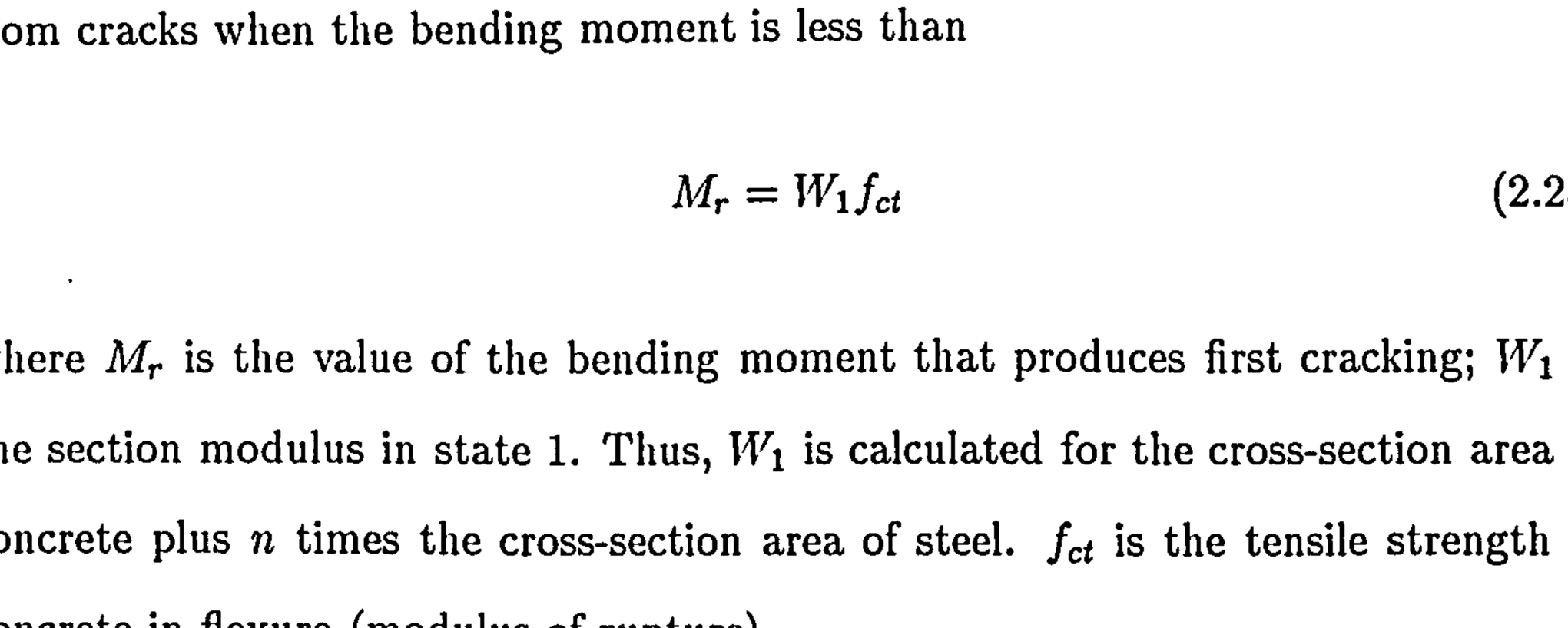


Figure 2.3 A reinforced concrete member in flexure: adapted from Ghali & Favre (1994)

For a bending moment $M > M_r$, cracking occurs and the steel stress varies from

BIBL
LONDON

a maximum value at the crack to a minimum value at the mid-way between the cracks. Assuming that the concrete between the cracks has the same effect on the mean strain in steel as in the case of an axial force, eq. 2.24 can be adopted. Thus,

$$\epsilon_{sm} = (1 - \zeta)\epsilon_{s1} + \zeta\epsilon_{s2} \tag{2.29}$$

where

$$\zeta = 1 - \beta_1\beta_2 \left(\frac{\sigma_{sr}}{\sigma_{s2}}\right)^2 = 1 - \beta_1\beta_2 \left(\frac{M_r}{M}\right)^2 \tag{2.30}$$

Here σ_{sr} and σ_{s2} are the steel stresses calculated for M_r and M, on the assumption that the section is fully cracked.

The curvature at an uncracked or a cracked section can be expressed in terms of the bending moment and flexural rigidity or in terms of strains as follows:

$$\psi = \frac{M}{EI} \tag{2.31}$$

or

$$\psi = \frac{\epsilon_s - (\epsilon_c)_{\text{top}}}{d} \tag{2.32}$$

where ψ is the curvature; E is the modulus of elasticity; I is the moment of inertia of the section; ϵ_s is the strain in the steel reinforcement; $(\epsilon_c)_{\text{top}}$ is the strain at the extreme fibre of the compression zone; and d is the distance between the steel in tension and the extreme compression fibre (Fig. 2.3).

It is assumed that the effect of cracking on curvature is similar to its effect on the strain in axial tension. Thus, the mean curvature is given by:

$$\psi_m = (1 - \zeta)\psi_1 + \zeta\psi_2 \tag{2.33}$$

where ψ_1 and ψ_2 are the curvatures in states 1 and 2, respectively, corresponding to a bending moment M. Thus, the coefficient ζ is employed to interpolate between the curvatures in states 1 and 2 to obtain the mean curvature. This is illustrated in the moment-curvature graph in Fig. 2.4. The cracked member has a mean flexural

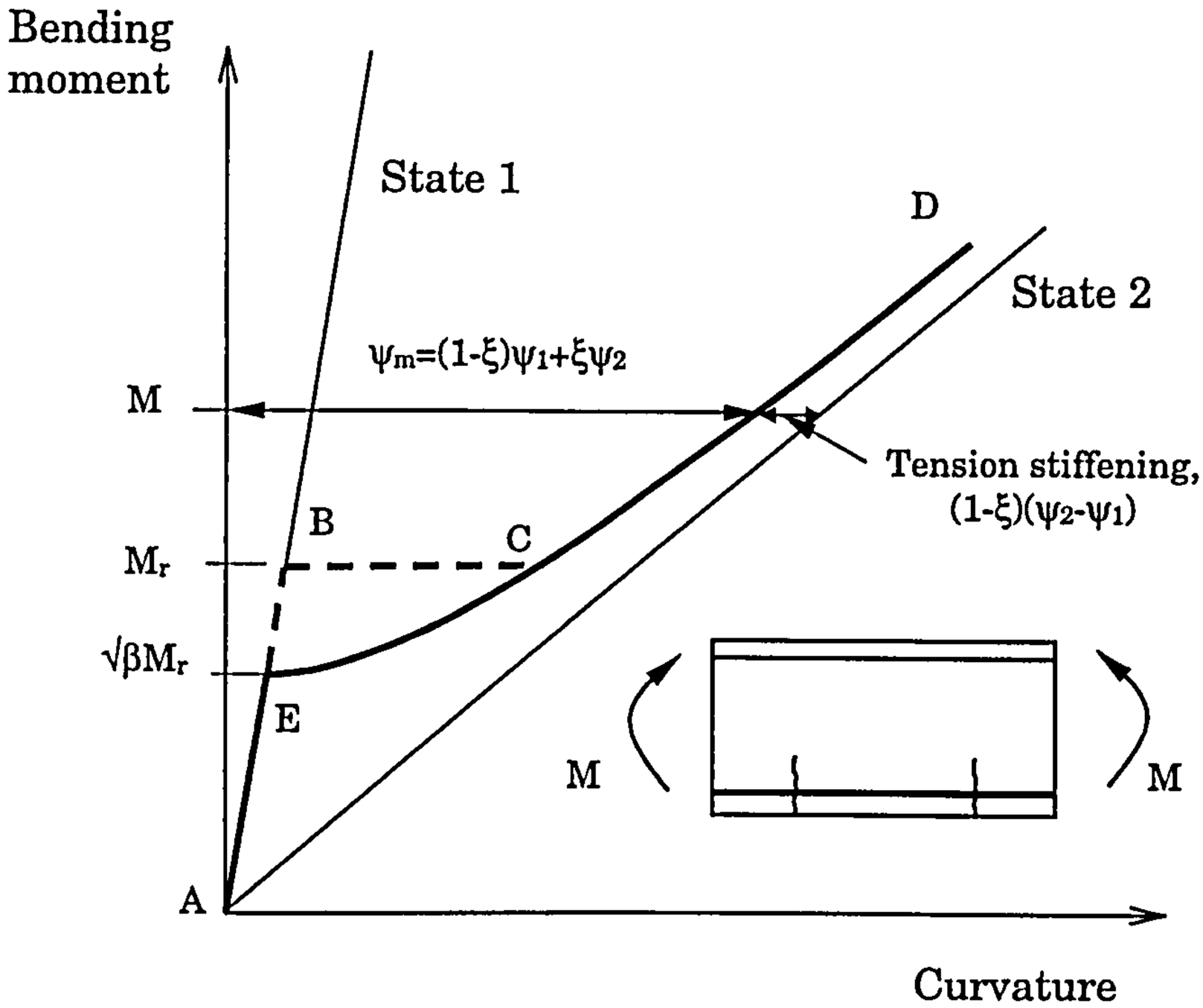


Figure 2.4 Moment versus curvature in a reinforced concrete member in flexure: adapted from Ghali & Favre (1994)

rigidity given by:

$$(EI)_m = \frac{M}{\psi_m} \tag{2.34}$$

The curvatures ψ_1 and ψ_2 are given by:

$$\psi_1 = \frac{M}{E_c I_1} \tag{2.35}$$

$$\psi_2 = \frac{M}{E_c I_2} \tag{2.36}$$

where I_1 and I_2 are, respectively, the moments of inertia of a transformed uncracked and fully cracked section about an axis through their respective centroids.

Provisions of codes

MC-90 (1993) and EC2-91 (1991) adopt eq. 2.33 to interpolate between state 1 and state 2 so as to calculate the mean curvature. EC2-91 uses of the same coefficient ζ with eq. 2.33, to calculate mean values for deformation parameters such as curvature, strain, rotation, or deflection.

MC-90 considers that the $M-\psi$ relation shown by the lines ABCD in Fig. 2.4 is

most representative of actual practice with the exception of the part EBC. This part is replaced by the line EC, which is an extension of the curve CD until it intersects AB at point E. Thus, for practical applications, the $M-\psi$ relation follows the straight line AE when $0 \leq M \leq (M_r\sqrt{\beta})$, where $(M_r\sqrt{\beta})$ represents the reduced cracking moment and $\beta = \beta_1\beta_2$.

When $(M_r\sqrt{\beta}) \leq M \leq M_y$, the $M-\psi$ relation is the nonlinear line ED, following the hyperbolic eq. 2.33, where M_y is the moment which produces yielding of the reinforcement. If the concrete is in a virgin state and the loading is of short-term character, the $M-\psi$ relation is more closely presented by the lines ABCD. Replacement of the part EBC by EC takes into consideration the behaviour of a member which has been cracked due to loads, shrinkage and temperature variations during construction.

MC-90 also differs from EC2-91 in the value of the coefficient β_2, which is considered equal to 0.8 instead of 1.0 for first loading.

2.9.3 Effective moment of inertia model

Branson (1976), (1977) proposed an equation similar to those used later by MC-90 (1993), EC2-91 (1991) to interpolate between state 1 and 2, although this equation interpolates between uncracked and fully cracked moments of inertia rather than curvatures. ACI 318-89 (1989) proposed that, for the calculation of deflection immediately after the application of load, an effective value of moment of inertia using Branson's equation should be used. ACI code used a power n=3 in Branson's equation:

$$I_e = \left(\frac{M_{cr}}{M_a}\right)^n I_g + \left[1 - \left(\frac{M_{cr}}{M_a}\right)^n\right] I_{cr} \qquad (2.37)$$

where I_g is the gross moment of inertia ($= h^3/12$) ignoring the presence of reinforcement. This is in contrast to the MC-90/EC2-91 approach where reinforcement is considered in state 1. I_{cr} is the moment of inertia of the fully cracked transformed section. M_a is the maximum moment in the member at the stage for which the

deflection is computed and M_{cr} is the cracking moment defined by

$$M_{cr} = \frac{f_r I_g}{y_t} \tag{2.38}$$

where $f_r = 7.5\sqrt{f'_c}$=modulus of rupture.

Branson uses the same equation as eq. 2.37 with a power n=4 when I_e is intended for calculation of curvature in an individual section.

Ghali (1993) suggests that this method is accurate in some cases, but that, in others, the predicted deflection can be in large in error. Examples of such cases are when the reinforcement ratio is low and variable, when the maximum moment is not substantially greater than the cracking moment and when the bending moment is constant over the major part of the structure. Ghali criticises the ignoring of tensile steel in state 1 and adds that any member, even that with a constant cross-section, behaves as a beam of variable rigidity because of cracking. It is impossible to find an expression for I_e that is equally accurate for all forms of variation of bending moment or reinforcement ratio over a member's length.

2.9.4 Gilbert model

Gilbert (1983), (1988) proposed an alternative approach for modelling tension stiffening. An area of concrete located at the tensile-steel level is assumed to be effective in providing tension stiffening. Figure 2.5 shows an average cross-section of a singly reinforced member. Like the other tension stiffening models, the properties of this average cross-section are between those of the fully cracked cross-section and the uncracked cross-section between the primary cracks. The tensile concrete area A_{ct}, which is assumed to contribute to the flexural stiffness after cracking, depends on the magnitude of the maximum applied moment M, the area of tensile reinforcement A_{st}, the amount of concrete below the neutral axis, the tensile strength of concrete (i.e. the cracking moment M_{cr}), and the duration of the sustained load.

Based on short-term test results, the following empirical for A_{ct} was proposed:

$$A_{ct} = \beta_1\beta_2 \left[0.21 b_w d - n A_{sn}\right] \left(\frac{M_{cr}}{M}\right)^2 \tag{2.39}$$

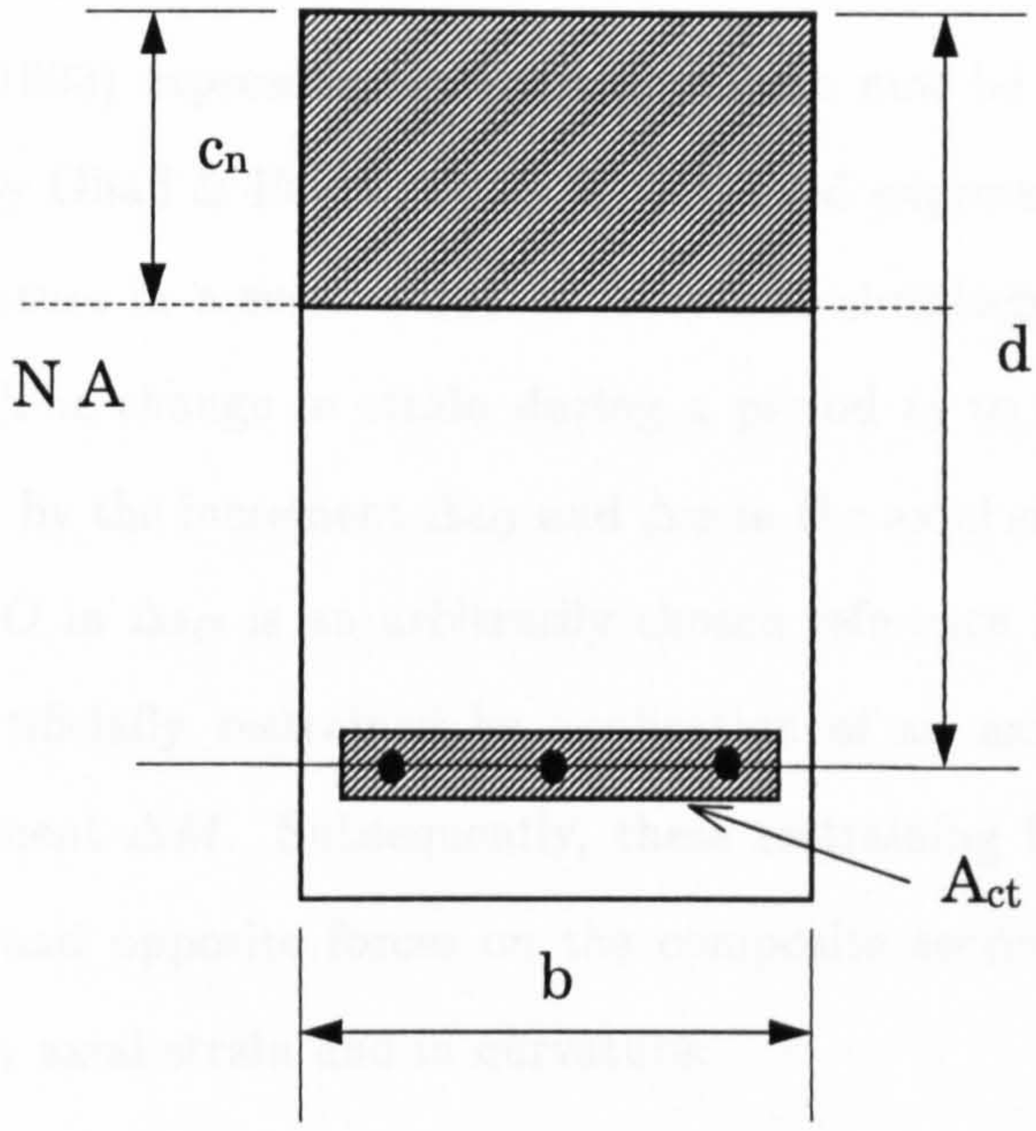


Figure 2.5 Gilbert's model: adapted from Gilbert (1988)

where β_1 and β_2 are same coefficients used in eq. 2.27. When $M < M_{cr}$, the term (M_{cr}/M) in eq. 2.39 is taken as unity.

2.10 Extension of MC-90 model to incorporate long-term effects

The methods proposed by MC-90 (1993) and EC2-91 (1991) to calculate the mean short-term curvature can also be extended to calculate long-term curvatures. The additional curvature due to creep and shrinkage can be calculated using the approach by Ghali & Favre (1994) described below combined with the curvatures for states 1 and 2 according to MC-90 (1993) approach at time t which are given by

$$\psi_1(t) = \psi_1(t_0) + \Delta\psi_1 \tag{2.40}$$

$$\psi_2(t) = \psi_2(t_0) + \Delta\psi_2 \tag{2.41}$$

so that the mean curvature at time t is given by

$$\psi_m(t) = (1 - \zeta)\psi_1(t) + \zeta\psi_2(t) \tag{2.42}$$

where ζ is given by eq. 2.30 with β_2=0.5.

These MC-90 (1993) expressions for curvatures can now be combined with the method proposed by Ghali & Favre (1994), who derived expressions for calculating the change of curvature in a section due to creep and shrinkage. Their derivation is presented here. The change in strain during a period t_0 to t due to creep and shrinkage is defined by the increment $\Delta\epsilon_O$ and $\Delta\psi$ in the axial strain and curvature respectively where O in $\Delta\epsilon_O$ is an arbitrarily chosen reference point. This change of strain is first artificially restrained by application of an axial force ΔN at O and a bending moment ΔM. Subsequently, these restraining forces are removed, by applying equal and opposite forces on the composite section, resulting in the following changes in axial strain and in curvature:

$$\begin{Bmatrix} \Delta\epsilon_O \\ \Delta\psi \end{Bmatrix} = \frac{1}{\bar{E}_c(t,t_0)(\bar{A}\bar{I}-\bar{B}^2)} \begin{bmatrix} \bar{I} & -\bar{B} \\ -\bar{B} & \bar{A} \end{bmatrix} \begin{Bmatrix} -\Delta N \\ -\Delta M \end{Bmatrix} \tag{2.43}$$

where $\bar{A}$ is the area of the age-adjusted transformed section, while $\bar{B}$ and $\bar{I}$ are, respectively, its first and second moments about an axis through reference point O. When the calculation is for long-term deflection, the modulus of elasticity of concrete is modified as follows:

$$\bar{E}_c(t,t_0) = \frac{E_c(t_0)}{1+\phi(t,t_0)\chi(t,t_0)} \tag{2.44}$$

where

$\bar{E}_c(t,t_0)$= age-adjusted modulus of elasticity of concrete at time t

$\phi(t,t_0)$= creep coefficient

$\chi(t,t_0)$= aging coefficient

$E_c(t_0)$= modulus of elasticity of concrete at time t_0

The modular ratio becomes:

$$\bar{n}(t,t_0) = \frac{E_s}{\bar{E}_c(t,t_0)} \tag{2.45}$$

The relaxation forces are calculated as the sum of two terms:

$$\left\{ \begin{array}{c} \Delta N \\ \Delta M \end{array} \right\} = \left\{ \begin{array}{c} \Delta N \\ \Delta M \end{array} \right\}_{\text{creep}} + \left\{ \begin{array}{c} \Delta N \\ \Delta M \end{array} \right\}_{\text{shrinkage}} \tag{2.46}$$

If creep were free to occur, the axial strain and curvature would increase during the period t_0 to t by the amount $\phi(t,t_0)\epsilon(t_0)$ and $\phi(t,t_0)\psi(t_0)$ respectively. If the centroid of the age-adjusted transformed section is selected as the reference point O, the force necessary to prevent these deformations is given by:

$$\left\{ \begin{array}{c} \Delta N \\ \Delta M \end{array} \right\}_{\text{creep}} = -\bar{E}_c(t,t_0)\phi(t,t_0) \left[\begin{array}{cc} A_c & A_c y_c \\ A_c y_c & I_c \end{array} \right] \left\{ \begin{array}{c} \Delta\epsilon_O(t_0) \\ \Delta\psi(t_0) \end{array} \right\} \tag{2.47}$$

where A_c is the area of the concrete section and I_c is the moment of inertia of this area about an axis through O, the centroid of the age-adjusted transformed section. y_c is the y-coordinate of the centroid of the concrete area measured in the downward direction from the point O. The forces required to prevent shrinkage are

$$\left\{ \begin{array}{c} \Delta N \\ \Delta M \end{array} \right\}_{\text{shrinkage}} = -\bar{E}_c(t,t_0)\epsilon_{cs}(t,t_0) \left\{ \begin{array}{c} A_c \\ A_c y_c \end{array} \right\} \tag{2.48}$$

The sum of eqs 2.47 and 2.48 gives the total forces required to restrain creep and shrinkage:

$$\left\{ \begin{array}{c} \Delta N \\ \Delta M \end{array} \right\} = -\bar{E}_c(t,t_0) \left\{ \begin{array}{l} \{\phi(t,t_0)[\epsilon_O(t_0) + \psi(t_0)y_c] + \epsilon_{cs}(t,t_0)\}A_c \\ \left[\phi(t,t_0)\left(\psi(t_0) + \epsilon_O(t_0)\frac{y_c}{r_c^2}\right) + \epsilon_{cs}(t,t_0)\frac{y_c}{r_c^2}\right] A_c r_c^2 \end{array} \right\} \tag{2.49}$$

The artificial restraint may now be eliminated by application of $-\Delta N$ and $-\Delta M$ on the age-adjusted transformed section. With the reference point chosen at the centroid of the section, the first moment of area B must be zero. The axial strain and curvature due to $-\Delta N$ and $-\Delta M$ can be calculated by eq. 2.43 giving

$$\left\{ \begin{array}{c} \Delta\epsilon_O \\ \Delta\psi \end{array} \right\} = \frac{1}{\bar{E}_c(t,t_0)} \left\{ \begin{array}{c} -\Delta N/\bar{A} \\ -\Delta M/\bar{I} \end{array} \right\} \tag{2.50}$$

Substitution of eq. 2.49 into 2.50 gives

$$\Delta\epsilon_O = \eta\{\phi(t,t_0)[\epsilon_O(t_0) + \psi(t_0)y_c] + \epsilon_{cs}(t,t_0)\} \tag{2.51}$$

$$\Delta\psi = \kappa\left[\phi(t,t_0)\left(\psi(t_0) + \epsilon_O(t_0)\frac{y_c}{r_c^2}\right) + \epsilon_{cs}(t,t_0)\frac{y_c}{r_c^2}\right] \tag{2.52}$$

where η and κ are the ratios of the area and moment of inertia of the concrete section to the area and moment of inertia of the age-adjusted transformed section, respectively (see below). They represent the effect of reinforcement in reducing the absolute value of the change in axial strain and in curvature respectively due to creep and shrinkage. Thus:

$$\eta = A_c/\bar{A} \tag{2.53}$$

$$\kappa = I_c/\bar{I} \tag{2.54}$$

Equations 2.53 and 2.54 are applicable to both states 1 and 2.

CEB manual on cracking and deformation (1985) provides a simpler equation to calculate long-term curvatures for both states 1 and 2:

$$\psi(t) = k_s(1 + k_\phi\phi)\psi_c + k_{cs}\frac{\epsilon_{cs}}{d} \tag{2.55}$$

The correction coefficients k_s, k_ϕ and k_{cs} are to take into account the amount of steel, creep and shrinkage respectively and can be obtained from the CEB manual. d is the effective depth and ϵ_{cs} is the shrinkage strain.

2.11 Concluding remarks

Considerable uncertainties exist within the design community over the selection of flat slab thickness. Different codes provide simplified equations to calculate long-term deflections. There are also provisions in codes for omitting deflection calculation altogether by following minimum safe thickness guidelines. These methods are relatively simple to adopt in design offices, but their accuracy is questionable since key parameters which affect deflection (e.g. construction sequence, material properties) are not included. Some codes and authors suggest multipliers, which vary

significantly, to calculate long-term deflections from instantaneous deflections. Field measurements of deflection also indicate a high level variability, the author believes that inherent variability in geometric and material properties are primarily responsible for this. Also, different construction approaches may lead to different final deflections. Perhaps, the most important factor that influences deflection is cracking. There are several models to calculate short-term deflections due to cracking, their derivation and assumptions were described in this chapter. MC-90 extends its method for calculating short-term deflections to incorporate long-term effects. These methods need to be incorporated into FE models to establish their suitability for predicting slab deflection. Furthermore, the literature review identified a need for developing an analysis method to model deflections due to a time-varying load history. Literature is reviewed on FE methods for calculating slab deflections in the next chapter.

Chapter 3

Review of FE models

3.1 Introduction

This chapter introduces the finite-element (FE) analysis method. It begins with a description of different FE methods and compares their performances and adaptability. Different FE approaches proposed by several authors to incorporate the effective stiffness method are described in detail with relevant derivations. Various formulae proposed by others for calculating the effective area of steel in the principal moment directions are presented and compared. These equations are required to determine the moment of inertia of uncracked and cracked concrete sections.

3.2 Finite-element analysis

In the FE method, the stiffness matrix of an element is evaluated from the equation:

$$[K] = \int_v [B]^t [D][B] \mathrm{dv} \tag{3.1}$$

where $[B]$ is the strain displacement matrix and $[D]$ is the material stiffness matrix. Theoretically, nonlinearity in the load-displacement response is caused by nonlinear strain-displacement relationships (i.e. large displacements) and/or nonlinear stress-strain relationships. Nonlinear strain-displacement relations are referred to as geometrically nonlinear behaviour (e.g. $P - \Delta$ effect). Nonlinear stress-strain

relationships are responsible for material nonlinearities. At service-load levels, geometric nonlinearity does not normally have a major effect on the behaviour of a structure whereas material nonlinearities (e.g. cracking, creep, shrinkage) have a significant influence on service-load deflections.

For a member subjected to non-uniform stress conditions such as bending, the stiffness of concrete changes throughout the member and, in general, depends on the stress level at a given location in the member. One approach to this problem is to analyse each "location" of the member, find its stiffness and then integrate over the volume of the member to find the total stiffness of the member. This can result in two main approaches: a "micro-element" approach where the structure is divided into many small elements, with each of these representing one "location", and the "macro-element" approach where each element represents both concrete and reinforcement and all the local phenomena are incorporated into a constitutive model to evaluate the stiffness matrix of a macro-element. The micro-element approaches include two-dimensional (2-D) (and sometimes even a three dimensional (3-D)) analysis for beams, and 3-D analysis for slabs and shells. For beams, plates and shells, the macro-element approaches result in layered models and effective-stiffness models. 3-D analysis is becoming more common with the increase in readily available computing power; however, the macro-element approaches are probably still more adaptable to both research and practical design situations because they require less computing resources and are simpler to implement and interpret. These macro-element methods have been successfully used for calculating the deflections of numerous reinforced concrete structures.

3.2.1 Effective-stiffness model

The effective-stiffness method can be used for structures subjected to bending or a combination of bending and in-plane forces, e.g. beams, slabs and shells. The behaviour of a reinforced concrete member, before cracking, is assumed to be linearly elastic. The curvature can be calculated by

$$\psi = \frac{M}{EI_g} \tag{3.2}$$

where, EI_g is the bending stiffness of a member before cracking and I_g is the second moment of area of the uncracked section (steel may or may not be included depending on the model used).

After the tensile stress in the section exceeds the modulus of rupture, cracks start to form in the tension region and the bending stiffness of the section, consequently, reduces. The contribution of the reinforcement to the stiffness of the section is now significant and also it is important to incorporate the effect of the uncracked concrete between successive cracks. It is possible to approximately represent the entire section with an effective-stiffness, EI_e. It is assumed that, after cracking, the value of the stiffness modulus E remains unchanged but the moment of inertia I is assumed to change and to depend on the applied moment and the reinforcement present in the section. Thus, the curvature of a cracked section can be calculated by

$$\psi = \frac{M}{EI_e} \tag{3.3}$$

where, EI_e is the effective bending stiffness of a member after cracking, as shown in Fig. 3.1.

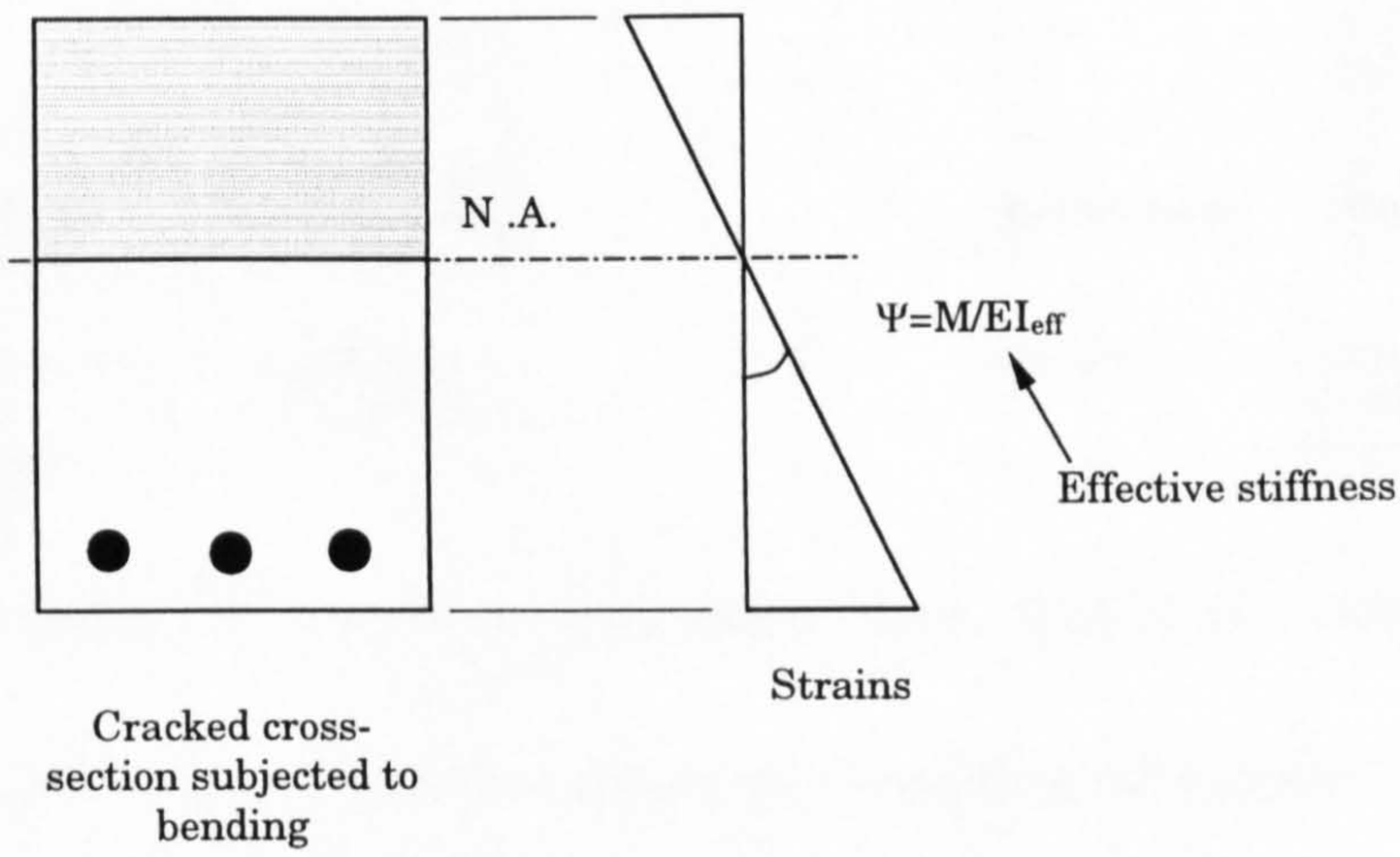


Figure 3.1 Effective-stiffness model: adapted from Polak *et al.* (1996)

The fully cracked second moment of area is calculated assuming that no tensile stress exists in the cracked concrete. But even after cracking, uncracked concrete between successive cracks provides some level of stiffness through bond between concrete and steel. In reality, the effective moment of inertia, I_e, of any cracked section lies between the moments of inertia of the uncracked and fully cracked sec-

tions. Several models have been proposed by different authors [(ACI Committee 318, 1989), (CEB-FIP, 1993), (Gilbert, 1988)] to define the effective stiffness of a cracked section, which were discussed in section 2.9.

3.2.2 Layered model

The stiffness matrix of a finite-element given by eq. 3.1 must be integrated over the volume of the element. Integration is carried out over the area and through the thickness of an element. The integration over the area of the element is usually done by either exact or numerical integration, where stresses, strains, material and stiffness coefficients are found at certain discrete points. Integration through the thickness is executed by dividing the element into layers and evaluating strains, stresses and material stiffness properties at midpoints of each layer (Fig. 3.2). The total stiffness matrix of an element is found by adding the stiffness contributions of all layers.

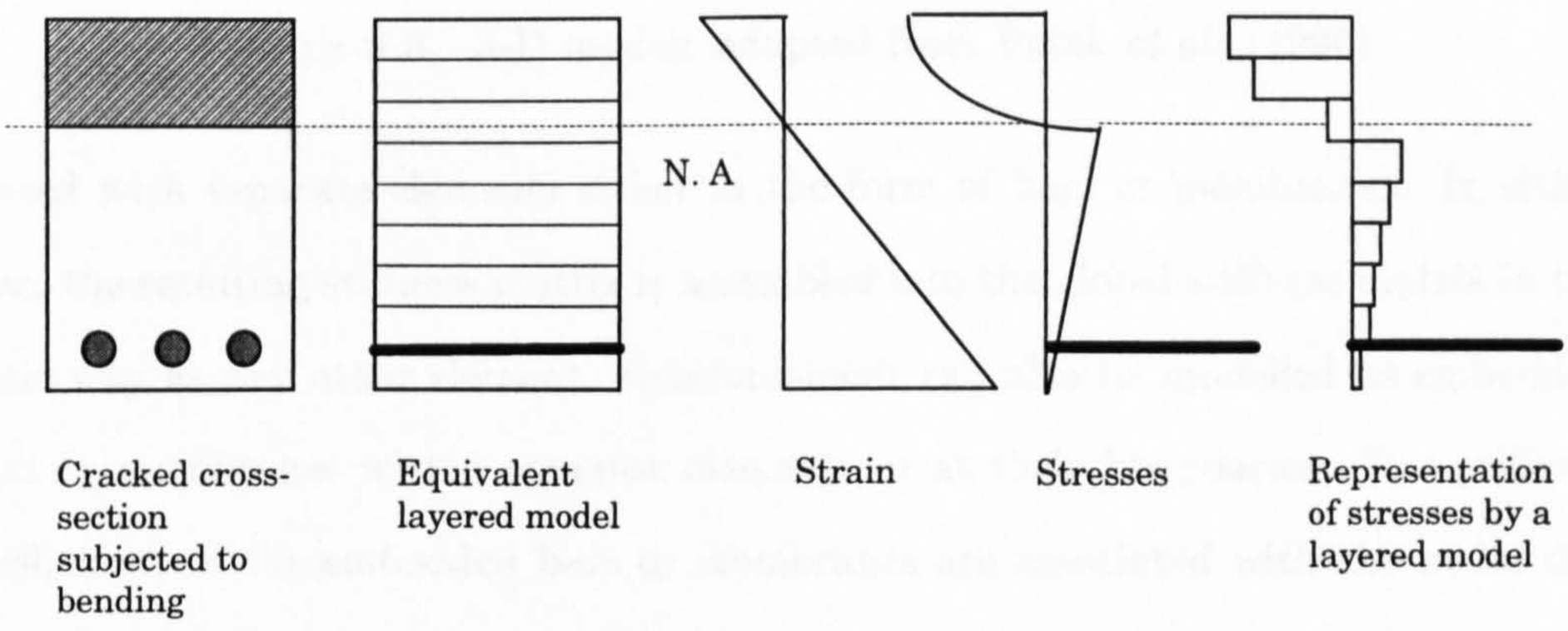


Figure 3.2 Layered model: adapted from Polak *et al.* (1996)

The analysis starts with certain assumptions regarding the stiffness of the structure (e.g. assumption of concrete being a linearly elastic material). From the initial analysis the strains and stresses are found at all the locations needed for integration, e.g. midpoints of each layer, gauss points. From these strains, the material model adopted and the iteration technique, a new stiffness matrix is found and the analysis is repeated until a desired convergence is attained.

3.2.3 3-D model

The stiffness matrix of a 3-D finite-element is integrated over its entire volume by an appropriate triple numerical integration rule associated with the 3-D global or local coordinate system. This results in a number of sampling points distributed throughout the element at which stresses, strains, material and stiffness coefficient and material damage states are calculated (Fig. 3.3). Reinforcement can be repre-

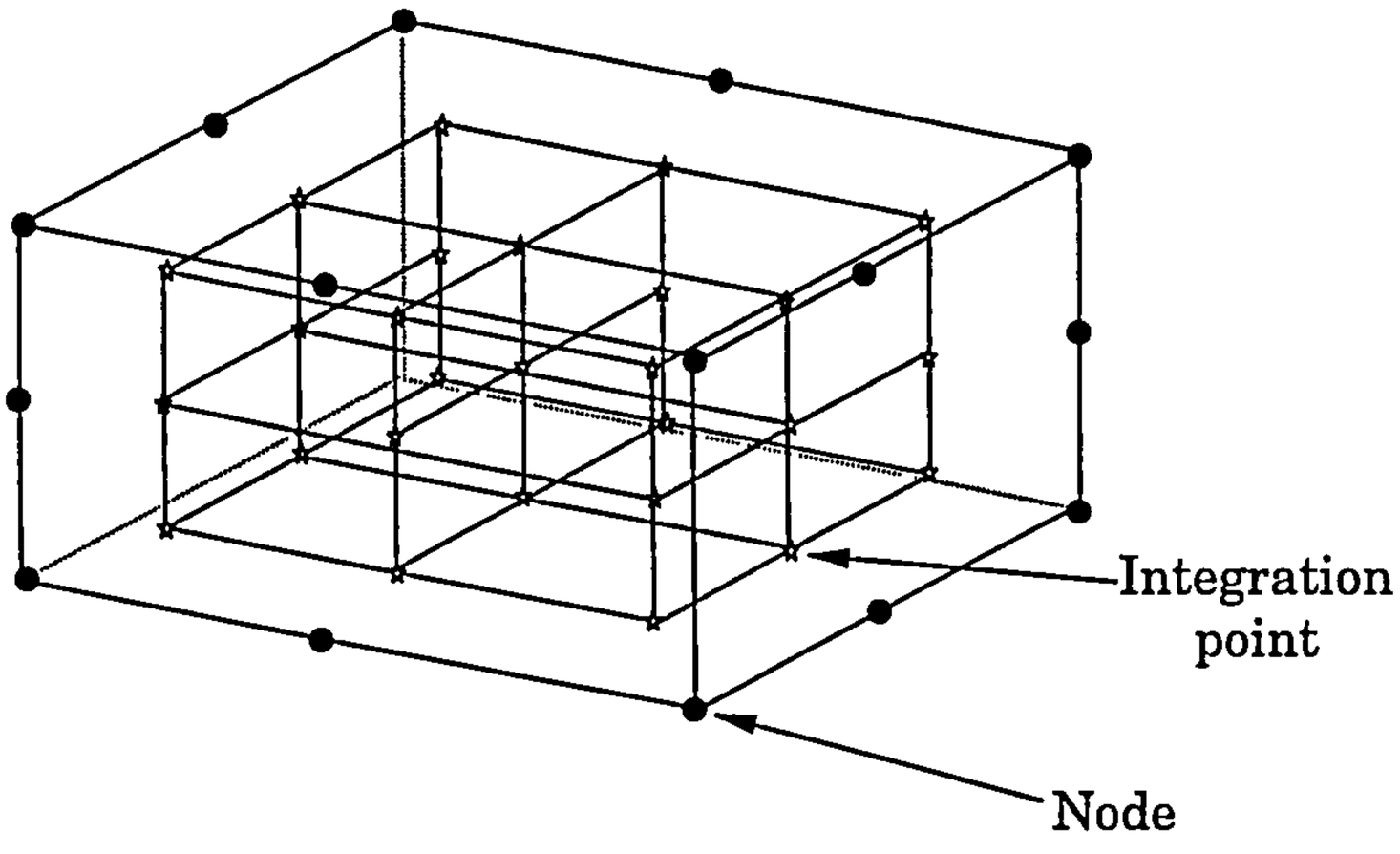


Figure 3.3 3-D model: adapted from Polak *et al.* (1996)

sented with separate elements either in the form of bars or membranes. In either case, the resulting stiffness matrix is assembled into the global stiffness matrix in the same way as any other element. Reinforcement can also be modelled as embedded bars or membranes within concrete elements or at their boundaries. The stiffness coefficients of the embedded bars or membranes are associated with the nodal displacement of the element in which they are embedded and hence can be summed directly into the element stiffness matrix.

The nonlinear iterative procedure for estimating the deflections for a given load in 3-D analysis is the same as that described above for the layered model.

3.2.4 Discussion

The 3-D, layered and effective-stiffness methods allow the calculation of the stiffness matrix of an element in the nonlinear deflection analysis. In layered and 3-D models the stiffness matrix of an element is estimated from local stress-strain relationships and consists of the contributions from all layers or sampling points. In the effective-

stiffness method the stiffness of an element is estimated in a more global sense from the moment-curvature relationship. The effective-stiffness method does not require integration of the stiffness matrix through the thickness of an element.

The layered and 3-D approaches are more powerful and versatile; as stiffness conditions are evaluated at discrete locations they are particularly suitable for modelling localised effects e.g. punching mechanisms. On the other hand, an effective-stiffness approach is applicable in modelling overall behaviour of structures and its use is restricted to the specific type of structural behaviour for which moment-curvature relationships have been developed.

Both layered and 3-D approaches require complex computer codes and the analyses are expensive in both computer run time and user time to prepare data and interpret results. A 3-D analysis usually involves a larger number of degrees of freedom for a given descretisation than for a layered model and is, therefore, more time consuming. On the other hand, the effective-stiffness approaches can be easily incorporated in an existing FE program, require less effort in creating input for the analysis and the analysis takes considerably less computer time.

Polak *et al.* (1996) presented a comparative study to evaluate the performance of several effective-stiffness formulations and that of a layered model. A comparison was made with results of tests on reinforced slabs. The effective-stiffness models considered in the analysis were developed by Scanlon & Murray (1982), Jofriet & McNeice (1971) and Polak (1996). It should be noted here that all the formulations used Branson's formula for effective-stiffness. The layered model employed in the study was developed by Polak & Vecchio (1993). A point-supported slab loaded with point load and a simply supported slab under uniformly distributed load were considered in the study. Polak *et al.* (1996) concluded that, for typical slabs and slab systems, the effective-stiffness formulations can provide results with accuracy comparable to the accuracy of the layered approaches.

3.2.5 Iteration Technique

There are two main approaches to stiffness evaluation in nonlinear analysis: the secant-stiffness and the tangential-stiffness formulations. The techniques can be

used for layered, effective-stiffness and 3-D models. In the secant formulations, the stiffness matrix $[K]$ relates total nodal forces $[F]$ to total displacements $[D]$. The tangential-stiffness matrix relates the increment of nodal displacement $[\Delta D]$ to the increments in nodal forces $[\Delta F]$. The choice of an appropriate stiffness-formulation technique depends on several factors. The material model adopted in the given FE formulation is one of the most important of them.

3.3 Scanlon & Murray approach

Scanlon & Murray (1982) proposed an FE method to model cracking in reinforced concrete slabs. The method utilised a secant-stiffness formulation and used a modified anisotropic plane-stress relationship to include the effect of cracking. Specialised for orthotropy, the stress-strain relationships are expressed by:

$$\begin{Bmatrix} \sigma_x \\ \sigma_y \\ \tau_{xy} \end{Bmatrix} = \begin{bmatrix} \frac{E_x}{(1-\nu_x\nu_y)} & \frac{\nu_x E_y}{(1-\nu_x\nu_y)} & 0 \\ \frac{\nu_y E_x}{(1-\nu_x\nu_y)} & \frac{E_y}{(1-\nu_x\nu_y)} & 0 \\ 0 & 0 & G_{xy} \end{bmatrix} \begin{Bmatrix} \epsilon_x \\ \epsilon_y \\ \gamma_{xy} \end{Bmatrix} \tag{3.4}$$

Moment-curvature relationships are obtained by integrating over the slab depth to obtain:

$$\begin{Bmatrix} M_x \\ M_y \\ M_{xy} \end{Bmatrix} = \begin{bmatrix} \frac{E_x h^3}{12(1-\nu_x\nu_y)} & \frac{\nu_x E_y h^3}{12(1-\nu_x\nu_y)} & 0 \\ \frac{\nu_y E_x h^3}{12(1-\nu_x\nu_y)} & \frac{E_y h^3}{12(1-\nu_x\nu_y)} & 0 \\ 0 & 0 & \frac{G_{xy} h^3}{12} \end{bmatrix} \begin{Bmatrix} \psi_x \\ \psi_y \\ \psi_{xy} \end{Bmatrix} \tag{3.5}$$

Based on the analysis of the uncracked slab, moments in x and y directions, M_x and M_y, can be calculated for each element.

Scanlon & Murray (1982) used the Branson's (1977) equations (eq. 2.37) with power n=3 to calculate the reduced flexural second moment of area in both x and y directions. Reduction in flexural stiffness in each direction can be accounted for using the ACI Building Code equation (eq. 2.37) in both x and y directions:

$$I_{ex} = \left(\frac{M_{cr}}{M_x}\right)^3 I_g + \left[1 - \left(\frac{M_{cr}}{M_x}\right)^3\right] I_{crx} \tag{3.6}$$

$$I_{ey} = \left(\frac{M_{cr}}{M_y}\right)^3 I_g + \left[1 - \left(\frac{M_{cr}}{M_y}\right)^3\right] I_{cry} \tag{3.7}$$

where M_{cr} can be obtained from eq. 2.38. Material properties are modified as follows to reflect the reduction in stiffness due to cracking:

$$E_x = \alpha_x E_c \tag{3.8}$$

$$E_y = \alpha_y E_c \tag{3.9}$$

$$\nu_x = \alpha_x \nu \tag{3.10}$$

$$\nu_y = \alpha_y \nu \tag{3.11}$$

where

$$\alpha_x = \frac{I_{ex}}{I_{gx}} \tag{3.12}$$

$$\alpha_y = \frac{I_{ey}}{I_{gy}} \tag{3.13}$$

The analysis is then repeated using the reduced elastic constants until a stable condition is achieved. Scanlon & Murray (1974) expected some reduction in effective shear modulus due to cracking. However, they used the uncracked value of shear modulus in the analysis before and after cracking since, according to them, a quantitative reduction is difficult due to the effects of dowel action and aggregate interlock. Tam & Scanlon (1986) also used an uncracked value of shear modulus in their analysis. It should be pointed out here that the slabs which the above authors' analysed were supported on four corners and the effect of torsional moment was insignificant. Kotsovos & Pavlović (1999), however, concludes from experimental results that there can be no contribution to the shear capacity through aggregate interlock at the interfaces of inclined crack or through the dowel action of steel bars.

Instead of considering principal moments, Scanlon & Murray's cracking criterion was based on M_x or M_y exceeding the cracking moment M_{cr}. As the calculation was limited to x and y directions, selection of steel in these two directions was straightforward. But Tam & Scanlon (1986) pointed out that, for the more general case involving irregular slabs and loading configurations, it would be essential to

consider the effects of principal moments.

3.4 Polak approach

Polak (1996) used a similar approach to that of Scanlon & Murray (1974) with Branson's (1977) equation (eq. 2.37) to calculate the reduced flexural second moment of area in both x and y directions, which led to eqs 3.6 and 3.7. Unlike Scanlon and Murray, Polak used shear-reduction factors to represent the values of the cracked shear moduli and proposed the following shear moduli after cracking:

$$G_1 = G\alpha_x\alpha_y \tag{3.14}$$

$$G_2 = G\alpha_x \tag{3.15}$$

$$G_3 = G\alpha_y \tag{3.16}$$

The shear-reduction factors are the products of the corresponding stiffness reduction factors in the x and y directions as given in eqs 3.12 and 3.13 with α_z assumed to be equal to unity.

Polak modified the material stiffness as follows:

$$[D] = \begin{bmatrix} \frac{E_x h^3}{12(1-\nu_x\nu_y)} & \frac{\nu_x E_y h^3}{12(1-\nu_x\nu_y)} & 0 & 0 & 0 \\ \frac{\nu_y E_x h^3}{12(1-\nu_x\nu_y)} & \frac{E_y h^3}{12(1-\nu_x\nu_y)} & 0 & 0 & 0 \\ 0 & 0 & \frac{G_1 h^3}{12} & 0 & 0 \\ 0 & 0 & 0 & G_2 h & 0 \\ 0 & 0 & 0 & 0 & G_3 h \end{bmatrix} \tag{3.17}$$

The procedure is based on the secant-stiffness formulation and consists of one iteration - the effective-stiffnesses are calculated based on the initial linear elastic moment distribution.

3.5 Jofriet & McNeice approach

Jofriet & McNeice (1971) presented an FE method using a bilinear moment-curvature relationship based on Branson's (1977) equation. The approach used a tangent-

stiffness formulation. The Branson formula does not yield directly the tangent-stiffness rigidity of a region after cracking but rather the secant rigidity. Using a least-square fit, an equivalent tangent-stiffness equation was proposed. Before cracking, the uncracked rigidity was defined by

$$R_u = E_c I_u \tag{3.18}$$

in which E_c= modulus of elasticity of concrete and I_u=the moment of inertia of the cross-section including the effect of reinforcement. After cracking, the rigidity was approximated as

$$R_c = \frac{(r-1) I_g I_{cr}}{r I_g - I_{cr}} E_c \tag{3.19}$$

in which r= a factor that is related to the reinforcing steel percentage, ρ. I_{cr} is the moment of inertia of the fully cracked transformed section given by

$$I_{cr} = \frac{1}{3} c_n^3 + \rho n d (d - c_n)^2 \tag{3.20}$$

where c_n is the depth of the neutral axis defined as

$$c_n = d \left[\sqrt{2\rho n + (\rho n)^2} - \rho n \right] \tag{3.21}$$

where, d = effective depth of section; n = modular ratio, E_s/E_c; ρ =steel ratio, $A_s/(bd)$. From a least-square fit, r was found to be approximately:

$$r = 4.5 - 280\rho + 11,000\rho^2 \tag{3.22}$$

The cracking criterion was based on principal moments M_n or M_t exceeding the cracking moment M_{cr}. Jofriet & McNeice (1971) used the rigidity matrix given by Huber (Timoshenko & Woinowsky-Krieger, 1959) which gives the following moment-

curvature relations in the principal directions:

$$\begin{Bmatrix} M_n \\ M_t \\ M_{nt} \end{Bmatrix} = \begin{bmatrix} \frac{E_c I_{cn}}{(1-\nu_c^2)} & \nu_c \frac{E_c \sqrt{I_{cn} I_{ct}}}{(1-\nu_c^2)} & 0 \\ \nu_c \frac{E_c \sqrt{I_{cn} I_{ct}}}{(1-\nu_c^2)} & \frac{E_c I_{ct}}{(1-\nu_c^2)} & 0 \\ 0 & 0 & \frac{E_c \sqrt{I_{cn} I_{ct}}}{2(1+\nu_c)} \end{bmatrix} \begin{Bmatrix} \psi_n \\ \psi_t \\ \psi_{nt} \end{Bmatrix} \tag{3.23}$$

in which I_{cn}= effective moment of inertia in major principal direction and I_{ct}= effective moment of inertia in minor principal direction. Huber defines the torsional stiffness of a reinforced concrete slab as:

$$D_{3,3} = \frac{1-\nu}{2} \sqrt{D_{1,1} D_{2,2}} \tag{3.24}$$

So, using Huber's equation, the torsional stiffness will vary with cracking and the cracked shear modulus in the principal directions will be

$$G_{nt} = \frac{\sqrt{E_n E_t}}{2(1+\sqrt{\nu_n \nu_t})} \tag{3.25}$$

where, E_n, E_t, ν_n and ν_t are modified elastic properties in principal directions as defined by eqs from 3.8 to 3.11.

It was assumed in the work that, once a crack forms at right angles to a principal moment direction, its orientation is unaltered during any increase of load as it was found that the greatest change in principal moment direction was actually less than 5°. Jofriet & McNeice suggested a transformation matrix to convert rigidities from principal directions to global directions. As this calculation was based on principal directions, Jofriet & McNeice proposed a set of equations to calculate the effective steel in the principal directions, and these are presented in section 3.7.1.

Transformation of $[E]$ matrix

Jofriet & McNeice (1971) proposed a method of transformation of the flexural rigidity matrix into global x and y directions from the principal directions. The relationships defined by eq. 3.4 may be rewritten in matrix form as:

$$[\sigma] = [E][\epsilon] \tag{3.26}$$

Also, for the principal directions, this becomes:

$$[\sigma'] = [E'][\epsilon'] \tag{3.27}$$

The stresses $[\sigma]$ in the x and y directions are related to the $[\sigma']$ in the principal directions by the transformation

$$\begin{Bmatrix} \sigma_n \\ \sigma_t \\ \tau_{nt} \end{Bmatrix} = \begin{bmatrix} c^2 & s^2 & -2cs \\ s^2 & c^2 & 2cs \\ cs & -cs & c^2 - s^2 \end{bmatrix} \begin{Bmatrix} \sigma_x \\ \sigma_y \\ \tau_{xy} \end{Bmatrix} \tag{3.28}$$

in which c and s refer to $\cos\theta$ and $\sin\theta$ respectively, θ being the angle between the major principal direction and the x direction. Obviously, τ_{nt} is zero as there is no shear stress in the principal directions. Equation 3.28 can be written as:

$$[\sigma'] = [C_1][\sigma] \tag{3.29}$$

Similarly for strains:

$$\begin{Bmatrix} \epsilon_n \\ \epsilon_t \\ \gamma_{nt} \end{Bmatrix} = \begin{bmatrix} c^2 & s^2 & -cs \\ s^2 & c^2 & cs \\ 2cs & -2cs & c^2 - s^2 \end{bmatrix} \begin{Bmatrix} \epsilon_x \\ \epsilon_y \\ \gamma_{xy} \end{Bmatrix} \tag{3.30}$$

or, simply,

$$[\epsilon'] = [C_2][\epsilon] \tag{3.31}$$

Substituting eqs 3.29 and 3.31 into eq. 3.27 yields

$$[C_1][\sigma] = [E'][C_2][\epsilon] \tag{3.32}$$

From eqs 3.32 and 3.26:

$$[C_1][E][\epsilon] = [E'][C_2][\epsilon] \tag{3.33}$$

Premultiplying both sides of eq. 3.33 with the matrix $[C_1]^{-1}[E]^{-1}$ yields

$$[\epsilon] = [C_1]^{-1}[E]^{-1}[E'][C_2][\epsilon] \tag{3.34}$$

from which it follows that

$$[E]^{-1}[C_1]^{-1}[E'][C_2] = [I] \tag{3.35}$$

The inverse of $[C_1]$ is the transpose of $[C_2]$; thus

$$[E] = [C_2]^t[E'][C_2] \tag{3.36}$$

3.6 Favre *et al.* approach

Favre *et al.* (1990),(1992) proposed an FE method which incorporates the MC-90 moment-curvature relationship using an iterative secant-stiffness algorithm. The method can estimate both short- and long-term deflections. The mean curvature of a cracked section ψ_m (instantaneous or long-term) is calculated by interpolating between the uncracked curvature ψ_1 and the fully cracked curvature ψ_2 using eq. 2.33. The curvatures in states 1 and 2 were determined using:

$$\psi_1(t) = k_{s1}(1 + k_{\phi 1}\phi)\psi_c + k_{cs1}\frac{\epsilon_{cs}}{d} \tag{3.37}$$

$$\psi_2(t) = k_{s2}(1 + k_{\phi 2}\phi)\psi_c + k_{cs2}\frac{\epsilon_{cs}}{d} \tag{3.38}$$

where ψ_c=the curvature calculated on the basis of gross concrete section. The correction coefficients $k_{s1}, k_{s2}, k_{\phi 1}, k_{\phi 2}, k_{cs1}, k_{cs2}$ which take into account the effects of the amount of reinforcement, creep and shrinkage can be obtained from the CEB manual on cracking and deformation (1985).

Favre *et al.* used the stiffness matrix proposed by Huber for the initial FE analysis based on the gross-section of concrete. For each element, curvatures in the principal directions were obtained on the basis of the gross concrete section. For both directions, curvatures were calculated in states 1 and state 2 using eqs 3.37

and 3.38 respectively. Mean curvatures were obtained in each principal direction by interpolating between state 1 and state 2 using eq. 2.33. Mean curvatures were then transformed from principal directions to global x and y directions to obtain ψ_{xm}, ψ_{ym} and ψ_{xym}. The elements of the rigidity matrix were then obtained by:

$$D_{xm} = \frac{M_x - D_{1m}\psi_{ym}}{\psi_{xm}} \tag{3.39}$$

$$D_{ym} = \frac{M_y - D_{1m}\psi_{xm}}{\psi_{ym}} \tag{3.40}$$

$$D_{1m} = \frac{2\nu D_{xym}}{1-\nu} \tag{3.41}$$

$$D_{xym} = \frac{M_{xy}}{2\psi_{xym}} \tag{3.42}$$

Favre *et al.* (1992) used the following equations based on Johansen's (1972) yield criterion to calculate the effective steel:

$$A_{sn} = A_{sx}\left[\cos^2\theta + \mu\sin^2\theta\right] \tag{3.43}$$

$$A_{st} = A_{sx}\left[\sin^2\theta + \mu\cos^2\theta\right] \tag{3.44}$$

where μ is the ratio of y and x directional steel and θ is the angle between major principal direction and x axis (see Fig. 3.4).

3.7 Effective steel for different crack orientation

For a low steel percentage, which is usually the case in slabs, the reinforcement contributes little to the moment resistance of an uncracked section. According to Jofriet & McNeice (1971) an uncracked region, therefore, may be treated as isotropic, regardless of the orientation and orthotropy of reinforcement. This may be true for short-term loading as contribution of reinforcement to stiffness of an uncracked section is not usually significant. But it may not be true for long-term analysis when it is important to consider the actual amount of reinforcement in the cross-section to calculate creep and shrinkage curvatures.

Jofriet & McNeice (1971) suggest that the orientations of cracks in the service-load range may be assumed to be normal to the principal moment directions and the orientation can be kept unaltered during any increase of load since, as mentioned

earlier, the greatest change in principal moment direction, obtained in their analysis, was less than 5°. Lenschow & Sozen (1966), and Cardenas & Sozen (1971) have shown that the crack orientation will only be normal to the planes of applied principal moments in isotropically reinforced slabs. Orthotropically reinforced slabs crack initially on planes normal to the principal moment but, as the load is increased, the orthotropy of the reinforcement makes the crack turn to a plane where the ratio of the applied moment to the resisting moment is a maximum. The results of Cardenas & Sozen (1971) indicate that the change in direction of a crack is as much as 18°. As the analysis under discussion is mainly intended for the analysis of concrete slabs at service-load, it is assumed, according to Cope & Clark (1984), that the effect of deviation of the crack direction from principal directions will not be significant.

3.7.1 Jofriet & McNeice approach to calculate effective steel areas across cracks

Based on the work of Lenschow & Sozen (1966), Jofriet & McNeice (1971) derived expressions for the equivalent areas of reinforcement steel normal to the cracks. A brief description of the derivation is presented here. Figure 3.4 shows a reinforced concrete plate region with an orthogonal steel arrangement in the x and y directions. The steel area per unit width in the x direction is A_{sx} and in the y direction μA_{sx}. If

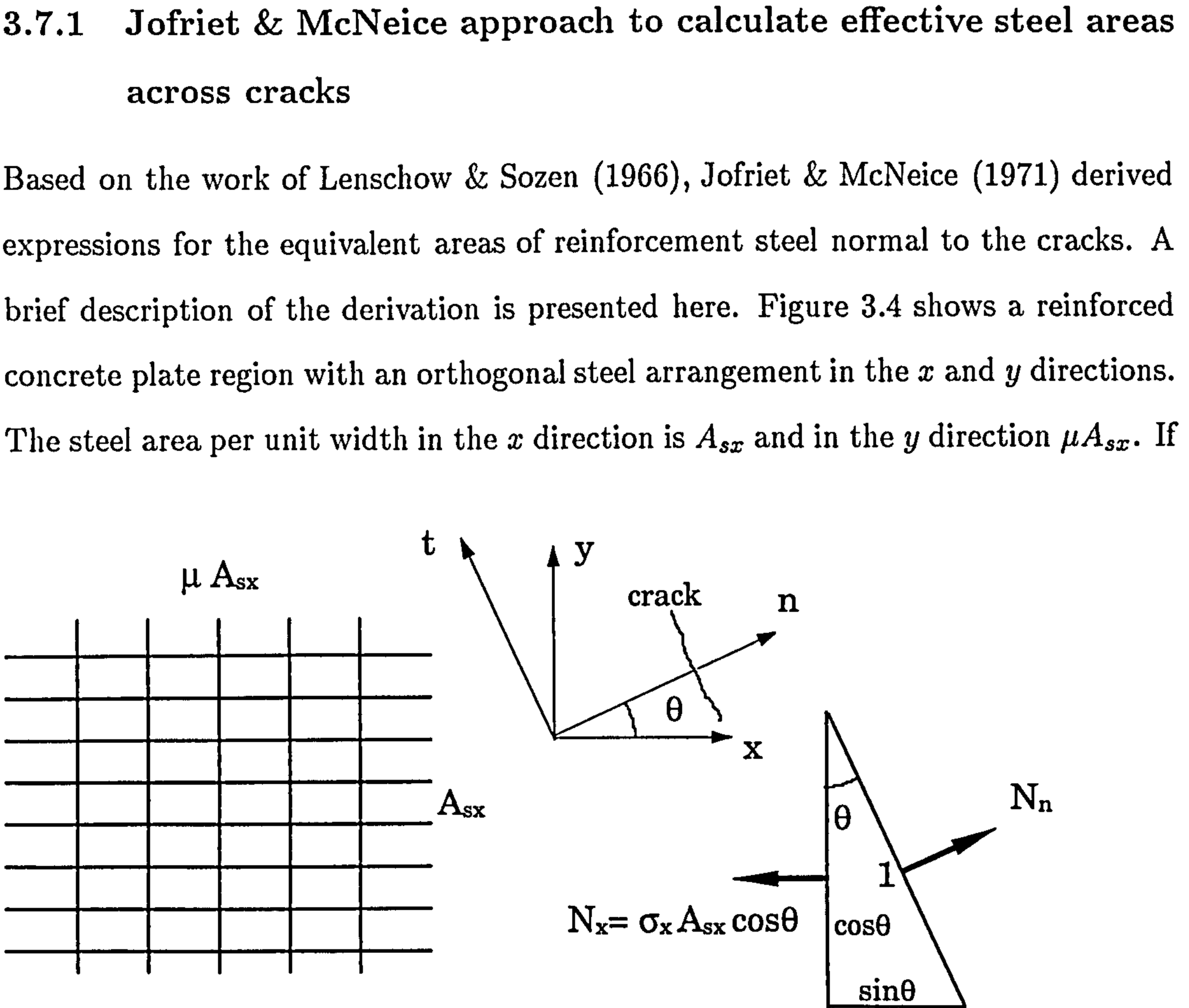


Figure 3.4 Effective steel area: adapted from Jofriet & McNeice (1971)

this reinforced concrete region is subjected to a set of principal direct tensile forces

N_n and N_t, the n direction being at an angle θ with the x direction, N_n and N_t can be expressed in terms of N_x and N_y as follows:

$$N_n = N_x \cos\theta + N_y \sin\theta \tag{3.45}$$

After the section is cracked, the full tension is taken by the steel alone:

$$N_x = E_s \epsilon_x A_{sx} \cos\theta \tag{3.46}$$

$$N_y = E_s \epsilon_y \mu A_{sx} \sin\theta \tag{3.47}$$

From Mohr's circle of strains:

$$\epsilon_x = \epsilon_n \cos^2\theta + \epsilon_t \sin^2\theta \tag{3.48}$$

$$\epsilon_y = \epsilon_n \sin^2\theta + \epsilon_t \cos^2\theta \tag{3.49}$$

Putting the values of ϵ_x and ϵ_y from eqs 3.48 and 3.49 into eqs 3.46 and 3.47, and the values of N_x and N_y from eqs 3.46 and 3.47 into eq. 3.45 result in

$$N_n = E_s A_{sx} \left[\epsilon_n\{\cos^4\theta + \mu \sin^4\theta\} + \epsilon_t\{1+\mu\}\cos^2\theta \sin^2\theta\right] \tag{3.50}$$

By rearranging terms and defining $\epsilon_n/\epsilon_t = r_{nt}$ = ratio of steel tensile strain in direction n to the steel tensile strain in direction t one obtains

$$\epsilon_n = \frac{N_n}{E_s A_{sx}\left[\cos^4\theta + \mu\sin^4\theta + \frac{1}{r_{nt}}(1+\mu)\cos^2\theta\sin^2\theta\right]} \tag{3.51}$$

As the effective steel in the n direction $A_{sn} = N_n/\epsilon_n E_s$ and in the t direction $A_{st} = N_t/\epsilon_t E_s$:

$$A_{sn} = A_{sx}\left[\cos^4\theta + \mu\sin^4\theta + \frac{1}{r_{nt}}(1+\mu)\cos^2\theta\sin^2\theta\right] \tag{3.52}$$

Jofriet & McNeice (1971) observed that cracks may occur in any section in three different ways: (a) one direction only; (b) two mutually orthogonal directions on the same side of the slab; and (c) two mutually orthogonal directions on opposite sides

of the slab. In case (a), as the value of r_{nt} in eq. 3.52 is quite large, the equivalent area of steel normal to the cracks may be expressed neglecting the last term:

$$A_{sn} = A_{sx}(\cos^4\theta + \mu \sin^4\theta) \tag{3.53}$$

In case (b) the equivalent area of steel in the major principal moment direction n may be obtained through eq. 3.52 and assuming $N_n/N_t = M_n/M_t$, so that the equivalent area of steel in the minor principal moment direction t is

$$A_{st} = A_{sn} r_{nt} \left|\frac{M_t}{M_n}\right| \tag{3.54}$$

where M_n = major principal moment; M_t = minor principal moment. r_{nt} can be expressed in terms of r_{xy} and angle θ:

$$r_{nt} = \frac{r_{xy}\cos^2\theta - \sin^2\theta}{\cos^2\theta - r_{xy}\sin^2\theta} \tag{3.55}$$

where r_{xy} is the ratio of steel strains in the x and y directions and can be approximated as

$$r_{xy} = \mu \left|\frac{M_x}{M_y}\right| \tag{3.56}$$

where M_x = moment in x-direction; M_y =moment in y-direction. In case (c) the equivalent steel area in the major principal moment direction is the same as for case (b) with the exception of the ratio of strains, r_{nt}. It must be replaced by a ratio r'_{nt} which may be approximated by:

$$r'_{nt} = -2.5 r_{nt} \tag{3.57}$$

3.7.2 Limitations of Jofriet & McNeice's approach

The author has found that Jofriet & McNeice's approach is inadequate for the following reasons:

1. The assumption $N_n/N_t = M_n/M_t$ is only true if the lever arms are equal in both principal directions.

2. The equation for A_{sn} is correct, but calculation of the ratio r_{nt} by eq. 3.55 is questionable. An attempt to include eq. 3.55 into the author's program failed since for certain combinations of r_{xy} and angle θ, the equation leads to very unrealistic values of r_{nt} (zero or negative even when both M_n and M_t are positive). Thus it is concluded that r_{nt} should be calculated in an iterative manner from actual steel strains in two principal directions rather than eq. 3.55.

3. Cardenas (1971) criticised the approach for case (c) because it assumes a depth to the neutral axis of $c_n = 0.4d$, which is not generally true. Also, he pointed out that slabs that are expected to crack at both top and bottom are usually reinforced on both levels. Consequently, the conditions of equilibrium have to be satisfied for both top and bottom layers of reinforcement. This is not the same as Jofriet & McNeice's case (b) where only top or bottom reinforcement is considered.

4. Jofriet & McNeice do not give any guideline for calculating the effective area of steel in the compression side or in the uncracked tensile region. This may not be important for short-term analysis but should be considered when creep and shrinkage are included in the long-term analysis.

3.7.3 Other approaches for calculating effective steel

Cope & Clark (1984) suggested that it is conservative to use eq. 3.53 for a single crack or two mutually orthogonal cracks on the same side of the slab and proposed a value of -1 for r_{nt} to be used in eq. 3.52 in the case of skew bending. But they also added that, for angles more than 25°, reinforcement stresses can be grossly overestimated and recommended a more accurate value of r_{nt} by using an iterative procedure.

Favre *et al.* (1990), (1992) used eqs 3.43 and 3.44 to calculate the effective steel in the principal directions.

3.8 Concluding remarks

Different FE methods have been discussed in this chapter with their formulations and assumptions. The objective of the current work is to develop a rather simple but accurate method of modelling deflection under service load. To this end, macro element method, particularly effective-stiffness method has been found most suitable. This is due to the fact that the crack models and long-term MC-90 model can be easily incorporated in this type of FE analysis. Secondly, as mentioned in section 3.4 that for typical slab systems, the effective-stiffness formulations can provide results with accuracy comparable to the accuracy of the layered approaches (Polak *et al.*, 1996).

Several authors' FE approaches with effective-stiffness formulations were discussed in details. Scanlon & Murray (1982) performed their calculations on the basis of stresses in x and y directions, allowed redistribution of stresses, however, did not modify the torsional rigidity term in the modified stiffness matrix. Polak (1996) also analysed in x and y directions, modified torsional rigidity term, but did not allow redistribution of stresses. Both the above approaches were based on secant stiffness approach and as a result Branson's equation was adopted without modification. However, Jofriet & McNeice (1971) used a tangent stiffness formulations and derived an equivalent bilinear relationship of the Branson's equation. Their calculations were done on the basis of principal stresses and they proposed method to calculate steel effective in the principal directions from x and y directional steels. Their work covered the formation of modified stiffness matrix in principal directions and transformation of them into global x and y directions. Limitation of their approach of calculating effective steel along with other proposed approaches has been discussed in section 3.7.2. Favre *et al.* (1990),(1992) proposed an FE method using an iterative secant-stiffness formulations to incorporate the MC-90 moment-curvature relationship. Their calculations are done in principal directions, mean curvatures were then transformed into x and y directions. They have employed simplified version of CEB equations (eq. 2.55), for states 1 and 2, rather than more accurate ones (eqs 2.41, 2.41 and 2.52). They have used eqs 3.43 and 3.44 based on Johansen's (1972) yield criterion to calculate steel in the principal directions.

Chapter 4

Incorporation of models in FE package and their performances

4.1 Introduction

In Chapter 2, three different short-term deflection models and the CEB-FIP Model Code (MC-90) long-term model were presented. Chapter 3 discussed incorporation of these models in FE analysis by other authors. The author has developed a similar method of incorporating these models in FE analysis which is described in detail in this chapter. Several methods of calculating effective steel areas in the principal directions are reviewed with particular emphasis on their capability of modelling measured deflections. The problem of convergence of the FE solution is discussed and an efficient convergence algorithm is proposed. Finally, the various models for predicting deflection are assessed using short- and long-term test data.

4.2 Comparison with other methods

The similarities and differences of the current work with previous works are as follows:

- The current method utilises principal stresses (or moments) to interpolate between uncracked and fully cracked states. This is logical because at lower load levels, cracks occur normal to these directions. Jofriet & McNeice (1971)

and Favre *et al.* (1990), (1992) also developed methods using calculations in the principal directions. Scanlon & Murray (1982) and Polak (1996) carried out similar analysis on the basis of x-y directional stresses.

- The method is based on a secant stiffness formulation, since it allows the use of the crack models and MC-90 model without any modification. Also, the directions of crack can change with the change in load which is not the case for Jofriet & McNeice's model where the initial direction of crack is retained in tangent stiffness formulations. Favre *et al.*, Scanlon & Murray and Polak approaches are all based on secant stiffness formulations.

- The present work incorporates ACI, Gilbert and MC-90 crack models. Also the MC-90 long-term model is included in the analysis with more accurate equations proposed by Ghali & Favre (1994). Favre *et al.* adopted MC-90 method with simplified equations.

- The author carried out a detailed comparative study on the use of different possible equations to calculate effective steel areas in the principal directions. Jofriet & McNeice proposed their own equations whereas Favre *et al.* used equations based on Johansen's yield criteria.

- In the present work, the $[E]$ matrices are modified to model cracking, creep and shrinkage in the principal directions and then transformed into global x-y direction according to the work of Jofriet & McNeice.

- The author identified a problem of non-convergence of FE solution and developed an efficient method to overcome it.

4.3 Incorporation of FE models

A program module has been developed by the author to incorporate the crack models and MC-90 long-term model discussed in sections 2.9 and 2.10 respectively. The module acts as an integral part of the FE package FE77 (Hitchings, 1994) and calculates modified elastic properties (to represent cracking, creep and shrinkage)

for each element, on the basis of stresses of FE solution, which are then fed back into the assembly module of the FE package.

4.3.1 Sequences of analysis

A flow chart describing the incorporation of the MC-90 model is shown in Fig. 4.1. First, the analysis is carried out on the slab with gross concrete section (without reinforcement). The FE solution gives deflections and stresses at all the nodes. Bending moments are calculated in principal directions from x-y directional stresses. For the two principal directions, the curvatures are calculated in states 1 and 2. If the analysis is for long-term, creep and shrinkage terms are also added to state 1 and 2 curvatures. Mean curvatures are calculated using M/M_r ratios in both principal directions. Factors to modify the $[E]$ matrices in the principal directions are calculated comparing mean curvature and corresponding gross curvature. The modified $[E]$ matrices are then transformed into global x-y directions from principal directions. The resulting $[E]$ matrices are then compared with $[E]$ matrices of corresponding elements in previous step and adjusted to ensure that the loss of stiffness is gradual. With the modified set of $[E]$ matrices, the FE package gives a solution of stresses and deflections and another set of modified elastic properties are obtained from the program module. The whole procedure is repeated until a stable condition is attained. At the stable condition, the modified elastic properties are close to the values determined in the previous step. This is checked by comparing deflections of successive steps, when there are no changes in deflections at all points of the slab, the program stops.

The sequences for ACI and Gilbert models are similar. For the ACI method effective moments of inertia are obtained in two principal directions by interpolating between gross and cracked moments of inertia. In the Gilbert method, extra amount of steel is added to cracked section to find the effective moments of inertia. In both cases, effective moments of inertia are compared with gross inertia to find the modification factors.

A detailed description of the program module is presented in this chapter. The incorporation of the ACI and Gilbert's models to calculate the effective moment of

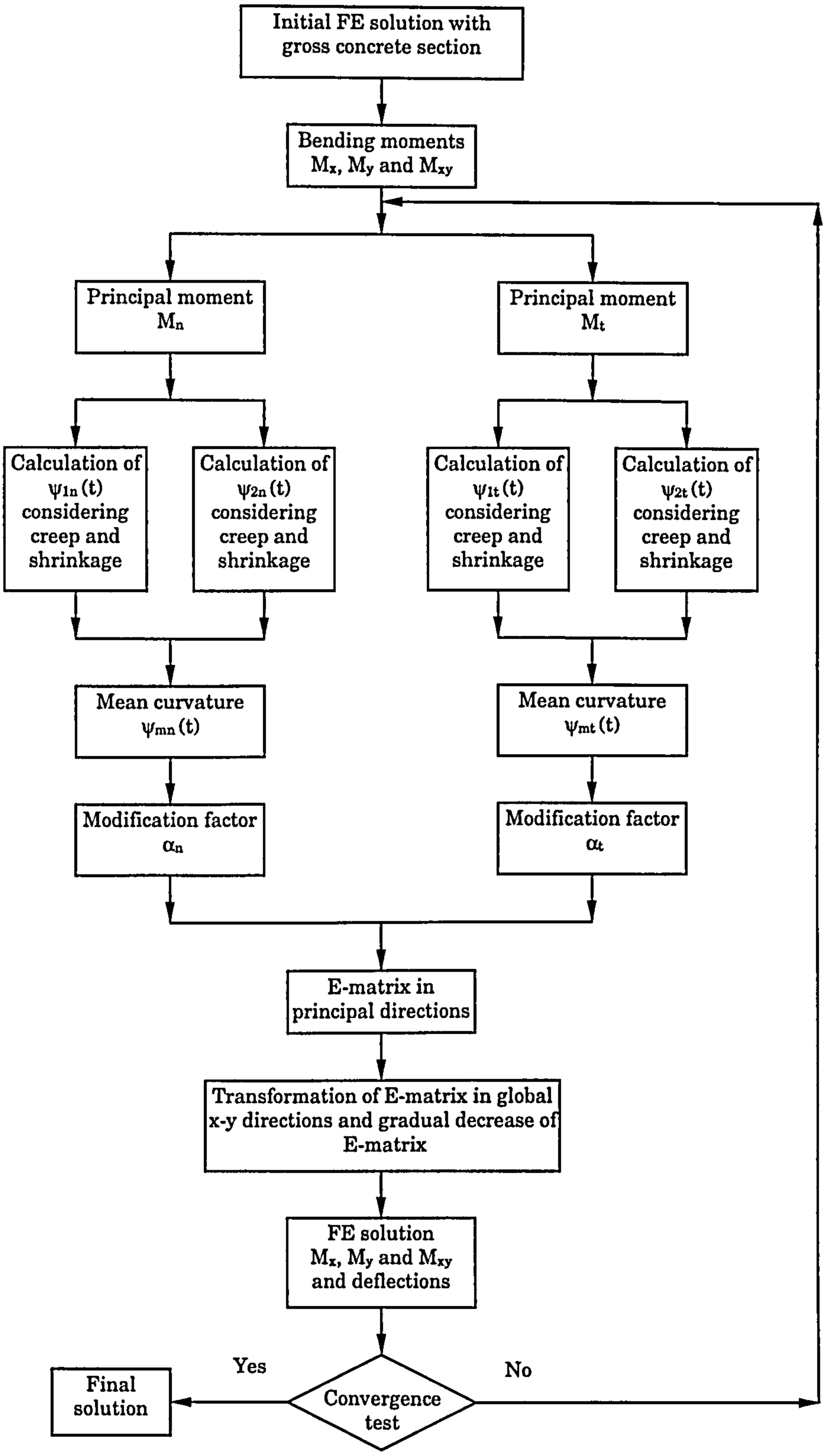


Figure 4.1 Flow chart showing the sequences of calculation

inertia are presented in section 4.7 and the MC-90 model for calculating the mean curvature are described in section 4.8. Once modification factors are calculated using either by eqs 4.29 and 4.30 or eqs 4.47 and 4.48, modified $[E]$ matrices are formed in the principal directions and then transformed into global x-y directions as described in section 4.9. The modified $[E]$ matrices in x-y coordinates are again adjusted according to section 4.11 by comparing $[E]$ of previous step so that the loss of stiffness is gradual and they are then fed back into the FE package which calculates redistributed stresses. The process is repeated until it yields a stable converged solution. A detailed study to find a suitable method of calculating steel effective in principal directions from x and y directional steel is presented in section 4.4.

4.3.2 Assumptions in the analysis of the slabs

An FE solution is carried out with QD09 (general shell and plate bending element with 9 nodes) elements. Initially, material of all the elements are defined as anisotropic and 6 X 6 elasticity $[E]$ matrices are defined for all the elements so that, later on the basis of calculations, they can have different E values in orthogonal directions to represent two levels of cracking in those directions.

It has been found that the middle node stresses of the QD09 element give a good average representation of all the nodal stresses when the mesh is reasonably fine. Therefore, the middle node stress has been used to calculate the principal stresses and moments. The FE package gives principal stresses, but it does not give their directions. Therefore, the principal stresses and their directions are calculated within the subroutine. The two principal stresses, which are close to the plane of the plate are considered in the analysis. The third principal stress which is close to the normal of the plate is ignored because it is small and has no effect on the flexural cracking.

Both 2-D and 3-D attributes were used to define the slab depending on the actual boundary conditions. If a slab is supported on column, the structure is defined as 3-D, otherwise a 2-D definition is sufficient. For a 2-D bending problem, the tensile and compressive stresses at the top and bottom fibres of a rectangular section are equal.

Hence, although all the models utilise moment values (M/M_{cr}), using extreme fibre stresses instead of moment yields the same result. In the present work, principal stresses are used to determine the effective moment of inertia (interpolation between state 1 and 2) using ACI and Gilbert's model and principal moments are used to calculate the effective curvature when using the MC-90 model. It should also be noted that when the slab is supported by columns, stresses may differ at the top and bottom surfaces of the slab. In this case, only the flexural components are used to calculate principal stresses and moments.

4.4 Equivalent steel areas

Section 3.7 presented approaches proposed by other authors to calculate effective steel areas. A study has been carried out to determine the best approach to find the effective steel. It has already been pointed out (see section 3.7.2) that the use of eq. 3.55 may produce unrealistic results. Hence, to remove this deficiency in Jofriet & McNeice's (1971) method, an iterative approach was adopted that used the actual strain ratio from the previous run. It was also pointed out in section 3.7 that Jofriet & McNeice's equations assume that the lever arms are equal in the two orthogonal directions, while the following derivation is more generalised as lever arms are derived from section calculation.

4.4.1 Derivation of equivalent steel areas for bending of plate

Equations similar to those proposed by Jofriet & McNeice (1971) can be derived for the general case of bending of a plate where the lever arms in the two principal directions are not equal. Figure 4.2 shows a reinforced concrete plate region with an orthogonal tensile steel arrangement in the x and y directions. The steel area per unit width in the x direction is A_{sx} and in the y direction μA_{sx}. If this reinforced concrete region is subjected to a set of principal moments M_n and M_t (n direction being at an angle θ with the x direction), M_n and M_t can be expressed in terms of M_x and M_y as follows:

$$M_n = M_x \cos\theta + M_y \sin\theta \tag{4.1}$$

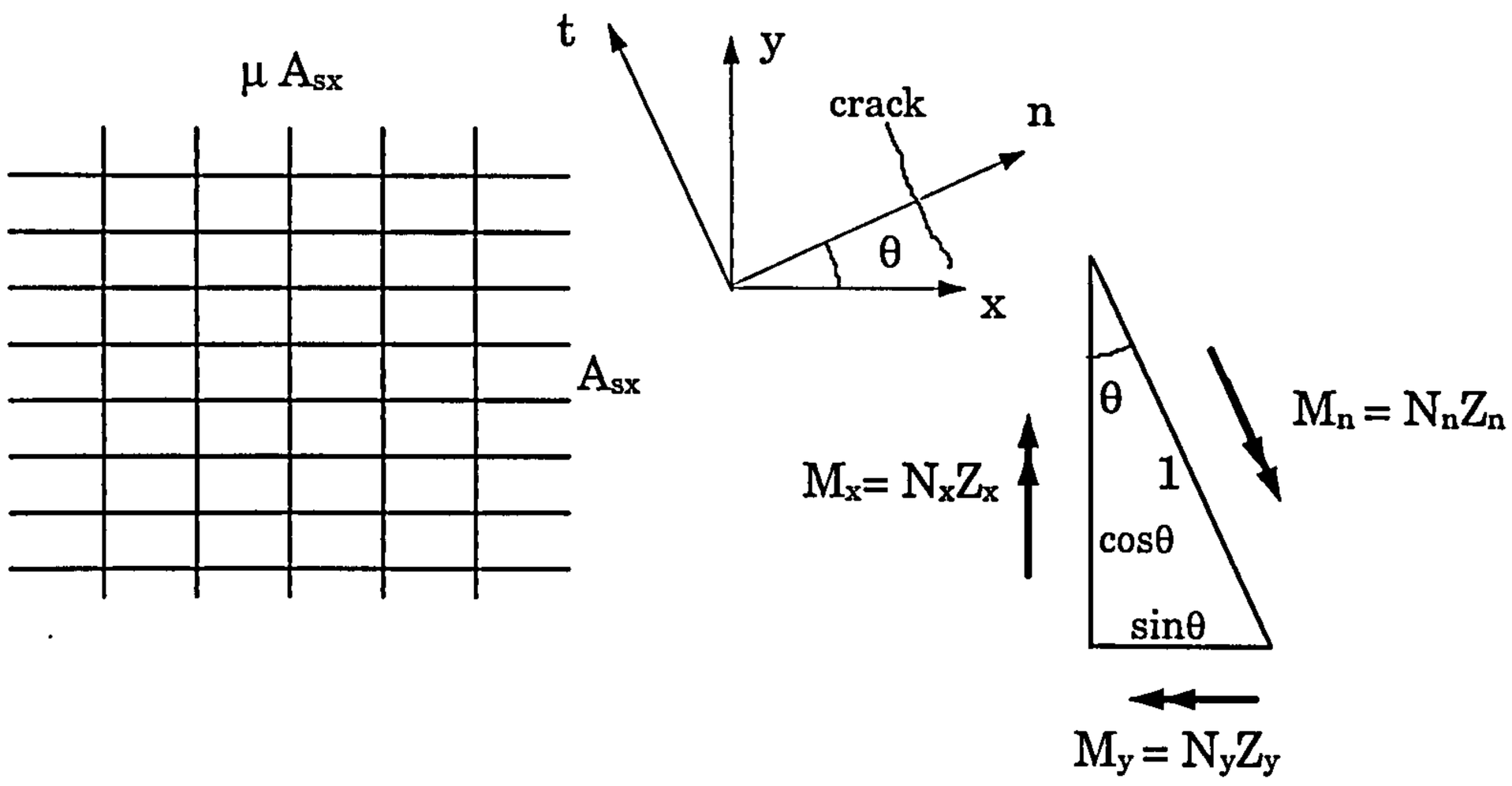


Figure 4.2 Equivalent steel area

The moments can be replaced by the tensile force in the reinforcement times the lever arm:

$$N_n Z_n = N_x \cos\theta Z_x + N_y \sin\theta Z_y \tag{4.2}$$

After the section is cracked, all the tension is taken by the steel and

$$N_x = E_s \epsilon_x A_{sx} \cos\theta \tag{4.3}$$

$$N_y = E_s \epsilon_y \mu A_{sx} \sin\theta \tag{4.4}$$

From Mohr's circle of strains:

$$\epsilon_x = \epsilon_n \cos^2\theta + \epsilon_t \sin^2\theta \tag{4.5}$$

$$\epsilon_y = \epsilon_n \sin^2\theta + \epsilon_t \cos^2\theta \tag{4.6}$$

Substituting the values of ϵ_x and ϵ_y from eqs 4.5 and 4.6 into eqs 4.3 and 4.4 and values of N_x and N_y from eqs 4.3 and 4.4 into eq. 4.2 one obtains

$$N_n Z_n = E_s A_{sx} \left[\epsilon_n \{\cos^4\theta Z_x + \mu \sin^4\theta Z_y\} + \epsilon_t \{Z_x + \mu Z_y\} \cos^2\theta \sin^2\theta\right] \tag{4.7}$$

By rearranging terms and letting $\epsilon_n/\epsilon_t = r_{nt}$ = ratio of steel tensile strain in direction n to the steel tensile strain in direction t, the following expression is obtained:

$$\epsilon_n = \frac{N_n}{E_s A_{sx}\left[\cos^4\theta\frac{Z_x}{Z_n} + \mu\sin^4\theta\frac{Z_y}{Z_n} + \frac{1}{r_{nt}}(\frac{Z_x}{Z_n} + \mu\frac{Z_y}{Z_n})\cos^2\theta\sin^2\theta\right]} \tag{4.8}$$

As the effective steel in the n direction is $A_{sn} = N_n/\epsilon_n E_s$:

$$A_{sn} = A_{sx}\left[\cos^4\theta\frac{Z_x}{Z_n} + \mu\sin^4\theta\frac{Z_y}{Z_n} + \frac{1}{r_{nt}}(\frac{Z_x}{Z_n} + \mu\frac{Z_y}{Z_n})\cos^2\theta\sin^2\theta\right] \tag{4.9}$$

An equation similar to Jofriet & McNeice's equation for the steel in the transverse direction (eq. 3.54) can be derived with varying the lever arms in two directions. Putting $\epsilon_t = \epsilon_n/r_{nt}$ in eq. 4.8

$$\epsilon_t = \frac{N_n}{E_s A_{sx}\left[\cos^4\theta\frac{Z_x}{Z_n} + \mu\sin^4\theta\frac{Z_y}{Z_n} + \frac{1}{r_{nt}}(\frac{Z_x}{Z_n} + \mu\frac{Z_y}{Z_n})\cos^2\theta\sin^2\theta\right] r_{nt}} \tag{4.10}$$

The tensile force N_n is related to N_t by:

$$\frac{N_n}{N_t} = \frac{M_n Z_t}{M_t Z_n} \tag{4.11}$$

Substitution of eq. 4.11 into eq. 4.10 leads to:

$$\epsilon_t = \frac{N_t}{E_s A_{sx}\left[\cos^4\theta\frac{Z_x}{Z_n} + \mu\sin^4\theta\frac{Z_y}{Z_n} + \frac{1}{r_{nt}}(\frac{Z_x}{Z_n} + \mu\frac{Z_y}{Z_n})\cos^2\theta\sin^2\theta\right] r_{nt}\frac{M_t Z_n}{M_n Z_t}} \tag{4.12}$$

and an expression for the equivalent steel area in the t direction of

$$A_{st} = A_{sx}\left[\cos^4\theta\frac{Z_x}{Z_n} + \mu\sin^4\theta\frac{Z_y}{Z_n} + \frac{1}{r_{nt}}(\frac{Z_x}{Z_n} + \mu\frac{Z_y}{Z_n})\cos^2\theta\sin^2\theta\right] r_{nt}\frac{M_t Z_n}{M_n Z_t} \tag{4.13}$$

or simply

$$A_{st} = A_{sn} r_{nt}\left|\frac{M_t Z_n}{M_n Z_t}\right| \tag{4.14}$$

If the lever arms in the n and t directions are assumed to be equal eq. 4.14 reduces to the Jofriet-McNeice equation (eq. 3.54) for the effective steel in the t direction.

A FORTRAN program was written to calculate effective steel areas using eqs 4.9

and 4.14 through an iterative approach based on steel strains which are determined from the section analysis. The effective depth d and the depth of the compression steel d' are taken as average of the x and y depths. The initial value of r_{nt} needs to be assumed to calculate the first values of A_{sn} and A_{st}. In this study, as an initial condition, either the areas of steel or the steel strains in both directions are assumed to be equal to calculate initial r_{nt}. During the iteration, the effective steel in the n and t directions A_{sn} and A_{st} are obtained using eqs 4.9 and 4.14 and r_{nt} is determined from the section calculation. In the case of skew bending (Jofriet & McNeice's case (c)), either ϵ_n or ϵ_t is compressive on a face, so that the actual value of r_{nt}, which is negative, is calculated for each face and used in the same equations (eqs 4.9 and 4.14). The whole section calculation is repeated with the r_{nt} obtained in the previous step until the steel areas obtained in the two successive steps converge.

4.4.2 Suitability of the different sets of equations

An investigation was carried out to check the suitability of eq. 4.14 along with 4.9 for isotropic meshes and meshes of different levels of orthotropy under biaxial and skew bending, the results of which are also presented in Appendix A. Four initial conditions have been considered:

- Case 1: with initial condition $\epsilon_n = \epsilon_t$ for the general case where the lever arms are initially assumed equal but derived from section analysis during iteration.
- Case 2: with initial condition A_{sn}=A_{st} for the general case where the lever arms are initially assumed equal but derived from section analysis during iteration.
- Case 3: with initial condition $\epsilon_n = \epsilon_t$ and assuming the lever arms to be equal in the two directions.
- Case 4: with initial condition A_{sn}=A_{st} and assuming the lever arms to be equal in the two directions.

It should be pointed out that cases 3 and 4 lead to the equations given by Jofriet & McNeice (1971) to calculate A_{sn} and A_{st} (eqs 3.52 and 3.54) since lever arms

are assumed equal, however in the current study an iterative approach was used to calculate r_{nt} from actual strains in principal directions instead of Jofriet & McNeice's equation (eq. 3.55). It has been found that eqs 4.9 and 4.14 do not produce an unique solution and that the solution depends very significantly on the initial conditions assumed in the analysis (i.e. cases 1 to 4). If A_{sn} is initially assumed to be equal to A_{st} (cases 2 and 4), the final steel areas are also equal in the two directions. The initial equal A_{sn} and A_{st} leads to $r_{nt}= M_n/M_t$ and $Z_n=Z_t$ (if calculated from analysis), which result in $A_{sn}=A_{st}$ at the end of each iteration. When ϵ_n and ϵ_t are assumed initially equal with lever arms derived from section analysis (case 1), the converged solution shows that the final conditions are $\epsilon_n Z_n=\epsilon_t Z_t$ (which is also the initial condition) and $A_{sn}/A_{st} = M_n/M_t$. When lever arms are assumed to be equal (even in case 3, where the initial value of A_{sn} is not equal to A_{st}), the solution always converges with $A_{sn}=A_{st}$ no matter what initial condition is selected. For case 3, initial condition, $\epsilon_n=\epsilon_t$ changes to $\epsilon_n/\epsilon_t=M_n/M_t$ and A_{sn} becomes equal to A_{st} after convergence. It is clear from this study that a unique solution for the effective steel is not possible with this set of equations since the effective steel area is dependent on the initial conditions adopted.

Another approach is also included the study as case 5 which is adopted by Favre [(1992), (1992)] in a similar analysis. This equations are based on Johansen's yield criterion (Johansen, 1972) which leads to eqs 3.43 and 3.44.

Also, it is suggested by Cope & Clark (1984) that it is conservative to use eq. 3.53 rather than eq. 3.52 for both one and two directional cracks. So to get an idea of the lowest possible steel the following equations are also considered in the study as case 6:

$$A_{sn} = A_{sx}\left[\cos^4\theta + \mu\sin^4\theta\right] \tag{4.15}$$

$$A_{st} = A_{sx}\left[\sin^4\theta + \mu\cos^4\theta\right] \tag{4.16}$$

4.5 Deflection comparison using different equations to calculate the effective steel

From the preceding section, it is clear that it is possible to calculate the effective steel areas in the two principal directions in three different ways. A comparative study has been performed to select the most suitable of these three possibilities which are:

- Case a: using Jofriet, McNeice's equations (eqs 4.9 and 4.14) which lead to equal steel in the n and t directions if the lever arms are assumed to be equal in the principal directions.

- Case b: using eqs 3.43 and 3.44 based on Johansen's yield criterion.

- Case c: using eqs 4.15 and 4.16 which is conservative to use as it leads to the lowest possible steel.

Deflections of several slabs with isotropic or orthotropic meshes and with different boundary and loading conditions were calculated using the three different sets of equations stated above. This enabled a comparative study of performance to be undertaken.

4.5.1 Short-term loading: McNeice slab

This slab, which is often used as a benchmark, was 36 in. square by 1.75 in. thick and reinforced with an isotropic mesh giving a reinforcement ratio $100A_s/bh = 0.85$. It was supported at four corners and loaded by a central point load. The slab was originally tested by McNeice (1967). All the material properties and geometric details are taken from Jofriet & McNeice (1971); as modulus of rupture is not specified in the paper, it is assumed to be $7.5\sqrt{f'_c}$, in accordance to ACI (1989). Details of the material properties, slab dimensions, reinforcement and the FE mesh used in the present analysis are given in Fig. 4.3. Analytical load versus instantaneous-deflection curves for four different nodes using the three sets of equations, as well as the relevant experimental results, are presented in Figs 4.4 to 4.7. From all the curves, it is evident that, at the lower load range, all the equations lead to deflections

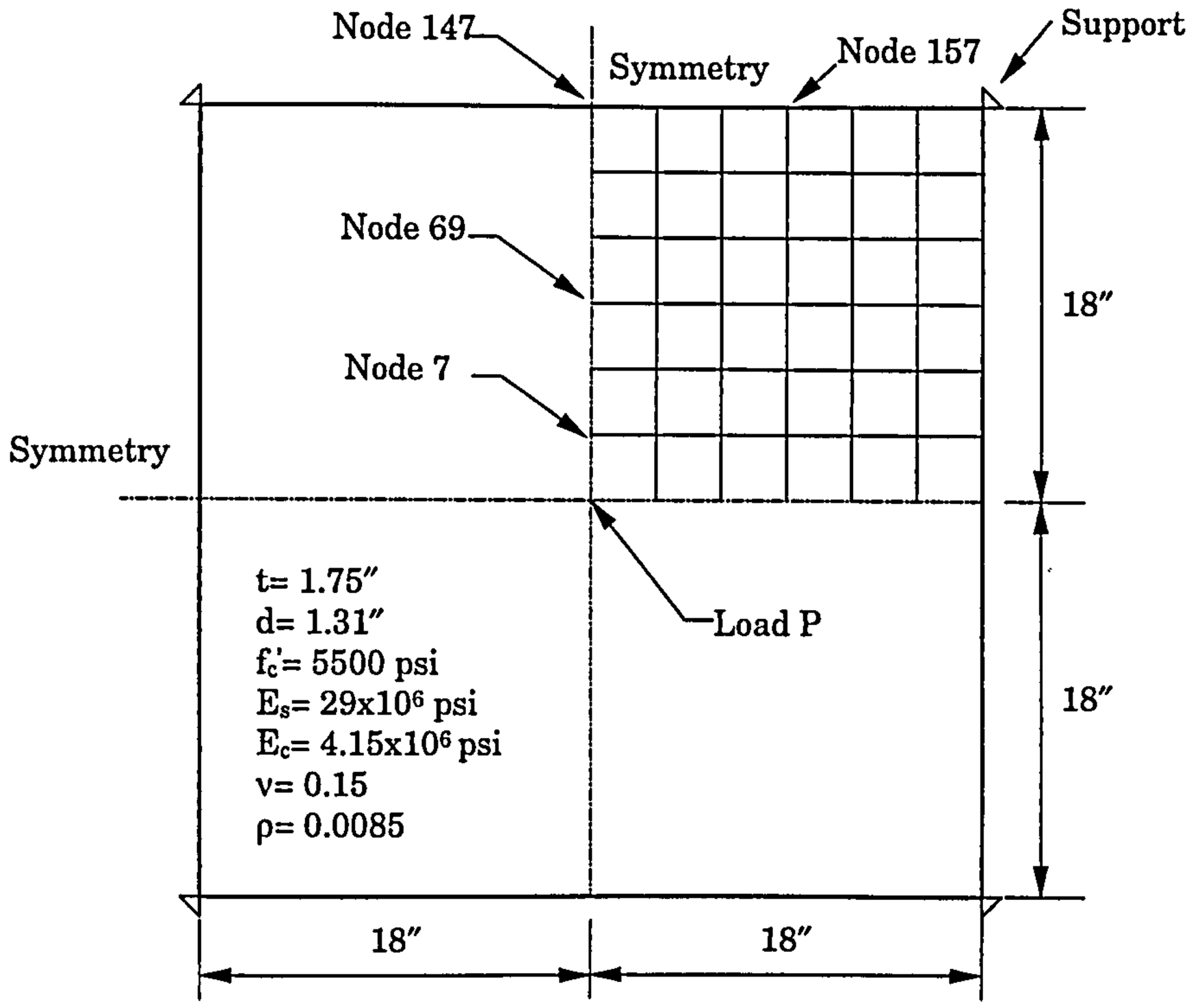


Figure 4.3 Details of corner-supported two-way slab tested McNeice: adapted from Jofriet & McNeice (1971)

of similar values but, as more cracking starts to appear with the increase in load, the deflections diverge. Case (c) gives the lowest area of steel and results in a considerably higher deflection compared to the experimental deflections. Cases (a) and (b) lead to similar deflections, with the latter case being closer to the experimental results.

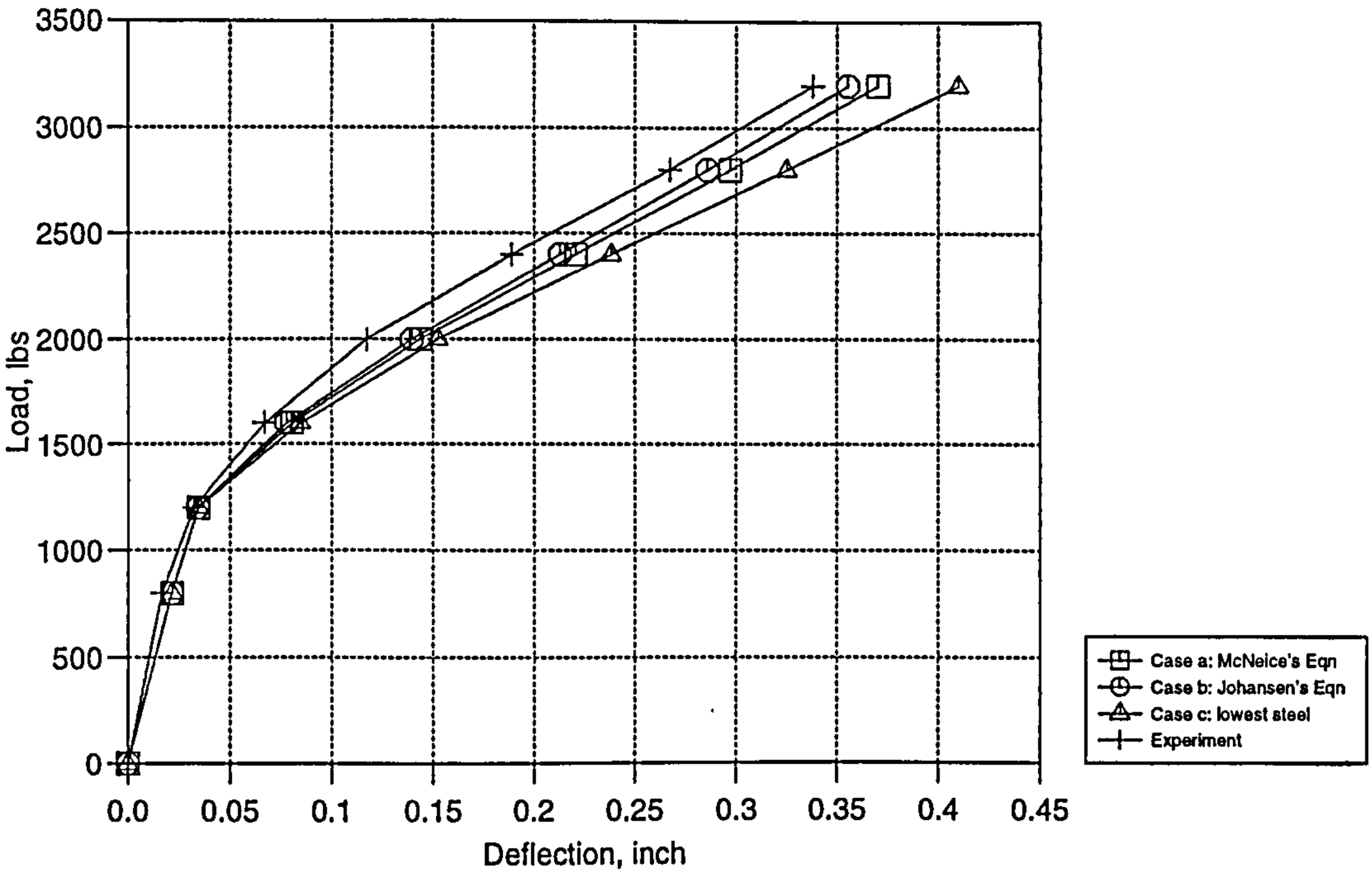


Figure 4.4 Load versus deflection curves for the corner-supported McNeice slab using different equations to calculate effective steel: node 7

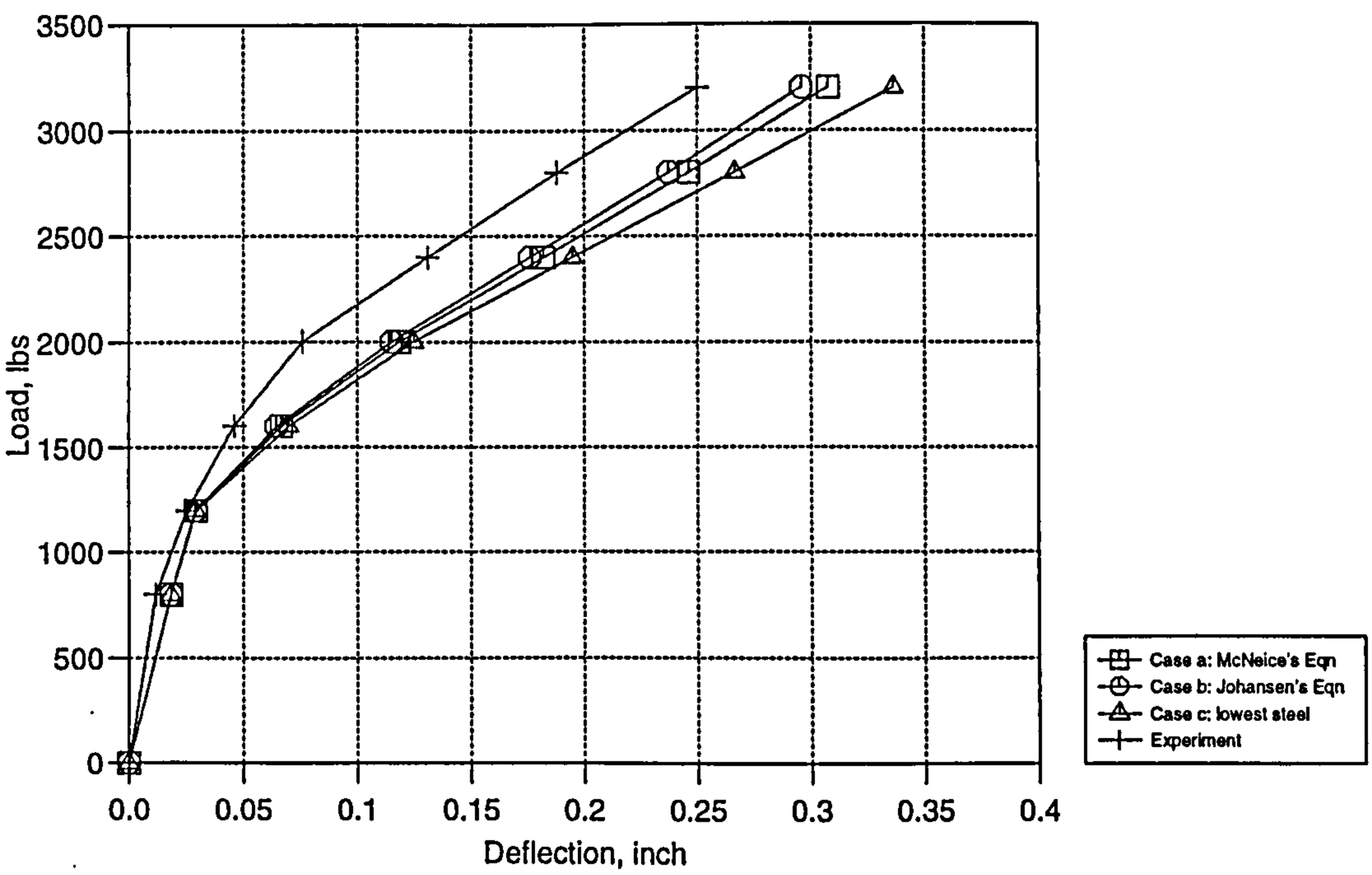


Figure 4.5 Load versus deflection curves for the corner-supported McNeice slab using different equations to calculate effective steel: node 69

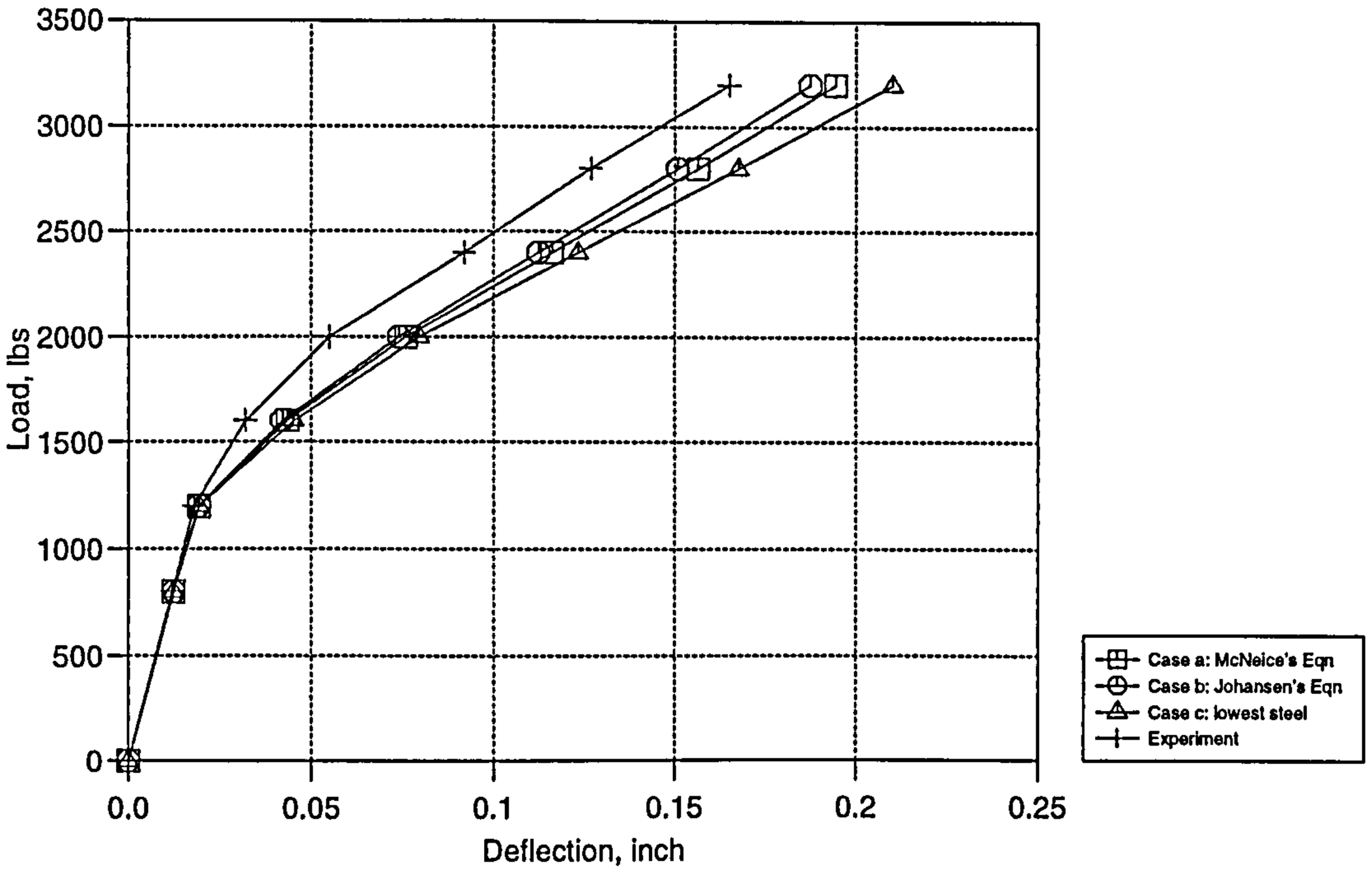


Figure 4.6 Load versus deflection curves for the corner-supported McNeice slab using different equations to calculate effective steel: node 147

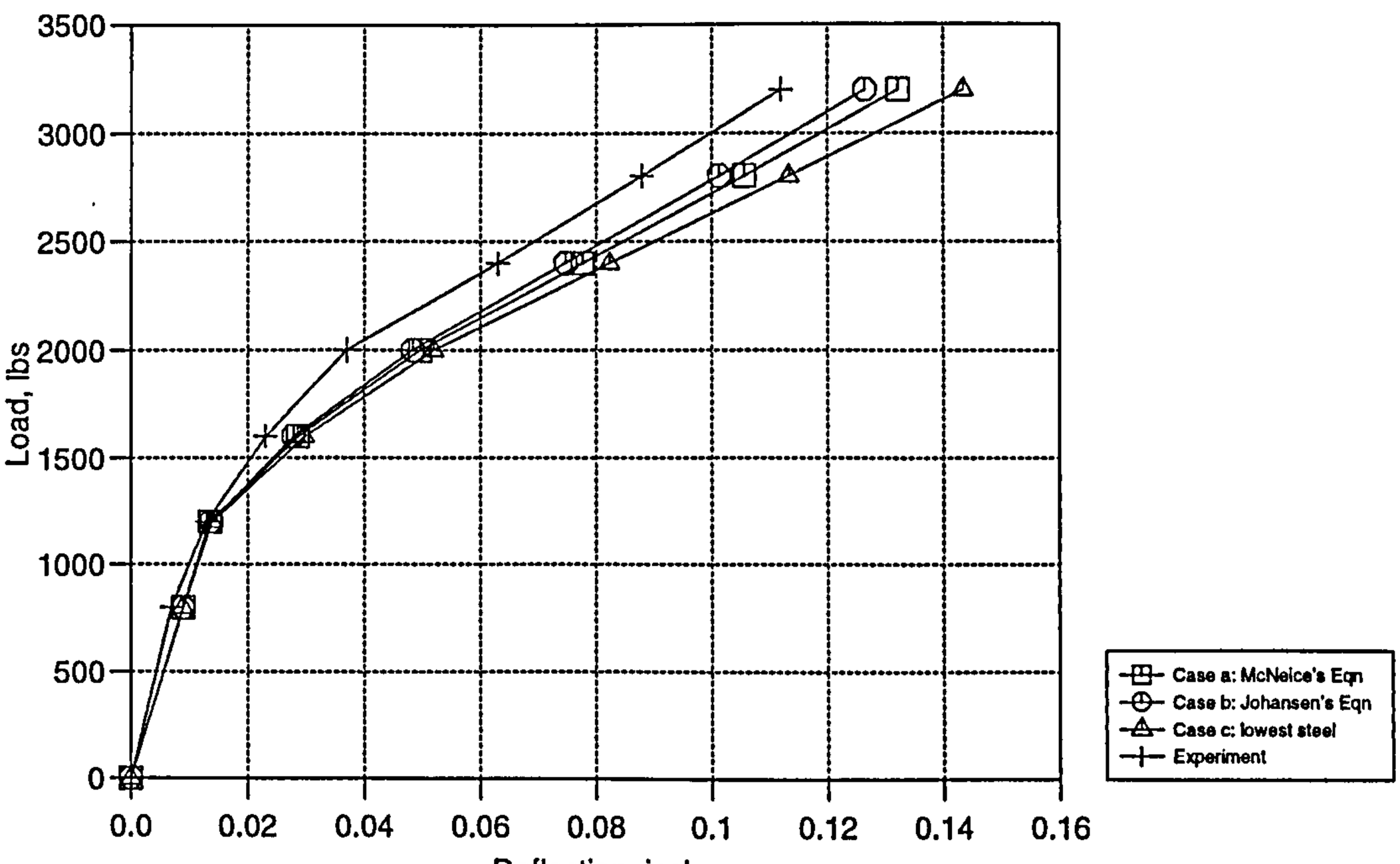


Figure 4.7 Load versus deflection curves for the corner-supported McNeice slab using different equations to calculate effective steel: node 157

4.5.2 Short-term loading: Shukla & Mittal slabs

Shukla & Mittal (1976) carried out a series of tests on two-way edge-supported slabs. All the slabs were 214 cm square and 8 cm thick. The slabs were supported on reinforced concrete walls with centre to centre span of 183 cm each way. Their corners were held down by means of 40 mm diameter steel rods anchored to the floor. Loads were applied to the test slab in increments of 2 tonnes each through an inverted waffle-tree system which transferred load at 16 equidistant point of the slab. Three slabs (S-8, S-11 and S-12) from this series have been analysed here. S-8 and S-11 were isotropically reinforced with 10 mm bars to provide 5.24 and 4.36 cm^2/m steel in each direction respectively. S-12 is reinforced with 10 and 6 mm bars to make an orthotropic slab with 5.24 and 1.35 cm^2/m steel in two directions. The amount of top steel is not specified by the authors and it is assumed to have the same amount of steel as the bottom layer. The three slabs differ in concrete strength which were 15.9 (S-8), 22.0 (S-11), 19.1 (S-12) N/mm^2. Moduli of rupture and elasticity were not reported and hence have been estimated using the ACI equations (in N/mm^2):

$$E_c = 4733\sqrt{f'_c} \tag{4.17}$$

$$f_r = 0.62\sqrt{f'_c} \tag{4.18}$$

Details of the slab dimensions and FE mesh are shown in Fig. 4.8.

Experimental and theoretical short-term load-deflection curves were compared for the central nodes of all the three slabs, and are presented in Figs 4.9 to 4.11. The results are similar to those for the McNeice slab, namely case (c) gives the lowest area of steel and overestimates experimental deflections. Cases (a) and (b) lead to similar deflections, with case (b) being closer to the experimental results.

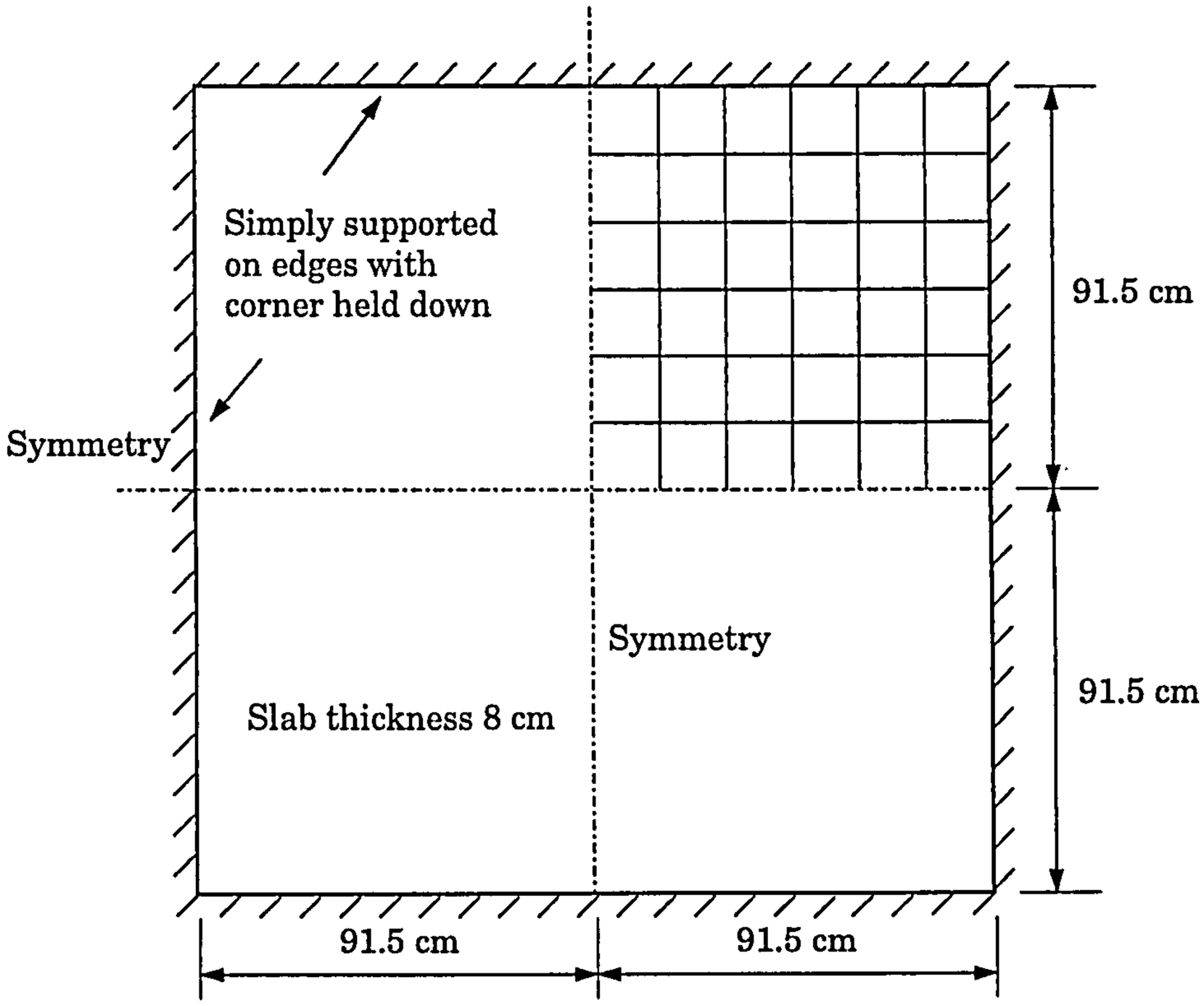


Figure 4.8 Details of edge-supported two-way slabs tested by Shukla & Mittal (1976)

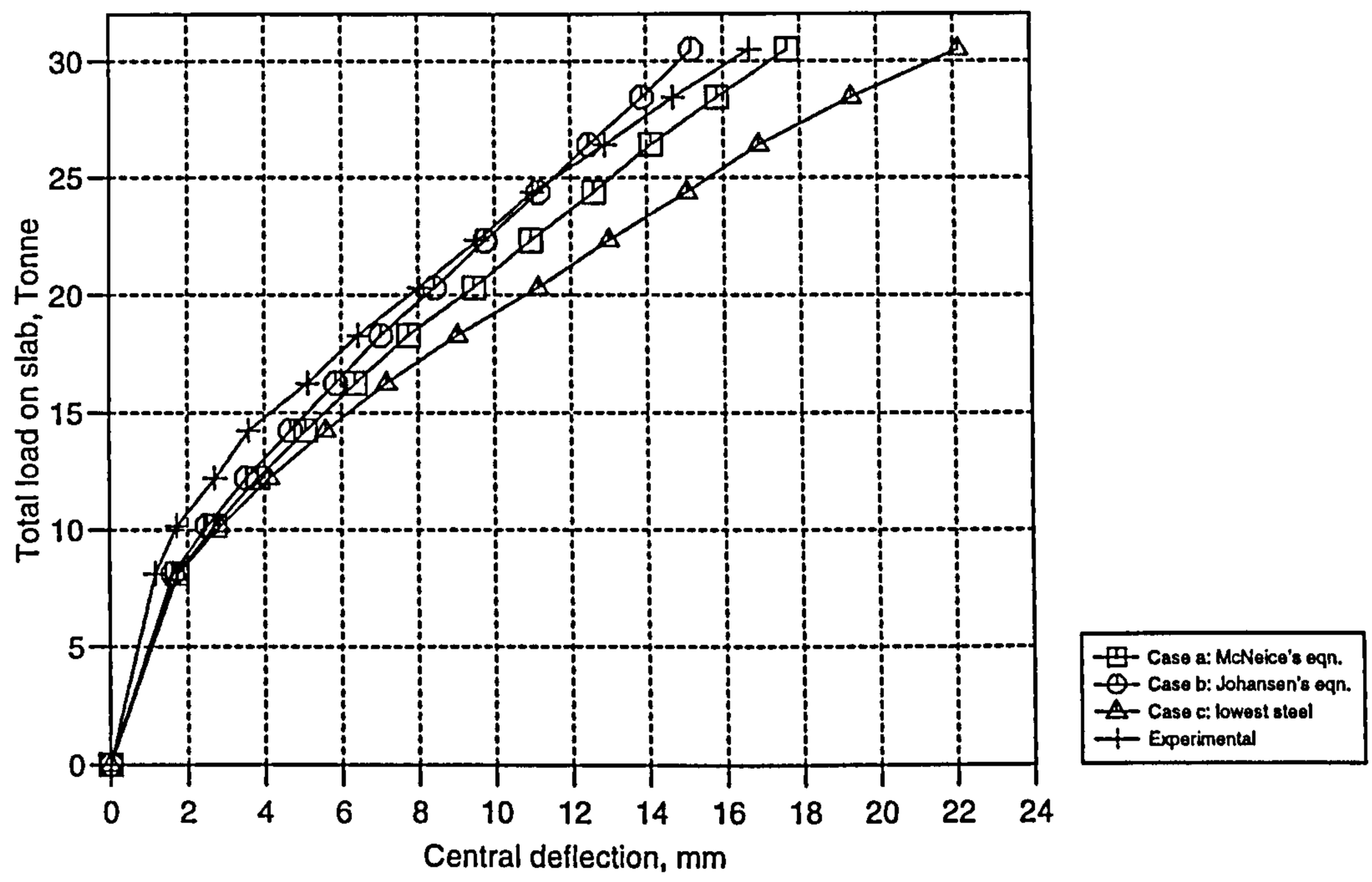


Figure 4.9 Load versus deflection curves for the edge-supported Shukla & Mittal slab S-8 using different equations to calculate the effective steel

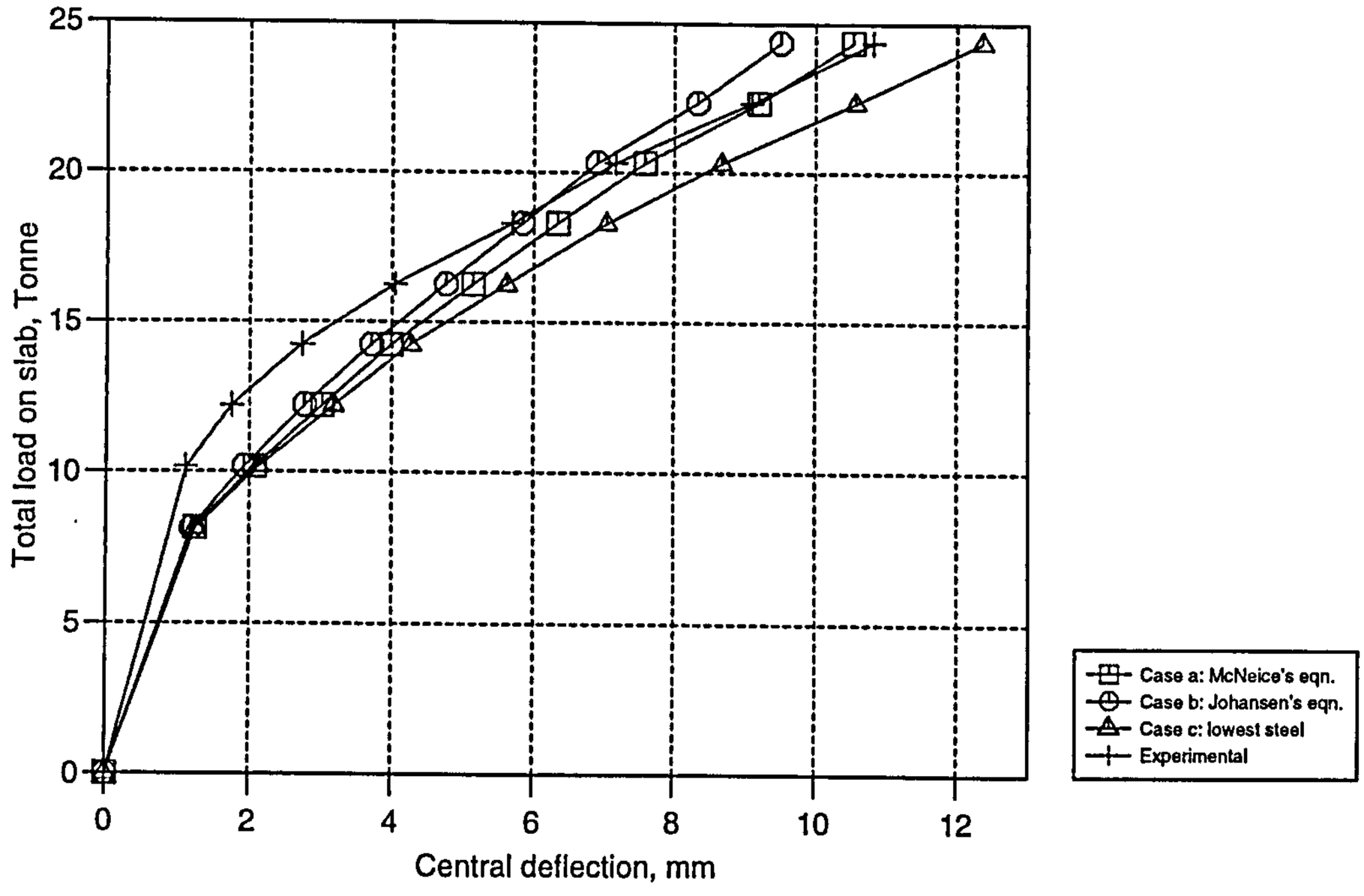


Figure 4.10 Load versus deflection curves for the edge-supported Shukla & Mittal slab S-11 using different equations to calculate effective steel

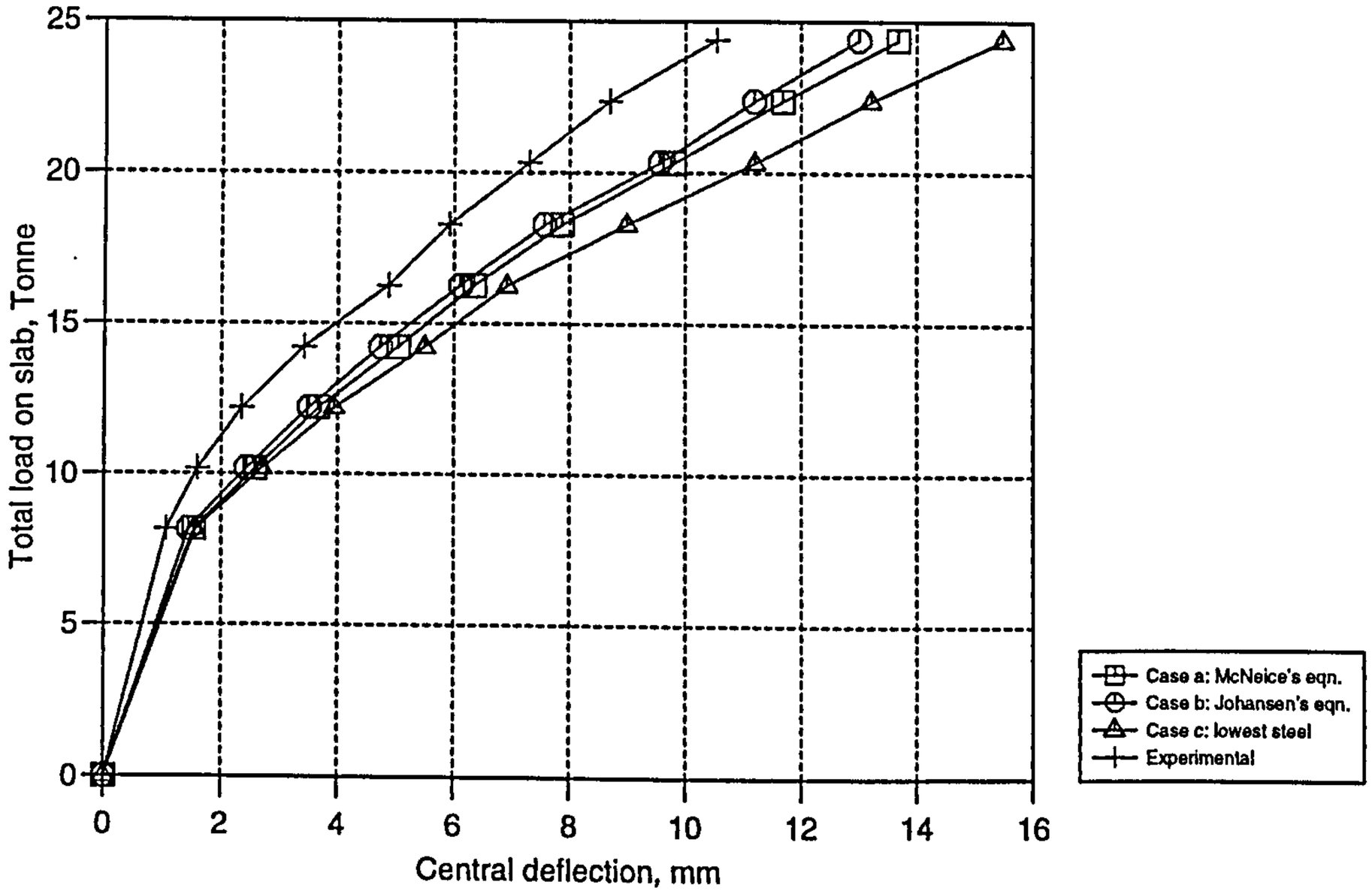


Figure 4.11 Load versus deflection curves for the edge-supported Shukla & Mittal slab S-12 using different equations to calculate effective steel

4.5.3 Long-term loading: Taywood slab

A high-strength concrete slab supported on monolithic columns was tested by Taywood (Whittle, 1996). The details of the slab are presented in Fig. 4.12 and the material properties are given in Table 4.1 . The slab was tested under a load sequence typical of that experienced in a building. The slab was stripped at 1 day and a 1.5 kN/m^2 construction load was applied at 4 days in several cycles and then sustained until 19 days. A test service load of 7 kN/m^2 was applied at 30 days in 3 cycles and immediately withdrawn. The test was completed at 71 days by measuring the deflection under self-weight. A simplified load history has been adopted for the FE analysis as shown in Fig. 4.13. Deflection with time curves for two different nodes using the three sets of equations, together with the experimental results are presented in Figs 4.14 and 4.16. The load versus deflection behaviour under the 30 day test service load mentioned above are presented in Figs 4.15 and 4.17. For this slab, the results are similar to those of previous slabs. Case (c) gives the highest deflections whereas cases (a) and (b) lead to very similar results.

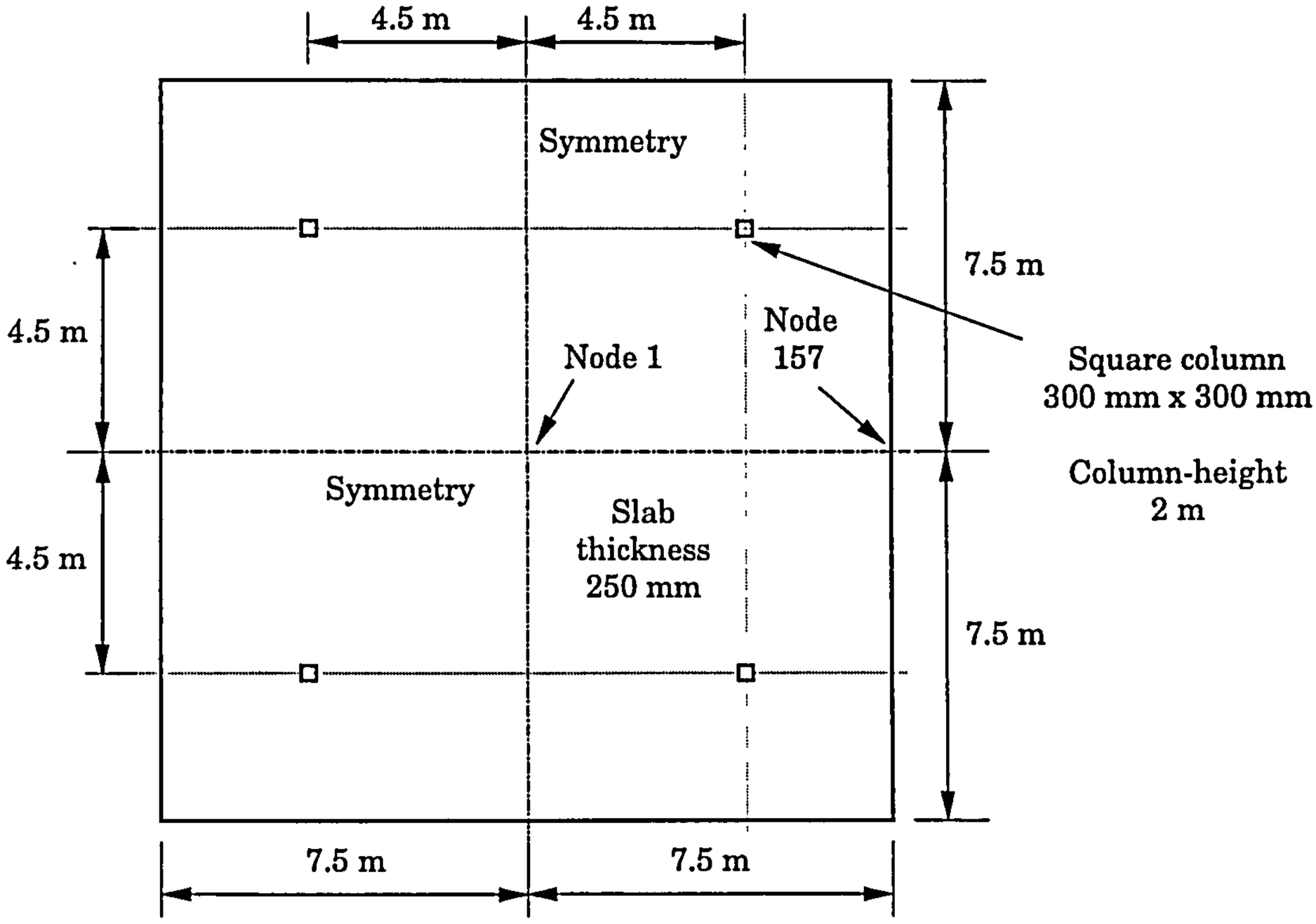


Figure 4.12 Details of Taywood slab: adapted from Whittle (1996)

Comments	Days	f_{cu} MPa	f_{ct} MPa	E_c GPa
Shutter stripped	1	104.5		39.36
18 hours after stripping	2	111		39.93
Construction loading	4	111		39.93
7 day reading	7	117	4.72	40.35
Test load	30	118	5.27	41.5
71 day reading	71	121		

Table 4.1 Properties of Taywood slab

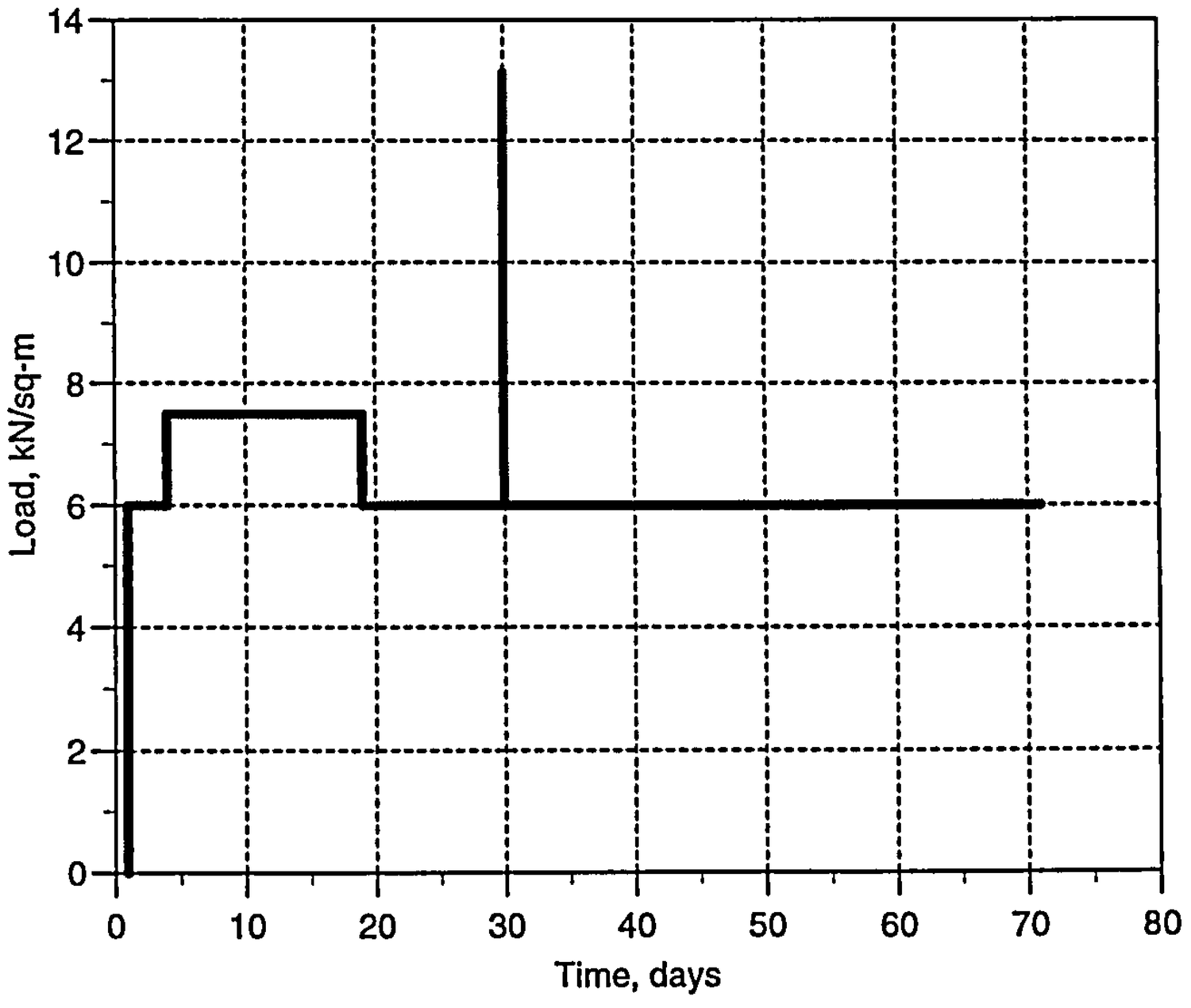


Figure 4.13 Simplified load history for Taywood slab

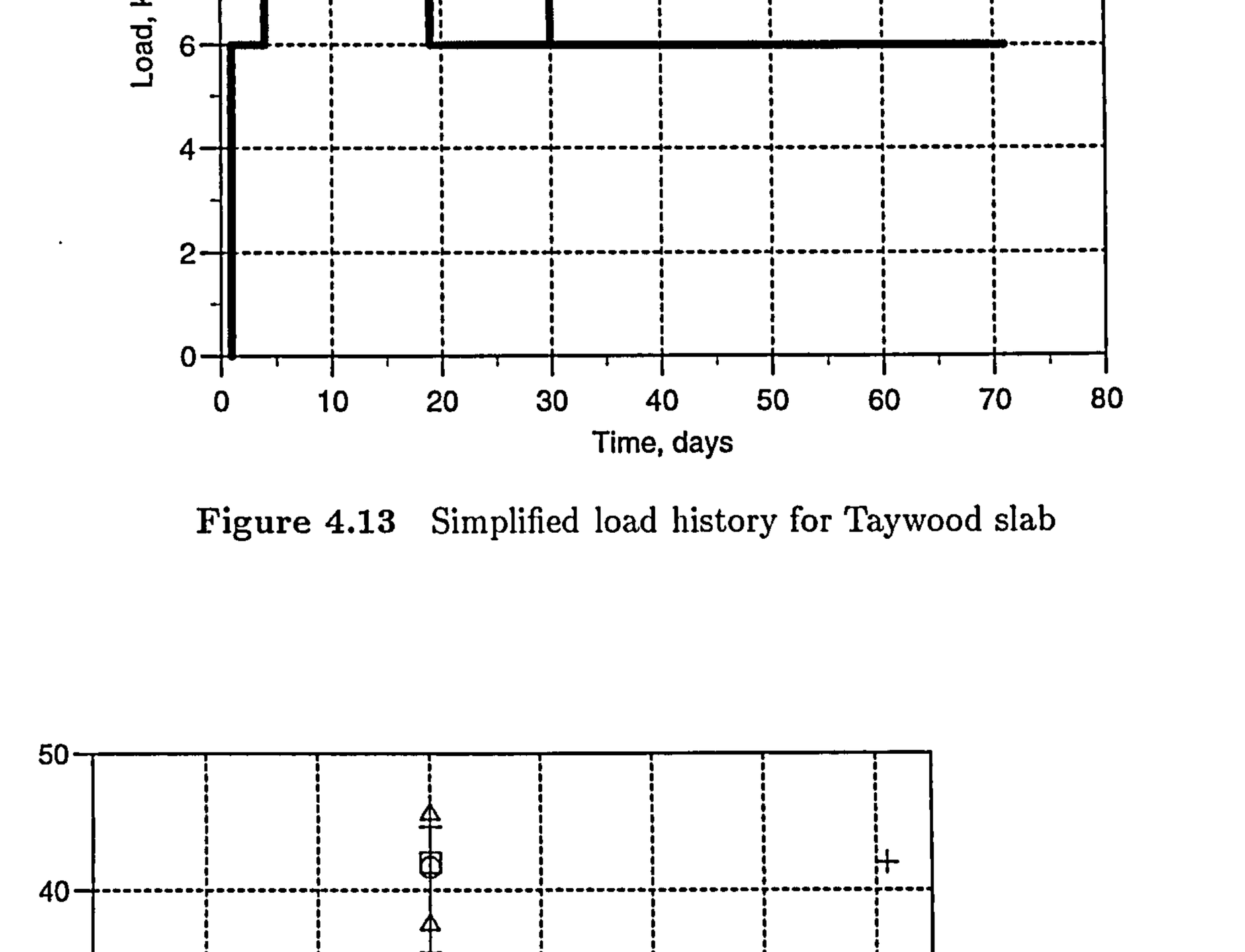


Figure 4.14 Deflection versus time curves for column-supported Taywood slab using different equations to calculate the effective steel: node 1

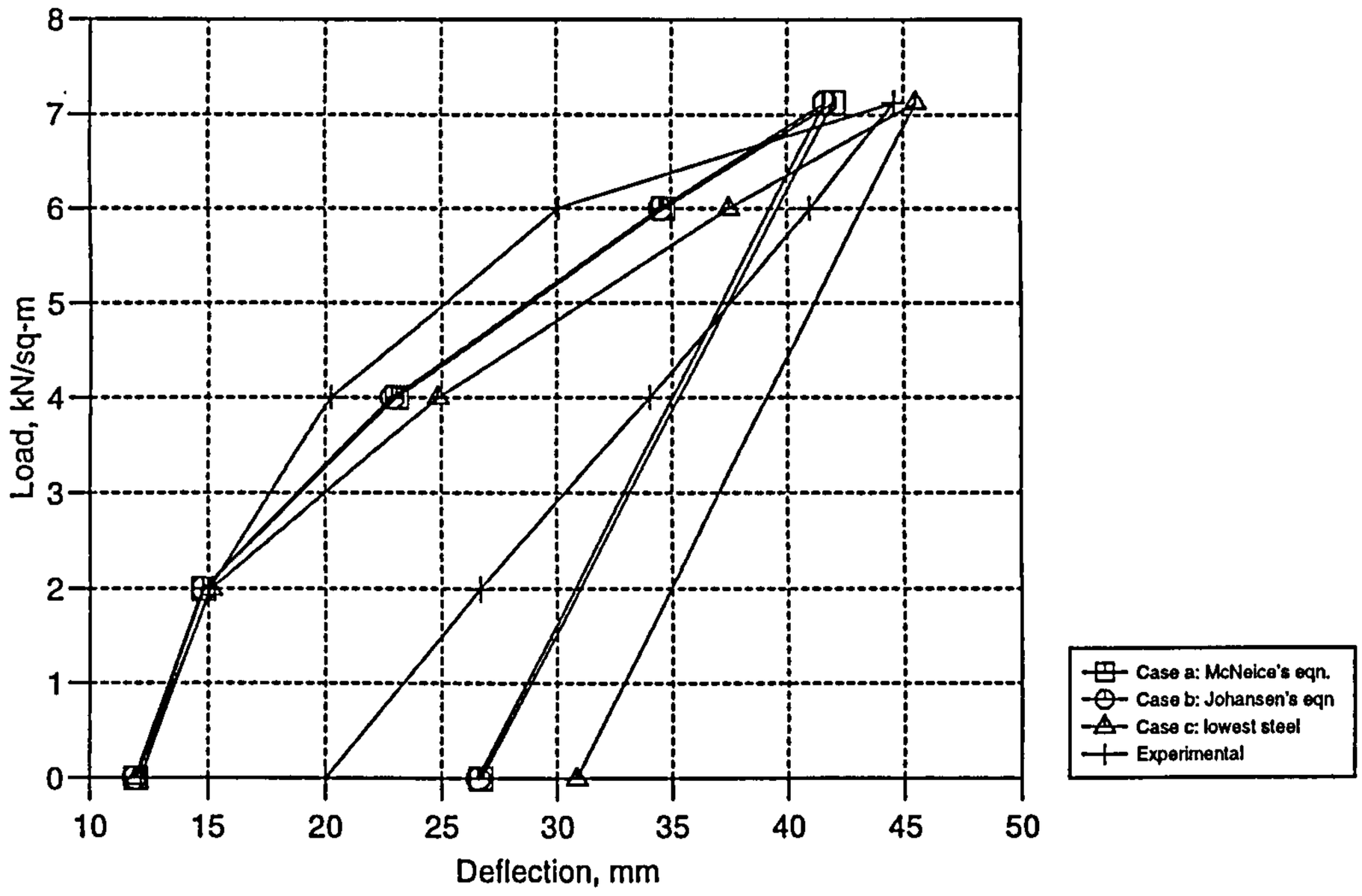


Figure 4.15 Service load versus deflection curves (at 30 days) for the column-supported Taywood slab using different equations to calculate the effective steel: node 1

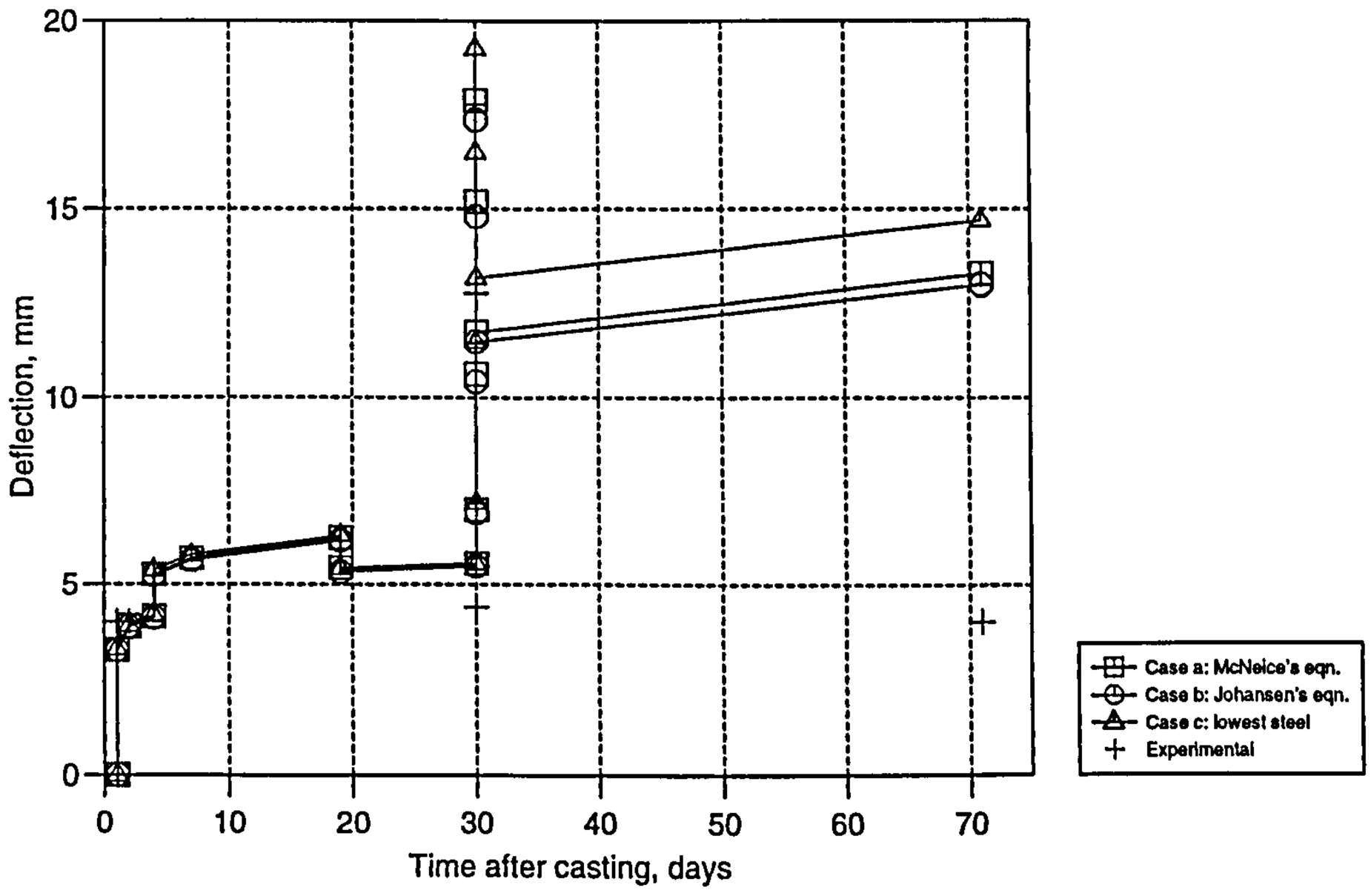


Figure 4.16 Deflection versus time curves for column-supported Taywood slab using different equations to calculate the effective steel: node 157

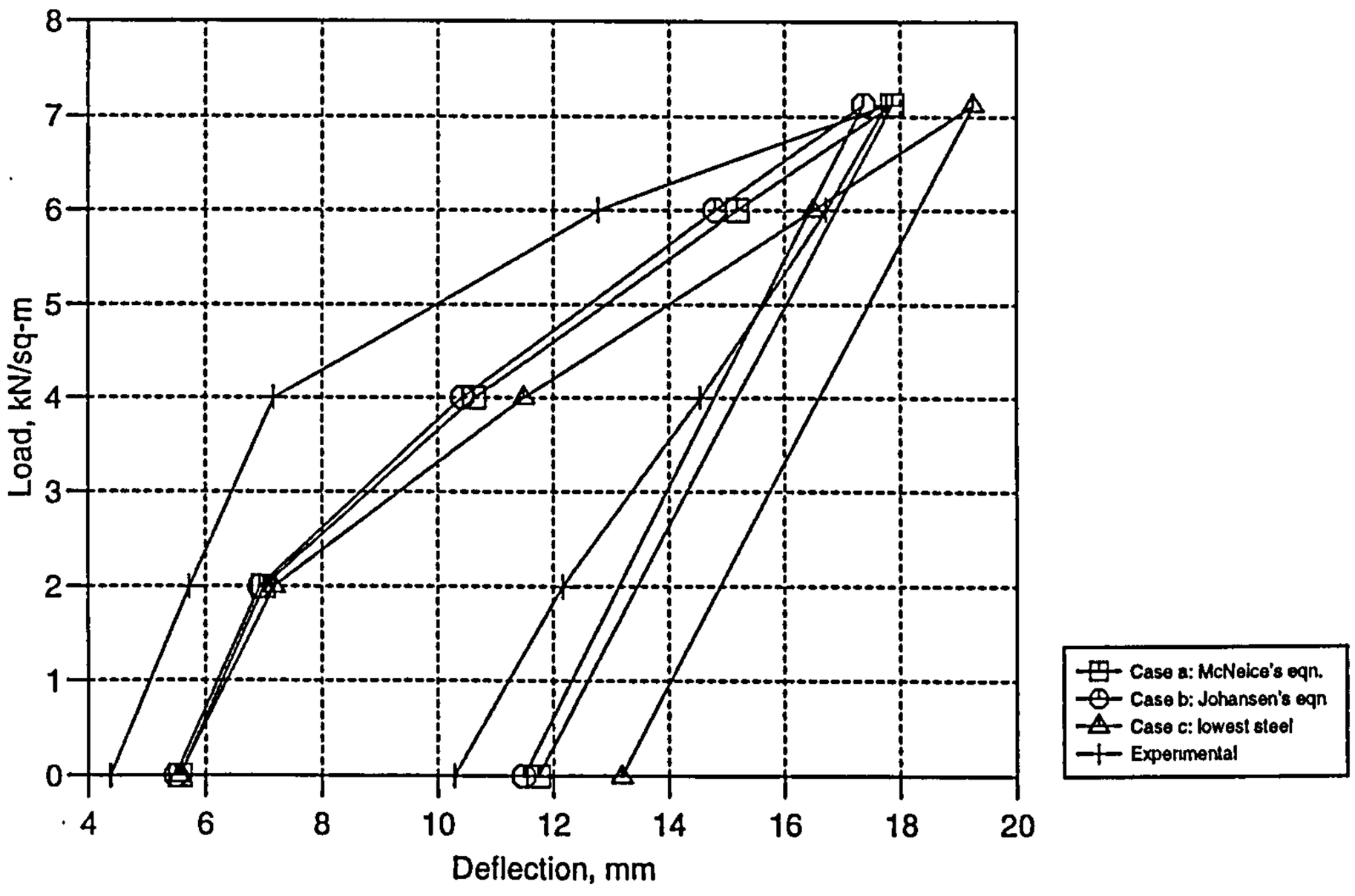


Figure 4.17 Service load versus deflection curves (at 30 days) for the column-supported Taywood slab using different equations to calculate the effective steel: node 157

4.6 Proposed approach for calculating the effective steel

It is apparent from the three comparative studies that case (c), which gives the lowest steel area may result in deflections being overestimated. Cases (a) and (b) lead to similar deflections, with case (b) being closer to the experimental value. However, case (a) may produce an unrealistic value of A_{st} because the condition $A_{sn} = A_{st}$ is not always physically viable. For example, if there is no steel present in the y direction and the principal directions coincide with the x and y directions, the approach will give $A_{sy} = A_{sx}$ which is certainly not correct. It is concluded that eqs 3.43 and 3.44 which are based on Johansen's yield criterion, should be used to calculate the effective area of steel in a cracked section. Deflections estimated using these equations are close to the experimental deflections.

Similar equations can be used to calculate the area of the compressive steel in the principal directions:

$$A_{snp} = A_{sxp}\left[\cos^2\theta + \mu_p \sin^2\theta\right] \tag{4.19}$$

$$A_{stp} = A_{sxp}\left[\sin^2\theta + \mu_p \cos^2\theta\right] \tag{4.20}$$

where A_{sxp} is the x-directional steel on the compression face and $\mu_p A_{sxp}$ is the y-directional steel on the same face.

4.7 Incorporation of ACI and Gilbert's method

The effective moment of inertia adopted by the ACI Building Code (1989) was discussed in section 2.9.3. The method uses the ratio of the section cracking moment to the applied moment to interpolate between uncracked and fully cracked states. In the present work, the ratio of modulus of rupture to principal tensile stress at the face of the section i.e. (f_r/σ_1) or (f_r/σ_2) is used instead of (M_{cr}/M) in eq. 2.37. The following equations are used to calculate the effective moment of inertia in the major and minor principal directions, respectively:

$$I_{e1} = \left(\frac{f_r}{\sigma_1}\right)^3 I_g + \left[1 - \left(\frac{f_r}{\sigma_1}\right)^3\right] I_{cr1} \tag{4.21}$$

$$I_{e2} = \left(\frac{f_r}{\sigma_2}\right)^3 I_g + \left[1 - \left(\frac{f_r}{\sigma_2}\right)^3\right] I_{cr2} \tag{4.22}$$

where σ_1 and σ_2 are the two principal stresses at the surface of slab and I_{cr} is the moment of inertia of the fully cracked transformed section. Jofriet & McNeice (1971) used eqs 3.21 and 3.20, respectively, to calculate the depth of neutral axis and the second moment of area of a fully cracked section. These equations do not take into account the presence of compression steel. In the present work, the depth of neutral axis and the second moment of area of a fully cracked section are calculated considering both tension and compression steel. The depth of neutral axis of a fully cracked section, considering both tension and compression steel, is given by:

$$c_n = \frac{-a_2 + \sqrt{{a_2}^2 - 4a_1a_3}}{2a_1} \tag{4.23}$$

where,

$$a_1 = b/2.$$

$$a_2 = nA_s + (n-1)A_{sp}$$

$$a_3 = -nA_sd - (n-1)A_{sp}d'$$

The second moment of area around the neutral axis is:

$$I_{cr} = \frac{b{c_n}^3}{3} + nA_s(d - c_n)^2 + (n-1)A_{sp}(d' - c_n)^2 \tag{4.24}$$

The Gilbert (1988) method has been discussed in section 2.9.4. In the present work, the area of concrete effective in tension is calculated using (f_r/σ_1) or (f_r/σ_2) instead of (M_{cr}/M) in eq. 2.39:

$$A_{ct1} = \beta_1\beta_2\,[0.21b_wd - nA_{sn}]\left(\frac{f_r}{\sigma_1}\right)^2 \tag{4.25}$$

$$A_{ct2} = \beta_1\beta_2\,[0.21b_wd - nA_{st}]\left(\frac{f_r}{\sigma_2}\right)^2 \tag{4.26}$$

The steel ratios are then modified by adding an excess amount of steel in the

principal directions, given by:

$$\rho_{m1} = \frac{A_{sn} + \frac{A_{ct1}}{n}}{bd} \tag{4.27}$$

$$\rho_{m2} = \frac{A_{st} + \frac{A_{ct2}}{n}}{bd} \tag{4.28}$$

The moment of inertia of a cracked section is calculated considering both increased tension steel determined as above and compression steel.

The modification factor

For the methods of ACI and Gilbert, the modification factors, to account for cracking, are obtained similarly to Scanlon & Murray approach (eqs 3.12 and 3.13) where calculations were performed in x and y directions. However, in the present work they are calculated in the major and minor principal directions:

$$\alpha_n = \frac{I_{e1}}{I_g} \tag{4.29}$$

$$\alpha_t = \frac{I_{e2}}{I_g} \tag{4.30}$$

where, α_n and α_t are the modification factors for major and minor principal directions respectively.

4.8 MC-90 method

The model proposed by MC-90 (1993), is used in the present work. This allows for the effects of cracking, shrinkage and creep. Moments and curvatures are calculated in the principal directions assuming the gross uncracked concrete section ignoring reinforcement.

$$\psi_g = \frac{M}{E_c I_g} \tag{4.31}$$

Curvatures are calculated in state 1 and state 2 considering reinforcement both in the tension and the compression zones (if the latter is present).

The curvature in state 1 at time of application of load, t_0 is given by:

$$\psi_1(t_0) = \frac{M}{E_c(t_0)I_1} \tag{4.32}$$

where

M= principal moment

$E_c(t_0)$=modulus of elasticity of concrete at time t_0

I_1= moment of inertia of uncracked transformed section around axis O_1 which is the centroid of the transformed section.

The curvature in state 2 at time t_0 is given by:

$$\psi_2(t_0) = \frac{M}{E_c(t_0)I_2} \tag{4.33}$$

where

I_2= moment of inertia of cracked transformed section around axis O_2 which is the centroid of the transformed section and lies on the neutral axis, calculated using eq. 4.24.

When short-term deflection is of interest, the mean curvature is calculated using eq. 2.33:

$$\psi_m(t_0) = (1-\zeta)\psi_1(t_0) + \zeta\psi_2(t_0) \tag{4.34}$$

where

$$\zeta = 1 - \beta_1\beta_2\left(\frac{M_r}{M}\right)^2 \tag{4.35}$$

4.8.1 Calculation for long-term deflection

When the calculation is for long-term deflection, the modulus of elasticity of concrete is modified for age-effect:

$$\bar{E}_c(t,t_0) = \frac{E_c(t_0)}{1+\phi(t,t_0)\chi(t,t_0)} \tag{4.36}$$

where,

$\bar{E}_c(t,t_0)$= age-adjusted modulus of elasticity of concrete at time t.

$\phi(t, t_0)$= creep coefficient of concrete, i.e. ratio of creep strain to the instantaneous strain due to a stress applied at time t_0 and sustained to time t.

$\chi(t, t_0)$= aging coefficient.

$E_c(t_0)$= modulus of elasticity of concrete at time t_0.

The equations required to calculate the creep coefficient are presented in Appendix B. Creep and aging coefficients are calculated in the program using subroutines developed by Ghali & Favre (1994).

The modular ratio is defined as:

$$\bar{n}(t, t_0) = \frac{E_s}{\bar{E}_c(t, t_0)} \tag{4.37}$$

4.8.2 Calculation for state 1

The following parameters are calculated: the area of the age-adjusted transformed uncracked section, $\bar{A}_1$; the centroid $\bar{O}_1$ below the top edge; the moment of inertia about an axis through $\bar{O}_1$, $\bar{I}_1$; the area of concrete, $\bar{A}_{c1}$; the y-coordinate of the centroid of the concrete area (measured downward from $\bar{O}_1$), $\bar{y}_{c1}$; the moment of inertia of $\bar{A}_{c1}$ about $\bar{O}_1$, $\bar{I}_{c1}$; and the radius of gyration, $\bar{r}_{c1} = \bar{I}_{c1}/\bar{A}_{c1}$.

The curvature-reduction factor k_1, which represents the effect of the reinforcement in reducing the absolute value of the change in curvature due to creep and shrinkage is given by:

$$k_1 = \frac{\bar{I}_{c1}}{\bar{I}_1} \tag{4.38}$$

The curvature at t_0 for the state 1 is ψ_1 and the corresponding axial strain at $\bar{O}_1$ is :

$$\epsilon_{\bar{O}1}(t_0) = \psi_1 * (\text{distance between } O_1 \text{ and } \bar{O}_1) \tag{4.39}$$

The change in curvature during the period t_0 to t is given by (Ghali & Favre, 1994):

$$\Delta\psi_1 = k_1 \left[\phi(t, t_0) \left\{\psi_1(t_0) + \epsilon_{\bar{O}1}(t_0)\frac{\bar{y}_{c1}}{\bar{r}_{c1}^2}\right\} + \epsilon_{cs}(t, t_0)\frac{\bar{y}_{c1}}{\bar{r}_{c1}^2}\right] \tag{4.40}$$

where

k_1= reduction factor for reinforcement as described by eq. 4.38.

$\epsilon_{cs}(t, t_0)$= shrinkage strain, which can be obtained using the equations given in Appendix B.

$\psi_1(t_0)$= curvature at time t_0 in state 1.

$\epsilon_{\bar{O}1}(t_0)$= normal strain at $\bar{O}_1$ at t_0 due to the initial curvature $\psi_1(t_0)$.

Then, the curvature for state 1 at time t is

$$\psi_1(t) = \psi_1(t_0) + \Delta\psi_1 \tag{4.41}$$

4.8.3 Calculation for state 2

The following parameters are calculated: the area of the age-adjusted transformed cracked section, $\bar{A}_2$; the centroid $\bar{O}_2$ below top edge; the moment of inertia about an axis through $\bar{O}_2$, $\bar{I}_2$; the area of the concrete compression zone, $\bar{A}_{c2}$; the y-coordinate of the centroid of the concrete of the compression zone (measured downward from $\bar{O}_2$), $\bar{y}_{c2}$; the moment of inertia of $\bar{A}_{c2}$ about $\bar{O}_2$, $\bar{I}_{c2}$; and the radius of gyration, $\bar{r}_{c2} = \bar{I}_{c2}/\bar{A}_{c2}$.

The curvature-reduction factor is

$$k_2 = \frac{\bar{I}_{c2}}{\bar{I}_2} \tag{4.42}$$

The curvature at t_0 for the state 2 is ψ_2 and the corresponding axial strain at $\bar{O}_2$ is :

$$\epsilon_{\bar{O}2}(t_0) = \psi_2 * (\text{distance between } O_2 \text{ and } \bar{O}_2) \tag{4.43}$$

The change in curvature during the period t_0 to t is given by (Ghali & Favre, 1994):

$$\Delta\psi_2 = k_2 \left[\phi(t, t_0) \left\{\psi_2(t_0) + \epsilon_{\bar{O}2}(t_0)\frac{\bar{y}_{c2}}{\bar{r}_{c2}^2}\right\} + \epsilon_{cs}(t, t_0)\frac{\bar{y}_{c2}}{\bar{r}_{c2}^2}\right] \tag{4.44}$$

where

k_2= reduction factor for reinforcement as described in eq. (4.42).

$\psi_2(t_0)$= curvature at time t_0 in state 2.

$\epsilon_{\bar{O}2}(t_0)$= normal strain at $\bar{O}_2$ at t_0 due to the initial curvature $\psi_2(t_0)$.

Then, the curvature for state 2 at time t is

$$\psi_2(t) = \psi_2(t_0) + \Delta\psi_2 \tag{4.45}$$

4.8.4 Mean curvature

The coefficient ζ used to interpolate between state 1 and state 2 for long-term curvature is obtained by means of eq. 2.30 using a value of 0.5 for β_2. The mean curvature at time t is given by:

$$\psi_m(t) = (1-\zeta)\psi_1(t) + \zeta\psi_2(t) \tag{4.46}$$

Mean curvatures (either short-term $\psi_m(t_0)$ or long-term $\psi_m(t)$) are calculated in both the principal directions.

4.8.5 The modification factor

The modification factors (to account for cracking, creep and shrinkage) for the major and minor principal directions, respectively, are given by:

$$\alpha_n = \frac{\psi_g}{\psi_{m-major}} \tag{4.47}$$

$$\alpha_t = \frac{\psi_g}{\psi_{m-minor}} \tag{4.48}$$

4.9 Formation of $[E]$ matrices

In the FE analysis, initially the 6*6 elasticity matrices for all the elements are defined as anisotropic so that they can have different values in orthogonal directions. These matrices are then modified for each element using the modification factors α_n and α_t to incorporate cracking, creep and shrinkage, by using either eqs 4.29 and 4.30 for the ACI and Gilbert model or eqs 4.47 and 4.48 for the MC-90 method. The

modified matrix in the principal directions thus follows:

$$[E'] = \begin{bmatrix} \frac{\alpha_n E_c}{(1-\alpha_n\alpha_t\nu^2)} & \frac{\alpha_n\nu\alpha_t E_c}{(1-\alpha_n\alpha_t\nu^2)} & 0 \\ \frac{\alpha_t\nu\alpha_n E_c}{(1-\alpha_n\alpha_t\nu^2)} & \frac{\alpha_t E_c}{(1-\alpha_n\alpha_t\nu^2)} & 0 \\ 0 & 0 & \frac{E_c\sqrt{\alpha_n\alpha_t}}{2(1+\nu\sqrt{\alpha_n\alpha_t})} \end{bmatrix} \tag{4.49}$$

These $[E']$ matrices are then transformed into global directions using eq. 3.36. A set of $3 * 3$ matrices for all the elements are obtained:

$$\begin{Bmatrix} \sigma_x \\ \sigma_y \\ \tau_{xy} \end{Bmatrix} = \begin{bmatrix} A & D & E \\ D & B & F \\ E & F & C \end{bmatrix} \begin{Bmatrix} \epsilon_x \\ \epsilon_y \\ \gamma_{xy} \end{Bmatrix} \tag{4.50}$$

The global $[E]$ matrix is then adjusted so that it can be used in the FE package (Hitchings, 1994). The FE package needs a $6 * 6$ $[E]$ matrix to define the elastic properties of a material, i.e. the stress-strain relations should be specified for all the 6 degrees of freedom although some of them may not be active in 2-D bending problems. The $3 * 3$ matrix is adjusted to the $6 * 6$ matrix as follows:

$$\begin{Bmatrix} \sigma_x \\ \sigma_y \\ \sigma_z \\ \tau_{xy} \\ \tau_{xz} \\ \tau_{yz} \end{Bmatrix} = \begin{bmatrix} A & D & 0 & E & 0 & 0 \\ D & B & 0 & F & 0 & 0 \\ 0 & 0 & 0 & 0 & 0 & 0 \\ E & F & 0 & C & 0 & 0 \\ 0 & 0 & 0 & 0 & C & 0 \\ 0 & 0 & 0 & 0 & 0 & C \end{bmatrix} \begin{Bmatrix} \epsilon_x \\ \epsilon_y \\ \epsilon_z \\ \gamma_{xy} \\ \gamma_{xz} \\ \gamma_{yz} \end{Bmatrix} \tag{4.51}$$

These $[E]$ matrices for all the elements are written in a file which is subsequently read by the FE package (Hitchings, 1994) in the next run and it modifies the global stiffness matrix accordingly. As the material elasticity, and hence the structural stiffness is modified, there will be redistribution of stresses. Another set of modified $[E]$ values can be obtained with the redistributed stresses. This procedure is continued until a state of equilibrium between stress redistribution and material properties is reached.

4.10 Effect of modifying the shear terms of the $[E]$ matrix

Several authors [Tam & Scanlon (1986), Scanlon & Murray (1974)] used a constant shear modulus for cracked and uncracked elements as they considered the effect of shear deformations related to twisting moments to be insignificant. On the contrary, Favre *et al.* (1990) modified the torsional stiffness in accordance with Huber's (Timoshenko & Woinowsky-Krieger, 1959) recommendations. Polak (1996) reduced the torsional and transverse shear moduli with factors described in section 3.4. To determine the effect of torsional stiffness on deflection, the present research has studied several slabs by analysing them with and without modified torsional stiffness. For McNeice's corner-supported slab (Jofriet & McNeice, 1971), the effect was found to be insignificant as the torsional moment is very small for this case. The central deflection was 0.355 and 0.345 inch with and without modified torsional stiffness respectively; the experimental deflection was 0.338 inch. Three edge-supported slabs S-8, S-11 and S-12 from Shukla & Mittal (1976) have also been analysed. The effect of modifying torsional stiffness is most pronounced for these slabs due to the presence of high torsional moments. Four cases were studied:

1. Keeping all the shear-related terms of the $[E]$ matrices (eq. 4.51) unchanged.

2. Keeping the torsional shear-related term [(4,4) term of the matrix of eq. 4.51] unchanged and modifying the transverse shear-related terms [(5,5) and (6,6) terms of the matrix of eq. 4.51]. The Huber equation (eq. 3.25) was used even though it defines the torsional stiffness.

3. Modifying the torsional shear term [(4,4) term of the matrix of eq. 4.51] using the Huber equation (eq. 3.25) and keeping the transverse shear-related terms [(5,5) and (6,6) terms of the matrix of eq. 4.51] unchanged.

4. Modifying all the shear-related terms [(4,4), (5,5) and (6,6) terms of the matrix of eq. 4.51] as already shown in section (4.9) using Huber's equation (eq. 3.25).

The central deflections of the three Shukla & Mittal slabs are shown in Table 4.2 for cases 1 to 4 along with the experimental results. It is evident from the study that

Slab	Central deflection, mm				
	Case 1	Case 2	Case 3	Case 4	Expt
S-8	8.75	9.33	14.88	15.18	16.7
S-11	5.74	6.10	9.38	9.50	10.82
S-12	6.49	7.10	12.78	13.01	10.55

Table 4.2 Effect of modifying the shear and torsional terms of the $[E]$ matrix

the effect of varying the transverse shear moduli is not very significant, but that the effect of modifying the torsional shear moduli is very important. A comparison with experimental results reveals that neglecting the reduction in torsional stiffness due to cracking will lead to very unconservative results. In the present work, therefore, all the shear terms are modified in accordance with case 4.

4.11 Selection of convergence procedure

It has been found that convergence does not occur if the E values are modified on the basis of stress levels used in successive FE runs because the solution fluctuates between two near equilibrium conditions. It seems that large changes in the value of stiffness make the structure numerically unstable. It is apparent that convergence can only be achieved if the stiffness is gradually reduced.

A study has been carried out to select a suitable convergence approach by analysing an edge panel of a flat slab, details of which are presented in Fig. 4.18. The deflection of four points of the flat slab were monitored for different convergence strategies, and the results are presented in Figs 4.19 to 4.22. The following approaches have been considered:

1. E values were calculated on the basis of stresses in the plate. A fluctuating deflection pattern was obtained. Highly stressed sections crack severely and lose stiffness in one iteration step. In the next step, the stress reduces at that section due to the loss of stiffness and stress redistributes to stiffer parts. As the magnitude of stress is lowered at that section, the section becomes stiffer in the next run and attracts more stress. Different parts of the slab gain and lose stiffness in successive iteration steps and sections that are cracked in one run

may become uncracked in the next run and vice versa. Convergence cannot be attained with this approach.

2. E values are derived from stresses but are only allowed to reduce. The solution converge rapidly but deflections are greater than those of case 1. The converged solution shows significant differences in E values from stress calculations and actual E values used. Deflections are overestimated because the E values are either equal to or lower than, E from stress. Convergence can be attained but deflections are overestimated because the stress reduction at a cracked section is neglected. In reality, cracking reduces stress levels at a section and thereby the severity of cracking will also be reduced.

3. Another approach has been considered where the E values are based on stresses but are not allowed to go below certain percentages (10, 20 and 50) of the E values derived in the previous step. With up to 50 percent reduction, deflections converge quickly though the deflection values are higher. With 10 and 20 percent reductions, the deflections are quite close to each other, but more than 40 and 20 runs are required for the 10 and 20 percent reductions respectively (Figs 4.19 to 4.22). It is evident that the more gradual the decrease of stiffness, the better the results are, although the time required to get a converged solution is higher. It should be pointed here that, even though the E values are gradually decreased, the magnitude of the stiffness reduction all over the slab is still overestimated. The more gradually the E value are reduced, the less the overestimation becomes. Thus, smaller deflections indicate a better solution, as the values of E used in the converged solution are closer to the values corresponding to stress.

4. To speed up the convergence and, at the same time, to get the smallest deflection possible (i.e. to obtain the least possible overestimation of the reduction of stiffness), another approach for gradually decreasing E values is proposed. Here, the amount of reduction in E values due to cracking, creep and shrinkage are calculated and, the greater the reduction, the smaller the fraction by which it is actually reduced. First, the changes in the elements of the $[E]$

matrices $\Delta E(i,j)$ are calculated comparing elements of the elasticity matrices calculated in the current iteration $E(i,j)_{calculated}$ and the same used in the previous run $E(i,j)_{last}$:

$$\Delta E(i,j) = E(i,j)_{last} - E(i,j)_{calculated} \tag{4.52}$$

The elasticity matrix to be actually used for the next iteration is then calculated:

$$E(i,j)_{use} = E(i,j)_{last} - \left[1 - \frac{\Delta E(i,j)}{E(i,j)_{last}}\right] \Delta E(i,j) \tag{4.53}$$

The factor $(1 - \frac{\Delta E(i,j)}{E(i,j)_{last}})$ determines the amount to be reduced: the greater the value of $\Delta E(i,j)$, the smaller will be the factor by which it will be actually reduced. However, the factor has been given a minimum certain value (0.4 and 0.6 shown here) that ensures that at least certain portion (40% and 60%) of $\Delta E(i,j)$ is always reduced. A converged solution can be attained quite rapidly: for example, 17 and 11 runs are required for minimum values of reduction of 0.4 and 0.6 respectively (Figs 4.19 to 4.22). In both cases, deflection values are quite close and they are also very close to the case where the E values were reduced by up to 10 percent in each run.

Case 4 has been found to perform well and, therefore, it is incorporated in the present work, i.e. in all further analysis. To take consideration of the steel present in the uncracked section, elasticity values are allowed to go up initially and the finally stiffness of the cracked section is reduced in a gradual manner. For the first few runs, the value of $E(i,j)_{use}$ can be greater or lower than $E(i,j)_{last}$, and then only the lower value is taken. After that, if the value of $E(i,j)_{use}$ is found to be greater than $E(i,j)_{last}$, it is taken equal to $E(i,j)_{last}$.

A subroutine has been written to check displacements of all the nodes in each step of the iteration. When all these displacements do not vary (strictly, the covariances of three successive deflection are less than 0.5%) between three successive runs the program stops. It should be noted that for one-way continuous slabs, the gradual method described in case 4 and an independent curvature integration calculation gave identical results.

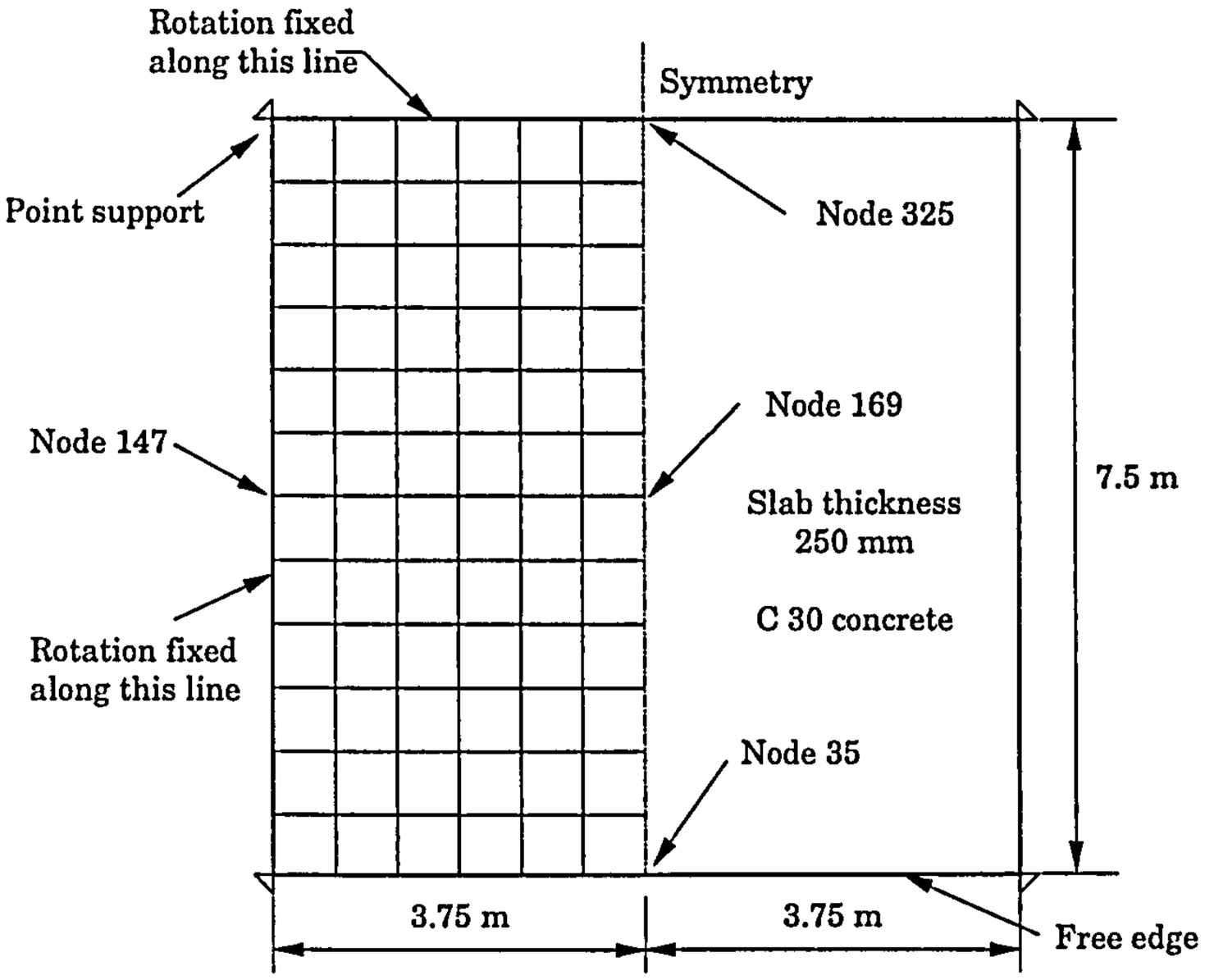


Figure 4.18 Details of flat slab used in the selection of the convergence procedure

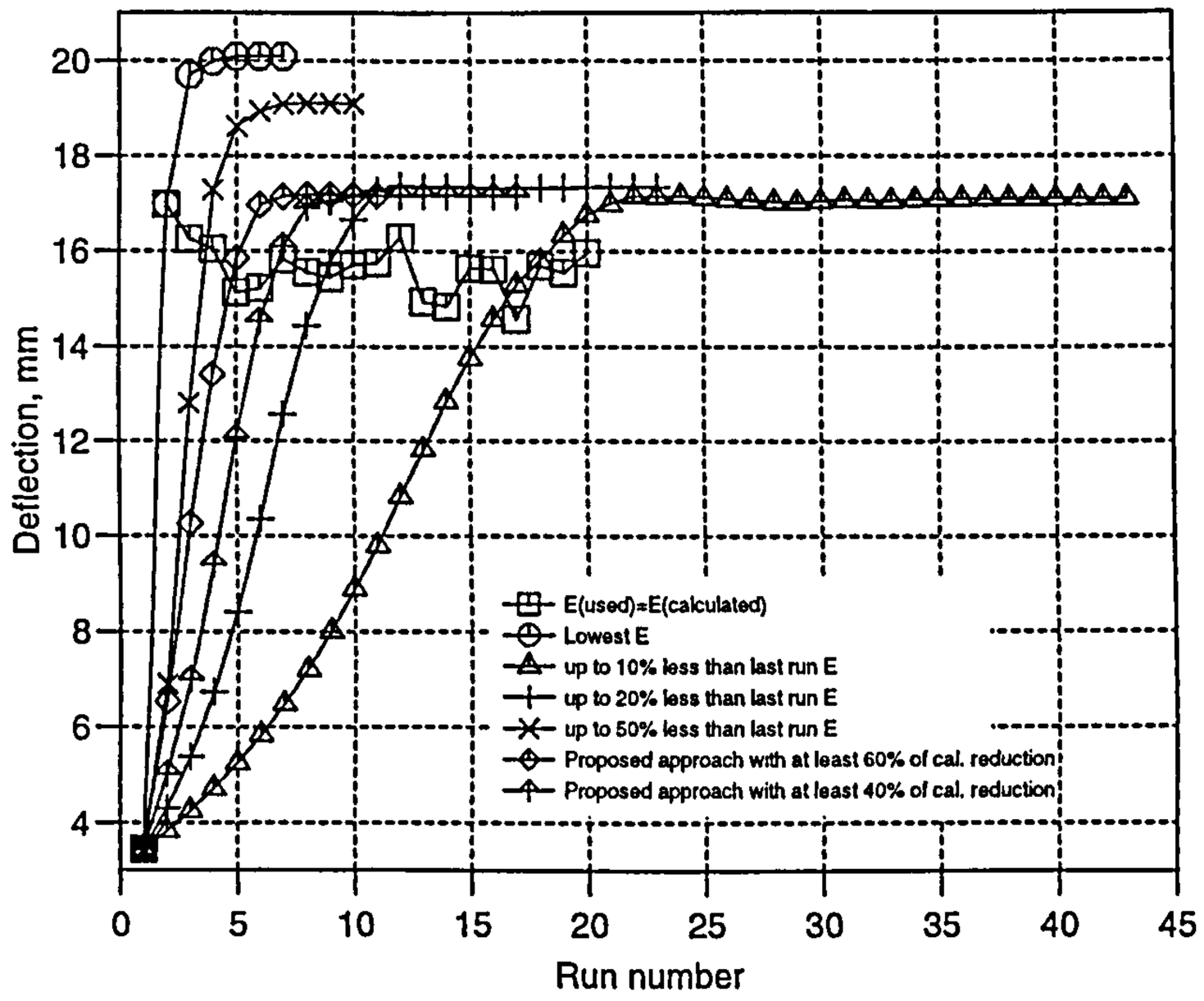


Figure 4.19 Different convergence approaches: node 35

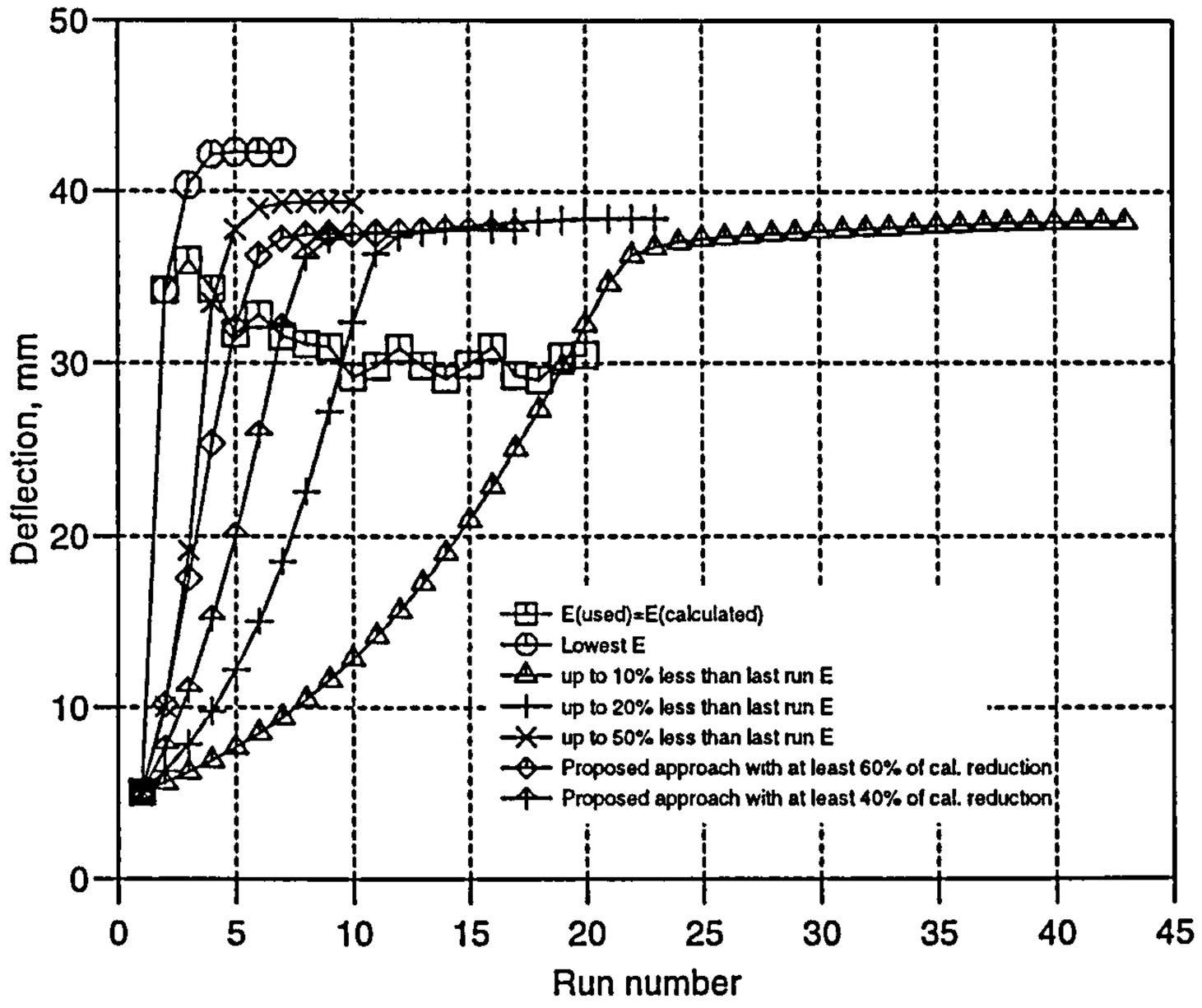


Figure 4.20 Different convergence approaches: node 147

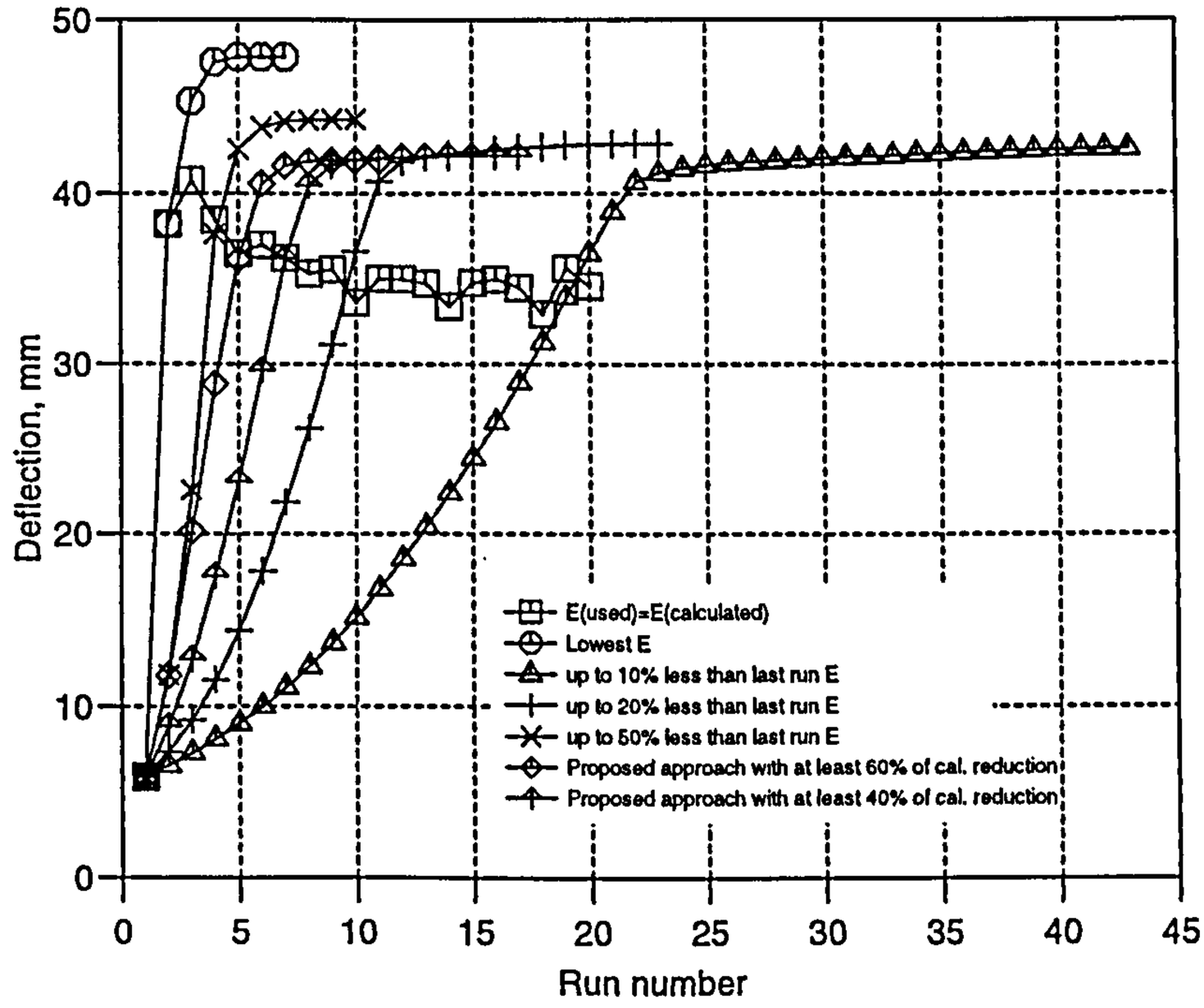


Figure 4.21 Different convergence approaches: node 169

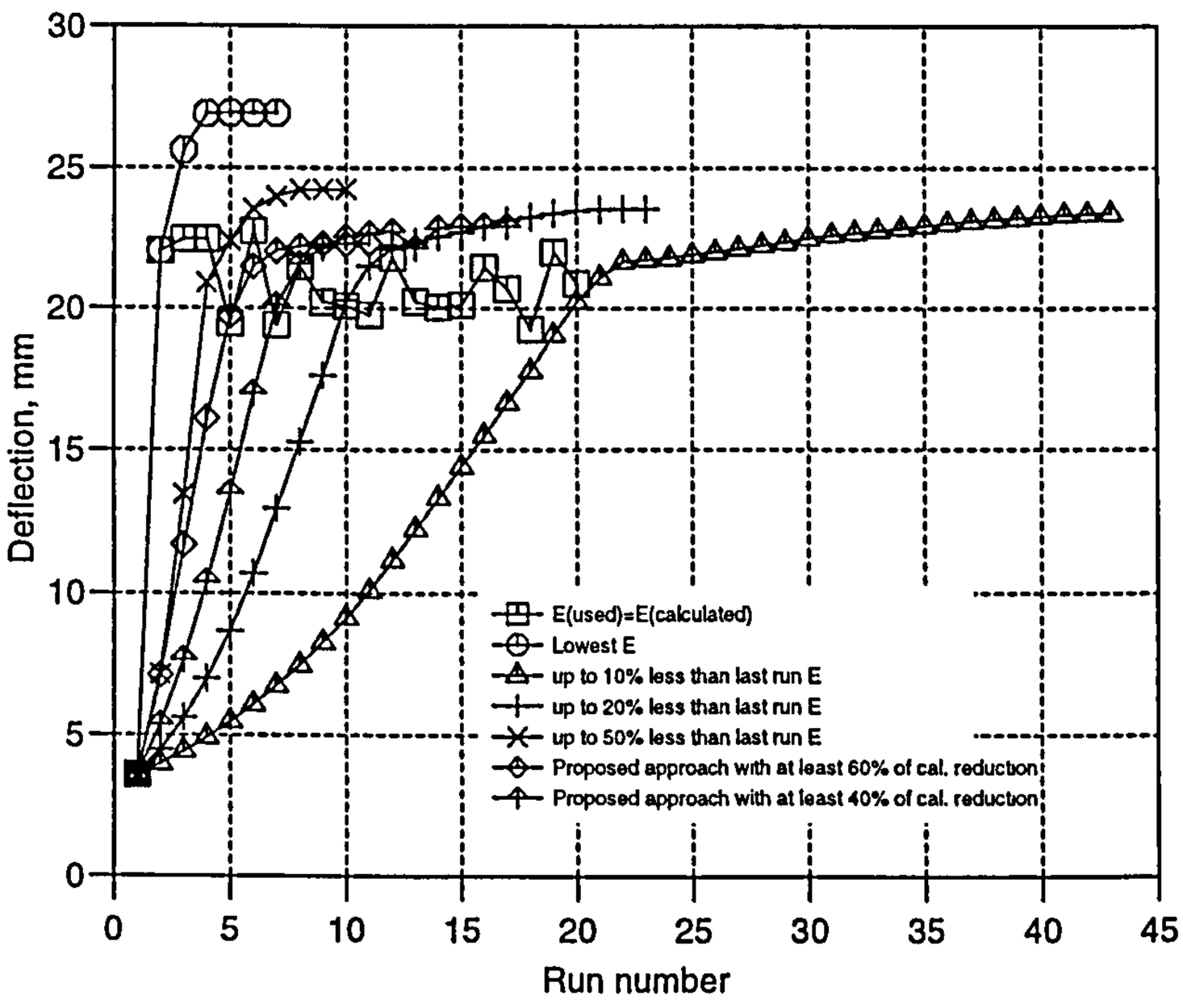


Figure 4.22 Different convergence approaches: node 325

4.12 Comparison with short-term experimental results

To demonstrate the capability of the secant-stiffness approach for reinforced concrete flexural members and, in particular, to establish which of the models, ACI, MC-90 or Gilbert, represent experimental results best, analyses were performed on seven case studies. These are presented below.

4.12.1 McNeice's two-way corner-supported slab

This is a square slab supported on four corners and loaded with a point load at the centre. The material properties of the slab are described in section 4.5.1 and the FE mesh is given in Fig. 4.3. Deflection of four nodes, calculated by the FE package with the three models, along with the experimental results, are compared in Figs 4.23 to 4.26.

For all the nodes, the ACI model predicts the lowest deflections. The Gilbert model gives the highest deflection for the lower load level but, as the load increases, the MC-90 model deflections are the highest. The ACI model gives the best estimate of the experimental deflection at node 7 at low loads. The ACI model progressively underestimates the deflection at node 7 as the load is increased further and the deflection tends towards that predicted by the MC-90 model. At other nodes, the ACI model gives the best estimate of the measured deflections, while deflections are overestimated by the Gilbert and MC-90 models. However, it should be noted that the accuracy of each method is dependent on the material properties which were only estimated and thus the study gives relative magnitudes of deflections for all the methods.

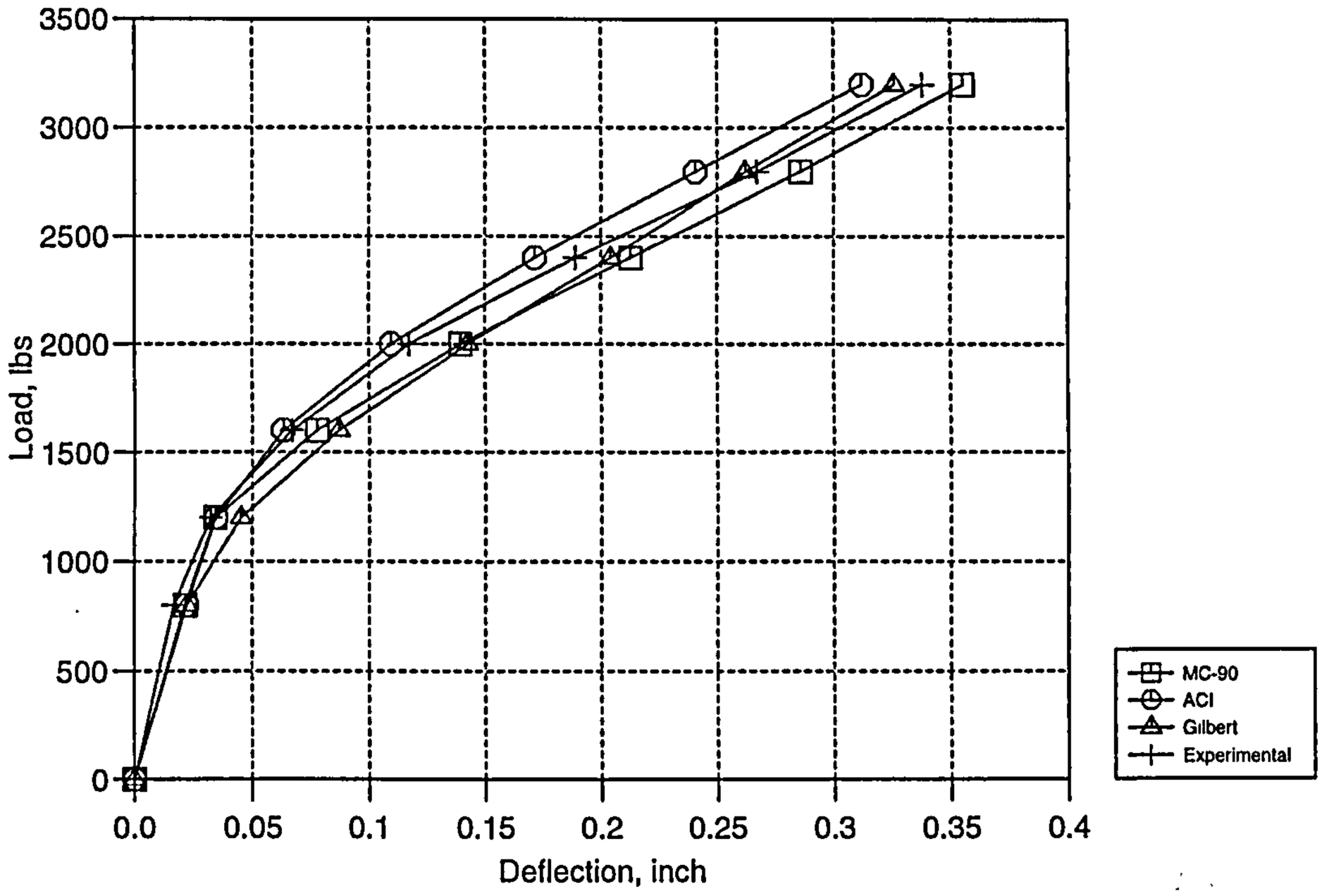


Figure 4.23 Load versus deflection curves for the corner-supported McNeice slab: node 7

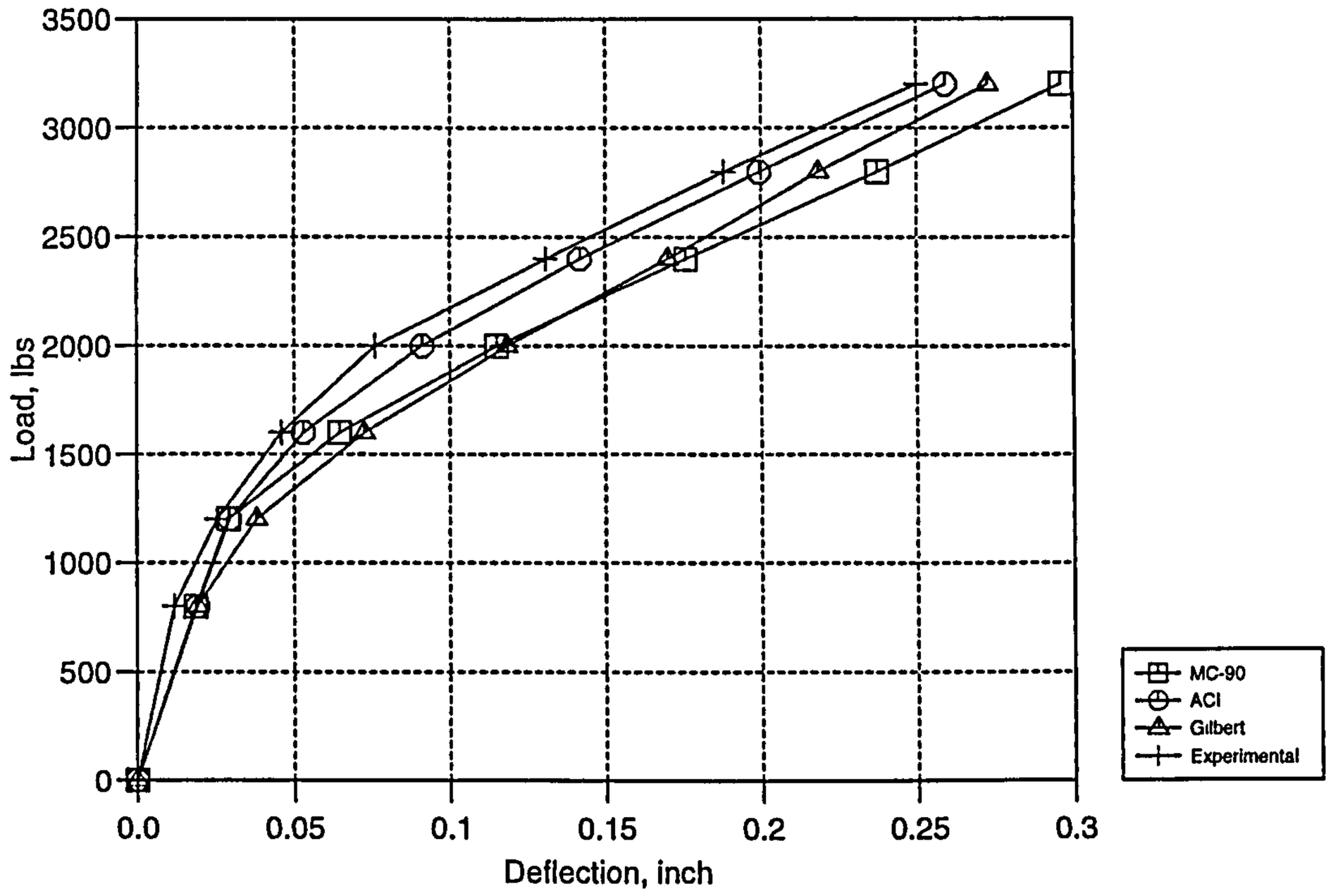


Figure 4.24 Load versus deflection curves for the corner-supported McNeice slab: node 69

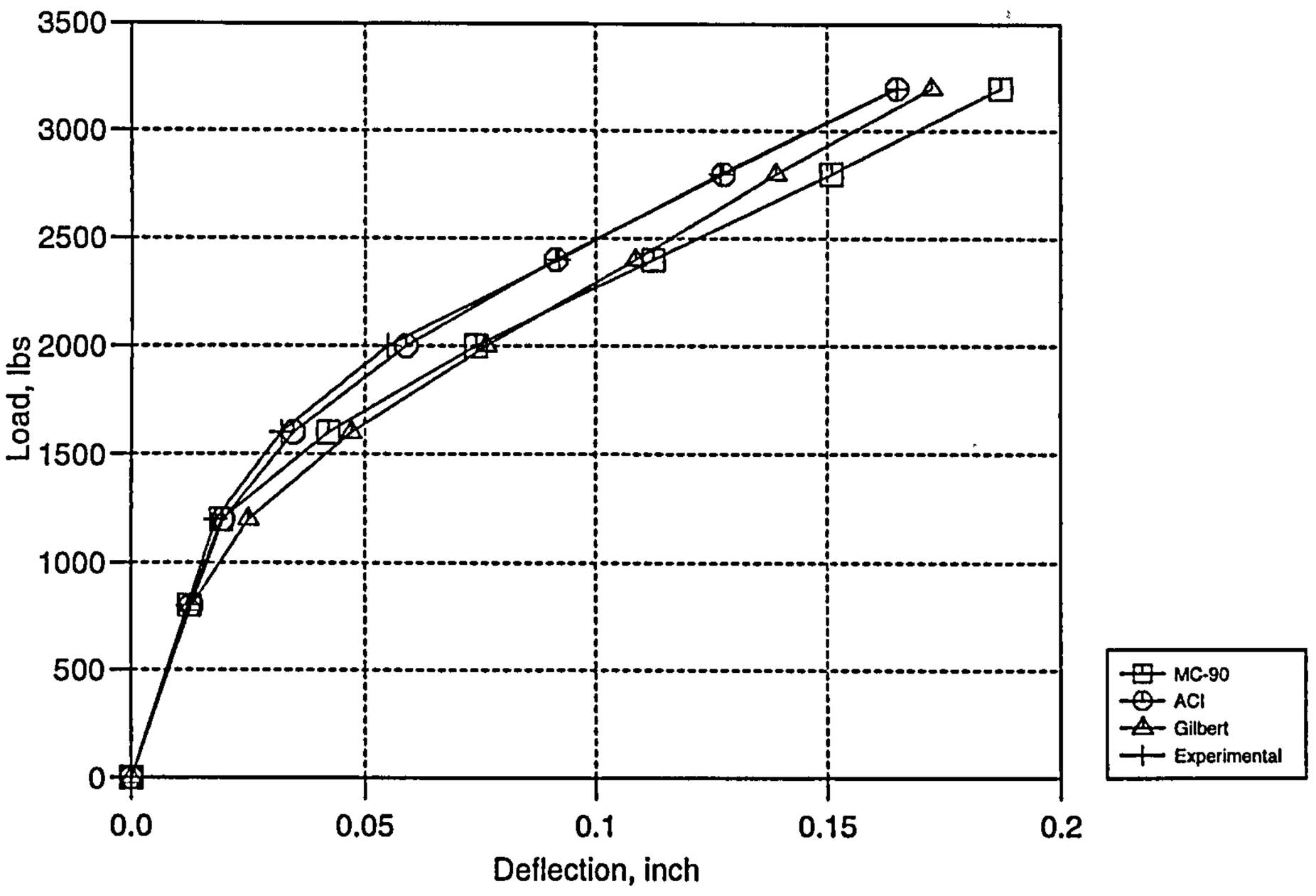


Figure 4.25 Load versus deflection curves for the corner-supported McNeice slab: node 147

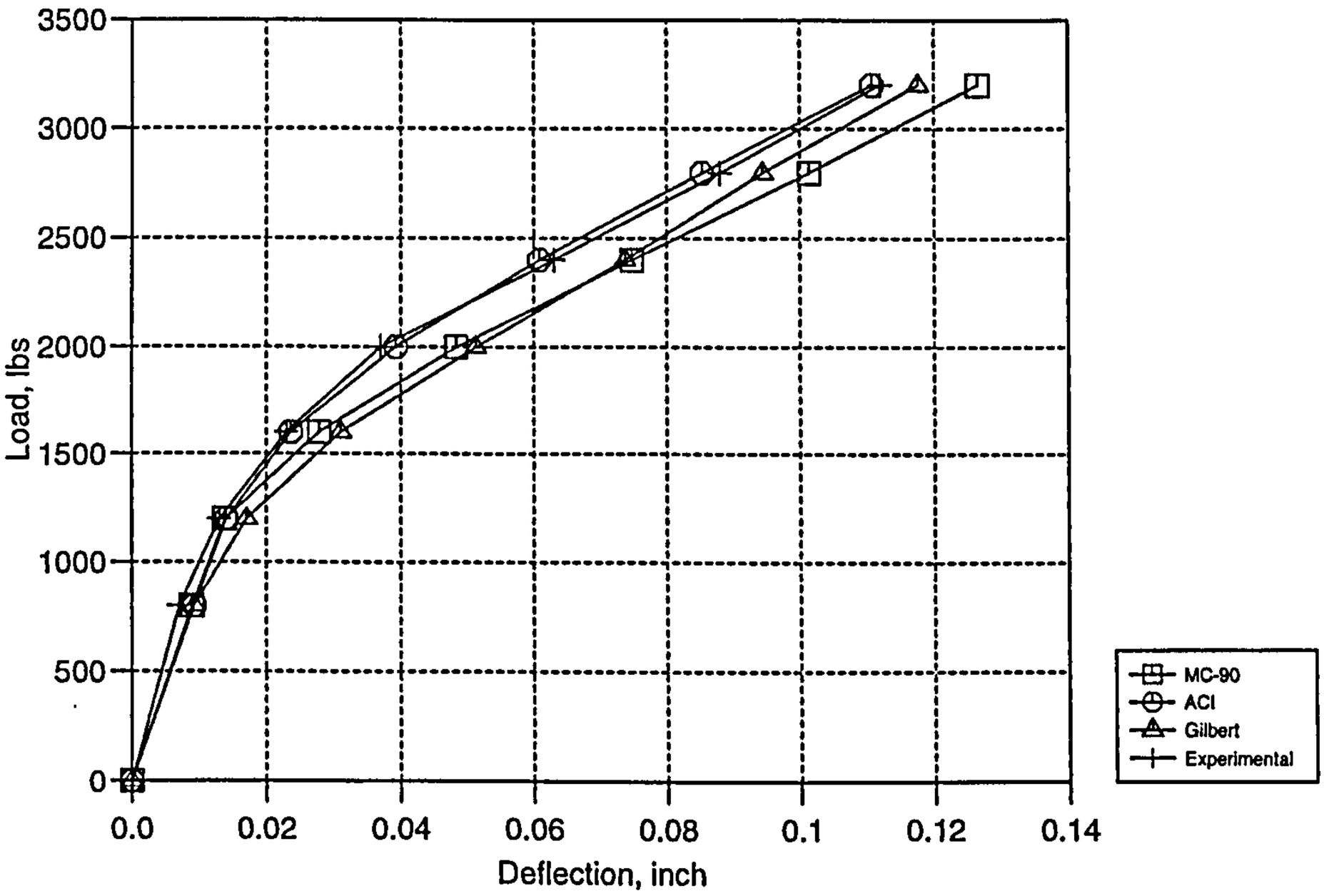


Figure 4.26 Load versus deflection curves for the corner-supported McNeice slab: node 157

4.12.2 McNeice's one-way slab

A one-way slab, 12 in. wide by 1.75 in. thick, simply supported with a span of 34 in. and reinforced with 0.8 percent steel, was tested by McNeice (1967). Details of the material properties and slab dimensions are shown in Fig. 4.27. Central deflections were estimated using the ACI, MC-90 and Gilbert models. The results are compared with their experimental counterparts in Fig. 4.28. The MC-90 model gives the highest deflection, the Gilbert model is quite good in the higher load range and the ACI model gives the best estimate of deflection at all load levels. Nevertheless, all the models predict similar deflections.

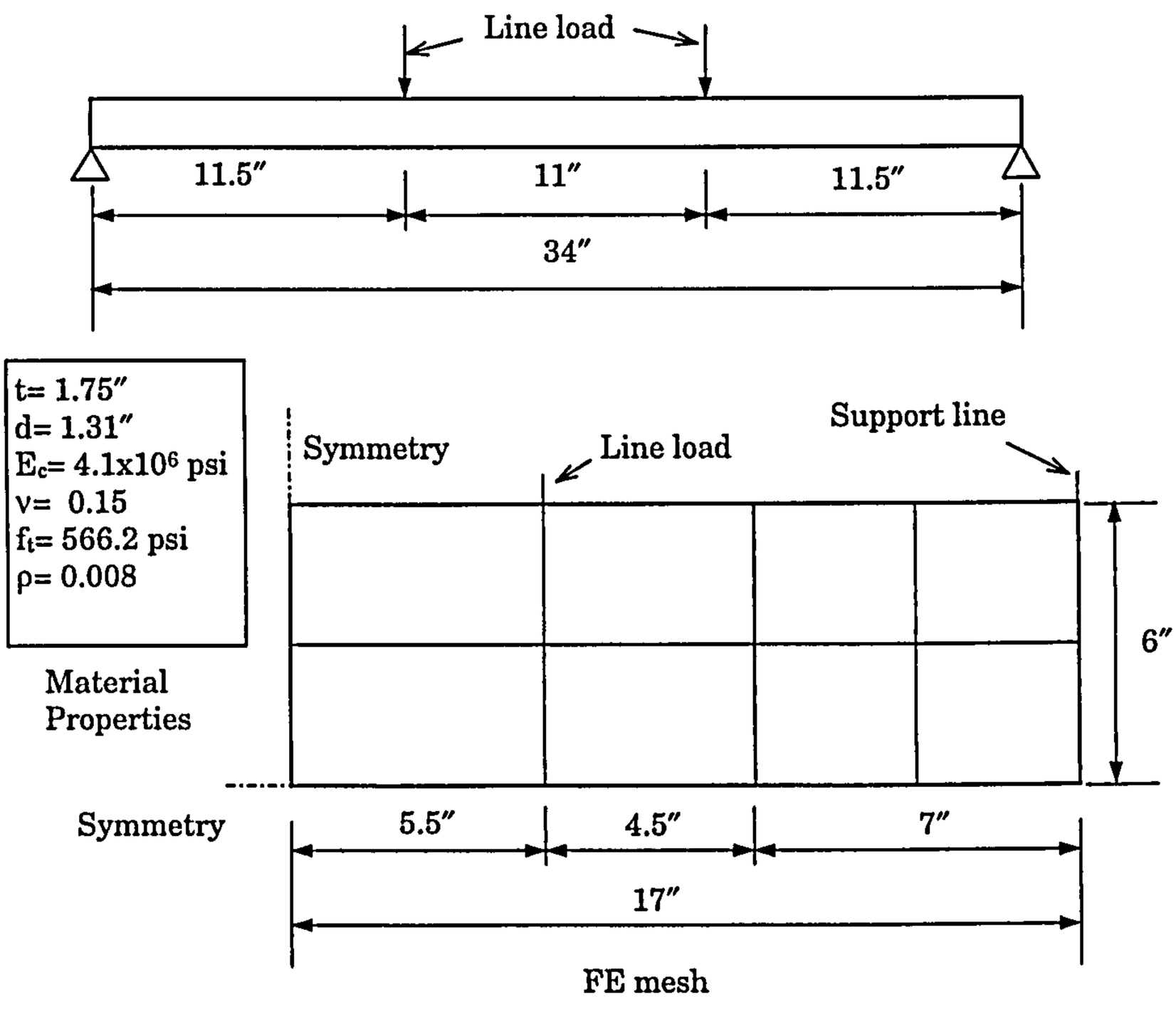


Figure 4.27 Details of simply supported one-way slab tested by McNeice: adapted from Jofriet & McNeice (1971)

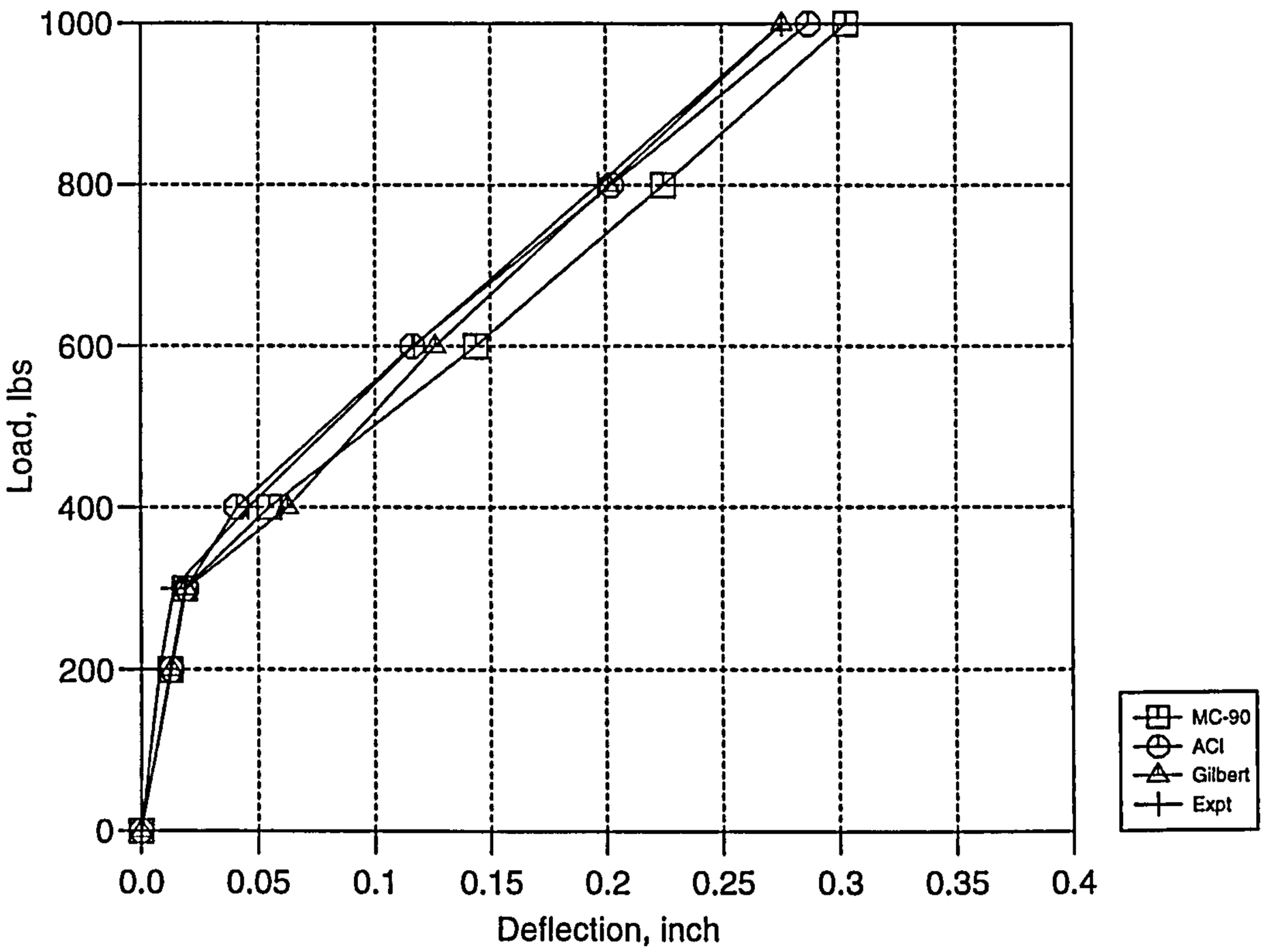


Figure 4.28 Load versus deflection curves for the simply supported one-way slab tested by McNeice

4.12.3 Cement and Concrete Association beam

Jofriet & McNeice used their FE program to predict the deflection of a beam tested at the Cement and Concrete Association (1966). The author has repeated the analysis of this beam using data from Jofriet & McNeice (1971). The beam was 7 in. wide by 15.25 in. deep and reinforced with 0.93 percent steel. The simply supported beam spanned 180 in. and was tested under a two-point loading. Details of the material properties, beam dimensions and loading are shown in Fig. 4.29. As the present analysis is intended for slabs, the whole procedure has been developed with plate elements. Hence this problem is treated as a one-way slab rather than a beam. Experimental deflections are given only for two load levels. All the three models predict very similar deflections, which are close experimental values.

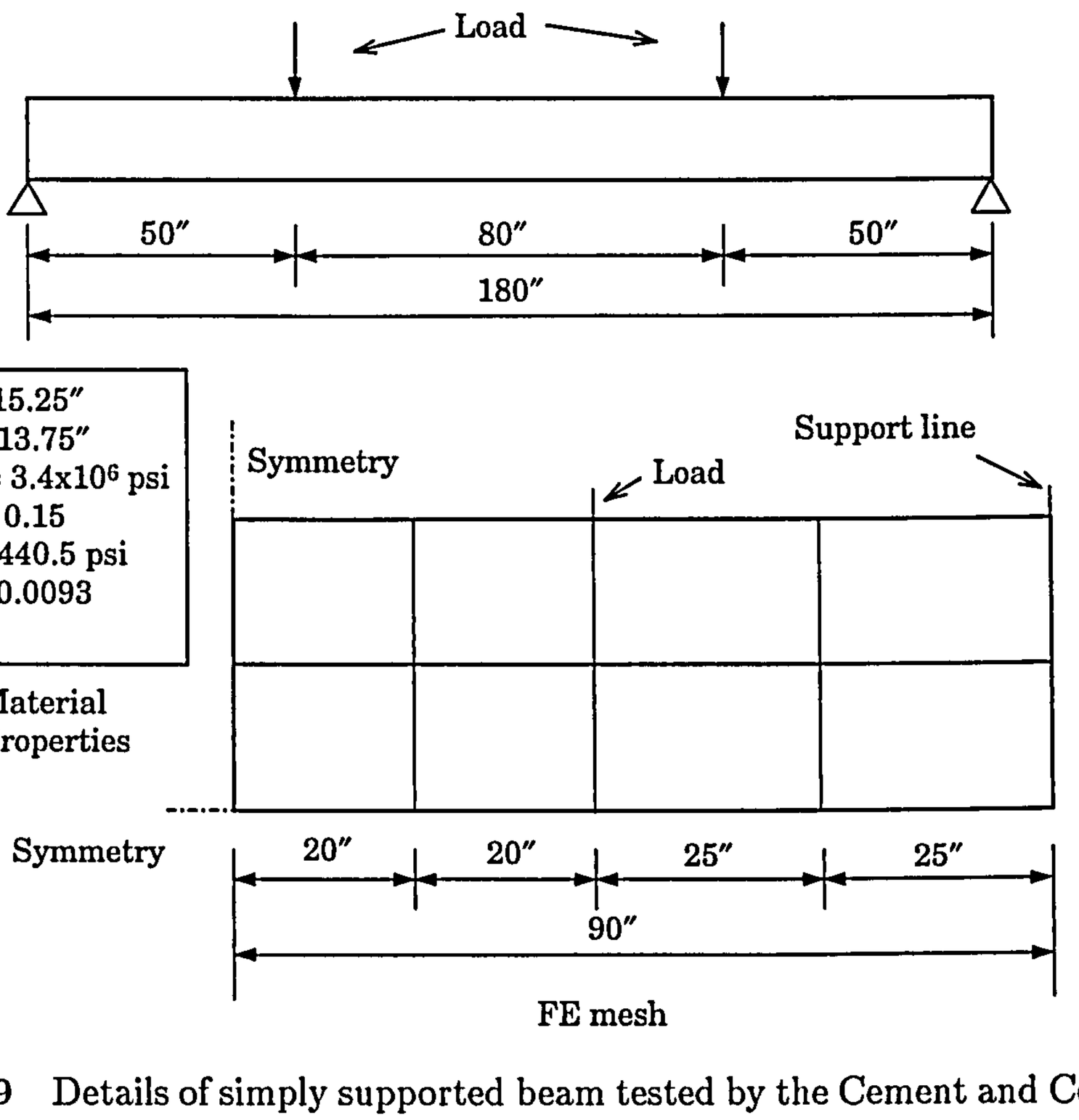


Figure 4.29 Details of simply supported beam tested by the Cement and Concrete Association: adapted from Jofriet & McNeice (1971)

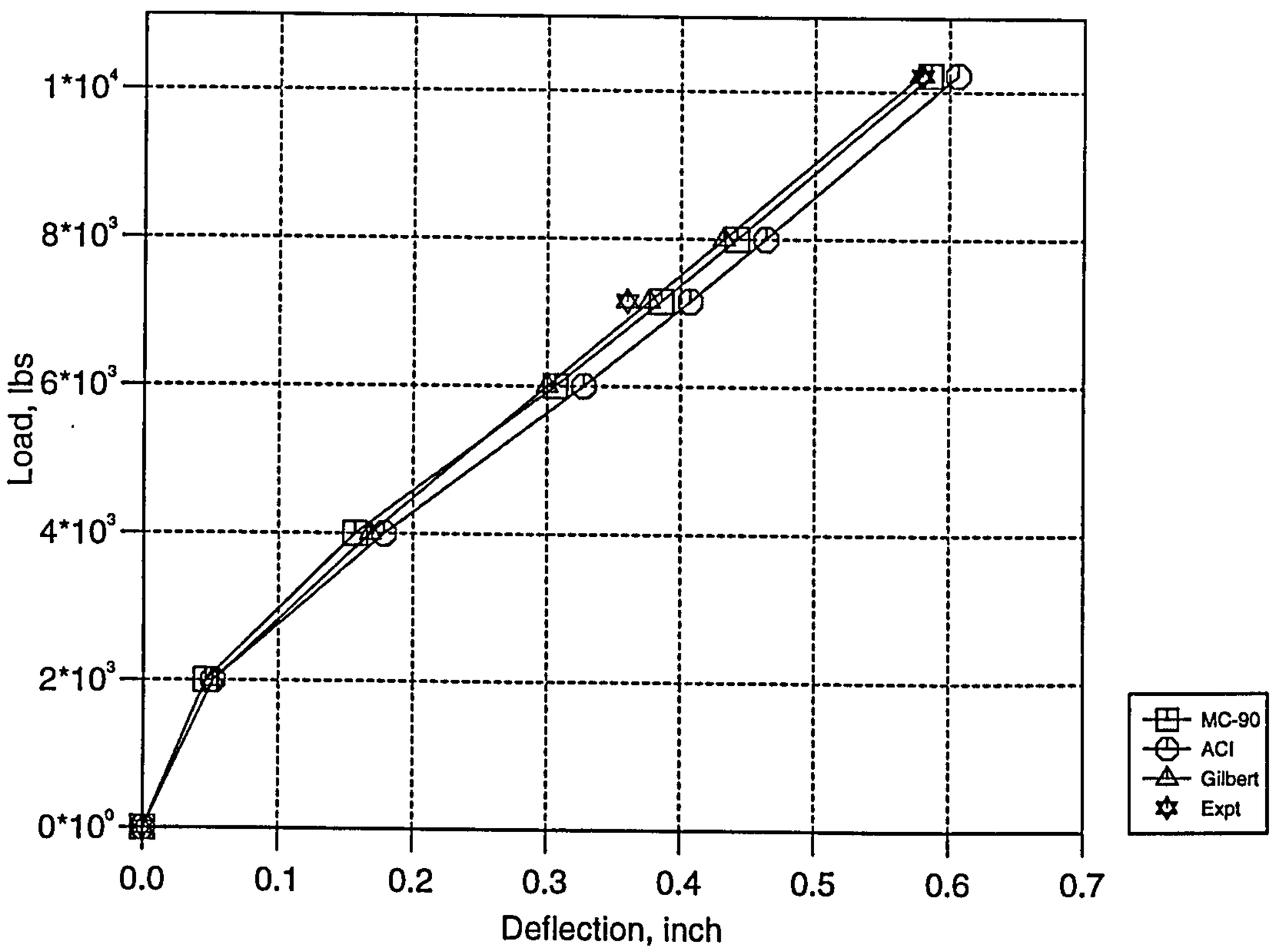


Figure 4.30 Load versus deflection curves for the beam tested by the Cement and Concrete Association

4.12.4 Jain & Kennedy's one-way slab

Jain & Kennedy (1974) tested a one-way slab which was 457.2 mm wide, and 38.1 mm thick, reinforced with 0.885 percent steel and simply supported with a span of 762 mm. Details of the slab dimensions and loadings are shown in Fig. 4.31. This slab has been analysed numerically by other researchers [Gilbert & Warner (1978), Crisfield (1982)]. The material properties and slab dimensions used in the current analysis were taken from the ABAQUS manual (1994). The slab was analysed using ABAQUS with different types of element and the results presented here have been taken from the manual. The post-cracked behaviour of the concrete, i.e. tension stiffening, was modelled in the ABAQUS analysis using an approach proposed by Crisfield (1982). The Crisfield model assumes a linear loss of strength after cracking until the concrete carries no tensile stress beyond a strain of 5.7×10^{-4} (about ten times the failure strain). The results are shown in Fig. 4.32 which is taken from the ABAQUS manual. The results are clearly improved when compared with the analysis with no tension stiffening (also shown in the manual, but not presented here) but, still, although the final deflection is accurately predicted, the ABAQUS analysis overestimates the initial stiffness and the loss of stiffness due to cracking is quite abrupt which is not the case in the actual experiment. The moment deflection curves obtained with the MC-90, ACI and Gilbert models are shown in Fig. 4.33. The curves show a gradual loss of stiffness after cracking. The deflections predicted by the three models are similar and compare well with the experimental results, thus being a clear improvement on the ABAQUS models.

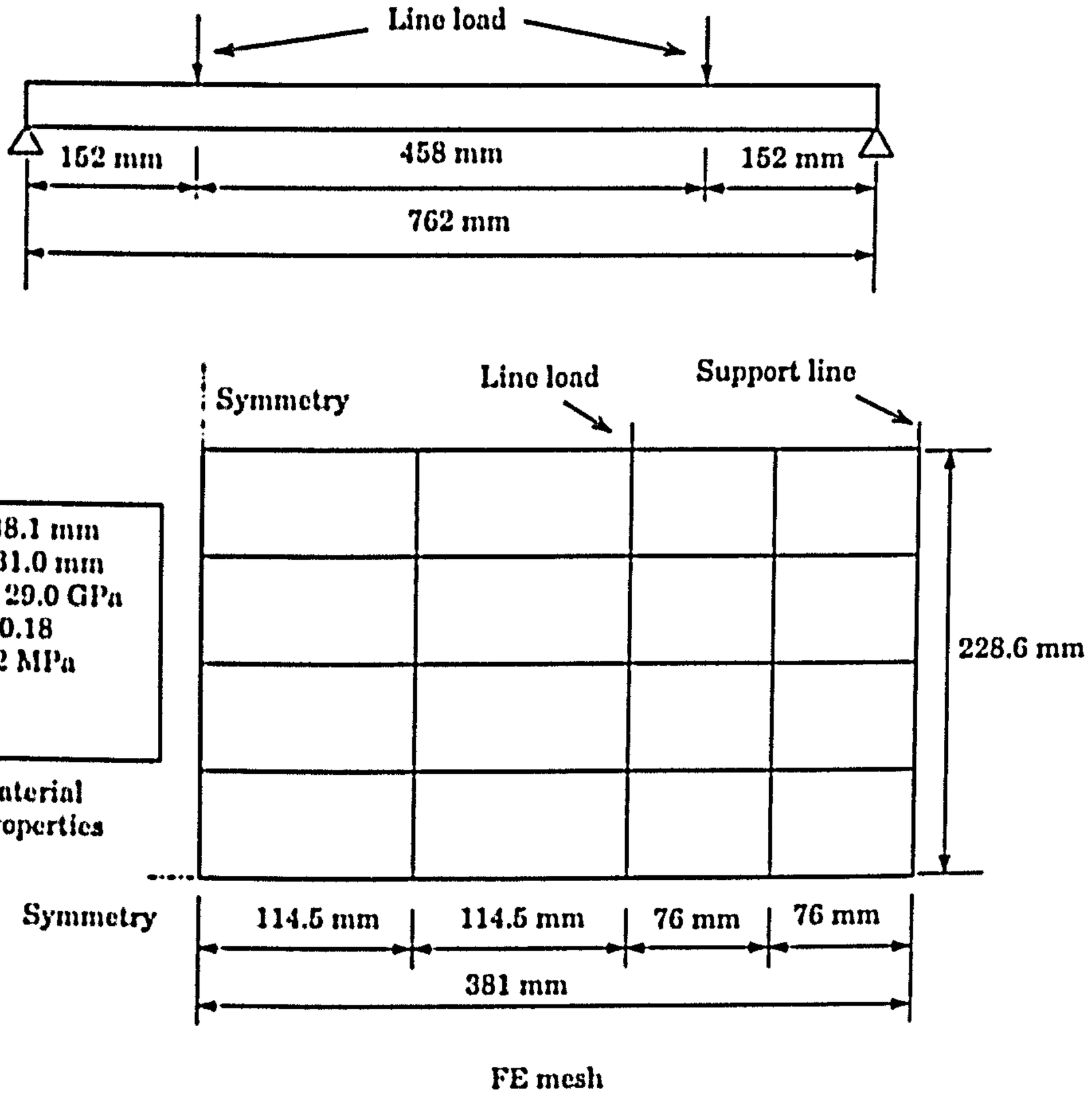


Figure 4.31 Details of simply supported one-way slab tested by Jain & Kennedy (1974)

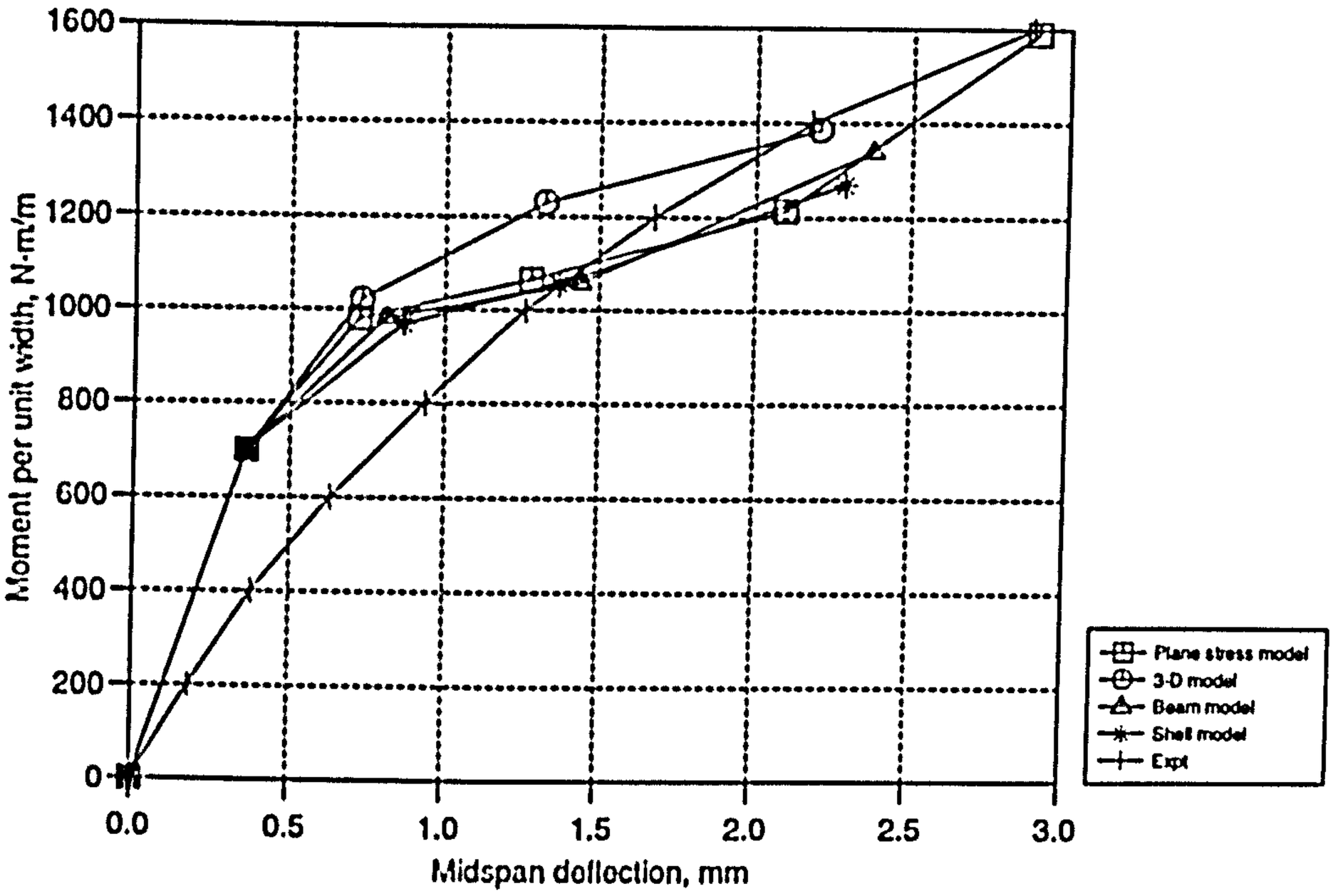


Figure 4.32 Moment versus deflection curves for the simply supported one-way slab tested by Jain & Kennedy: taken from the ABAQUS manual (1994)

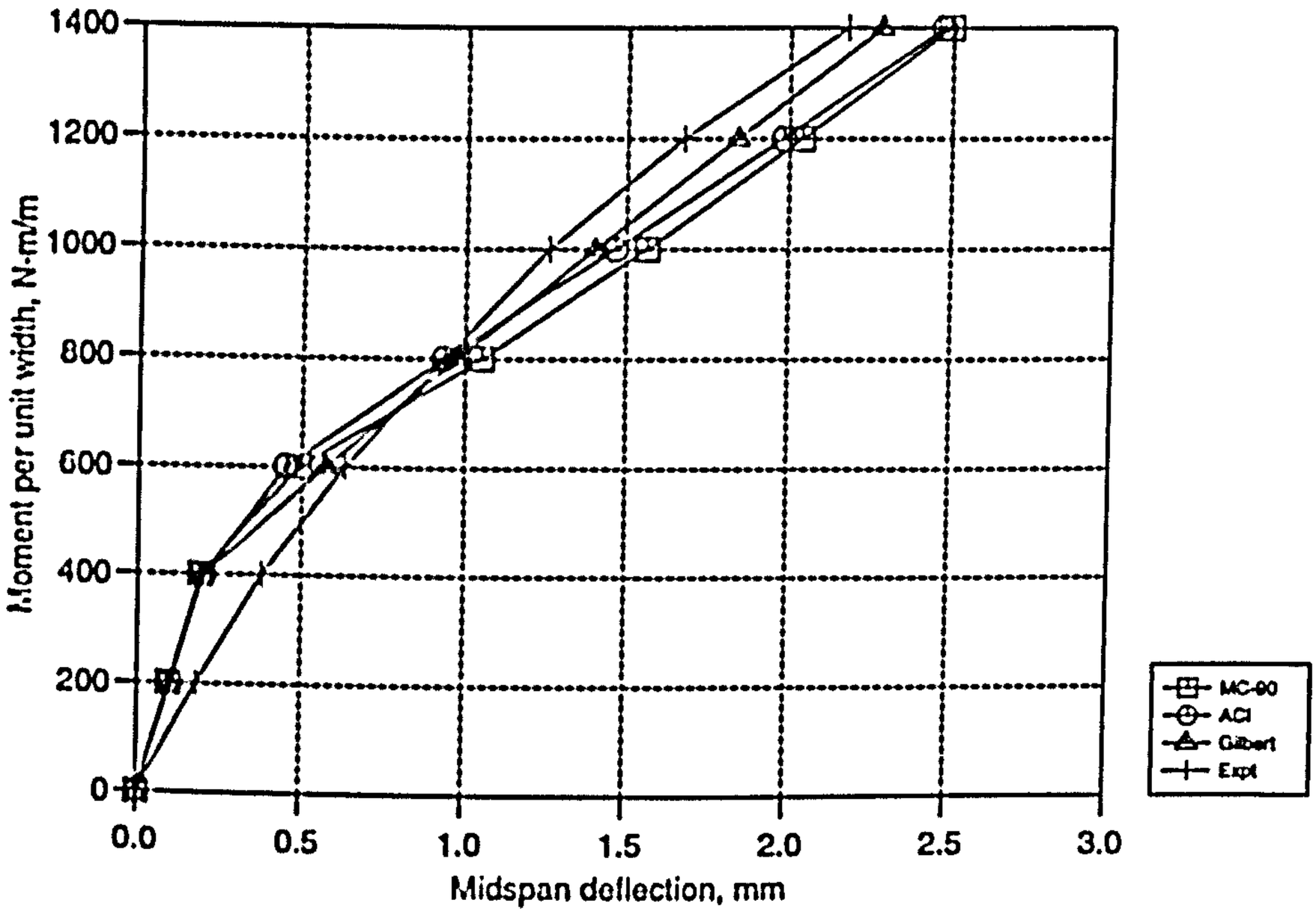


Figure 4.33 Moment versus deflection curves for the simply supported one-way slab tested by Jain & Kennedy

4.12.5 Elstner & Hognestad corner-supported slab

Elstner & Hognestad (1956) reported test results of 39 slabs with dimensions 6 ft square by 6 in. thick which were loaded through a centrally located column stub. The support details were varied in the tests. The slab considered in the present analysis was designated A-7a. It was loaded centrally through a 10 in. square column and was supported at each corner on 3.5 x 3.5 in. oak blocks. The concrete average cylinder strength was 3820 psi. The slab had 2.47 and 1.15 % steel at the tension and compression faces respectively. Moduli of rupture and elasticity were not reported and hence have presently been estimated (in psi) using the ACI equations:

$$E_c = 57,000\sqrt{f'_c} \tag{4.54}$$

$$f_r = 7.5\sqrt{f'_c} \tag{4.55}$$

The slab failed suddenly near three of the corner supports. Details of the slab dimensions and FE mesh are shown in Fig. 4.34. The author has estimated slab deflections using the ACI, MC-90 and Gilbert models. Predicted deflections, at the centre of the slab, are compared with the measured deflections in Fig. 4.35. The deflections obtained using the different models are close to each other but the experimental deflections were greater for the whole load range including the uncracked region. It is evident that the assumed values of moduli of elasticity and rupture made the slab stiffer than actual experiment.

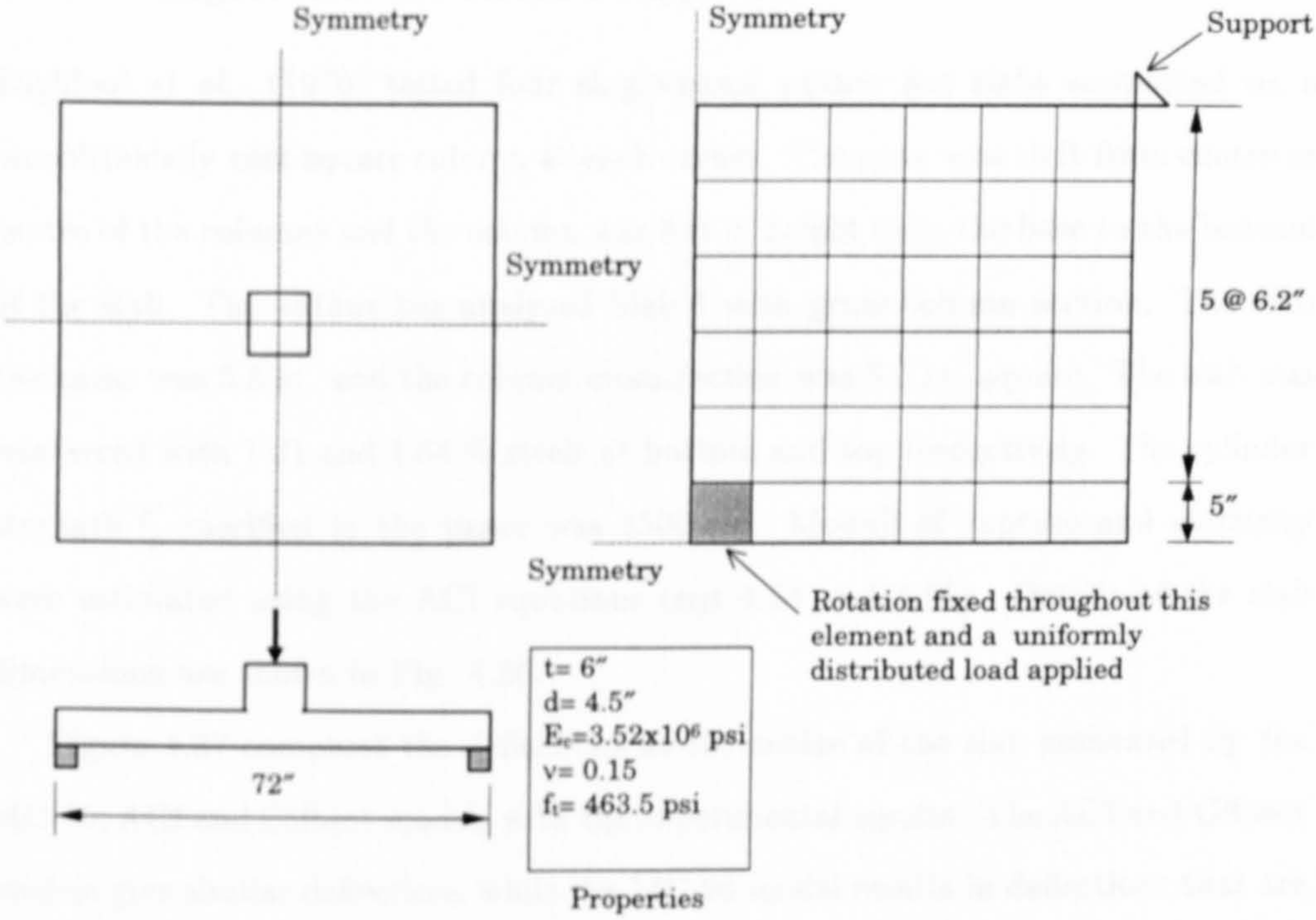


Figure 4.34 Details of the corner-supported two-way slab tested by Elstner & Hognestad (1956)

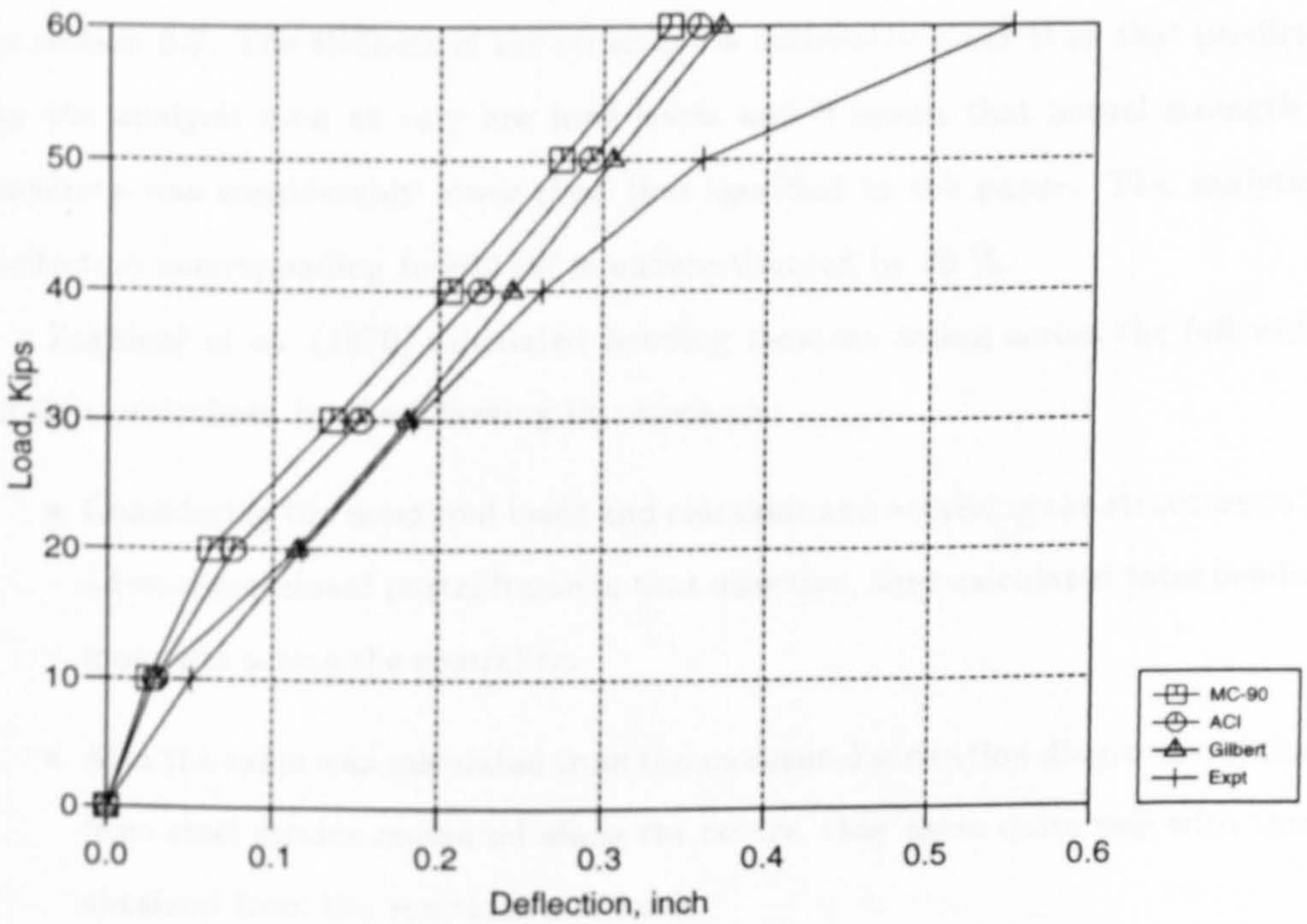


Figure 4.35 Load versus deflection curves for the corner supported slab tested by Elstner & Hognestad

4.12.6 Zaghlool *et al.* column-supported slab

Zaghlool *et al.* (1970) tested four single-panel square flat slabs supported on a monolithically cast square column at each corner. The span was 10 ft from centre to centre of the columns and the column was 5 ft in height from the base to the bottom of the slab. The author has analysed Slab 1 with gross column section. The slab thickness was 5.5 in. and the column cross-section was 5.5 in. square. The slab was reinforced with 1.31 and 1.64 % steels at bottom and top respectively. The cylinder strength f'_c specified in the paper was 3500 psi. Moduli of rupture and elasticity were estimated using the ACI equations (eqs 4.54 and 4.55). Details of the slab dimensions are shown in Fig. 4.36.

Figure 4.37 compares the deflections at the centre of the slab estimated by the MC-90, ACI and Gilbert models with the experimental results. The ACI and Gilbert models give similar deflections while the MC-90 model results in deflections that are lower than these values. For all the models, the predicted deflections are lower than the experimental values even at low loads. The columns were only cracked at higher loads and the effect of not modelling column cracking is insignificant as will be shown in section 5.7. The stiffness of the structure is noticeably lower than that predicted by the analysis even at very low load levels and it seems that actual strength of concrete was considerably lower than that specified in the paper. The analytical deflection corresponding to 800 psf is underestimated by 30 %.

Zaghlool *et al.* (1970) calculated bending moment acting across the full width of slab centrelines by the following two methods.

- Considering the measured loads and reactions and assuming the structure to be a two-dimensional portal frame in that direction, they calculated total bending moments across the centreline.

- Also the same was calculated from the moment-distribution diagrams obtained from steel strains measured along the centre, they agree quite well with those obtained from the reactions and loads.

Total bending moments, across the full width at centreline, obtained from the current analysis by means of all the three models agree very well with the experimentally

obtained bending moments (from reaction and load) as shown in Fig. 4.38.

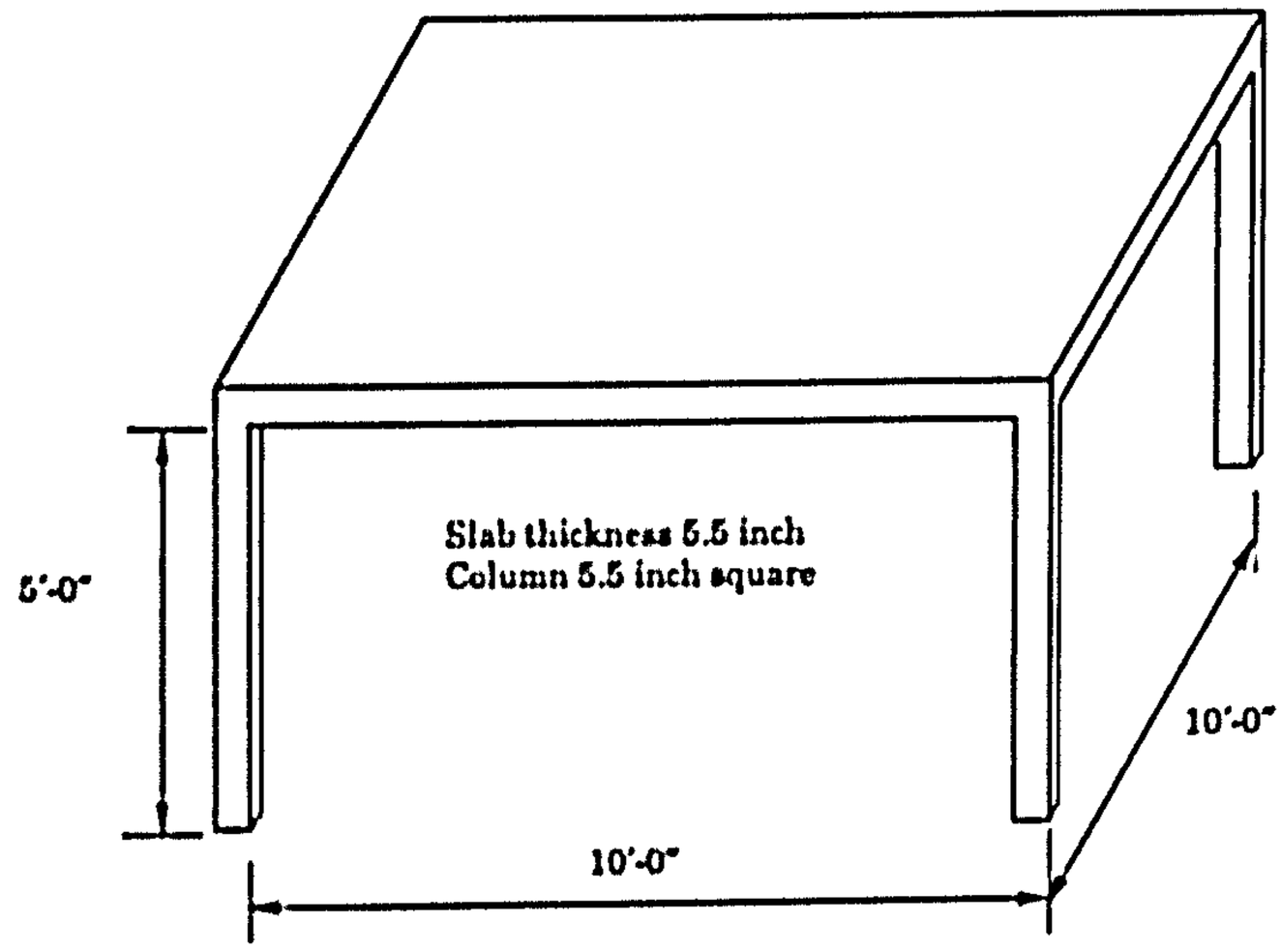


Figure 4.30 Details of the column-supported slab tested by Zaghlool *et al.* (1970)

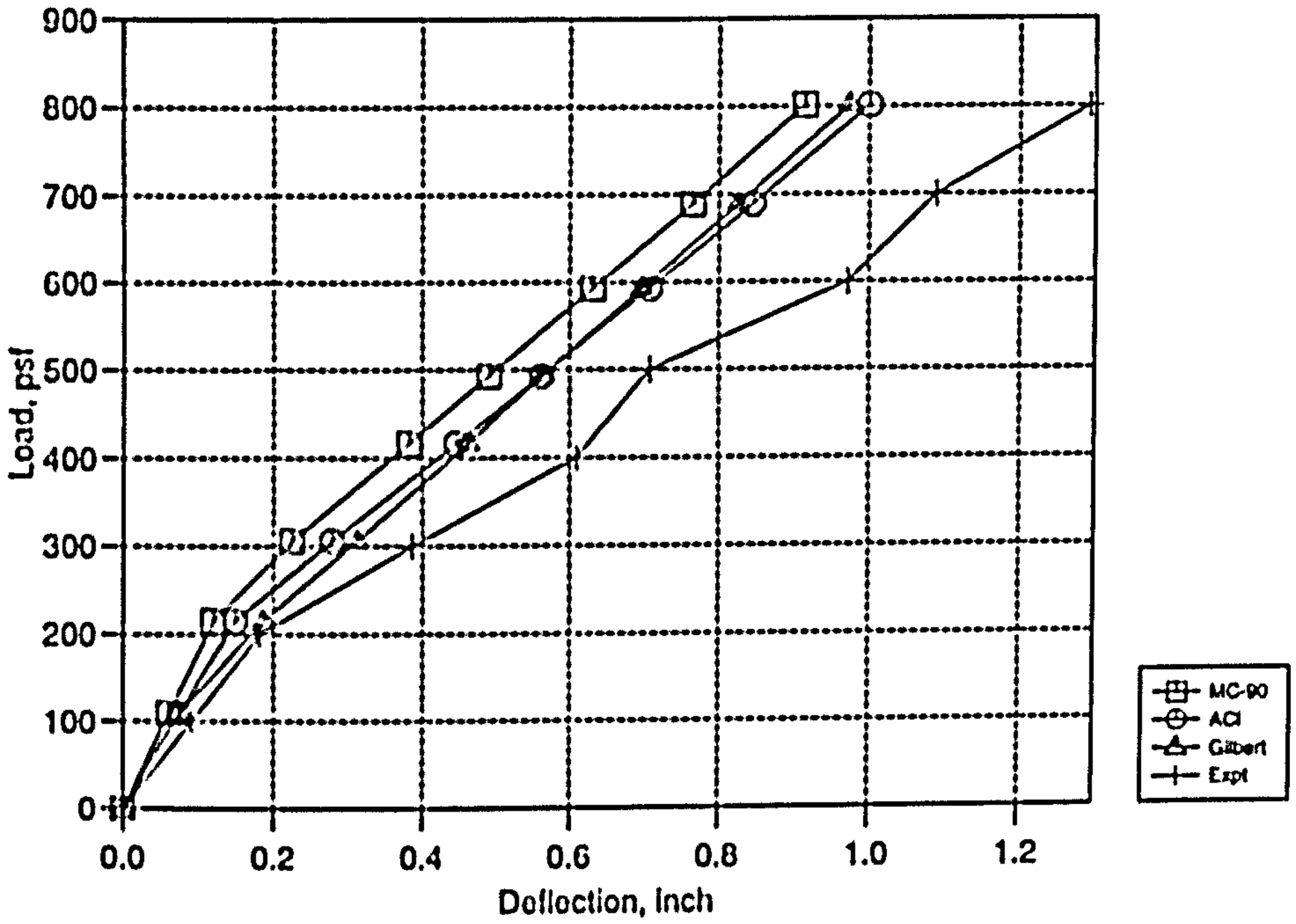


Figure 4.37 Load versus deflection curves for the column-supported slab tested by Zaghlool *et al.*

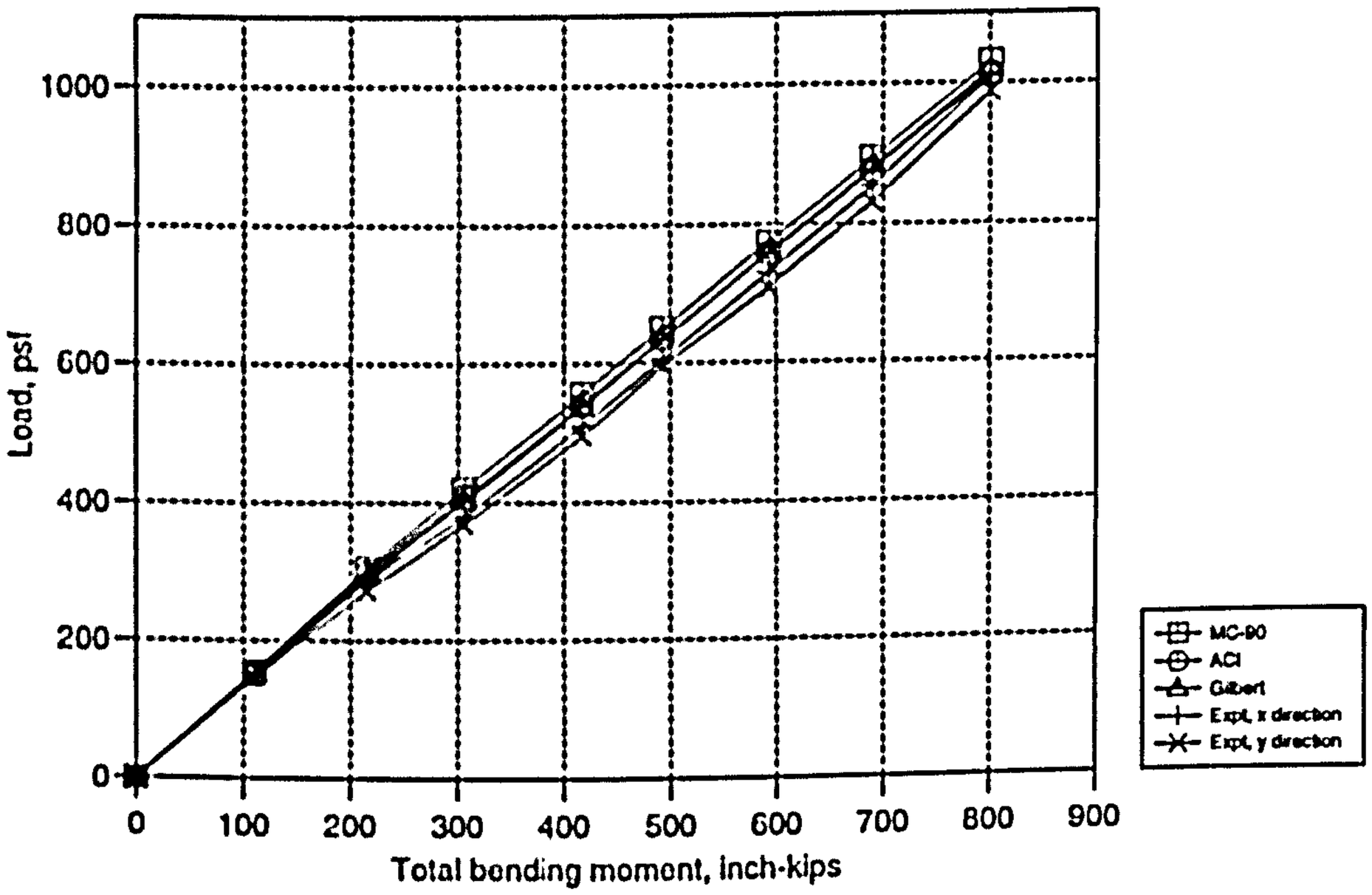


Figure 4.38 Variation of total central moment with load for the column-supported slab tested by Zaghlool *et al.*

4.12.7 Shukla & Mittal two-way edge-supported slab

A series of square slabs supported on edges were tested by Shukla & Mittal (1976). The dimensions of the slabs are identical but they differ in material properties and reinforcement arrangements. Three of the these slabs have been analysed in the present work, and the deflections calculated using the MC-90, ACI and Gilbert models have been compared with the experimental results. Slabs S-8 and S-11 are isotropically reinforced whereas the reinforcement mesh of S-12 is orthotropic. Details of the slabs were given in section 4.5.2 and the mesh used for the FE analysis appeared in Fig. 4.8. The load versus central-point deflection curves using the different models are presented in Figs 4.39 to 4.41. It can be seen that the correlation between analysis and experiment is quite good in all cases.

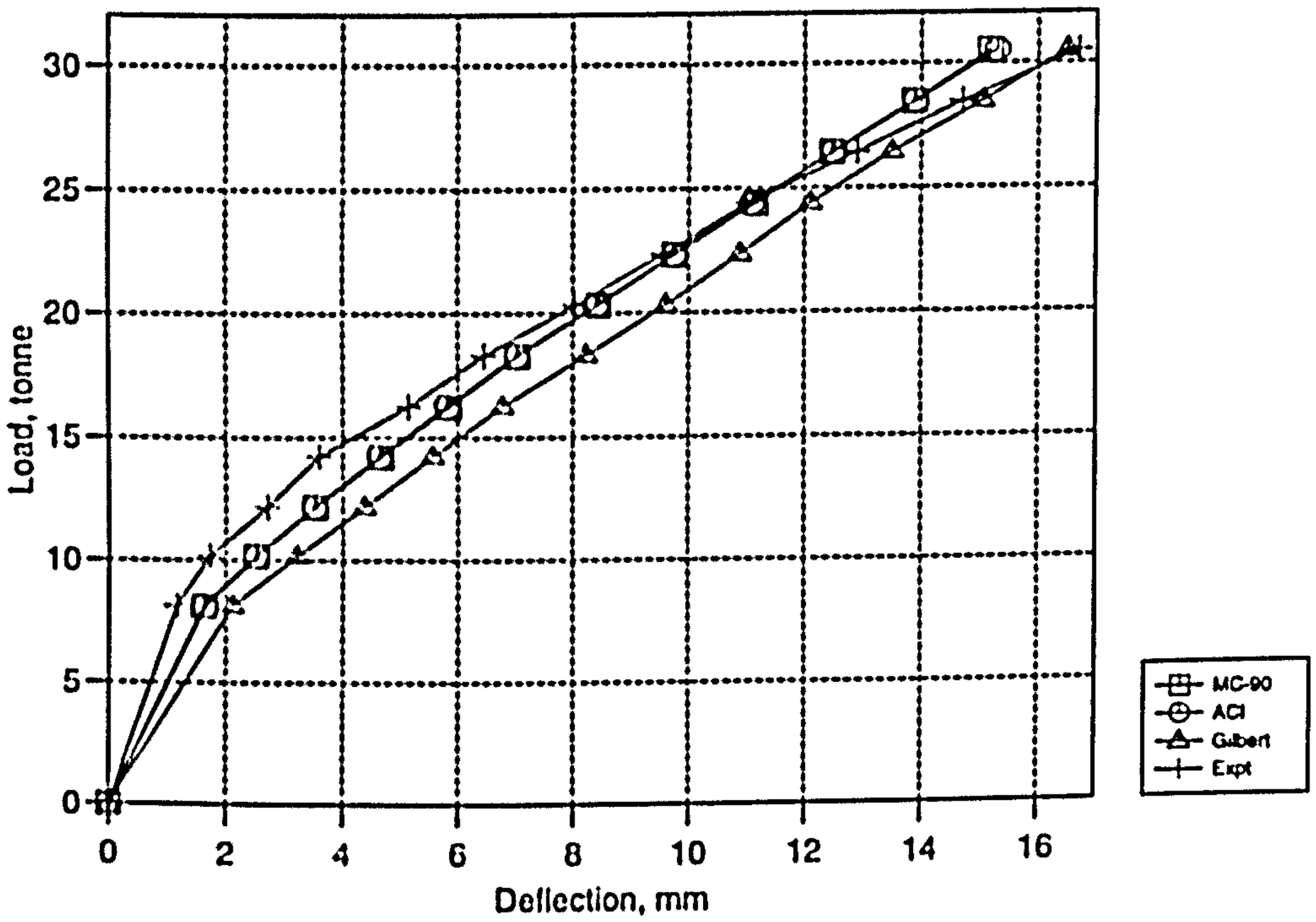


Figure 4.39 Load versus deflection curves for the edge-supported Shukla & Mittal slab S-8

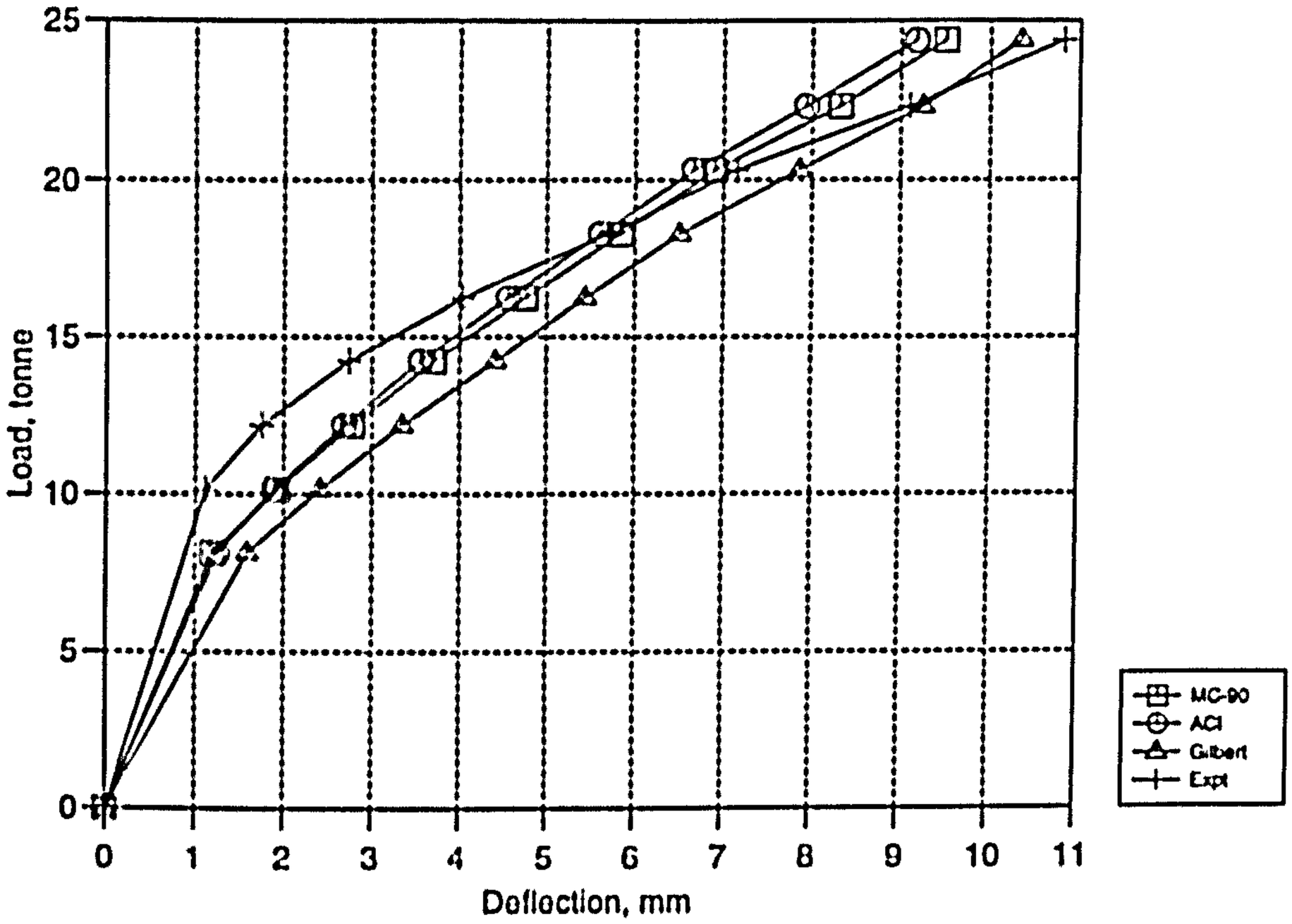


Figure 4.40 Load versus deflection curves for the edge-supported Shukla & Mittal slab S-11

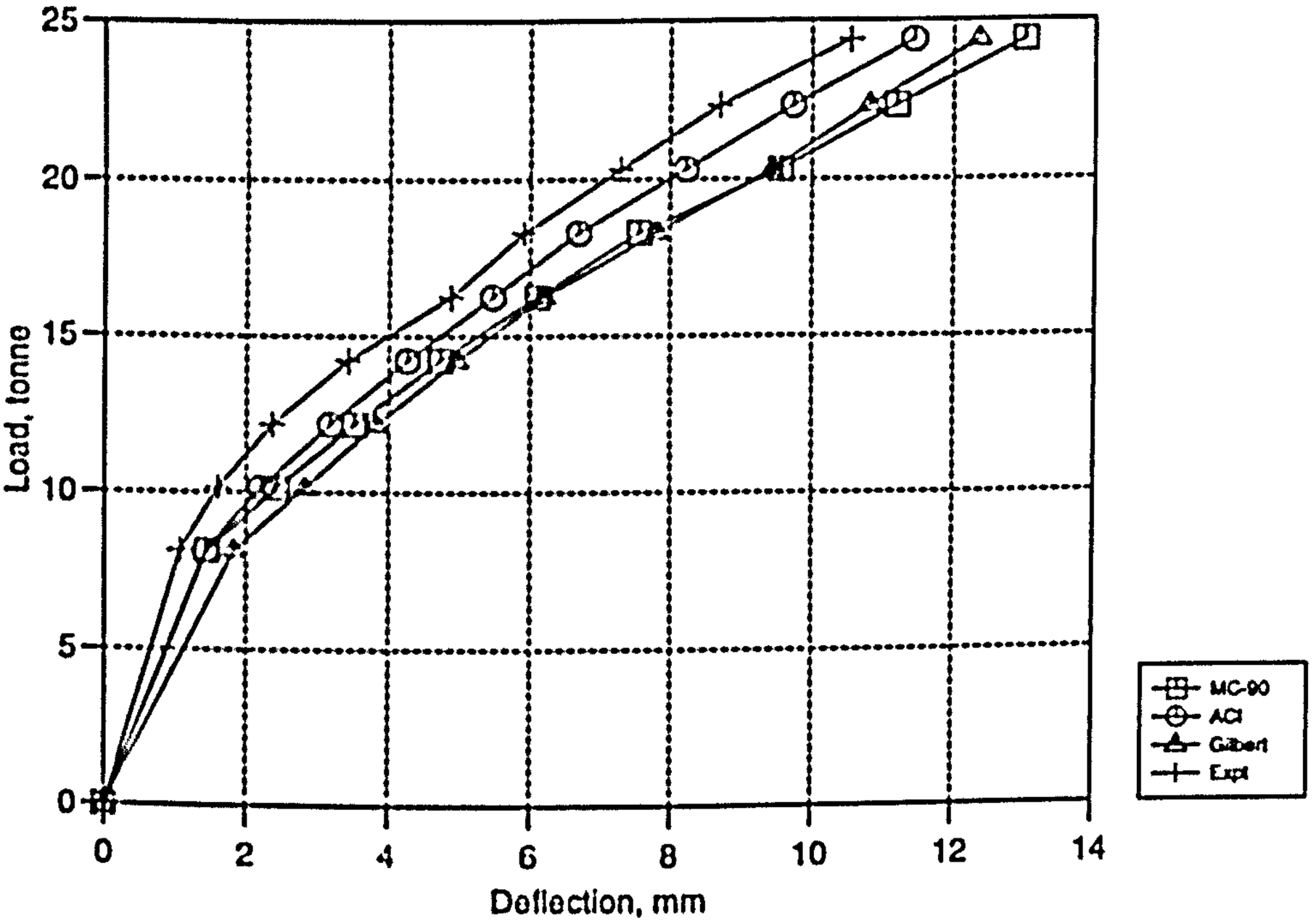


Figure 4.41 Load versus deflection curves for the edge-supported Shukla & Mittal slab S-12

4.13 Comparison with long-term experimental results

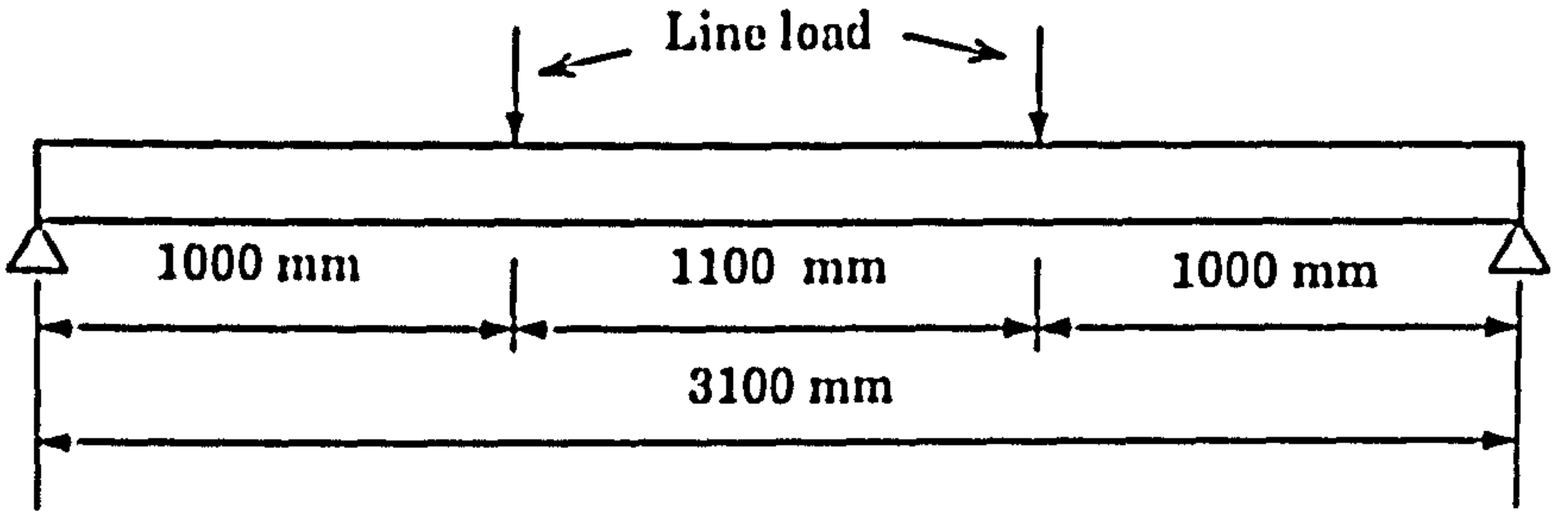
4.13.1 Favre *et al.* slab

Slab details

Favre *et al.* (1990) performed long-term tests on a series of 16 one-way slabs identical in geometry and reinforcement. Details of the material properties, slab dimensions and the reinforcement are given in Fig. 4.42. They were all 750 mm wide by 160 mm deep and simply supported over a span of 3100 mm. The principal reinforcement represents a ratio of $\rho = 0.58\%$. The transverse reinforcement consisted of ϕ 8 mm stirrups at intervals of 200 mm in the central zone. Different types of concrete, ranging from normal concrete typically used in building construction to high-strength concrete with or without silica fume, were considered. The compressive strengths of concrete for slabs A1 and CF4 were reported as 28 and 71.4 MPa at 28 days. The bending moment due to permanent load varied 20, 30, 50 and 75% of the conventional ultimate moment M_u. M_u is calculated to be 32.3 kN-m with f_{yk}=460 MPa. Of the total of 16 slabs, 11 were cast with the tensile reinforcement placed near the lower surface during concreting and 5 were made with tensile reinforcement at the top. All the slabs were tested with the tensile reinforcement at the bottom. Thus, 11 slabs simulated the span region and the remaining 5 slabs simulated the support region of a continuous slab.

Analysis details

Slabs A1 and CF4 were considered in the present analysis. Slab A1 was made from standard concrete and slab CF4 with high-strength concrete with silica fume. Both the actual creep coefficient and shrinkage strains and the values given by the equations in the MC-90 were used in the analysis. Figures 4.43 and 4.44 give experimental and predicted creep coefficients and shrinkage strains respectively for the concrete used in slabs CF4 and A1. Comparison of the values shows that the MC-90 equations overestimate the creep strain but underestimate the shrinkage strain. Ganeswaran & Rangan (1996) came to the same conclusion. Figures 4.45 and 4.46 show the moment-curvature relationship after 1 year derived using the MC-90 equations with experimental creep and shrinkage data. The relative deformation to the



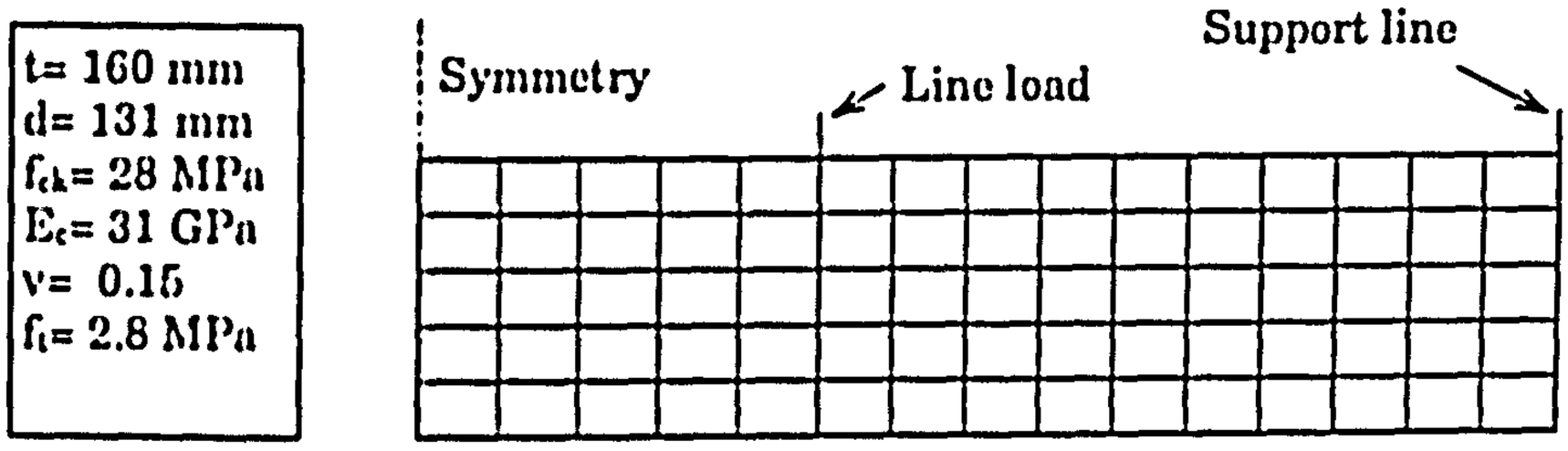


Figure 4.42 Details of one-way simply-supported slab tested by Favre *et al.* (1990)

surface of the concrete, on the upper and lower surfaces were measured in the experiment, from which it was possible to deduce the curvatures. The predicted curvatures agree very well with the experimental results. Deflections are plotted against time for slabs with A1 and CF4 concrete for a moment level of $M/M_u = 0.75$ in Figs 4.47 and 4.48. Experimental deflections for both positive and negative moments are also plotted. The deflections obtained using the creep and shrinkage strains calculated using the MC-90 equations agree reasonably well with those calculated using the actual creep and shrinkage strains. These analytical predictions also agree quite well with the experimental deflections under positive moment. It is interesting to note, however, that, while the model predicts the deflections of slabs A1 and CF4 well under positive moment conditions, the experimental deflections of both A1 and CF4 concrete slabs under negative moment conditions are considerably greater (by some 20%) than the predicted values. The reason for this seems to be that the tensile strength of the concrete is less at the cast surface than the bottom surface of the slab. The tests of Favre *et al.* (1990) suggest that the position of steel relative to the cast face should be taken into account in the calculation of the deflection of continuous members.

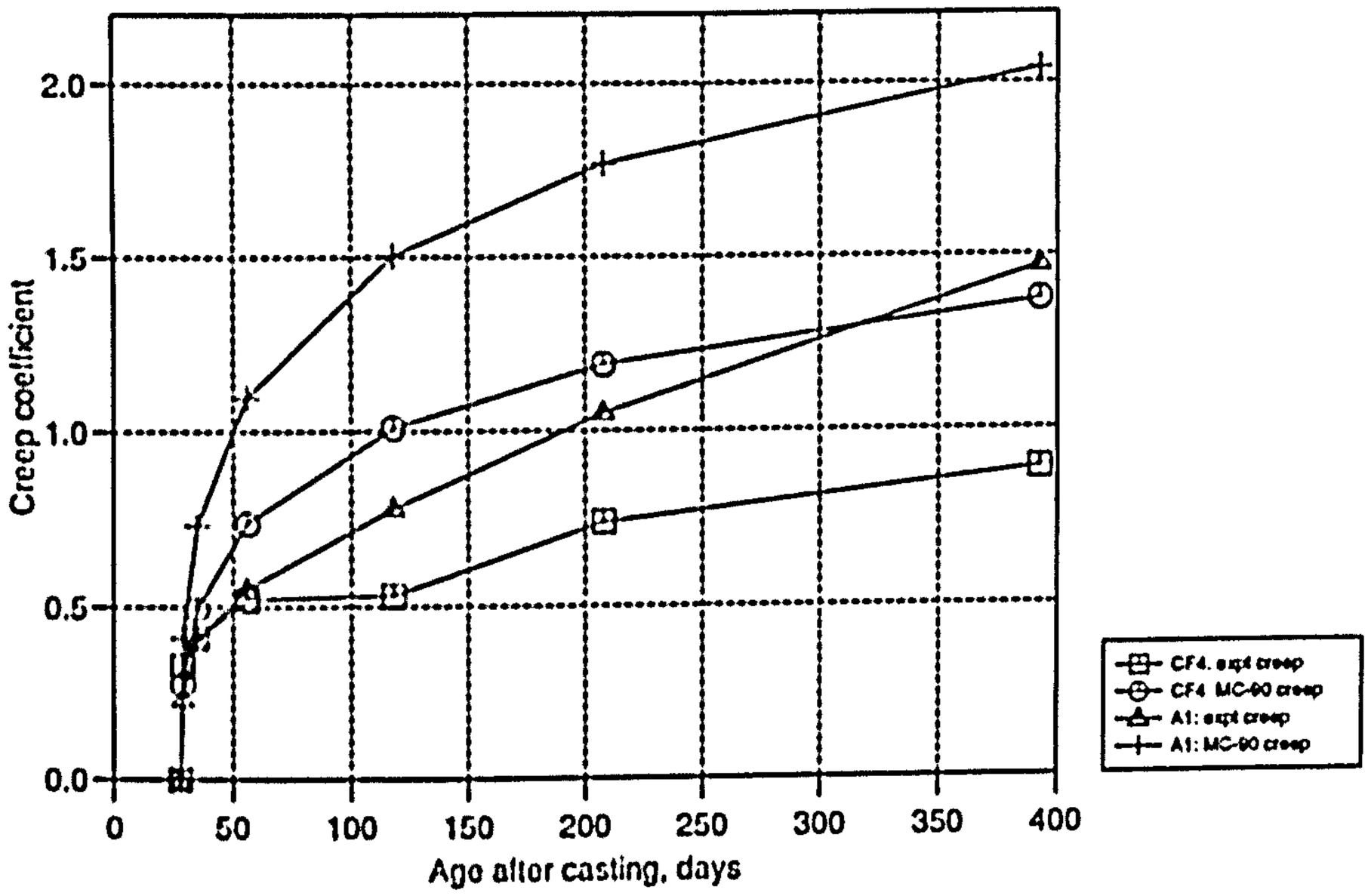


Figure 4.43 Experimental and MC-90 creep coefficient for concrete for slabs CF4 and A1

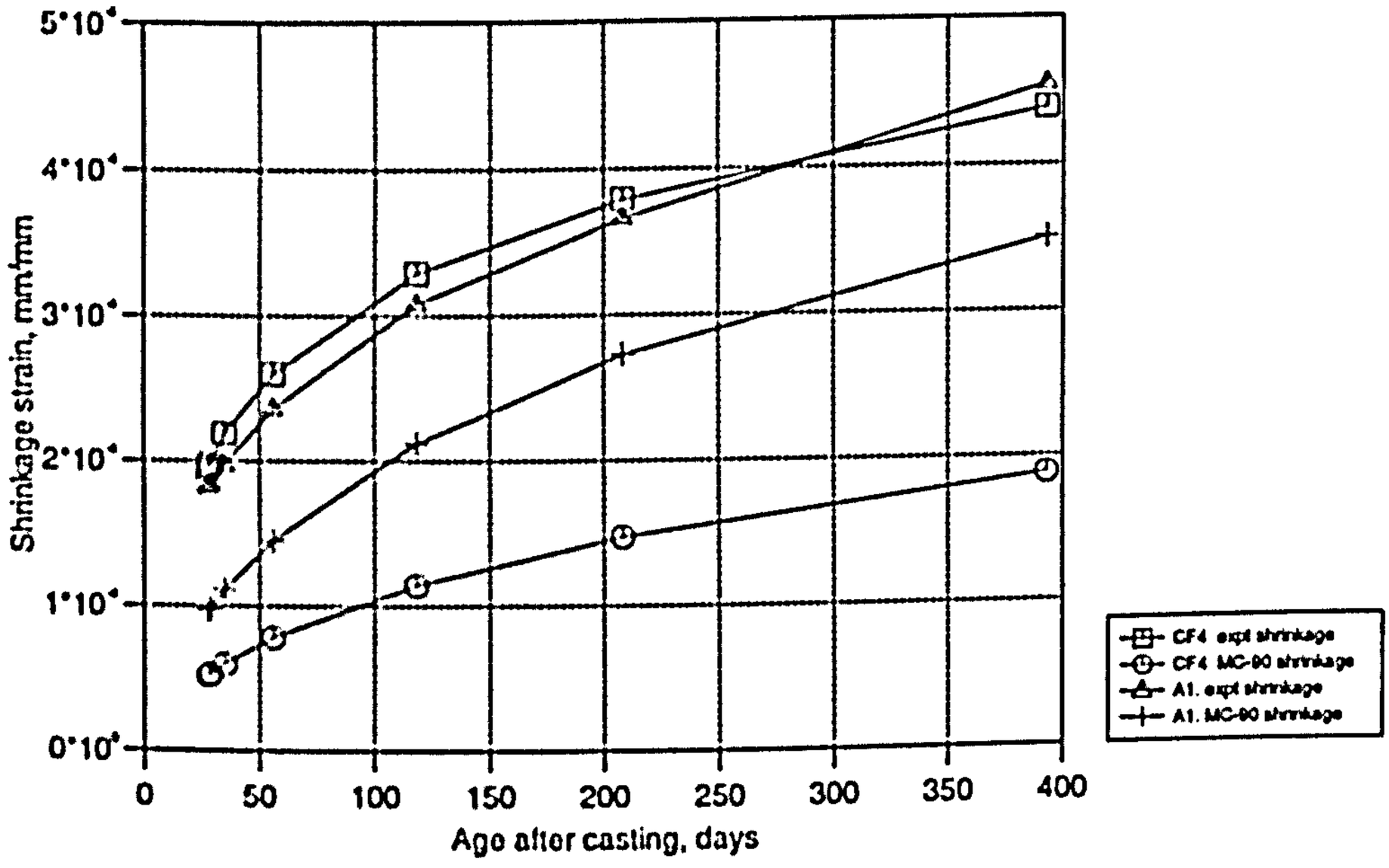


Figure 4.44 Experimental and MC-90 shrinkage strain for concrete for slabs CF4 and A1

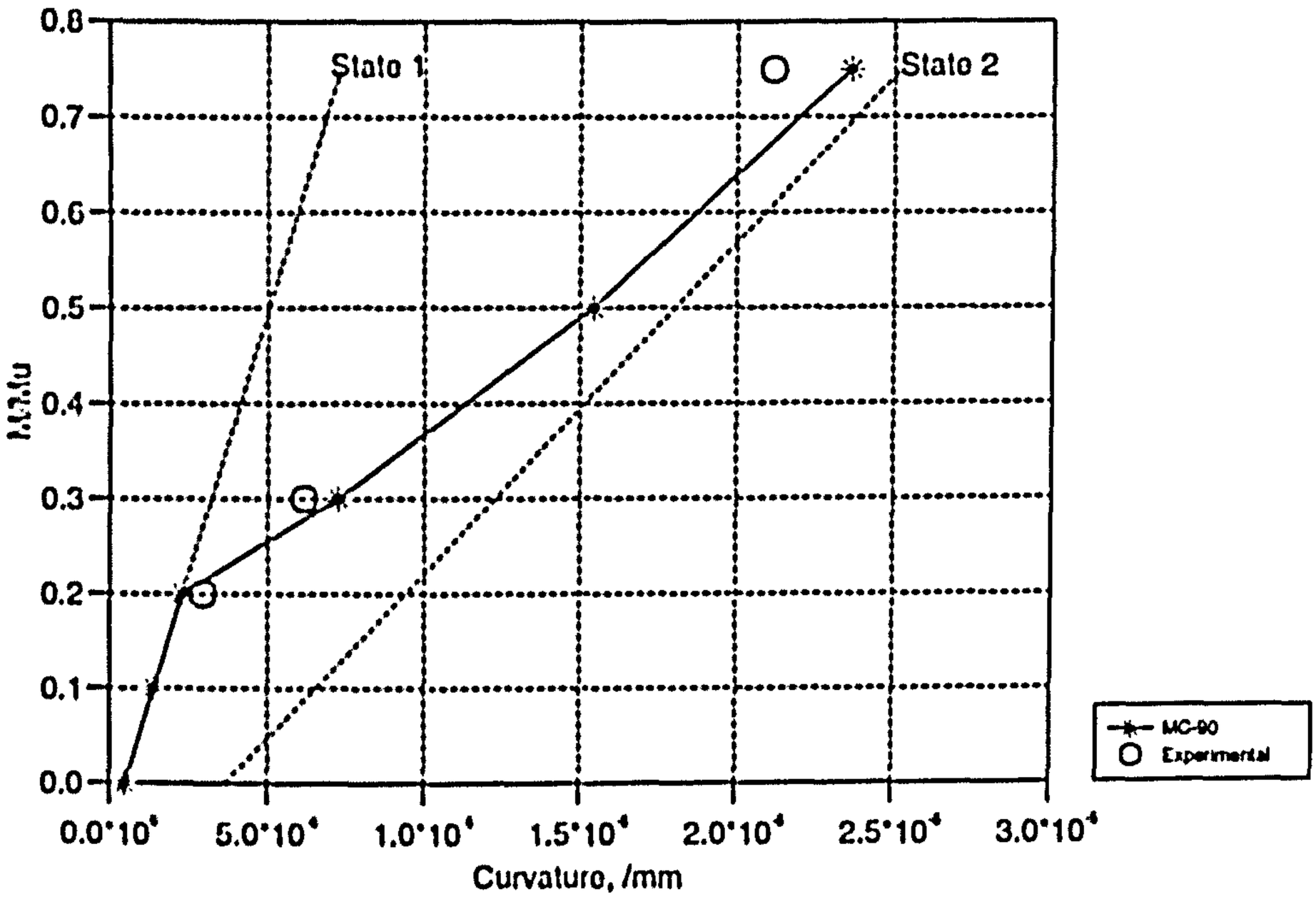


Figure 4.45 Moment-curvature relationship: Favre *et al.* slab A1

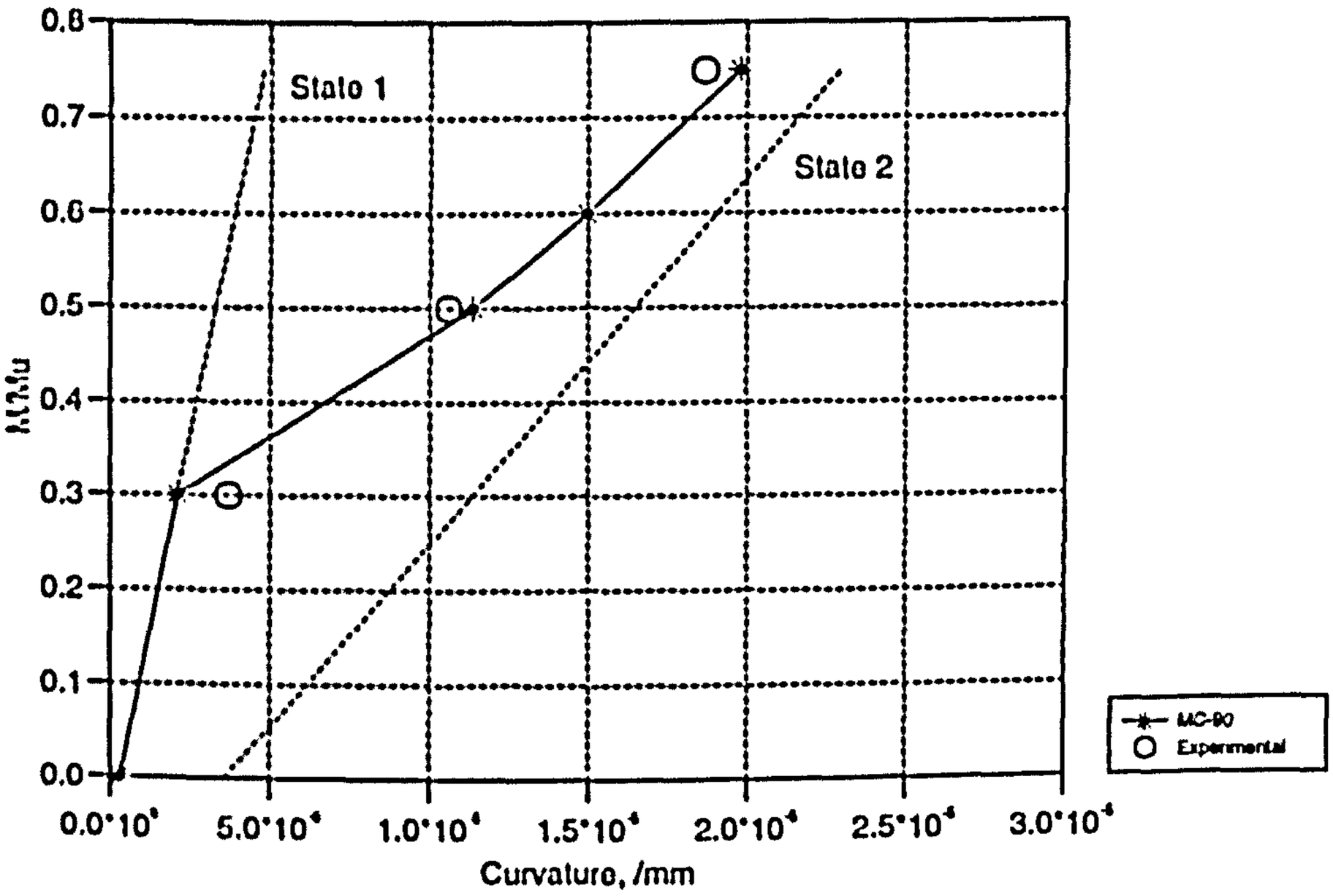


Figure 4.46 Moment-curvature relationship: Favre *et al.* slab CF4

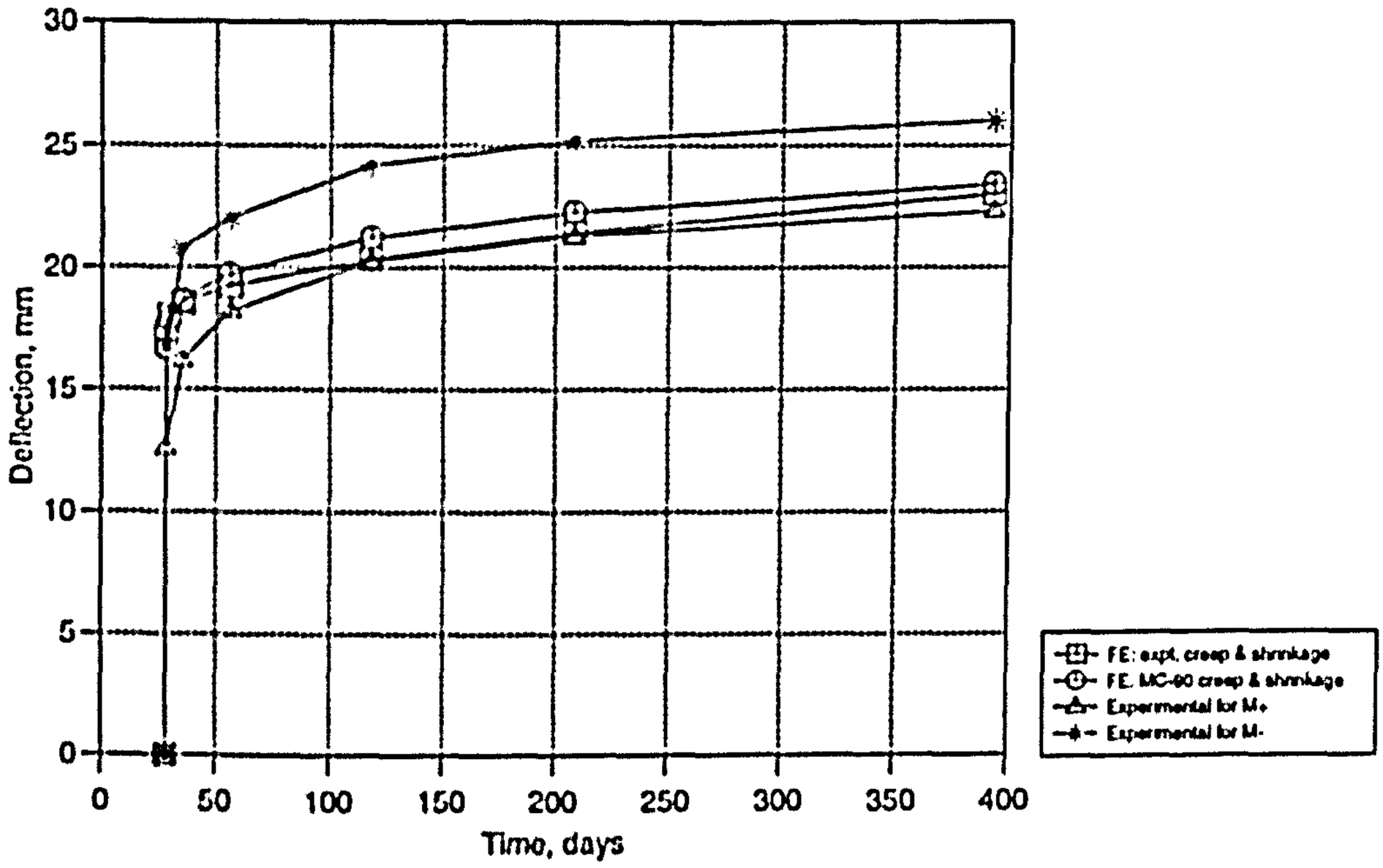


Figure 4.47 Deflection versus time: Favre *et al.* slab A1

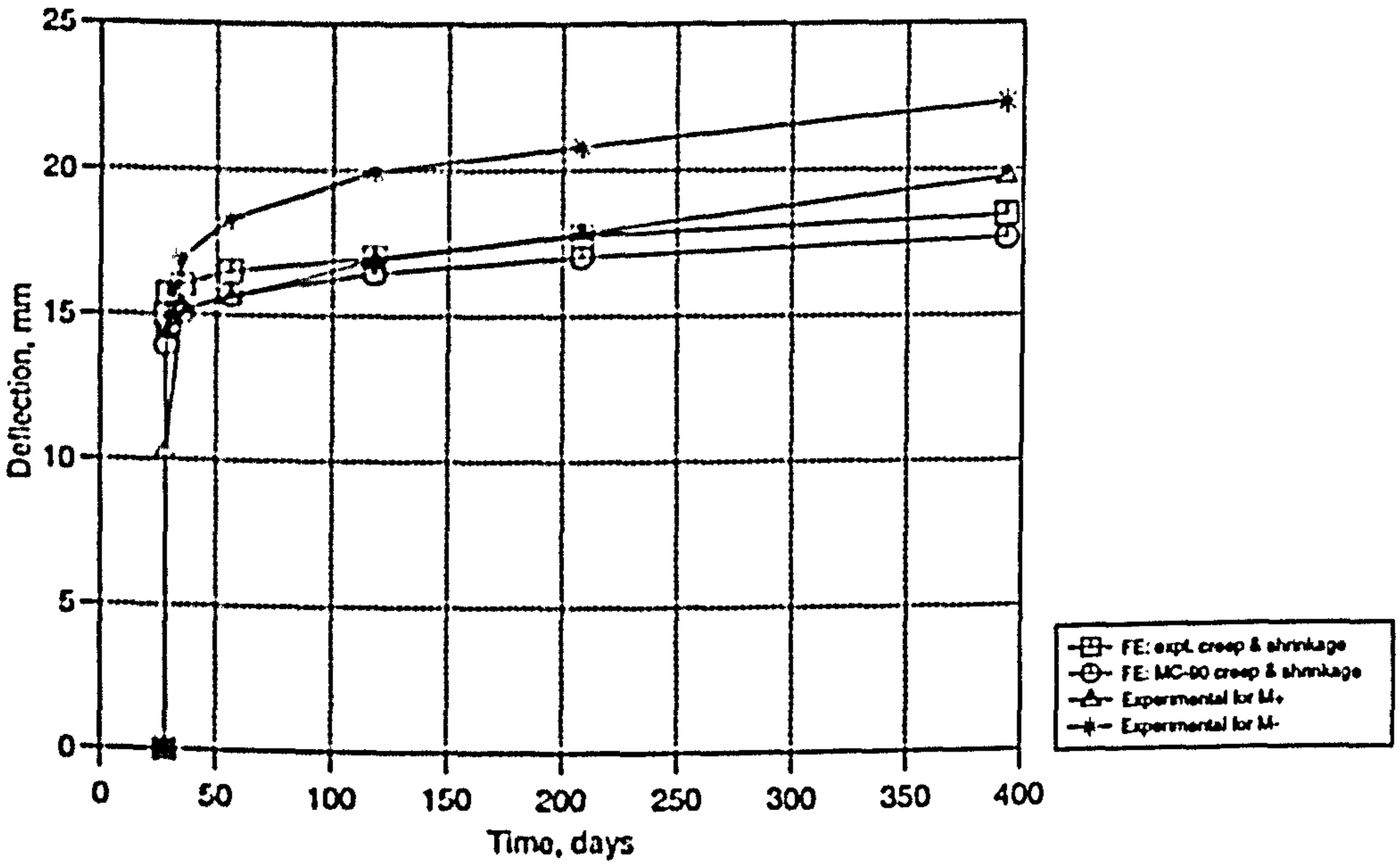


Figure 4.48 Deflection versus time: Favre *et al.* slab CF4

4.13.2 Ganeswaran & Rangan one-way slab

Slab details

Ganeswaran & Rangan (1996) performed a series of long-term tests on beams and one-way slabs. Three one-way spanning simply supported slabs with similar dimensions, but varying tensile steel percentages, have been considered in the present analysis. Details of the material properties, slab dimensions and the reinforcement are given in Fig. 4.49. The slabs were 500 mm wide, 2450 mm long and 100 mm thick, with a centre to centre span of 2300 mm. The percentages of tensile steel were 0.63, 0.80 and 0.98 and the slabs are designated as S/62-0.63, S/62-0.80, S/62-0.98 respectively. The slabs were made of high-strength concrete with a compressive strength of 62 MPa. Slabs were cured for 7 days and each were loaded at the third points of the span at 29 days with three different load levels according to their ultimate load capacity.

Analysis details

Ganeswaran & Rangan (1996) carried out creep and shrinkage tests on control specimens. They found that the MC-90 (1993) underestimated significantly (by about 35 to 55 percent) the shrinkage strains and overestimated the creep strains by as much as 50 percent. Similar conclusions have been drawn for the Favre *et al.* slab in section 4.13.1. The same pattern is obtained from the current analysis, and the creep and shrinkage strains obtained from experiment are compared with those obtained from the MC-90 equations in Figs 4.50 and 4.51. Predicted deflections along with experimental results are plotted against time for the three slabs in Figs 4.52 to 4.54. Deflections have been calculated using creep and shrinkage coefficients obtained both experimentally and with those obtained using the MC-90 equations presented in Appendix B. Deflections obtained with experimental coefficients are always higher than those obtained with the MC-90 coefficients. However, both predictions compare reasonably well with the actual deflection. Deflections were also calculated neglecting shrinkage. The results are given in Figs 4.52 to 4.54 which show.that a significant amount of the actual long-term deflection was due to shrinkage, which was not the case with the MC-90 which underestimates shrinkage.

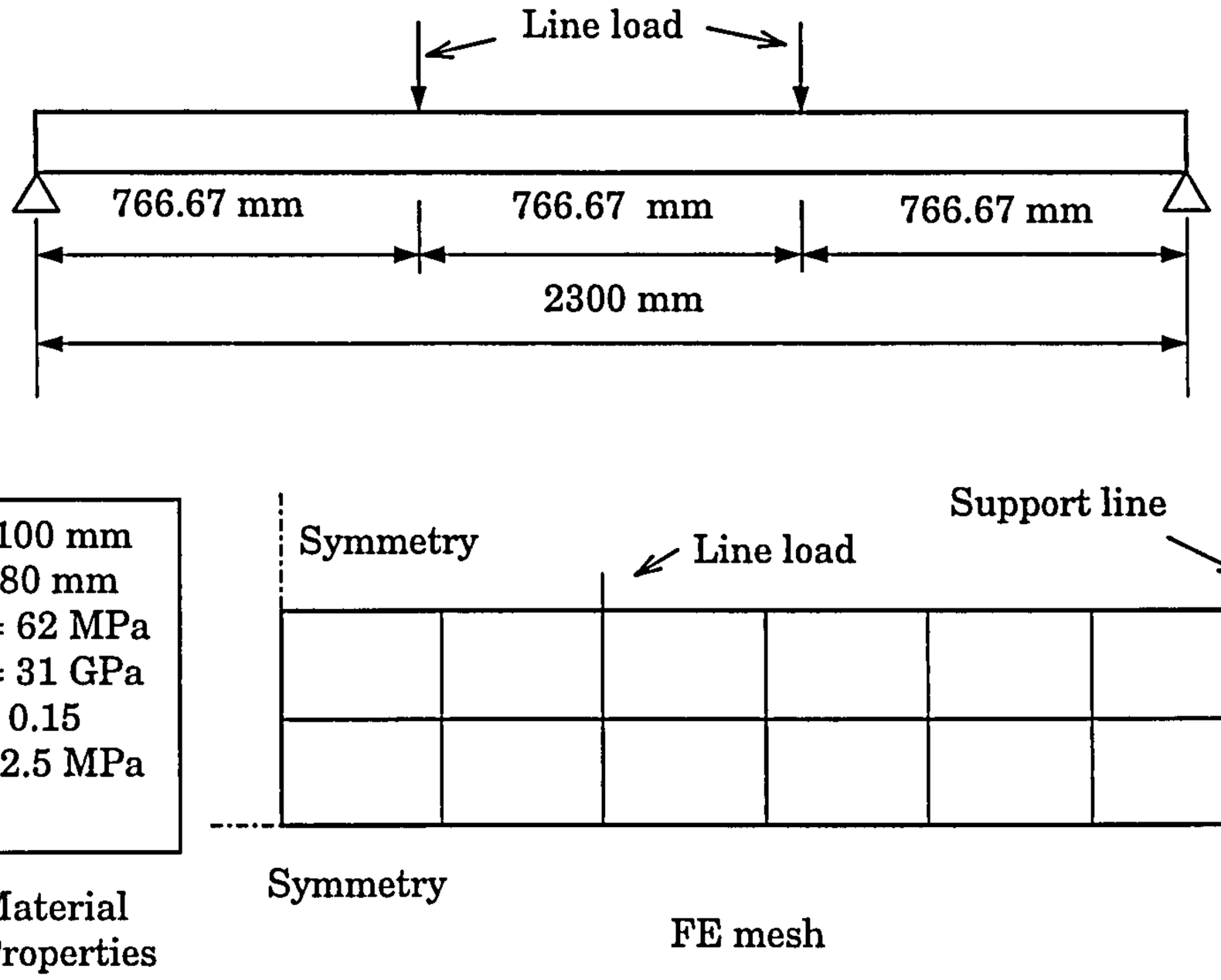


Figure 4.49 Details of one-way simply-supported slabs tested by Ganeswaran & Rangan (1996)

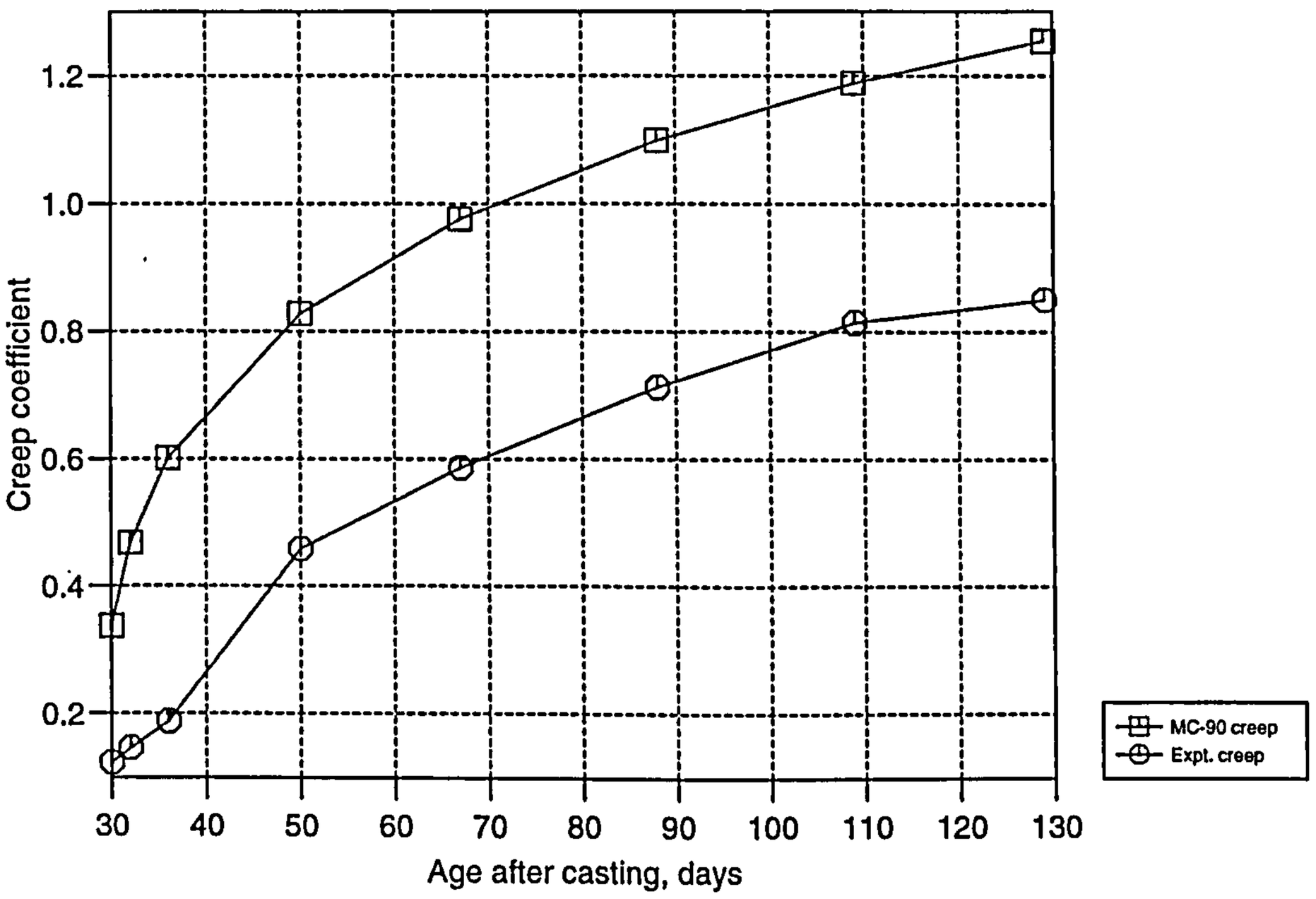


Figure 4.50 Experimental and MC-90 creep coefficient for concrete S/62

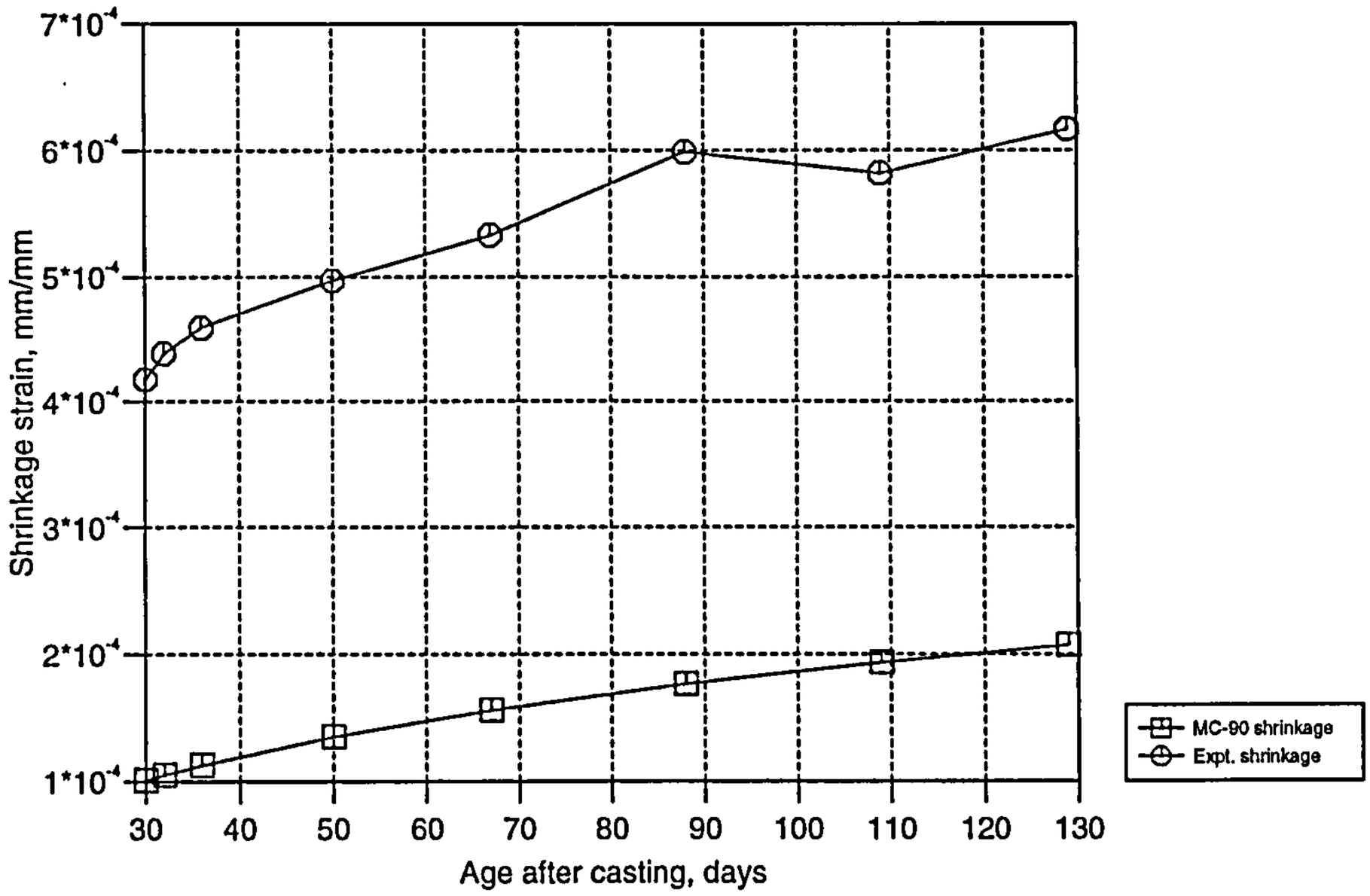


Figure 4.51 Experimental and MC-90 shrinkage strain for concrete S/62

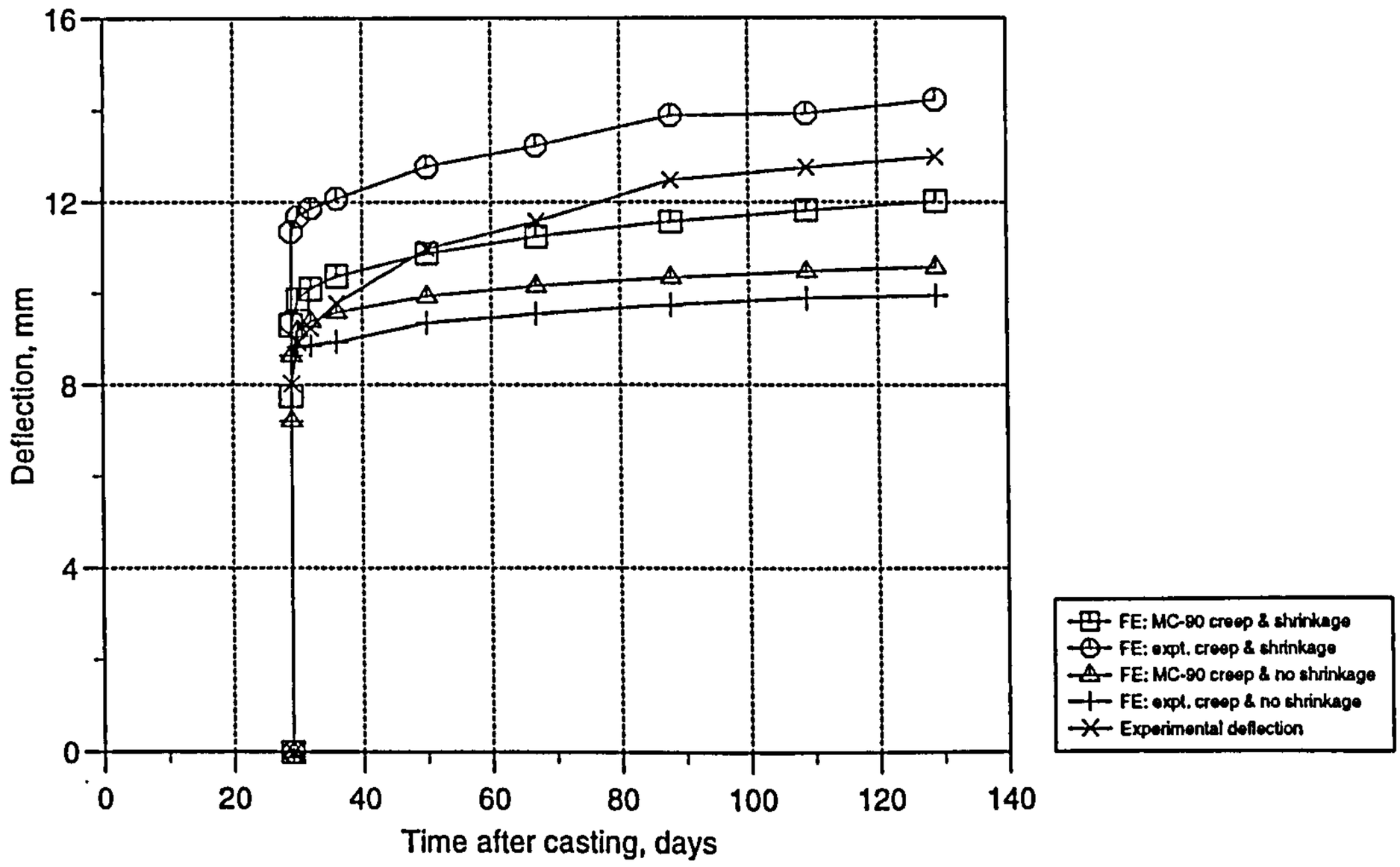


Figure 4.52 Deflection versus time: Ganeswaran & Rangan slab S/62-0.63

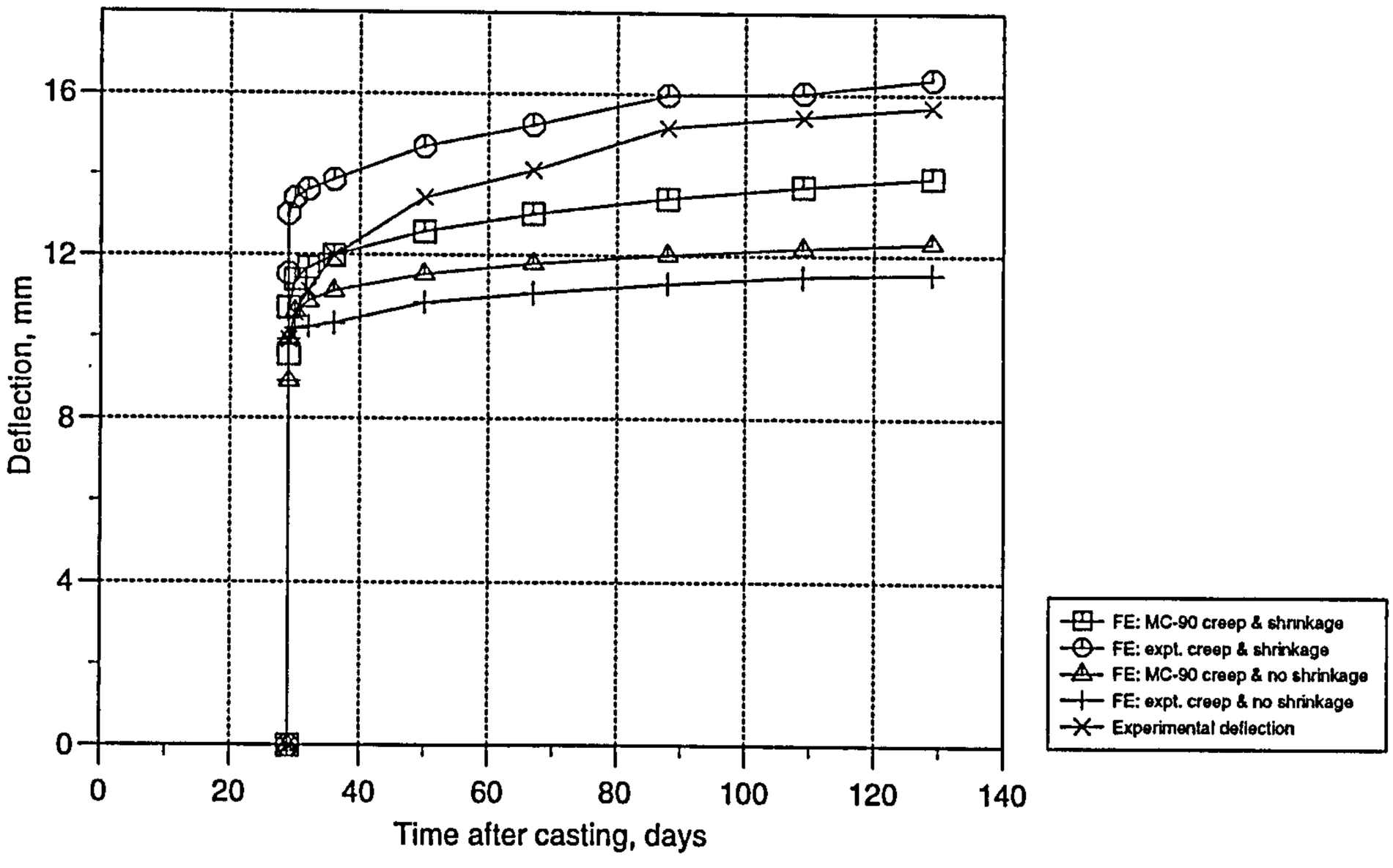


Figure 4.53 Deflection versus time: Ganeswaran & Rangan slab S/62-0.80

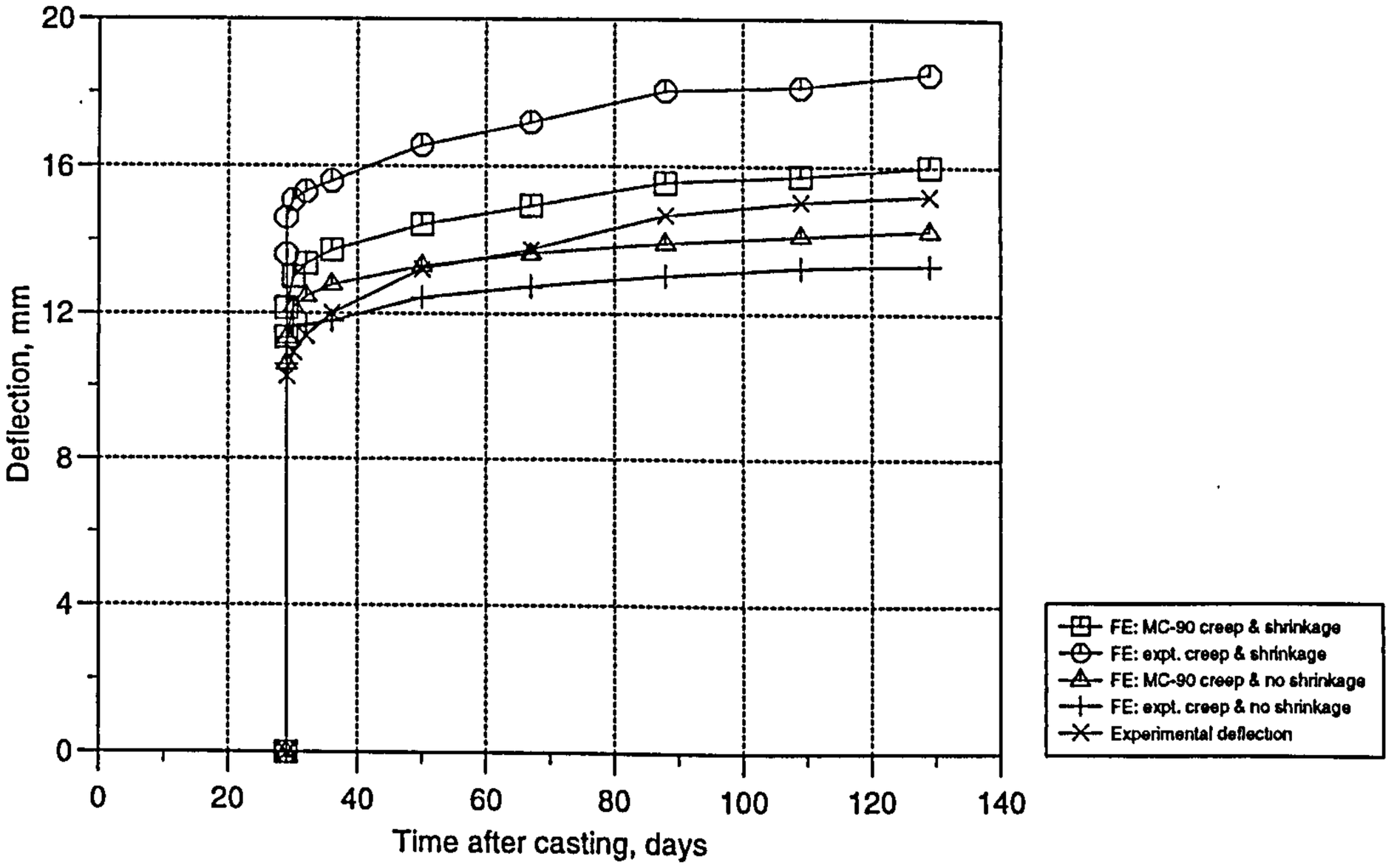


Figure 4.54 Deflection versus time: Ganeswaran & Rangan slab S/62-0.98

4.14 Concluding remarks

Several crack models and MC-90 long-term models have been successfully incorporated in an existing FE package. Details of their inclusion with relevant expressions used in the programming were presented in the chapter. Effect of modifying shear terms of $[E]$ matrix were studied and appropriate modified $[E]$ matrix was selected.

A thorough study was carried out to select a suitable method to find the effective steel in the principal directions from x and y directional steels. Different short- and long-term experiments were modelled with different possible equations. It has been found that equations obtained from Johansen's yield line criteria are the most suitable for predicting deflections.

Problems were also detected while modifying $[E]$ matrices on the basis of stress in any run of the iteration. The analysis fluctuates between two conditions. Gradually reducing section stiffness is shown to solve this problem of non-convergence. Several possible methods of reducing section stiffness were studied and a quick method was proposed which gives similar results to very gradually reducing stiffness.

Seven short-term and two long-term experimental deflections were modelled using the author's program. All the short-term models result in almost similar deflections. The predictions were very good for both short- and long-term deflections.

Chapter 5

Performance of ACI and MC-90 models for biaxial bending and compression

5.1 Introduction

In Chapter 4, both the ACI and MC-90 models were successfully incorporated in an FE package. The performances of both of these models in estimating flexural rigidities of a cracked section have been found to be adequate as deflection predictions by the FE package compared well with experimental results. The presence of an axial force complicates the estimate of curvature because the neutral axis is no longer at the centre of gravity of the section. Thus, the second moment of area of the fully cracked section becomes dependent on both the moment and the axial load applied. Sakai & Kakuta (1980) developed a method of calculating curvatures for one directional eccentricity using ACI effective moment of inertia relationship and CEB-FIP Model Code moment-curvature relationship and compared the predictions with their experimental results. A similar method, however, more generalised with the capabilities of modelling curvature due to an axial load applied with two directional eccentricity is developed by the author. This will be useful in predicting curvatures of columns due to cracking, creep and shrinkage under a two-directional eccentric load. A computer program has been developed to determine the depth of

the neutral axis of the fully cracked section under biaxial moment and compression by trial and error. The MC-90 and ACI equations are then incorporated to calculate the mean curvature by interpolating between uncracked and fully cracked sections. A simplified FE method with equivalent sections, obtained from mean curvatures, has also been proposed.

5.2 Assumptions

The present numerical analysis is based on the following assumptions:

1. Plane sections remain plane during bending.

2. The stress-strain relations for the concrete and steel making up the column are known.

3. Perfect bond exists between steel and concrete elements.

4. The effect of crushing of concrete is not considered.

5. All the displacements are small enough to neglect second-order effects.

5.3 Short-term analysis

5.3.1 Curvature in state 1

Consider a concrete section reinforced by a number of layers of steel and subjected to a compressive load N at A as shown in Fig. 5.1, point A being in a position to create biaxial bending moment. When the section is uncracked (i.e. the maximum tensile stress is less than the tensile strength), the eccentric normal force can be replaced by a normal force acting on the centroid of the transformed section and two bending moments. The position of the centroid and the moment of inertia about the x and y axes are calculated on the basis of the transformed section. Moments M_{xx} and M_{yy} are calculated about two orthogonal axes passing through the centroid and the curvatures are found by dividing them by the respective flexural rigidity :

$$\psi_{1x}(t_0) = \frac{M_{xx}}{E_c(t_0) * I_{xx}} \tag{5.1}$$

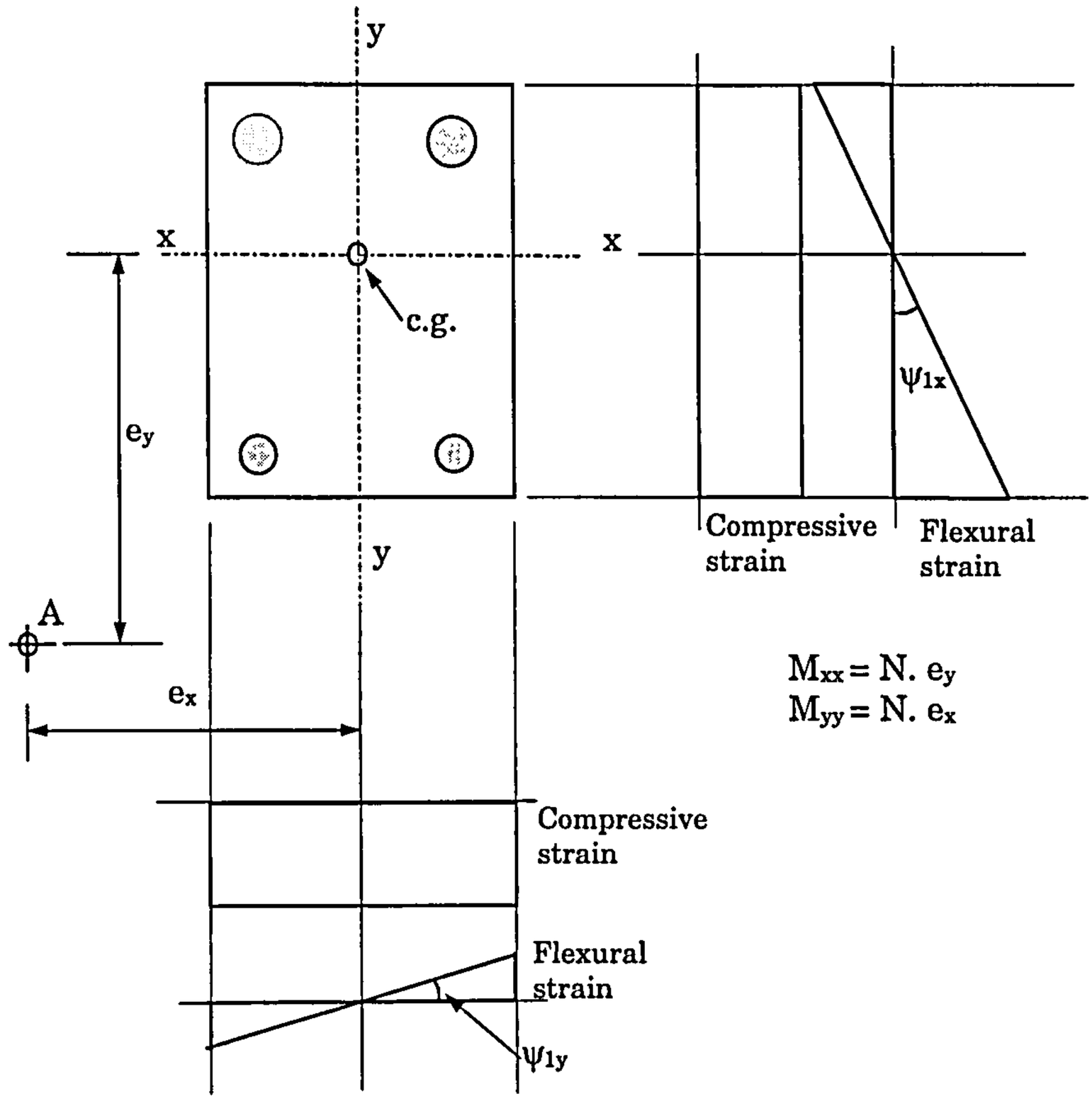


Figure 5.1 Curvature in state 1

$$\psi_{1y}(t_0) = \frac{M_{yy}}{E_c(t_0) * I_{yy}} \tag{5.2}$$

The resultant curvature and its direction is obtained by

$$\psi_1(t_0) = \sqrt{\psi_{1x}^2(t_0) + \psi_{1y}^2(t_0)} \tag{5.3}$$

$$\theta_1(t_0) = \tan^{-1} \frac{\psi_{1y}(t_0)}{\psi_{1x}(t_0)} \tag{5.4}$$

Unlike the MC-90 method, the ACI method neglects the reinforcement in the calculation of the second moment of area of the uncracked section.

5.3.2 Curvature in state 2

Consider the same concrete section subject to an eccentric compressive load that produces biaxial bending where the maximum tensile stress exceeds the tensile strength to cause cracking. The cracked section and accompanying strain diagram are shown

in Fig. 5.2. Assuming the perpendicular distance from the concentrated load to

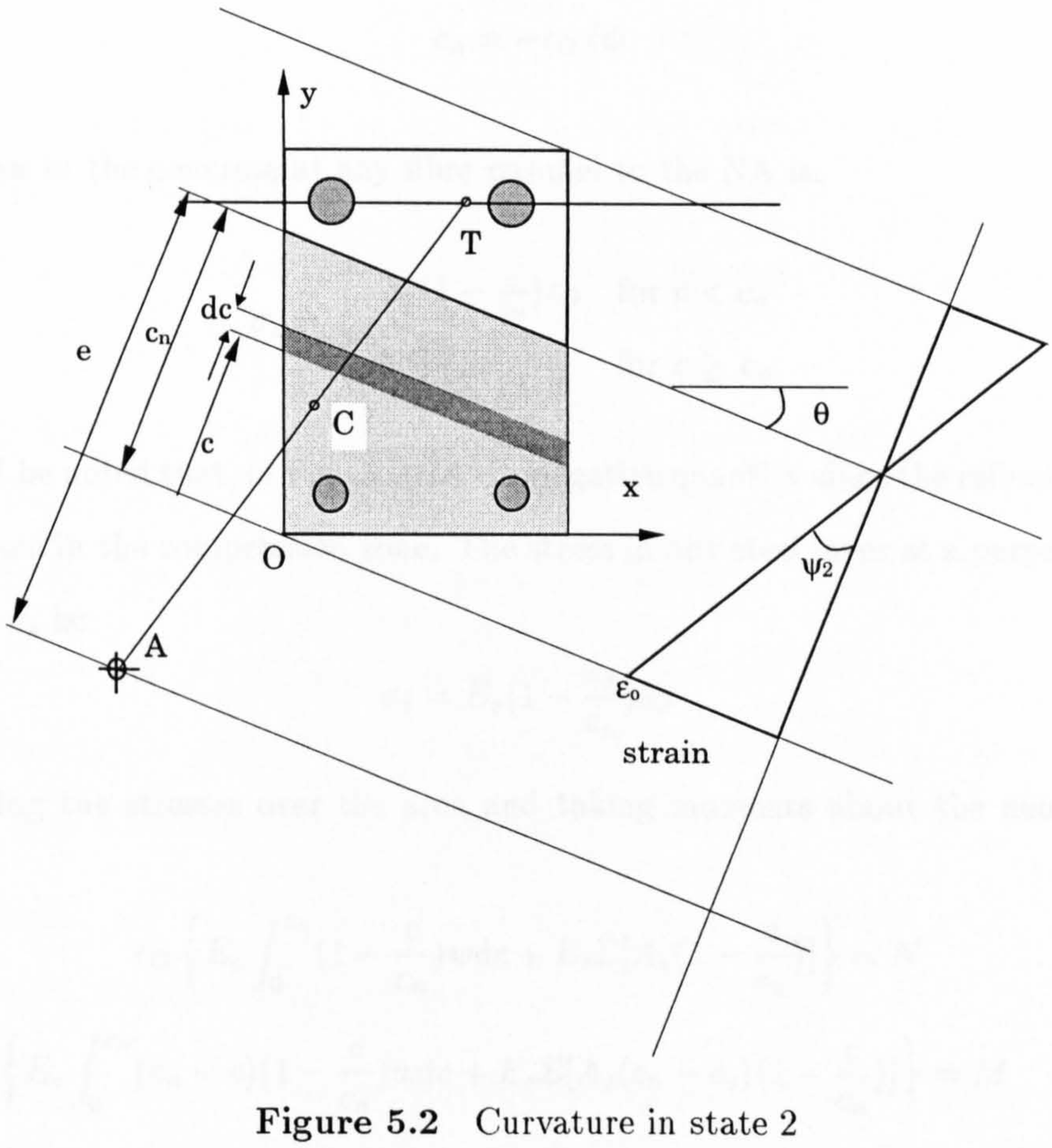


Figure 5.2 Curvature in state 2

the neutral axis to be e, the moment about the neutral axis is:

$$M = N.e \tag{5.5}$$

The location and orientation of the neutral axis depends on the value of e, not on the separate values of M and N. In the analysis presented below, the area considered effective in resisting the internal forces is composed of the area of the concrete compression zone plus the area of the reinforcement. The equations given below enable the determination of the depth c_n and the orientation angle θ_n of the neutral axis. The bottom left corner of the section is taken as the reference point to measure all the distances and θ is measured clockwise from the x axis.

The strain at any fibre (Fig. 5.2) is:

$$\epsilon = \epsilon_O + c\psi \tag{5.6}$$

The perpendicular distance of the neutral axis from the reference point is:

$$c_n = -\epsilon_O/\psi \tag{5.7}$$

The stress in the concrete at any fibre parallel to the NA is:

$$\sigma_c = \begin{cases} E_c(1-\frac{c}{c_n})\epsilon_O & \text{for } c < c_n \\ 0 & \text{for } c \geq c_n \end{cases} \tag{5.8}$$

It should be noted that, in Fig. 5.2, ϵ_O is a negative quantity since the reference point O is chosen in the compression zone. The stress in any steel layer at a perpendicular distance c_s is:

$$\sigma_s = E_s(1-\frac{c_s}{c_n})\epsilon_O \tag{5.9}$$

Integrating the stresses over the area and taking moments about the neutral axis gives:

$$\epsilon_O\left\{E_c\int_0^{c_n}(1-\frac{c}{c_n})w\mathrm{d}c + E_s\Sigma[A_s(1-\frac{c}{c_n})]\right\} = N \tag{5.10}$$

$$\epsilon_O\left\{E_c\int_0^{c_n}(c_n-c)(1-\frac{c}{c_n})w\mathrm{d}c + E_s\Sigma[A_s(c_n-c_s)(1-\frac{c}{c_n})]\right\} = M \tag{5.11}$$

where

$\mathrm{d}c$ = infinitesimal thickness of concrete elemental area in compression

w = width of concrete elemental area in compression

A_s and c_s = the area of a reinforcing bar and its perpendicular distance to a line passing through reference point and parallel to the neutral axis

c_n = depth of the neutral axis

E_s and E_c = the moduli of elasticity of steel and concrete

The summations in eqs 5.10 and 5.11 are for all the reinforcing bars.

When $N \neq 0$, the neutral axis does not coincide with the centroid of the transformed section. The equation to be solved for c is obtained by division of eq. 5.11 by eq. 5.10:

$$\frac{\int_0^{c_n}(c_n-c)^2w\mathrm{d}c + \alpha\Sigma[A_s(c_n-c_s)^2]}{\int_0^{c_n}(c_n-c)w\mathrm{d}c + \alpha\Sigma[A_s(c_n-c)]} - e = 0 \tag{5.12}$$

When the load is applied to produce biaxial bending, an additional condition is

needed to find the two unknowns, i.e. the depth and orientation of the neutral axis c_n and θ_n. The second condition is that the applied load, and the resultants of the compressive and tensile stresses should lie on a straight line. It should be noted that for biaxial bending, axis of bending is no longer parallel to neutral axis but perpendicular to line joining centres of tensile and compressive stress resultants.

The following iterative procedure is adopted in the computer program to find c_n and θ_n by trial and error:

1. The lower and upper limits of c and θ and the increments by which they are to be varied are selected for the analysis; initially c is varied from zero to the uncracked neutral axis depth, and θ is varied from 0 to 90°.

2. For each set of c and θ, the perpendicular distance from the applied load to the assumed position of the neutral axis e is found and the transformed areas subjected to compression and tension are calculated.

3. An arbitrary value of strain ϵ_0 is assumed at the reference point and the corresponding stress is computed.

4. Using this stress and assuming a linear stress diagram having zero value at the neutral axis, the total compressive and tensile stress resultants C and T, and their coordinates, are found.

5. Distances from the load to the compressive and tensile resultants are found and by multiplying these distances with the compressive and tensile resultants, the resulting compressive and tensile moment M_C and M_T at the load point are found.

6. For each set of c and θ, the value of $(M_C - M_T)$ and the slope and distance of the line connecting C, T and N are calculated.

7. When $(M_C - M_T)$ becomes zero and C, T and the external load N lie on the same line for a particular set of c and θ, the set defines the position and orientation of the neutral axis.

8. If these two conditions are not satisfied simultaneously, the lower and upper values of c and θ which are close to satisfying the two conditions by some level

of tolerance are selected as the limits of step 1. At the same time increments are made smaller.

9. Steps 1 to 8 are repeated until step 7 is satisfied. The lower and upper limits of the trial become closer to each other with increments and level of tolerance becoming smaller in each iteration. The whole iteration process is reasonably fast and converges to a set of c and θ to define the position and orientation of the neutral axis quite rapidly.

After obtaining the required solutions, the actual concrete strain at the reference point is obtained by:

$$\epsilon_0 = \frac{N}{E_c(C-T)} \tag{5.13}$$

The curvature of the fully cracked section at time t_0 then follows:

$$\psi_2(t_0) = \frac{\epsilon_0}{c_n} \tag{5.14}$$

Numerical example

Brøndum-Nielsen (1997) adopted a modified Newton-Raphson iteration technique for a similar serviceability analysis of a concrete section under biaxial bending. His work is different from the present work in two ways. First, his objective was to perform the stress calculation on a cracked section without any tension in concrete where as in the present work section calculation is carried with an aim to find the mean curvature considering tension stiffening. Secondly, he used a modified Newton-Raphson method and the current work is based on trial and error iteration technique. However, his works gave an opportunity to check the author's method of finding neutral axis and stresses in steel. Brøndum-Nielsen presented a numerical example for five separate cases for the cross-section shown in Fig. 5.3, varying the position of the eccentric load and the reinforcement as follows:

- Case 1: Pentagonal compression zone
- Case 2: Trapezoidal compression zone with parallel sides in the x-direction
- Case 3: Triangular compression zone

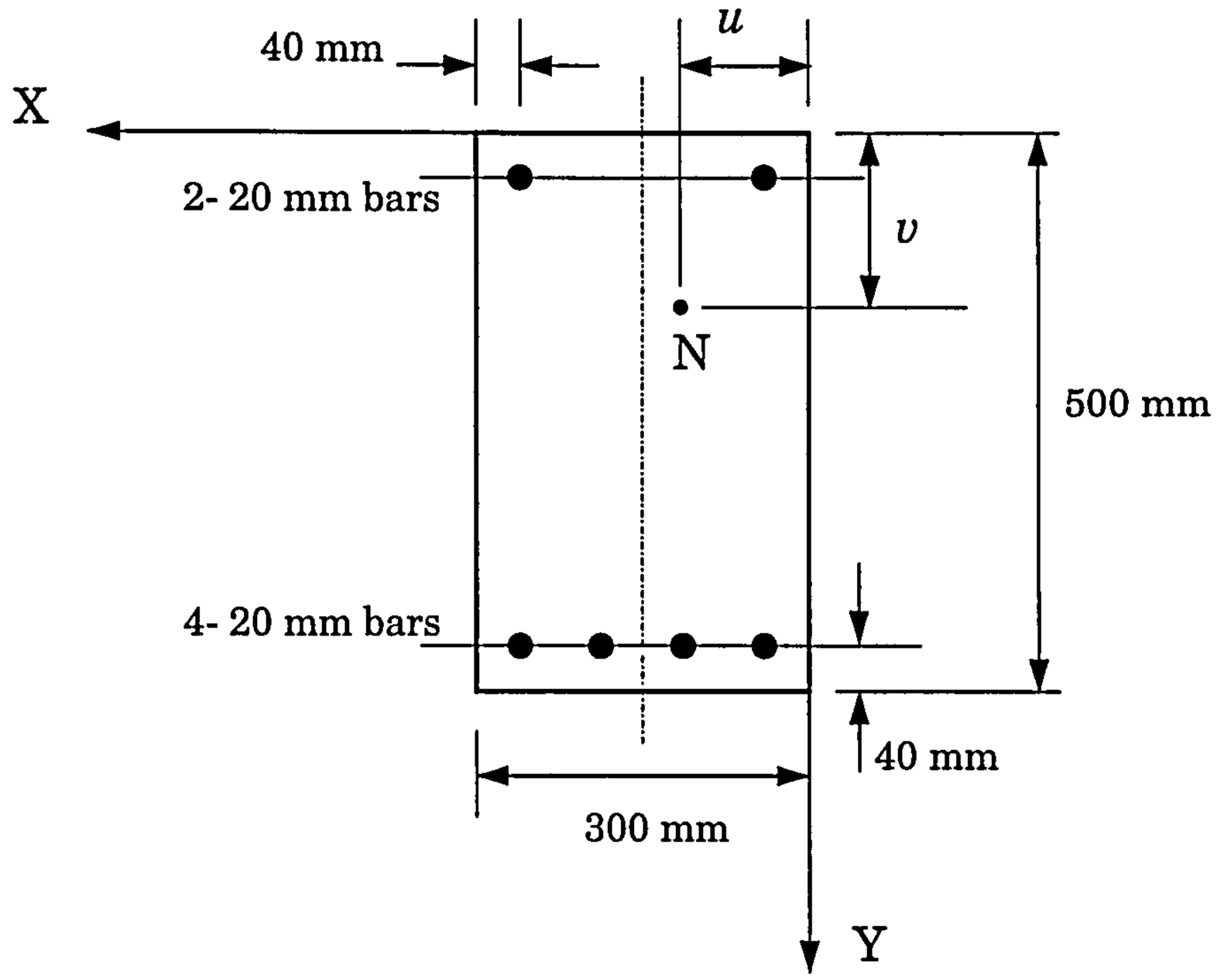


Figure 5.3 Cross-section analysed in numerical example: adapted from Brøndum-Nielsen (1997)

- Case 4: Trapezoidal compression zone with parallel sides in the y-direction

- Case 5: Identical to case 4 with the sole exception that the bottom reinforcement only consists of the two corner bars

The same five cases have been analysed using the present method with the trial and error solution technique. The position and orientation of the neutral axis (see Fig. 5.4) and the maximum tension and compression in the reinforcement calculated are presented in Table 5.1 with Brøndum-Nielsen's values shown in brackets. Both the analyses lead to almost the same results, the slight difference being due to the different iteration techniques.

Parameter	Unit	Case 1	Case 2	Case 3	Case 4	Case 5
u	mm	100	-100	-100	100	100
v	mm	150	150	-300	-150	-150
c_n	mm	374.9 (375.3)	138.2 (137.6)	221.4 (220.9)	283.5 (283.0)	233.5 (232.77)
θ_n	degree	55.9 (55.9)	85.6 (85.6)	60.4 (60.5)	23.6 (23.7)	19.6 (19.5)
Max σ_s	MPa	7.48 (7.37)	93.7 (93.5)	152.9 (152.1)	57.9 (57.7)	97.7 (97.3)
Min σ_s	MPa	-24.3 (-24.0)	-57.0 (-56.4)	-110.2 (-109.1)	-55.2 (-54.6)	-62.1 (-61.4)

Table 5.1 Position and orientation of neutral axis and steel stresses for different load cases

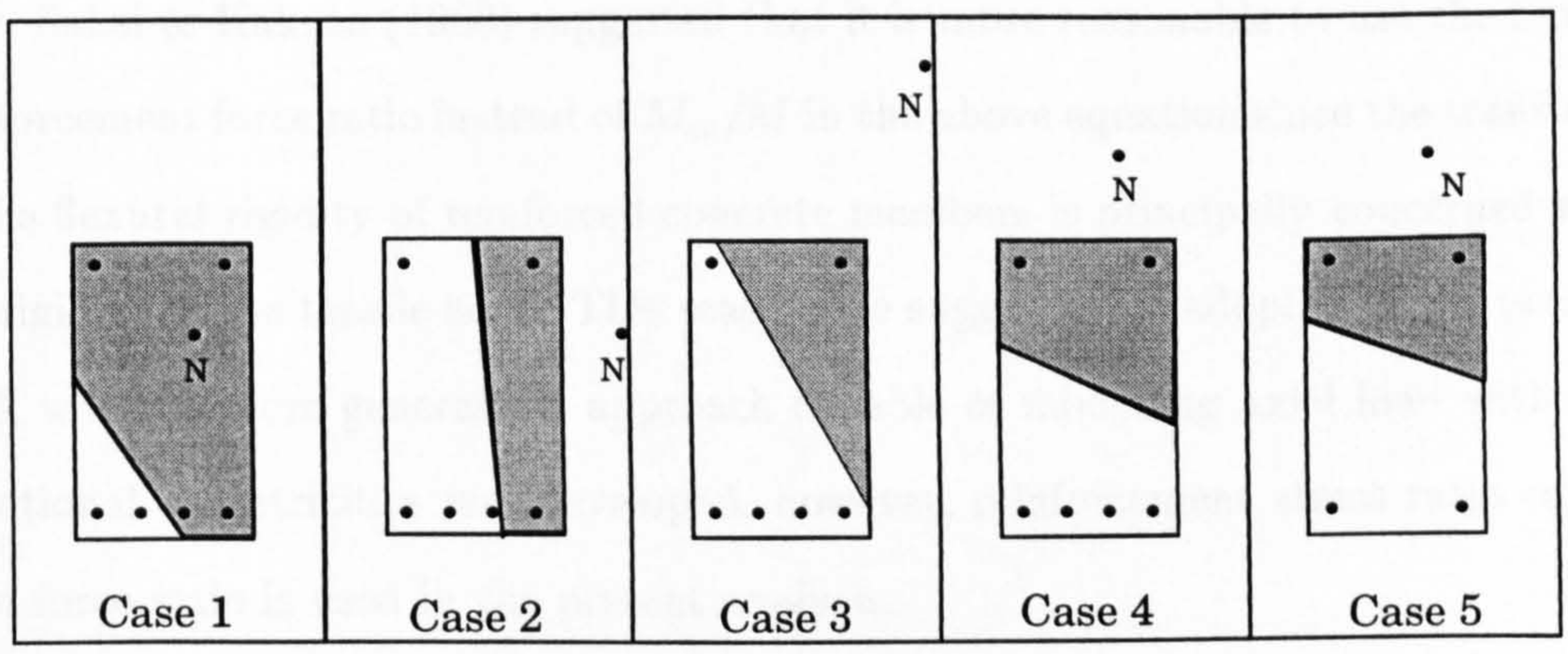


Figure 5.4 Location of axial loads and neutral axis

5.3.3 Mean inertia by ACI equations

ACI adopted Branson's equation to calculate the effective moment of inertia I_e using the gross inertia I_g and the cracked inertia I_{cr} in the following form:

$$I_e(t_0) = \left(\frac{M_{cr}}{M}\right)^m I_g(t_0) + \left(1 - \frac{M_{cr}}{M}\right)^m I_{cr}(t_0) \tag{5.15}$$

$I_g(t_0)$ can be obtained from the moment and curvature around the gross uncracked neutral axis by:

$$I_g(t_0) = \frac{M}{E_c \psi_g(t_0)} \tag{5.16}$$

Similarly, $I_{cr}(t_0)$ can be calculated from the moment and curvature around the fully cracked neutral axis by:

$$I_{cr}(t_0) = \frac{M}{E_c \psi_2(t_0)} \tag{5.17}$$

The values of $\psi_g(t_0)$ and $\psi_2(t_0)$ in the above eqs 5.16 and 5.17 can be obtained from eqs 5.3 (ignoring reinforcement) and 5.14 respectively. It should be noted here that moments in the above equations are, in fact, components of moments acting around neutral axis and as result calculated $I_g(t_0)$ and $I_{cr}(t_0)$ are equivalent moments of area around neutral axis.

Sakai & Kakuta (1980) presented a similar work using the above eq. 5.15, however, their work was limited to axial load applied with one directional eccentricity only. Sakai & Kakuta (1980) suggested that it is more reasonable to use the tensile reinforcement force ratio instead of M_{cr}/M in the above equation since the transition of the flexural rigidity of reinforced concrete members is principally concerned with the rigidity in the tensile zone. This reasonable suggestion is adopted in the present work where a more generalised approach capable of modelling axial load with two directional eccentricities was developed, however, reinforcement stress ratio rather than force ratio is used in the present analysis:

$$I_e(t_0) = \left(\frac{\sigma_{sr}}{\sigma_s}\right)^m I_g(t_0) + \left(1 - \frac{\sigma_{sr}}{\sigma_s}\right)^m I_{cr}(t_0) \tag{5.18}$$

where σ_{sr} and σ_s express the maximum tensile reinforcement stresses in the cracked

section at cracking and at applied load levels respectively. The ψ_2 is obtained corresponds to the rupture load found on the basis of gross uncracked section, and the maximum steel tensile stresses are found for this ψ_2.

A value of 3 for m is used in the present analysis according to the suggestions of Sakai & Kakuta (1980) as this value is compatible with their test results. The moment M around the neutral axis at state 2 is obtained and the mean curvature is found by dividing it by the mean rigidity:

$$\psi_m(t_0) = \frac{M}{E_c(t_0) I_e(t_0)} \tag{5.19}$$

The adoption of ACI method for column is different from that of slab in the use of stress ratio to interpolate between gross inertia and cracked inertia. In the case of slab (see section 4.7), a ratio of stress at the outer face of the gross concrete plate (found from FE analysis) and modulus of rupture was used. Whereas for column, the maximum tensile reinforcement stresses on the basis of cracked section are used and the ratio is calculated comparing stresses at cracking and at applied load levels.

5.3.4 Mean curvature by MC-90 equations

The mean curvature given by MC-90 guidelines is:

$$\psi_m(t_0) = (1 - \zeta)\psi_1(t_0) + \zeta\psi_2(t_0) \tag{5.20}$$

It should be noted that states 1 and 2 curvatures in the above equation are in two different directions. However, it has been observed that there directions are not significantly different and hence a scalar sum is employed instead of a more correct vector addition. Also, a mean angle θ_m is calculated from states 1 and 2 angles using a similar relationship like eq. 5.20. The coefficient ζ is employed to interpolate between the state 1 and 2 to obtain the mean. ζ is given by:

$$\zeta = 1 - \beta_1\beta_2 \left(\frac{\sigma_{sr}}{\sigma_s}\right)^2 \tag{5.21}$$

The ψ_2 is obtained corresponds to the rupture load found on the basis of state 1, and the maximum steel tensile stresses are found for this ψ_2.

The adoption of MC-90 method for column is different from that of slab in the use of stress ratio to interpolate between curvatures of states 1 and 2. In the case of slab (see section 4.8), a ratio of moments calculated on the basis of the gross concrete plate (i.e. M) and on the basis of transformed state 1 section reaching modulus of rupture at the face (i.e. M_r) was used. Whereas for column, the maximum tensile reinforcement stresses on the basis of cracked section are used and the ratio is calculated comparing stresses at cracking and at applied load levels.

5.4 Comparison with short-term experimental results

5.4.1 One-directional eccentricity: experiment by Sakai & Kakuta

Sakai & Kakuta (1980) performed a series of tests on reinforced concrete members with eccentric compressive axial force. The shapes and dimensions of the specimens used in their experiments are shown in Fig. 5.5. Table 5.2 indicates the identification and properties of the specimens. Sakai & Kakuta used eq. 5.15 to calculate theoretical moment-curvature relations, and in their analysis they assumed tensile strengths of concrete using both ACI and CEB-FIP Model Code equations. In the present study, both ACI (eq. 5.15) and MC-90 (eq. 5.20) equations have been considered and the corresponding provisions for the modulus of rupture or tensile strength have been adopted. Two levels of steel percentages (i.e. 0.932 and 0.596) were used in the tests. Moment-curvature curves calculated in the present work using both ACI and MC-90 equations are presented along with Sakai & Kakuta experimental results in Figs 5.6 and 5.7 for two different sets of reinforcement percentages. The curves are plotted with characteristic moments (M_c/bd^2f_c) against characteristic curvature (curvature times effective depth). A line defining the fully cracked section (i.e. state 2, no tension in concrete) is also plotted. Results obtained in the current analysis with both ACI and MC-90 models compare very well with experimental curvatures. Sakai & Kakuta's analytical results (not shown on the curves) are similar to those curvatures obtained in corresponding current analysis.

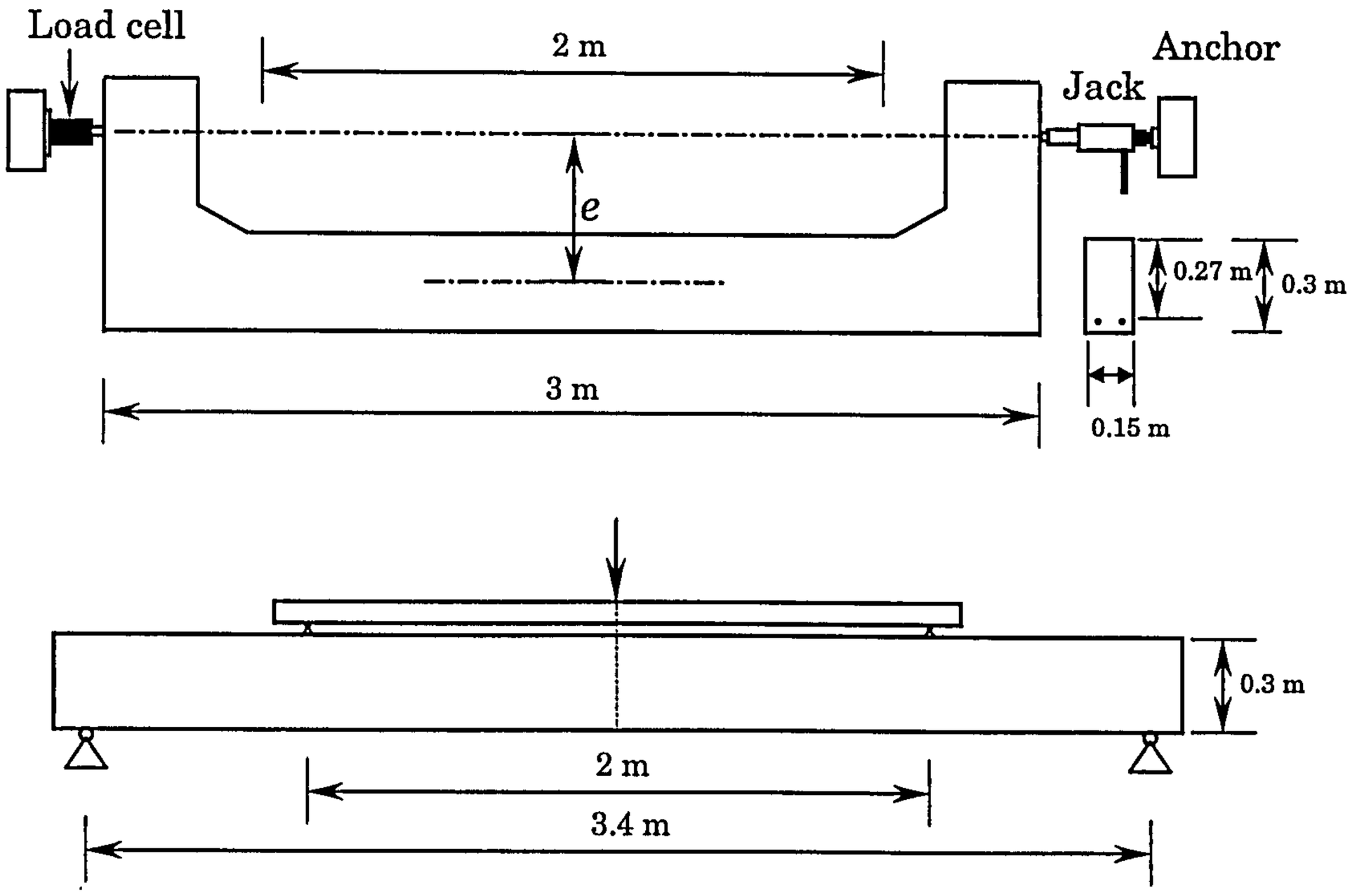


Figure 5.5 Test specimen and loading method, experiment by Sakai & Kakuta (1980)

Specimen	Eccentricity of load e, cm	Steel percentage ρ	Comp. strength of concrete f_c', kg/cm^2	Mod. of elasticity of concrete E_c (10^5), kg/cm^2
MN-35-16	35	0.932	313	2.75
MN-55-16	55	0.932	319	2.84
MN-65-16	65	0.932	298	2.91
MN-75-16	75	0.932	340	2.89
MN-85-16	85	0.932	319	3.09
MN-35-13	35	0.596	316	3.00
MN-55-13	55	0.596	313	2.94
MN-75-13	75	0.596	323	2.97

Table 5.2 Identification and properties of the Sakai & Kakuta specimens

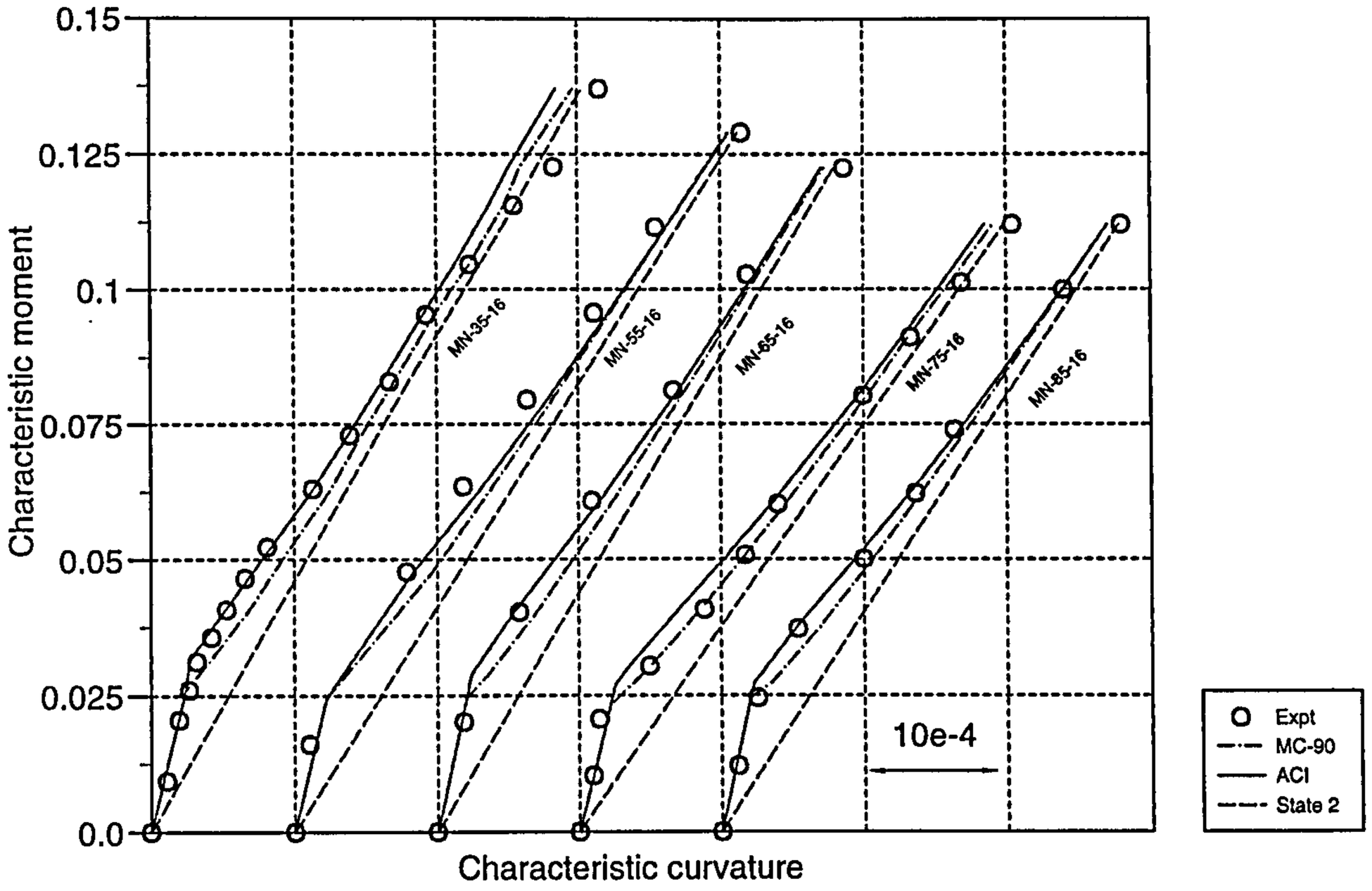


Figure 5.6 Moment-curvature curves for steel percentage 0.932 (experiment by Sakai & Kakuta)

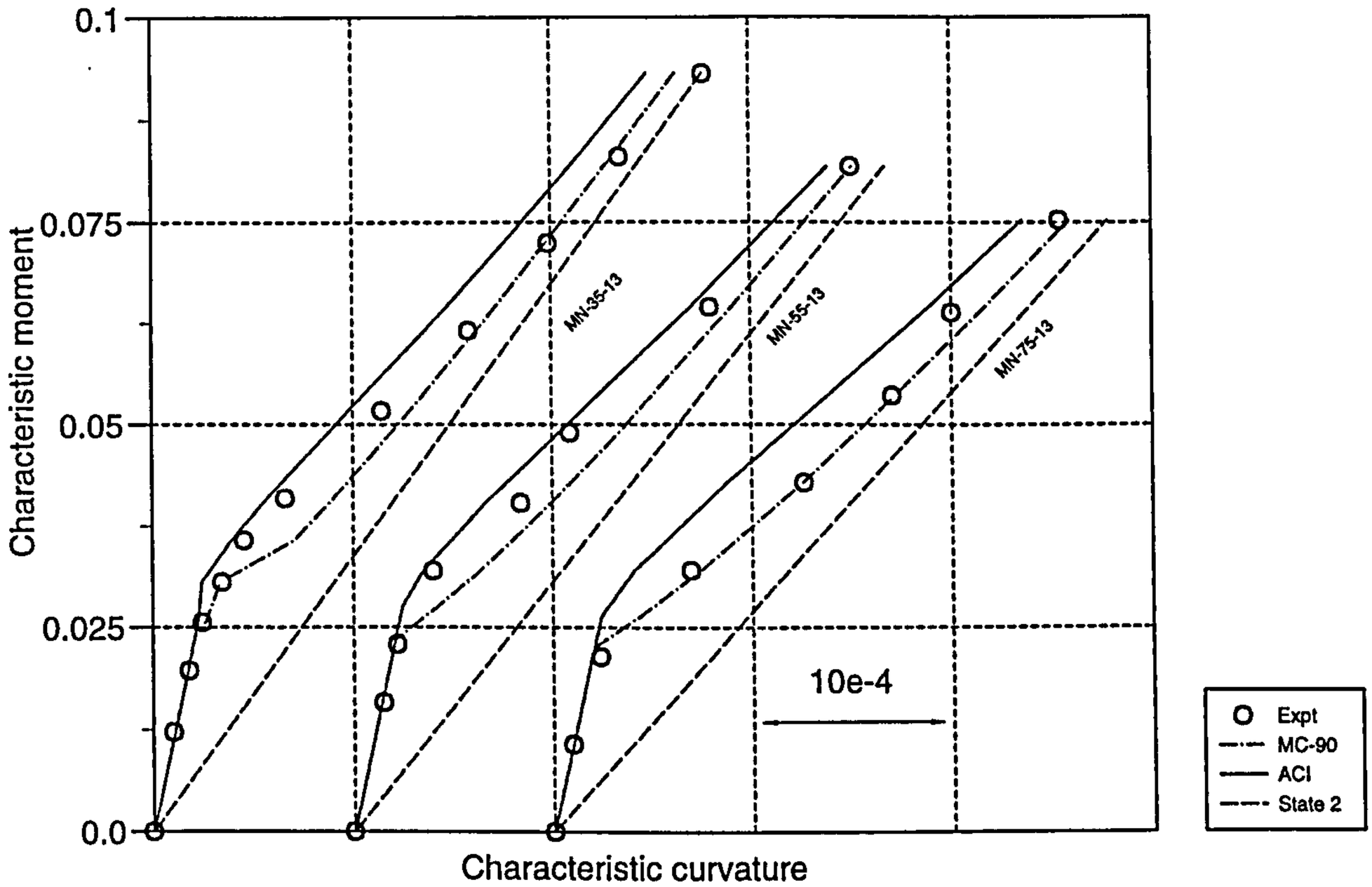


Figure 5.7 Moment-curvature curves for steel percentage 0.596 (experiment by Sakai & Kakuta)

5.4.2 Two-directional eccentricity: analysis by Hsu & Mirza

Hsu & Mirza (1973) presented a numerical example involving moment-curvature characteristics of structural concrete sections subjected to combined biaxial bending moment and axial load. They used a modified Newton-Raphson method to obtain convergence of solution satisfying equilibrium and compatibility conditions. The stress-strain curves for concrete including strain softening and the steel reinforcing including strain hardening were idealised using piece-wise linear approximation of the constitutive relationship, as a result their method is capable of modelling crushing of concrete or yielding of steel. Two cases have been studied by them, the first one with equal eccentricities in both directions and the second one with different eccentricities. Details of the column and material properties are presented in Fig. 5.8. Moment-curvature curves obtained using MC-90 and ACI models are shown along with the analytical results by Hsu & Mirza in Fig. 5.9 for the same eccentricity in both directions and in Figs 5.10 and 5.11 for different eccentricities in the two orthogonal directions. For the symmetric eccentric case, the prediction by Hsu & Mirza agrees very well with the current analysis. For the case with different eccentricities, the current analysis prediction agrees very well with those of Hsu & Mirza in the lower load range, but as the load increases Hsu & Mirza's curvatures are higher than those for the current analysis which does not include concrete crushing or steel yielding. The limitation of the present work is that it cannot model the failure at ultimate load. However, it is simpler than Hsu & Mirza method and the primary aim of the present work is to model behaviour at service load level for which it is proved quite accurate.

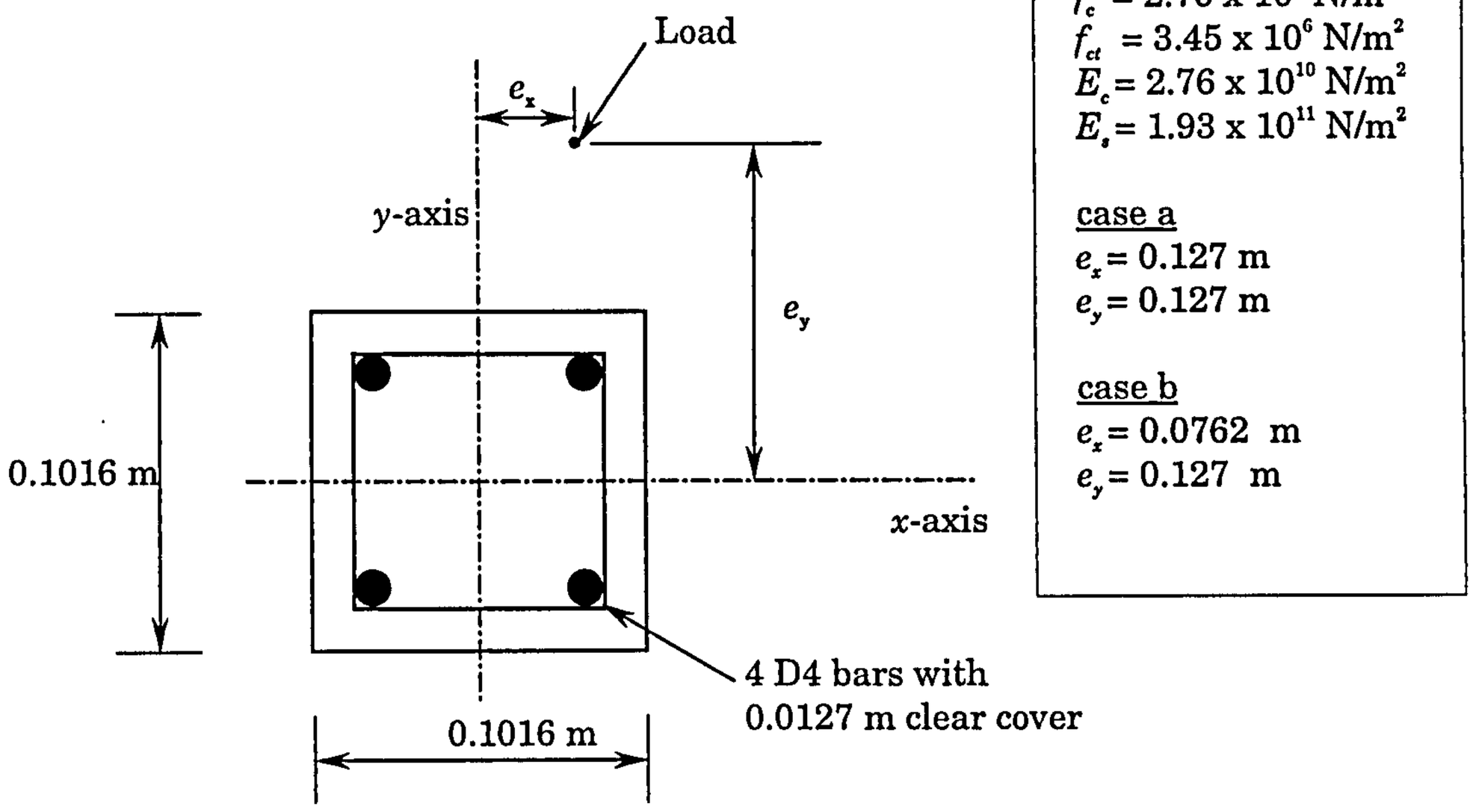


Figure 5.8 Details of section with material properties, analysis by Hsu & Mirza (1973)

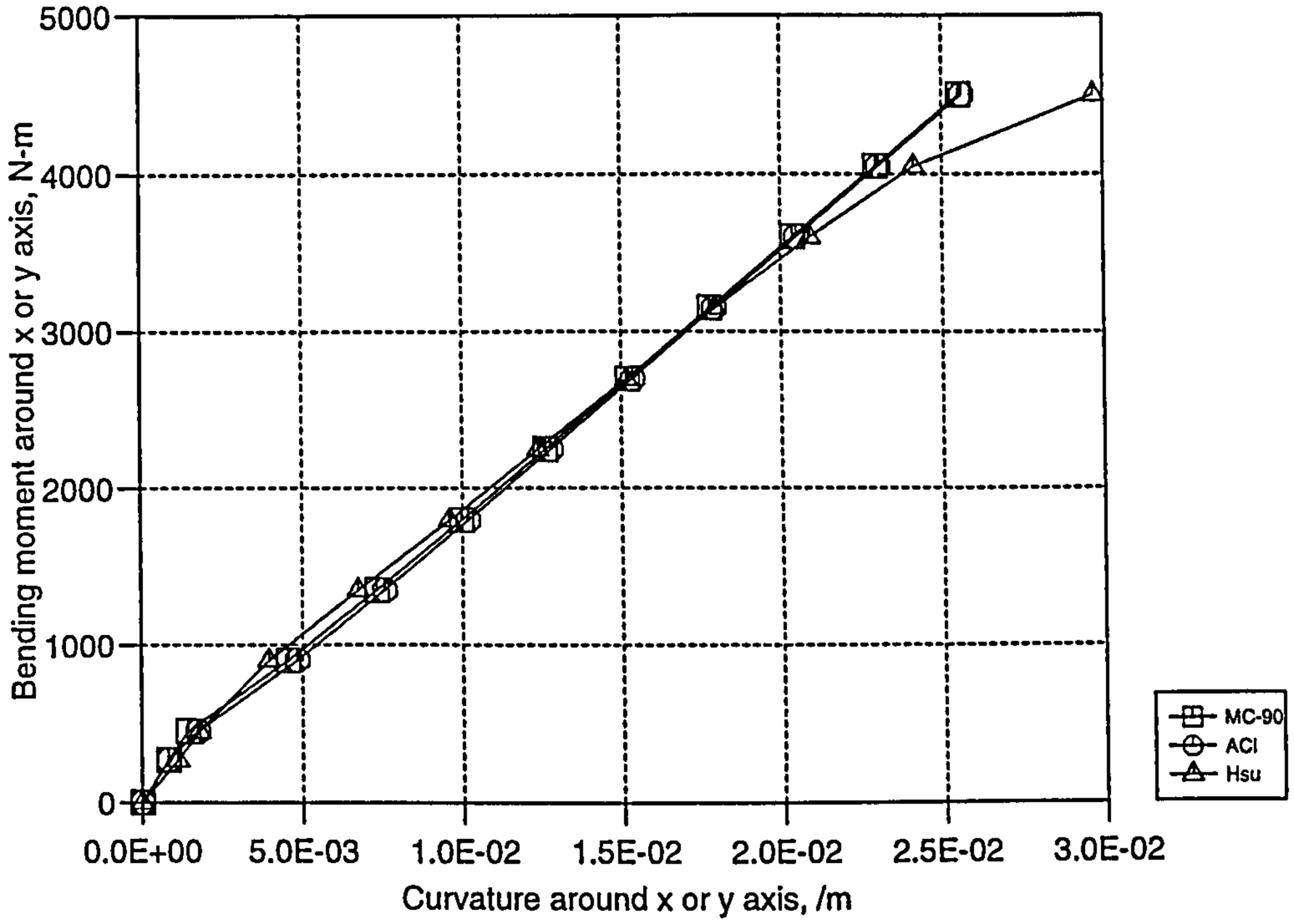


Figure 5.9 Moment-curvature curves: around x- or y-axis, analysis by Hsu & Mirza, ACI and MC-90 model

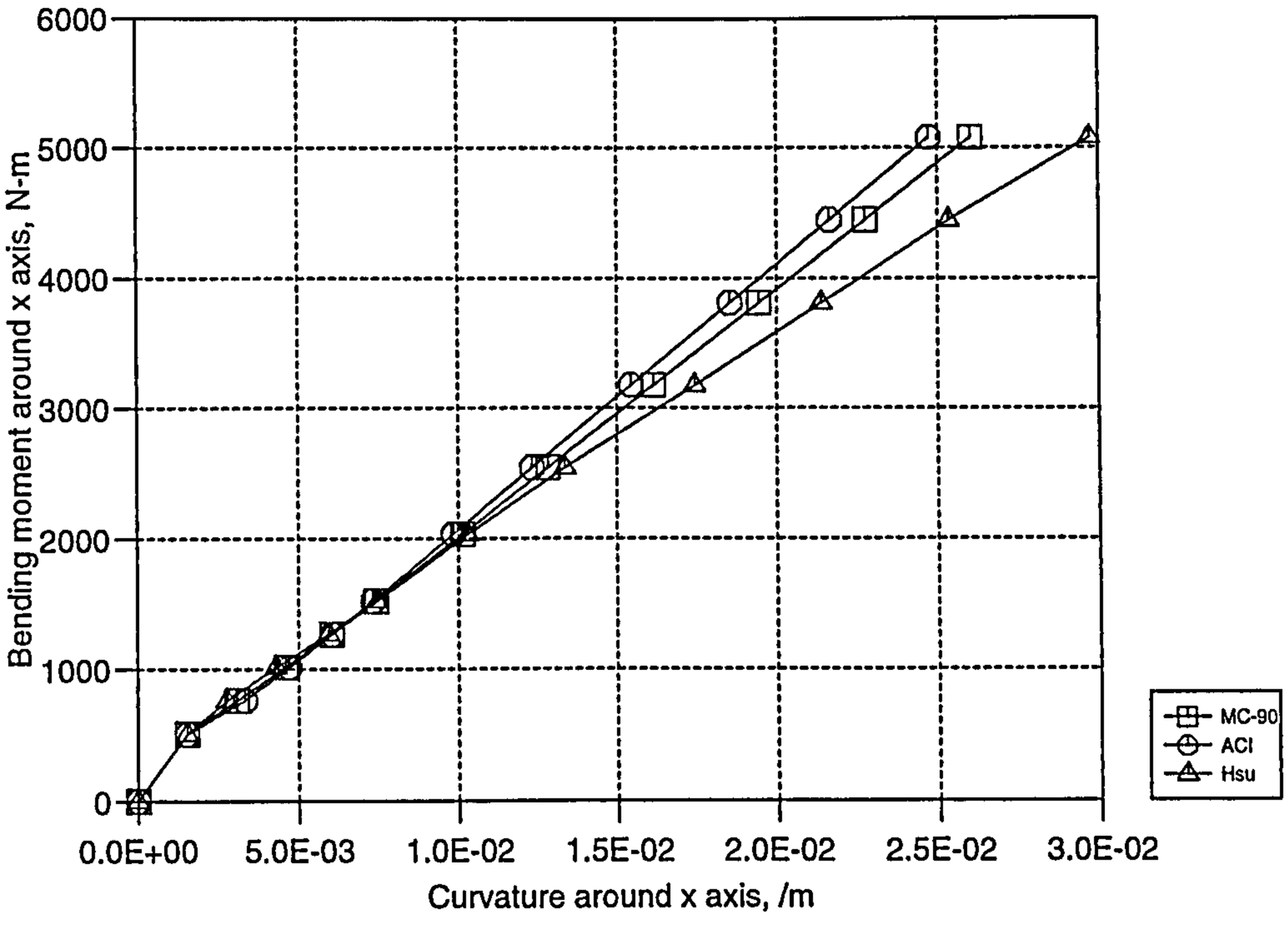


Figure 5.10 Moment-curvature curves: around x-axis, analysis by Hsu & Mirza, ACI and MC-90 model

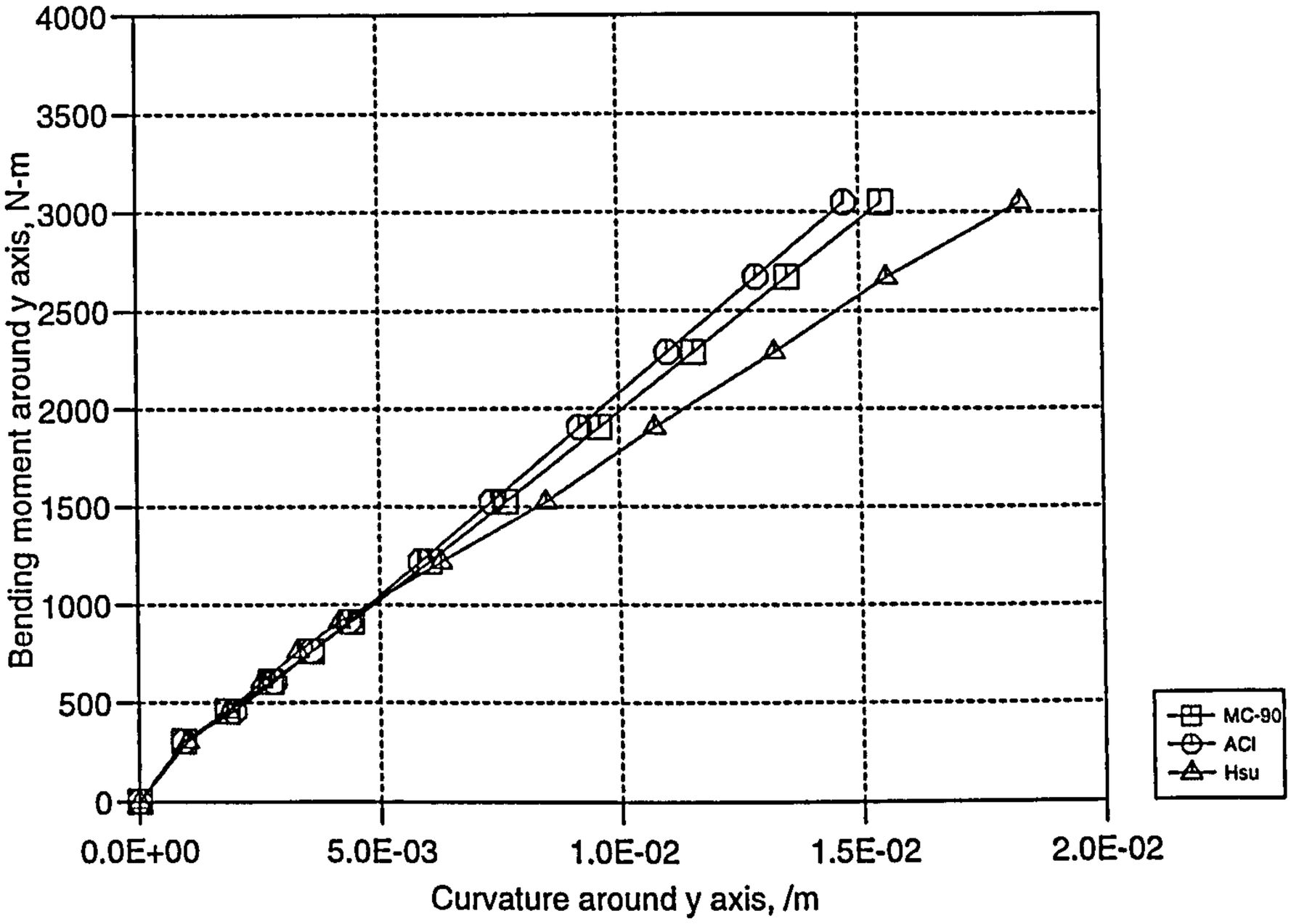


Figure 5.11 Moment-curvature curves: around y-axis, analysis by Hsu & Mirza, ACI and MC-90 model

5.4.3 Two-directional eccentricity: Experiment by Wang *et al.*

Wang *et al.* (1992) carried out tests on six biaxially loaded columns. The results of one of them, U-5, were presented in detail. The column was loaded in a way that it had different eccentricities in the x and y directions. Details of the column and material properties are presented in Fig. 5.12. Moment-curvature curves obtained using MC-90 and ACI equations are shown with experimental results in Figs 5.13 and 5.14 for around x and y directions. The agreement between experiment and current analysis is reasonably good particularly in the lower load range. The difference in the higher load range was due to the fact that concrete crushing has not been included in the present work while, in the experiment at higher load levels, concrete began to crush and eventually the column failed.

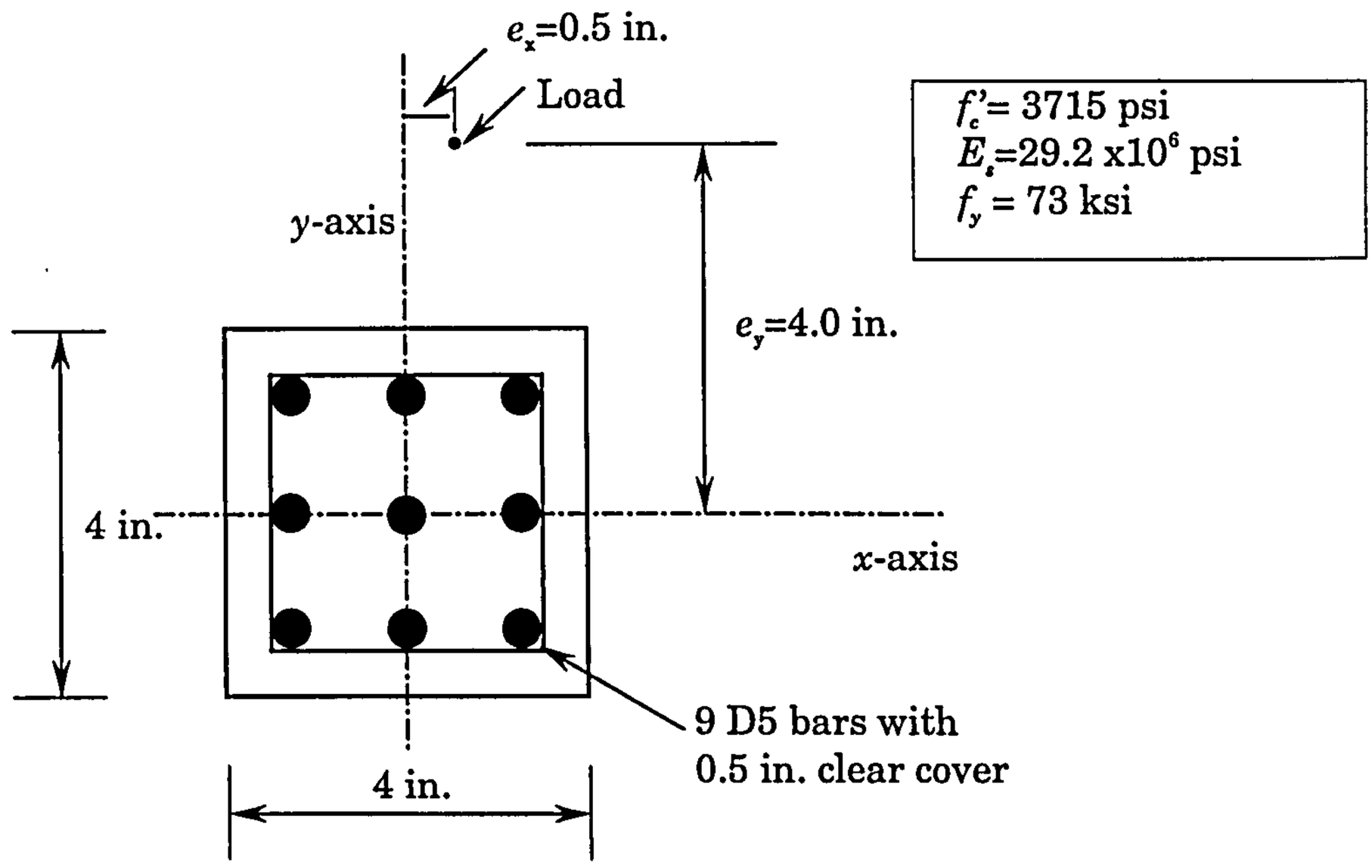


Figure 5.12 Details of column U-5 with material properties, tested by Wang *et al.* (1992)

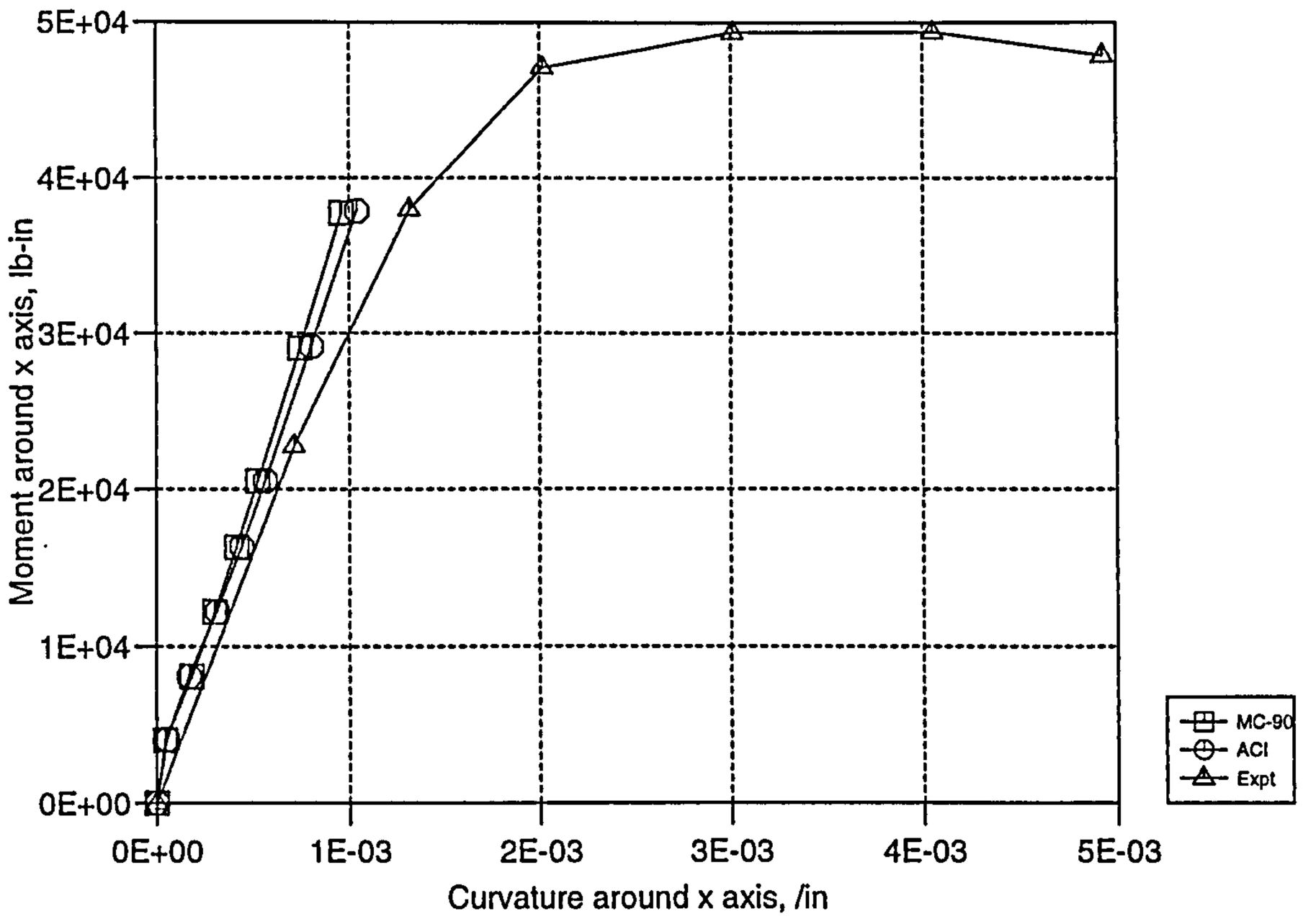


Figure 5.13 Moment-curvature curves: around x-axis, experiment by Wang *et al.*

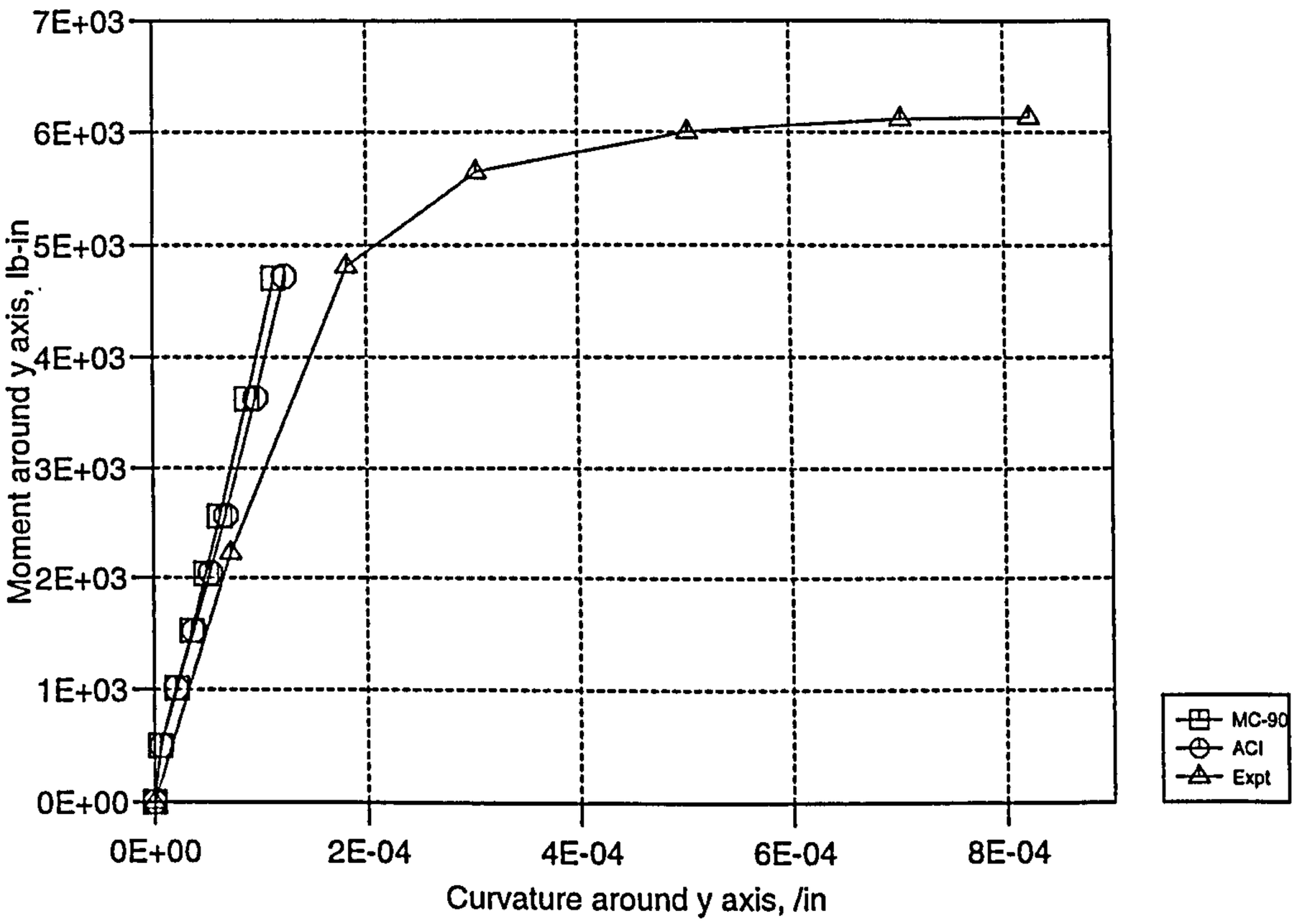


Figure 5.14 Moment-curvature curves: around y-axis, experiment by Wang *et al.*

5.5 Long-term analysis

5.5.1 Calculation for long-term in state 1

The uncracked transformed section at time t_0 is now modified for the age-adjusted modulus of elasticity of concrete. Coordinates of the centroid $\bar{O}_1$ of the uncracked age-adjusted transformed area $\bar{A}_1$ and those of the centroid O_{c1} of the concrete area A_{c1} are found. The second moment of area of the transformed section $\bar{I}_{o1}$ and of the concrete section I_{co1} around $\bar{O}_1$ are then calculated. The radius of gyration of the concrete section, $r_{c1}^2 = I_{co1}/A_{c1}$ is thus obtained. The curvature reduction factor is

$$\kappa_1 = \frac{I_{co1}}{\bar{I}_{o1}} \tag{5.22}$$

The curvature at t_0 for the state 1 is $\psi_1(t_0)$ and the corresponding axial strain at $\bar{O}_1$ is

$$\epsilon_{\bar{O}1}(t_0) = \psi_1 * (\bar{O}_1 O_1) \tag{5.23}$$

where O_1O_1= perpendicular distance from O_1 to the neutral axis at time t_0. The change in curvature during the period t_0 to t is

$$\Delta\psi_1 = \kappa_1 \left[\phi(t,t_0)\left\{\psi_1(t_0) + \epsilon_{\bar{O}1}(t_0)\frac{y_{c1}}{r_{c1}^2}\right\} + \epsilon_{cs}(t,t_0)\frac{y_{c1}}{r_{c1}^2}\right] \tag{5.24}$$

where y_{c1}= distance between two lines passing through O_{c1} and $\bar{O}_1$ and parallel to the neutral axis of state 1 at time t_0. Then, the curvature for state 1 at time t is

$$\psi_1(t) = \psi_1(t_0) + \Delta\psi_1 \tag{5.25}$$

5.5.2 Calculation for long-term in state 2

The fully cracked transformed section at time t_0 is now modified for the age-adjusted modulus of elasticity of concrete. Coordinates of the centre of gravity $\bar{O}_2$ of the fully cracked age-adjusted transformed area $\bar{A}_2$ and those of the centroid O_{c2} of the concrete area A_{c2} are found. The second moment of area of the transformed section $\bar{I}_{o2}$ and of the concrete section I_{co2} around $\bar{O}_2$ are calculated. The radius of gyration

of the concrete section, $r_{co2}^2 = I_{co2}/A_{c2}$, is then obtained. The curvature reduction factor is

$$\kappa_2 = \frac{I_{co2}}{\bar{I}_{o2}} \tag{5.26}$$

The curvature at t_0 for the state 2 is $\psi_2(t_0)$ and the corresponding axial strain at $\bar{O}_2$ is

$$\epsilon_{\bar{O}2}(t_0) = \psi_2(t_0) * (\bar{O}_2 O_2) \tag{5.27}$$

where $\bar{O}_2 O_2$= perpendicular distance from $\bar{O}_2$ to the neutral axis at time t_0. The change in curvature during the period t_0 to t is given by

$$\Delta\psi_2 = \kappa_2 \left[\phi(t,t_0)\left\{\psi_2(t_0) + \epsilon_{\bar{O}2}(t_0)\frac{y_{c2}}{r_{c2}^2}\right\} + \epsilon_{cs}(t,t_0)\frac{y_{c2}}{r_{c2}^2}\right] \tag{5.28}$$

where y_{c2}= distance between two lines passing through O_{c2} and $\bar{O}_2$ and parallel to the neutral axis of state 2 at time t_0. Then, the curvature for state 2 at time t is

$$\psi_2(t) = \psi_2(t_0) + \Delta\psi_2 \tag{5.29}$$

5.5.3 Mean curvature

The interpolation coefficient ζ between state 1 and state 2 for long-term curvature is obtained by eq. 5.21 using a value of 0.5 for β_2. Then, the mean curvature at time t is given by

$$\psi_m(t) = (1-\zeta)\psi_1(t) + \zeta\psi_2(t) \tag{5.30}$$

5.6 FE analysis

5.6.1 Equivalent section

From the mean curvature obtained above, an equivalent elastic section is generated which incorporates the effects of cracking, creep and shrinkage. The equivalent section is formed with brick and line element assembly shown in Fig. 5.15. The curvatures in the x and y directions are given by:

$$\psi_{mx} = \psi_m \cos\theta_m \tag{5.31}$$

$$\psi_{my} = \psi_m \sin\theta_m \tag{5.32}$$

where θ_m is the average of angles of neutral axes at state 1 and state 2.

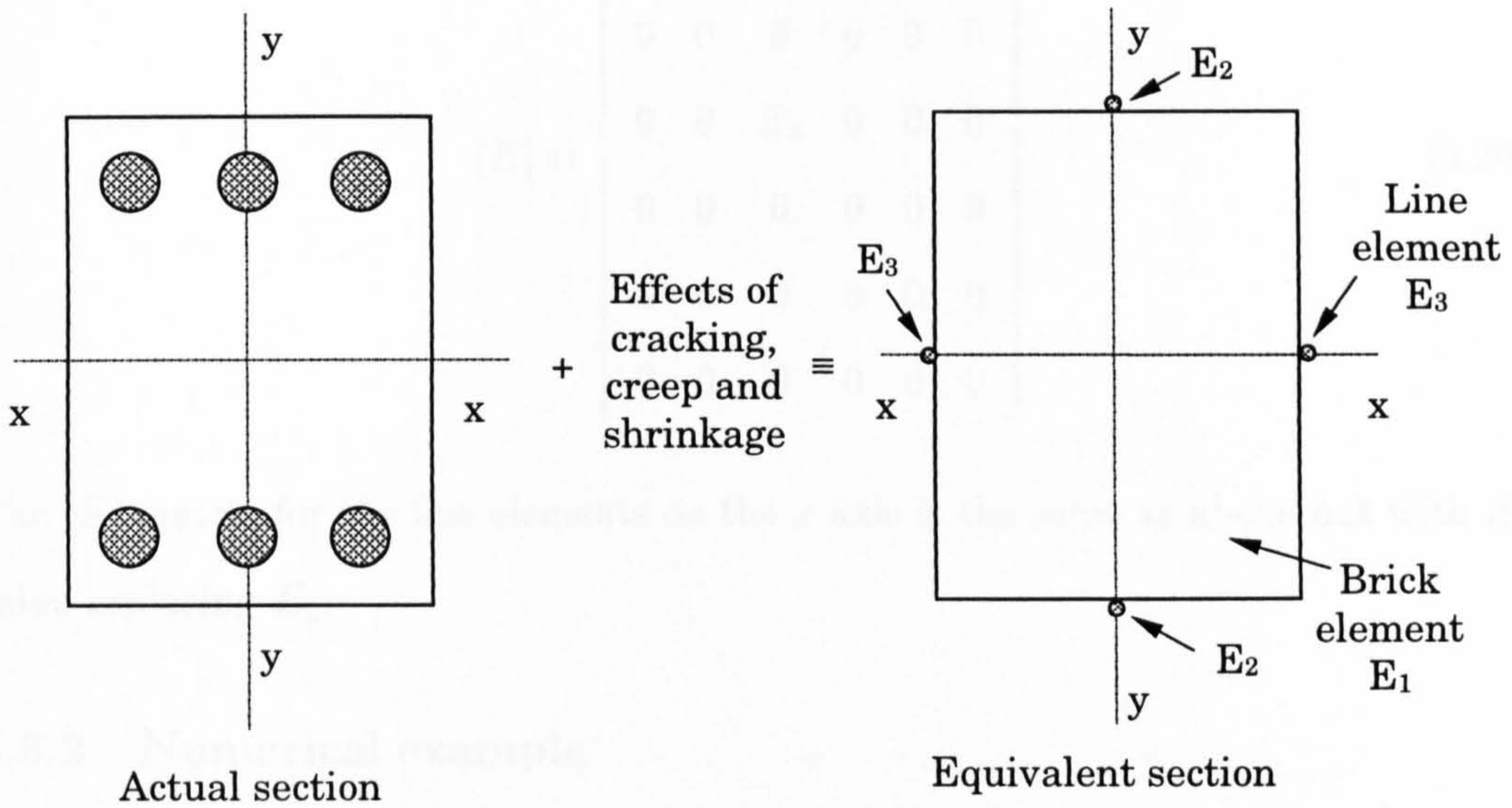


Figure 5.15 Equivalent section for FE analysis

The flexural rigidities of the equivalent section in the x and y directions are given by:

$$EI_{eqx} = \frac{M_{xx}}{\psi_{mx}} \tag{5.33}$$

$$EI_{eqy} = \frac{M_{yy}}{\psi_{my}} \tag{5.34}$$

where M_{xx} and M_{yy} are the moments around the symmetry lines of the equivalent section.

To obtain the EI_{eqx} and EI_{eqy} calculated above, the modulus of elasticity in the z direction of the brick element E_1, and those of the line elements E_2 and E_3 are adjusted accordingly. Thus the $[E]$ matrix for the brick elements becomes:

$$[E] = \begin{bmatrix} \frac{E_c(1-\nu)}{(1+\nu)(1-2\nu)} & \frac{E_c\nu}{(1+\nu)(1-2\nu)} & \frac{E_1\nu}{(1+\nu)(1-2\nu)} & 0 & 0 & 0 \\ \frac{E_c\nu}{(1+\nu)(1-2\nu)} & \frac{E_c(1-\nu)}{(1+\nu)(1-2\nu)} & \frac{E_1\nu}{(1+\nu)(1-2\nu)} & 0 & 0 & 0 \\ \frac{E_1\nu}{(1+\nu)(1-2\nu)} & \frac{E_1\nu}{(1+\nu)(1-2\nu)} & \frac{E_1(1-\nu)}{(1+\nu)(1-2\nu)} & 0 & 0 & 0 \\ 0 & 0 & 0 & \frac{E_c}{(1+\nu)} & 0 & 0 \\ 0 & 0 & 0 & 0 & \frac{E_c}{(1+\nu)} & 0 \\ 0 & 0 & 0 & 0 & 0 & \frac{E_c}{(1+\nu)} \end{bmatrix} \tag{5.35}$$

and that for the line elements on the y axis is:

$$[E] = \begin{bmatrix} 0 & 0 & 0 & 0 & 0 & 0 \\ 0 & 0 & 0 & 0 & 0 & 0 \\ 0 & 0 & E_2 & 0 & 0 & 0 \\ 0 & 0 & 0 & 0 & 0 & 0 \\ 0 & 0 & 0 & 0 & 0 & 0 \\ 0 & 0 & 0 & 0 & 0 & 0 \end{bmatrix} \tag{5.36}$$

The $[E]$ matrix for the line elements on the x axis is the same as above but with E_3 value replacing E_2.

5.6.2 Numerical example

An example is given here to demonstrate the approach. A 5 m long cantilever reinforced concrete column is fixed at the bottom and loaded with 5000 kN at the corner of the top free face. The intensity of the load was chosen extremely high to create substantial amount of sway. In reality a load of this magnitude would create second-order effects, but the objective of this example is to compare results of the FE analysis with that of curvature calculations and hence second order effects are neglected. The concrete section with reinforcement arrangement is shown in Fig. 5.16.

The instantaneous mean curvature obtained by MC-90 equations is $1.715 * 10^{-5}$ /mm and the mean angle of the neutral axes in state 1 and state 2 is 62.66 degree. ψ_{mx} and ψ_{my} are $7.88 * 10^{-6}$ /mm and $1.52 * 10^{-5}$ /mm respectively. The equivalent rigidities around x and y direction are:

$$EI_{eqx} = \frac{5000 * 10^3 * 400}{7.88 * 10^{-6}} = 2.54 * 10^{14} \tag{5.37}$$

$$EI_{eqy} = \frac{5000 * 10^3 * 200}{1.52 * 10^{-5}} = 6.56 * 10^{13} \tag{5.38}$$

The equivalent section is assumed to have dimensions as shown in Fig. 5.16, and the area of line elements is assumed to be 1000 mm^2. To obtain the equivalent rigidities around the x and y directions calculated by eqs 5.37 and 5.38, the E values of the

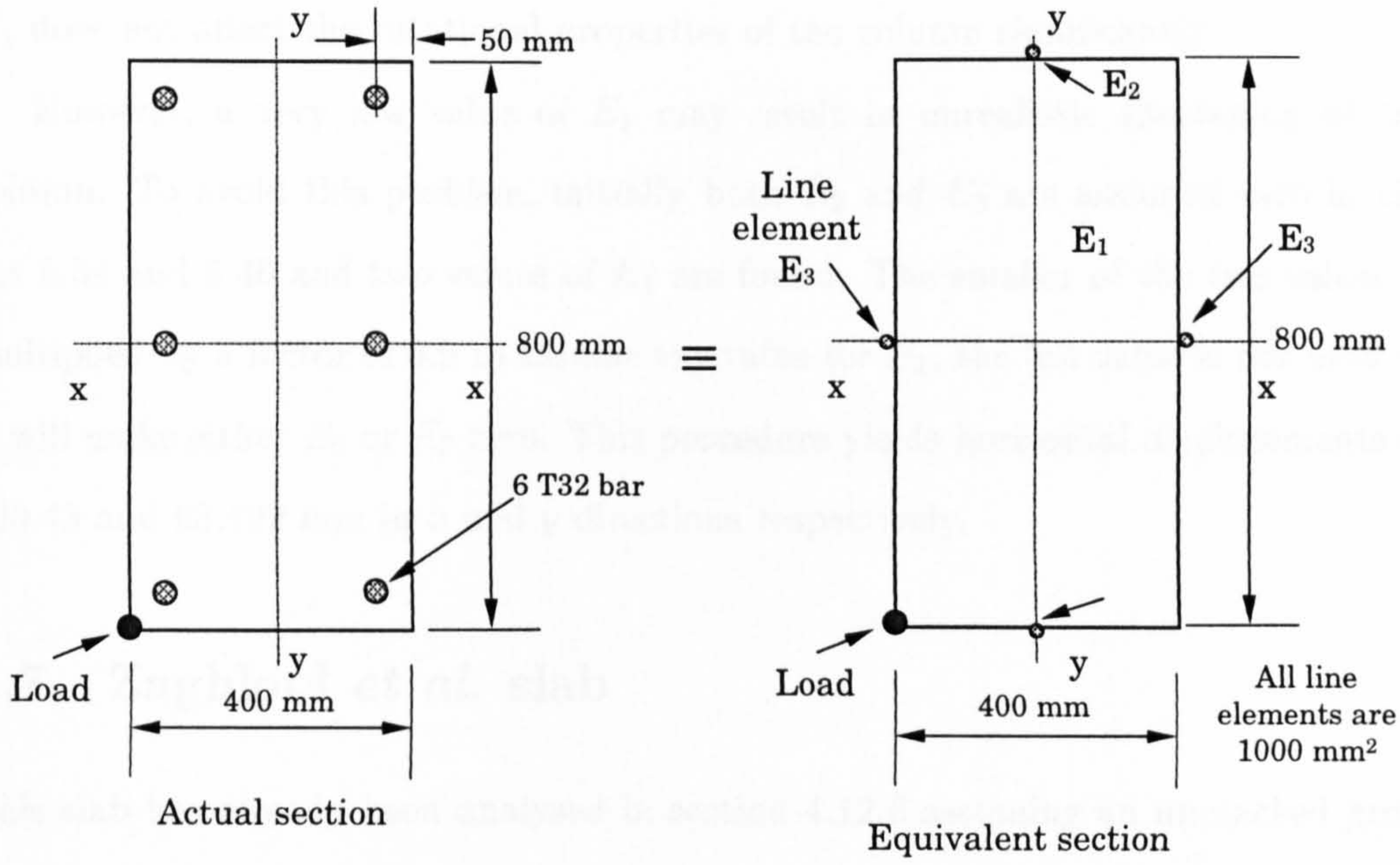


Figure 5.16 Column section and equivalent section

equivalent section should follow these two equations:

$$2.54 * 10^{14} = E_1 * 400 * 800^3/12 + 2 * E_2 * 1000 * 400^2 \tag{5.39}$$

$$6.56 * 10^{13} = E_1 * 800 * 400^3/12 + 2 * E_3 * 1000 * 200^2 \tag{5.40}$$

There are three unknowns in the above two eqs 5.39 and 5.40, to solve this problem, two different values of E_1 are arbitrarily chosen to find its effect on rotational properties.

First, E_1 is assumed to be $0.4 * E_c$ and from eqs 5.39 and 5.40, we get $E_2 = 153.46 * 10^3$ N/mm^2 and $E_3 = 180.44 * 10^3$ N/mm^2. These values are used to form the $[E]$ matrices for the brick and the line elements using eqs 5.35 and 5.36. From the FE analysis, the horizontal displacements of the top of the column are 190.45 and 98.49mm in the x and y directions respectively.

Secondly, E_1 is selected to be $0.1 * E_c$ and $E_2 = 633.46 * 10^3$ N/mm^2 and $E_3 = 660.45 * 10^3$ N/mm^2 are found. The FE analysis, with this set of E values, gives horizontal displacements of 190.91 and 98.59mm in the x and y directions respectively.

From curvature calculations, the corresponding displacements are 190.45 and 98.46mm. It is thus evident from above results that assuming an arbitrary value for

E_1 does not affect the rotational properties of the column significantly.

However, a very low value of E_1 may result in unrealistic shortening of the column. To avoid this problem, initially both E_2 and E_3 are assumed zero in the eqs 5.39 and 5.40 and two values of E_1 are found. The smaller of the two values is multiplied by a factor of 0.9 to assume the value for E_1, the full value is not used as it will make either E_2 or E_3 zero. This procedure yields horizontal displacements of 190.43 and 98.492 mm in x and y directions respectively.

5.7 Zaghlool *et al.* slab

This slab has already been analysed in section 4.12.6 assuming an uncracked gross cross-section for the column. The analysis has been repeated here to consider the effect of tensile cracking in the column with the MC-90 model for biaxial bending with axial force. The effect of modelling the column's tensile cracking on slab deflection and on total central moment are presented in Figs 5.17 and 5.18. It seems that considering tensile cracking in the column does not significantly affect either the deflection or the total moment. Deflections at lower load levels are reduced by an almost negligible amount when reinforcement is included, while at higher loads increased slightly as column starts to crack in tension. Deflections obtained from the analysis are significantly lower than those obtained from the experiment. Zaghlool *et al.* (1970) observed tensile cracking near the top of the column at fairly low loads, and their cracked column showed cracking at the top of column at 50 psf. It seems that the actual strength of the concrete was much lower than that specified in the paper.

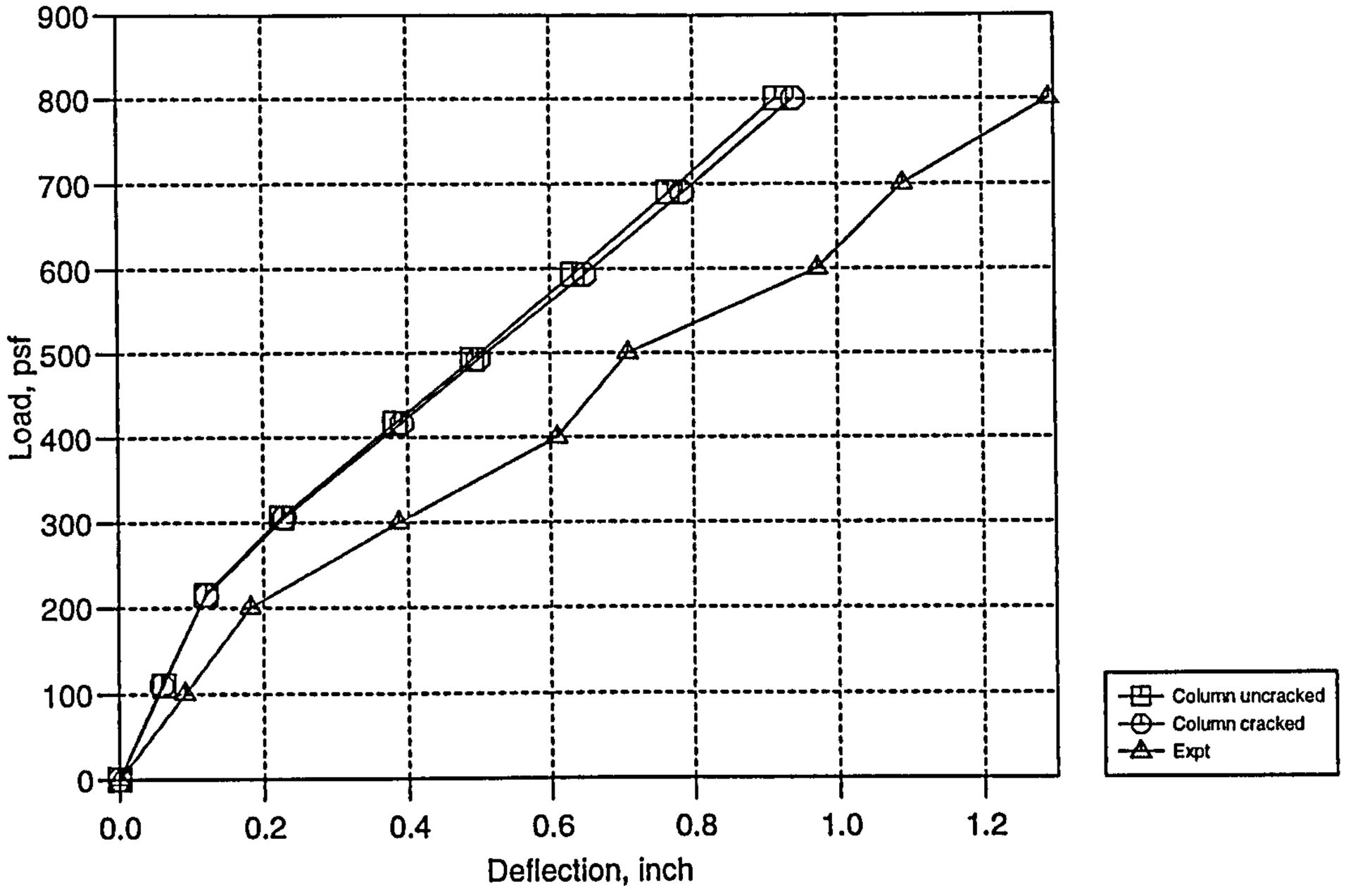


Figure 5.17 Effect of modelling column cracking on deflection: slab tested by Zaghlool *et al.*

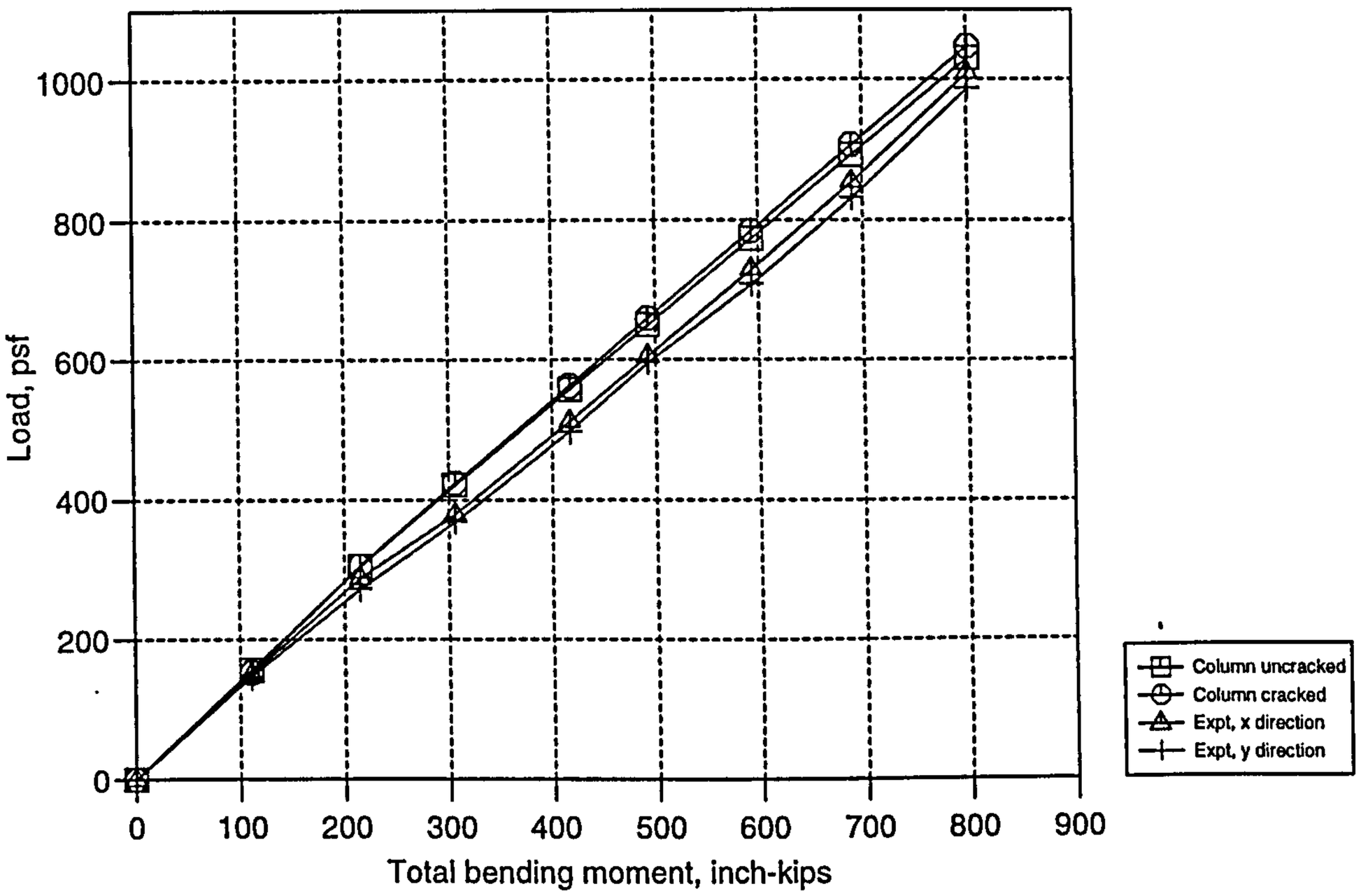


Figure 5.18 Effect of modelling column cracking on central moment: slab tested by Zaghlool *et al.*

5.8 Parker & Bullman slab

Parker & Bullman (1998) performed six full-scale tests on reinforced concrete flat-slab to edge column connections. The columns were all 300 X 300 mm in section, reinforced with 4T25 main steel, while the depth of the flat slabs tested ranged from 175mm-300mm. The specimens were cast and tested upside down, as shown in Fig. 5.19, and details of the slab reinforcement are shown in Fig. 5.20. The test details are given in Table 5.3. The modulus of elasticity and the tensile strength for the concrete were assumed using EuroCode EC2-91 (1991).

All the slabs have been analysed for three cases with MC-90 moment-curvature relationship equations. For the first two cases a mean value is assumed for the tensile strength of the concrete, while for the third case a low tensile strength is used according to EC2-91. The three cases are as follows:

1. Cracking is modelled only in the slab, while the column remains as a gross section.

2. Cracking is modelled both in the slab and in the column.

3. Same as case 2, but with a low tensile strength.

Case 2 has been analysed with the column section modified both on the basis of elastic stresses without any redistribution and on the basis of redistributed stresses. They yield almost identical result since the moments in the column are statically determinate.

Deflection versus load curves for the six slabs are plotted in Figs 5.21 to 5.26. Other than slab 6a, predictions are very good for all the slabs, particularly in the lower load ranges. The effect of modelling column crack is more important for slabs 6c and 6f where the axial load is zero, however, the effect is not very significant in lower load ranges.

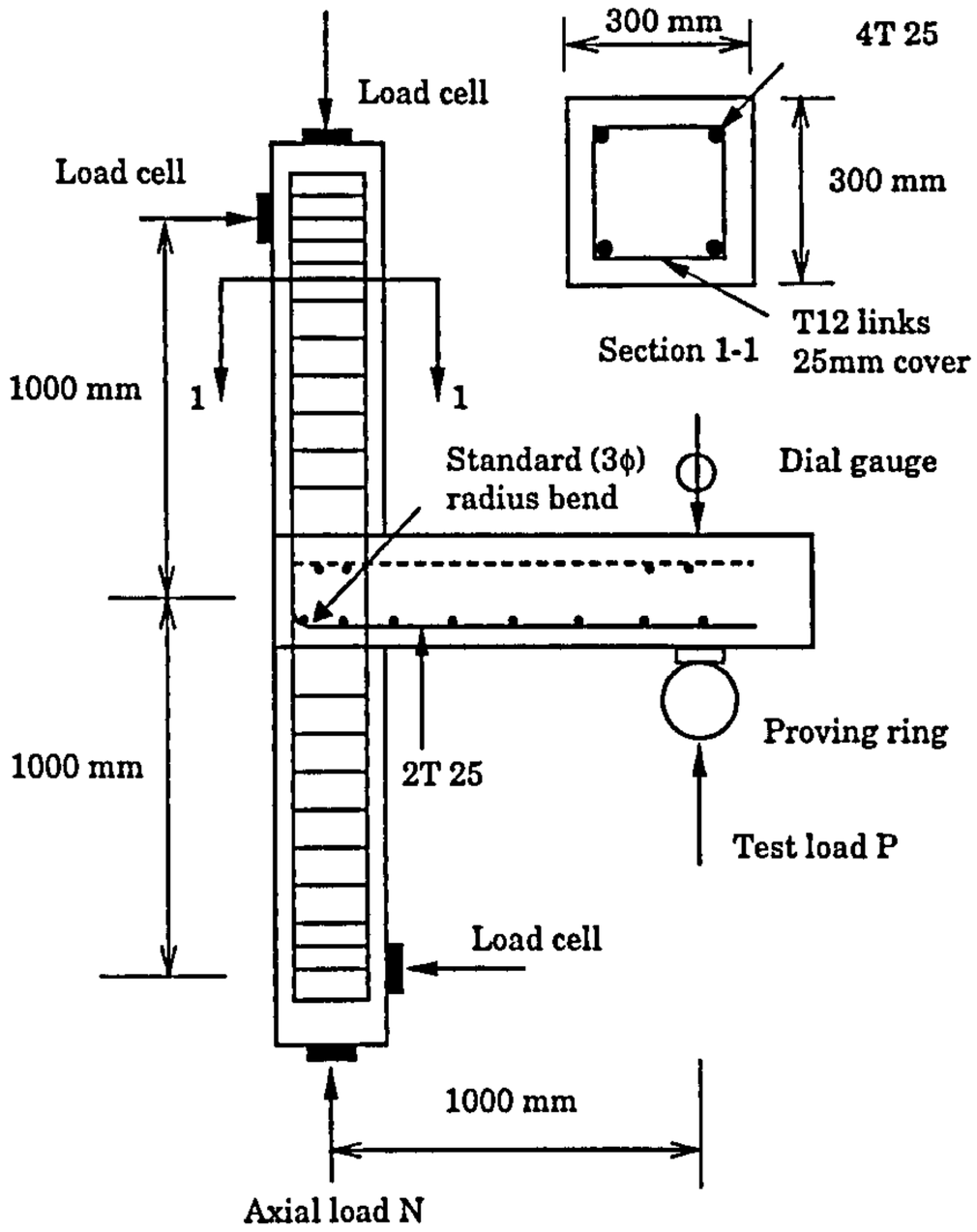


Figure 5.19 Test arrangement: slab tested by Parker & Bullman (1998)

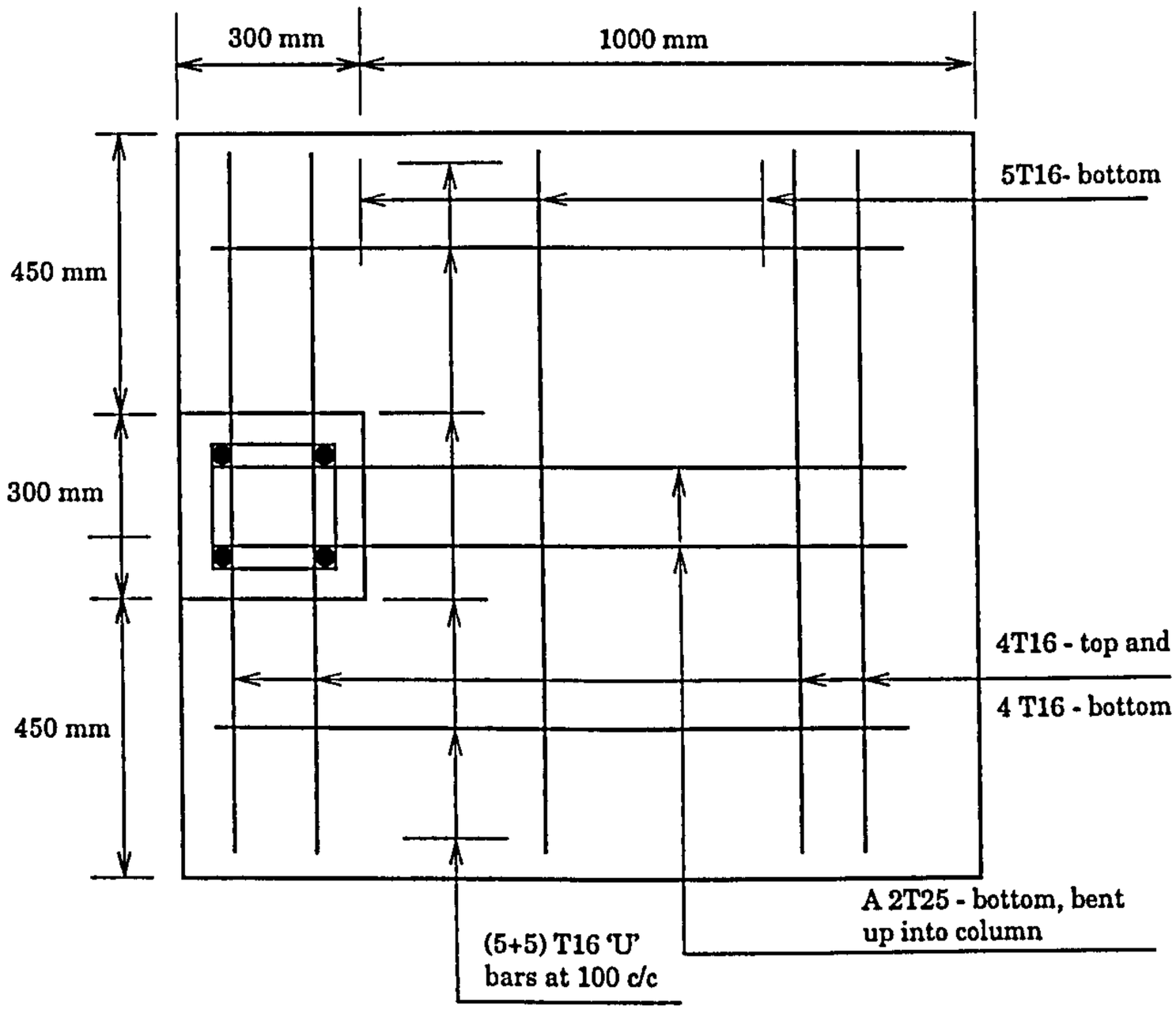


Figure 5.20 Slab reinforcement: slab tested by Parker & Bullman (1998)

Test ref.	Slab depth mm	Concrete f_{cu} MPa	Axial load N kN	Maximum slab load P kN	Assumed E_c GPa	Assumed mean f_{ct} MPa	Assumed low f_{ct} MPa
6a	300	55	600	253	33.5	3.76	2.55
6b	275	56	300	242	33.5	3.76	2.55
6c	250	57	0	193	33.5	3.76	2.55
6d	225	50	600	216	32.4	3.52	2.39
6e	200	55	300	182	33.5	3.76	2.55
6f	175	53	0	150	32.4	3.52	2.39

Table 5.3 Geometric and material properties: Parker & Bullman slab

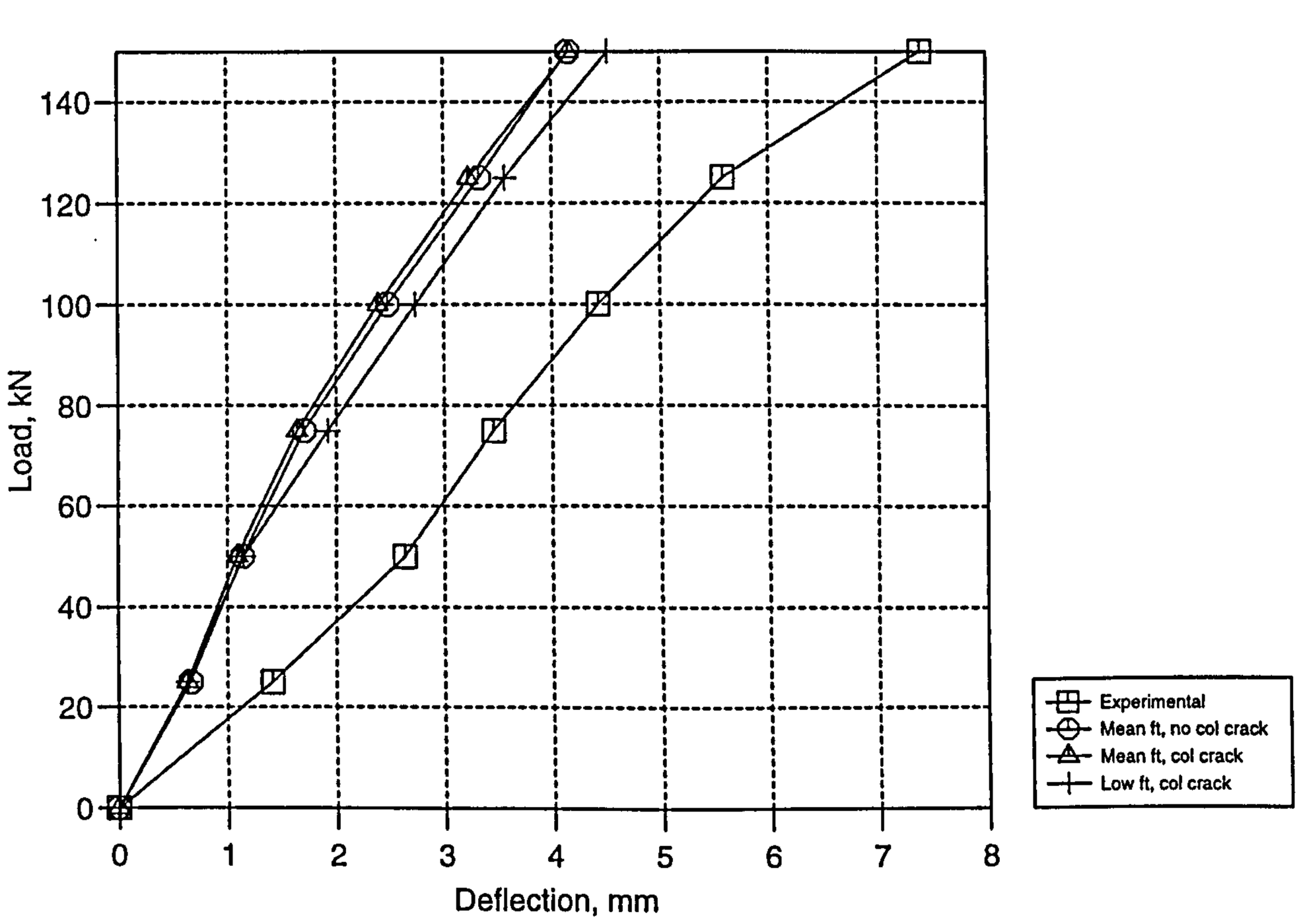


Figure 5.21 Load-deflection curves: Parker & Bullman slab 6a

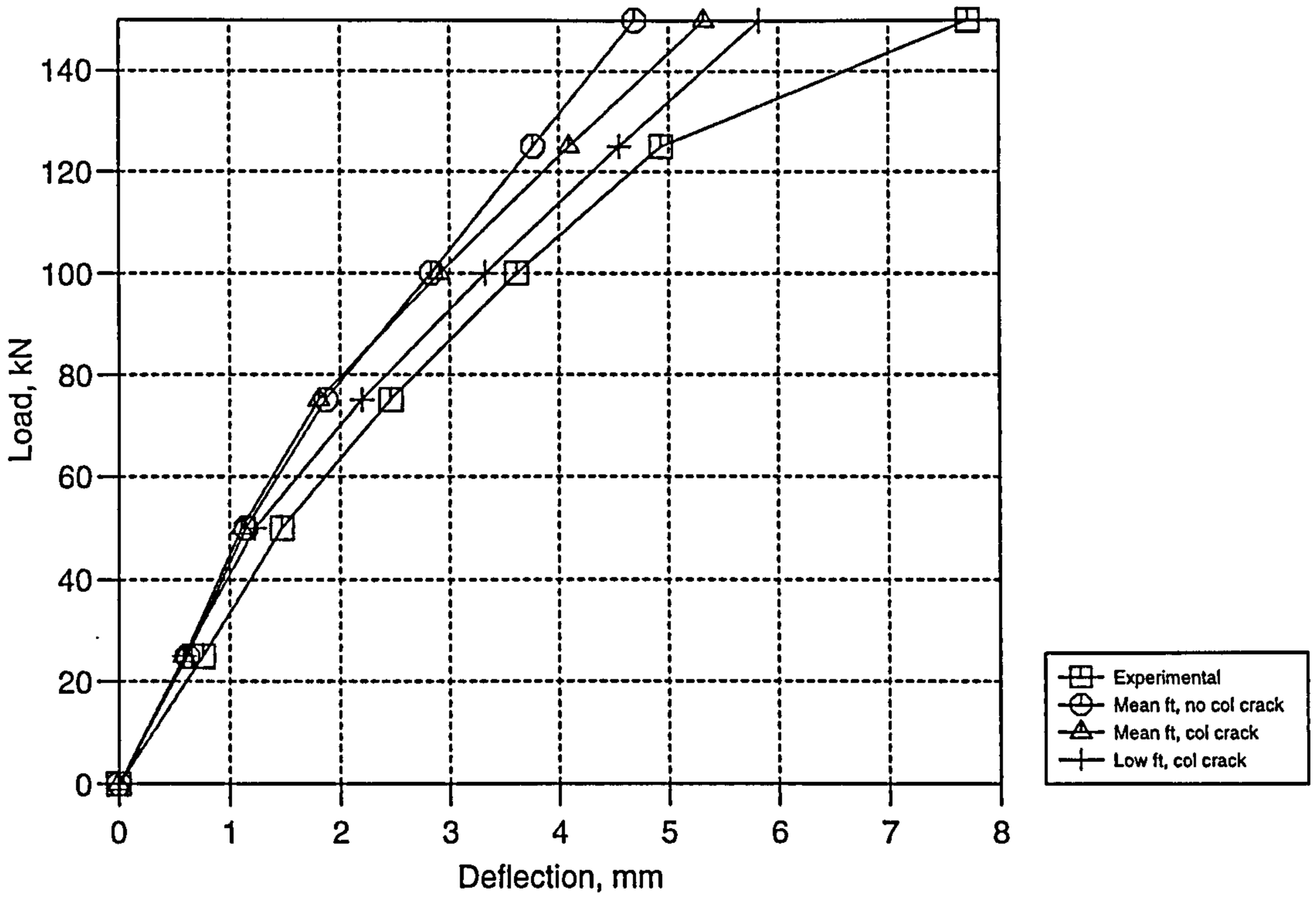


Figure 5.22 Load-deflection curves: Parker & Bullman slab 6b

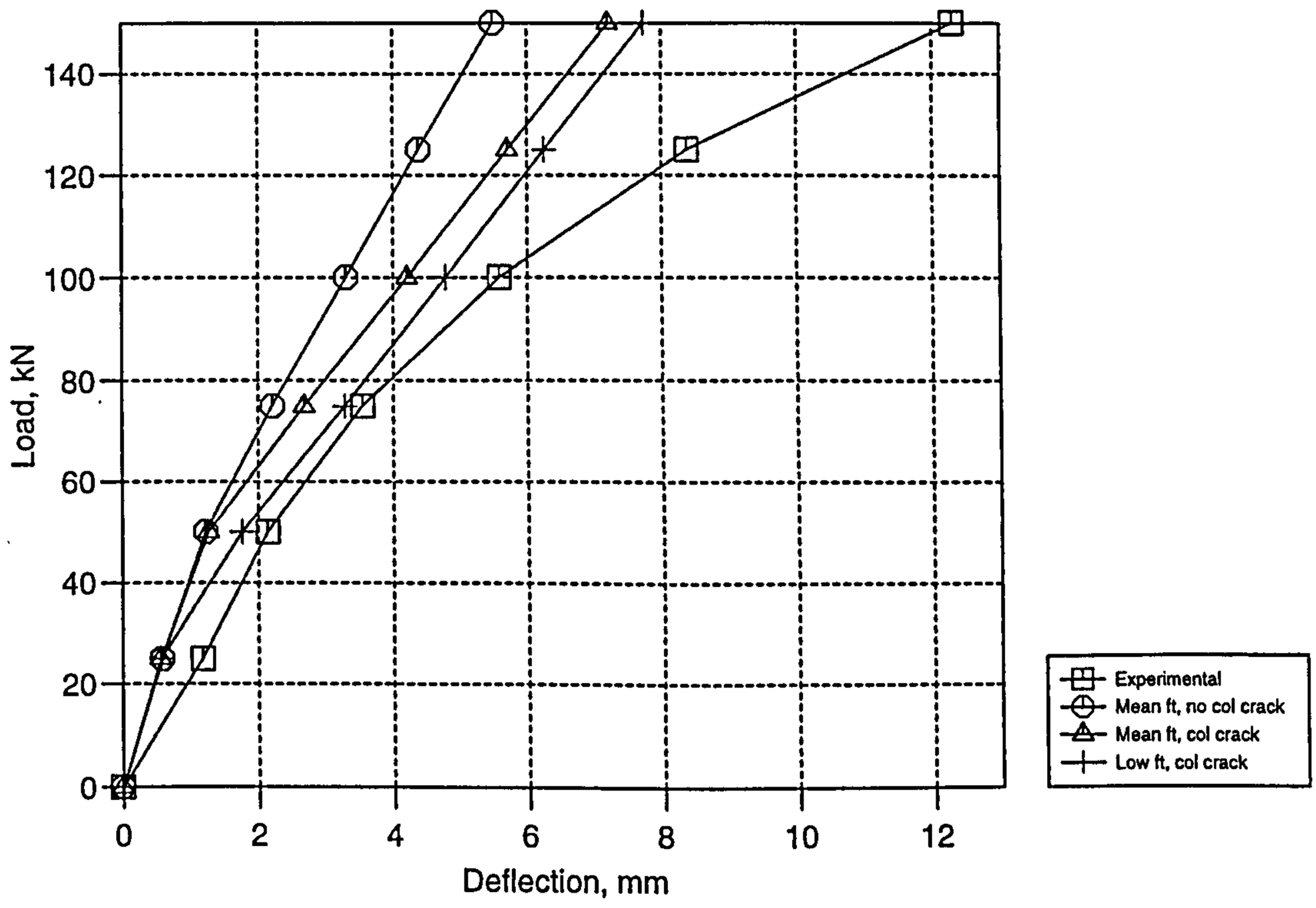


Figure 5.23 Load-deflection curves: Parker & Bullman slab 6c

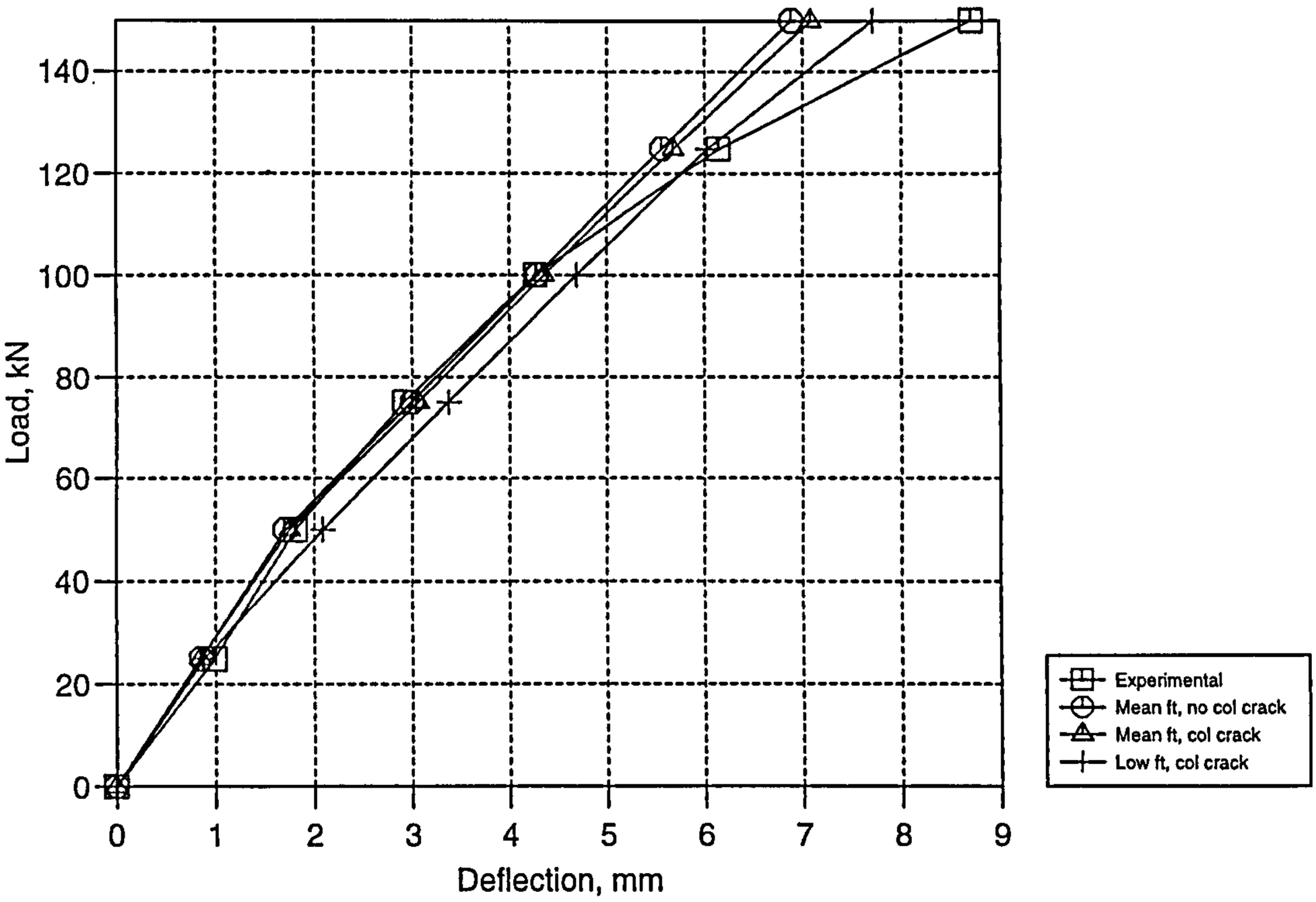


Figure 5.24 Load-deflection curves: Parker & Bullman slab 6d

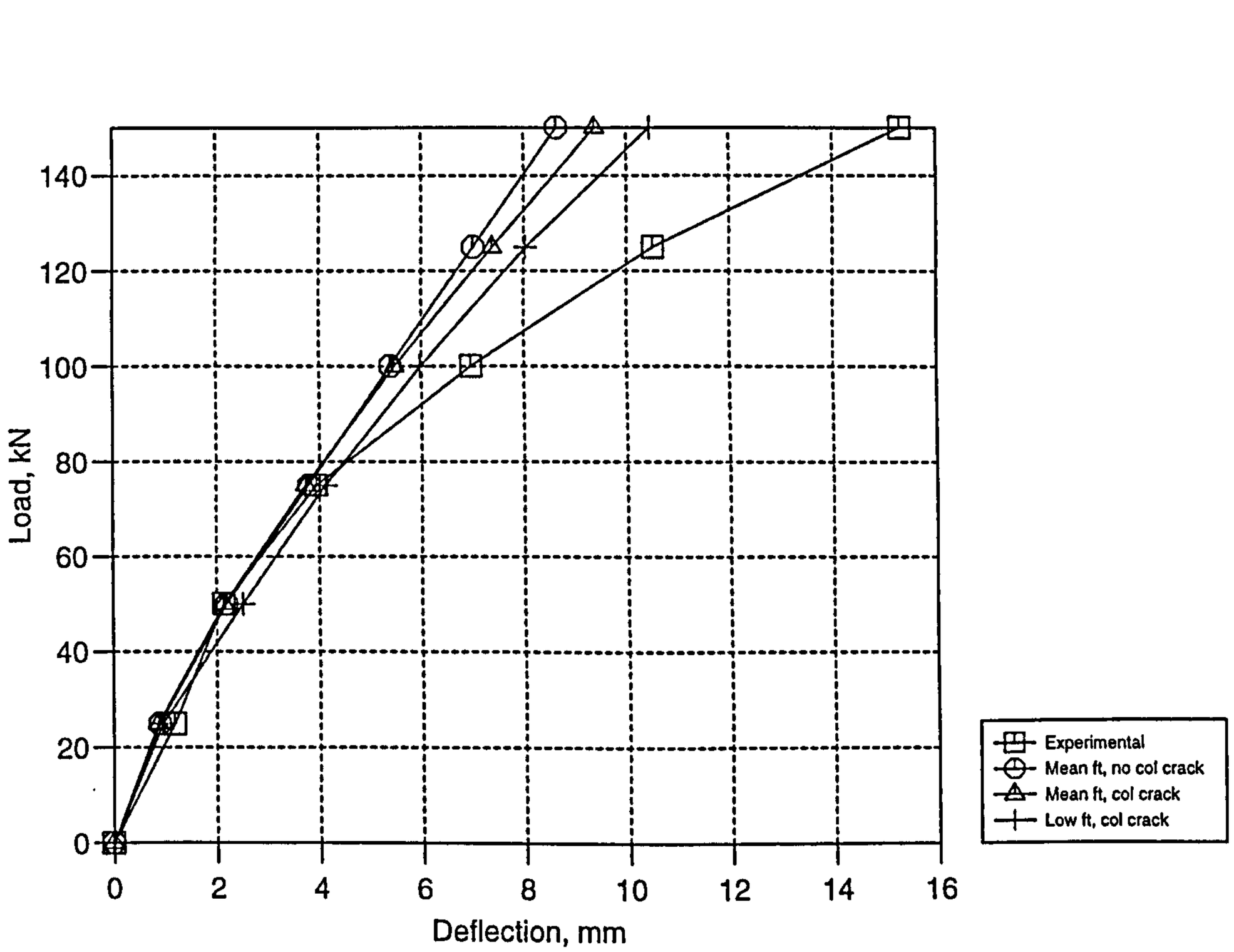


Figure 5.25 Load-deflection curves: Parker & Bullman slab 6e

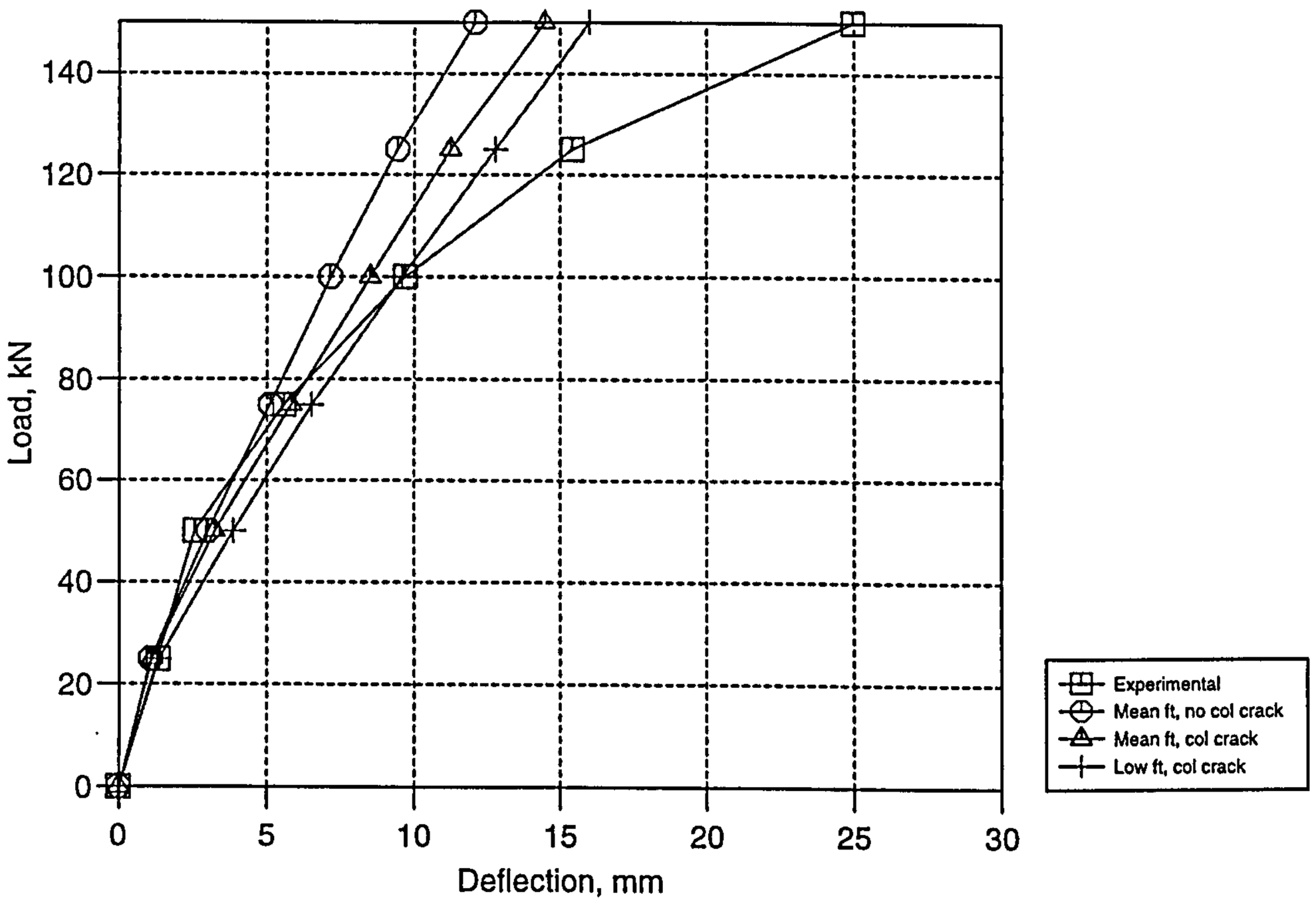


Figure 5.26 Load-deflection curves: Parker & Bullman slab 6f

5.9 Conclusions

The objective of this chapter was to develop a method to model cracking, creep and shrinkage in column. It was different from slab due to the presence of axial force which makes the problem more complicated. The position of the neutral axis, in state 2, depends on the magnitude of the load and its position. An iterative method based on trial and error has been developed by the author to find the neutral axis of a section loaded with an axial force having two-directional eccentricity. The approach has been checked with the results of analyses of Brøndum-Nielsen (1997), who developed a similar method with a modified Newton-Raphson iteration technique.

Both the ACI and the MC-90 equations are adopted to find the mean curvature once state 2 is defined by the above method. Although the method is more generalised and can model a situation where load is applied with two directional eccentricities, Sakai & Kakuta experiments which are essentially with one directional eccentricity were modelled successfully. The method was also checked with Hsu & Mirza analysis and Wang *et al.* experiments. The method is also extended to incorporate long-term effects using MC-90 equation following Ghali & Favre approach, similarly as slabs.

An FE method was proposed by the author to find an equivalent section of column using brick and line elements. Mean curvatures of the column sections are modelled by assigning appropriate E values to the brick and line elements. The equivalent section method has been found to give the same result as curvature calculations.

The method was applied to a slab tested by Zaghlool *et al.* and it was found that modelling column cracking had no significant effect on deflection. Parker & Bullman slabs were also modelled with and without column cracking. Modelling column cracking increased deflections, particularly for slabs without any axial load in the upper column. The effect of cracking is more prominent at higher load ranges. The author believes that for service load analysis, modelling column with gross concrete section without any change in material properties (for cracking, creep and shrinkage) should be reasonably adequate.

Chapter 6

Time-varying load history

6.1 Introduction

In Chapter 4, three short-term models were incorporated into the FE package. It was shown that all the models give reasonable estimates of deflections measured in tests. Also, it was shown that the MC-90 method gives good predictions of long-term deflections for constant loading. However, in reality, a slab undergoes a time-varying load during its construction and operational life, which needs to be accounted for if long-term deflections are to be modelled realistically.

Construction loads are dependent on the method of re-propping adopted and the number of floors which are back-propped. Different systems of back-propping and resulting construction loads have been discussed in section 2.7. When stripped, depending on the repropping system adopted, the weight of the slab is transmitted in two ways: 1) The reprops are loosely fitted and the slab is allowed to carry its own weight, 2) The reprops are tightly fitted and, as a result, part of the self weight of the slab is transmitted to the slabs below. When the next slab is cast, in both cases, the weight of fresh concrete is distributed between the slabs in the supporting assembly below. With repropping system 1, any slab in the supporting assembly carries only its own weight and part of the freshly cast concrete. Whereas, for system 2, lower slabs accumulate high loads as parts of weight of all above slabs pass through it. It has already been pointed out in section 2.7 that, construction loads on the lower slab in the supporting assembly may often be several times larger

than the self-weight of the slab due to the construction sequence. It is important to take account of construction loads in the calculation of deflection because early-age striking can result in severe cracking of the immature slab due to its low tensile strength.

This chapter presents a novel method that the author has developed to simulate the deflection behaviour of slabs throughout their construction and service life. The method is based on the MC-90 moment curvature relationship for cracking, creep and shrinkage. The method divides the load history into steps, corresponding to changes in either load or in time. The approach is based on the principle of superposition and is capable of modelling any loading or unloading sequence. The method is based on the secant-stiffness formulation and is novel in that it stores curvatures, moments and the extent of cracking from previous load steps and then calculates the additional curvature for moment or time increments.

6.2 Assumptions

The assumptions involved in this analysis are:

1. Increments in moment can be calculated using the method of superposition. This implies that the directions of the principal moments under different loading stages are the same.

2. Superposition of curvature is valid.

3. Superposition of creep and shrinkage is valid.

4. Second-order effects are negligible.

6.3 Analysis method for time-varying load history

A subroutine is written as a part of an existing FE package to calculate the modified elastic properties of each element taking consideration of all present and past load steps. The modified properties are then fed back into the assembly module of the FE package which gives another solution that is used to calculate another set of modified

elastic properties. The whole procedure is repeated until convergence occurs. At this point, the modified elastic properties corresponding to the current stress state are very close to the values calculated in the previous step.

The analysis method presented in this chapter is intended for a time-varying load history similar to that in Fig. 6.1.

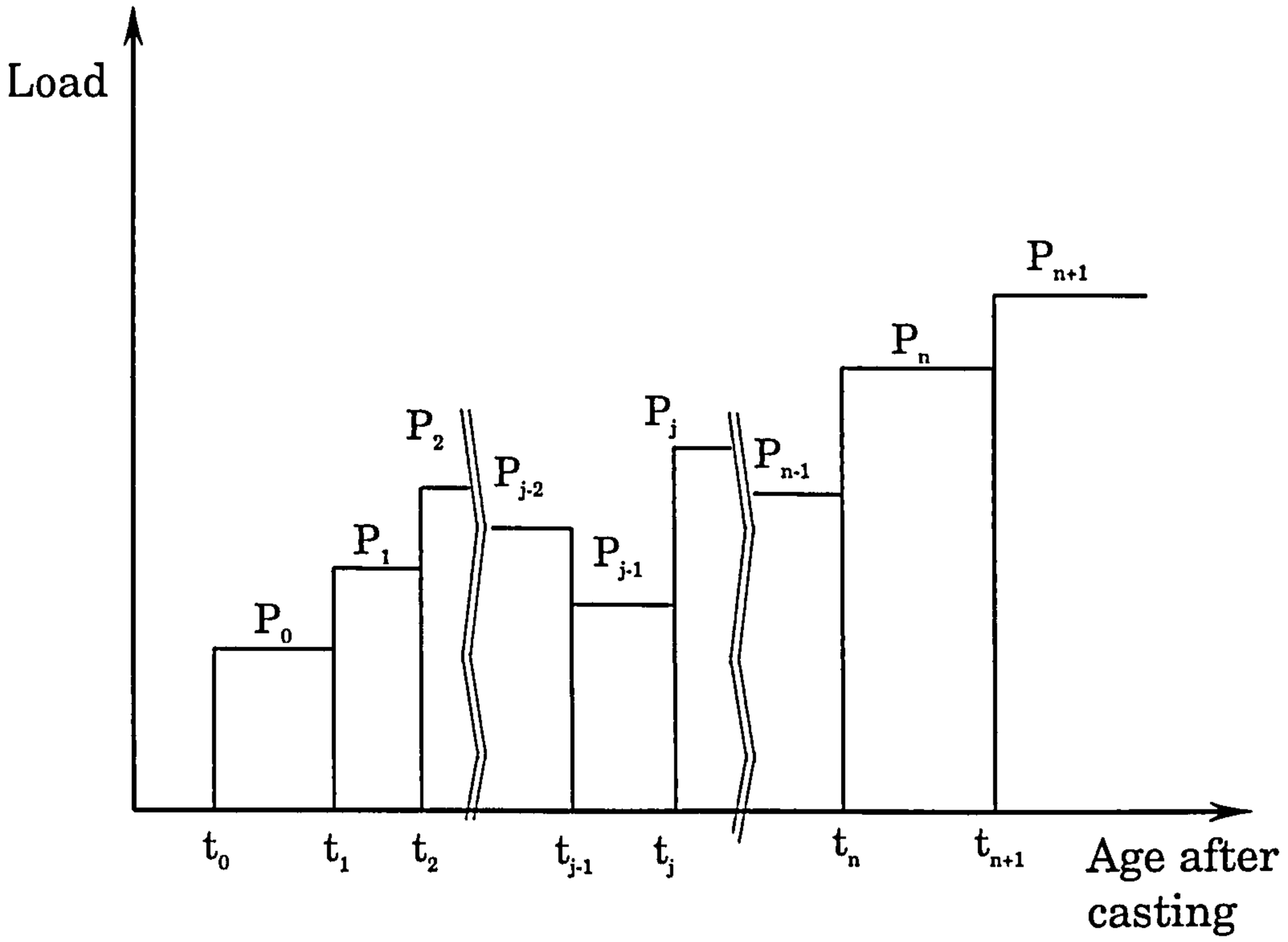


Figure 6.1 Time-varying load

6.3.1 Instantaneous change in curvature due to load increment

The mean curvature at time t_n, just after the load jumps from P_{n-1} to P_n, is given by:

$$\psi_m(t_n) = \psi_m(t_n^-) + \Delta\psi_m \tag{6.1}$$

where $\psi_m(t_n^-)$ is the mean curvature stored at the end of the last step at time t_n^-, i.e. just before the load P_n is applied, and $\Delta\psi_m$ is the change in curvature due to the change in load from P_{n-1} to P_n. $\Delta\psi_m$ is given by:

$$\Delta\psi_m = \psi_m^*(t_n) - \psi_m^*(t_n^-) \tag{6.2}$$

$\psi^*_m(t_n)$ is the mean instantaneous curvature calculated for the moment $M_n(t_n)$. The moment $M_n(t_n)$ corresponds to the load P_n at time t_n.

$\psi^*_m(t^-_n)$ is the mean instantaneous curvature calculated for the moment $M_{n-1}(t^-_n)$. The moment $M_{n-1}(t^-_n)$ corresponds to the load P_{n-1} at time t^-_n.

6.3.2 Change in curvature with time under constant load

The mean curvature at time t^-_{n+1} (a minus sign indicates that the time is just before application of further load) corresponding to P_n is given by:

$$\psi_m(t^-_{n+1}) = \psi_m(t_n) + \Delta\psi_m \tag{6.3}$$

where $\psi_m(t_n)$ is the mean curvature stored at the end of the last step (i.e. at time t_n immediately after the load P_n is applied), and $\Delta\psi_m$ is the change in curvature due to creep and shrinkage between times t_n and t^-_{n+1}. $\Delta\psi_m$ is taken as:

$$\Delta\psi_m = \psi^*_m(t^-_{n+1}) - \psi^*_m(t_n) \tag{6.4}$$

$\psi^*_m(t^-_{n+1})$ is the mean curvature due to P_n at time t^-_{n+1} which is calculated by interpolating between states 1 and 2 curvatures using eq. 6.10. The curvatures in states 1 and 2 are taken as the sum of the instantaneous curvatures due to $M_n(t^-_{n+1})$, the curvatures due to creep between t_0 to t^-_{n+1} and the curvature due to shrinkage between t_s to t^-_{n+1}. The curvature due to creep is calculated by superposition.

$\psi^*_m(t_n)$ is the mean curvature corresponding to P_n at time t_n which is calculated by interpolating between states 1 and 2 curvatures using eq. 6.12. The curvatures in states 1 and 2 are calculated using the same procedure as for $\psi^*_m(t^-_{n+1})$. The moments $M_n(t_n)$ and $M_n(t^-_{n+1})$ (both due to load P_n) are not in general equal since some redistribution of moment occurs between time t_n to t^-_{n+1}. The values of ζ used in eqs 6.10 and 6.12 differ in general since neither the moments nor β values are equal at t_n and t^-_{n+1}.

6.4 Analysis method for slab

The analysis starts when the load P_0 is applied instantly at time t_0. The first step corresponds to the instantaneous change in load from zero to P_0 at time t_0. The analysis is similar to that presented in section 4.8. After convergence, moments $M_0(t_0)$ and mean curvatures at time t_0, $\psi_m(t_0)$ for each element for the two principal directions are stored in files for later use.

The second step starts at t_0 and ends at time t_1^- when the load is still P_0. Although there is no change in load, the moment changes due to stress redistribution. The moment increment for the second step is $[M_0(t_1^-) - M_0(t_0)]$. $\Delta\psi_m$ is given by:

$$\Delta\psi_m = \psi_m^*(t_1^-) - \psi_m^*(t_0) \tag{6.5}$$

where $\psi_m^*(t_0)$ is the instantaneous curvature due to $M_0(t_0)$. $\psi_m^*(t_1^-)$ comprises:

- The instant curvature due to $M_0(t_1^-)$.
- Creep due to $M_0(t_0)$ from time t_0 to t_1^-.
- Creep due to $[M_0(t_1^-) - M_0(t_0)]$ from time t_0 to t_1^-.
- Shrinkage from time of drying to t_1^-.

The analysis procedure for any subsequent load step, when P_n is applied at t_n and sustained until t_{n+1}^-, can be generalised as:

1. Read the principal moments $M_n(t_n)$ and mean curvatures $\psi_m(t_n)$ corresponding to end of the previous load step (i.e. time t_n) from storage files.
2. Calculate the principal moments $M_n(t_{n+1}^-)$ corresponding to the current load P_n at time t_{n+1}^- and hence calculate the changes in moments $[M_n(t_{n+1}^-) - M_n(t_n)]$.
3. Calculate the instantaneous curvatures for states 1 and 2, $\psi_{1_n}(t_{n+1}^-)$, $\psi_{2_n}(t_{n+1}^-)$ due to moment $M_n(t_{n+1}^-)$ and $\psi_{1_n}(t_n)$, $\psi_{2_n}(t_n)$ due to moment $M_n(t_n)$. Material properties (tensile strength and elasticity modulus) corresponding to time t_n are used.

4. Calculate creep curvatures for states 1 and 2 between t_0 and t_{n+1}^- (corresponding to the stepped load history) using the principal of superposition.

   For any instantaneous load step P_j (incremental moment $[M_j(t_j) - M_{j-1}(t_j)]$), creep curvatures are calculated assuming that the load step is sustained from time t_j to time t_{n+1}^-.

The modulus of elasticity of concrete is modified for load step P_j :

$$\bar{E}_c(t_{n+1}^-, t_j) = \frac{E_c(t_n)}{1 + \phi(t_{n+1}^-, t_j)\chi(t_{n+1}^-, t_j)} \tag{6.6}$$

where

$\bar{E}_c(t_{n+1}^-, t_j)$= age-adjusted modulus of elasticity of concrete for load step P_j at time t_{n+1}^-.

$E_c(t_n)$= modulus of elasticity of concrete at time t_n.

$\phi(t_{n+1}^-, t_j)$= creep coefficient of concrete at time t_{n+1}^- due to a stress applied at time t_j.

The modular ratio becomes:

$$\bar{n}(t_{n+1}^-, t_j) = \frac{E_s}{\bar{E}_c(t_{n+1}^-, t_j)} \tag{6.7}$$

Using the cross-section calculation with age-adjusted modulus of elasticity of concrete and modified modular ratio as obtained by eqs 6.6 and 6.7, the changes in state 1 curvature due to creep for the moment increment corresponding to load step P_j during the period t_j to t_{n+1}^- are given by:

$$\Delta\psi_{1_j}(t_{n+1}^-, t_j) = k_1 \left[\phi(t_{n+1}^-, t_j)\left\{\delta\psi_{1_j} + \epsilon_{\bar{O}_1}(t_j)\frac{\bar{y}_{c1}}{\bar{r}_{c1}^2}\right\}\right] \tag{6.8}$$

where

k_1= reduction factor for reinforcement (see eq. 4.38).

$\delta\psi_{1_j}$= instantaneous increment in state 1 curvature at time t_j due to moment increment corresponding to load step P_j.

$\epsilon_{\bar{O}_1}(t_j)$= increment in normal strain at $\bar{O}_1$ at t_j corresponding to the increment in curvature $\delta\psi_{1_j}$.

The change in state 2 curvature due to creep for the moment increment corresponding to load step j during the period t_j to t_{n+1}^- is given by:

$$\Delta\psi_{2_j}(t_{n+1}^-, t_j) = k_2\left[\phi(t_{n+1}^-, t_j)\left\{\delta\psi_{2_j} + \epsilon_{\bar{O}_2}(t_j)\frac{\bar{y}_{c2}}{\bar{r}_{c2}^2}\right\}\right] \tag{6.9}$$

where

k_2= reduction factor for reinforcement (see eq. 4.42).

$\delta\psi_{2_j}$= instantaneous increment in curvature at time t_j in state 2 due to moment increment for load step j.

$\epsilon_{\bar{O}_2}(t_j)$= normal strain increment at $\bar{O}_2$ at t_j due to the increment in curvature $\delta\psi_{2_j}$.

5. Resultant curvatures are calculated in both states 1 and 2, by adding the
   - instantaneous curvatures i.e. $\psi_{1_n}(t_{n+1}^-)$ and $\psi_{2_n}(t_{n+1}^-)$ for states 1 and 2 respectively, due to principal moments $M_n(t_{n+1}^-)$.
   - incremental creeps, found in step 4, corresponding to all moment increments (e.g. $\Delta\psi_{1_j}(t_{n+1}^-, t_j)$ and $\Delta\psi_{2_j}(t_{n+1}^-, t_j)$ for states 1 and 2 respectively, for moment increment due to load step P_j) for all the load steps before time t_{n+1}^-.
   - shrinkage curvatures occurring in states 1 and 2 between time t_s and t_{n+1}^-.

The mean curvature ${\psi^*}_m(t_{n+1}^-)$ is then calculated interpolating between resultant curvatures in states 1 and 2:

$$\begin{aligned}{\psi^*}_m(t_{n+1}^-) &= (1-\zeta)\left[\psi_{1_n}(t_{n+1}^-) + \textstyle\sum_{j=1}^{n}\Delta\psi_{1_j}(t_{n+1}^-, t_j) + k_1\epsilon_{cs}(t_{n+1}^-, t_s)\frac{\bar{y}_{c1}}{\bar{r}_{c1}^2}\right] \\ &\quad +\zeta\left[\psi_{2_n}(t_{n+1}^-) + \textstyle\sum_{j=1}^{n}\Delta\psi_{2_j}(t_{n+1}^-, t_j) + k_2\epsilon_{cs}(t_{n+1}^-, t_s)\frac{\bar{y}_{c2}}{\bar{r}_{c2}^2}\right]\end{aligned} \tag{6.10}$$

Shrinkage curvatures are calculated using cross-sectional properties (i.e. $k_{1 \text{ or } 2}$, $\bar{y}_{c1 \text{ or } c2}$ and $\bar{r}_{c1 \text{ or } c2}^2$ in state 1 or 2) corresponding to the first load step. This

is an approximation which is justified by the observation that selecting cross-sectional properties related to the final step does not make any significant difference in the long-term deflection results. Also, the contribution of shrinkage to long-term deflection is not as significant as that of creep as will be demonstrated in section 8.5.

The magnitude of the interpolation coefficient ζ should be based on the actual level of cracking which depends on both the moment and concrete tensile strength as explained in detail in section 6.5.3. A check is carried out to determine the critical load step for cracking by comparing the current value of $M_n(t^-_{n+1})/\sqrt{\beta}M_r$ with all previous $M/\sqrt{\beta}M_r$ ratios and the critical (the biggest $M/\sqrt{\beta}M_r$ ratio) is used to find:

$$\zeta = 1 - \left(\frac{\sqrt{\beta}M_r}{M}\right)^2_{critical} \tag{6.11}$$

where $\beta = \beta_1\beta_2$. The β_1 coefficient takes into account the bond properties of bars; both Model Code-90 (MC-90) (1993) and Euro Code (EC2) (1991) recommend that β_1 should be taken as 1 and 0.5 for high-bond and plain bars respectively. The β_2 coefficient takes into account the deterioration of tension stiffening for long-term and repeated loads. MC-90 uses 0.8 for first loading and 0.5 for long-term or a large number of load cycles. EC2 suggests 1 and 0.5 respectively under similar conditions.

6. The mean curvature at the start of the current step, t_n, is then calculated using the procedure given in step 5. For load step P_j, creep curvatures are calculated similarly to step 4 except the load is sustained from time t_j to time t_n instead of t_j to t_{n+1}. Curvatures $\Delta\psi_{1_j}(t_n, t_j)$ and $\Delta\psi_{2_j}(t_n, t_j)$ are found for state 1 and state 2. Instantaneous curvatures are calculated for principal moments $M_n(t_n)$ and the incremental creep curvatures and shrinkage curvatures between time t_s and t_n are added to obtain the resultant curvatures in states 1 and 2. The mean curvature ${\psi^*}_m(t_n)$ is calculated as described in step 5, i.e.:

$${\psi^*}_m(t_n) = (1-\zeta)\left[\psi_{1_n}(t_n) + \textstyle\sum_{j=1}^{n} \Delta\psi_{1_j}(t_n, t_j) + k_1\epsilon_{cs}(t_n, t_s)\frac{\bar{y}_{c1}}{\bar{r}^2_{c1}}\right]$$

$$+\zeta\left[\psi_{2_n}(t_n)+\sum_{j=1}^{n}\Delta\psi_{2_j}(t_n,t_j)+k_2\epsilon_{cs}(t_n,t_s)\frac{\bar{y}_{c2}}{\bar{r}_{c2}^2}\right] \quad (6.12)$$

The ζ is taken as the greatest of either $M_n(t_n)/\sqrt{\beta}M_r$ or all previous values of $M/\sqrt{\beta}M_r$

7. Considering the curvature at the end of the last step $\psi_m(t_n)$, the mean curvature at time t_{n+1}^- is given by:

$$\psi_m(t_{n+1}^-)=\psi_m(t_n)+\psi^*{}_m(t_{n+1}^-)-\psi^*{}_m(t_n) \quad (6.13)$$

8. The modification factors α_{major} and α_{minor} (to account for cracking, creep and shrinkage) for major and minor principal directions are then:

$$\alpha_{major}=\frac{\psi_g}{\psi_{m-major}} \quad (6.14)$$

$$\alpha_{minor}=\frac{\psi_g}{\psi_{m-minor}} \quad (6.15)$$

where $\psi_g = M_n(t_{n+1}^-)/E_c(t_n)I_g$.

6.5 Calculation for unloading and reloading

The unloading and reloading parts of the load history are treated as follows:

1. Instantaneous changes in curvature on unloading and reloading are calculated using Rotilio's (1998) modified CEB-FIP Model Code 90 (1993).

2. The changes in curvature due to creep recovery are calculated using the method of superposition. Recovery creep curves are scaled down with a recovery factor to account for the fact that recovery strains are less than creep strains due to a load increment.

These points are explained below.

6.5.1 Instantaneous unloading

Rotilio (1998) suggested that the unloading branch proposed in CEB-FIP Model Code 90 moment-curvature relationship (see Fig. 6.2) is inaccurate. He proposed

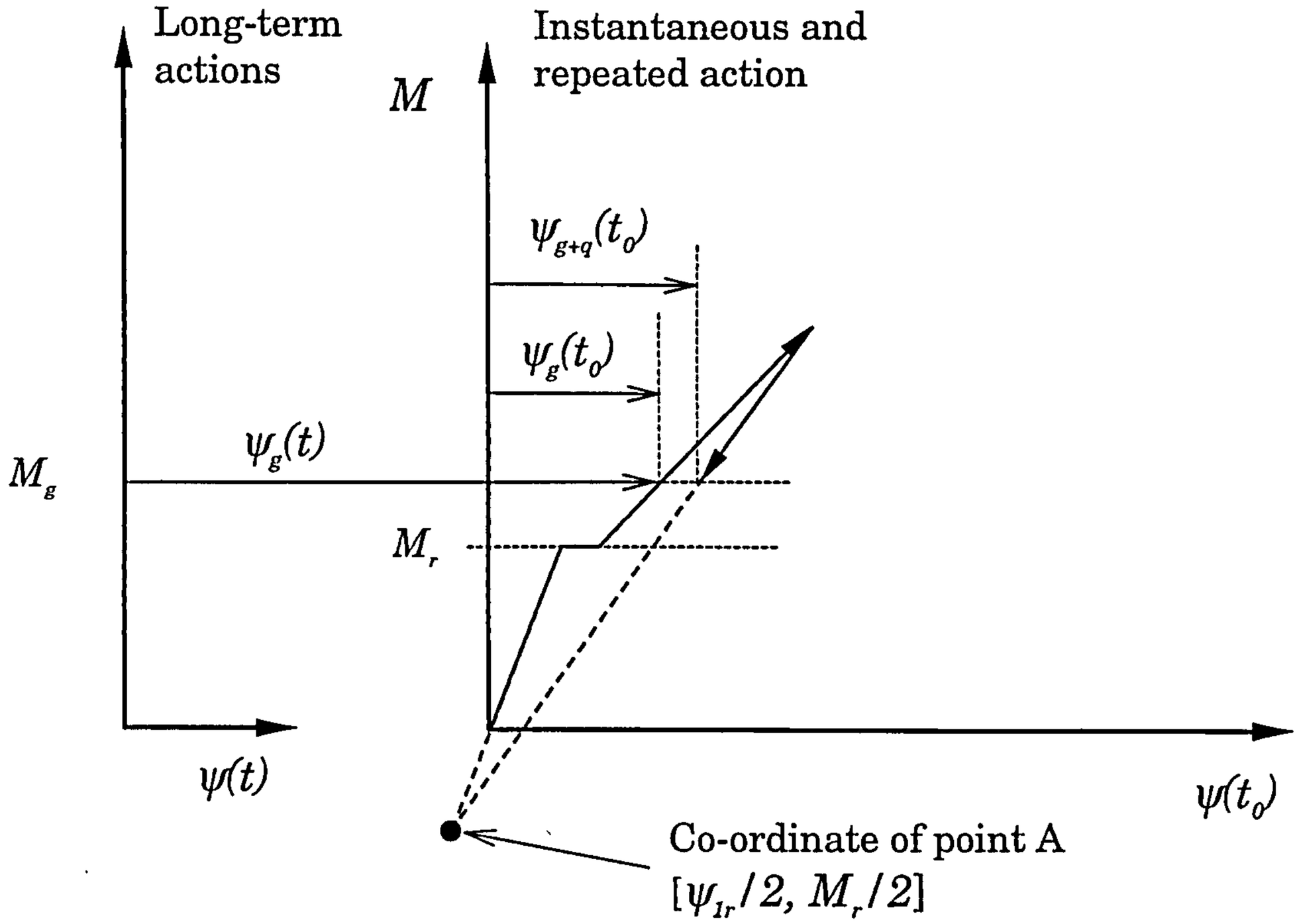


Figure 6.2 Moment-curvature relationship proposed by Model Code 90 (1993)

the adjusted unloading curve shown in Fig. 6.3. Based on his test results, he defined a pivot point (point A in Fig. 6.3) on the state 1 line with a moment coordinate equal to the negative value of the maximum moment reached before unloading. All the unloading branches converge towards this pivot point irrespective of the maximum load level, amount of reinforcement or shape and size of the element. This unloading branch is employed in the current work. For any instantaneous change in moment, the program compares the values of $M/\sqrt{\beta}M_r$ ($\beta = \beta_1\beta_2$; β_2= 1 for instantly applied load and 0.5 for cyclic load) of the current step with all previous steps. If unloading is detected, i.e. $M/\sqrt{\beta}M_r$ from a previous step is found to be higher than for the current step, curvatures are calculated using the unloading branch.

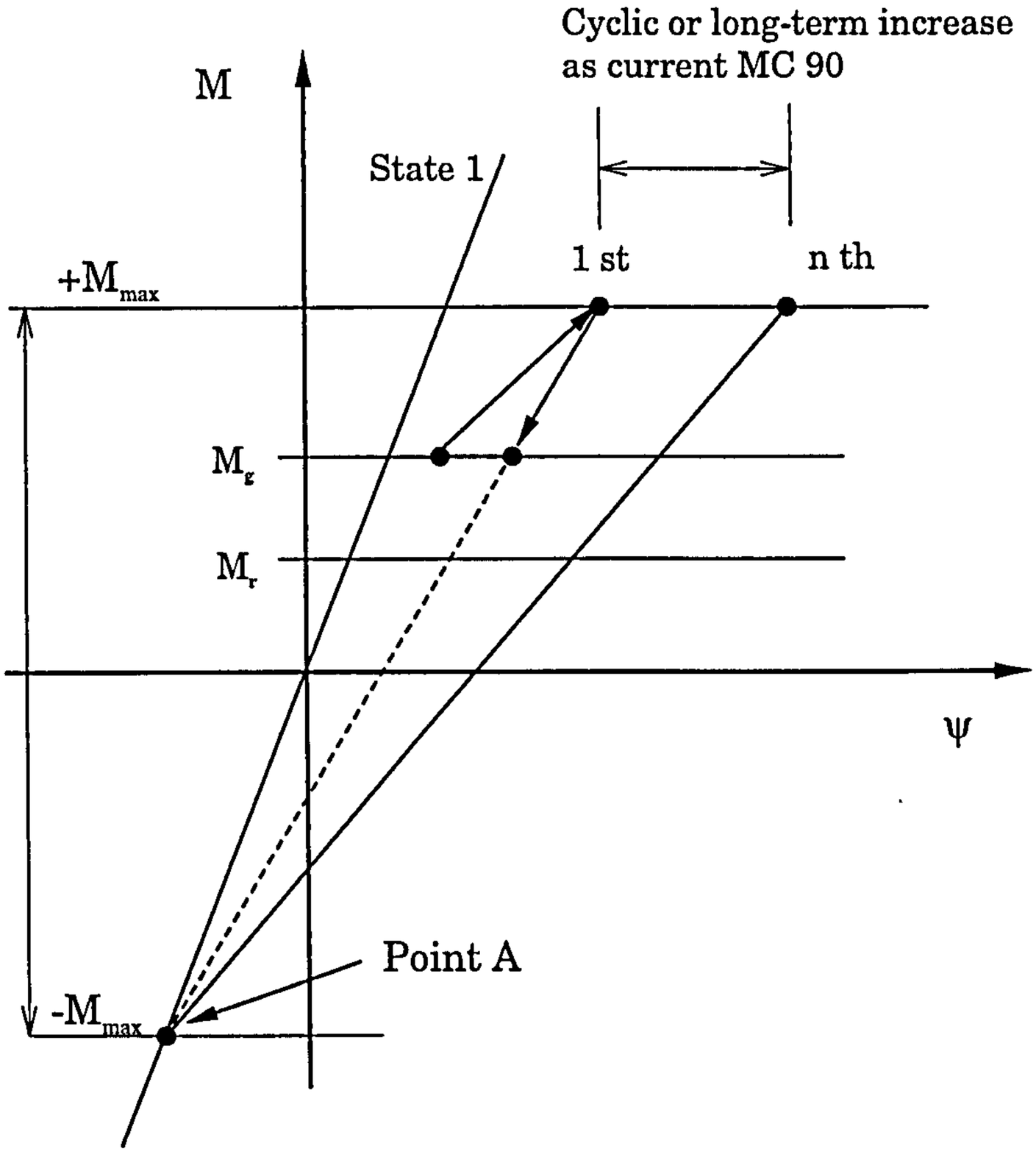


Figure 6.3 Moment-curvature relationship proposed by Rotilio (1998)

6.5.2 Long-term after unloading: creep recovery

The principle of superposition of creep curvatures adopted in the current analysis is illustrated in Fig. 6.4. Gilbert (1988) reported that, for increasing stress histories,

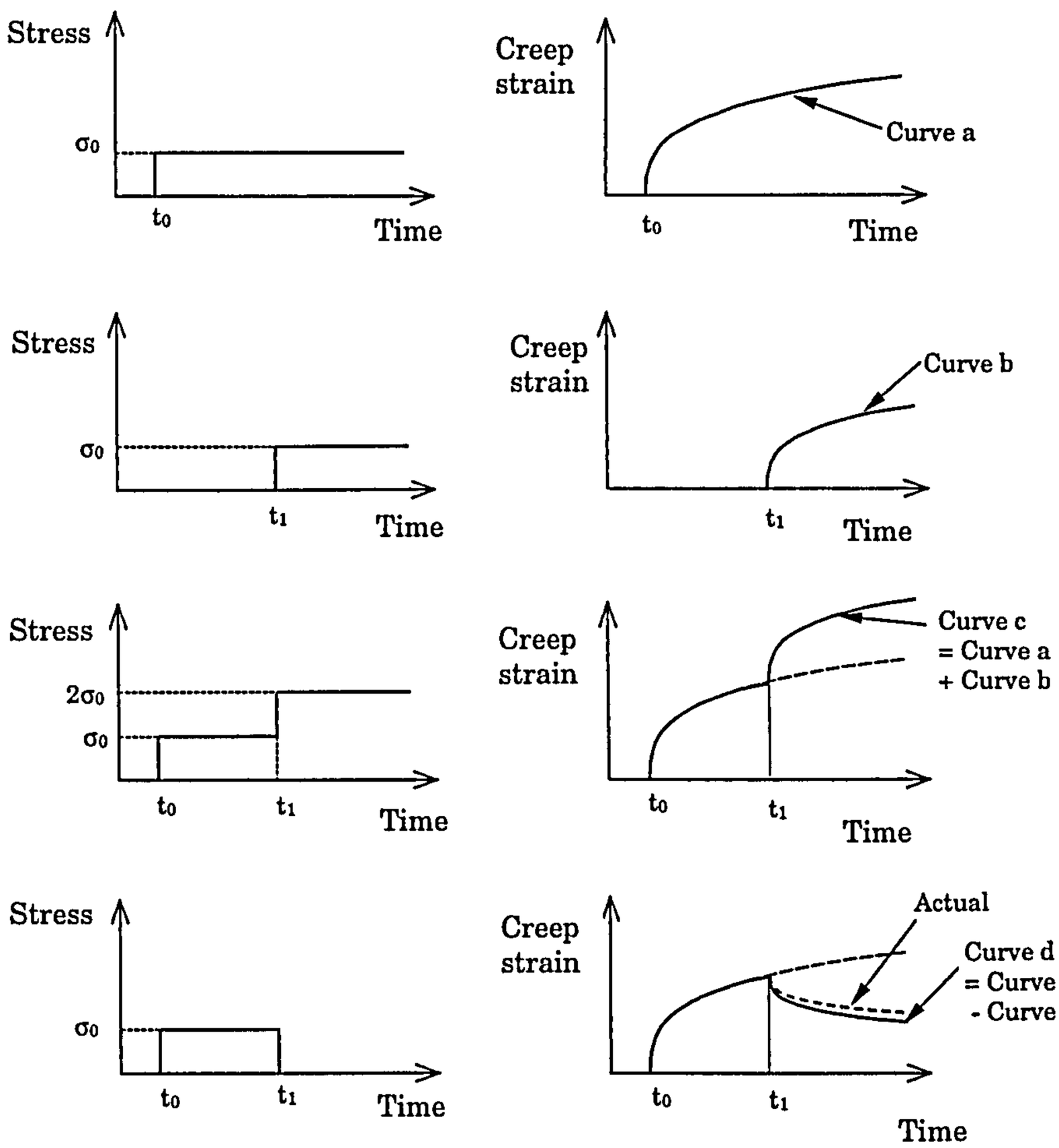


Figure 6.4 Principle of superposition of creep curvatures: adapted from Gilbert (1988)

the principle of superposition agrees well with experimental observations. However, for a reducing stress history, the principle of superposition overestimates creep recovery because only a portion of the creep strain is actually recoverable, while usually a larger portion is irrecoverable or permanent. The recoverable part of the creep is referred to as the delayed elastic strain, $\epsilon_d(t)$. This delayed elastic strain is thought to be caused by the elastic aggregate acting on the viscous cement paste after stress is removed. According to Gilbert (1988), if a concrete specimen is unloaded after a long period under load, the magnitude of the recoverable creep is of the order of 10 to 30 percent of the total creep strain. The majority of creep strain is irrecoverable

and is often termed as flow, $\epsilon_f(t)$. The creep strain at any time can therefore be expressed as the sum of the delayed elastic and flow components:

$$\epsilon_c(t) = \epsilon_d(t) + \epsilon_f(t) \tag{6.16}$$

Figure 6.5 shows recoverable and irrecoverable creep components.

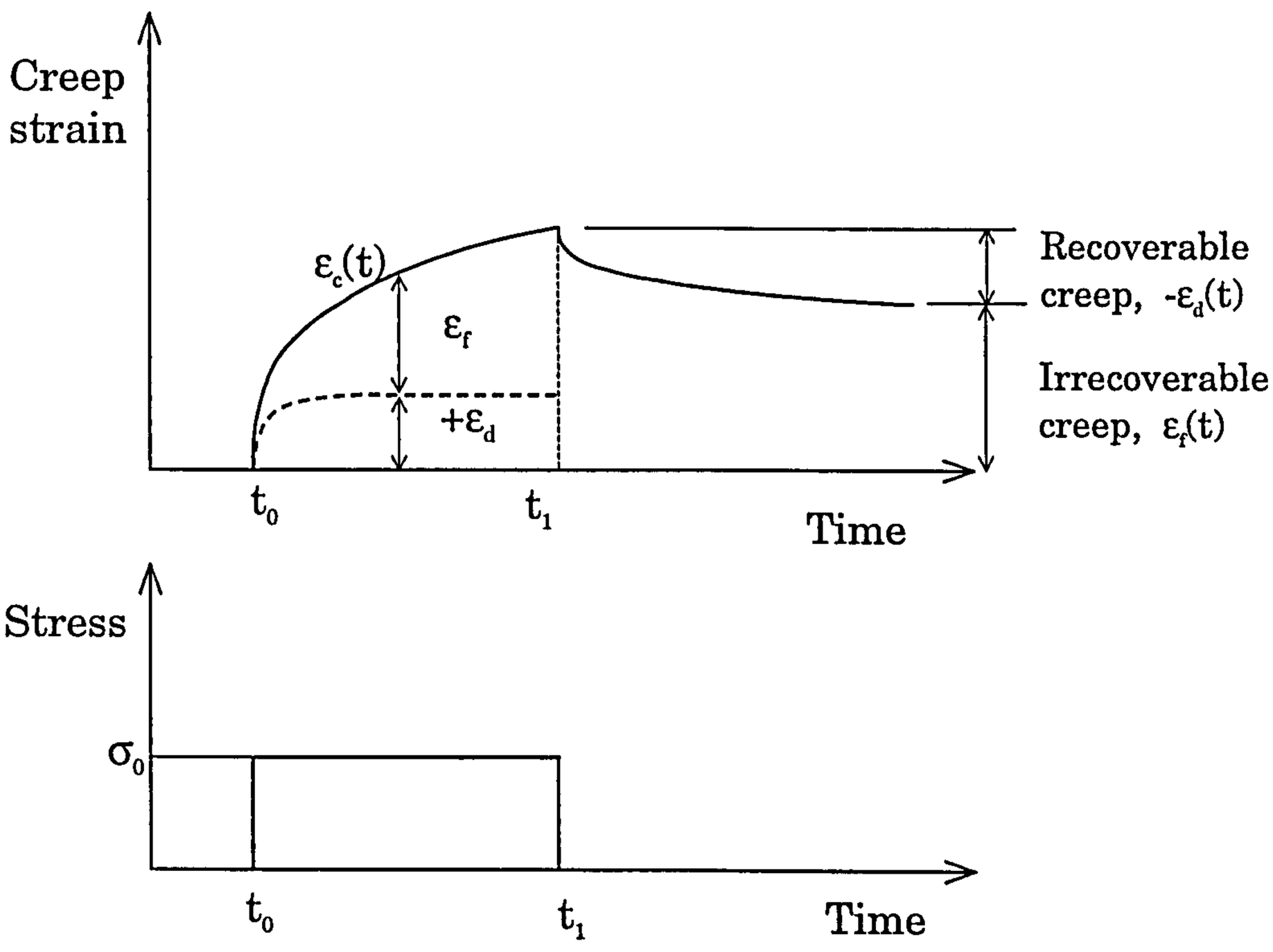


Figure 6.5 Recoverable and irrecoverable creep components: adapted from Gilbert (1988)

The principal of superposition described in the previous section is also valid for unloading steps. For an unloading step, the moment increment can be treated as a negative term and creep curvatures resulting due to this negative increment of moment (as obtained by eq. 6.8 or eq. 6.9) will also be negative. This calculated negative creep curvature is less than the actual creep, since the negative load is applied later than the positive load. The principal of superposition overestimates creep recovery. Therefore, a recovery factor R is used to scale down the negative creep curvatures to model the delayed elastic strain which is the only recoverable component of creep.

6.5.3 Long-term after unloading: interpolation coefficient

The interpolation coefficient used to calculate the mean curvature (eq. 6.11) at any time t needs to be based on the actual level of cracking which may not correspond to the current loading. The level of cracking depends on both the load and the concrete tensile strength.

This can be seen by considering three otherwise identical one-way slabs with three different loading or cracking cases. Figure 6.6 shows a loading and unloading long-term moment-curvature relationship for a slab element. To simplify the argument

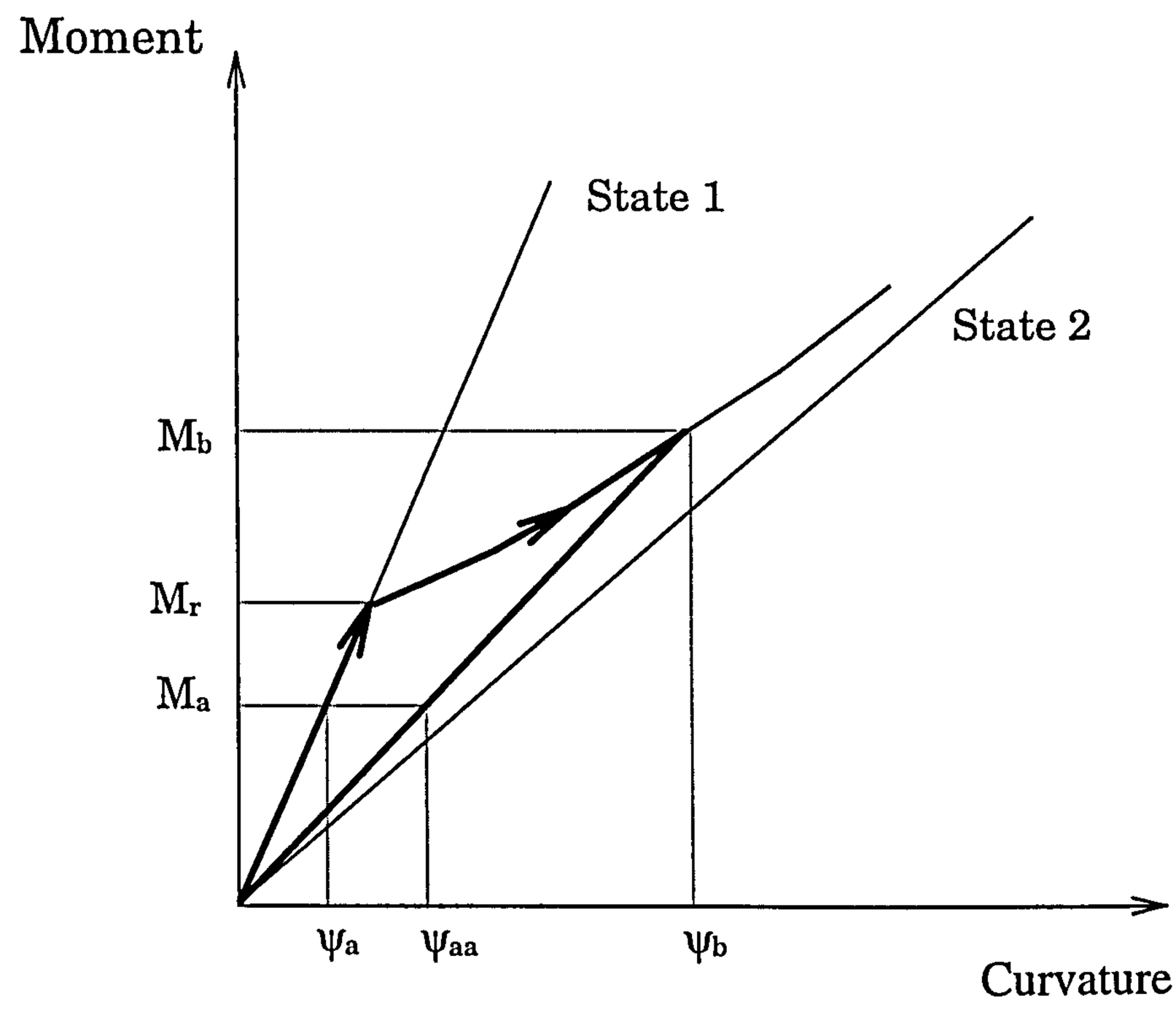


Figure 6.6 Moment-curvature relationship: loading and unloading

it is assumed that unloading does not produce any permanent deformation. Three cases are considered:

1. The first slab is loaded under self-weight at t_1 days and is assumed to not crack. The moment due to self-weight is M_a and the corresponding curvature at t_2 days is ψ_a. ψ_a includes instantaneous, creep and shrinkage curvatures.

2. The second slab is loaded to a higher load to produce M_b at time t_1 days

where M_b is greater than M_r. The corresponding curvature at t_2 days, ψ_b, is calculated by interpolating between states 1 and 2 using the ratio $M_b/\sqrt{\beta}M_r$ in eq. 6.11.

3. The third slab is loaded under self-weight at t_1 days, but with the assumption that the extent of cracking is similar to case 2, i.e. it has been subjected to a moment M_b prior to the current load when the cracking moment was M_r. Therefore, the moment-curvature relationship will follow the unloading line shown in Fig. 6.6. The moment due to self-weight is M_a and the corresponding curvature at t_2 days, ψ_{aa}, should be calculated by interpolation between states 1 and 2 using the ratio $M_b/\sqrt{\beta}M_r$ in eq. 6.11.

To take into account the history of cracking of the slab, the maximum values of $(M/\sqrt{\beta}M_r)_{max}$ for all the elements for the two principal directions are stored in a file. For any particular step, $M/\sqrt{\beta}M_r$ is calculated for each element in each direction and, if the ratio is less than the maximum $(M/\sqrt{\beta}M_r)_{max}$ already stored in file for previous steps, the latter is used in eq. 6.11 in place of $M/\sqrt{\beta}M_r$. If $M/\sqrt{\beta}M_r$ is higher than stored value, $M/\sqrt{\beta}M_r$ is used in eq. 6.11 and the value replaces the previous value stored as the maximum $(M/\sqrt{\beta}M_r)_{max}$ ratio.

6.6 Effect of subdivision of load step: slab

A computer program was developed to model time-varying load history using the method described in section 6.4. To determine the effect of subdivision of load step, a statically determinate one-way slab and an indeterminate square fixed-edge slab have been analysed. First, the program was used to analyse the one-way slab loaded with a uniform load. The load was artificially divided into different number of time steps to check if the step analysis method was correctly implemented. When the load step is divided, the incremental moment is calculated for each step by subtracting the previous step moment from the current step moment. For statically determinate slabs, as there is no moment redistribution, the deflection should be independent of the number of time subdivisions of the load step. Therefore, a determinate structure is analysed to check the accuracy of programming. However, for indeterminate slabs,

due to cracking, creep and shrinkage, moment redistribution occurs even under a uniform load. As a result, the incremental moments and time of application are dependent on the number of subdivisions of the load step. The study indicates the effect of subdividing the load step on deflection.

6.6.1 Statically determinate one-way slab

A 7.5 m square one-way slab with 250 mm thickness (see Fig. 6.7) has been considered in the analysis to demonstrate that the program developed to model time-varying load history works. The load is assumed to be applied at 1 day and sustained for 1000 days. The tensile strength of concrete is taken as 2.0 MPa and modulus of elasticity as 30.0 GPa. A concrete compressive cylinder strength of 40 MPa and a relative humidity of 50 percent were used to calculate the creep coefficient and shrinkage strain of concrete by means of the MC-90 equations. Shrinkage is assumed to start from 1 day. To create a substantial deflection, a very high-intensity uniformly distributed load of 20 kN/m^2 is applied. 0.8 percent top and bottom reinforcement are used throughout the slab. One quarter of the slab is taken for the FE analysis.

Four cases have been studied with different numbers of load steps. For the first case, the analysis was done with the assumption that the load was applied at 1 day and sustained until 1000 days. For the second case, first, an FE analysis was carried out with the load being sustained from 1 to 500 days. Next, another FE analysis was performed with load sustained from 500 to 1000 days and curvatures and moments stored in the first analysis were used in the calculations. Intervals of 250 and 100 days have been used for cases three and four respectively.

Deflections are monitored at two nodes (1 and 17) as shown in Fig. 6.7. The deflection at 1000 days for the two monitoring points are not influenced by the number of intervals used as there is no moment redistribution for a statically determinate structure. This is shown in Figs 6.8 to 6.9. The results clearly indicate that the programming, particularly the reading to and writing from the storage files was working properly. It should be noted here, for this one-way slab, that the solutions are checked in two different ways. First, the modified E values are gradually

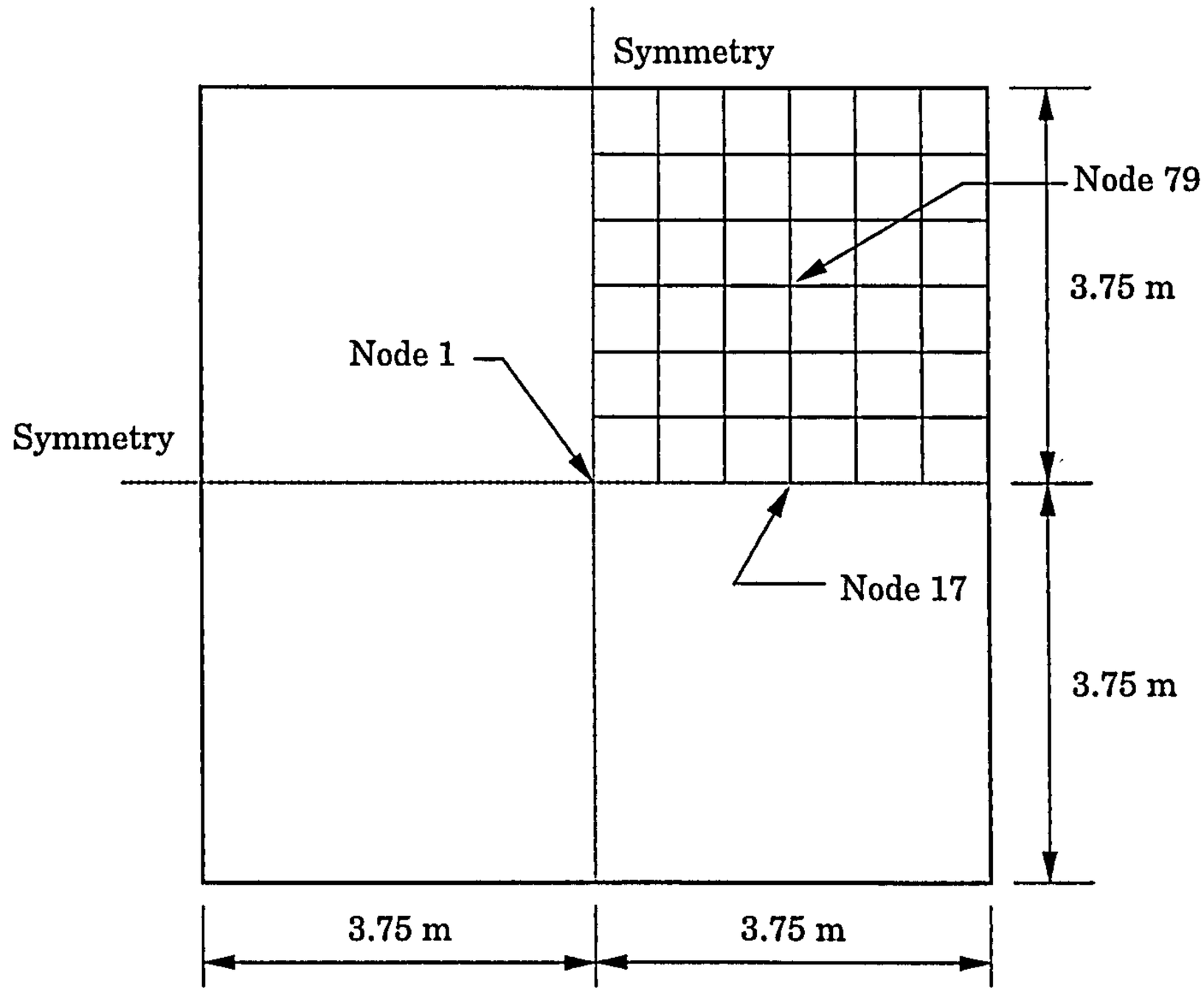


Figure 6.7 FE mesh for the fixed-edge and one-way slab

decreased in different FE runs until convergence and, secondly, modified E values are fed back without any gradual change into the FE package to get the solution in second run. Both cases yield identical results.

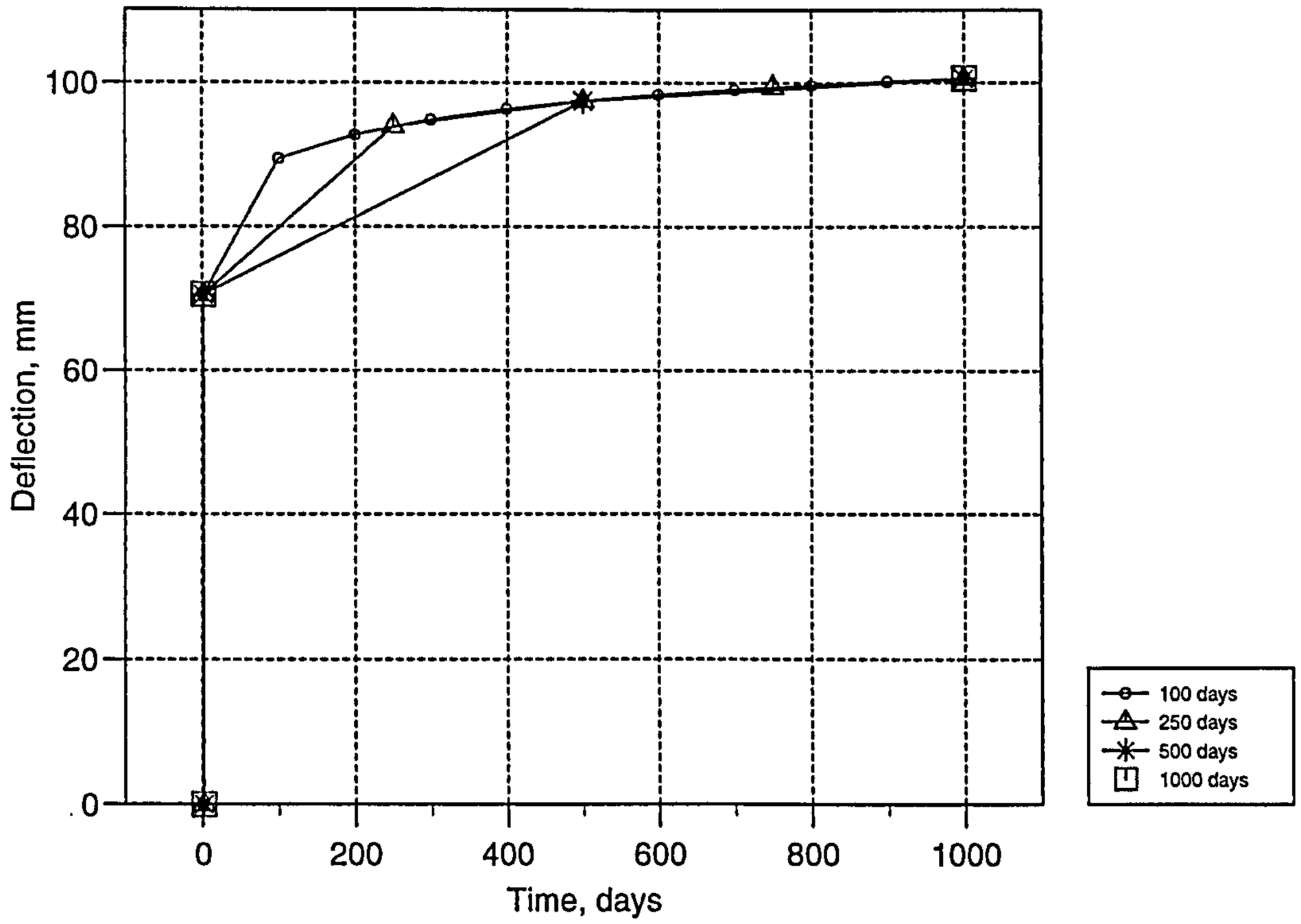


Figure 6.8 One-way slab: node 1 deflection with time

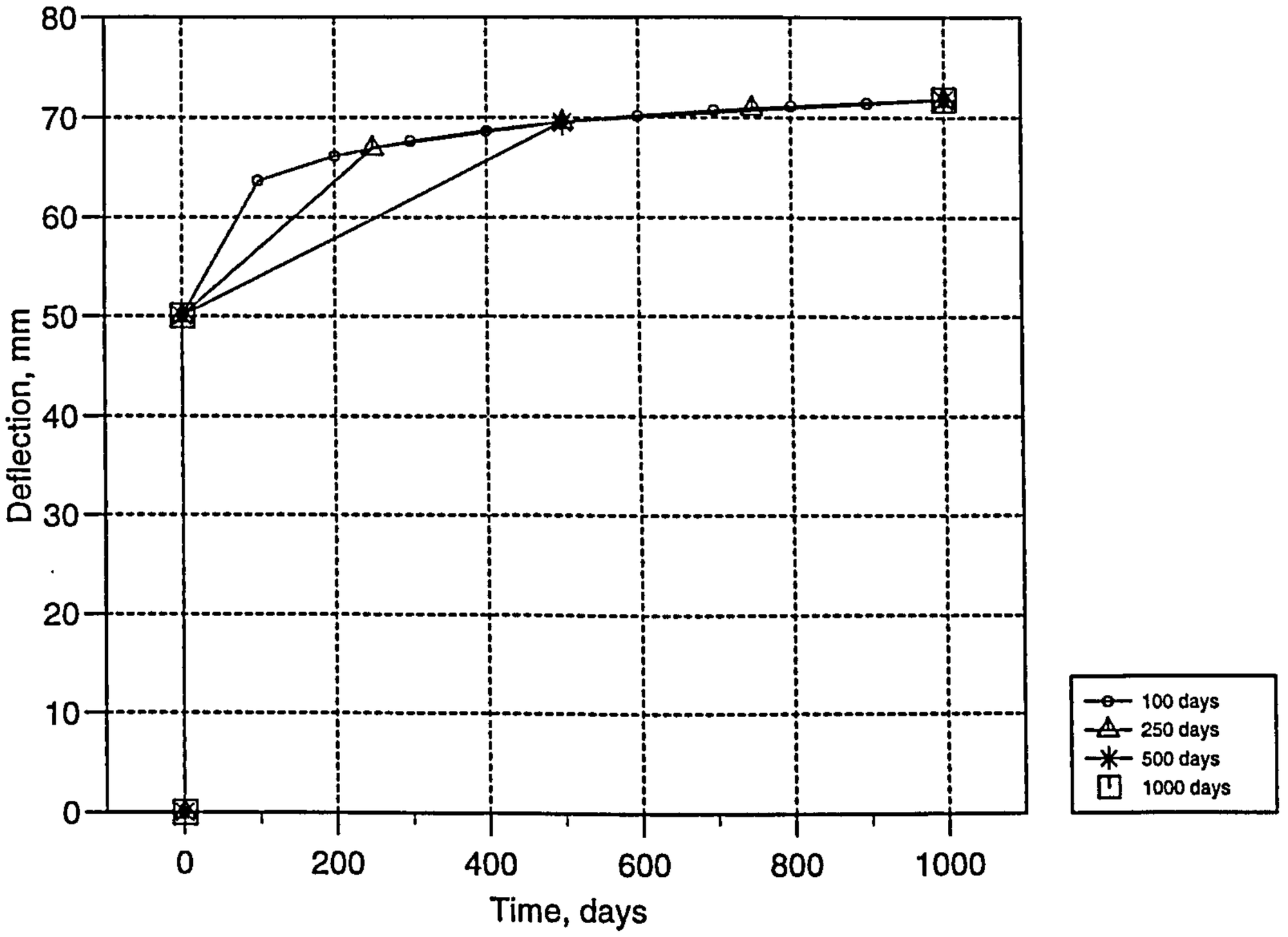


Figure 6.9 One-way slab: node 17 deflection with time

6.6.2 Statically indeterminate fixed-edge slab

The same slab as above is used here but now it is supported as a fixed-edge slab. The load applied remains the same. Three nodes (1,17 and 79), as shown on Fig. 6.7, are taken to monitor the deflections. The level of cracking varied over the slab resulting in a redistribution of moment in each subdivision of the load step. With different creep and shrinkage properties at different subdivisions, the resulting incremental moments are also different.

Deflections at the monitoring points are plotted against time in Figs 6.10 to 6.12. With the increase in the number of time intervals, 1000 day deflections increase, and the maximum increase has been found for the analysis with 100 day intervals. For nodes 1, 17 and 79, these increases are 6.0, 6.7 and 6.6% respectively. The moment distribution at any time depends on the applied load, level of cracking, creep and shrinkage, therefore, there are differences in moments between successive loading steps. This example shows that the final deflection is relatively insensitive to the number of subdivision of the load step. Therefore, if the deflection due to a constant load step is required at time t, it is not necessary to subdivide the load step into steps less than t. The author also found the instantaneous deflection by dividing the load step of 20 kN/m^2 into ten steps, the method gives exactly the same deflection that was obtained with a single step as shown in Figs 6.10 to 6.12. This is due to the fact that all the $\psi^*{}_m$-s cancel out to leave ψ_m corresponding to full 20 kN/m^2 load. So, the redistribution of stresses due to load change is implicitly incorporated in the approach.

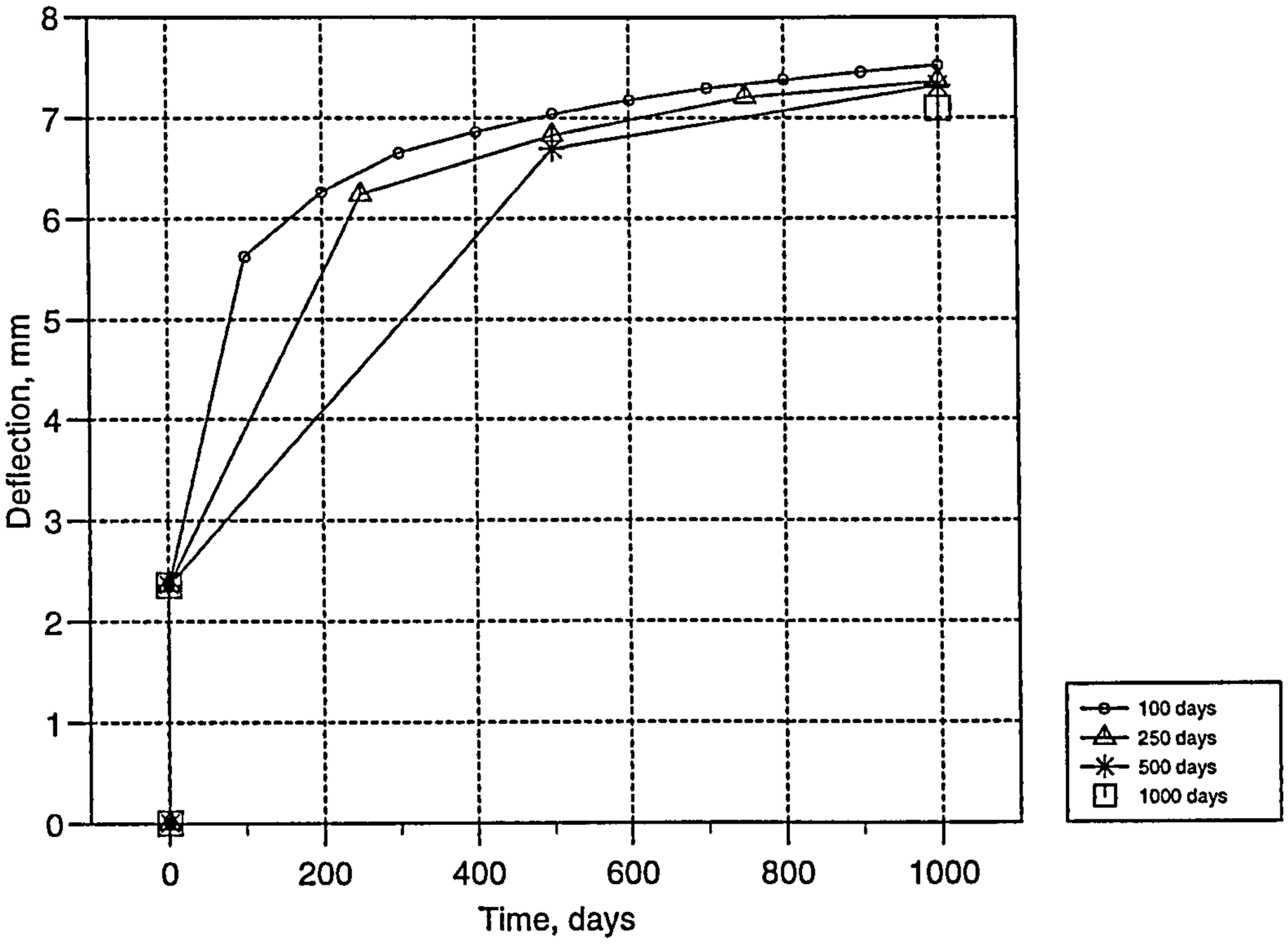


Figure 6.10 Fixed-edge slab: node 1 deflection with time

Figure 6.11 Fixed-edge slab: node 17 deflection with time

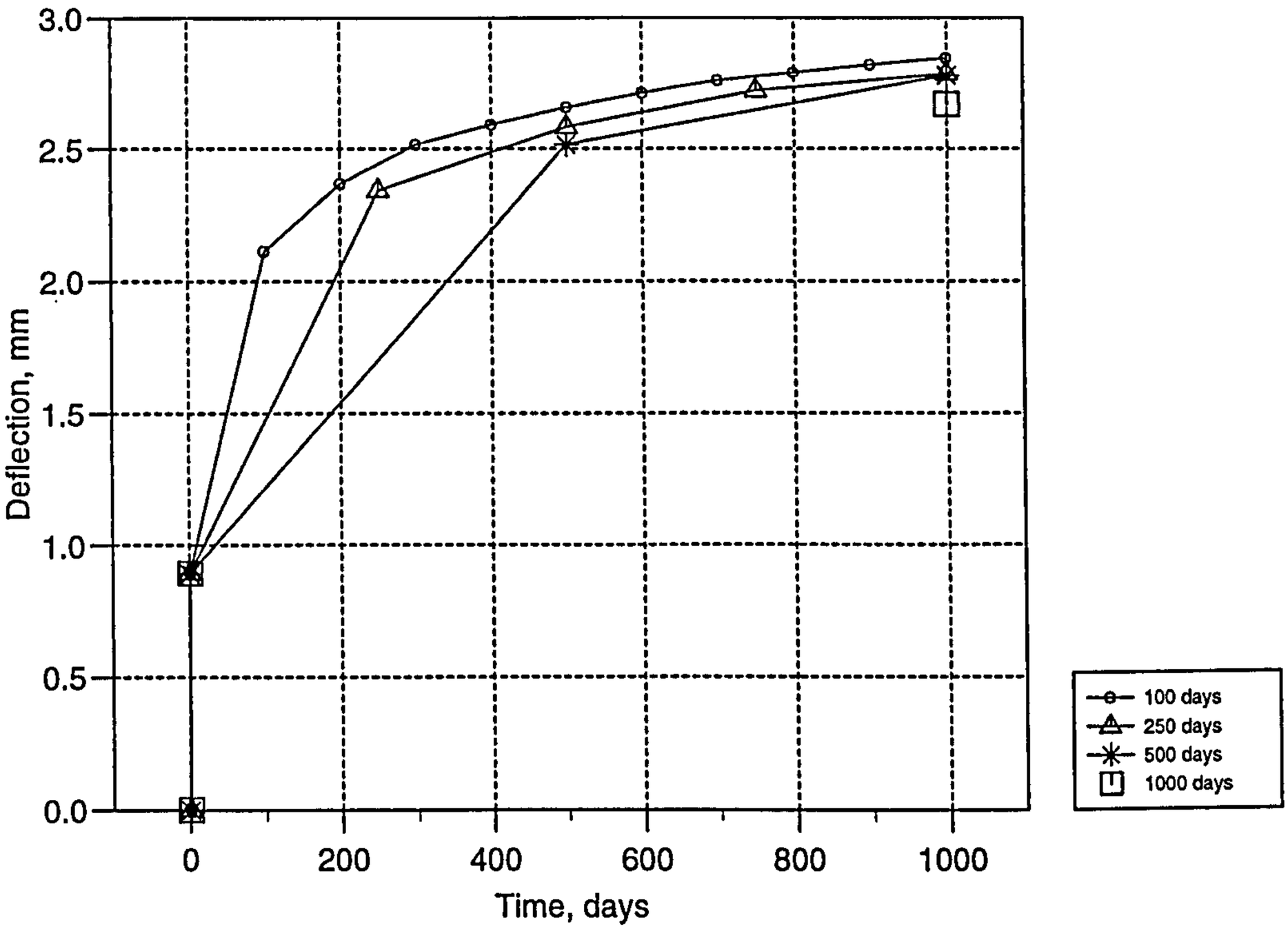


Figure 6.12 Fixed-edge slab: node 79 deflection with time

6.7 Analysis method for column

The method of analysis used to find the change in deflection with time for an eccentrically loaded column is similar to that of a slab described in section 6.4. The analysis starts with the load P_1 applied instantly at time t_1. As no previous load step is present, the analysis is similar to the analysis presented in section 5.5. After convergence, the axial force $N_1(t_1)$ and the mean curvature $\psi_m(t_1)$ for each brick element are stored in files for later use.

The mean curvature at the end of any load step, when P_n is applied at t_n and sustained until t_{n+1}^-, can be obtained as follows:

1. Axial forces $N_n(t_n)$ and curvatures $\psi_m(t_n)$ corresponding to time t_n, when the previous load step ends, are read from files.

2. Magnitudes and positions of axial forces $N_n(t_{n+1}^-)$ for the current load step P_n are calculated from stresses stemming from the current FE analysis, and changes in forces $[(N_n(t_{n+1}^-) - N_n(t_n)]$ are calculated.

3. Instantaneous curvatures for state 1 and state 2, $\psi_{1_n}(t_{n+1}^-)$ and $\psi_{2_n}(t_{n+1}^-)$ due to $N_n(t_{n+1}^-)$ and $\psi_{1_n}(t_n)$ and $\psi_{2_n}(t_n)$ due to $N_n(t_n)$, are calculated.

4. Creep curvatures are calculated for all the incremental axial forces assuming that they are sustained from their loading time to the end of the step under consideration i.e. time (t_{n+1}^-).

   For any load step P_j (the incremental force $[N_j(t_j) - N_{j-1}(t_j)]$), the creep curvatures are calculated assuming that P_j is sustained from time t_j to time t_{n+1}^-. The creep curvatures in states 1 and 2, $\Delta\psi_{1_j}(t_{n+1}^-, t_j)$ and $\Delta\psi_{2_j}(t_{n+1}^-, t_j)$, due to the force increment for load step P_j during the period t_j to t_{n+1}^-, are calculated similarly as described for the slab in section 6.4.

5. The mean curvature $\psi^*{}_m(t_{n+1}^-)$ is calculated assuming a single load step for normal force $N_n(t_{n+1}^-)$ by interpolating between states 1 and 2. Incremental creeps in states 1 and 2 due to all force increments for all the load steps before time t_{n+1}^-, as found in previous steps, are added to instantaneous curvatures

$\psi_{1n}(t^-_{n+1})$ and $\psi_{2n}(t^-_{n+1})$:

$$\begin{aligned}\psi^*{}_m(t^-_{n+1}) &= (1-\zeta)\left[\psi_{1n}(t^-_{n+1}) + \textstyle\sum_{j=1}^{n}\Delta\psi_{1_j}(t^-_{n+1},t_j) + k_1\epsilon_{cs}(t^-_{n+1},t_s)\frac{\bar{y}_{c1}}{\bar{r}^2_{c1}}\right] \\ &\quad +\zeta\left[\psi_{2n}(t^-_{n+1}) + \textstyle\sum_{j=1}^{n}\Delta\psi_{2_j}(t^-_{n+1},t_j) + k_2\epsilon_{cs}(t^-_{n+1},t_s)\frac{\bar{y}_{c2}}{\bar{r}^2_{c2}}\right] \quad (6.17)\end{aligned}$$

The shrinkage curvatures are calculated using section properties corresponding to the first load step.

The interpolation coefficient ζ is based on the current $\sigma_{sn}(t^-_{n+1})/\sigma_{sr}$ value or any critical value of σ/σ_r corresponding to a previous loading step:

$$\zeta = 1 - \beta_1\beta_2\left(\frac{\sigma_r}{\sigma}\right)^2_{critical} \quad (6.18)$$

where σ_{sr} and $\sigma_{sr}(t^-_{n+1})$ express the maximum tensile reinforcement stresses in the cracked section at cracking and at the applied axial load $N_n(t^-_{n+1})$ respectively. ψ_2 is obtained corresponding to the rupture load found on the basis of state 1 and the maximum steel tensile stresses are found for this ψ_2.

6. The amount of creep occurring between the application of the force increment and the starting time of the current step is then calculated. For the load step P_j, creep curvatures are calculated similarly as step 4 but now assuming that they are sustained from time t_j to time t_n. For state 1 and state 2, curvatures $\Delta\psi_{1_j}(t_n,t_j)$ and $\Delta\psi_{2_j}(t_n,t_j)$ are found. The mean curvature $\psi^*{}_m(t_n)$ is calculated similarly as for step 5 but this time for a normal force of $N_n(t_n)$:

$$\begin{aligned}\psi^*{}_m(t_n) &= (1-\zeta)\left[\psi_{1n}(t_n) + \textstyle\sum_{j=1}^{n}\Delta\psi_{1_j}(t_n,t_j) + k_1\epsilon_{cs}(t_n,t_s)\frac{\bar{y}_{c1}}{\bar{r}^2_{c1}}\right] \\ &\quad +\zeta\left[\psi_{2n}(t_n) + \textstyle\sum_{j=1}^{n}\Delta\psi_{2_j}(t_n,t_j) + k_2\epsilon_{cs}(t_n,t_s)\frac{\bar{y}_{c2}}{\bar{r}^2_{c2}}\right] \quad (6.19)\end{aligned}$$

The interpolation coefficient ζ is based on the $\sigma_{sn}(t_n)/\sigma_{sr}$ value or any previous critical load condition.

7. Considering the curvature at the end of the last step $\psi_m(t_n)$, the mean curva-

ture at time t_{n+1}^- is obtained using:

$$\psi_m(t_{n+1}^-) = \psi_m(t_n) + \psi^*{}_m(t_{n+1}^-) - \psi^*{}_m(t_n) \tag{6.20}$$

8. From the mean curvature obtained above, an equivalent section with brick and line elements is generated as described in section 5.6.1.

For unloading steps, creep recovery is treated similarly as described in section 6.5.2 for the case of slabs. The maximum ratios of σ/σ_{sr} for all the brick elements are also stored to take into account cracking in previous steps.

6.8 Effect of subdivision of load step: column

The method described in section 6.7 was incorporated in the computer program to model time-varying load history for a column. To determine the effect of subdivision of a load step, a statically determinate cantilever column and an indeterminate propped cantilever have been analysed. A uniform load step was considered which was artificially subdivided into a number of steps. When the load step is divided, the axial force increment in each step is calculated by subtracting the previous step force from the current step force. For the statically determinate cantilever column, as there is no stress redistribution, the displacements should be independent of the number of time subdivisions of the load step. Therefore, the cantilever column was analysed to check if the analysis method was correctly implemented. However, for the indeterminate propped cantilever column, due to cracking, creep and shrinkage, stress redistribution occurs even under a uniform force. Hence, the axial force increments are dependent on the number of subdivisions of the load step. The study shows the effect of subdivision of load step on column displacements.

6.8.1 Statically determinate cantilever

An eccentrically loaded cantilever column is loaded at the corner with a load of 5000 kN. The column is 5 m long having a section 800 x 400 mm. Six 32 mm bars are used in the section as shown in the Fig. 5.16. 40 MPa concrete is used with a

modulus of elasticity of 30 GPa and tensile strength of 2.5 MPa. Shrinking of the column starts from 1 day.

Four cases have been studied with different number of load steps. For the first case, the analysis was done with the assumption that the load was applied at 1 day and sustained until 1000 days. For the second case, the load was applied at 1 day and sustained until 500 days and then again was re-applied at 500 days and sustained until 1000 days. An interval of 250 and 100 days have been used for case three and four respectively. x and y direction sways of the top of the cantilever have been monitored for different time intervals.

Elasticity properties are modified in two ways: first, they are modified gradually according to section 4.11 and, secondly, they are modified on the basis of elastic stresses. For both approaches, the deflections at 1000 days for all the monitoring points are not at all influenced by the number of intervals used and both approaches produce exactly same displacements. This is shown in Figs 6.13 and 6.14.

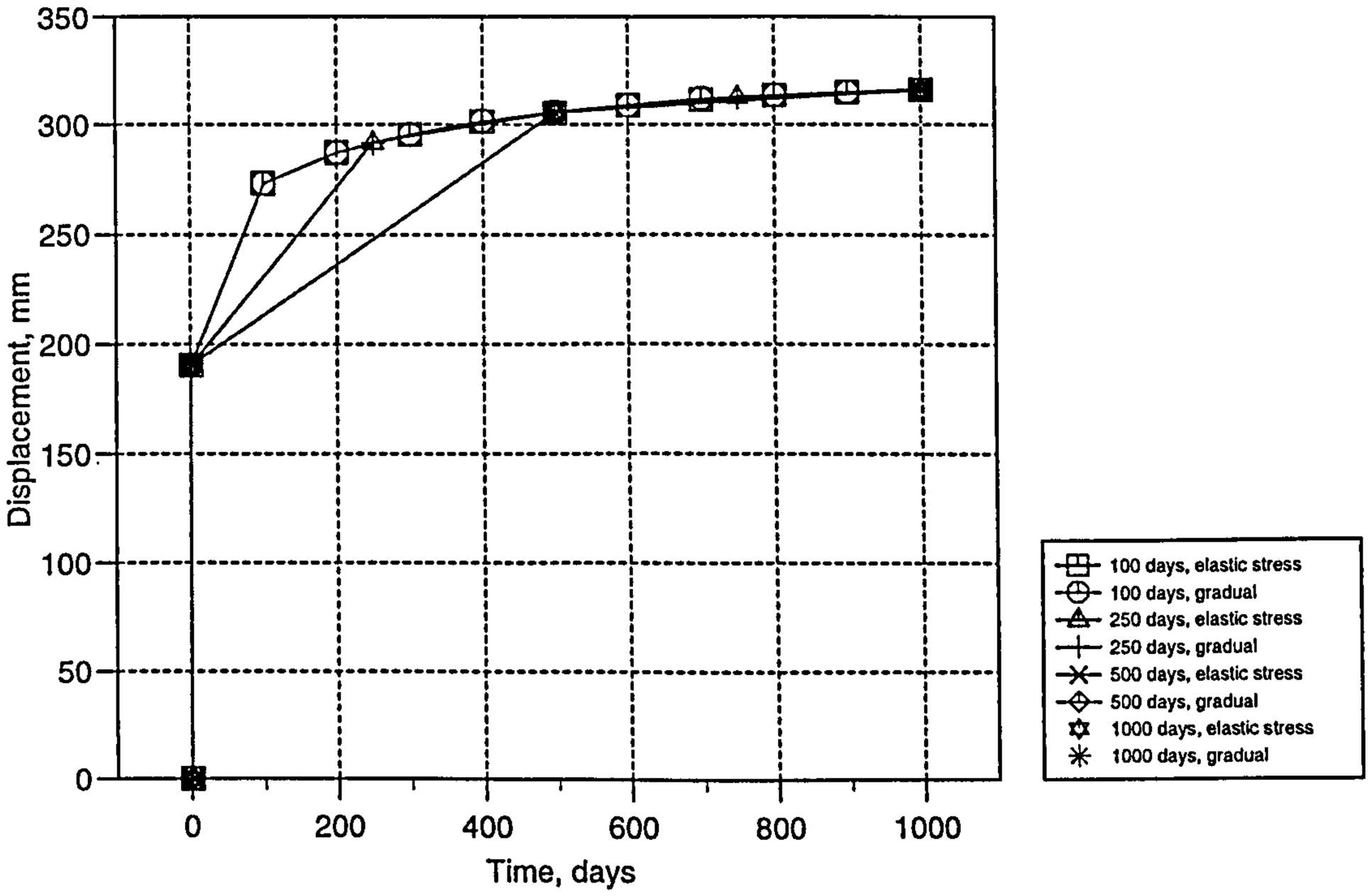


Figure 6.13 X directional sway of top of the cantilever with time

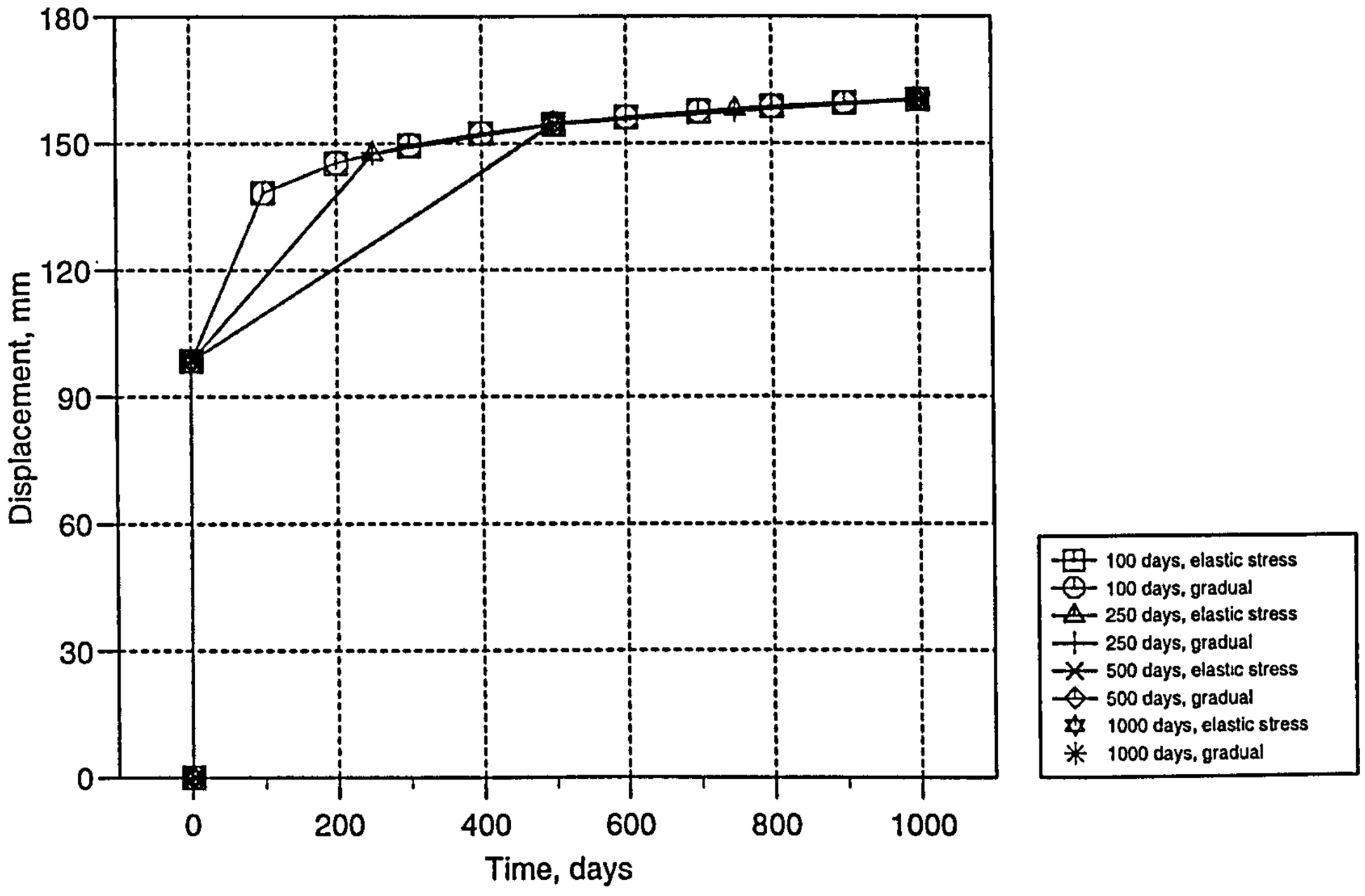


Figure 6.14 Y directional sway of top of the cantilever with time

6.8.2 Statically indeterminate propped cantilever

The same column, but now propped at the top against x and y sways, is now loaded at the corner. To create a substantial amount of sway, a very high intensity load of 60000 kN is applied. x and y directional sways at the mid-height of the cantilever were monitored.

Four cases have been studied with different number of load steps. Elasticity properties of the brick and line elements are gradually decreased to allow for possible redistribution of stress. The same analysis was carried with elasticity properties changed only once on the basis of elastic stresses and thus allowing no stress redistribution. x and y directional sways with time for the centre of the section at mid-height are plotted in Figs 6.15 and 6.16. The differences between sways calculated on gradually modified E and on E calculated using elastic stress, are less than 1.8%. Increasing the number of steps has also very negligible effect on x and y directional sways.

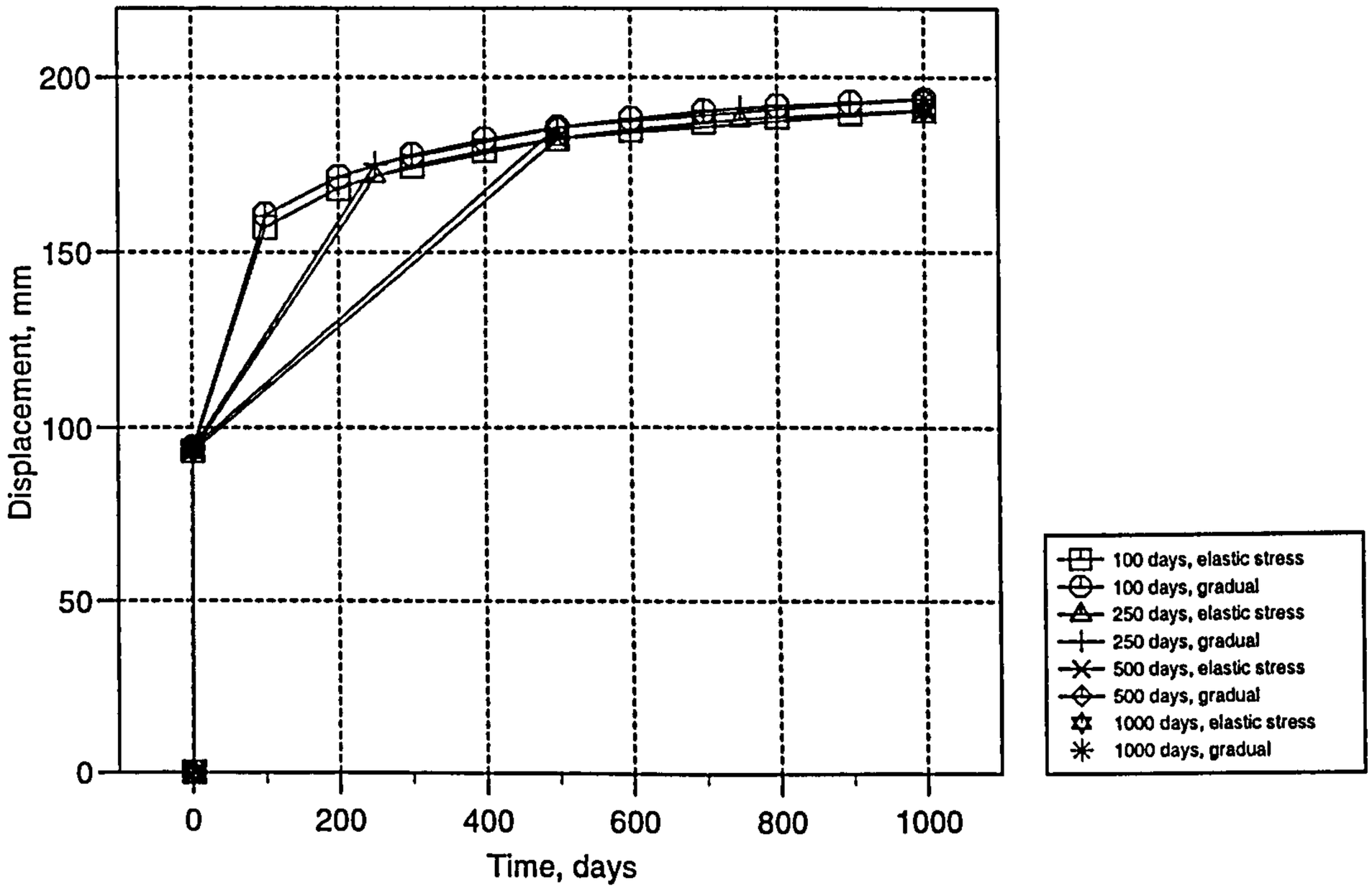


Figure 6.15 X directional sway of middle of the propped cantilever with time

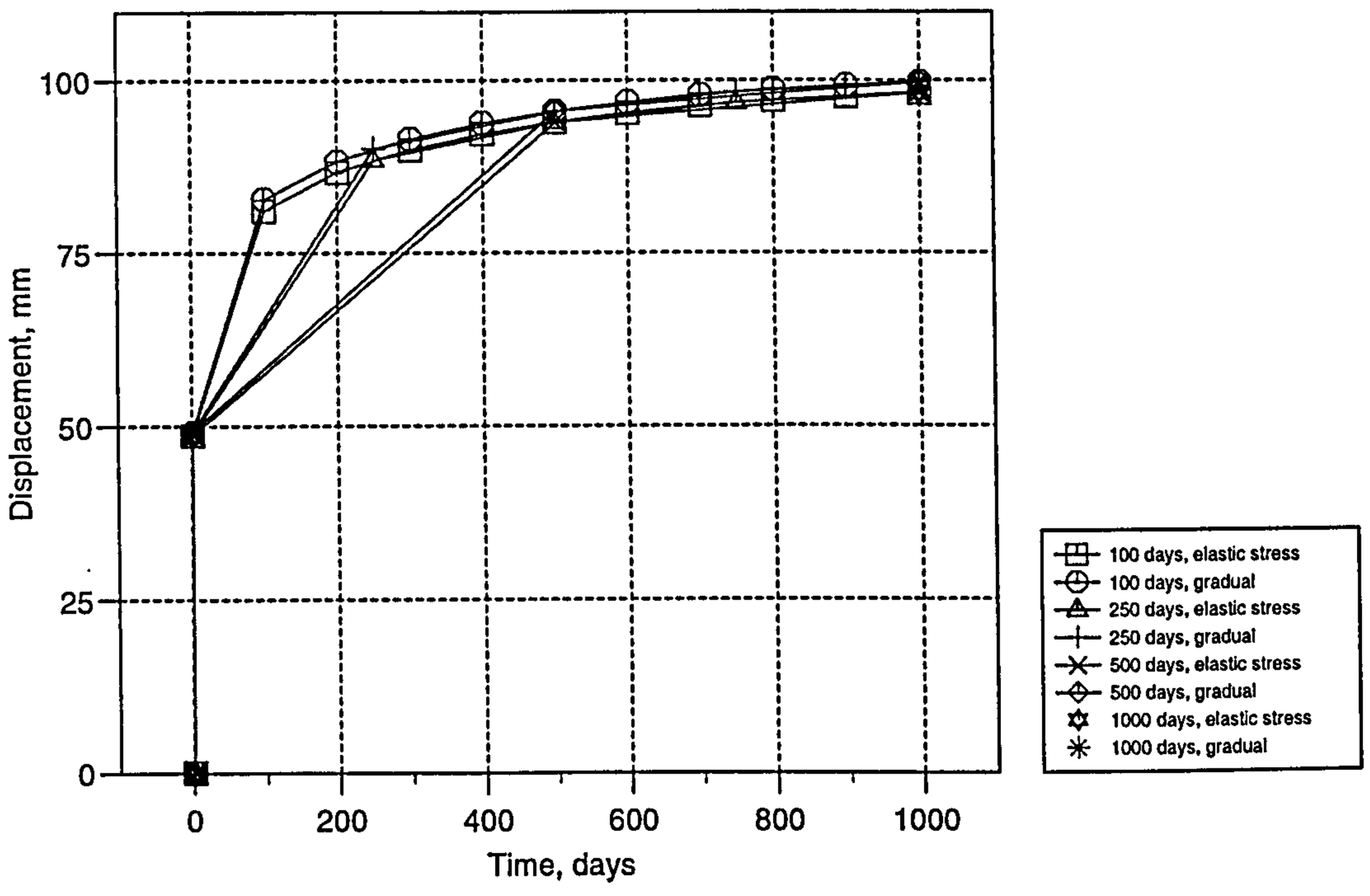


Figure 6.16 Y directional sway of middle of the propped cantilever with time

6.9 Taywood slab

A high-strength concrete slab supported on monolithic columns was tested by Taywood (Whittle, 1996). The details of the slab have already been presented in section 4.5.3 (with geometric details in Fig. 4.12 and material properties in Table 4.1). The slab was tested under a load sequence representative of the load history a slab might undergo in practice. The experimental loading sequence has been described in section 4.5.3 and the simplified load history that has been adopted for the FE analysis is shown in Fig. 4.13.

This slab has been analysed in this section to find the following:

1. The effect of modelling cracking, creep and shrinkage in the columns.
2. The effect of redistribution of stresses in both column and slab.
3. The effect of creep recovery.
4. The effect of cyclic load.

6.9.1 Selection of mesh

A sensitivity analysis has been carried out to determine the effect of mesh size and to find a suitable mesh for subsequent analyses. Three different meshes were considered for modelling one quarter of the slab:

- Mesh 1: 81 plate elements and 12 brick elements as shown in Fig 6.17.
- Mesh 2: 196 plate elements and 12 brick elements as shown in Fig 6.18.
- Mesh 3: 85 plate elements and 12 brick elements as shown in Fig 6.19.

In all the cases, 96 line elements are connected to the 12 brick elements to model cracking, creep and shrinkage in the column.

A uniform load of 13 kN/m^2 was applied to the slab at one day and sustained for 71 days. A uniform reinforcement mesh was used throughout the sensitivity study for selecting the mesh. All other material properties correspond to those given in Table 4.1. For all the meshes, elastic, instantaneous and 71 day deflections at the centre and the edge of the slab are presented in Table 6.1. Mesh 2 is the finest of the

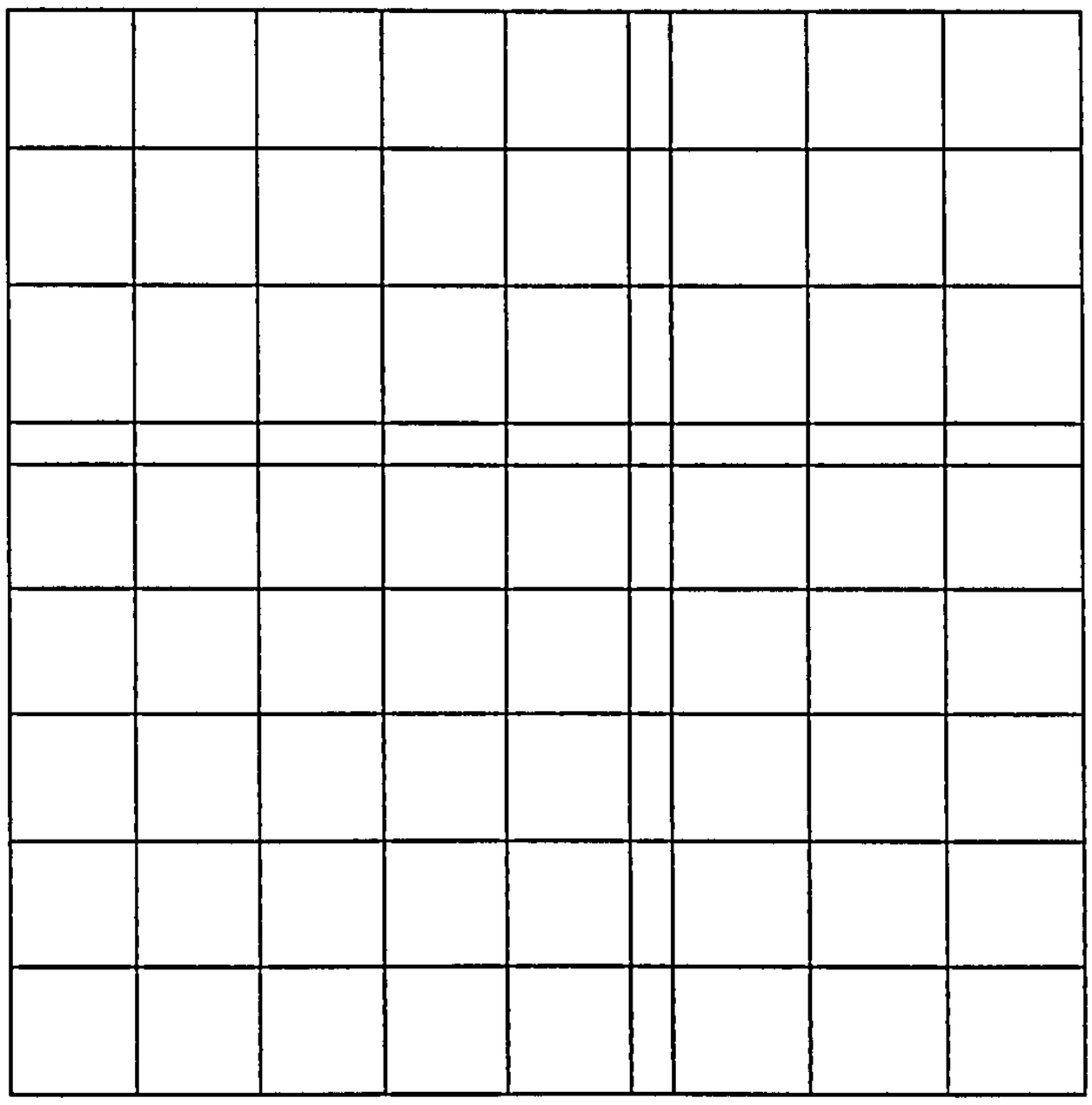


Figure 6.17 Sensitivity analysis: mesh 1

Position	Deflection	Mesh 1	Mesh 2	Mesh3
Centre	elastic	15.016	15.178	15.055
	instantaneous	24.571	26.011	25.372
	71 day	35.888	37.638	37.079
Edge	elastic	6.7842	6.9093	6.8467
	instantaneous	10.922	11.941	11.985
	71 day	16.435	17.851	18.277

Table 6.1 Mesh sensitivity: Taywood slab

three, meshes 1 and 3 have a similar number of elements, but mesh 3 is finer around the column. For elastic deflection, all the mesh arrangements give similar results. Meshes 2 and 3 give similar instantaneous and 71 day deflections, the maximum difference is within 3%. Mesh 1 gives smaller deflections compared with the other two. Mesh 3 is selected for further analysis because with less than half the number of elements of the finer Mesh 2, the results are very close and time required for the analysis of Mesh 3 is significantly lower.

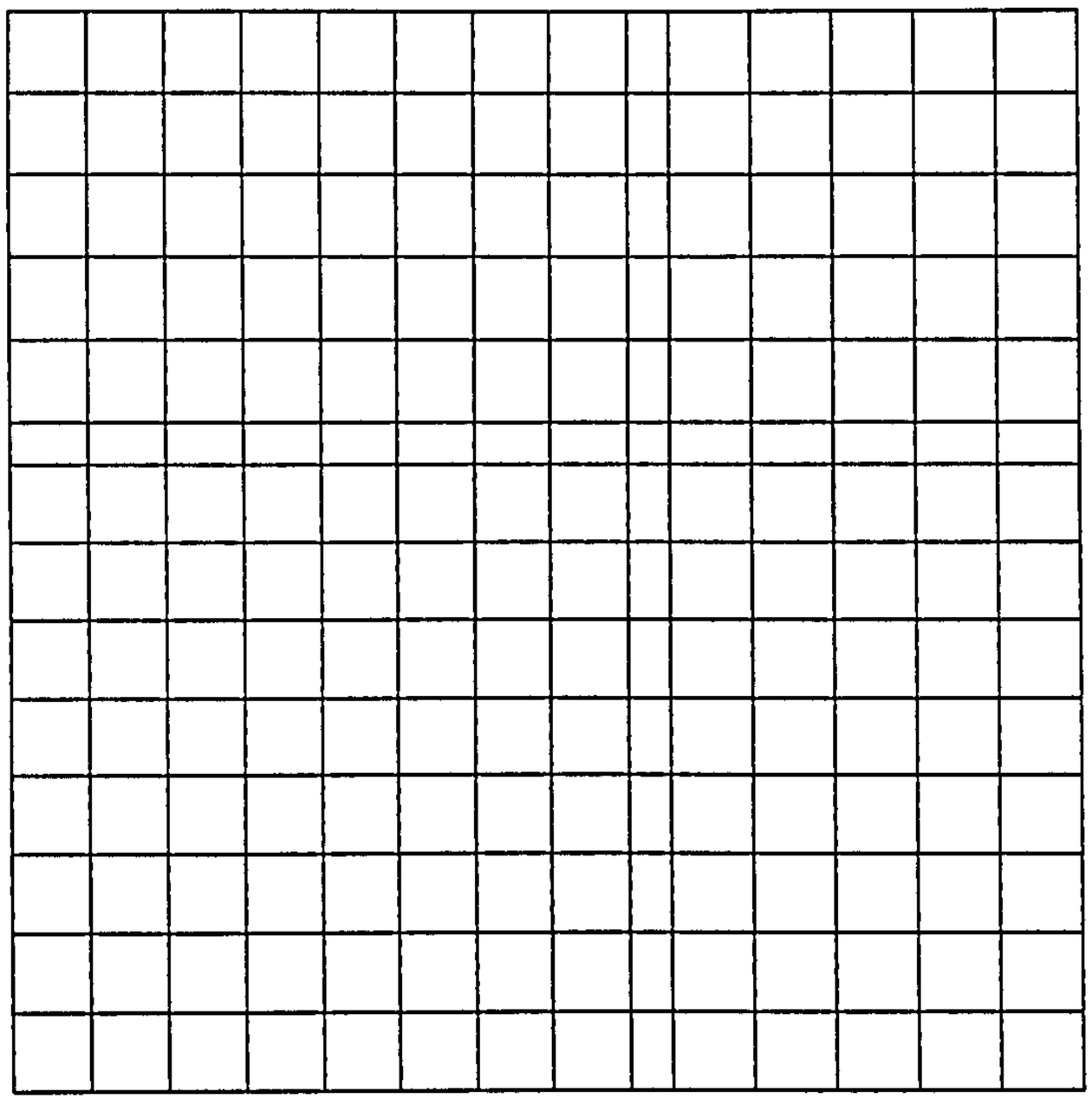


Figure 6.18 Sensitivity analysis: mesh 2

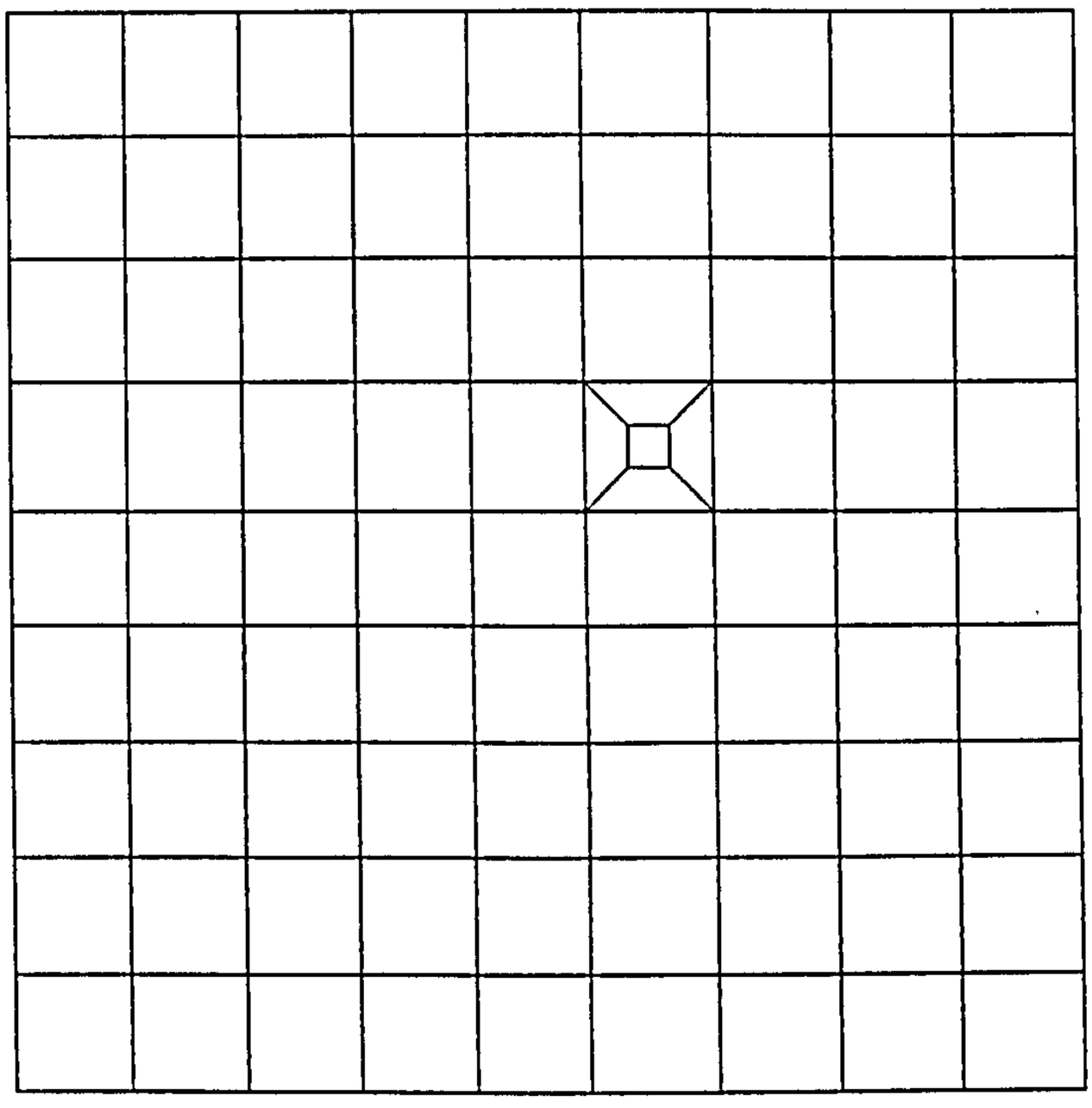


Figure 6.19 Sensitivity analysis: mesh 3

6.9.2 The effect of modelling a column for cracking, creep and shrinkage

To find the effect of modelling cracking, creep and shrinkage in the column, two cases have been considered.

1. The gross column section is used without any change in E values. E values of the slab elements are modified and gradually decreased until convergence.

2. The E values for both slab and column are modified using the approaches described in sections 6.7 and 6.4. For both the slab and column (brick and line elements), E values are gradually decreased to obtain a converged solution.

β_2 is taken as 0.5 when test loads are applied in cycles and at 71 days. The creep recovery factor was also taken as 0.5.

Deflections are plotted against time at the centre (node 1, see Fig. 4.12) and mid point of edge (node 157) of the slab in Figs 6.20 and 6.22 for cases 1 and 2 along with experimental results. Deflections under test load are presented separately in Figs 6.21 and 6.23.

The effect of modelling the column is not very significant at either node. At node 157, the 71 day deflection with the gross column is only 2.3% less than that obtained using the modified column. At the central node 1, modifying the column properties increases the 71 day deflection by 8.7%. The increase in test-load deflection is 5.9%. Results obtained with modified column properties are closest to the experimental test load deflections.

Modelling the column for cracking, creep and shrinkage increases the solution time in two ways: first, the total number of elements increases due to the inclusion of line elements and, secondly, the distance and orientation of the neutral axis, which are found by using the iterative technique described in section 5.3.2, is significantly time consuming. So, for a quick estimate of deflection, an analysis with gross concrete column section can be performed with reasonable accuracy.

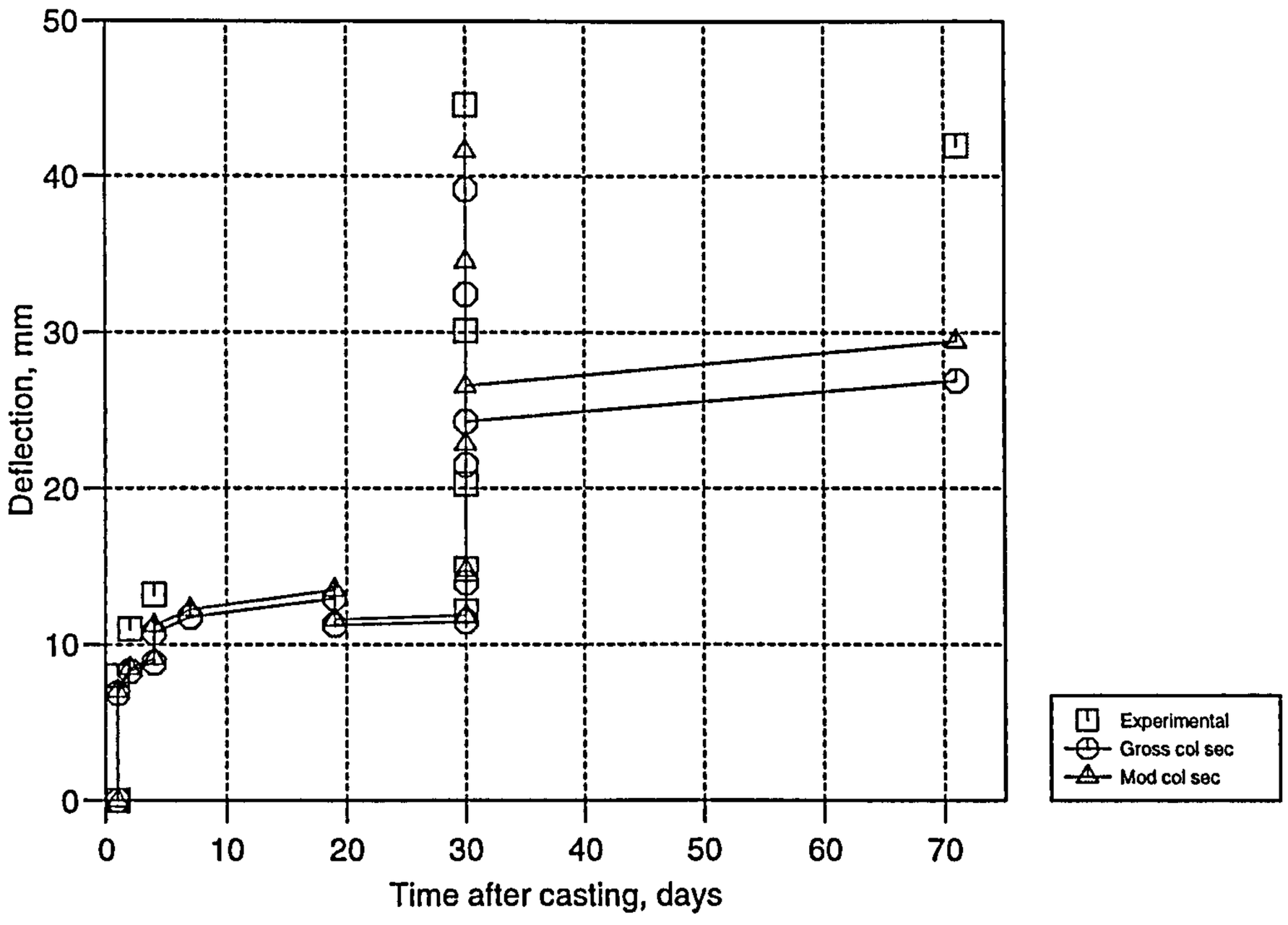


Figure 6.20 Effect of modelling a column: deflection with time for the Taywood slab, node 1

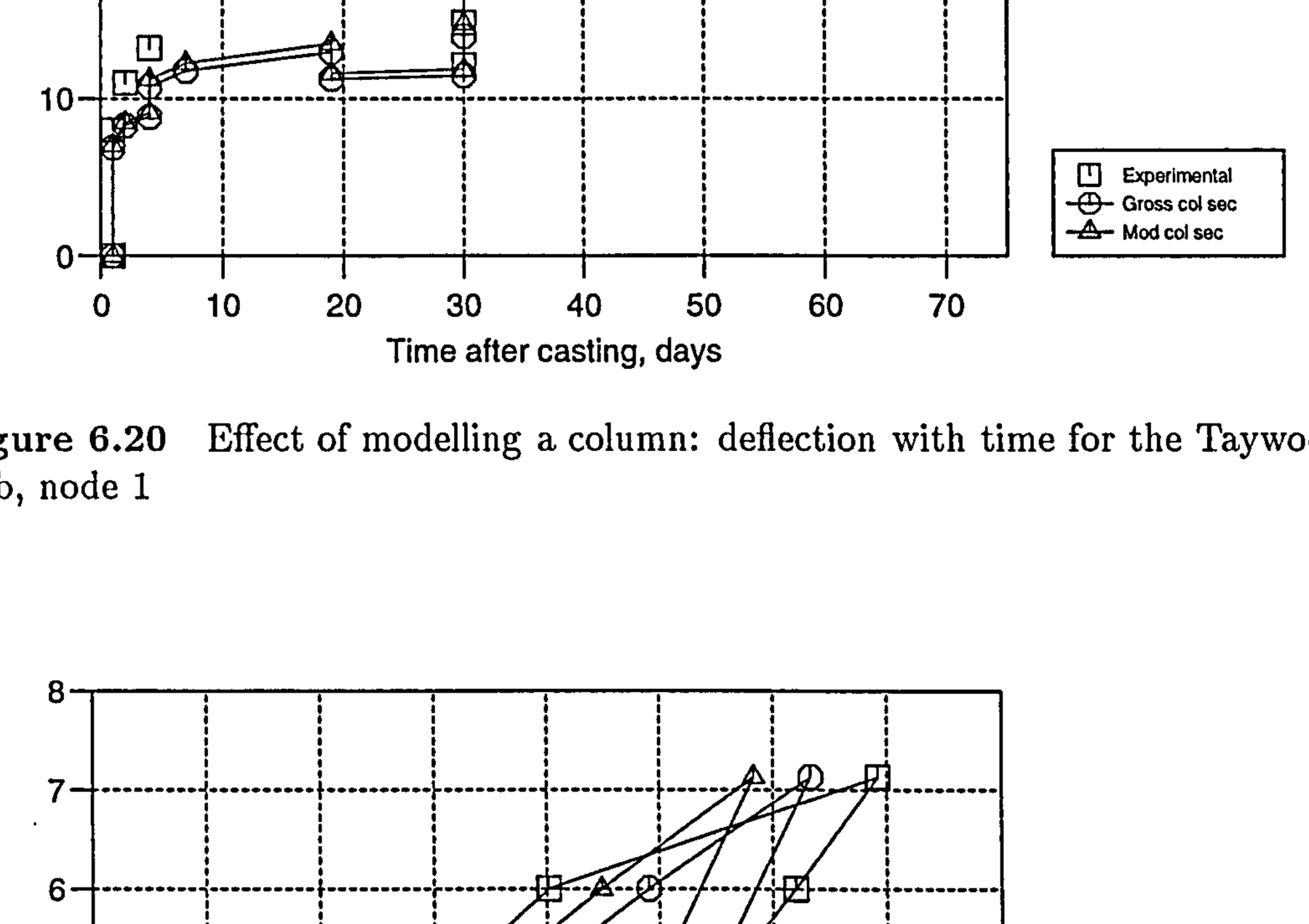


Figure 6.21 Effect of modelling a column: service load-deflection (at 30 days) for the Taywood slab, node 1

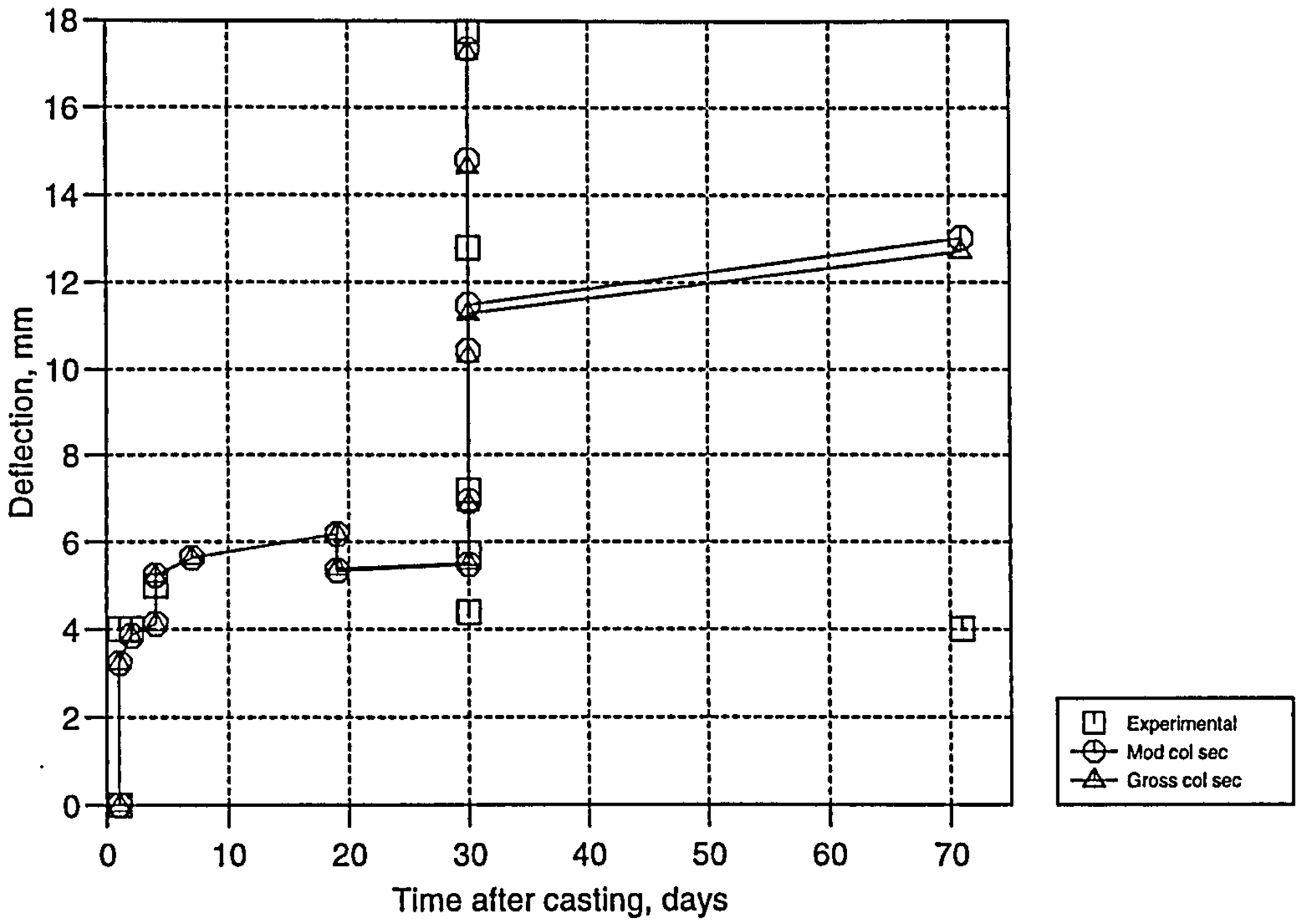


Figure 6.22 Effect of modelling a column: deflection with time for the Taywood slab, node 157

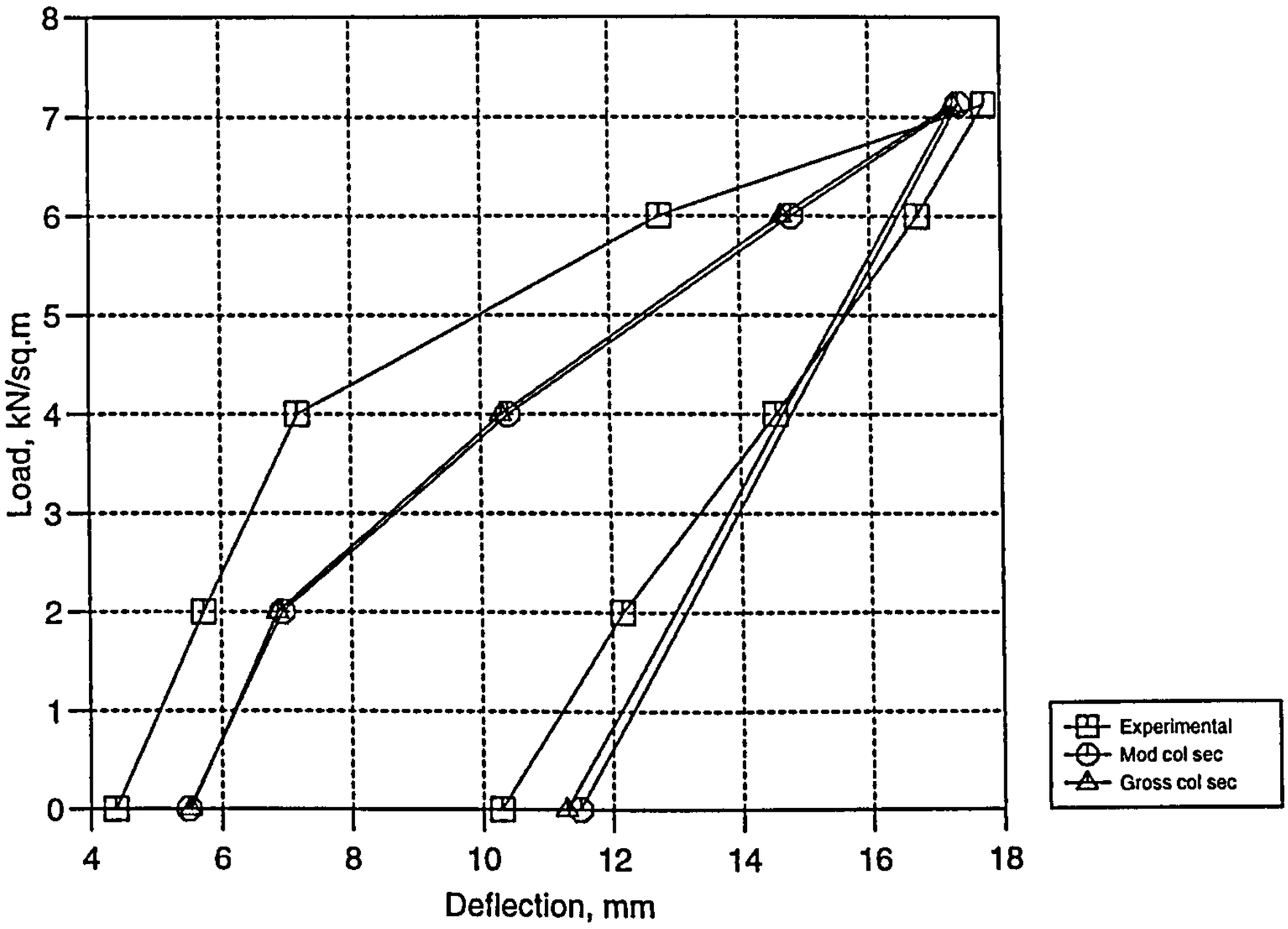


Figure 6.23 Effect of modelling a column: service load-deflection (at 30 days) for the Taywood slab, node 157

6.9.3 The effect of redistribution of stresses in column and slab

To determine the effect of stress redistribution in column and slab, three cases have been studied.

1. Redistribution of stress is not allowed in either slab or column, and the solution is obtained in the second run using E values modified on the basis of elastic stresses found in the first run with gross concrete section.

2. Stresses are allowed to redistribute in slab elements only, and slab E values are gradually decreased, while the column E values are based on elastic stresses.

3. E values for both column and slab are gradually decreased to allow stress redistribution in the whole structure.

0.5 is used for β_2 when test loads are applied in cycles and at 71 days. 0.5 is also used as the recovery factor.

The development of deflection with time calculated for the above three cases, along with experimental results for the centre (node 1) and edge (node 157) of the slab, are presented in Figs 6.24 and 6.26. Deflections under test load are presented separately in Figs 6.25 and 6.27.

Until 30 days, with just construction load and before the application of the test load, all the cases produce almost identical deflection as the slab was predominately uncracked and there was little stress redistribution. The agreement with experimental deflection is also good at striking, 2, 4 and 30 days.

Case 1 deflection at 71 days for the centre node is 18.6% higher and for the edge node it is 4.2% lower in comparison with Case 3 results. For the test peak load they are 15.6% higher and 3% lower respectively. The analysis time required for Case 1 is about one tenth of that required for Case 3. So, for a very quick estimate of deflection, Case 1 can be utilised.

Cases 2 and 3 yield similar deflections, which compare very well with experimental results under test load at 30 days. For the peak test load, Case 2 deflections for centre and edge are 4% and 2% higher respectively in comparison with Case 3 deflections.

At 71 days, the deflections for Cases 2 and 3 are still similar. Case 2 deflections are 4.5% and 0.3% higher than Case 3 for the centre and the edge respectively. This indicates that it is not necessary to model the stress redistribution in column for deflection calculations.

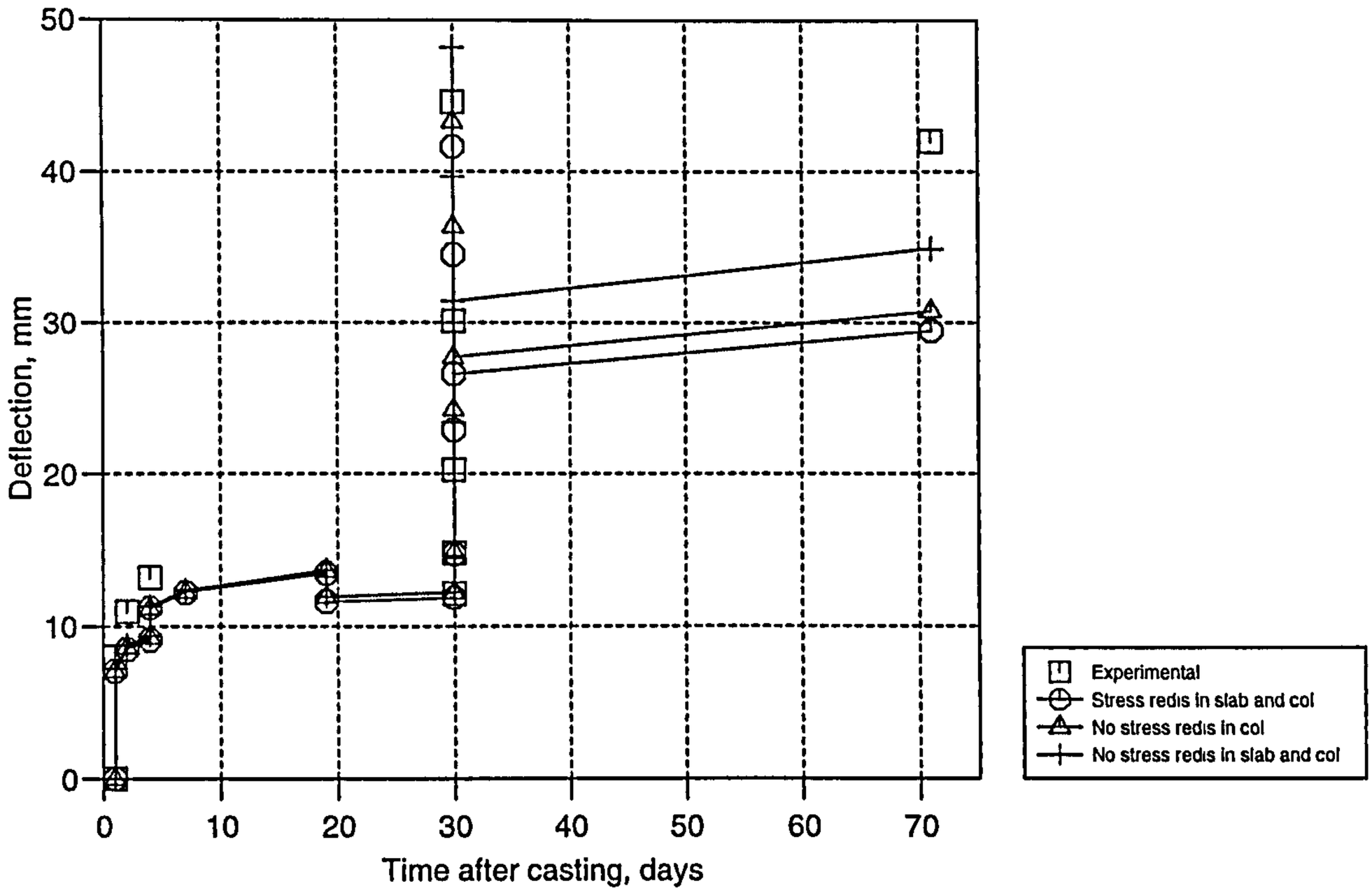


Figure 6.24 Effect of redistribution of stresses: deflection with time for the Taywood slab, node 1

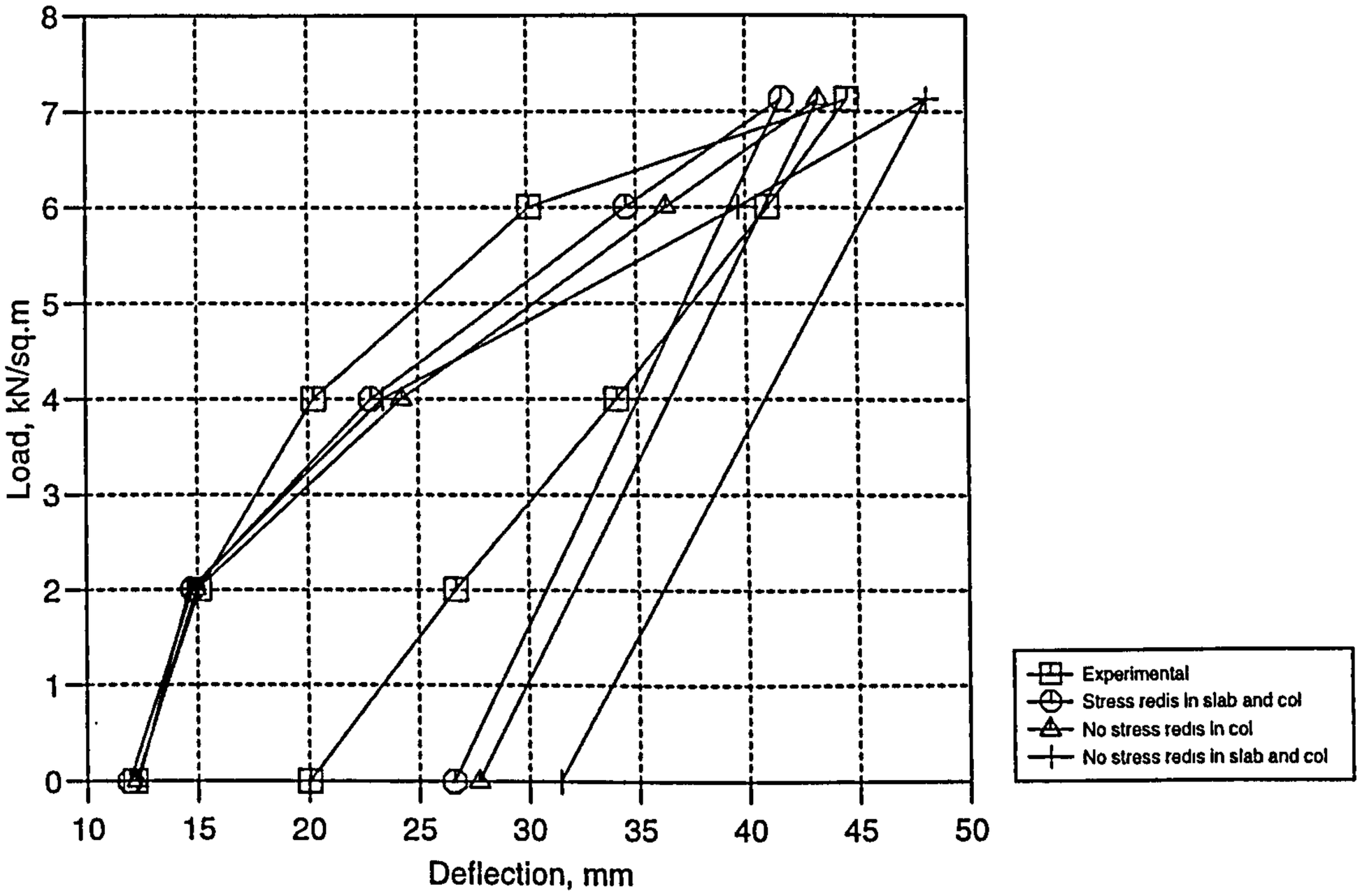


Figure 6.25 Effect of redistribution of stresses: service load-deflection (at 30 days) for the Taywood slab, node 1

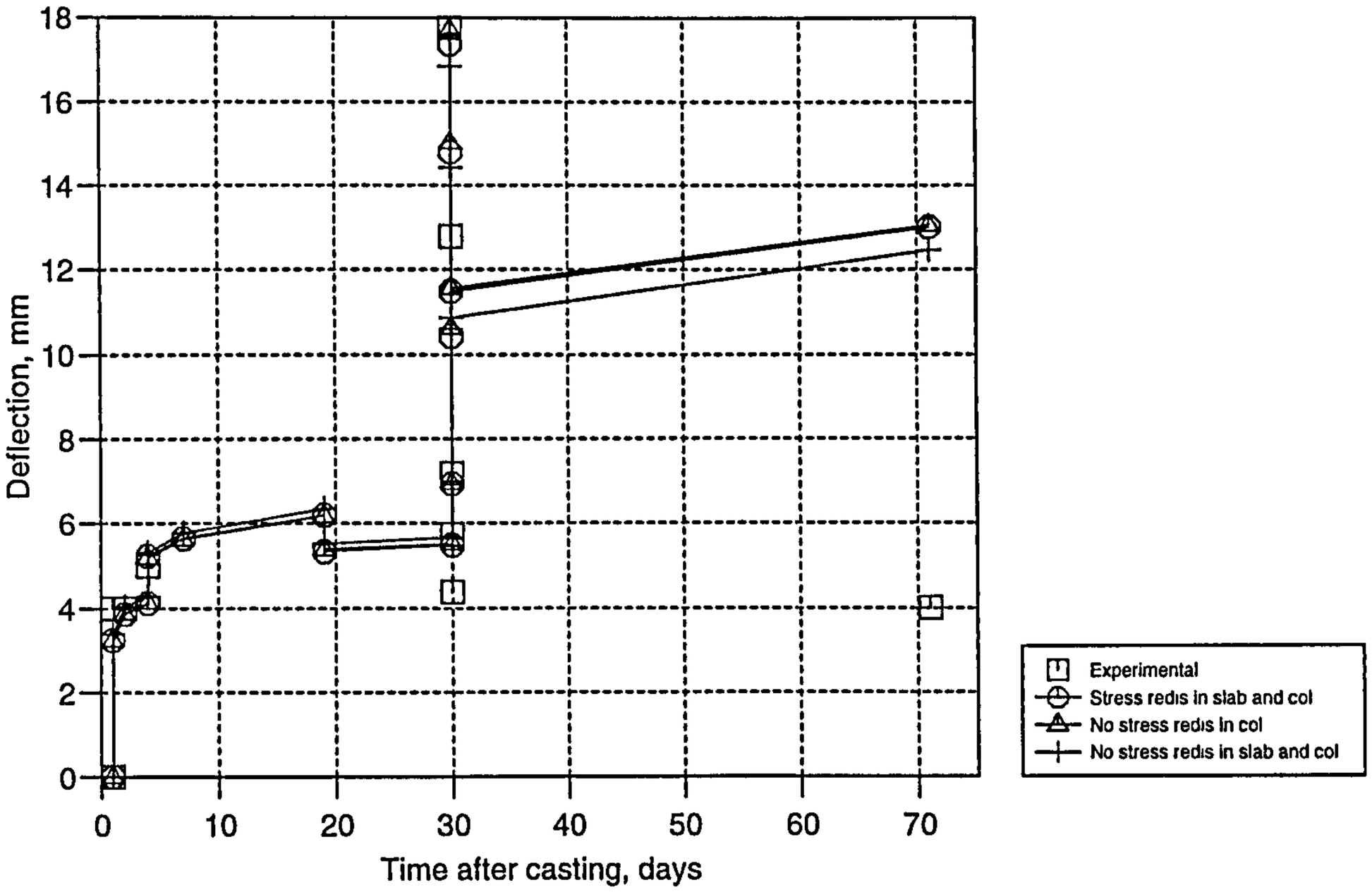


Figure 6.26 Effect of redistribution of stresses: deflection with time for the Taywood slab, node 157

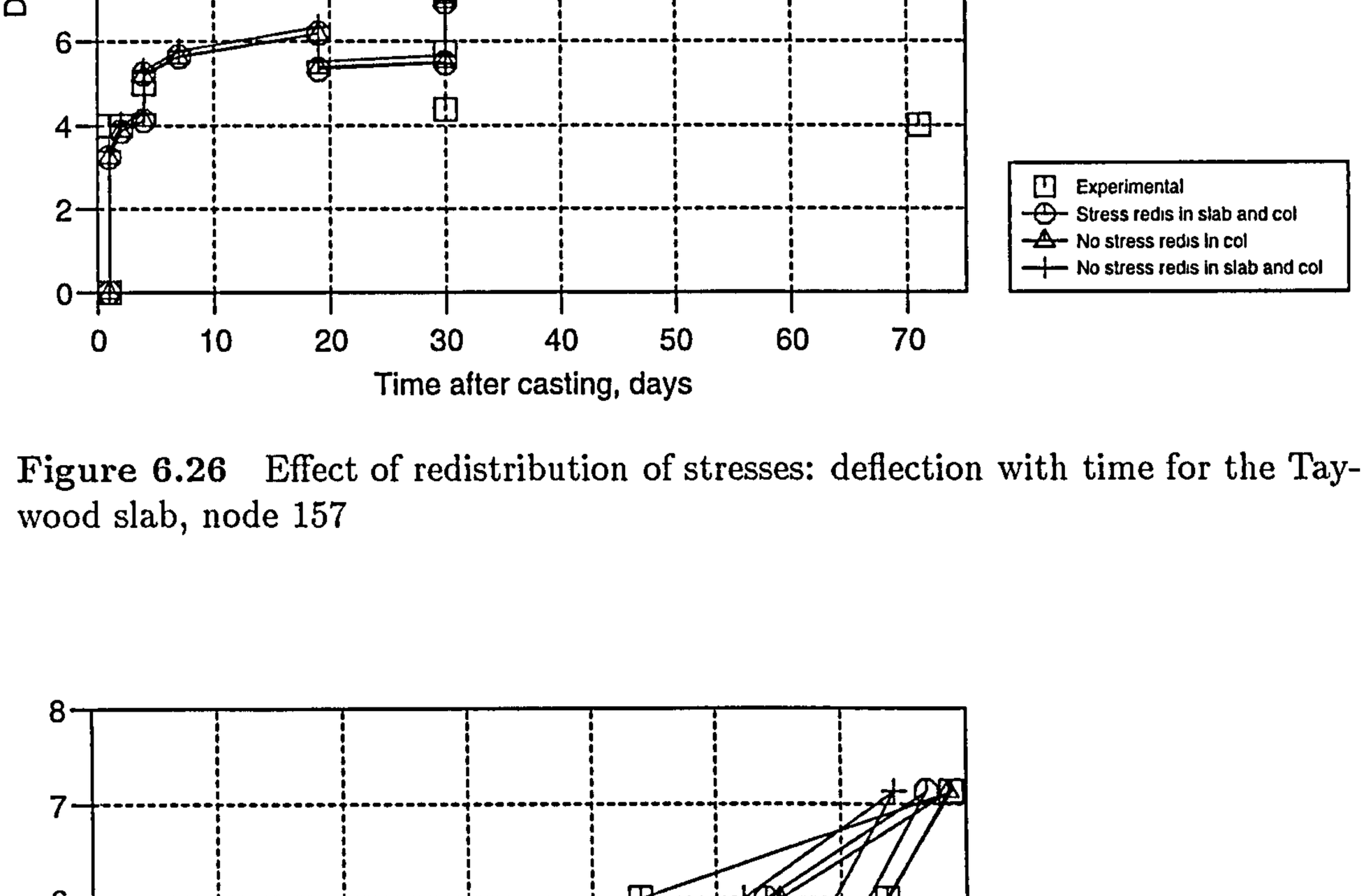


Figure 6.27 Effect of redistribution of stresses: service load-deflection (at 30 days) for the Taywood slab, node 157

6.9.4 The effect of creep recovery

To determine the effect of the creep recovery factor, two cases have been studied.

1. Recovery factor= 1 is used in the calculation for a negative load increment.

2. Recovery factor= 0.5 is used in the calculation for a negative load increment to scale down the creep curve to simulate creep recovery.

Both analyses are performed with E values gradually modified for the slab only while the column E values are based on elastic stresses.

The development of deflection with time calculated for the above two cases, along with experimental results for the centre (node 1) and edge (node 157) of the slab, are presented in Figs 6.28 and 6.30. Deflections under test load are presented separately in Figs 6.29 and 6.31.

A construction load of 1.5 kN/m^2 was applied at 4 days and removed at 19 days. Until 30 days, the amount of creep recovery is not significant as only 11 days have passed, both the cases yield almost identical deflections. The pattern is similar in the test load region as the load was applied almost instantaneously. At 71 days, the effect of using different factors becomes significant as another 41 days have elapsed and there is extensive cracking due test load, also a $\beta_2 = 0.5$ is used for 71 days. A recovery factor of 0.5 yields 10.9% and 14 % higher deflection at 71 days for centre and edge respectively in comparison with the same obtained with a factor 1.

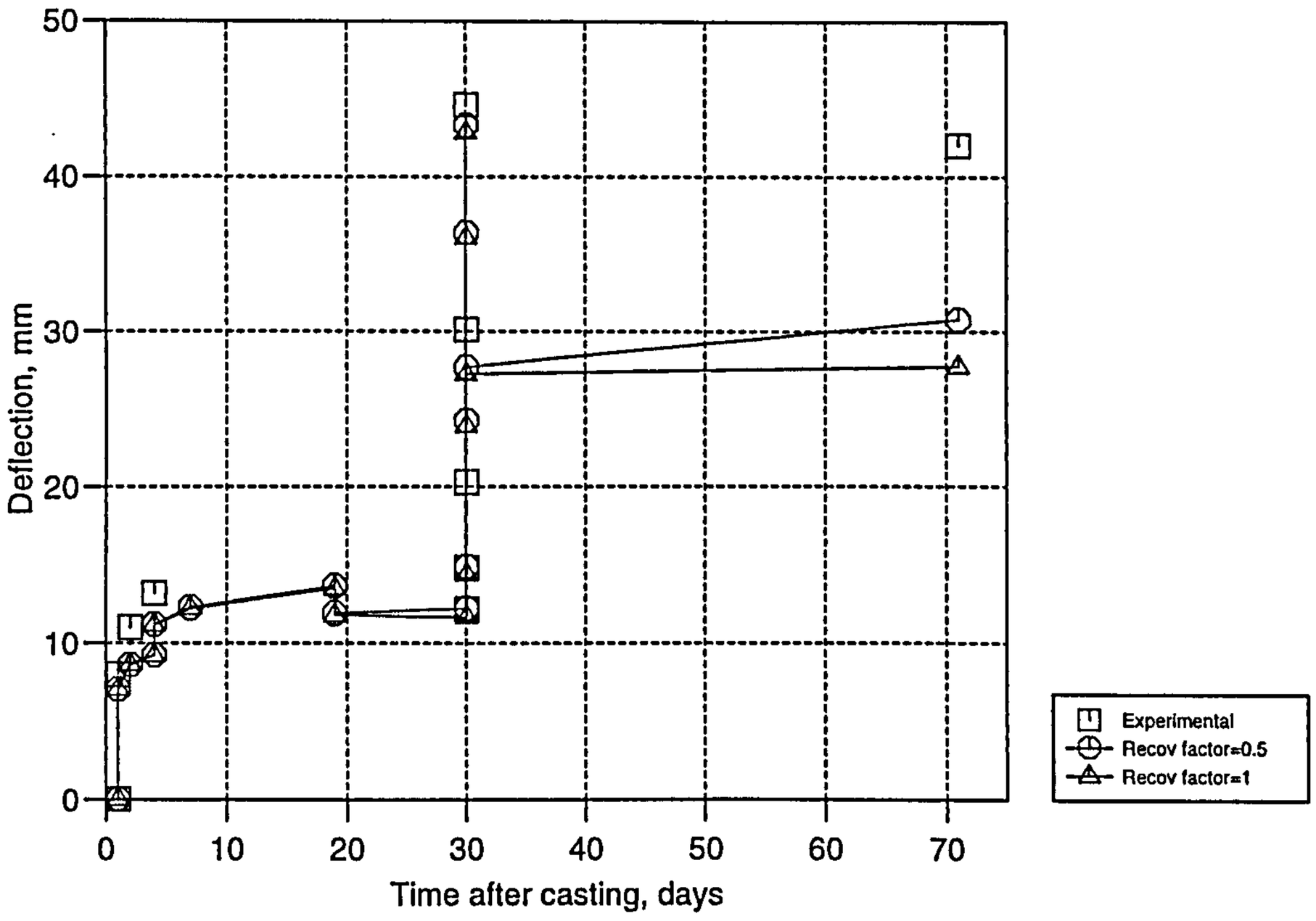


Figure 6.28 Effect of creep recovery: deflection with time for the Taywood slab, node 1

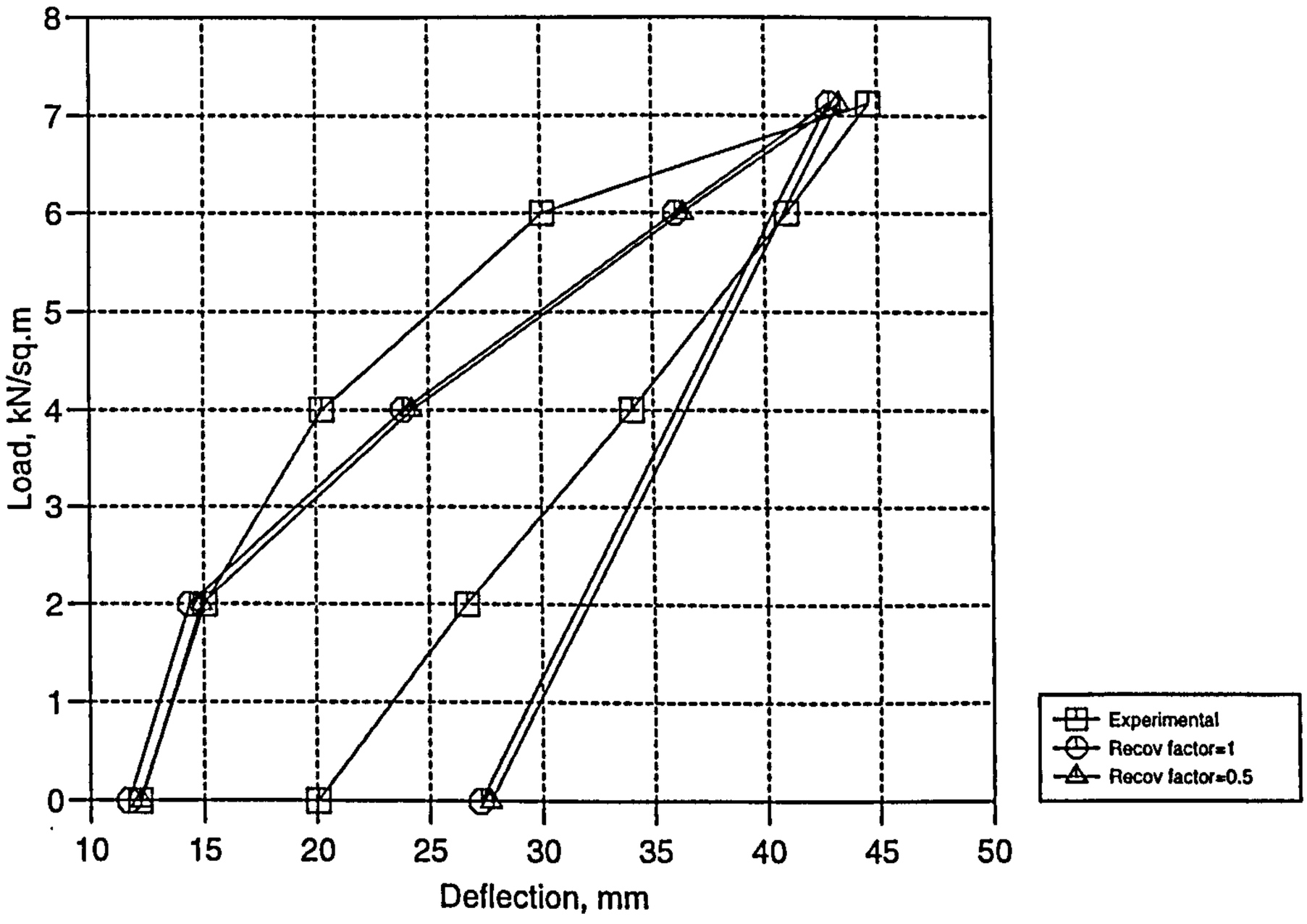


Figure 6.29 Effect of creep recovery: service load-deflection (at 30 days) for the Taywood slab, node 1

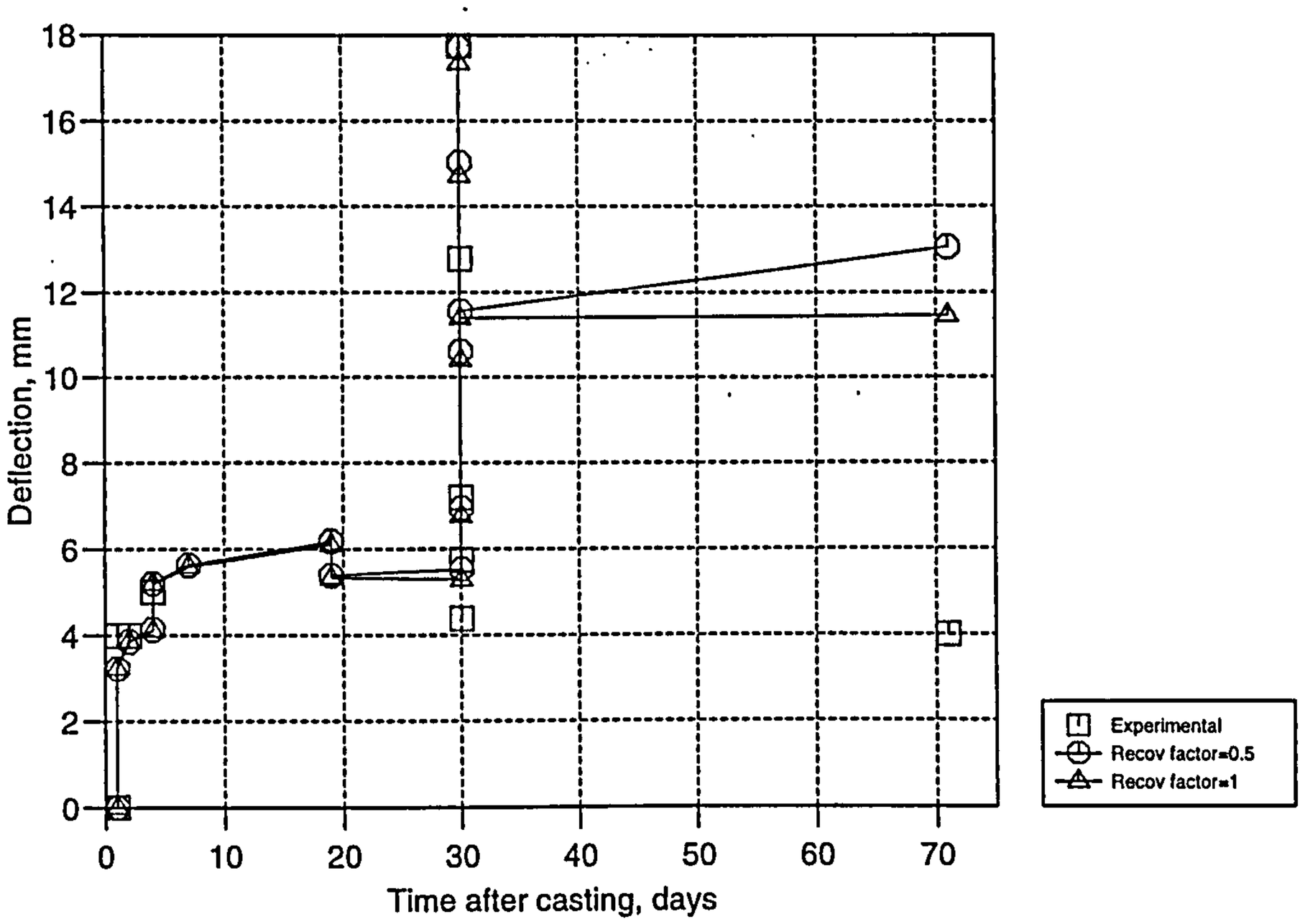


Figure 6.30 Effect of creep recovery: deflection with time for the Taywood slab, node 157

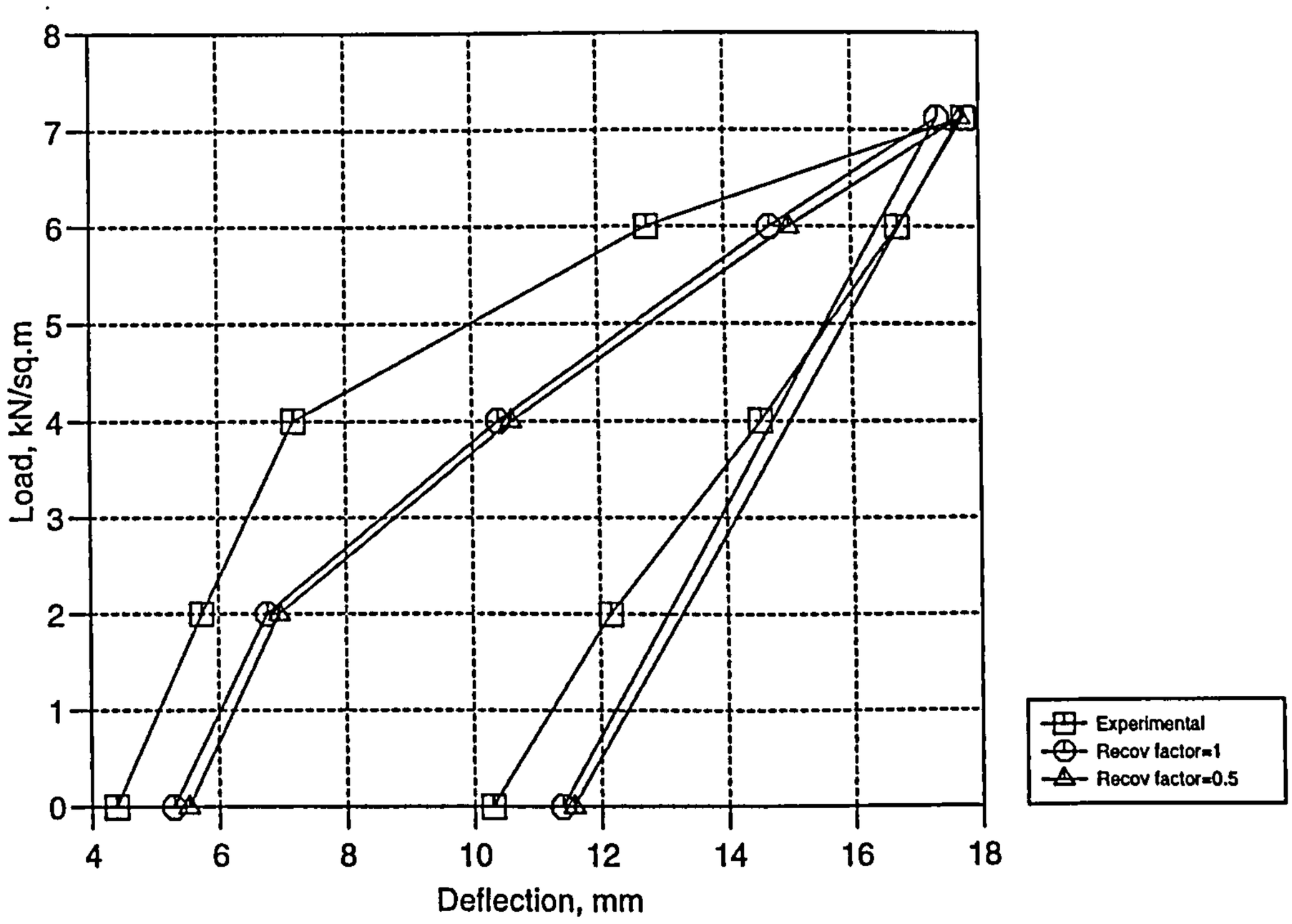


Figure 6.31 Effect of creep recovery: service load-deflection (at 30 days) for the Taywood slab, node 157

6.9.5 The effect of the β_2 factor

The β_2 factor is used in the Model Code 90 (1993) moment-curvature relationship to take into account the effect of deterioration of tension stiffening for long-term and repeated loads. For short-term loading, MC-90 suggests a value of 0.8 while EC2 proposes a value of 1.0 under similar conditions. Both codes uses a value of 0.5 for a very large number of cycles or for long time. To determine the effect of this β_2 factor, two cases have been studied.

1. β_2= 1 is used in the mean curvature calculation throughout the analysis.

2. β_2= 0.5 is used for cyclic test loads at 30 days and final deflection calculation at 71 days.

Both analyses are performed with E values gradually modified for both slab and column to allow for stress redistribution. 0.5 is used as the recovery factor.

The development of deflection with time calculated for the above two cases, along with experimental results for the centre (node 1) and edge (node 157) of the slab, are presented in Figs 6.32 and 6.34. Deflections under test load are presented separately in Figs 6.33 and 6.35.

Until 30 days, before application of the test load, both cases produce identical deflection, as β_2= 1 is assumed for both cases (i.e. both refer to short-term).

The effect of using β_2= 0.5 is very significant, and the effect becomes more prominent, particularly when the load is high. For the test peak load, Case 2 deflection is 53% and 27.9% higher than Case 1 for centre and edge respectively. And finally the 71 day deflections are 53.7% and 23.4% higher for Case 2 for centre and edge respectively.

Case 2 deflections agree very well with experimental results, particularly in the cyclic test-load region. However, it should be noted that there were only three cycles of test load in the experiment and a value of β_2= 0.5, in fact overestimates the loss in tension stiffening. Although the current analysis shows a maximum tensile stress of 213 MPa in the column steel under peak load, local yielding of column steel has been reported in the experiment, which is believed to be the reason for the extra loss of stiffness.

It should be noted here that both the unloading branches using β_2=1 and β_2= 0.5 converge to a pivot point on the state 1 line (very close to the first part of the loading line) with the second coordinate being negative of total peak load of 13.125 kN/m^2. This is, in fact, the assumed shape of the unloading branch proposed by Rotilio (1998) which is developed on basis of series of experiments and adopted in the present work (see section 6.5.1).

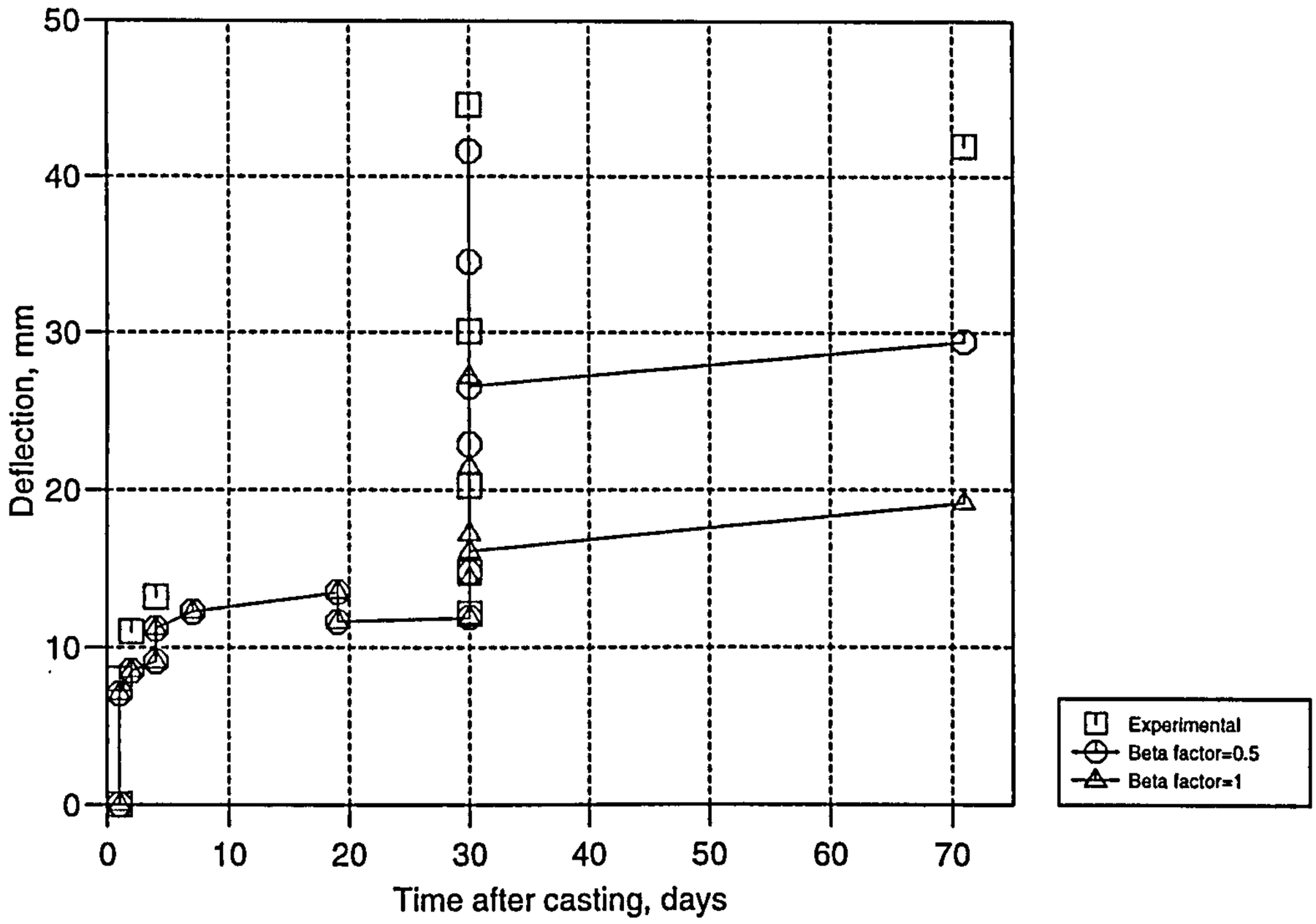


Figure 6.32 Effect of the β_2 factor: deflection with time for the Taywood slab, node 1

Figure 6.33 Effect of the β_2 factor: service load-deflection (at 30 days) for the Taywood slab, node 1

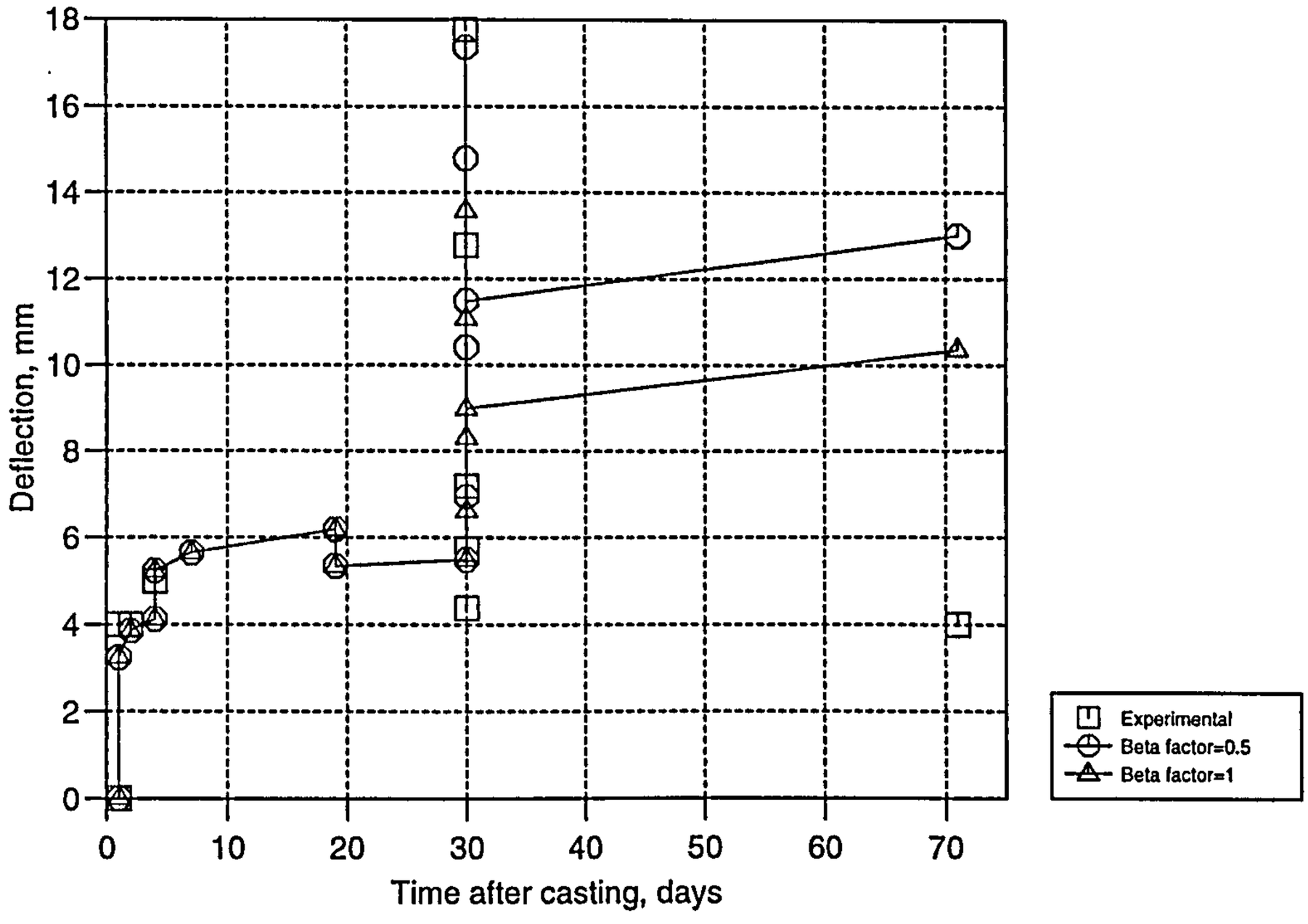


Figure 6.34 Effect of the β_2 factor: deflection with time for the Taywood slab, node 157

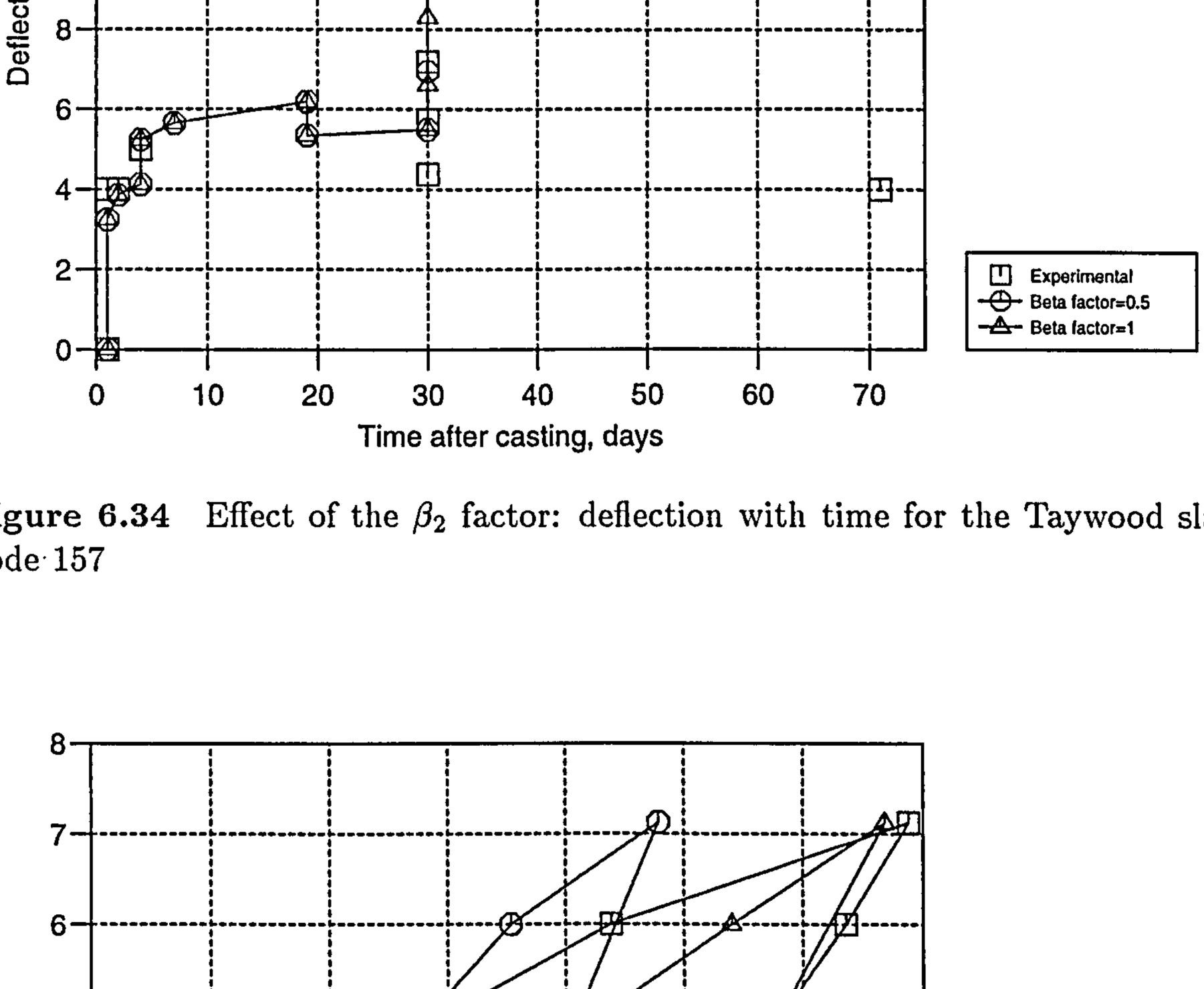


Figure 6.35 Effect of the β_2 factor: service load-deflection (at 30 days) for the Taywood slab, node 157

6.10 Conclusions

A novel method of modelling non uniform load history, based on the MC-90 moment-curvature relationship (for uniform load) describing cracking, creep and shrinkage, has been presented in this chapter. The method will be useful because a slab, in reality, undergoes time-varying non uniform load history during its construction and operational life. The long-term total and incremental deflections depend on the full load history of the slab. Most importantly, construction loads can be very high depending on the re-propping method employed and can cause severe cracking of slabs with relatively low tensile strength. In such cases, the long-term deflection will be very high compared to a slab where construction load does not produce any significant extra cracking. With the use of the author's new method it is possible to model the deflection development for the full load history which includes the striking of slab, the construction loading and unloading, creep recovery, application of imposed load and the final deflection with considering loss of tensile stiffening.

The formulation of the method has been described in the chapter with the assumptions. The method has been checked by analysing determinate structures with different number of subdivisions of a uniform load. Same study was carried out for an indeterminate structures which showed that the effect of subdividing a uniform load step was not significant.

The proposed method was used to analyse the slab tested by Taywood and different parameters were varied to identify their effects on deflections. Good deflection predictions were obtained for the slab, particularly the test load deflection were accurately estimated. But as there was reporting of yielding of steel in the experiment, the final deflection for the centre was higher than estimated. The effect of modelling cracking, creep and shrinkage in column was found less important and a gross column section without any material modification has been found to be sufficient for a adequate estimation. The effect of allowing stress redistribution, particularly in slab has been found to have some effect on deflection though not very significant and in column, the effect is negligible. The use of the β_2 factor to model loss of tension stiffening due to cyclic application of load or elapse of long time is very crucial. A

value of β_2=0.5 was found to be very good in modelling the cyclic application of test load on the Taywood slab.

Chapter 7

Parametric study

7.1 Introduction

The design of reinforced concrete floor systems is usually governed by the need to limit long-term deflections under service loads. The calculation of long-term deflections of reinforced concrete slabs is a complex problem even in a controlled environment under constant loading. It is even more complicated to estimate deflections in real buildings because deflections are influenced by a wide range of factors, many of which are not known to the designer. Even though some of these factors are interconnected, they can be classified into the broad categories of geometric factors, material properties, construction factors and service-life factors.

7.1.1 Geometric parameters (including reinforcement)

Slab dimensions, i.e. slab thickness and span in either direction, are the most important geometric parameters. Some other key factors that influence slab deflection are slab reinforcement and arrangement, column dimensions (i.e. cross-section, height and reinforcement). In this chapter, four thicknesses of slab with three levels of concrete strength are considered in order to determine the effect of varying thickness on instantaneous and long-term deflections. The efficiency of the common practice of providing more bottom steel than required to reduce deflection is checked. Also, the effect of distribution of reinforcement over column and span are studied.

7.1.2 Material properties

Material properties include modulus of elasticity of concrete and reinforcing steel and tensile strength of concrete. Long-term deflections are influenced by the creep and shrinkage properties of concrete. All the properties of concrete are related to its compressive strength; generally all of them improve with increasing strength. Two types of parametric studies were carried out for material properties. First, three levels of concrete strength (i.e. C30, C50 and C80) were considered in the analysis with four thicknesses to study the effect of concrete strength on elastic (on the basis of gross concrete section without reinforcement and cracking), instant and long-term deflections. The mean values of key concrete properties- i.e. tensile strength, creep coefficient, shrinkage strain and modulus of elasticity- were derived using the equations in CEB-FIP Model Code 90 (MC-90) (1993). Secondly, deflections were also calculated using lower characteristic, mean and upper characteristic values of material properties to demonstrate the likely variation in deflections due to inherent variability in material properties. The study was carried out for two cases: a) the material properties were varied to their upper and lower characteristic value one at a time (keeping other properties at mean value) to find the sensitivity of deflection to each parameter; b) they were all varied together to form the best and worst possible combination of properties to get an idea of extreme variation of deflections. This also reveals the interrelation of different parameters.

7.1.3 Construction factors

Some of the factors which influence slab deflection during the construction phase are a) curing condition, b) variation in cover to steel and slab thickness, c) age at striking, and d) construction loads. Assuming good construction practice, probably the most significant factors influencing deflections in the field are striking time and construction loading. Investigators including Sbarounis (1984c), Jokinen & Scanlon (1987), Scanlon & Murray (1982), Graham & Scanlon (1986) report that long-term field deflections are often considerably greater than predicted by models calibrated on the basis of laboratory tests. Some of the discrepancy is no doubt due to the difficulty in assessing creep and shrinkage in the field. More significantly, it appears

that additional deflections develop owing to the effects of additional cracking due to construction loads [(Sbarounis, 1984c), (Jokinen & Scanlon, 1987)], which are often greater than service loading. The effect of construction loading may be significant as they are applied to a relatively young slab with lower tensile strength.

The effect of adopting different construction sequences on final deflection is studied here. Contribution to deflections due to early creep corresponding to construction load and its recovery over time and the relative contribution of residual deflection after unloading is considered. A simplified load history and a single-step method to predict long-term deflection considering construction loading are also proposed.

7.1.4 Service-life factors

The magnitude, type of loading (cyclic or static), time of imposed loading and relative humidity are the important service-life factors that influence slab deflections. To study their effect on deflection, imposed loads with different magnitudes and time of application were considered.

7.2 Details of the slab used in parametric study

7.2.1 Loading and design

A flat slab system with 3 panels in each direction was designed in accordance with EC2 (1991). The edge panel is used in all the parametric studies of this chapter, the FE mesh with boundary conditions was shown in Fig. 4.18. The panels are 7.5 m square and the thickness, according to the code l/d ratio, was found to be 300 mm. The design was based on the assumption that 16 mm bars were used with 25 mm clear cover. BS 6399 (1984) requires general office areas to be designed for a minimum characteristic imposed load of 2.5 kN/m^2 whereas corridors must be designed for a characteristic imposed load of 4 kN/m^2 and storage areas for a minimum of 5 kN/m^2. The need to design different areas of a floor for different loading complicates the design procedure and to avoid such problems office floors are often designed for a total imposed load of 5 kN/m^2 which includes an allowance of 1 kN/m^2 for partitions. Design imposed loads adopted in the UK are generally

higher than those adopted in Europe and US. In the current analysis, imposed live load was taken as 2.5 kN/m^2. An allowance of 2 kN/m^2 was adopted for raised floor ceiling, services and demountable partitions. The ultimate load was calculated using appropriate load factors (i.e. 1.35 for self weight and floor finishes and 1.5 for imposed load). The design was carried out using the equivalent frame method described in BS 8110 (1997). A 7.5 m wide equivalent beam was analysed. Design span and column moments were found using different pattern loadings and the peak column moments were reduced by 20%. According to code requirement, the hogging moment over the column was distributed between the column and middle strips by 75 and 25% respectively. The corresponding distribution of total sagging moment in the span are 55 and 45%. A minimum of 0.15% steel was also provided as nominal steel. For thickness other than 300 mm, reinforcements are adjusted according to the need for strength.

7.2.2 Material properties

Different concrete strengths (i.e. C30, C50 and C80) were adopted in the study and the yield strength of steel was assumed to be 500 MPa. Material properties are calculated using MC-90. Relative humidity was assumed to be 50% for creep and shrinkage calculations. Characteristic compressive strength of concrete at any time t is calculated using the MC-90 equation:

$$f_{ck}(t) = \beta_{cc} f_{ck}(28) \tag{7.1}$$

where $f_{ck}(28)$ is the 28-day characteristic strength and β_{cc} is the time function defined by:

$$\beta_{cc} = \exp\left[s(1 - \sqrt{\frac{28}{t}})\right] \tag{7.2}$$

where t is the time in days, with s being a coefficient depending on type of cement: s is equal to 0.2, 0.25 and 0.38, respectively, for rapidly hardening high-strength cements, for normal and rapidly hardening cements, and for slowly hardening cements. A value of 0.25 is taken in the current analysis. Mean tensile strength and

modulus of elasticity of concrete are estimated from the characteristic strength:

$$f_{ct}(t) = 1.4\left[\frac{f_{ck}(t)}{10}\right]^{2/3} \tag{7.3}$$

$$E_c(t) = \sqrt{\beta_{cc}} E_c(28) \tag{7.4}$$

where $E_c(28)$ is the modulus of elasticity of concrete at 28-days and is calculated by:

$$E_c(28) = 9.5\left[f_{ck}(28) + 8\right]^{1/3} \tag{7.5}$$

7.2.3 Imposed load

Austin (1998), Fitzpatrick *et al.* (1992) showed that, in practice, actual floor loadings are usually less than 1 kN/m^2 and therefore considerably less than the characteristic design imposed load. EC2 acknowledges this by allowing the designer to calculate deflections using a reduced imposed load. The reduction factor is dependent on floor use. For example, a reduction factor of 0.3 is recommended for offices. In the current analysis, an imposed load of 3 kN/m^2 represents the permanent component of the service load. It includes allowances of 1 kN/m^2 for raised floor, services and ceilings and 1 kN/m^2 for partitions. It is assumed that the permanent component of the characteristic design imposed load of 2.5 kN/m^2 is 1 kN/m^2. This is considered typical of the actual component of the imposed load in the office building. The self-weight of slab plus this 3 kN/m^2 imposed loads are applied at 28 days and sustained for 10-years to calculate instantaneous and long-term deflections in most of the analyses of this chapter unless otherwise specified. Descriptions are presented where a full load history was considered.

7.3 Effect of geometric properties

7.3.1 Effect of slab thickness

Objective

Slab thickness is the most important geometric property which is likely to be considered in design for deflection. Most design codes give span-to-depth rules for ensuring that slab deflections are within tolerable limits. In the current study, four slab thicknesses (i.e. 250, 275, 300 and 325 mm) were considered with three sets of concrete strengths (i.e. C30, C50 and C80).

Result

Elastic (on the basis of gross concrete section without reinforcement), instant and long-term (10 years) deflections for different thicknesses and concrete strengths are plotted in Figs 7.1 to 7.3 respectively. Table 7.1 also compares the deflections due to change in thickness.

Analysis	Slab thickness	Deflection, % for concrete strengths		
		C30	C50	C80
Elastic	250 mm	100.0	100.0	100.0
	275 mm	80.6	80.6	80.6
	300 mm	67.5	67.5	67.5
	325 mm	55.7	55.7	55.7
Instantaneous	250 mm	100.0	100.0	100.0
	275 mm	61.7	78.0	78.1
	300 mm	41.9	61.4	63.8
	325 mm	29.6	50.0	51.7
Long-term	250 mm	100.0	100.0	100.0
	275 mm	76.9	67.3	75.4
	300 mm	61.2	49.4	60.9
	325 mm	44.1	38.4	47.9

Table 7.1 Effect of slab thickness

The elastic deflection reduces as the slab thickness is increased since the second moment of area increases in proportion with the cube of slab thickness whereas the self-weight of the slab is proportional to slab thickness. Table 7.1 shows that in-

creasing slab thickness reduces instant and long-term deflections more than elastic deflections. This is the case because cracking reduces with increase in slab thickness. The reduction in short-term deflection due to increased slab thickness is most pronounced for C30 concrete. For C50 and C80 concrete, the slabs are lightly cracked and the reductions in short-term cracking due to increase in thickness, are less significant. Table 7.1 also shows that the reduction in deflection due to 25 mm increment in slab thickness reduces as the slab thickness increases since both increase in moments of inertia and reductions in cracking becomes less prominent. For C30 concrete, long-term deflections are less sensitive than instant deflections to increase in slab thickness since β_2=0.5 makes all the slabs more cracked in long-term calculations. However, for C50 and C80, long-term deflections appear to be more sensitive to thickness increase in comparison to their instant counterpart. Use of β_2=0.5 makes the 250 mm slab more cracked whereas the other slabs are predominately uncracked. A similar pattern was found when a slab with 9 m span was considered.

Conclusion

An efficient method of reducing deflection is to increase the slab thickness. This is most effective when increasing the slab thickness reduces cracking. Increasing slab thickness is less efficient if the slab is already uncracked.

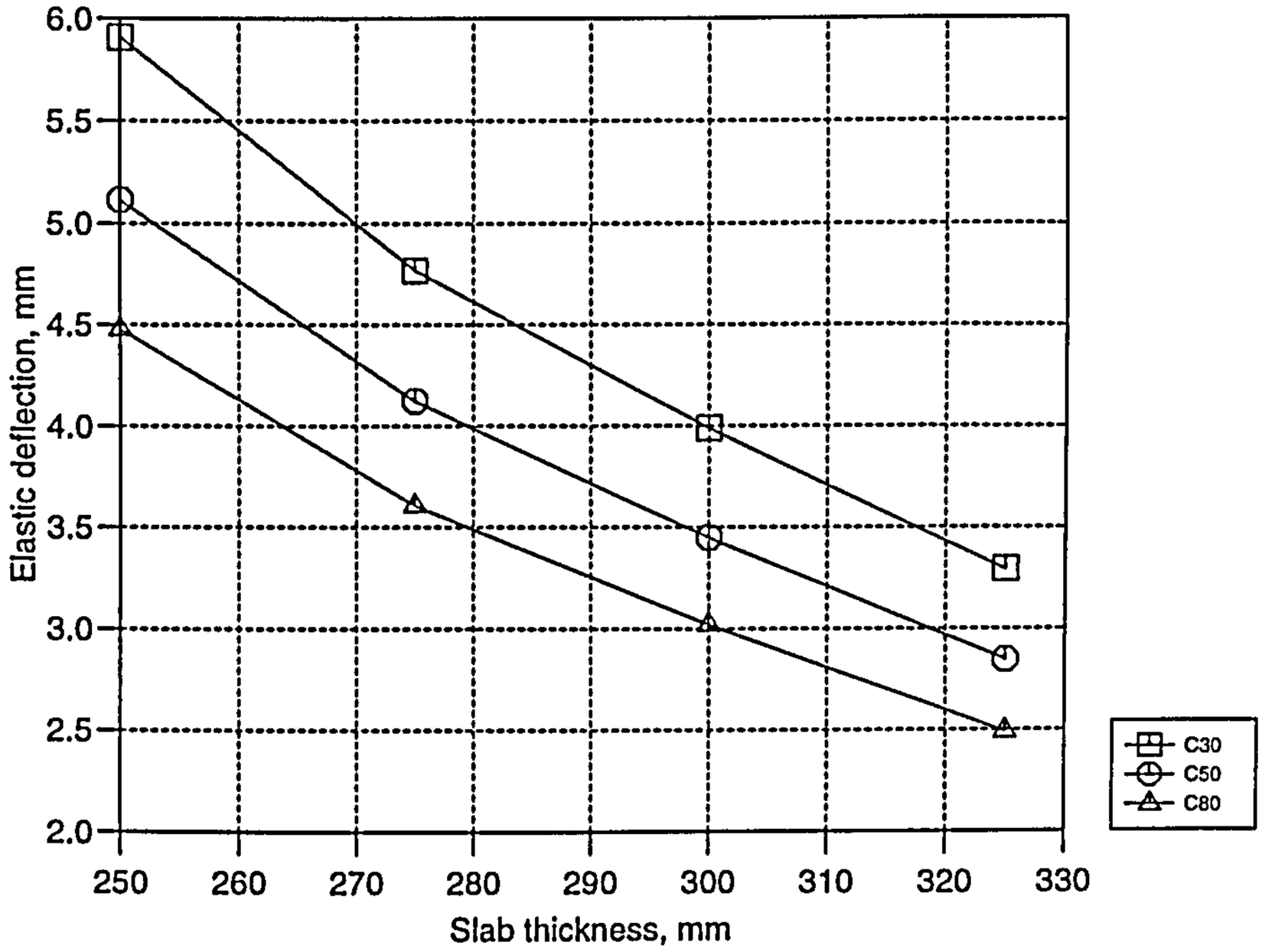


Figure 7.1 Effect of slab thickness on elastic deflection

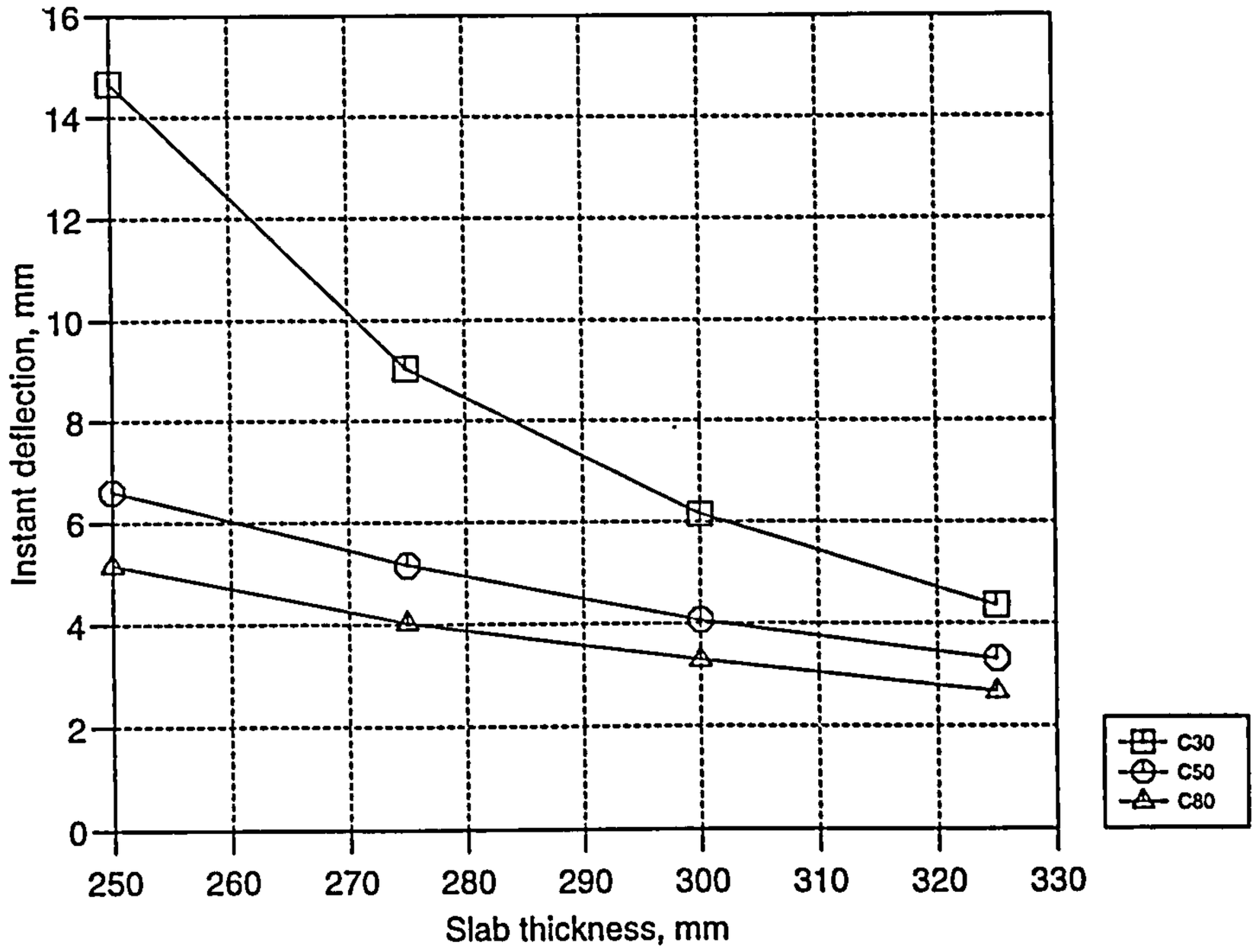


Figure 7.2 Effect of slab thickness on instant deflection

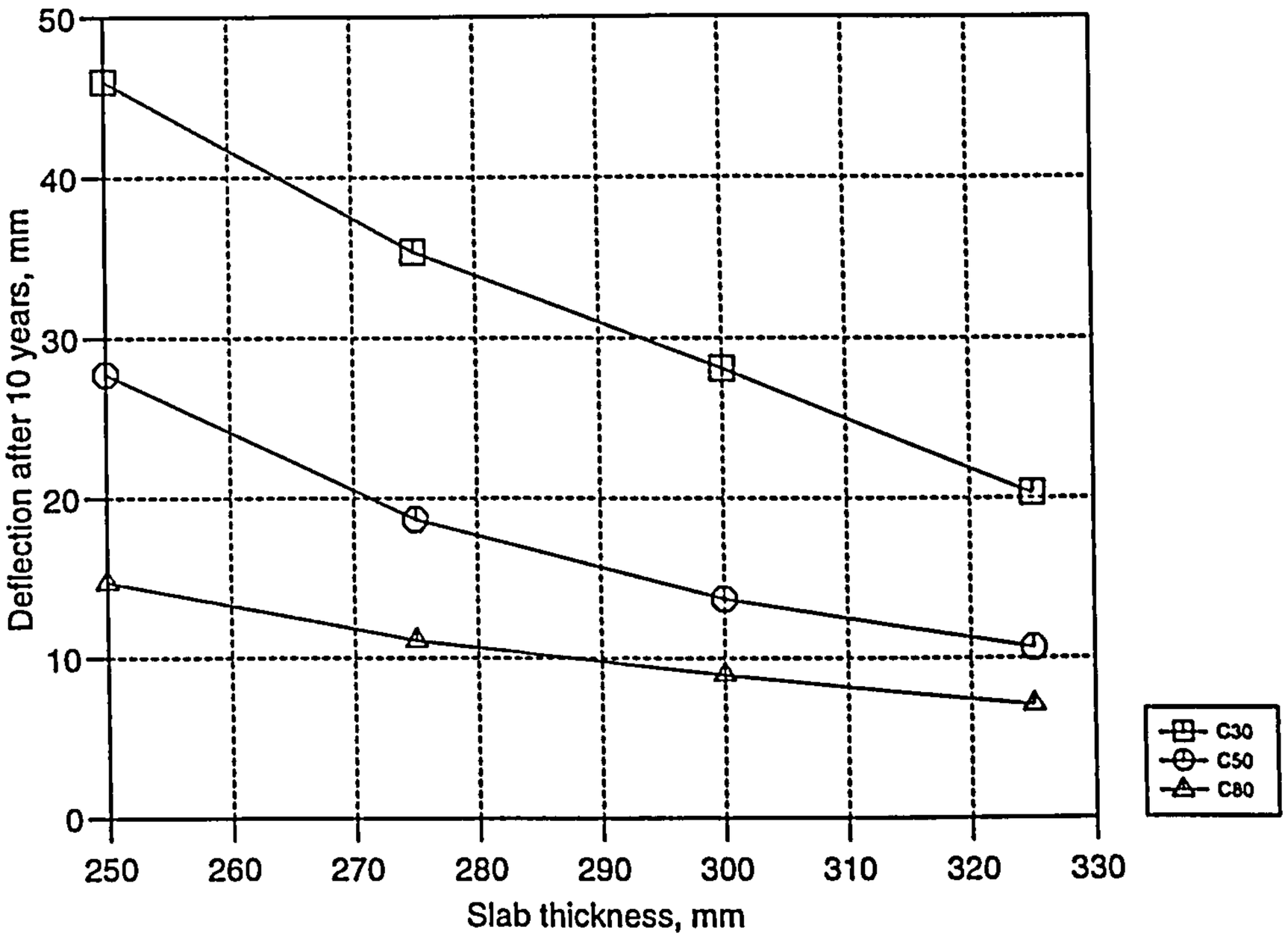


Figure 7.3 Effect of slab thickness on long-term deflection

7.3.2 Effect of providing more bottom steel than required

Objective

The objective of this study is to check the efficiency of the common practice of providing more bottom steel than is required for strength to reduce deflection. BS 8110 (1997) and EC2 (1991) ensure acceptable deflection by specifying maximum permissible l/d ratios which are dependent on the amount of tensile steel provided in the slab at mid-span. In this study, the area of bottom reinforcement was increased by 20 and 40% over and above that required for strength for four different slab thicknesses.

Result

The effect of providing more bottom steel than required on instant and long-term deflection for four thicknesses is shown in Figs 7.4 and 7.5. Comparison of deflections obtained with more bottom steel than required for strength are also made in Table 7.2. A similar pattern was found when the span was increased to 9 m.

Analysis	Bottom reinforcement	Deflection, % for different thicknesses			
		250 mm	275 mm	300 mm	325 mm
Instantaneous	Design for strength	100.0	100.0	100.0	100.0
	20% higher	94.1	97.1	96.4	99.3
	40% higher	89.0	92.6	95.2	98.8
Long-term	Design for strength	100.0	100.0	100.0	100.0
	20% higher	95.7	96.1	95.4	96.9
	40% higher	92.5	93.1	92.6	94.4

Table 7.2 Effect of providing more bottom steel than required

Conclusion

The effect of providing more bottom steel than required for strength has very little effect on deflection. The effect is most significant if the slab is cracked. It is more efficient to reduce deflections by increasing slab thickness or use higher concrete strength. A similar conclusion is also drawn by Vollum & Hossain (1998) from a parametric study on a one-way slab.

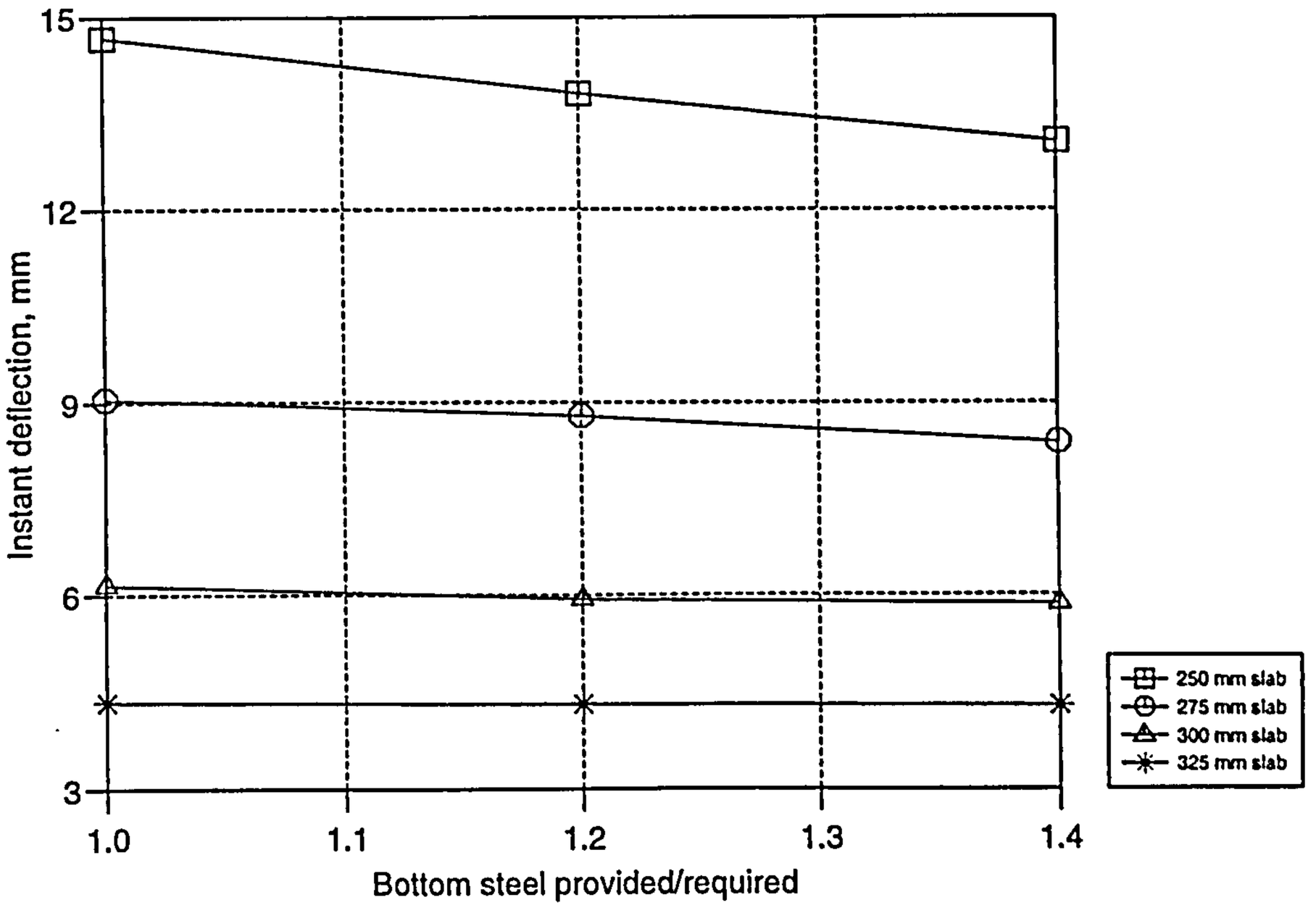


Figure 7.4 Effect of providing more bottom steel than required for strength on instant deflection

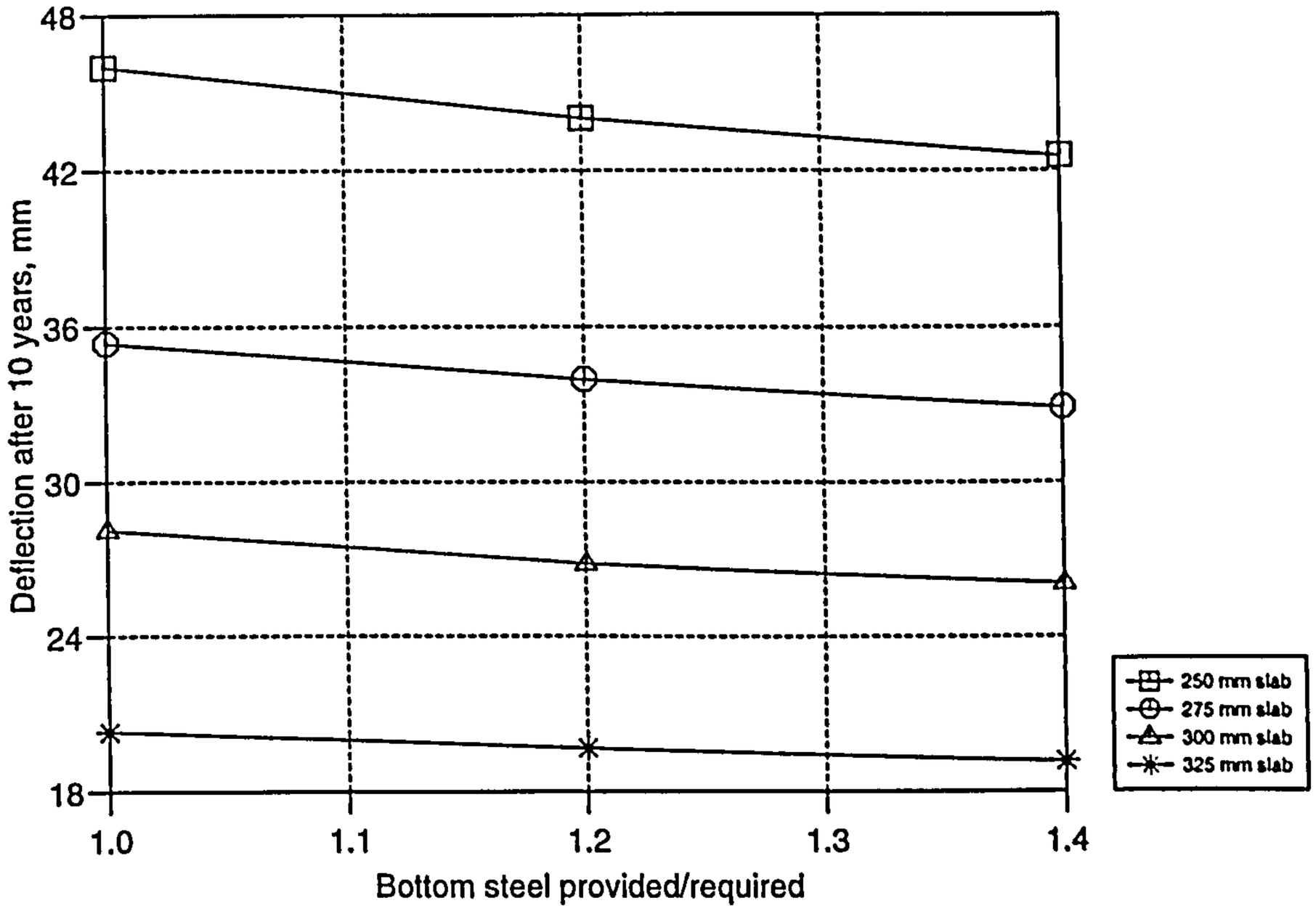


Figure 7.5 Effect of providing more bottom steel than required for strength on long-term deflection

7.3.3 Effect of distribution of reinforcement

Objective

In order to study the effect of distributing reinforcement over hogging and sagging regions, five different meshes were considered with four slab thicknesses. In other sections of the chapter, slabs were designed with the column peak moments being reduced to 80% of the original value and span moments were adjusted accordingly. In the current analysis, the peak column moments were multiplied by five different factors (i.e. 0.6, 0.8, 1.0, 1.2 and 1.4) to obtain different moment diagrams and corresponding reinforcement meshes were obtained. Factors less than 1.0 leads to reduced column moment and increased span moment and vice versa. Reinforcement was assumed to remain elastic. A minimum of 0.15% steel was provided as nominal steel.

Result

The variations in deflection with different reinforcement meshes are shown in Figs 7.6 and 7.7 and compared in Table 7.3. Providing more top steel in the slab over the column, which is more cracked than the span, reduces deflections. The effect is greater for the thinner slabs since they are more cracked. However, the effect is not significant.

Analysis	Multiplication factor	Deflection, % for different thicknesses			
		250 mm	275 mm	300 mm	325 mm
Instantaneous	0.6	106.7	105.2	106.7	103.5
	0.8	105.1	102.8	102.4	101.7
	1.0	100.0	100.0	100.0	100.0
	1.2	97.4	98.1	98.2	98.3
	1.4	95.1	95.7	96.6	96.9
Long-term	0.6	104.3	106.2	103.4	102.5
	0.8	101.6	103.3	102.3	100.3
	1.0	100.0	100.0	100.0	100.0
	1.2	99.0	98.5	97.4	97.7
	1.4	98.2	97.1	96.5	97.3

Table 7.3 Effect of distribution of reinforcement

Conclusion

Placing more steel over the column appears to slightly reduce the deflection of thinner slabs as it increases the second moment of area of the cracked section. However, the effect is not significant.

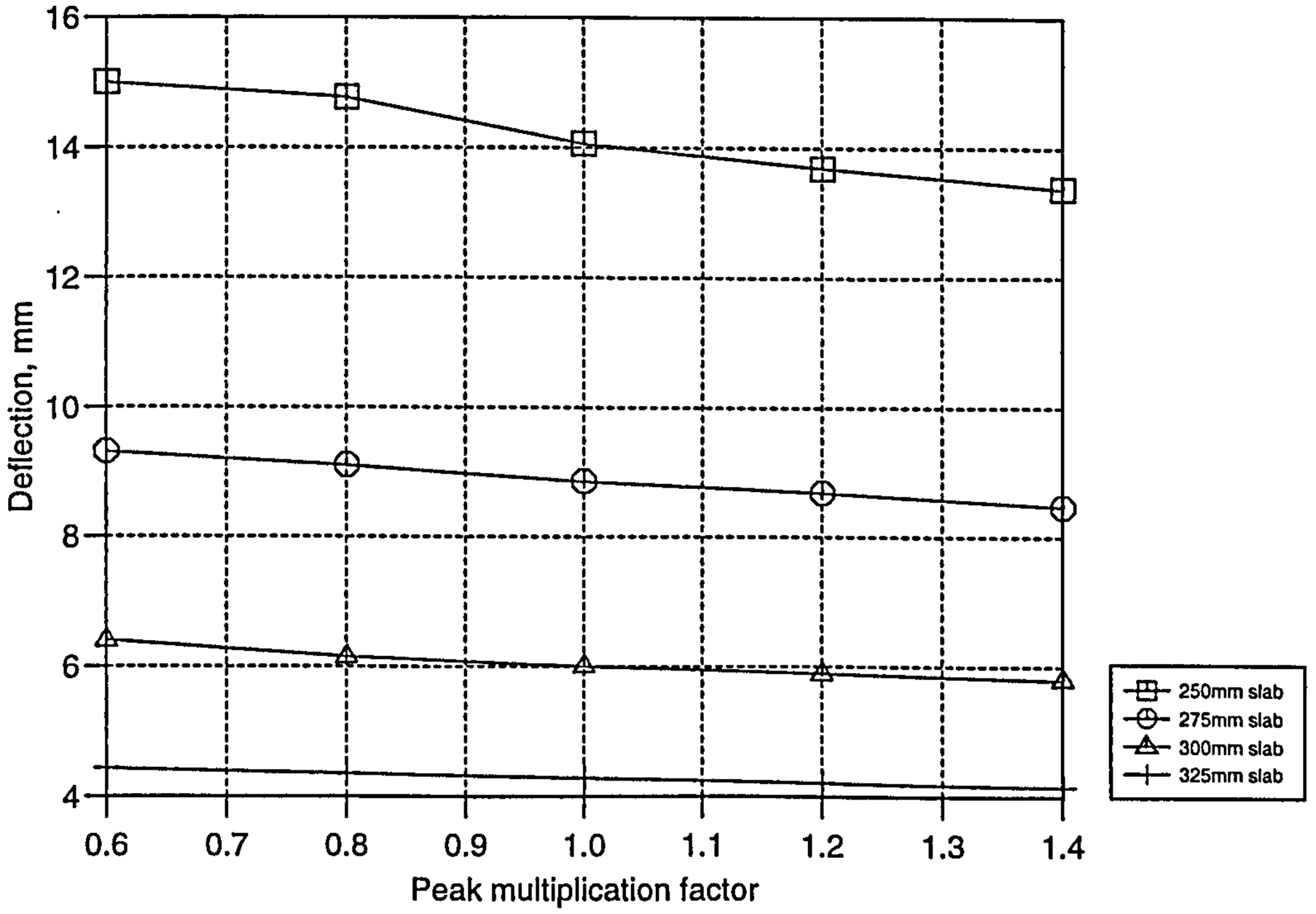


Figure 7.6 Effect of distribution of reinforcement on instant deflection

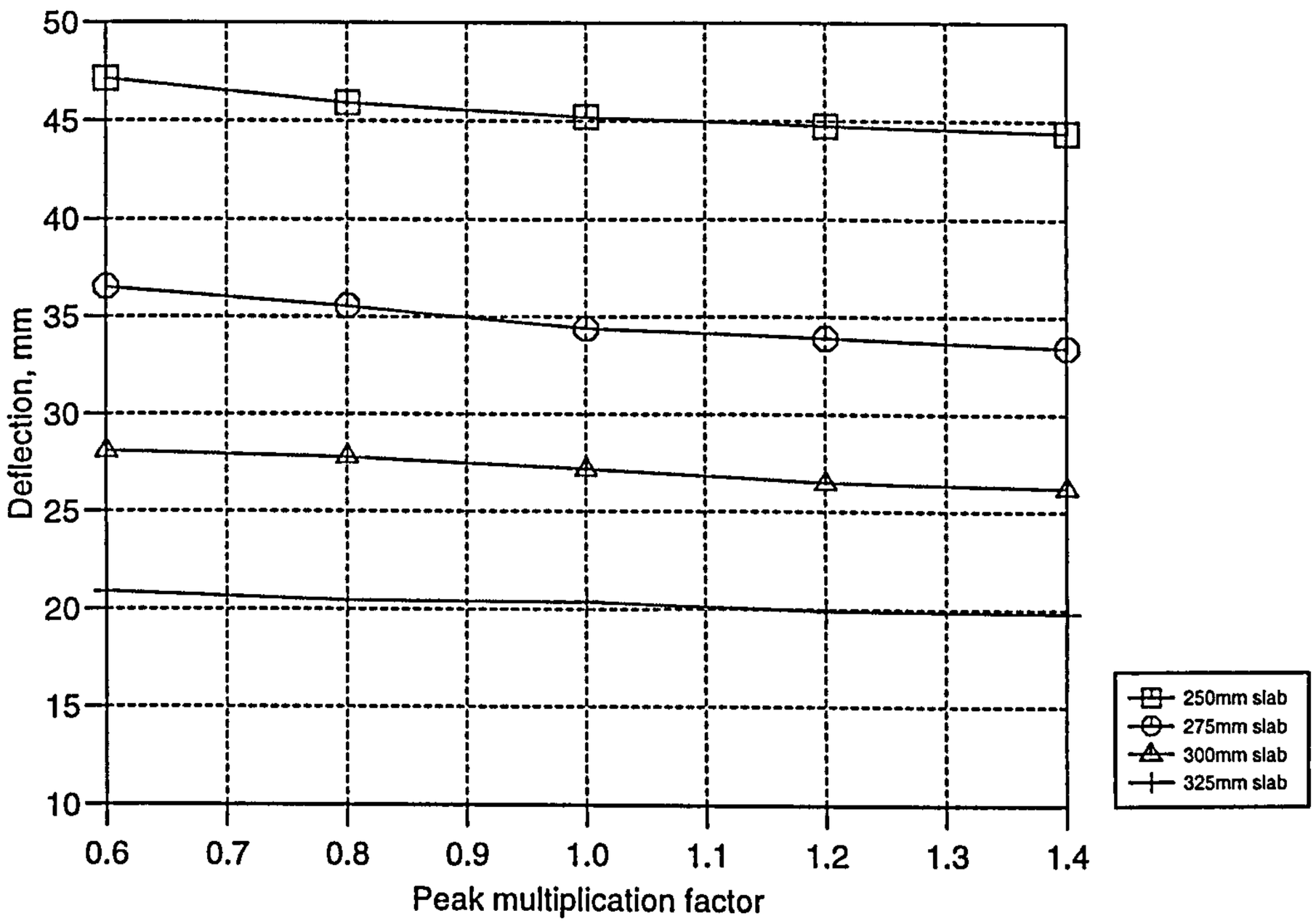


Figure 7.7 Effect of distribution of reinforcement on long-term deflection

7.3.4 Effect of column dimensions

Objective

All the results presented in this chapter are obtained from analyses of an edge panel supported on point supports. To study the effect of modelling actual columns, three column sizes were considered in the current analysis with four slab thicknesses. Top and bottom columns are assumed with contraflexure points at the mid-heights of 3.5 m high columns. Reinforcement, creep, shrinkage and cracking were neglected in column analysis.

Result

Changes in elastic, instantaneous and long-term deflections with the changes in column sizes are presented in Figs 7.8 to 7.10. Comparison of deflections with different column sizes and those obtained with point support are also shown in Table 7.4. Column shortening is subtracted from the FE results.

Analysis	Column size	Deflection, % for different thicknesses			
		250 mm	275 mm	300 mm	325 mm
Elastic	No column	100.0	100.0	100.0	100.0
	200 mm	99.0	99.4	100.0	100.2
	400 mm	93.5	94.6	95.5	96.0
	600 mm	85.3	86.9	88.4	89.4
Instantaneous	No column	100.0	100.0	100.0	100.0
	200 mm	89.9	87.7	88.0	90.6
	400 mm	66.8	72.4	79.8	85.1
	600 mm	50.1	57.7	68.0	75.0
Long-term	No column	100.0	100.0	100.0	100.0
	200 mm	92.6	93.0	94.6	91.7
	400 mm	72.2	70.6	73.1	74.9
	600 mm	58.6	58.1	61.8	64.3

Table 7.4 Effect of column size

Conclusion

Column size has a significant effect on deflections and the modelling of the column is important in predicting deflections accurately. However, it was shown in section

6.9.2 that a more detailed modelling of the column with reinforcement, cracking and long-term effects is not particularly important for the serviceability state.

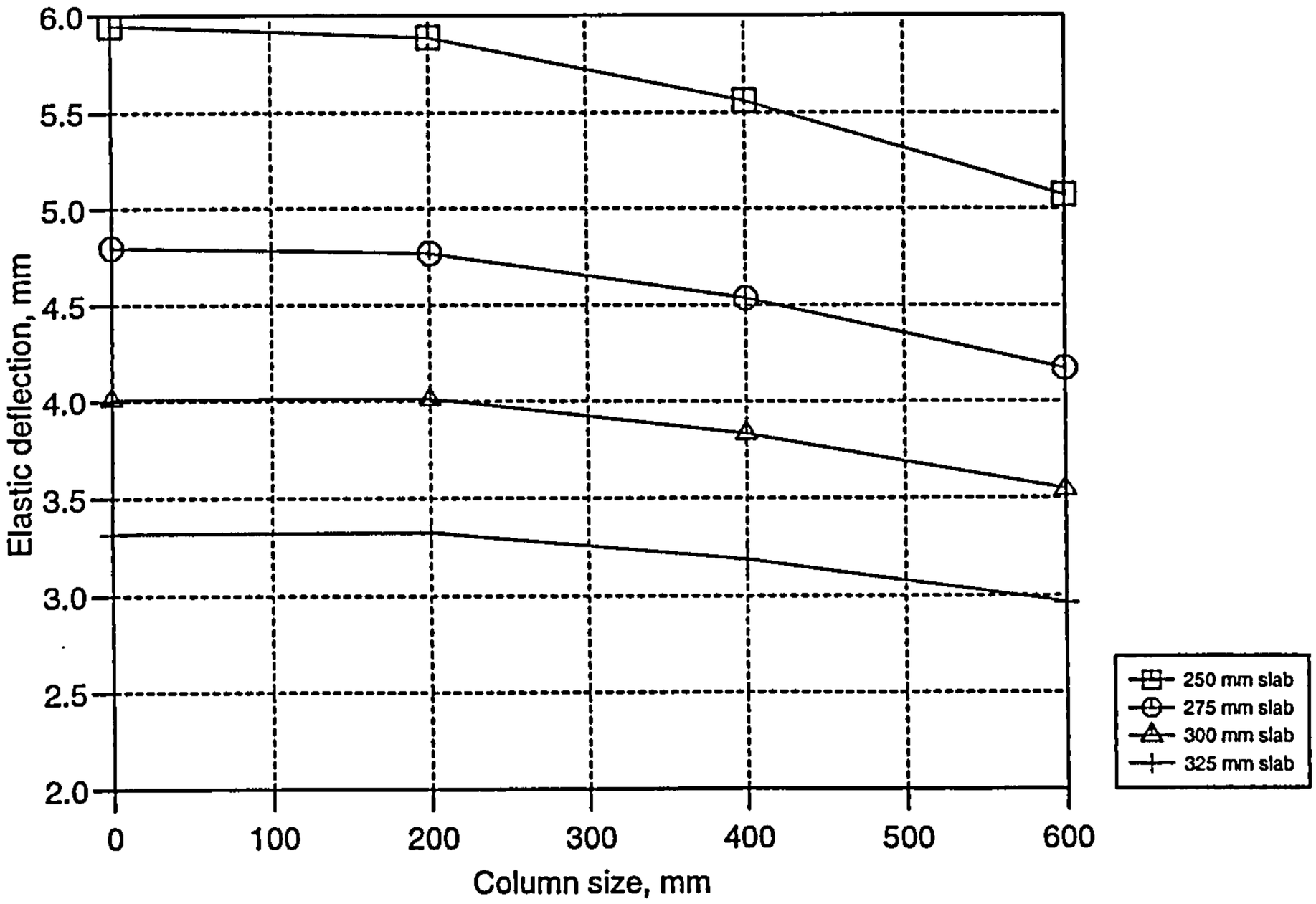


Figure 7.8 Effect of column size on elastic deflection

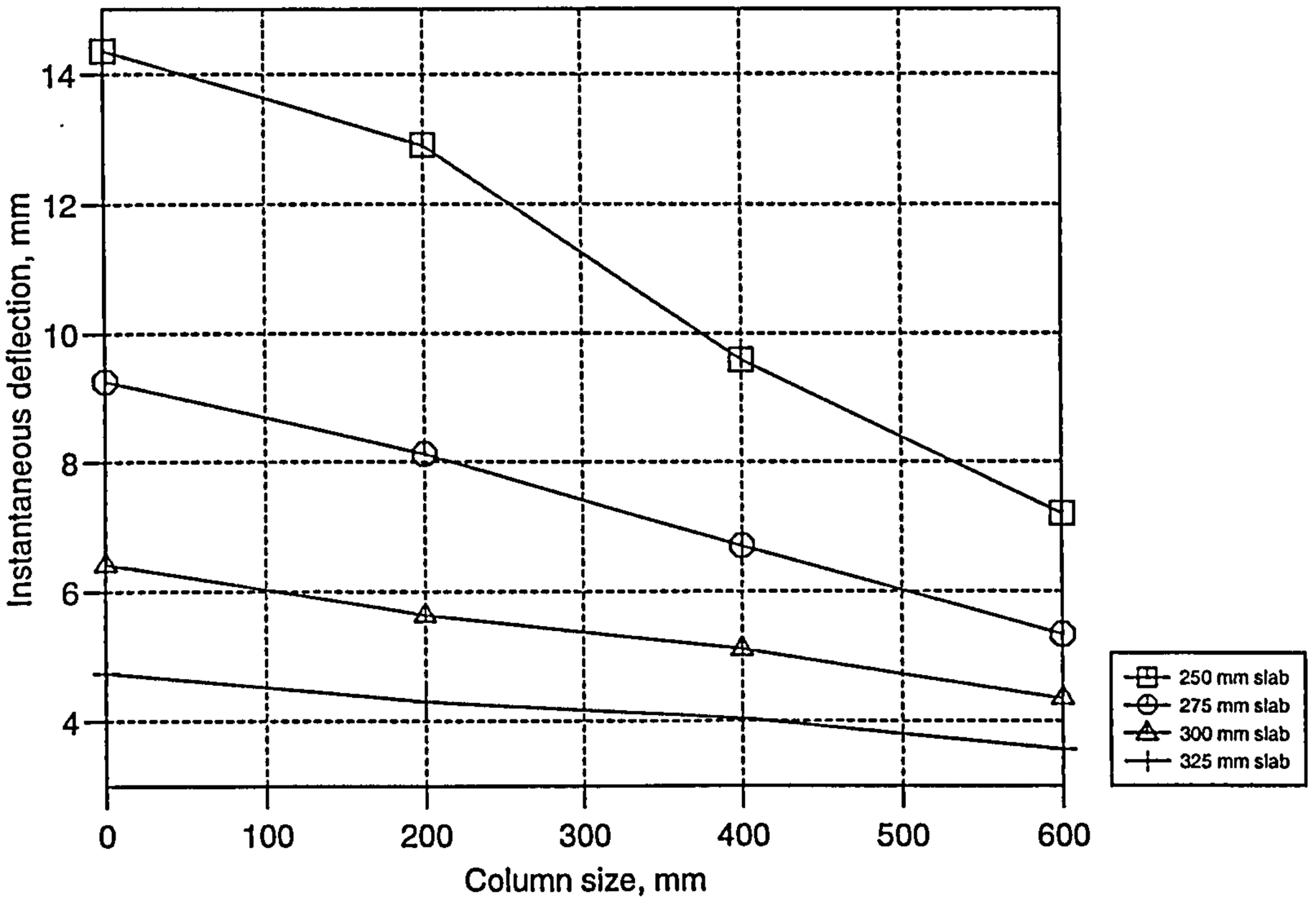


Figure 7.9 Effect of column size on instantaneous deflection

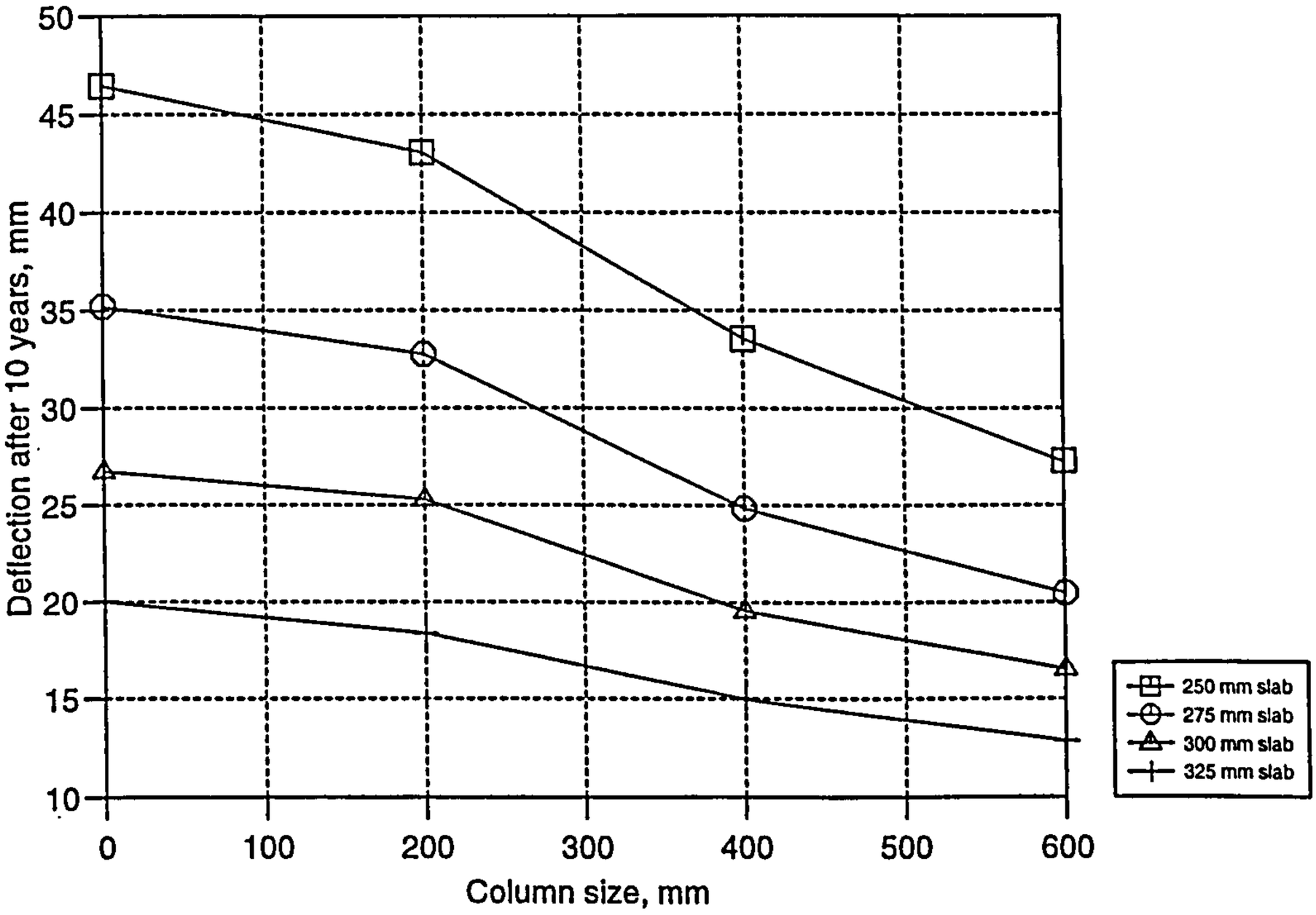


Figure 7.10 Effect of column size on long-term deflection

7.4 Effect of material properties

7.4.1 Effect of concrete strength

Objective

Material properties which are very important in determining deflections, i.e. tensile strength, modulus of elasticity, creep and shrinkage, are all connected to the characteristic compressive strength of concrete. This study will give an idea how this single parameter can influence deflection. Four slab thicknesses and three concrete characteristic strength (i.e. C30, C50 and C80) were used in the analysis. Mean material properties adopted are calculated using MC-90.

Result

The changes in elastic, instant and long-term deflections as functions of the changes in concrete strength (for four thicknesses) are plotted in Figs 7.11 to 7.13 and compared in Table 7.5. Elastic deflections are not greatly affected by increases in concrete strength since they only depend on the modulus of elasticity. Instantaneous deflections reduce significantly with increases in concrete strength since the amount of cracking reduces due to the increase in tensile strength. This is more pronounced for thinner slabs, which are more cracked, where an increase in tensile strength significantly reduces cracking and hence deflections.

Increasing concrete strength also reduced long-term deflections drastically for all four slabs. Here, the improvement in creep and shrinkage properties contributes to the reduction in deflection in addition to the increase in modulus of elasticity and tensile strength.

Conclusion

Deflections can be very significantly reduced by increasing the concrete strength. This is particularly so for thin slabs where the extent of cracking can be reduced greatly by increasing the concrete strength.

Analysis	Concrete strength	Deflection, % for different thicknesses			
		250 mm	275 mm	300 mm	325 mm
Elastic	C30	100.0	100.0	100.0	100.0
	C50	86.5	86.5	86.5	86.5
	C80	75.7	75.7	75.7	75.7
Instantaneous	C30	100.0	100.0	100.0	100.0
	C50	45.1	57.0	65.9	76.1
	C80	35.1	44.5	53.4	61.3
Long-term	C30	100.0	100.0	100.0	100.0
	C50	60.3	52.8	48.7	52.5
	C80	32.0	31.4	31.9	34.7

Table 7.5 Effect of concrete strength

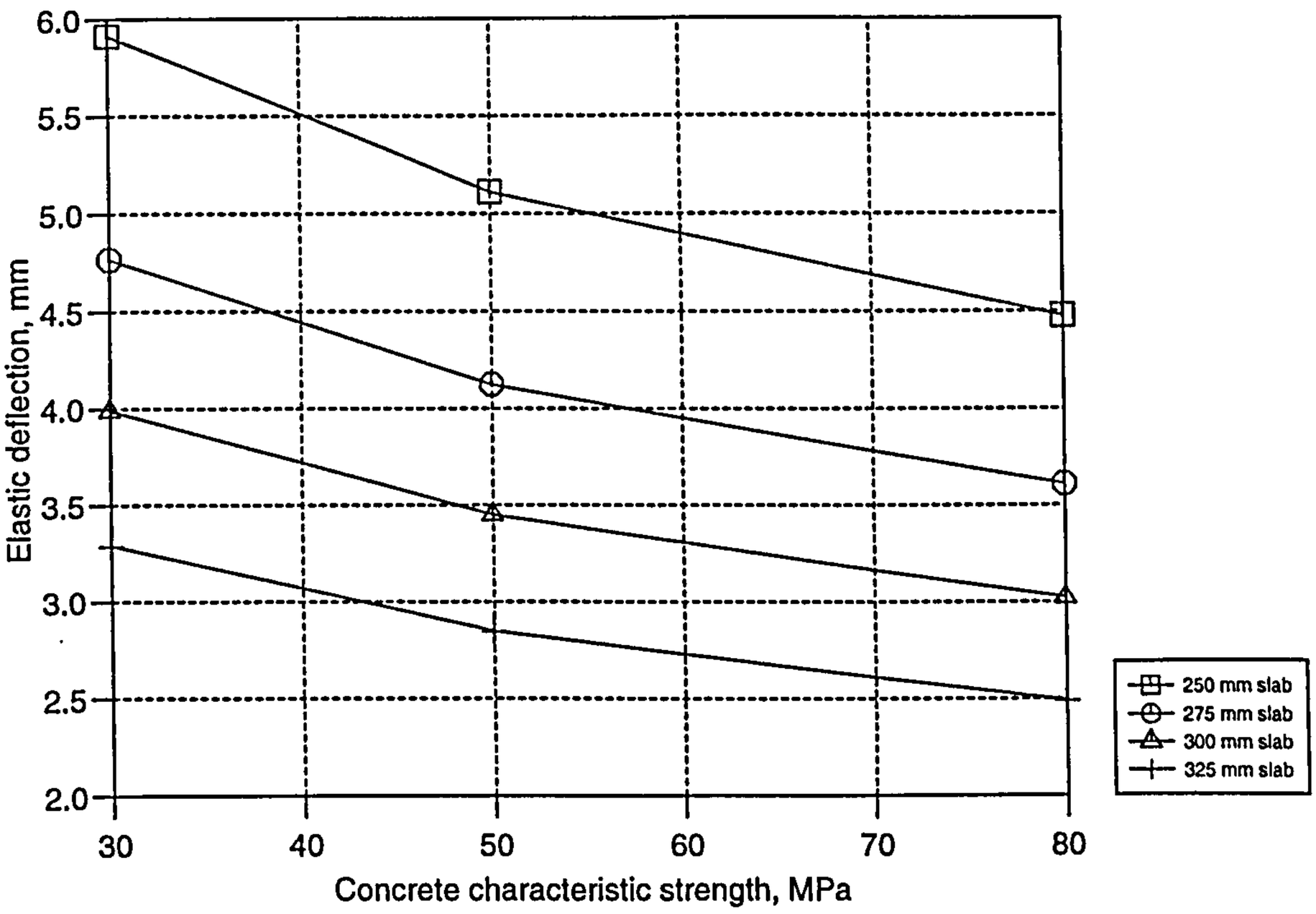


Figure 7.11 Effect of concrete strength on elastic deflection

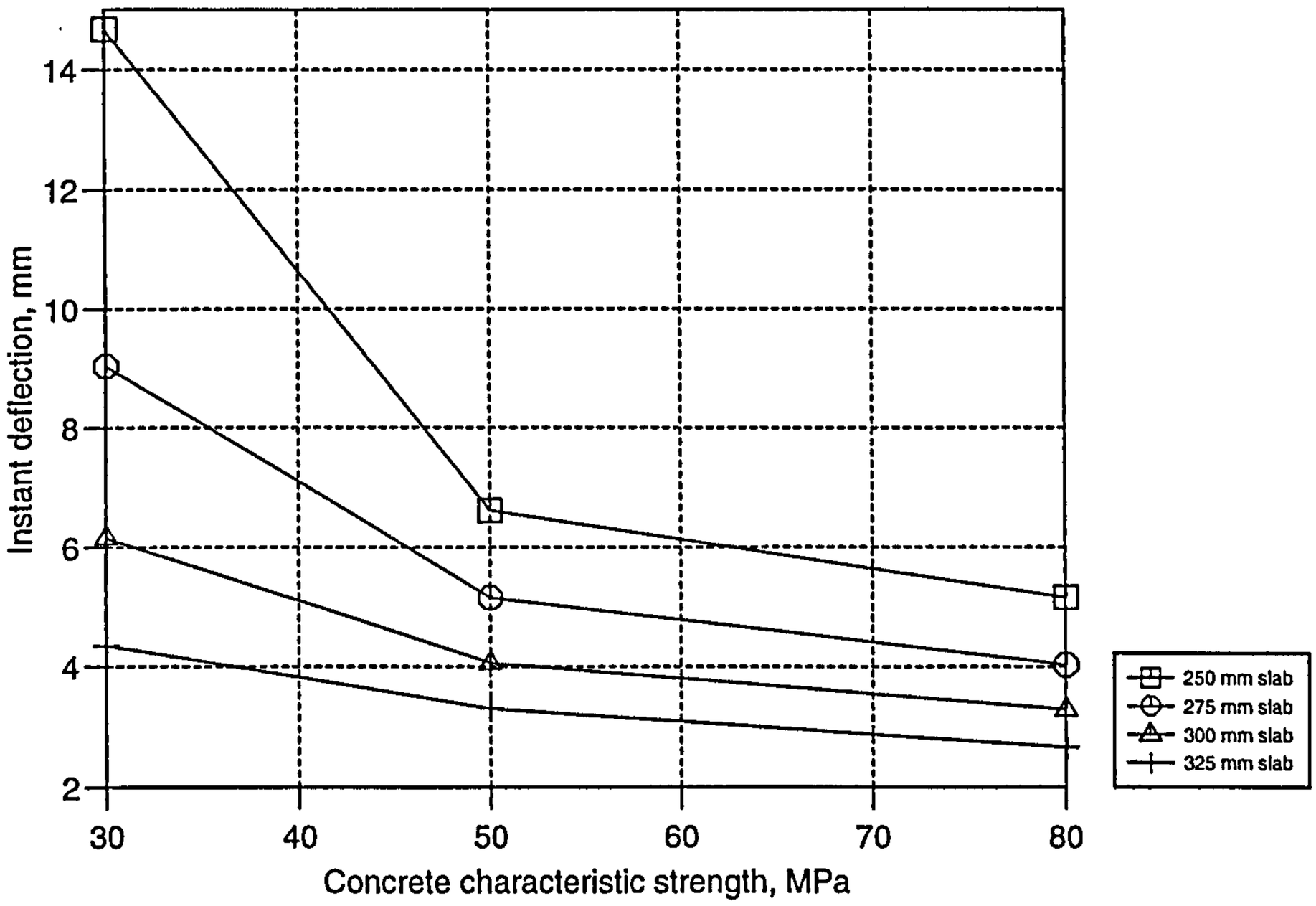


Figure 7.12 Effect of concrete strength on instantaneous deflection

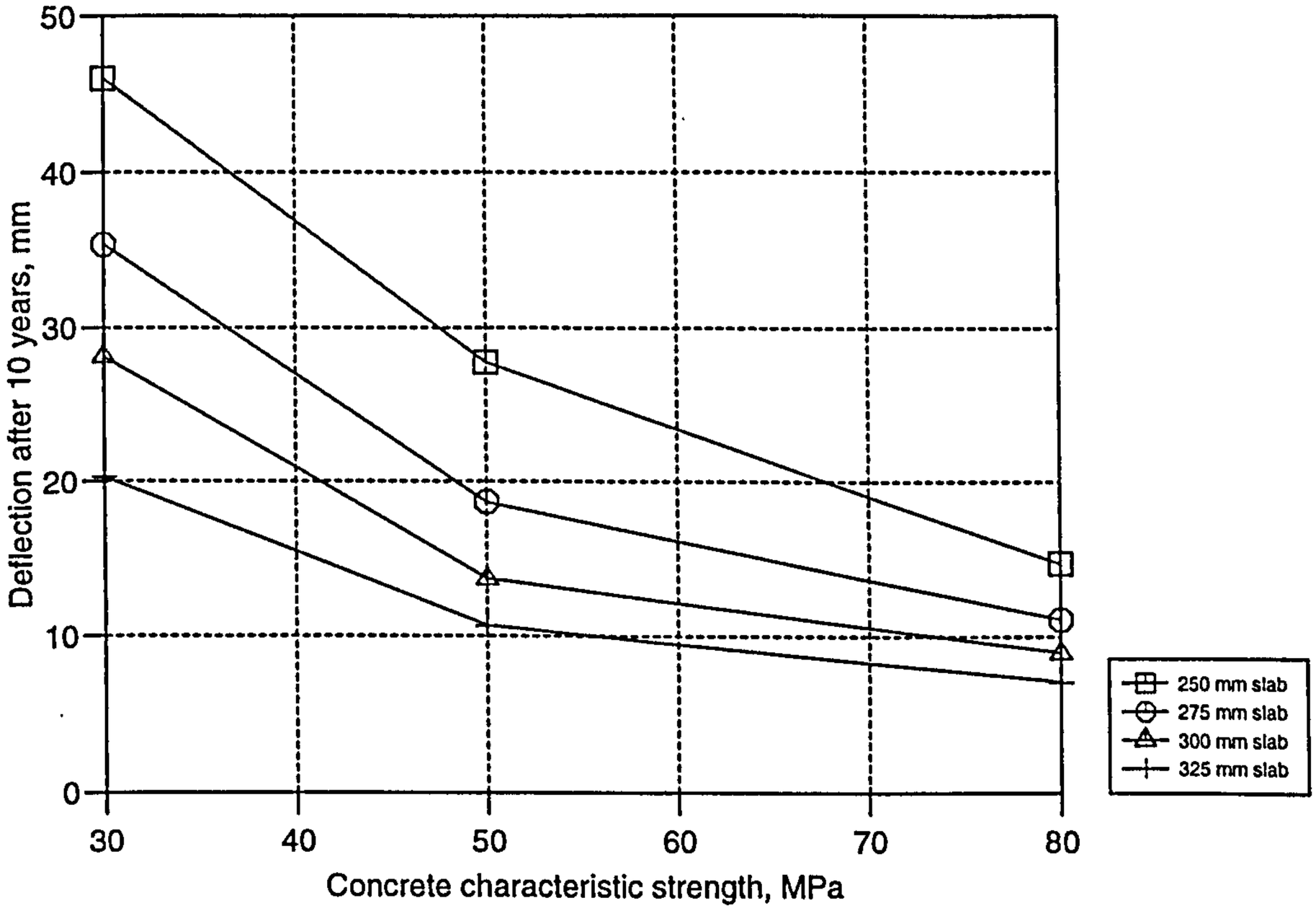


Figure 7.13 Effect of concrete strength on long-term deflection

7.4.2 Effect of variation in tensile strength

Objective

Tensile strength is the most important material property in deflection calculations since it determines the extent of cracking. According to MC-90, it can vary ± 33% of the mean tensile strength for a given compressive strength assuming a normal distribution of all available test data with 5% cut-off points. Here, it is varied between these ranges for a C30 concrete to demonstrate how the statistical variation in f_{ct} can influence instant and long-term deflections.

Result

The variations in instant and long-term deflections with concrete tensile strength are plotted in Figs 7.14 and 7.15 for four slab thicknesses. Three values of concrete tensile strengths were used, i.e. 1.97, 2.90 and 3.83 MPa, where 2.90 MPa is the mean value specified by MC-90. A comparison of deflections calculated with different values of tensile strength are also presented in Table 7.6. The effect of tensile strength on instant deflection is very significant, particularly for thin slabs where cracking is more critical. A similar pattern is also obtained for long-term deflections calculated with β_2=1. Reductions are more prominent for thinner slabs where the extent of cracking is greatly reduced by the improvement in f_{ct}.

Analysis	Tensile strength, MPa	Deflection, % for different thicknesses			
		250 mm	275 mm	300 mm	325 mm
Instantaneous	1.97	167.7	204.9	232.4	241.6
	2.90	100.0	100.0	100.0	100.0
	3.83	54.0	66.2	79.2	87.9
Long-term $\beta_2 = 1$	1.97	141.9	153.1	158.8	152.7
	2.90	100.0	100.0	100.0	100.0
	3.83	76.4	82.9	87.5	90.9
Long-term $\beta_2 = 0.5$	1.97	128.3	133.6	137.4	150.2
	2.90	100.0	100.0	100.0	100.0
	3.83	78.0	74.2	69.8	73.0

Table 7.6 Effect of tensile strength

The effect of loss of tension stiffening on deflection (i.e. using a value of β_2=0.5)

is presented in Table 7.7 and Fig. 7.15. It is concluded that the effect of loss of

Analysis	β_2 value	Deflection, % for different thicknesses			
		250 mm	275 mm	300 mm	325 mm
Long-term	$\beta_2 = 1$	100.0	100.0	100.0	100.0
f_{ct}=1.97 MPa	$\beta_2 = 0.5$	124.2	129.0	132.2	141.8
Long-term	$\beta_2 = 1$	100.0	100.0	100.0	100.0
f_{ct}=2.90 MPa	$\beta_2 = 0.5$	137.3	147.8	152.8	144.2
Long-term	$\beta_2 = 1$	100.0	100.0	100.0	100.0
f_{ct}=3.83 MPa	$\beta_2 = 0.5$	140.3	132.3	121.9	115.7

Table 7.7 Effect of loss of stiffness: using $\beta_2 = 0.5$

tension stiffening is greatest when M=M_r and reduces as level of cracking increases due to either an decrease in thickness or an decrease in f_{ct}. The effect of loss of tension stiffening (with time or due to repeated load) is greater if the section is slightly cracked which is often the case for slabs.

Conclusion

For a specified characteristic strength, the likely statistical variation in f_{ct} can appreciably affect deflection. Long-term analysis has been carried out with β_2=1 and 0.5 to isolate the deflection that results from loss of tension stiffening with time. The increase in long-term deflection due to loss of tension stiffening is particularly significant for thin slabs.

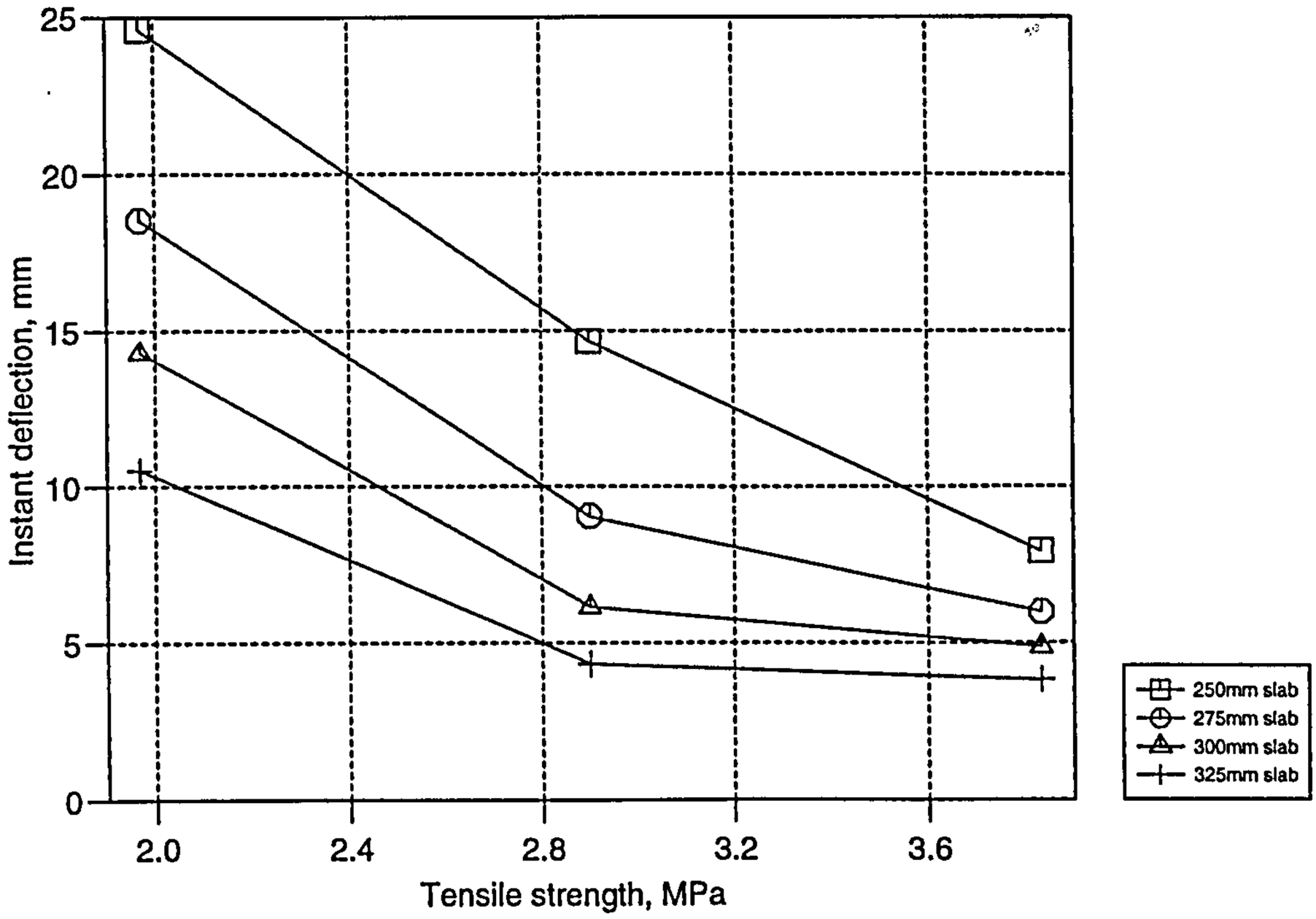


Figure 7.14 Effect of tensile strength on instant deflection

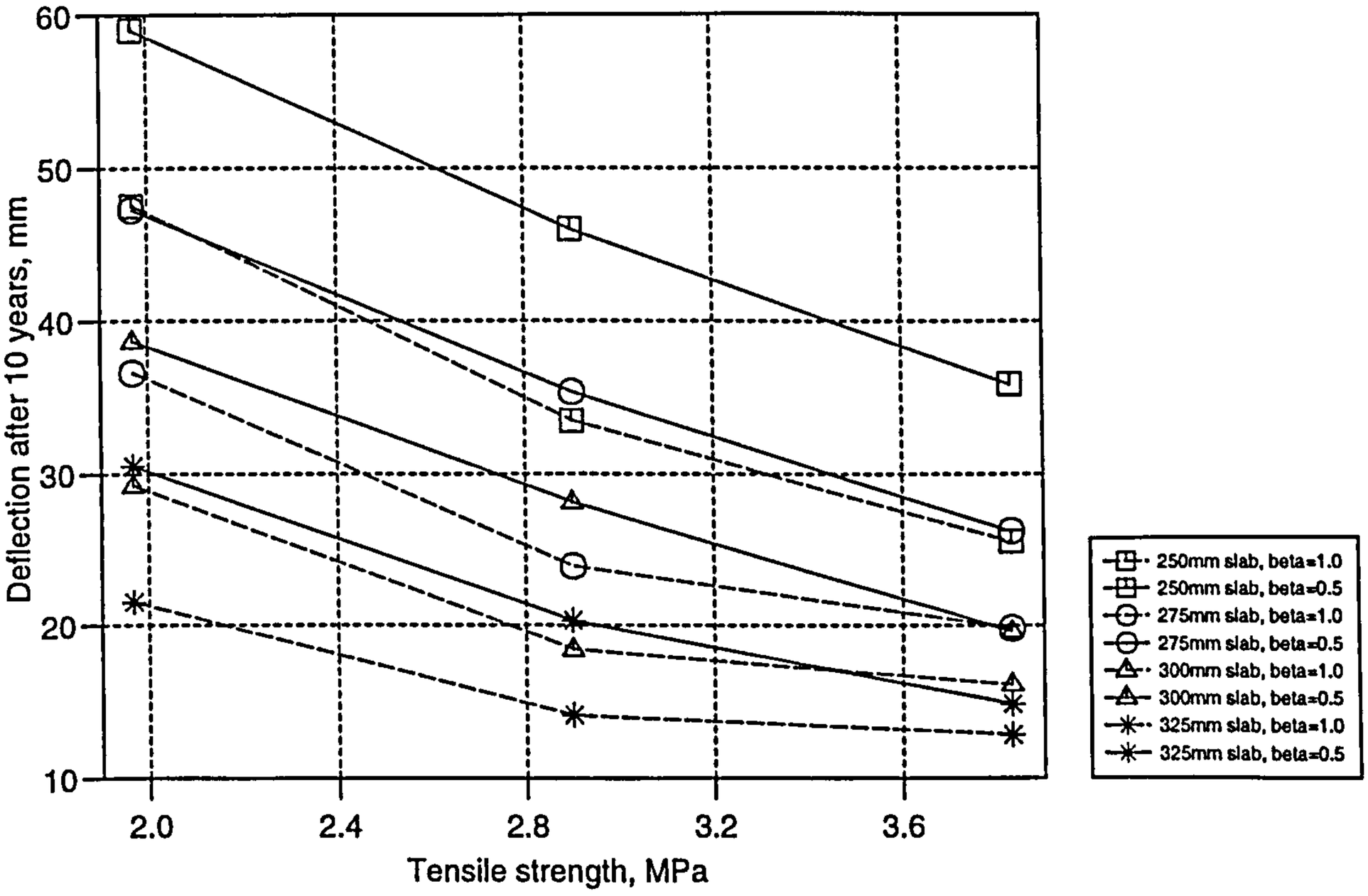


Figure 7.15 Effect of tensile strength on long-term deflection

7.4.3 Effect of variation in creep coefficient

Objective

The creep coefficient determines the amount of long-term deflection due to creep of concrete. MC-90 provides equations to calculate the mean creep coefficient at any time t for a concrete specimen loaded at t_0. The other parameters included in the equations are type of cement, characteristic cylinder strength of concrete at 28 days, notional size of the specimen and relative humidity. Assuming a normal statistical distribution of all the available test data and 5% cut-off points, the code also proposes maximum and minimum values for creep which are ± 33% of the mean creep coefficient for a given compressive strength. To determine how this statistical variation affects the deflection, the creep coefficient is varied between these ranges for a C30 concrete.

Result

The long-term deflection variation with variation of creep coefficient by ± 33% are presented in Fig. 7.16. A comparison of deflections calculated with three values of creep coefficient is also presented in Table 7.8.

Analysis	Creep coefficient	Deflection, % for different thicknesses			
		250 mm	275 mm	300 mm	325 mm
Long-term	$0.66\phi_{MC-90}$	90.3	90.5	87.2	86.8
	$1.00\phi_{MC-90}$	100.0	100.0	100.0	100.0
	$1.33\phi_{MC-90}$	109.5	109.1	108.4	114.1

Table 7.8 Effect of creep coefficient

Conclusion

For a specified characteristic strength, the likely statistical variation in creep coefficient results in an almost linearly variation in long-term deflection. The almost parallel curves for different thicknesses indicate that the variation type is similar for any thickness. The statistical variation of creep coefficient affects long-term deflection, but the effect is not as significant as the tensile strength. A variability of

deflection within ± 15% of the mean can be expected due to the variability of the creep coefficient.

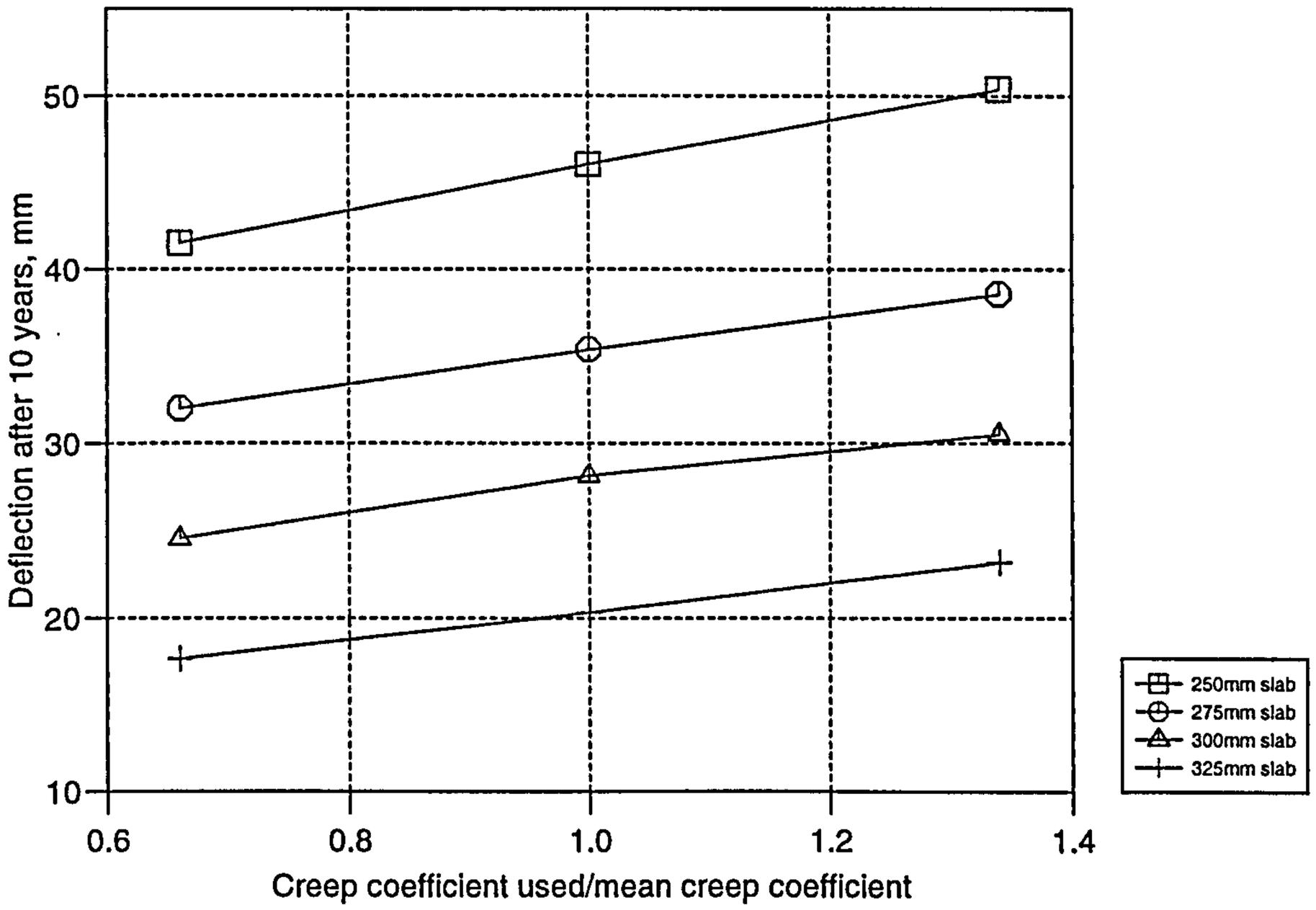


Figure 7.16 Effect of creep coefficient on long-term deflection

7.4.4 Effect of variation in shrinkage strain

Objective

The shrinkage strain determines the amount of long-term deflection due to shrinkage of concrete. MC-90 provides equations to calculate the mean shrinkage strain of a concrete specimen at time t for drying from time t_s. The other parameters included in the equations are type of cement, characteristic cylinder strength of concrete at 28 days, notional size of the specimen and relative humidity. The code also identifies the maximum and minimum ranges within which the shrinkage strain can vary by considering all available test data assuming a normal statistical variation with 5% cut-off. The ranges are $0.42\epsilon_{cs}$ to $1.58\epsilon_{cs}$ for a given compressive strength where ϵ_{cs} is the mean shrinkage strain. Here it is varied between these ranges for a C30 concrete.

Result

The variation in long-term deflection with shrinkage strain is presented in Fig. 7.17. A comparison of deflections calculated with three values of shrinkage strains is also shown in Table 7.9.

Analysis	Shrinkage strain	Deflection, % for different thicknesses			
		250 mm	275 mm	300 mm	325 mm
Long-term	$0.42\epsilon_{cs-MC-90}$	90.1	90.2	88.6	92.9
	$1.00\epsilon_{cs-MC-90}$	100.0	100.0	100.0	100.0
	$1.58\epsilon_{cs-MC-90}$	110.5	110.7	109.1	107.8

Table 7.9 Effect of shrinkage strain

Conclusion

The variation in long-term deflection, due to the statistical variation in shrinkage strain for a specified characteristic strength, is similar for different thicknesses. Deflections vary almost linearly with shrinkage strain. The variation in shrinkage strain ranges between ± 58% which is greater than the variation in creep coefficient. However, the variation it causes in deflections is only about 10%, which is less than the variation in deflection due to variation in the creep coefficient.

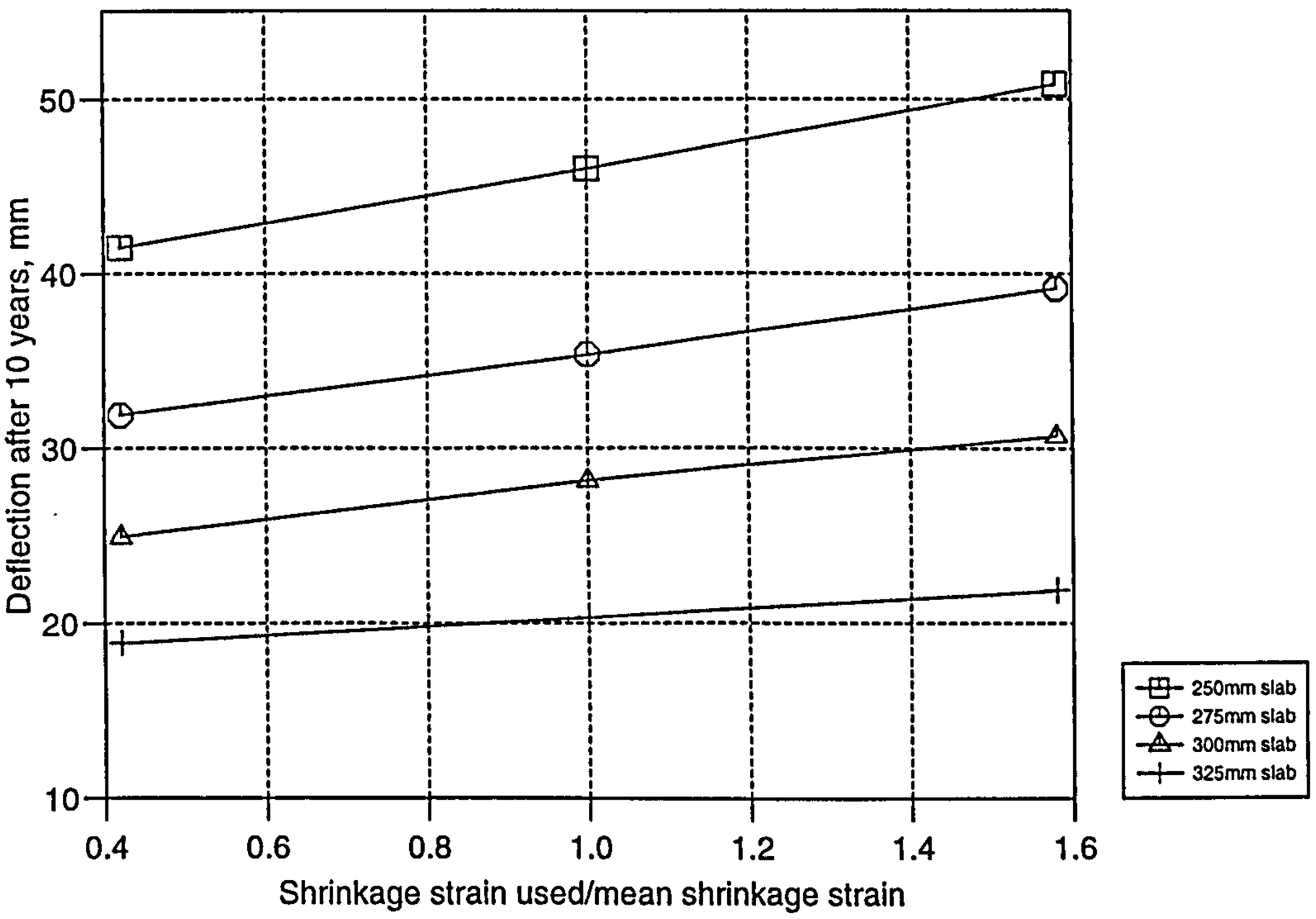


Figure 7.17 Effect of shrinkage strain on long-term deflection

7.4.5 Effect of variation in modulus of elasticity of concrete

Objective

The modulus of elasticity of concrete affects short- and long-term deflections. According to MC-90, depending on the aggregate used, it can vary from $0.7E_m$ to $1.2E_m$ where E_m is the mean value of modulus of elasticity for a given compressive strength. Here it is varied between these ranges for a C30 concrete.

Result

The variation in instant and long-term deflections with modulus of elasticity of concrete for the four slab thicknesses are shown in Figs 7.18 and 7.19. Deflections are also compared in Table 7.10. The slab deflections do not reduce in inverse proportion to E since the reinforcement contributes less to the slab stiffness as modular ratio is reduced due to increase in E. Thinner slabs are less sensitive to the variations in elasticity modulus than thicker slabs since they contain more steel than thicker ones and are more cracked. Long-term deflections are less sensitive than instant deflections to changes in E since use of β_2=0.5 makes all the slabs more cracked and addition of creep and shrinkage reduces the significance of the instant part of the deflection.

Analysis	Modulus of elasticity of concrete	Deflection, % for different thicknesses			
		250 mm	275 mm	300 mm	325 mm
Instantaneous	$0.70E_{m-MC-90}$	113.1	121.2	126.2	136.5
	$1.00E_{m-MC-90}$	100.0	100.0	100.0	100.0
	$1.20E_{m-MC-90}$	94.2	93.3	86.7	85.5
Long-term	$0.70E_{m-MC-90}$	113.6	113.5	113.0	118.8
	$1.00E_{m-MC-90}$	100.0	100.0	100.0	100.0
	$1.20E_{m-MC-90}$	93.8	95.0	93.3	93.2

Table 7.10 Effect of modulus of elasticity of concrete

Conclusion

For a specified characteristic strength, instant and long-term deflections can vary appreciably due to the likely variation in modulus of elasticity resulting from using different aggregates. The effect on instant deflection is most prominent.

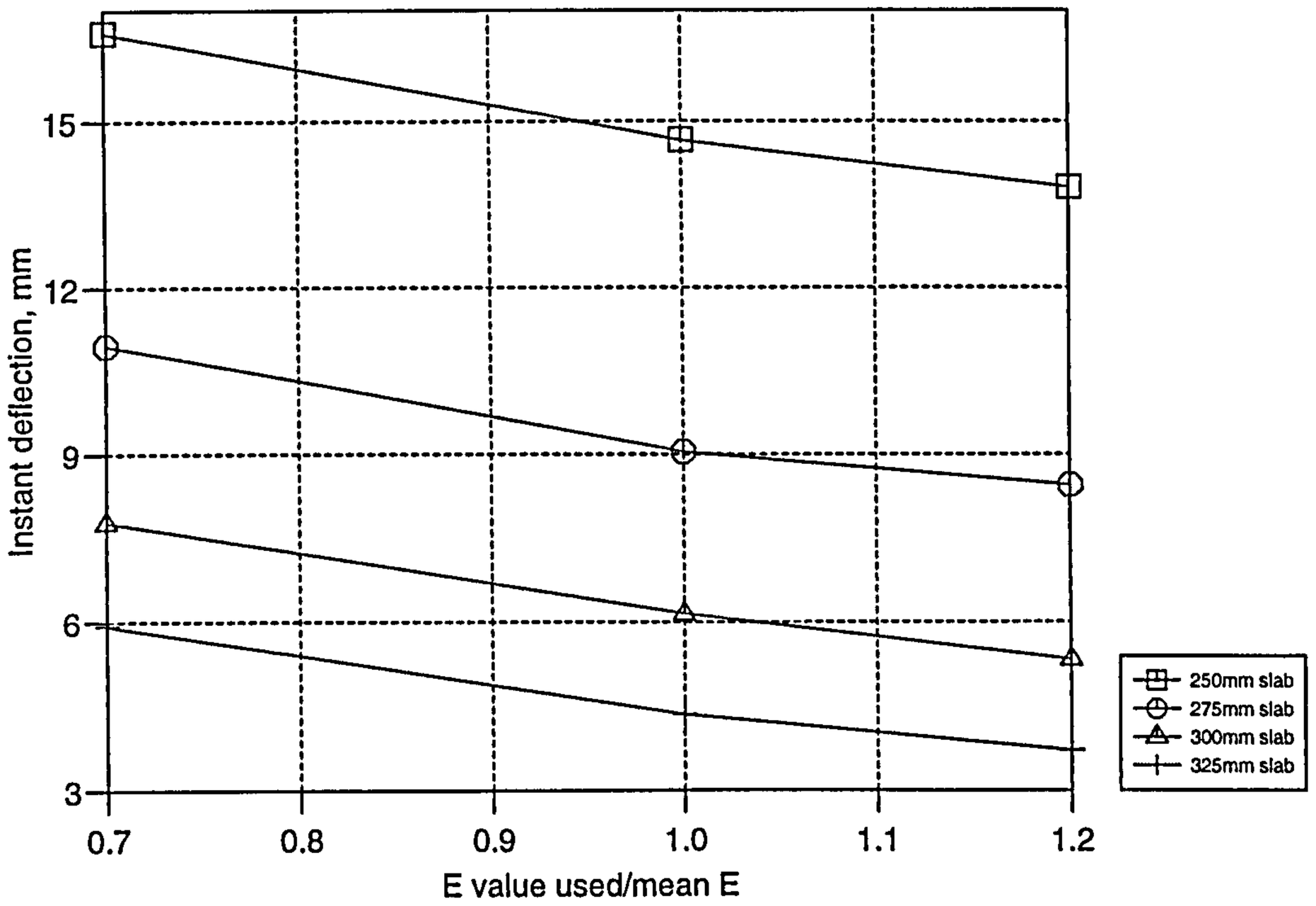


Figure 7.18 Effect of elasticity of concrete on instant deflection

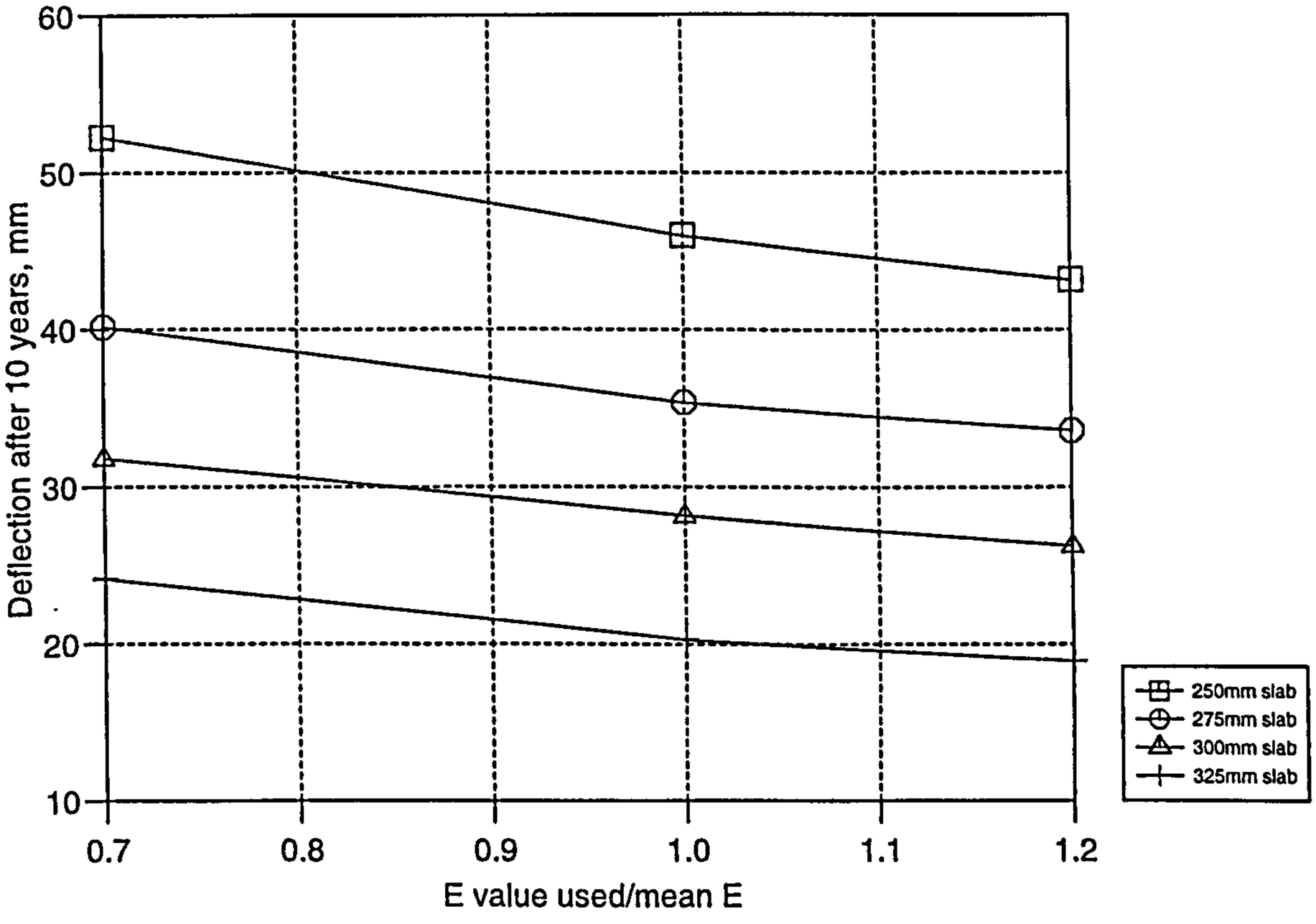


Figure 7.19 Effect of elasticity of concrete on long-term deflection

7.4.6 Varying material properties to extremes

Objective

In the previous studies, different concrete properties (i.e. f_{ct}, E, ϕ, ϵ_{cs}) were varied individually between extremes values given in MC-90. In the current study, they are all varied together to give the best and worst possible combinations to find their joint effect on short- and long-term deflections. Also, to see the interaction between different concrete parameters, deflection changes due to properties varied separately are added to or subtracted from deflections obtained with mean properties.

Result

The instantaneous and long-term deflections with best and worst possible combinations of concrete properties are plotted in Figs 7.20 and 7.21 respectively. Also, comparisons between them are presented in Table 7.11. Most of the variation in deflections is due to the variation in f_{ct}. Deflections obtained by superimposing separate contributions due to changes in f_{ct}, E, ϕ, ϵ_{cs} (only f_{ct}, E for instantaneous deflection) on deflections with mean properties agree well with those obtained with the extreme properties combinations (shown in brackets in Table 7.11). This indicates that the effects of the properties are almost independent.

Conclusion

The effect of using different concrete grades on deflections is very prominent as shown in section 7.4.1. However, even for a specified characteristic strength, the likely variation in material properties can also affect the short- and long-term deflections very significantly. Therefore, for important structures, testing is recommended to determine concrete properties more accurately before design. If the deflection changes due to different properties are superimposed on the deflection corresponding to mean properties, the values are close to the deflections obtained with the extreme properties combinations. This indicates that the different properties affect deflections almost independently.

Analysis	Material properties of concrete	Deflection, % for different thicknesses			
		250 mm	275 mm	300 mm	325 mm
Instant: properties worse than mean	Mean (MC-90)	100.0	100.0	100.0	100.0
	Increases due to f_{ct}	+67.7	+104.9	+132.4	+141.6
	Increase due to E	+13.1	+21.2	+26.2	+36.5
	Added to mean=	180.8	226.1	258.5	278.1
	(Worst combination)	(183.5)	(227.6)	(260.1)	(272.0)
Instant: properties better than mean	Mean (MC-90)	100.0	100.0	100.0	100.0
	Decrease due to f_{ct}	-46.0	-33.8	-20.8	-12.1
	Decrease due to E	-5.8	-6.7	-13.3	-14.5
	Deducted from mean=	48.2	59.5	65.9	73.4
	(Best combination)	(46.7)	(56.1)	(67.1)	(74.3)
Long-term: properties worse than mean	Mean (MC-90)	100.0	100.0	100.0	100.0
	Increases due to f_{ct}	+28.3	+33.6	+37.4	+50.2
	Increase due to E	+13.6	+13.5	+13.0	+18.8
	Increases due to ϕ	+9.5	+9.1	+8.4	+14.1
	Increase due to ϵ_{cs}	+10.5	+10.7	+9.1	+7.8
	Added to mean=	161.9	166.9	167.9	190.9
	(Worst combination)	(165.9)	(173.1)	(177.0)	(196.7)
Long-term: properties better than mean	Mean (MC-90)	100.0	100.0	100.0	100.0
	Decreases due to f_{ct}	-22.0	-25.8	-30.2	-27.0
	Decrease due to E	-6.2	-5.0	-6.7	-6.8
	Decreases due to ϕ	-9.7	-9.5	-12.8	-13.2
	Decrease due to ϵ_{cs}	-9.9	-9.8	-11.4	-7.1
	Deducted from mean=	52.1	49.9	38.9	45.9
	(Best combination)	(57.0)	(51.4)	(47.0)	(47.1)

Table 7.11 Effect of varying material properties to extremes

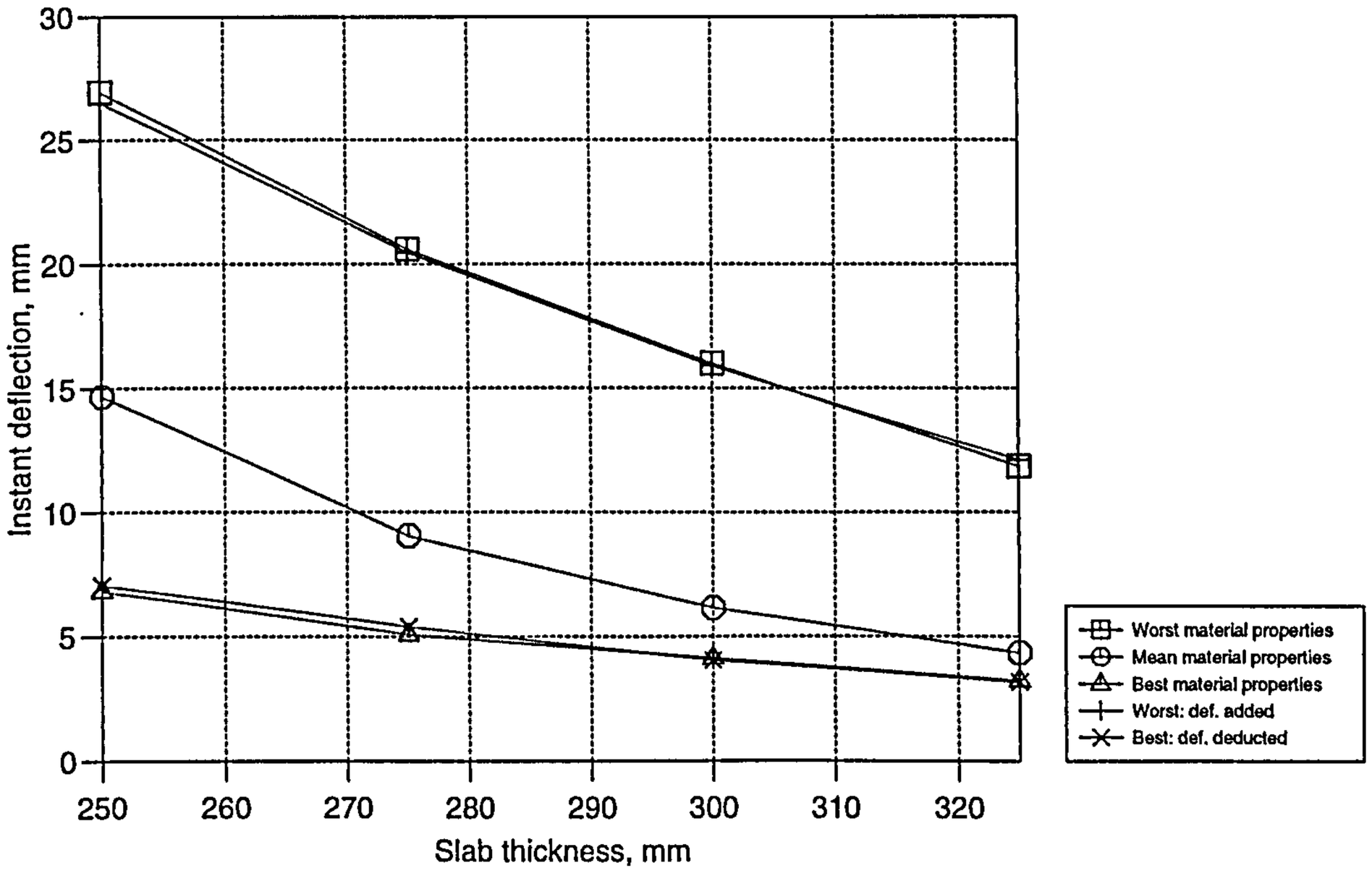


Figure 7.20 Effect of varying material properties to extremes on instant deflection

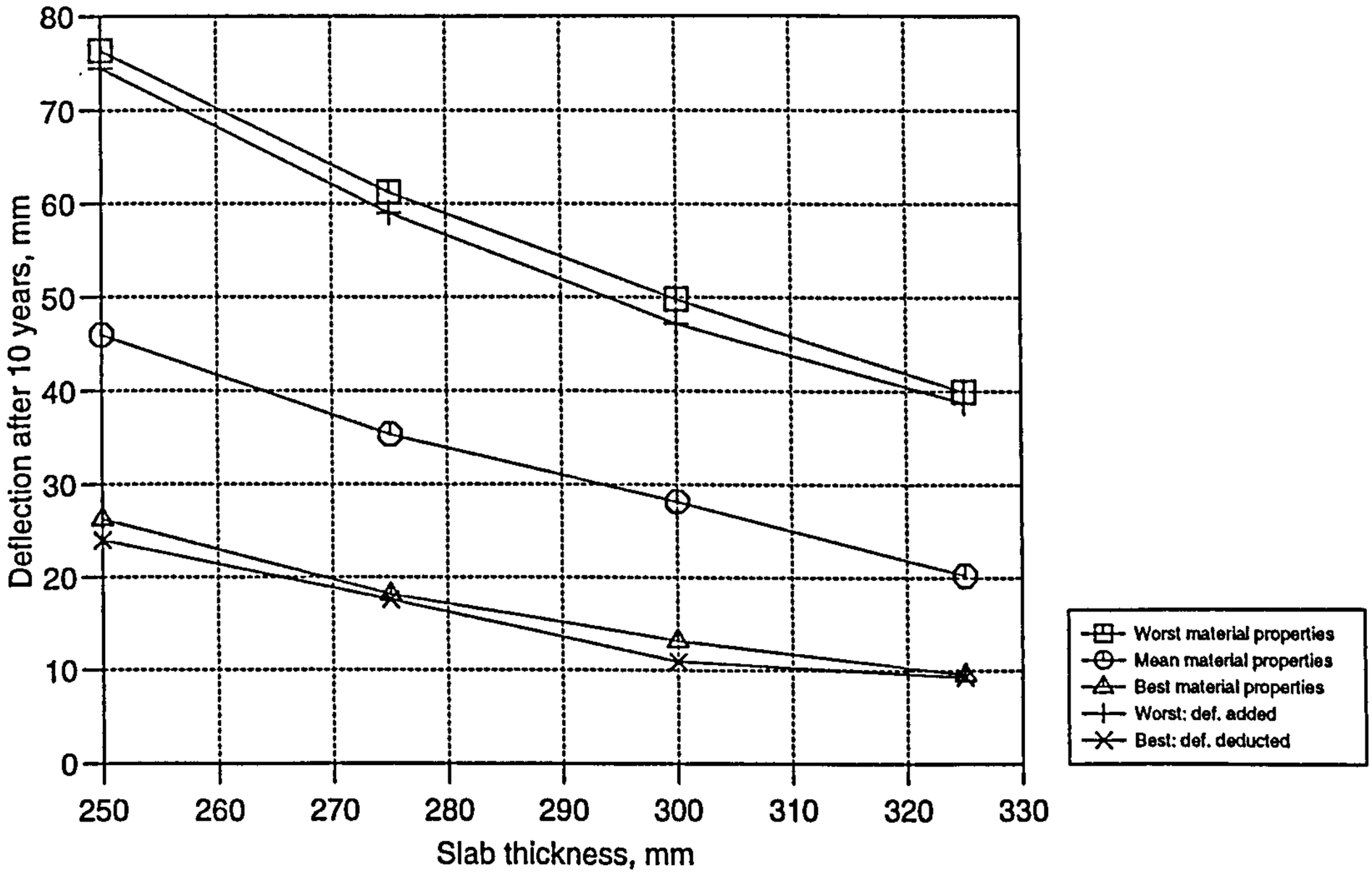


Figure 7.21 Effect of varying material properties to extremes on long-term deflection

7.5 Effect of construction load sequences and their timings

7.5.1 Adopting different construction sequences

An unfavourable construction sequence can result in relatively young slabs being subjected to loading several times their dead load with the possibility of severe cracking developing before the imposed load is applied. A number of researchers have worked on quantifying construction loads and determining their effect on short- and long-term deflections of flat slabs (see section 2.7).

Three different construction sequences- i.e. three shores method, one shore plus two reshores method and Cardington building construction approach (see Fig. 7.22)- were considered in the current analysis to determine the effect of different construction methods on deflections. Grundy & Kabaila (1963) developed a simplified method of analysis which was used to calculate the construction load of a multi-floor building using three levels of shores for a 7-day casting cycle with stripping after 5 days. The assumption of the analysis is that the shores are rigid and tightly fixed under the slabs and all the slabs deflects identically. Using the same simplifying method, Agarwal & Gardner (1974) and Marosszeky (1972) analysed the construction loads for shore and reshore method. The reshore technique involves using typically only one level of shore and several levels of reshores. Basically, the shores are removed from beneath a slab, allowing it to deflect and carry its own weight; reshores are then installed, allowing the load during concrete placement to be shared among the various slabs in the system. The slab loads imposed using one shore and two reshores method are much less than using three shores method. The construction load was measured from the prop force for the Cardington method where also a shore and reshore method was employed.

A 250 mm slab was considered in the analysis with three levels of tensile strength (i.e. 1.97, 2.90 and 3.83 MPa). Also, two values (i.e. 0.5 and 1.0) of creep recovery factor, R (see section 6.5.2) are used.

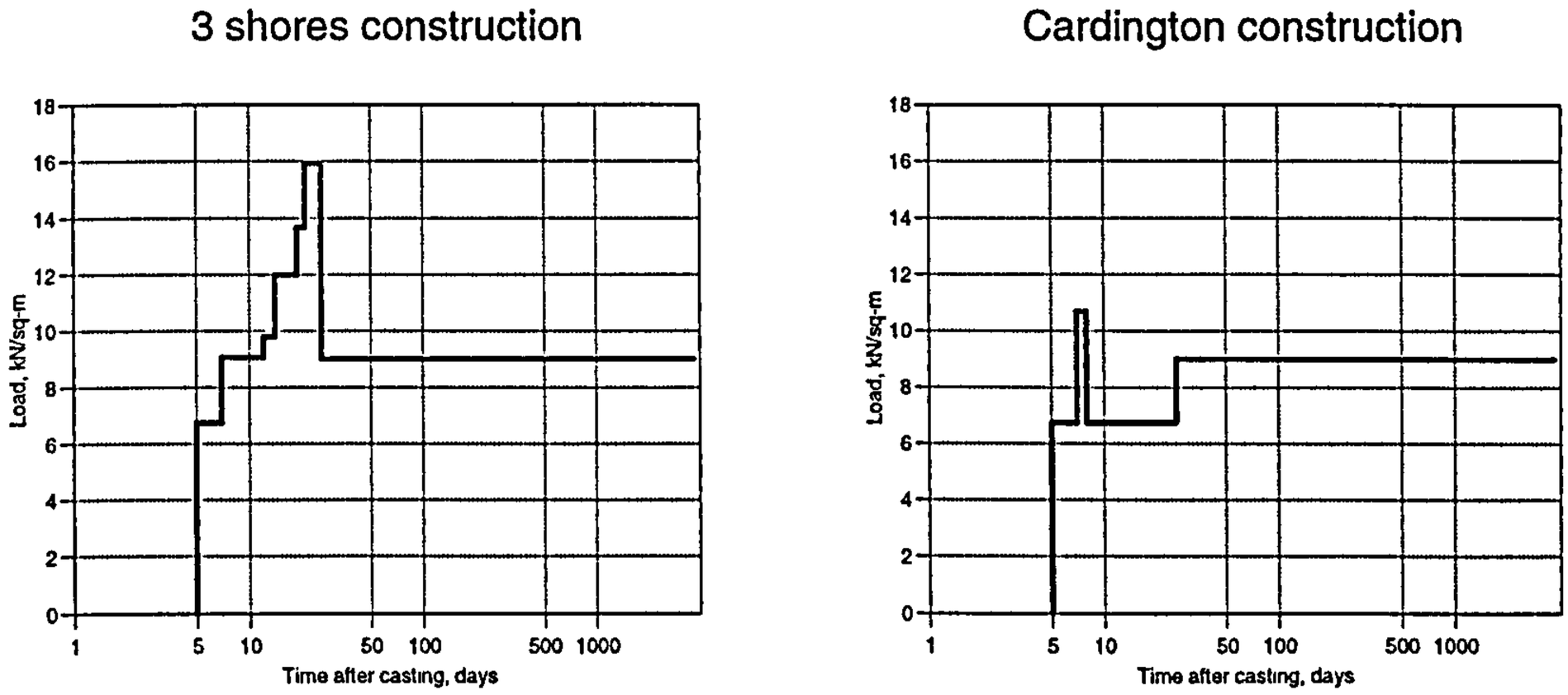


Figure 7.22 Different construction sequences

Result

The effect of different construction sequences on deflections are shown in Figs 7.23 to 7.28. Table 7.12 compares the final deflection obtained using different construction sequences and those found without any construction load. The three shore method gives significantly higher deflection than the other two methods. The one shore plus two reshores method has the smallest effect on final deflection and using a value of R=1.0 appears to be unrealistic for this method as it results in slightly smaller deflections than obtained without construction load. Increase in deflection due to Cardington construction sequence is also reasonably small.

Analysis	Slab thickness	Deflection, % for tensile strengths		
		Low	Mean	High
Long-term R=0.5	No constr. load	100.0	100.0	100.0
	3 shores	144.3	155.6	163.1
	1 shore + 2 reshores	109.8	111.6	112.3
	Cardington	114.9	117.4	116.7
Long-term R=1.0	No constr. load	100.0	100.0	100.0
	3 shores	132.8	138.5	142.1
	1 shore + 2 reshores	100.1	99.5	98.9
	Cardington	105.5	106.0	102.9

Table 7.12 Effect of construction sequences

Conclusion

The influence of construction sequence on long-term deflection can be very significant and is often overlooked in the design. Coordination between designer and contractor to adopt a suitable construction method to ensure the safety of the designed slab is extremely important as pointed out by Stivaros & Halvorsen (1992).

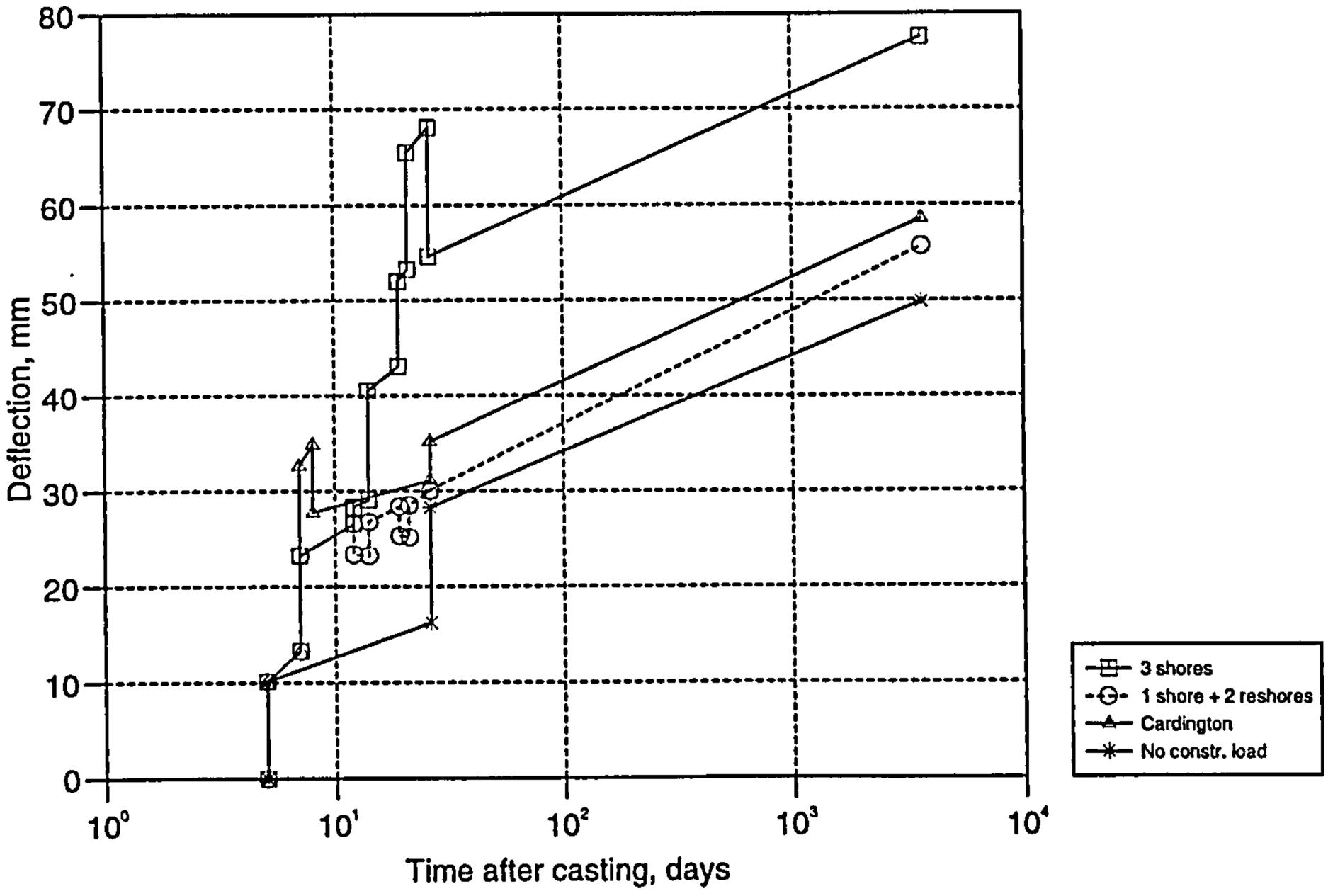


Figure 7.23 Effect of different construction sequences: mean f_{ct}, R =0.5

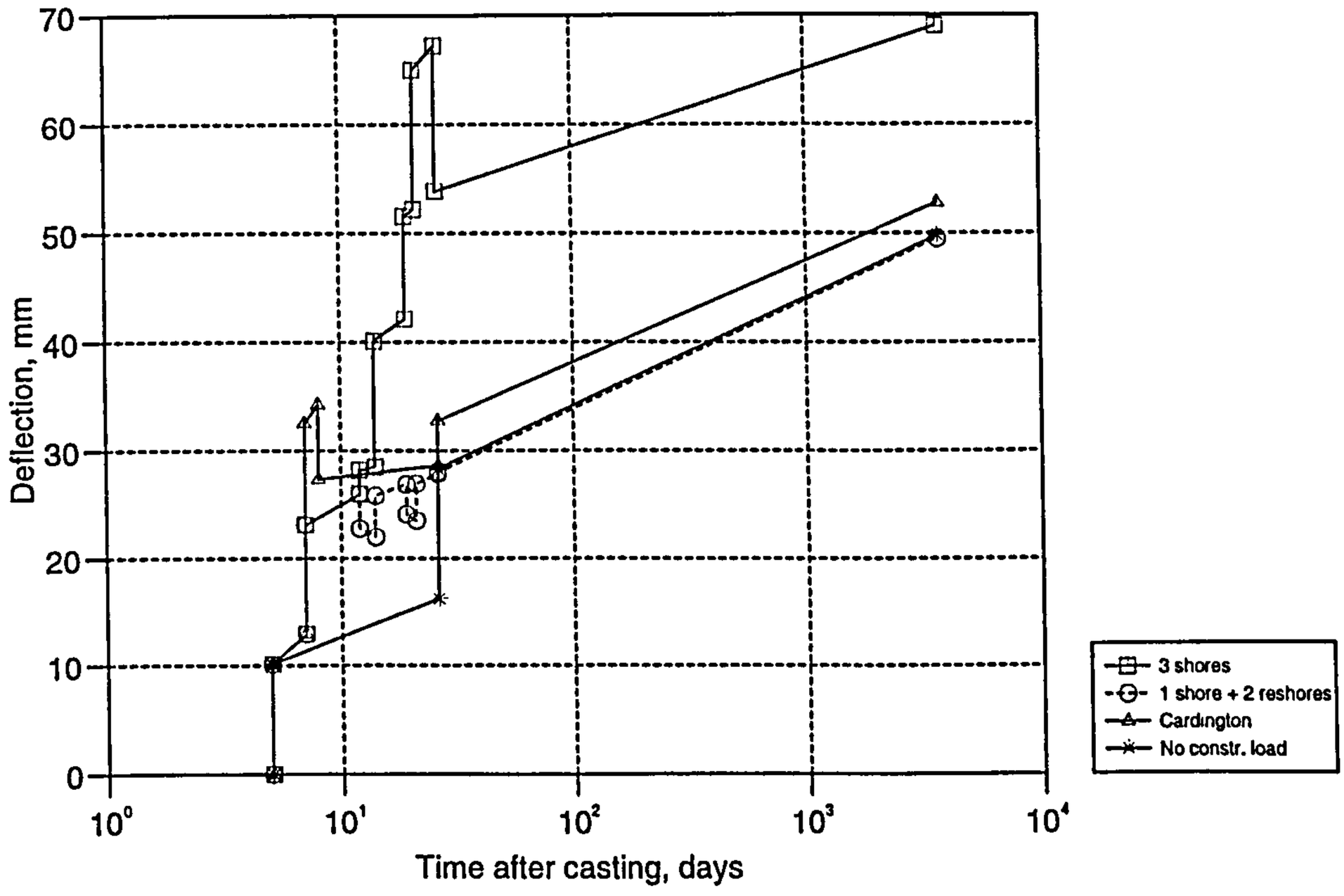


Figure 7.24 Effect of different construction sequences: mean f_{ct}, R =1.0

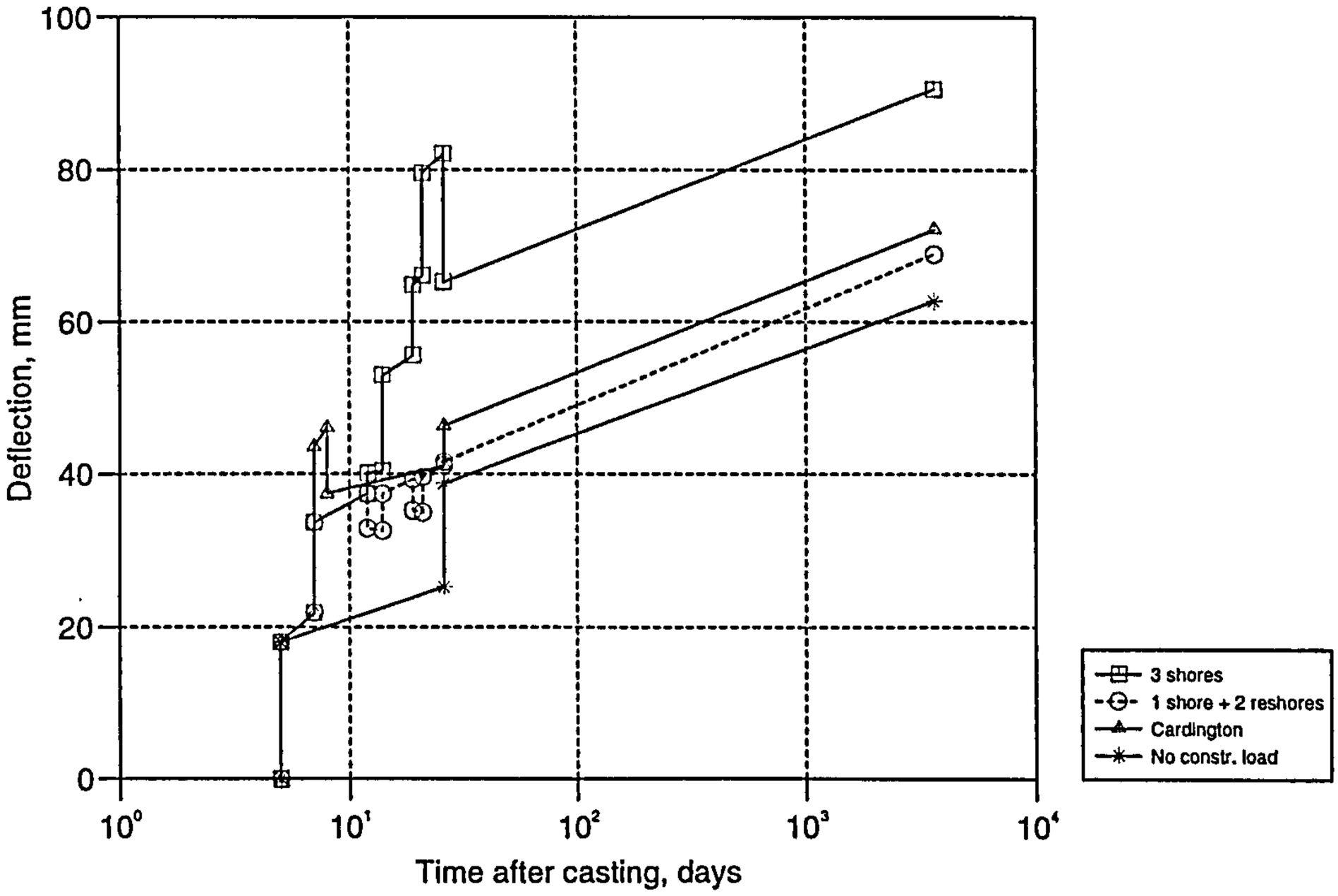


Figure 7.25 Effect of different construction sequences: low f_{ct}, R =0.5

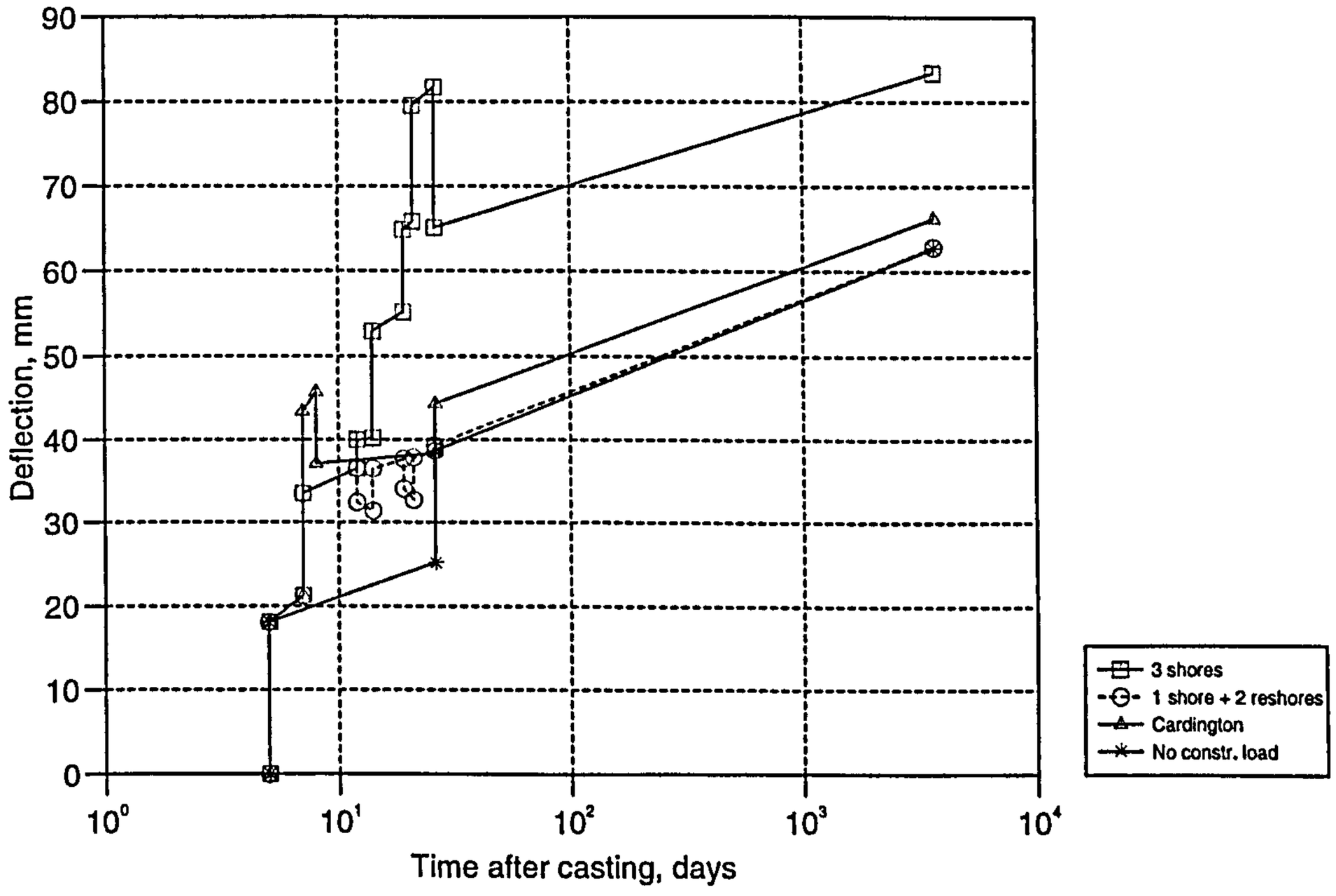


Figure 7.26 Effect of different construction sequences: low f_{ct}, R =1.0

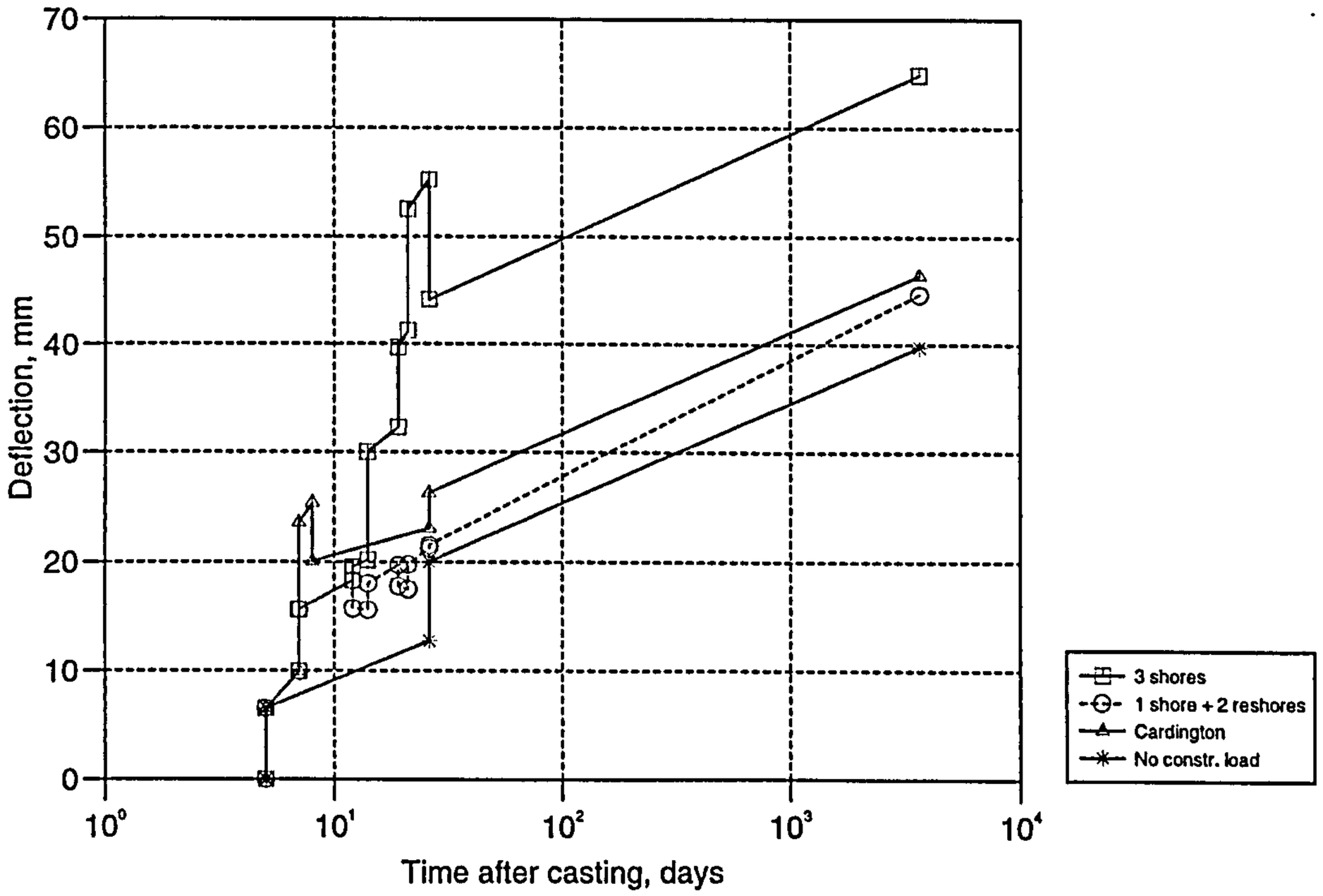


Figure 7.27 Effect of different construction sequences: high f_{ct}, R =0.5

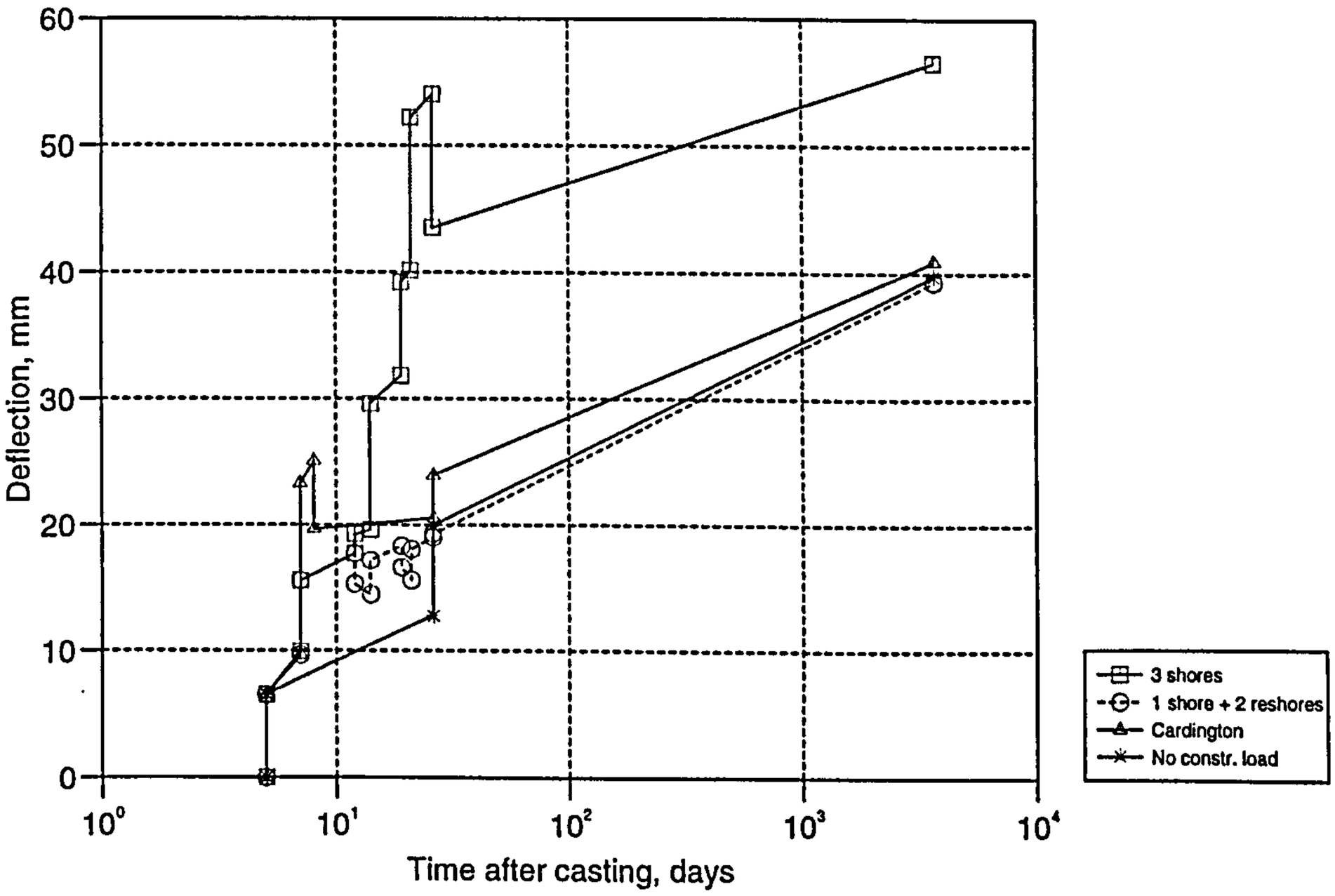


Figure 7.28 Effect of different construction sequences: high f_{ct}, R =1.0

7.5.2 Early creep and recovery

Objective

Gardner & Fu (1987) pointed out that early creep due to construction load on relatively young slabs may lead to high long-term deflections. To identify the amount of creep due to construction load and to study the effect of partial creep recovery with time, all three construction sequences were analysed (for the 250 mm slab) with recovery factors R (see section 6.5.2) equal to 0, 0.5 and 1.0. A recovery factor of R =0 means construction loads continue to induce creep after they are removed (see Fig. 7.29). A value of R =1 means that the creep induced by a negative increment of load is equal to that induced by a positive load. In this case, the recovery is less than 100% since the negative load increment is applied later than the positive load. Also a value of R =0.5 is used in the analysis.

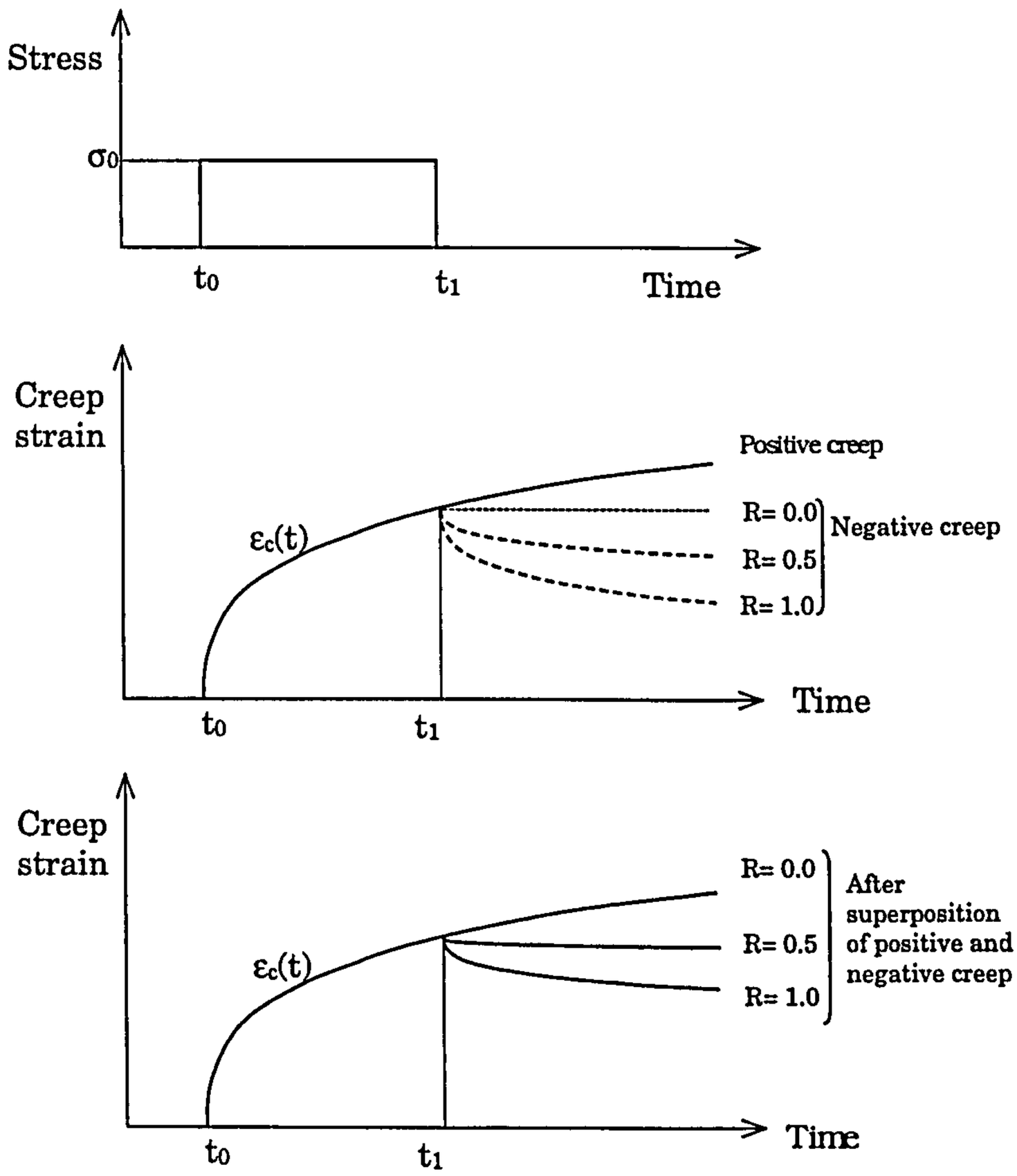


Figure 7.29 Creep recovery: superposition with different R factors

Result

The influences of the recovery factor are shown in Figs 7.30 to 7.32 for the three construction sequences. Comparisons of 10-year deflection calculated using three recovery factors are presented in Table 7.13 for three shores, one shore-two reshores and Cardington construction methods.

Analysis	Recovery factor	Deflection, % for different construction methods		
		3 shores	1 shore + 2 reshores	Cardington
Long-term	R =0	125.6	123.6	121.8
	R =0.5	112.3	112.2	110.8
	R =1.0	100.0	100.0	100.0

Table 7.13 Effect of recovery factor

The results show that there are significant differences between calculations with different R values. Figures 7.30 and 7.32 also show that for all the construction methods, creep deflections due to construction loads are small. For the three shores method, creep deflection due to construction load and self-weight during the construction period is 8.2 mm which is 12.1% of the 26-days deflection. For the Cardington method, the same contribution is only 5.1%.

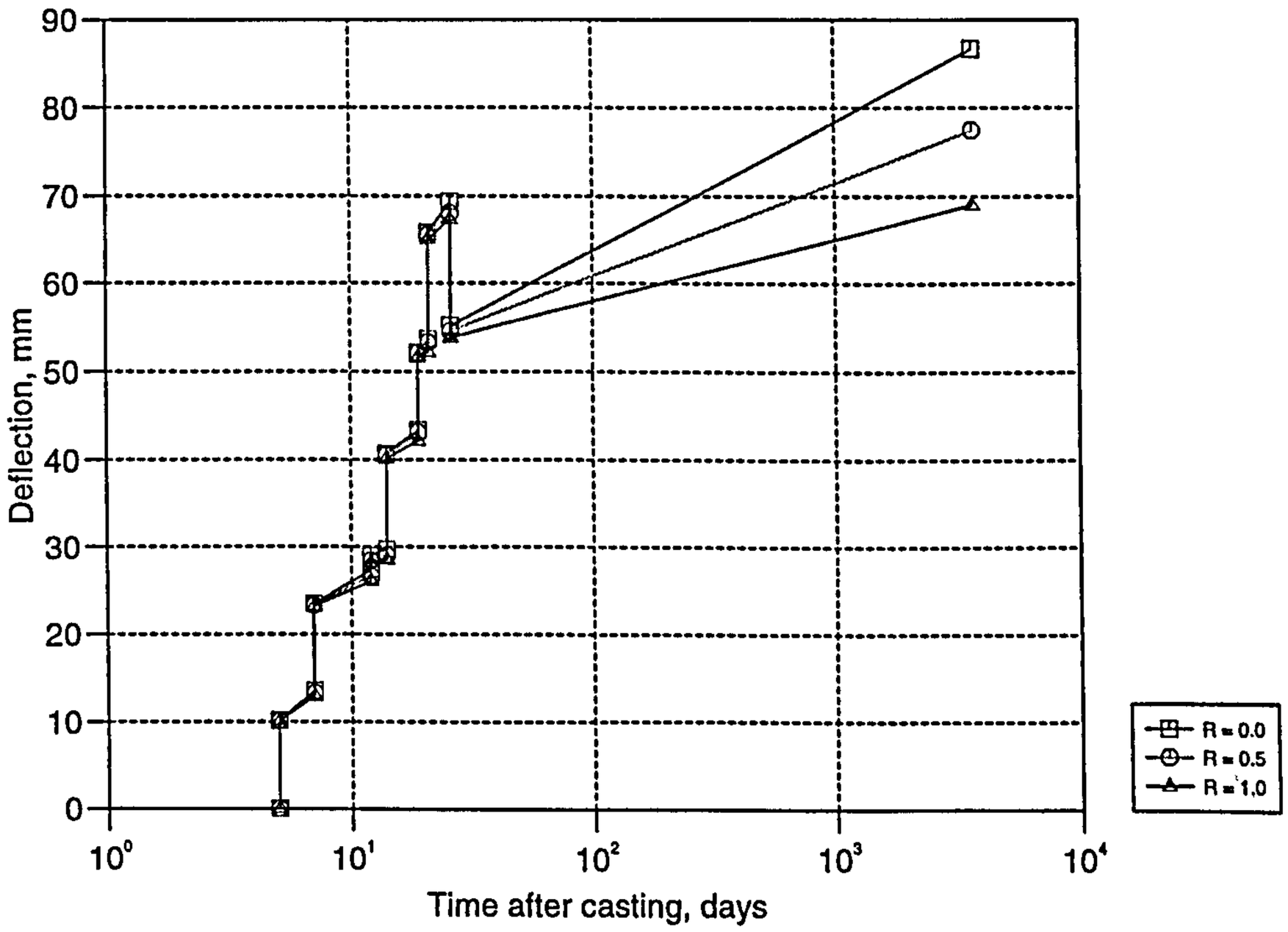


Figure 7.30 Effect of recovery factor, R: 3 shores method

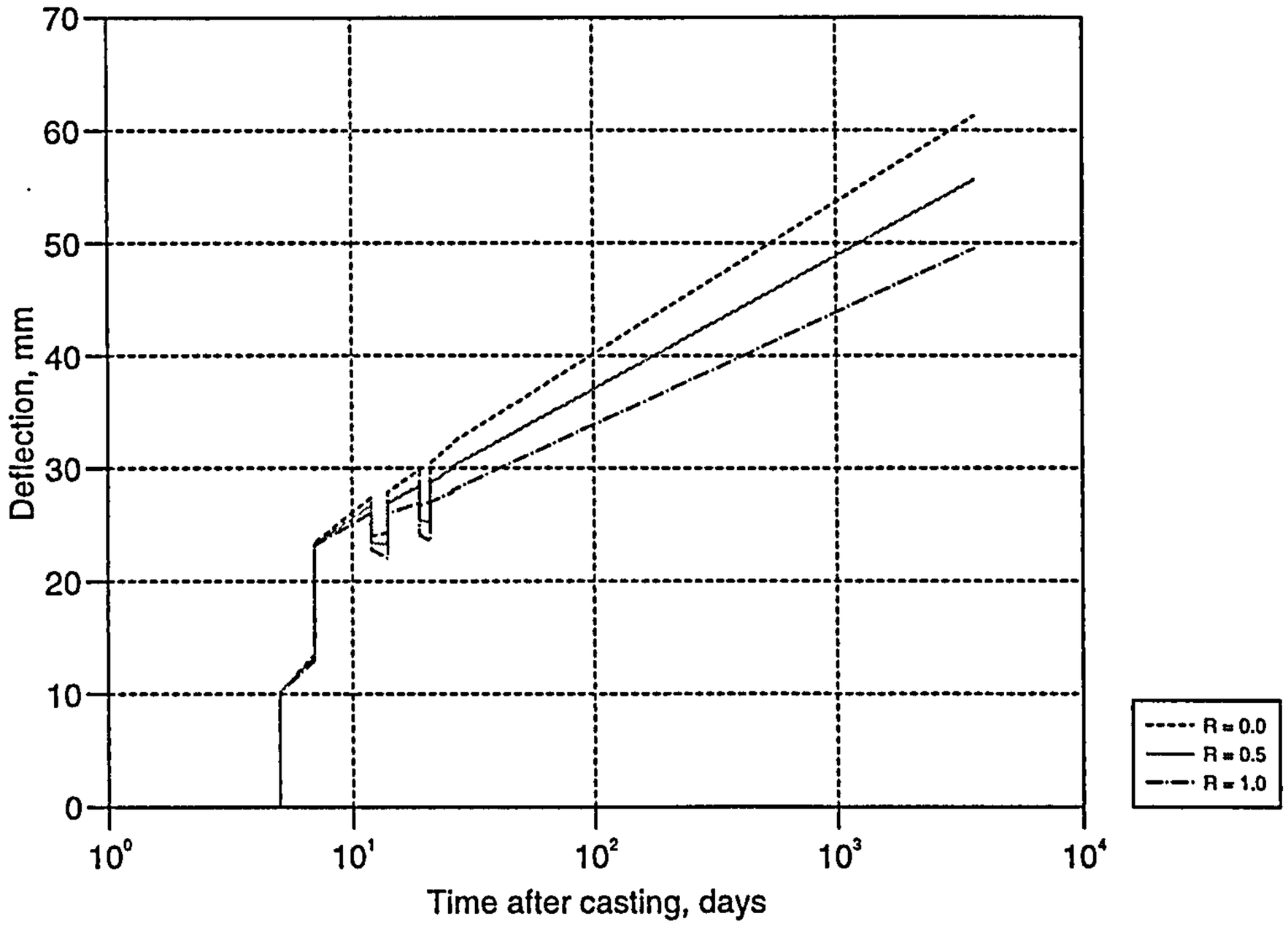


Figure 7.31 Effect of recovery factor, R: 1 shore-2 reshores method

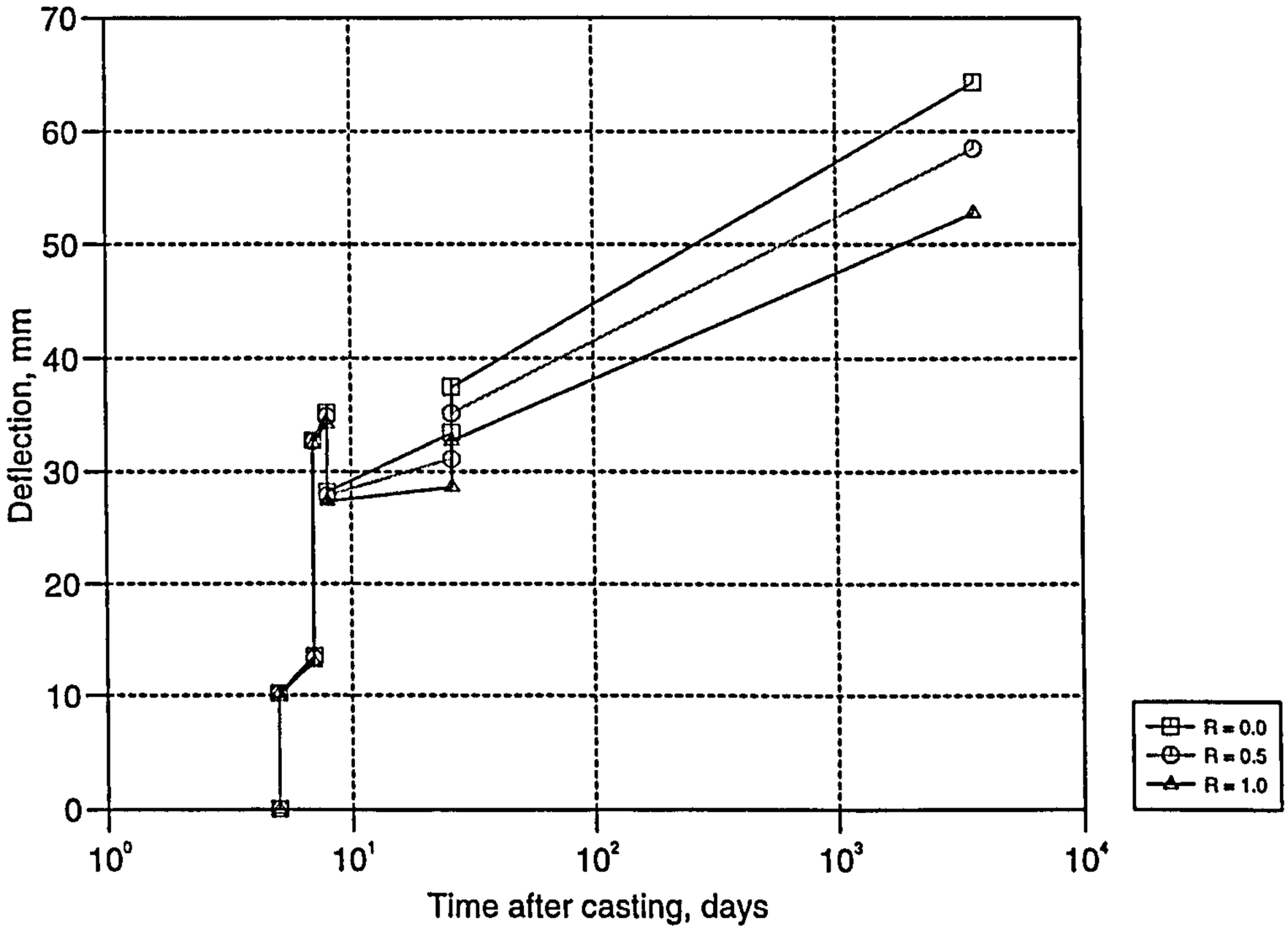


Figure 7.32 Effect of recovery factor, R: Cardington loading

Another study was carried out to determine the amount of creep due to construction load and to select the most realistic R value to model creep recovery due to unloading. The 250 mm slab was analysed with the simplified load history shown in Fig. 7.33. Here 6.9 kN/m^2, which corresponds to peak construction load (three shores method), was applied to the structure at 12 days and sustained up to 26 days. Then it is unloaded to a very low value (0.05 kN/m^2) which is sustained until 10 years. The whole analysis was done on the uncracked section without any shrinkage to identify the effect of creep only. A constant value of E was assumed throughout the analysis.

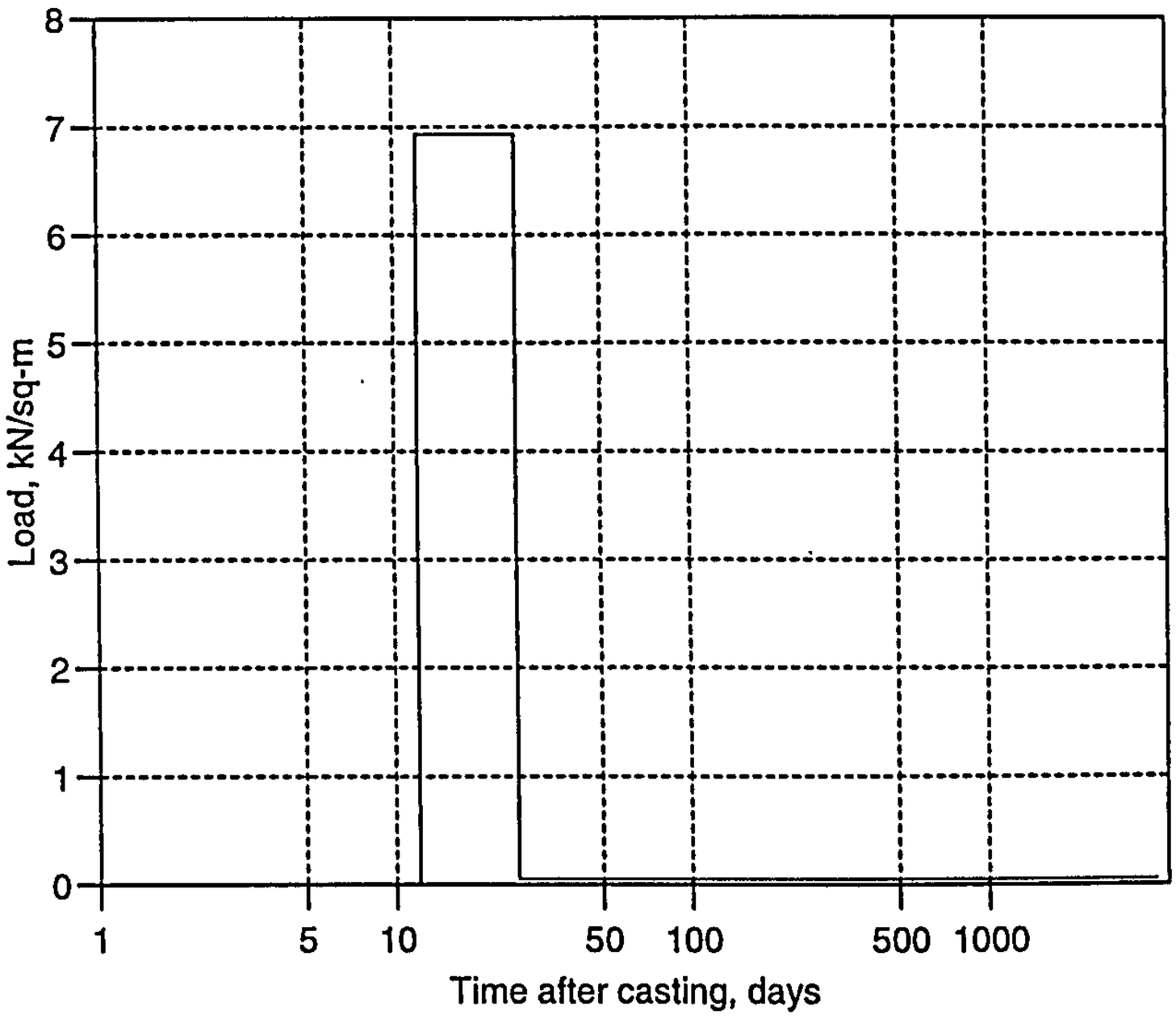


Figure 7.33 Creep recovery: simplified load history

Instant deflection at 12 days was 5.19 mm and at 26 days it was 9.89 mm which indicates a small creep of 4.7 mm. The deflection immediately after unloading at 26 days is 4.7 mm which is essentially the deflection due to creep and a negligible amount due to the 0.05 kN/m^2 load. Deflections and recovery percentages at 10-years and 71 days found for recovery factors ranging for 0 to 1 are presented in Table 7.14. For 10-years, a value of R =0.5 does not lead to any recovery at all, rather some extra creep is added which indicate that the positive creep components are governing. A value of R =1.0 resulted in 75.1% recovery which is high. According

Recovery factor	10 years		71 days	
	Deflection	% recovered	Deflection	% recovered
1	1.17	75.1	1.11	77.4
0.9	2.37	49.6	1.65	65.4
0.75	4.16	11.5	2.52	46.4
0.5	7.15	-52.2	3.98	15.4
0.0	13.13	-179.4	6.89	-46.5

Table 7.14 Amount of creep recovery

to Gilbert (1988), if a concrete specimen is unloaded after a long period under load, the magnitude of the recoverable creep is of the order of 10 to 30 percent of the total creep strain. If the load is sustained for a short period the recoverable part is higher. It has been found that as the creep curves are not parallel to each other, using superposition for unloading leads to unrealistic results. Figure 7.34 shows the unloading branches using different R values, in all cases deflections are higher at 10-years than 71-days which is not acceptable. However, R=0.9 leads to 10-years deflection to be 1.17 mm which means a 49.5% recovery of 4.7 mm creep deflection which is reasonable for a load of short duration. Thus, a value close to 1.0 would be a good choice for a 10-year period. For 71 days, a value of 0.5 is a good selection as the amount of creep recovery is less. In any case, however, the amount of creep due construction load and its recovery are relatively insignificant. Creep recovery is likely to be underestimated if R is taken as less than 0.5.

Conclusion

Construction loading only increase deflections significantly when it leads to cracking and governs the long-term cracking level. It is very important for the designer to either specify or take account of the construction method adopted by the contractor in the field. Certain construction methods can lead to very high long-term deflections which should be allowed for. However, the effect of creep due to construction loads is relatively unimportant and can be ignored in the calculations. A value close to 1 for R may be used in the analysis for long-term deflection calculations if creep due to construction load is considered.

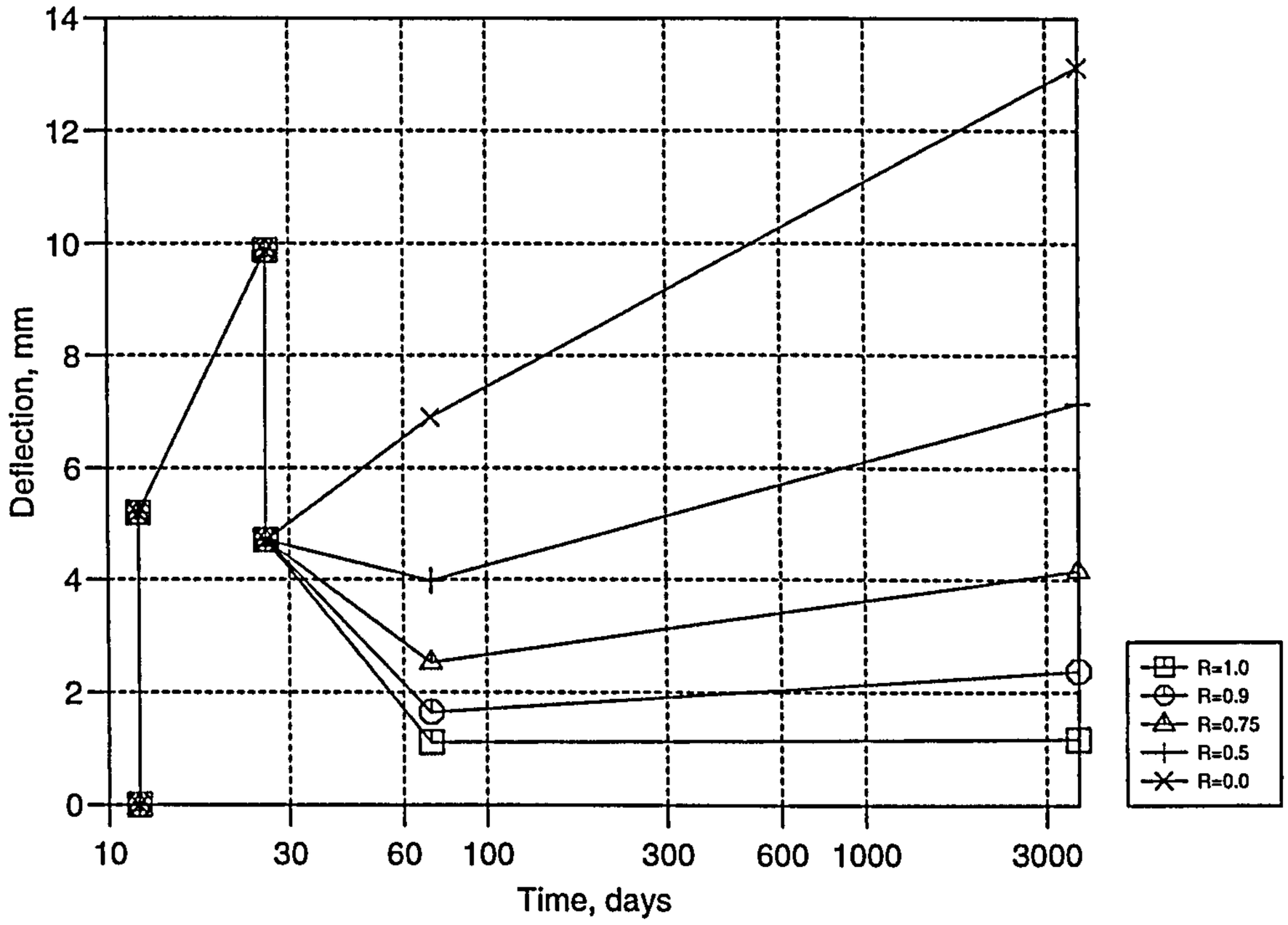
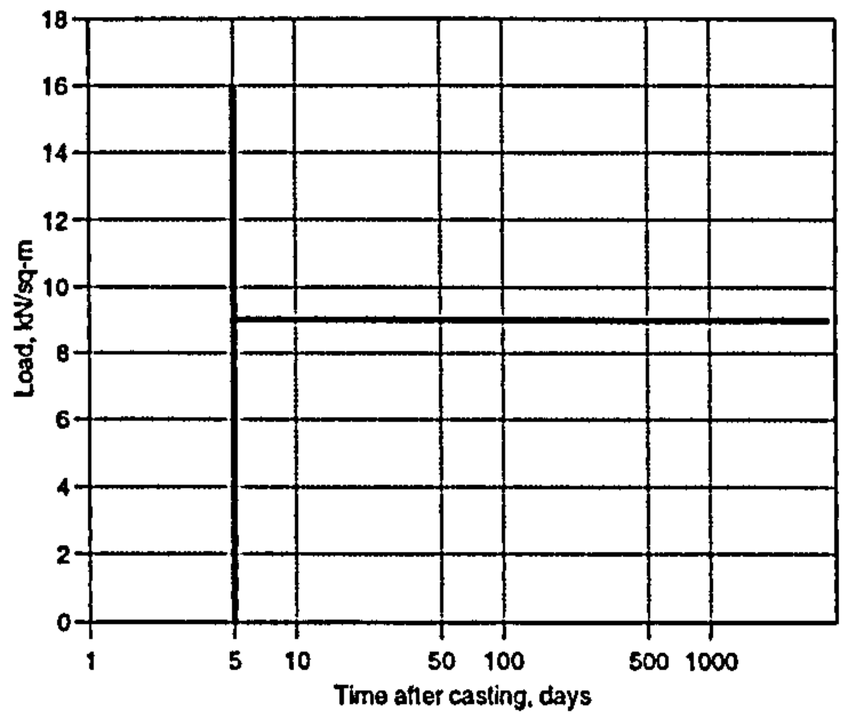


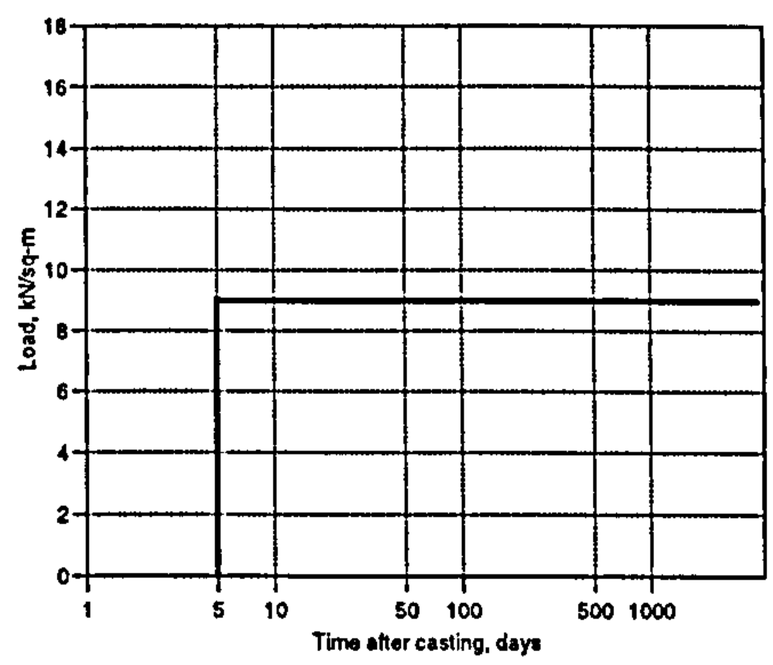
Figure 7.34 Creep recovery: different R factors

7.5.3 A simplified method to model construction loading

The method of modelling construction load described in section 7.5.1 is quite time-consuming. A simplified method to model construction load is proposed here. Construction load affects long-term deflection in two ways. First, it leads to some early creep, part of which is recovered on unloading. It has been shown in section 7.5.2 that the contribution of creep from construction load is not significant. Secondly, construction loading can lead to early cracking. Cracking due to construction load increases deflection by: 1) reducing the stiffness of the structure and 2) residual deflections remain after unloading.

To determine the relative contributions of items 1 and 2 to deflection, the simplified load history shown in Fig. 7.35 is adopted. The peak construction load is applied as a spike at striking. The construction load is then reduced to the level of the imposed load which is sustained for 10-years. f_{ct} is taken as that at peak loading for the spike and then values at the time of sustained load application were assumed. E values corresponding to striking time were assumed throughout. This simplified load considers the effect of cracking due to peak construction load (item 1 and 2 as above), but it neglects the creep due to construction load; however, the imposed load is applied at striking which overestimates the creep due to imposed load.





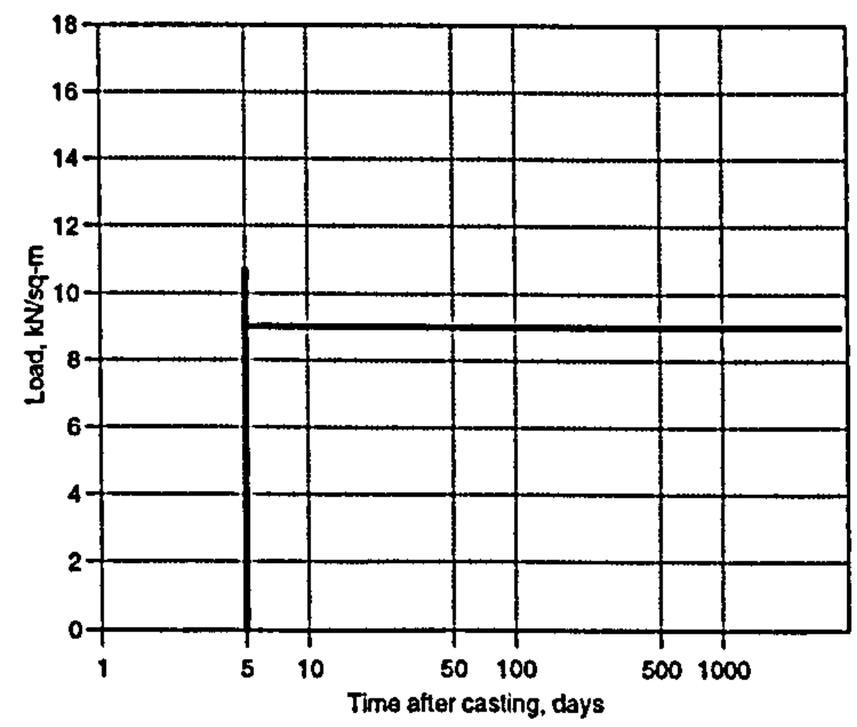


Figure 7.35 Simplified load history: different construction sequences

Example

Three simplified load histories corresponding to three shores, one shore-two reshores and Cardington loading method were considered with mean, low and high f_{ct}. Also, the analysis was performed with and without the Rotilio loading unloading curve (see section 6.5.1) to isolate the residual deflection from unloading. The results are shown in Table 7.15. The results with loading-unloading curve agree very well with those obtained by the more rigorous step analysis (shown in brackets for R=1.0 and 0.5), particularly with the recovery factor 1, as shown in Figs 7.23 to 7.25. A recovery factor 0.5, in fact, overestimates the long-term curvature as shown in section 7.5.2.

Therefore, this simplified approach is justifiable since it gives a good estimate of long-term deflection much quicker than the more rigorous step analysis. It should also be noted here that effect of residual deflection is more significant for the three shores method than the other two methods since much more cracking is induced by the three shores construction load.

f_{ct}: step analysis	Time	Deflections, mm: Rotilio on			Deflections, mm: Rotilio off		
		3 shores	1 shore-2 reshores	Card.	3 shores	1 shore-2 reshores	Card.
Mean: simplified	5 day	54.6	20.2	28.9	54.6	20.2	28.9
	5+ day	38.9	19.7	24.9	29.9	19.4	23.3
	10 yrs	70.4	52.4	55.0	60.4	51.6	53.2
Mean: rigorous	10 yrs, R=1	(69.0)	(49.5)	(52.8)			
	10 yrs, R=0.5	(77.5)	(55.6)	(58.5)			
Low: simplified	5 day	68.7	30.1	40.3	68.7	30.1	40.2
	5+ day	50.4	29.5	35.5	37.8	29.3	32.8
	10 yrs	83.6	64.7	68.5	71.1	64.6	65.8
Low: rigorous	10 yrs, R=1	(83.4)	(62.9)	(66.2)			
	10 yrs, R=0.5	(90.6)	(68.9)	(72.2)			
High: simplified	5 day	42.1	12.3	20.5	42.1	12.3	20.5
	5+ day	28.6	10.9	16.9	22.5	10.8	15.8
	10 yrs	57.5	41.6	43.8	50.3	41.4	42.6
High: rigorous	10 yrs, R=1	(56.5)	(39.3)	(40.9)			
	10 yrs, R=0.5	(64.9)	(44.7)	(46.4)			

Table 7.15 Comparison between results from simplified load history and rigorous step analyses

7.5.4 A single-step method to calculate long-term deflection

It has been shown that creep due to construction loads has little significance for long-term slab deflections. A reasonable approximation is to assume that the imposed load is sustained from first striking. A simplified single-step approach is proposed here which uses the critical cracking level to interpolate between states 1 and 2.

The simplified method is based on a modified tensile strength f_{ct-mod} that takes into account the effect of cracking due to peak load. The modified f_{ct-mod} should be the smallest of following three expressions:

$$f_{ct-mod} = f_{ct-str} * \frac{w_{imp}}{w_{str}} * \sqrt{\beta_{str}} \quad (7.6)$$

$$f_{ct-mod} = f_{ct-con} * \frac{w_{imp}}{w_{cons}} * \sqrt{\beta_{cons}} \quad (7.7)$$

$$f_{ct-mod} = f_{ct-imp} * \sqrt{\beta_{imp}} \quad (7.8)$$

where w_{str}, w_{cons} and w_{imp} are uniformly distributed striking, construction and imposed load respectively. The value of β_{str} (at striking) and β_{cons} (corresponds to peak construction load) are 1.0 unless the load is applied in a repeated number of cycles. β_{imp} is equal to 0.5 when the imposed load is sustained for a long period of time.

Example

All the three construction sequences considered earlier were analysed with the single-step approach. The modified tensile strengths are shown in Table 7.16. For the three shores method, cracking due to construction peak load was critical. For one shore-two reshores method and Cardington loading, cracking corresponding to imposed load was critical.

Table 7.17 compares the deflections obtained by the single-step method with other methods. For one shore-two reshores and Cardington construction methods, the effect of cracking due to construction loading is less significant, analysis with and without Rotilio unloading curve giving similar deflections and these compare well with the more rigorous step analysis with R=1. The single-step method also gives good agreement with these results. However, the agreement is not very good

f_{ct}	eq. used	Modified f_{ct-mod}, MPa		
		3 shores	1 shore-2 reshores	Card.
Mean	7.6	3.09	3.09	3.09
	7.7	1.60(Critical)	2.45	2.07
	7.8	2.04	2.04(Critical)	2.04(Critical)
Low	7.6	2.10	2.10	2.10
	7.7	1.09(Critical)	1.66	1.41
	7.8	1.39	1.39(Critical)	1.39(Critical)
High	7.6	4.09	4.09	4.09
	7.7	2.12(Critical)	3.24	2.74
	7.8	2.70	2.70(Critical)	2.70(Critical)

Table 7.16 Single-step load: selecting f_{ct-mod}

for the three shores method since the effect of residual deflection on unloading is greater. The deflection calculated for the three shores method by the single-step method agrees well with that obtained by the simplified method without the Rotilio unloading curve. This is due to the fact that residual deflections from unloading are neglected in both cases.

f_{ct}	Method used	Deflection after 10 yrs, mm		
		3 shores	1 shore-2 reshores	Card.
Mean	single-step	60.2	51.8	51.8
	simplified without Rotilio	60.4	51.6	53.2
	simplified with Rotilio	70.4	52.4	55.0
	rigorous step with R =1	(69.0)	(49.6)	(52.8)
	rigorous step with R =0.5	(77.5)	(55.6)	(58.5)
Low	single-step	71.8	64.5	64.5
	simplified without Rotilio	71.1	64.6	65.8
	simplified with Rotilio	83.6	64.7	68.5
	rigorous step with R =1	(83.4)	(62.9)	(66.2)
	rigorous step with R =0.5	(90.6)	(68.9)	(72.2)
High	single-step	50.5	41.3	41.3
	simplified without Rotilio	50.3	41.4	42.6
	simplified with Rotilio	57.5	41.6	43.8
	rigorous step with R =1	(56.5)	(39.3)	(40.9)
	rigorous step with R =0.5	(64.9)	(44.7)	(46.4)

Table 7.17 Single-step load: comparison with the results of simplified and rigorous step analyses

7.5.5 Effect of age at striking

Objective

Early striking creates more cracking and creep. To find the effect of age at striking, the following two cases were considered: 1) the effect of varying the striking time with no superimposed construction loading, 2) the effect of varying the striking time with superimposed construction loading.

Different striking time without any construction load

To identify the effect of early striking, the slab was struck at 1, 3, 7 and 14 days and allowed to take only self-weight until 90 days when a load of 3 kN/m^2 was applied and sustained for 10 years. Rigorous step analyses were carried out with the following parameters : 1) $\beta_2 = 1$ for instant application of load and 0.5 for 90 days and 10 years. 2) $\beta_2 = 0.5$ throughout the analysis. The results of the first and second cases are shown in Figs 7.36 and 7.37 respectively. The value of 0.5 for β_2 changes instant deflections significantly, but their contribution to the long-term deflection (which is calculated with 0.5 in both cases) is very small, since cracking under long-term loading is critical. All the deflections reduce significantly when the striking time is increased from 1 day to 7 days. Thereafter, the rate of reduction in deflection is smaller since the rate of increase in strength becomes slower. Also, the influence of increasing striking time is less on the 10-year deflection since the cracking under 10-year loading appears to be critical for the striking times at and after 3 days.

Different striking time with construction load

As shown in the previous section, early striking increases long-term deflection, the effect is more pronounced if the construction load produces further cracking. To show this, the Cardington type loading was applied with three different striking times, i.e. 1, 5 and 28 days. A load (self-weight plus construction) of 10.7 kN/m^2 was applied 2 days after striking. The slab was analysed with 1) cracking and 2) assuming no cracking to isolate the contributions of cracking and creep to long-term

deflections. The results of the first and second cases are shown in Figs 7.38 and 7.39 respectively. The reduction in deflection due to striking later is most significant for very early striking times (i.e. less than 3 days). The benefit of striking later decreases rapidly once the the slab gains significant strength. The influence of cracking due to early age loading is more significant than that of creep.

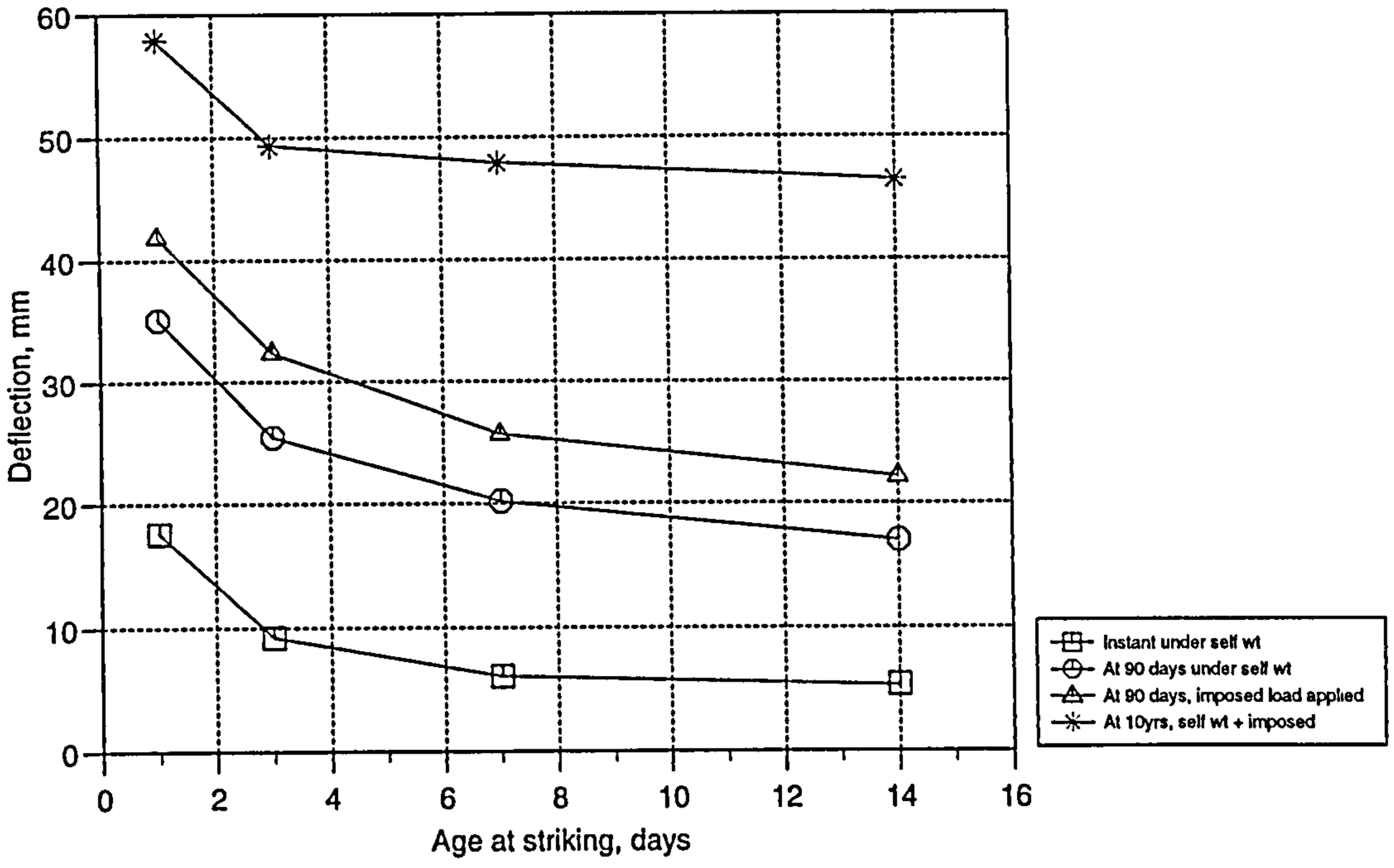


Figure 7.36 Effect of age at striking: β_2=1 and 0.5 for instant and long-term respectively (with no construction load)

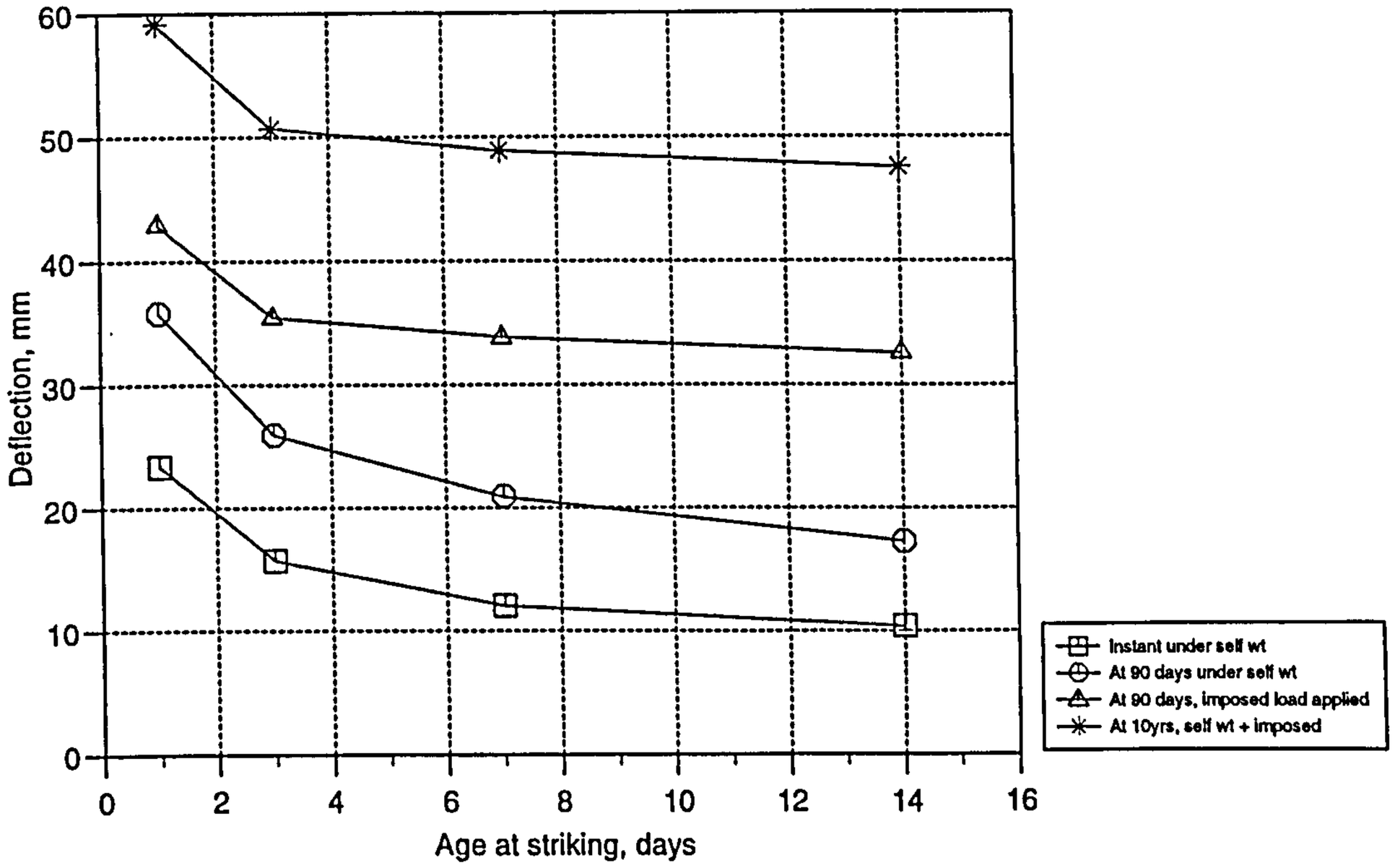


Figure 7.37 Effect of age at striking: β_2=0.5 for both instant and long-term (with no construction load)

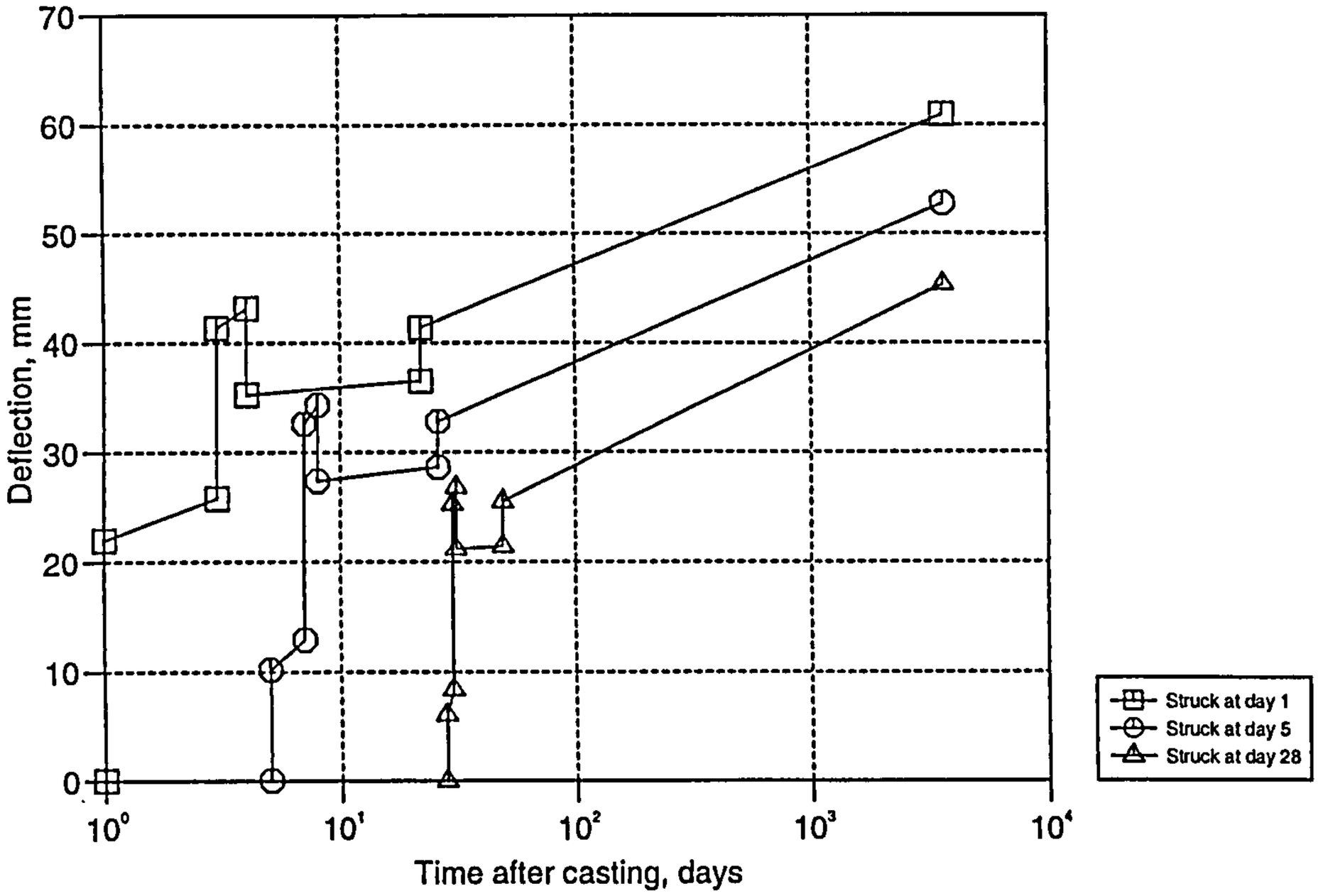


Figure 7.38 Influence of striking time: Cardington loading

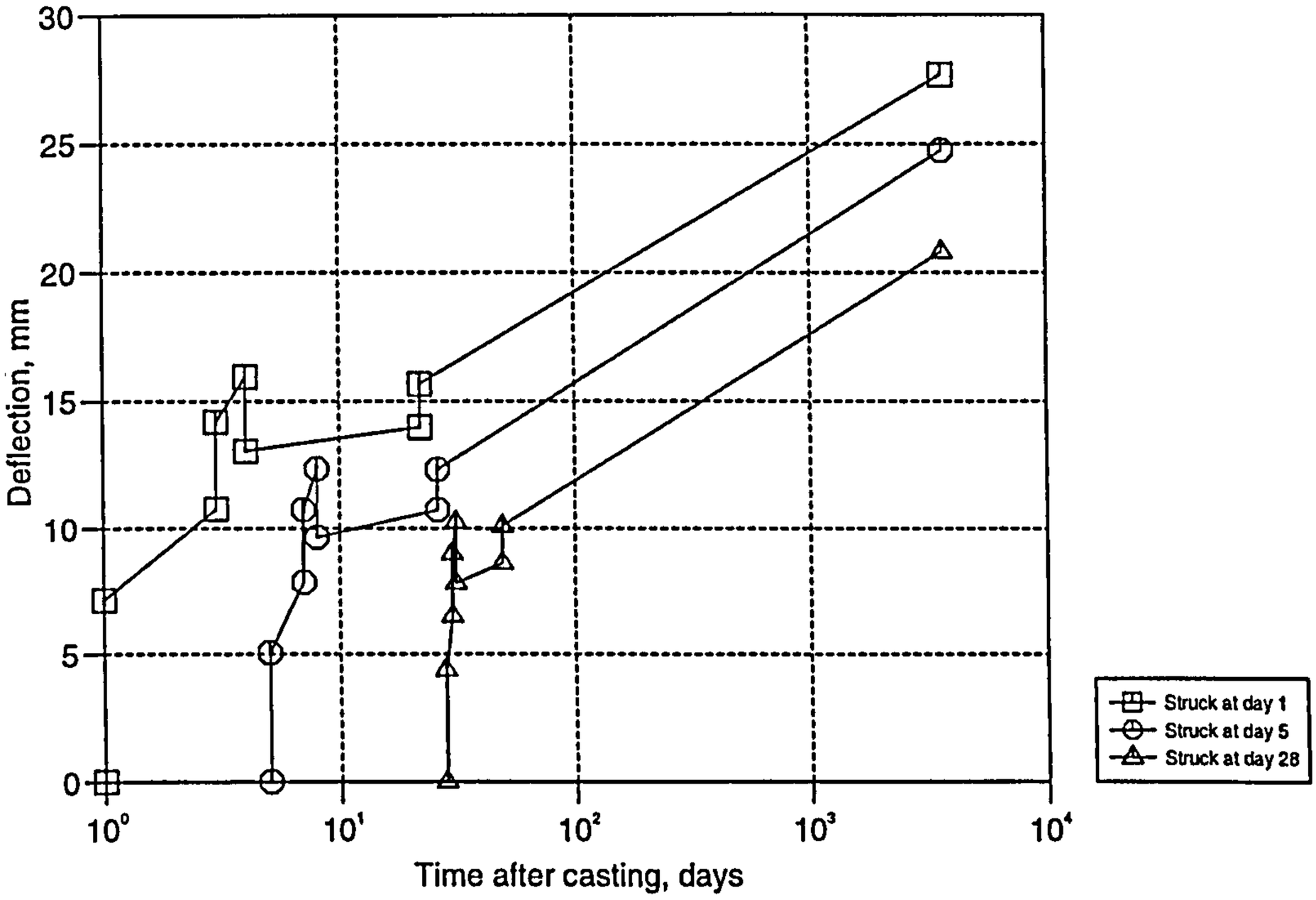


Figure 7.39 Influence of striking time: Cardington loading, uncracked slab

7.6 Effect of service-life factors

7.6.1 Effect of magnitude of imposed load and application time

Objective

To determine the effect of the magnitude and time of application of imposed load on long-term deflections, a study was carried out with the Cardington type construction load. Up to 8 days (when construction load is removed), the load history remains the same as Fig. 7.22 and three levels of imposed load (i.e. 8, 9 and 10 kN/m^2) were applied at either 26 days or 95 days. An analysis was also carried out without any imposed load. Recovery factor R was assumed to be 1.0 in the analyses and β_2=0.5 at 10 years and elsewhere it was assumed 1.0.

Result

Figure 7.40 presents load-deflection curves at the time the imposed load was first applied and after 10 years. Instantaneous load-deflection curves for both 26 and 95 days are perfectly straight since the critical level of cracking at this stage was governed by the level of cracking due to the construction load. It is interesting to note that the reduction in 10-year deflections is marginal when the imposed load is applied at the later date of 95 days. Table 7.18 shows the material properties (calculated using eqs 7.1 to 7.5) used in the analyses, which clearly suggest that the improvements in material properties from 26 to 95 days are small. Creep coefficients ϕ are also multiplied by corresponding load increment (since instant curvature increments can be assumed proportional to the load increments) to show that the difference in amounts of creep for the two loading times is small. 10-years load-deflection curves are not straight as the cracking levels corresponding to 10-years with β_2=0.5 become critical.

Conclusion

The magnitude of imposed load influences the long-term deflection significantly. However, if the cracking levels at the construction load remain critical even at long-term, the effect of imposed load would be linear on deflection. Applying imposed

load at a later date does not appear to provide any substantial benefit.

Property	26 days	95 days
f_{ct}, MPa	2.89	3.14
E_c, GPa	31.8	33.8
ϕ	5 to 3650 days=3.49 26 to 3650 days=3.017	5 to 3650 days=3.49 95 to 3650 days=2.504
ϕ x load (10 kN/m^2)	3.49x6.75+3.017x(10-6.75) =33.36	3.49x6.75+2.504x(10-6.75) =31.69

Table 7.18 Effect of imposed load: comparison of material properties

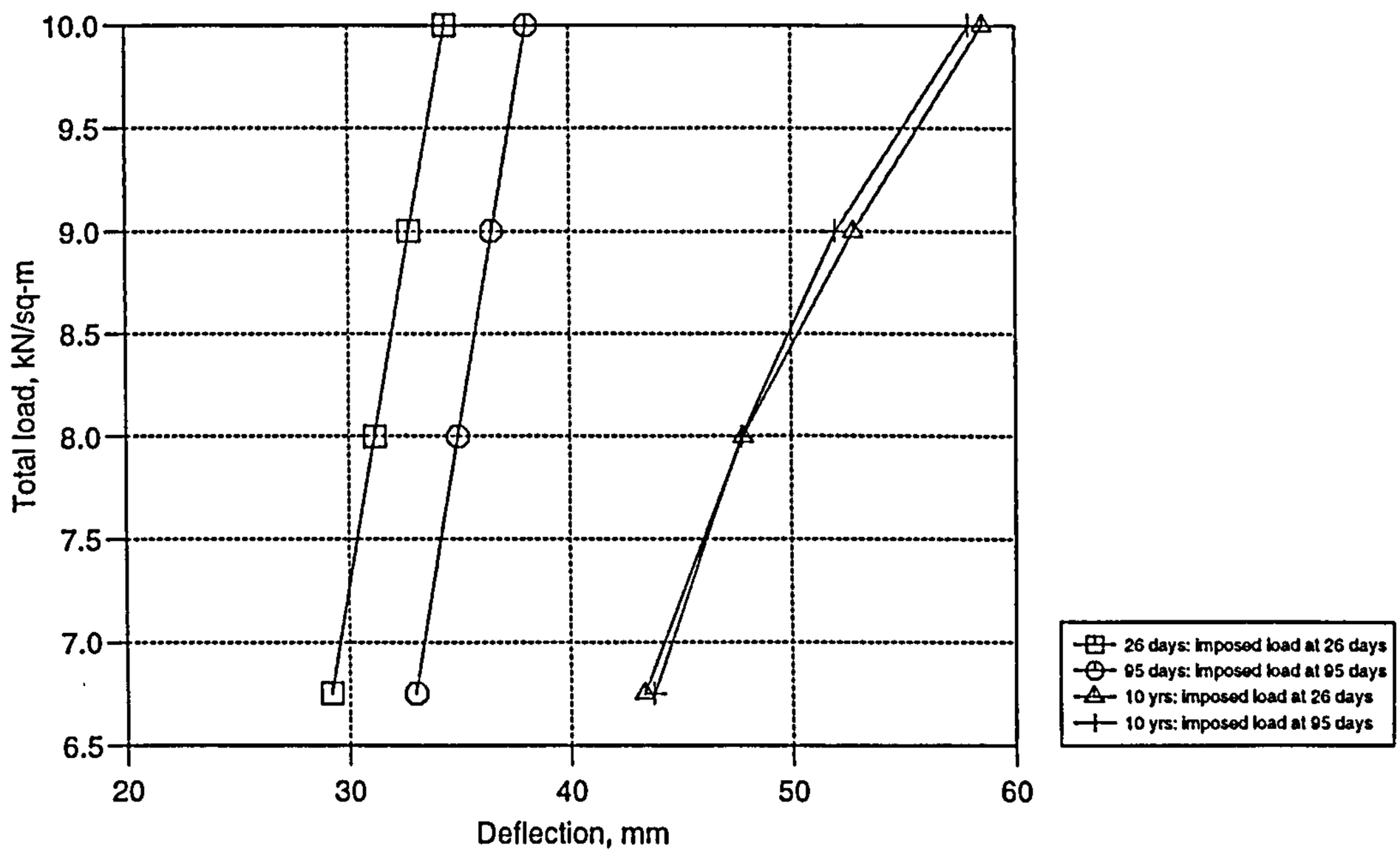


Figure 7.40 Effect of magnitude of imposed load and their application time: Cardington loading

7.6.2 Effect of relative humidity

Objective

Relative humidity is the most important environmental parameter to influence slab deflections since it influences creep and shrinkage of concrete. MC-90 equations for calculating the creep coefficient and the shrinkage strain are presented in sections B.2 and B.3. To study the effect of relative humidity, three levels of humidities (i.e. 50, 70 and 90%) were considered in the analyses with four slab thicknesses.

Results

Deflections after 10-years with different humidities are plotted in Fig. 7.41. Table 7.19 also compares the deflections for different humidities. Relative humidity influences deflections significantly. However, the influence is similar for all the thicknesses.

Analysis	Relative humidity, %	Deflection, % for different thicknesses			
		250 mm	275 mm	300 mm	325 mm
Long-term	50	100.0	100.0	100.0	100.0
	70	90.3	90.9	90.1	91.3
	90	76.5	76.9	75.9	76.5

Table 7.19 Effect of relative humidity

Conclusions

Humidity affects long-term deflections significantly. A good estimation of relative humidity is important in deflection calculations.

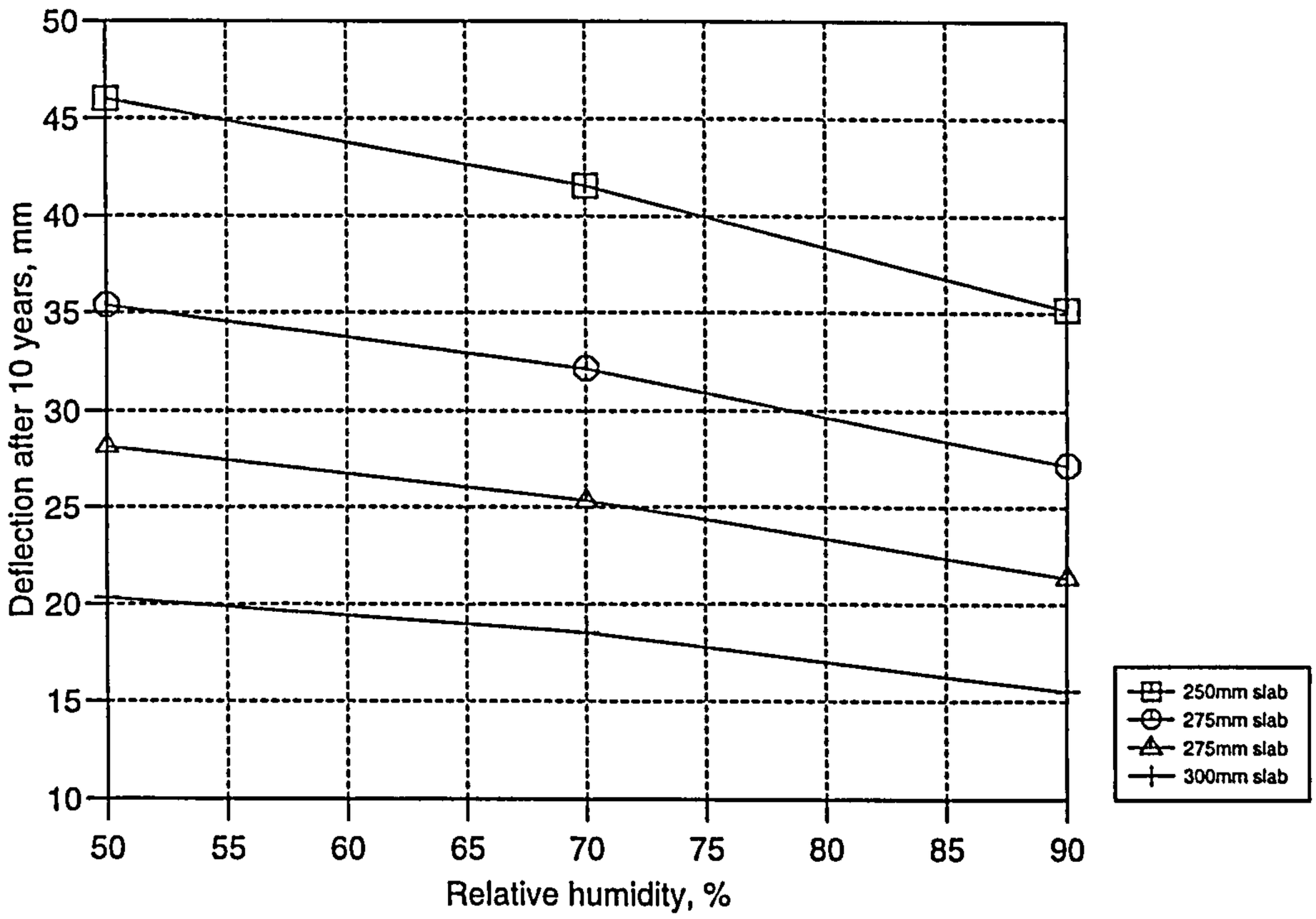


Figure 7.41 Effect of relative humidity on long-term deflection

7.7 Conclusions

7.7.1 Geometric properties

The summary of the parametric study on geometric properties is presented in Table 7.20. The influence of slab thickness is very significant on instant and long-term deflections. The effect is most pronounced when an increase in slab thickness decreases cracking. It is a common practice to provide more bottom steel than that required for strength in order to reduce slab deflections, (e.g. EC2 has provisions for increasing the permissible l/d ratio if the area of bottom steel is increased in the span). However, it was found that providing more bottom steel has a very small effect on deflection and the effect is least for thicker slabs. The distribution of steel does not significantly influence deflection. Modelling the column cross-section is found to be important in predicting deflections accurately. However, it was shown in section 6.9.2 that a more detailed modelling of column with reinforcement, cracking and long-term effects is not particularly important at the serviceability state.

Parameter and section	Description of analyses	Contribution on deflections
Slab thickness section 7.3.1	4 slab thicknesses were analysed with 3 concrete strengths to compare elastic, instant and long-term deflections	Very significant
Bottom reinforcement section 7.3.2	Bottom steel were increased by 20 and 40% for 4 thicknesses with C30 concrete to compare instant and long-term deflections	Not significant
Reinforcement distribution section 7.3.3	5 reinforcement arrangements were considered for 4 thicknesses with C30 concrete to compare instant and long-term deflections	Not significant
Column dimensions section 7.3.4	4 column cross-sections were considered for 4 thicknesses and C30 concrete to compare instant and long-term deflections	Significant

Table 7.20 Summary of parametric study: geometric properties

7.7.2 Material properties

All the concrete properties (i.e. f_{ct}, E, ϕ, ϵ_{cs}) are related to compressive strength. Different levels of concrete strength were used to analyse the same slabs to determine its effect on deflections. The summary of the analysis is presented in Table 7.21.

Parameter and section	Description of analyses	Contribution on deflections
Concrete compressive strength section 7.4.1	3 concrete strengths were considered for 4 slab thicknesses to compare elastic, instant and long-term deflections	Very significant
Tensile strength f_{ct} section 7.4.2	f_{ct} was varied between ±33% of the mean for 4 thicknesses with C30 concrete to compare instant and long-term deflections	Very significant
Creep coefficient, ϕ section 7.4.3	ϕ was varied between ±33% of the mean for 4 thicknesses with C30 concrete to compare long-term deflections	Not very significant
Shrinkage strain, ϵ_{cs} section 7.4.4	ϵ_{cs} was varied between ±42% of the mean for 4 thicknesses with C30 concrete to compare long-term deflections	Not very significant
Modulus of elasticity, E_c section 7.4.5	E_c was varied between -30% to +20% of the mean for 4 thicknesses with C30 concrete to compare instant and long-term deflections	Not significant
Combination of f_{ct}, ϕ, ϵ_{cs}, E_c section 7.4.6	f_{ct}, ϕ, ϵ_{cs}, E_c were varied combinedly for 4 thicknesses with C30 concrete to compare instant and long-term deflections	Very significant and effects of f_{ct}, ϕ, ϵ_{cs}, E_c are mostly independent

Table 7.21 Summary of parametric study: material properties

The concrete tensile strength, f_{ct}, determines the level of cracking and is, perhaps, the most important parameter in determining deflection. It is essential to estimate f_{ct} as accurately as possible. However, due to its inherent variability, it can vary appreciably around the mean which, in turn, makes variability of deflection significant. It is important to include the variability of f_{ct} and other concrete properties in the analysis to minimise the risk of deflections exceeding tolerable limits. It has been found that all the material properties affect deflection almost independently.

The effect of loss of tension stiffening, which is modelled by assigning a value of 0.5 to β_2, is found to increase long-term deflection greatly. The author believes that there is scope to study the loss of tension stiffening more extensively by experiments and the value of 0.5 should be replaced by a more logical expression to represent a gradual loss of stiffness with time.

7.7.3 Construction parameters

The magnitude and time of application of construction load is very important in determining the deflection of the slab. Excessive construction loads can lead to severe cracking of a relatively young slab and result in very high long-term deflections. A summary of the parametric studies on construction factors is given in Table 7.22. It has been shown that significant differences can occur in long-term deflections due to differences in construction methods. The contribution of creep due to construction load is very small and a simplified load history is proposed which gives deflections similar to those obtained from a more rigorous step analysis. A single-step analysis is also proposed with a modified concrete tensile strength which gives good prediction of deflection.

7.7.4 Service-life parameters

Table 7.23 summarises the studies on service-life factors. The magnitude of imposed load is very important in determining long-term deflections and needs to be estimated with reasonable accuracy. The time of application of the imposed load appears to have less effect on deflections. Relative humidity influences long-term deflection significantly.

Item and section	Description of analysis	Conclusions
Construction method section 7.5.1	3 construction sequences were considered for 250 mm slab with 3 f_{ct} to compare deflections for the full load history	Very significant differences due to construction method
Early creep and recovery section 7.5.2	3 R factors were considered for 3 construction sequences with mean f_{ct} to compare deflections for the full load history	Creep due to construction load is small, R=1 is reasonable
Simplified load history section 7.5.3	The load-history was applied for 3 construction sequences with 3 f_{ct} to compare long-term deflections	Yields deflections which are similar to those obtained from more rigorous analysis
Single-step method section 7.5.4	The method was applied for 3 construction sequences with 3 f_{ct} to compare long-term deflections	Compares well with simplified load history without Rotilio curve
Age at striking section 7.5.5	4 striking times were considered without construction load to compare the deflections for the full load history	Very early striking leads to increased deflections, very late striking may not be useful
	3 striking times were considered with construction load for cracked and uncracked slab, to compare deflections for the full load history	Early striking is more detrimental with high construction load, creep due to construction is less significant

Table 7.22 Summary of parametric study: construction factors

Item and section	Description of analysis	Conclusions
Magnitude and time of imposed load in section 7.6.1	4 magnitudes of imposed load were used with 2 different timings of application to compare the deflections for the full load history	Imposed load increases deflection significantly and timing is less important
Relative humidity in section 7.6.2	3 levels of relative humidities were considered for four thicknesses with C30 concrete to compare long-term deflections	Significant effect on deflections

Table 7.23 Summary of parametric study: service-life factors

Chapter 8

Modelling of full scale testing: Cardington ECBP building

8.1 Introduction

It has been shown in section 4.13 that the MC-90 model gives good predictions of the long-term deflection of reinforced concrete slabs under constant loading in a controlled environment. A novel method was proposed in Chapter 6 which extends the MC-90 method to model deflection development under time-varying loading. It was shown in section 6.9 that the method gives good results for the Taywood slab. Chapter 7 investigates the influence of key parameters on deflection, and shows that certain parameters can affect deflections drastically. It is more difficult to predict deflections in real buildings because many of the factors (including material properties, position of reinforcement, slab thickness and loading) that influence deflections can only be estimated at the time of design. In addition, there are considerable difficulties in estimating deflections for a realistic load-time history. Up to now, researchers have been faced with the problem that there is a lack of accurate and well-documented data on deflections in real buildings to calibrate their models. This has changed with the construction of the seven-storey in-situ reinforced concrete framed test building (European Concrete Building Project, ECBP) at the Cardington Large Building Test Facility (see Fig. 8.1). A unique opportunity is presented to measure the deflection of flat slabs in a typical commercial building,



Figure 8.1 Cardington building, source: BRE

under specified loading, and with different reinforcement layouts over a minimum period of two years. Early stages of the author's work are presented in Vollum *et al.* (1998) and Vollum and Hossain (1998). In this chapter, the method proposed in Chapter 6 to calculate deflections under a time-varying load history is used to model the deflection behaviour of the Cardington slabs throughout their construction and operational life. The performance of the simplified single-step method to estimate the final deflection (see section 7.5.4) has also been checked for this building. Field measurements obtained so far from Cardington are presented along with analytical results. A limited parametric study was also carried out to study the effect of cracking, creep, shrinkage, reinforcement and pattern loading. In reality, the imposed load has been applied only on panels between grid-lines 2 and 4 (see Fig. 8.2). All the FE results presented in this chapter other than those in section 8.7 are for imposed load on all panels. The FE results shown in section 8.7 correspond to imposed load on panels between grid-lines 2 and 4 and times of application of imposed load were also adjusted to mimic actual loading. Measured deflections after the application of imposed load are plotted in section 8.7 only.

8.2 Description of the ECBP building

The test building is a seven-storey in-situ reinforced concrete building of flat-slab construction. Construction of the ECBP building started on January 12 1998 and was completed in just 14 weeks. The grid is 7.5 m square and the slab is 250 mm thick. The floor plan and grid for deflection measurements is shown in Fig. 8.2. The slabs were all cast in a single day. The floors were designed by different designers using different methods and also different reinforcement arrangements were adopted. Thus, the floors are different due to variations in concrete mix design, reinforcement areas and their arrangements as shown in Table 8.1.

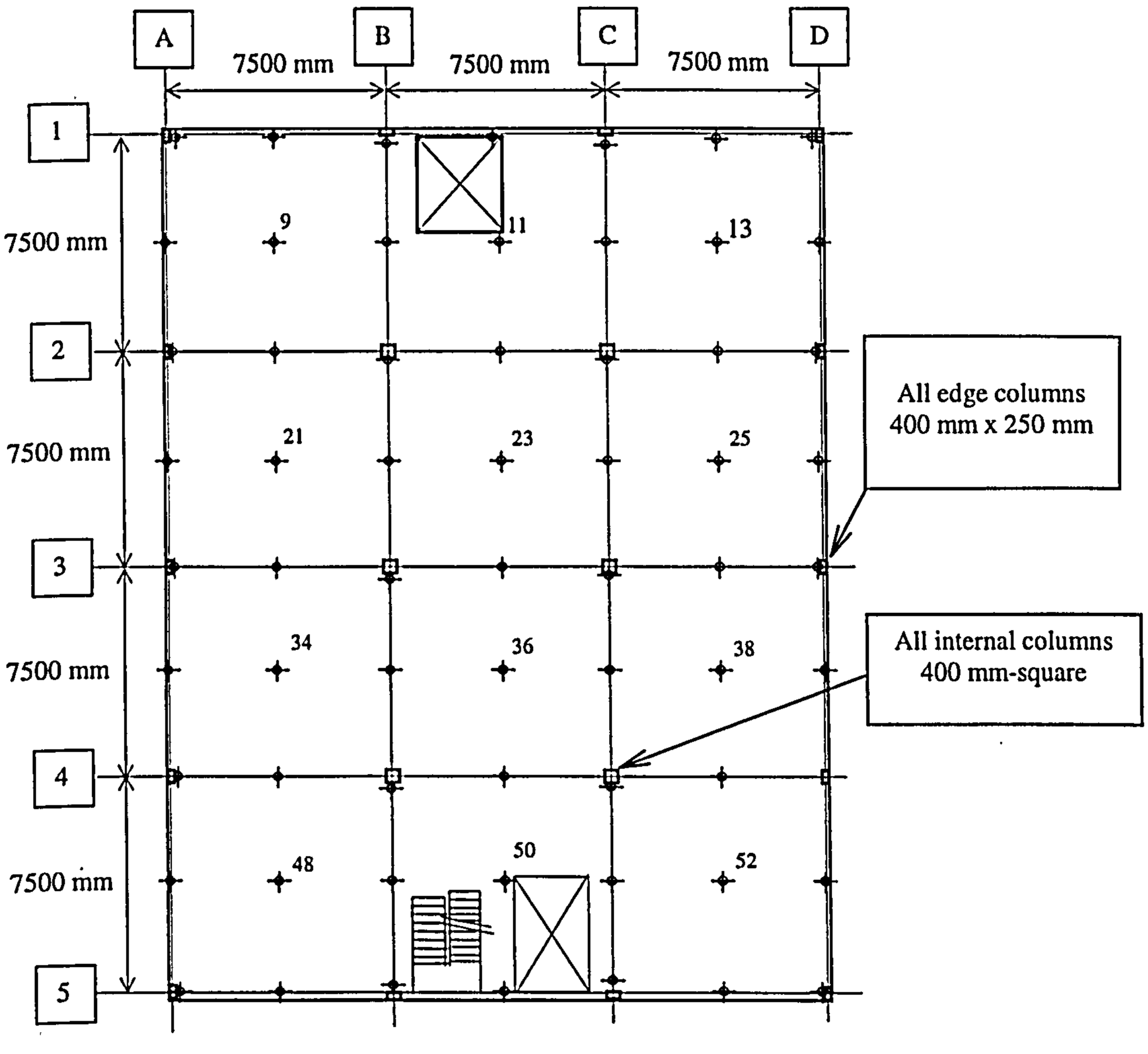


Figure 8.2 Floor plan and deflection measurement grid, source: BRE

The slabs designed using equivalent frame method 1 and yield-line analysis complied with the span-to-depth rules given in EC2. The procedure adopted is sum-

Floor	Concrete mix	Design method	Reinforcement arrangements
1	C37N	Equivalent frame 1	Traditional loose bar
2	C37N	Equivalent frame 1	Traditional loose bar
3	C37P	Equivalent frame 2	Rationalised loose bar
4	C37F	Equivalent frame 1 /yield-line	Blanket cover loose bar
5	C37N	Equivalent frame 1	One-way mats
6	C37F	Equivalent frame 1 /FE	Blanket cover one-way mats

1. N=normal mix, P=mix with plasticiser, F= mix with PFA

2. Four separate designs were produced as described above. Equivalent frame 1 and yield-line design complied with EC2 span-to-depth ratios. No deflection checks were made in other designs.

Table 8.1 Details of concrete mix and reinforcement arrangements at each floor

marised below:

1. A slab thickness of 250 mm was specified by the client.

2. The slab reinforcement was designed for the ultimate limit state and the required area of reinforcement A_{sreq} was calculated.

3. Actual and permissible span-to-depth ratios were calculated.

4. The basic span-to-depth ratio was increased to the actual value by increasing the area of tensile steel provided in the span A_{sprov} in accordance with:

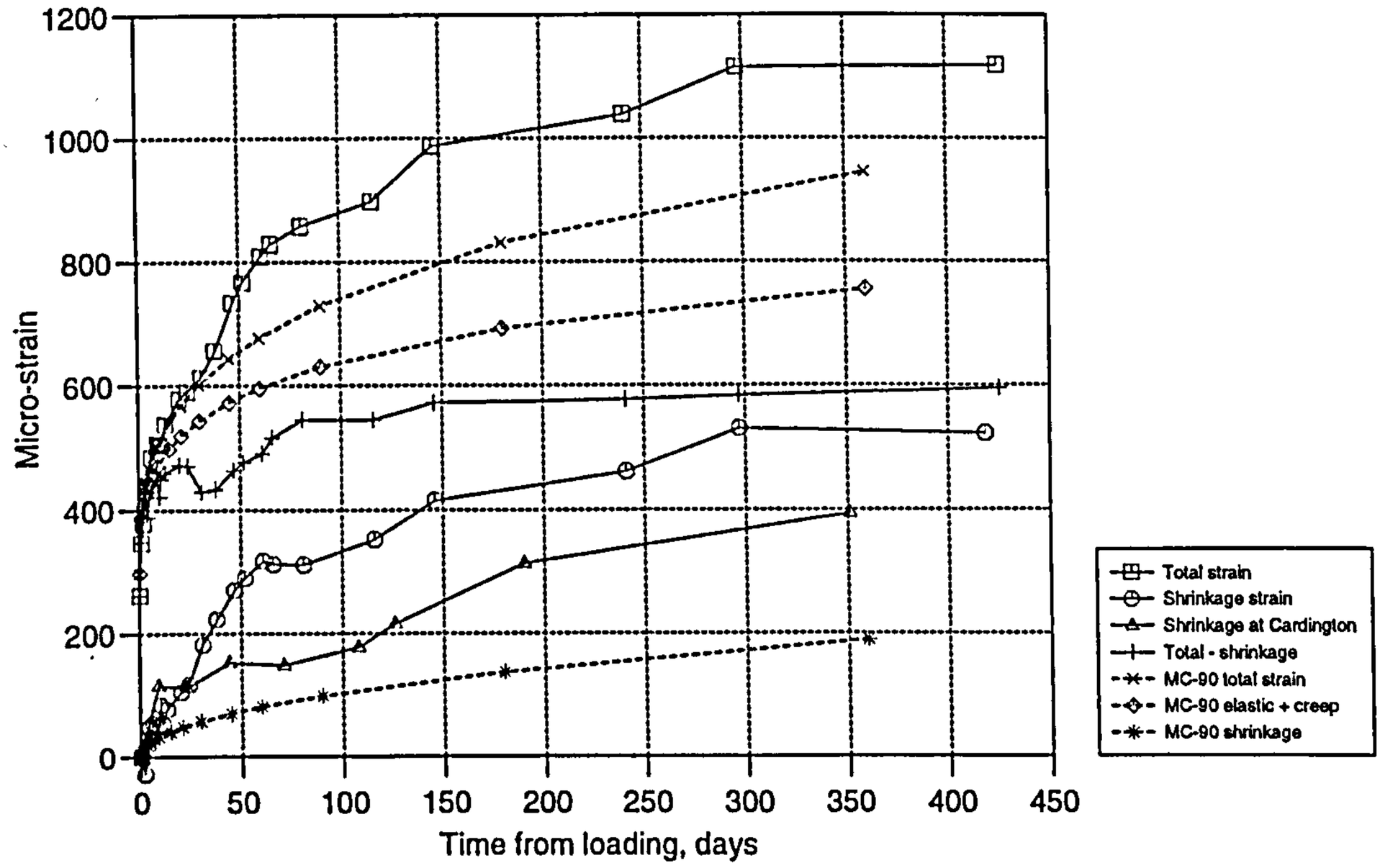
$$\left(\frac{l}{d}\right)_{permissible} = \frac{400}{f_{yk}} \frac{A_{sprov}}{A_{sreq}} \left(\frac{l}{d}\right)_{basic} \tag{8.1}$$

The area of tension steel in the span was increased by factors ranging between 1.35 to 1.7 in equivalent frame method 1. The multiplication factors were less in the yield-line design because the design moments were calculated on the basis that a straight yield-line formed at the face of columns. This assumption led to lower design

moments in the yield-line design with the consequence that the permissible span-to-depth ratio (which depends on A_s/bd), was greater than in the equivalent frame method. Therefore, the required value of the multiplication factor A_{sprov}/A_{sreq} was less in the yield-line design. The area of tension steel was increased by factors of 1.00 and 1.18 in the internal and external spans respectively in the yield-line design.

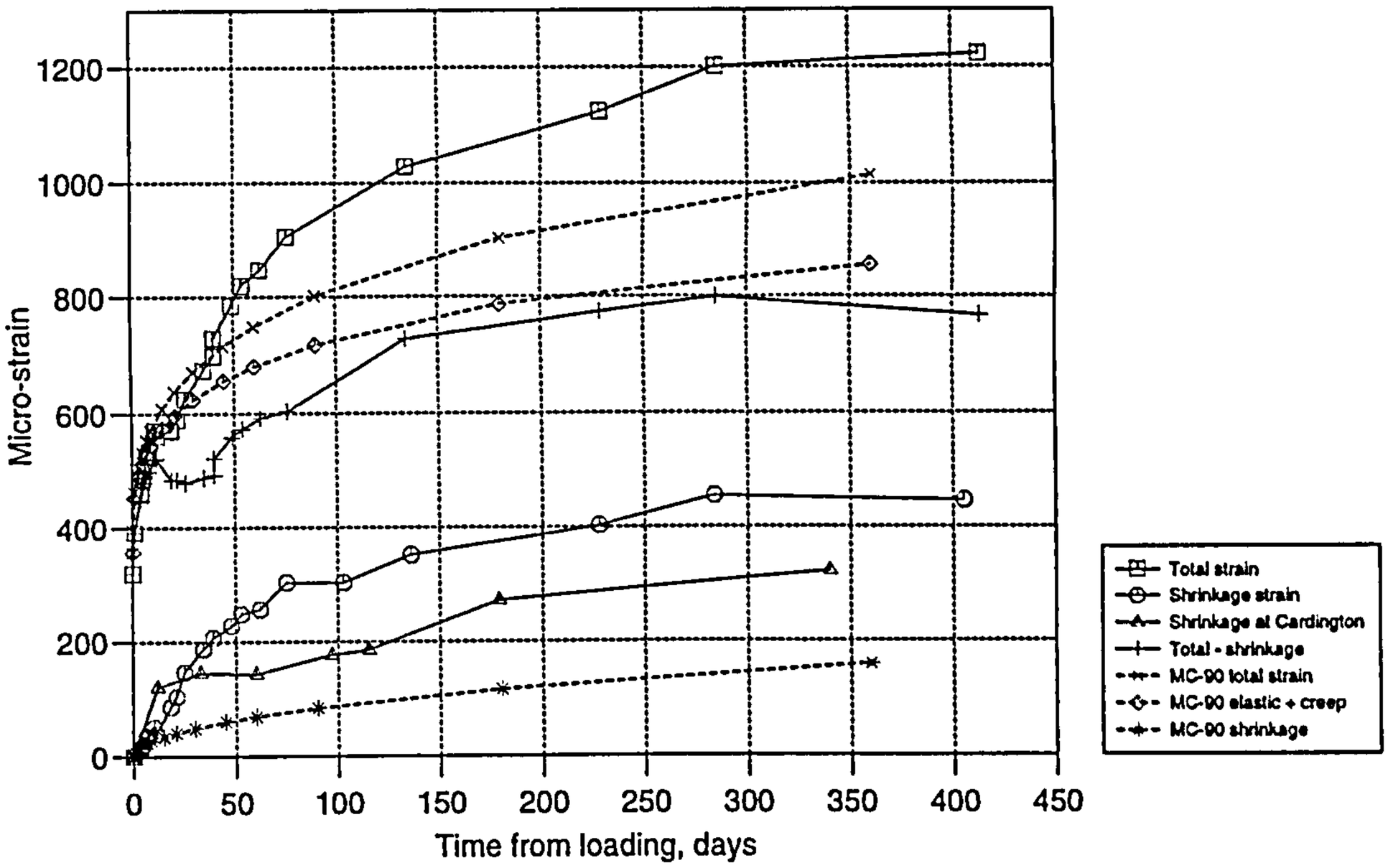
8.2.1 Material properties

A comprehensive test programme is being carried out by Vollum (1998) to determine the creep and shrinkage properties of the concrete. A total of six creep and nine shrinkage tests are being carried out on concrete cylinders from each floor. The creep tests were started at the time of striking and when the permanent service load was applied. The strains measured so far are compared with those obtained by CEB-FIP Model Code (MC-90) equations in Figs 8.3 to 8.5.



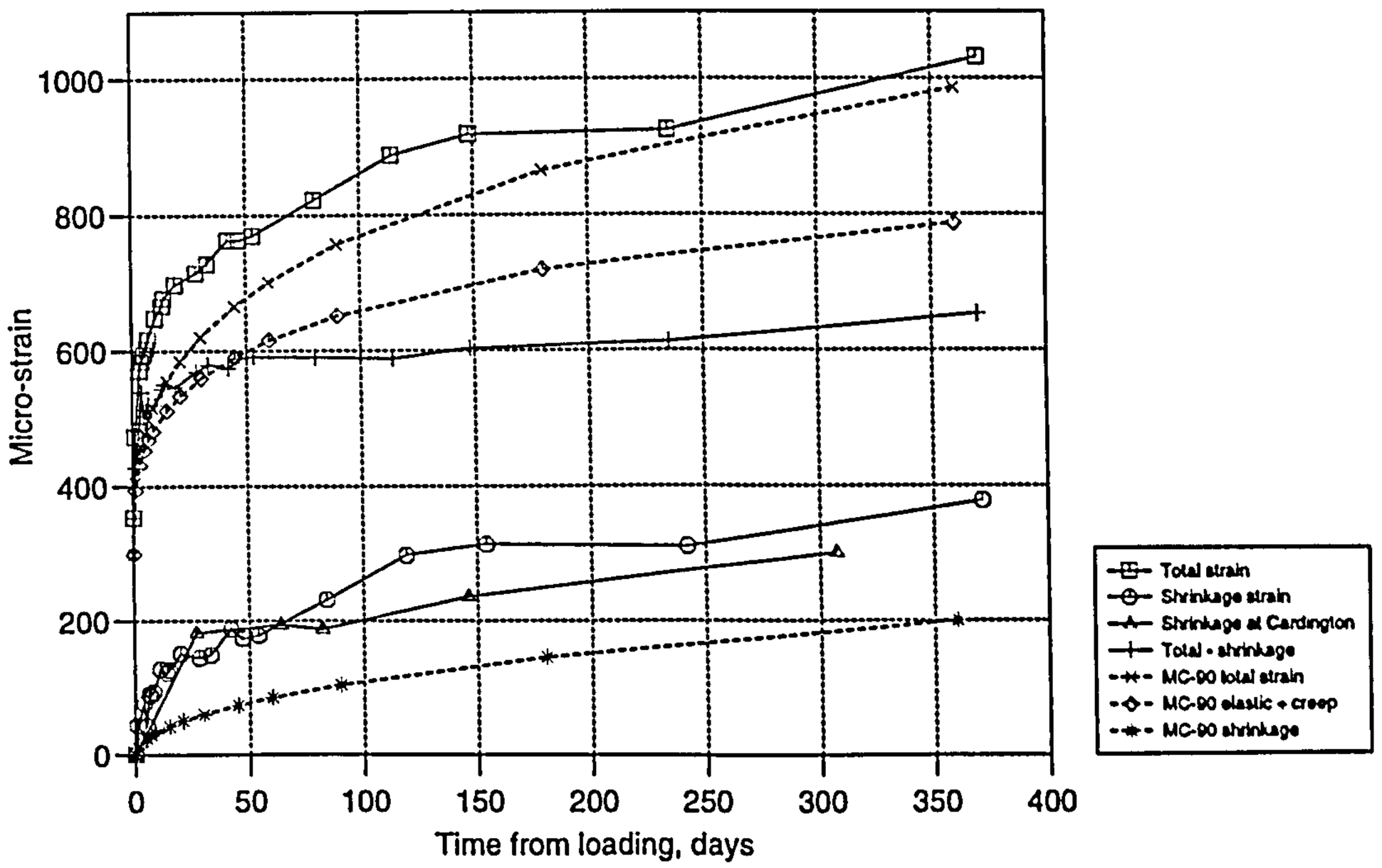
Notes:
1. Stress= 6 MPa
2. Specimen loaded at 2 days
3. RH assumed to be 44% for all predicted strains

Figure 8.3 Comparison of creep and shrinkage properties: measured and MC-90 predictions for floor 3: adapted from Vollum (1998)



Notes:
1. Stress= 8 MPa
2. Specimen loaded at 3 days
3. RH assumed to be 44% for all predicted strains

Figure 8.4 Comparison of creep and shrinkage properties: measured and MC-90 predictions for floor 4: adapted from Vollum (1998)



Notes:
1. Stress= 8 MPa
2. Specimen loaded at 10 days
3. RH assumed to be 44% for all predicted strains

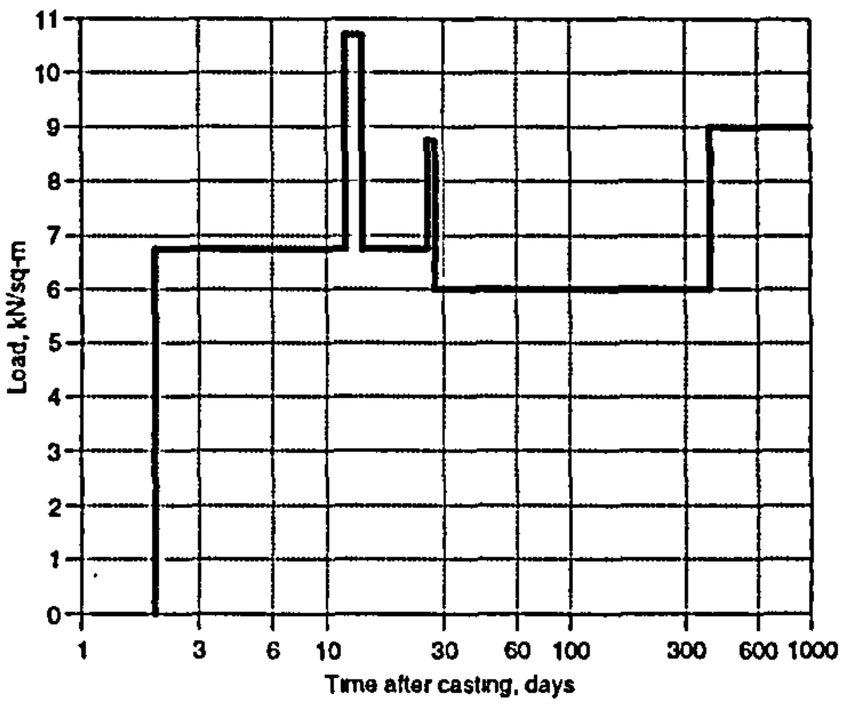
Figure 8.5 Comparison of creep and shrinkage properties: measured and MC-90 predictions for floor 6: adapted from Vollum (1998)

8.2.2 Loading

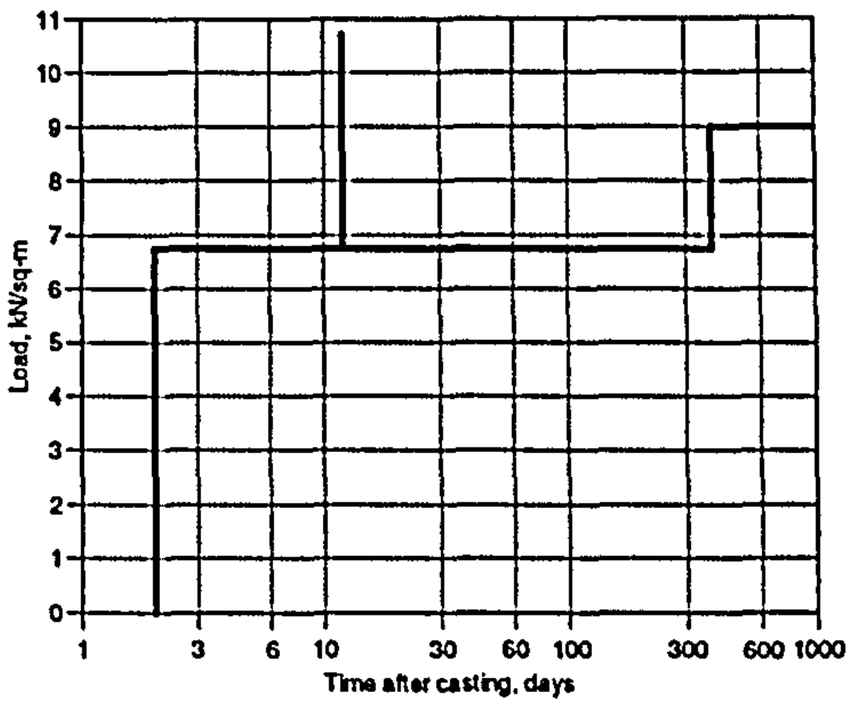
All the slabs were struck very early (at 2 or 3 days) and subsequently carried their self-weight. The slabs were back-propped before the next slab was cast. The back-props were placed in position but not tightened so that the back-props were theoretically only loaded when additional loads were applied. As a result the magnitudes of the construction load were relatively low. Beeby (1998) carried out research on the slabs at Cardington to investigate early striking of form-work and back-propping. Beeby proposed methods for the assessment of form-work striking times and for the assessment of loading that could be applied to young slabs. During construction, prop and back-prop forces were monitored. In the present work, these measurements were used to find the construction load on slabs.

One of the main aims of the Cardington project is to determine long-term slab deflections under loading representative of that in a typical office. To this end, the permanent imposed load applied to the structure has been taken as 3 kN/m^2. The imposed load of 3 kN/m^2 includes allowances of 1 kN/m^2 for raised floor, services and ceilings and 1 kN/m^2 for partitions. The permanent imposed load was applied in March 1999. Service loads were applied with sand bags, on the panels between grid-lines 2 and 4, as shown in Fig. 8.2, at floors 1 to 6. In reality, the imposed load is 3.27 kN/m^2, but 3 kN/m^2 is used in the analysis. Figure 8.6 shows the idealisation of actual and simplified (for FE analysis) load history of floors 3, 4 and 6. A load of 6.75 kN/m^2 (at striking) includes self-weight of slab (6.0 kN/m^2) and weight of form-work (0.75 kN/m^2).

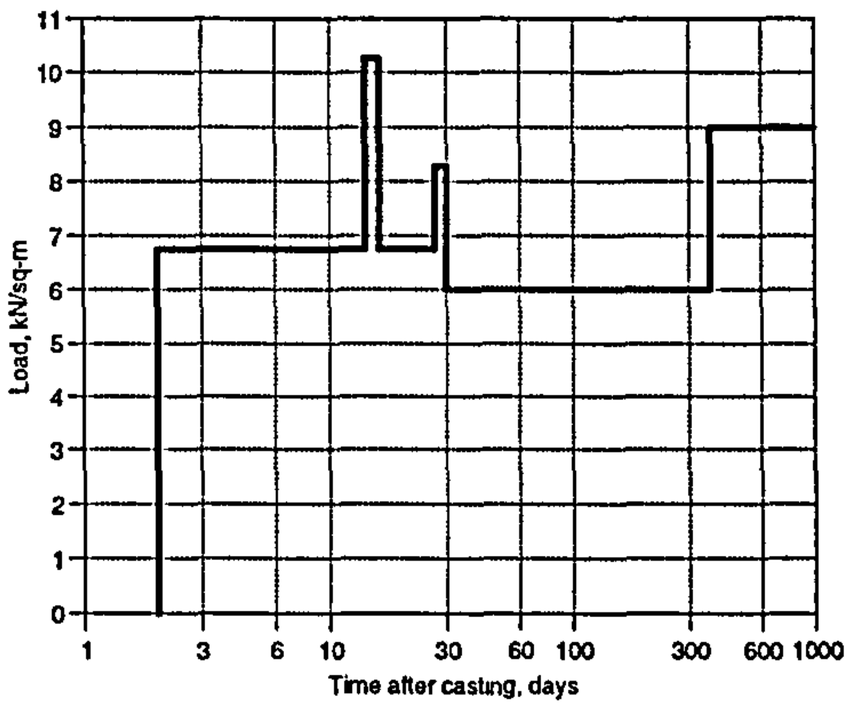
Floor 3: idealisation of actual load



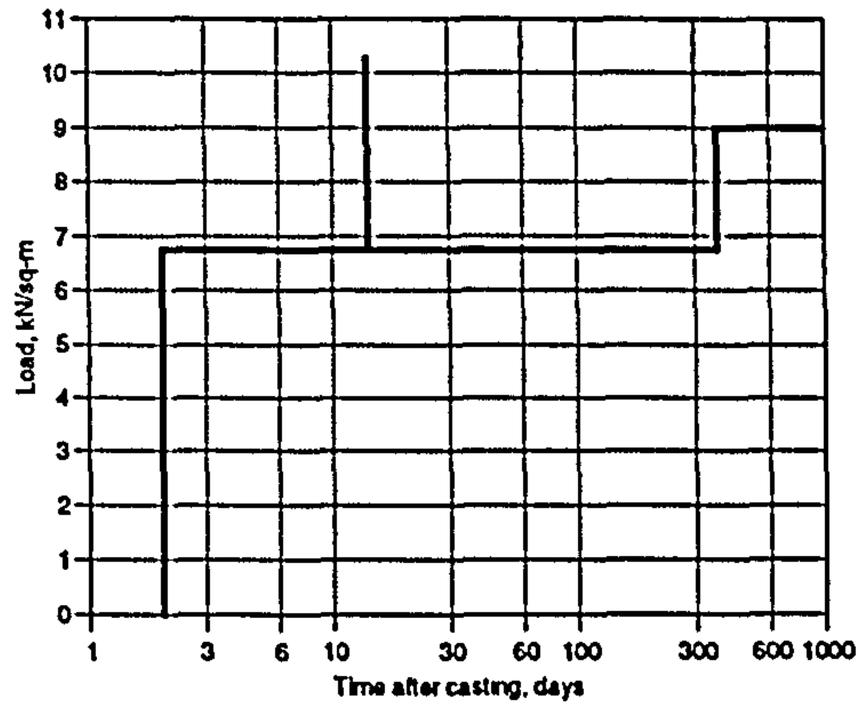
Floor 3: simplified load



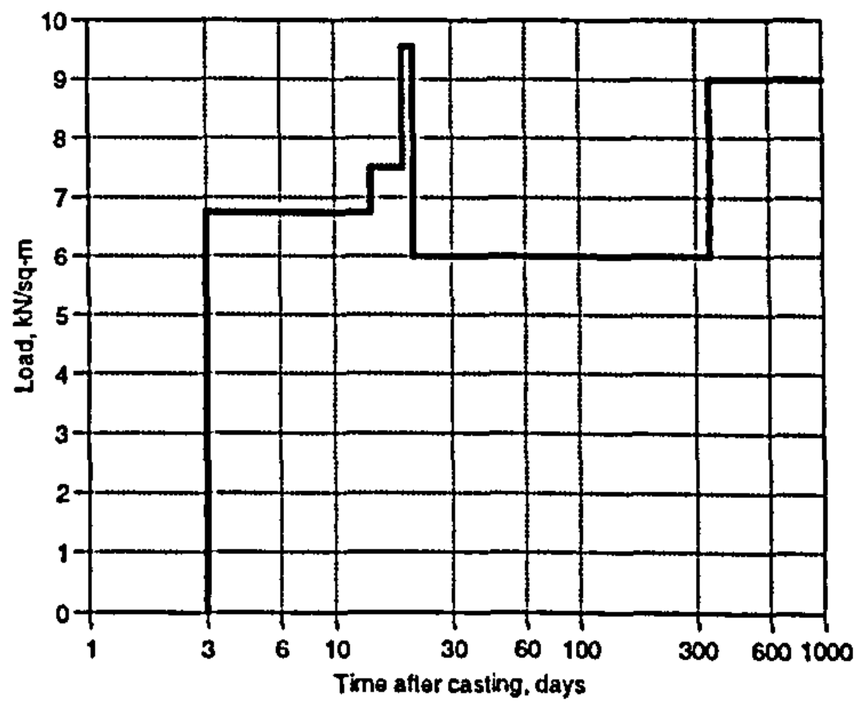
Floor 4: idealisation of actual load



Floor 4: simplified load



Floor 6: idealisation of actual load



Floor 6: simplified load

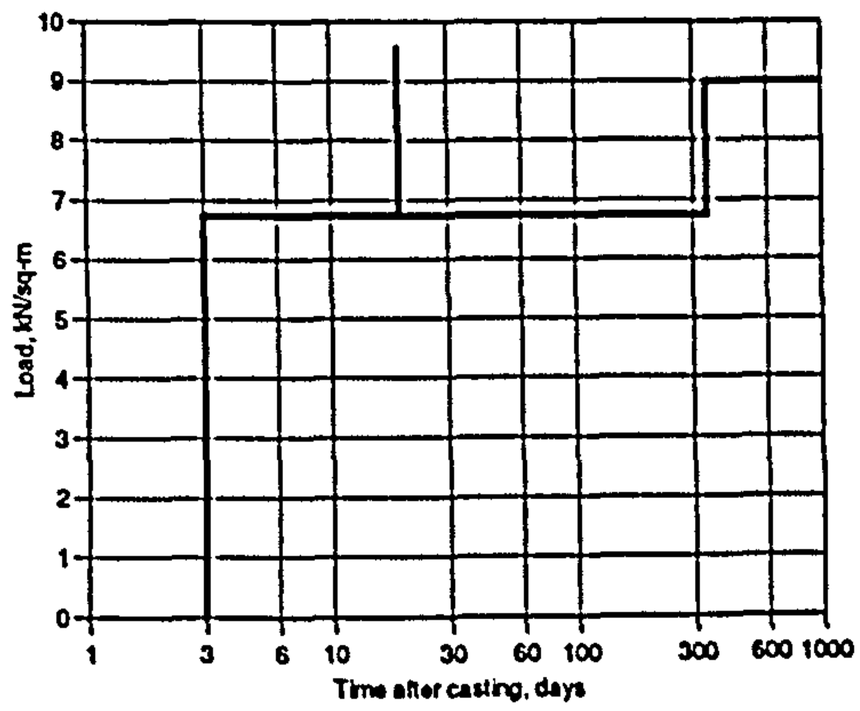


Figure 8.6 Actual and simplified load histories of floors 3, 4 and 6.

8.2.3 Deflection measurement

Deflections are being measured at 60 test points (see Fig. 8.2) by precise levelling. The instrument used is a Wild NA2 automatic level with parallel plate micrometer that enables levels to be measured to 0.001 cm. The instrument is used with a Wild invar staff fitted with a spirit level and an aluminium bipod which allows the staff to be held truly vertical. All the levels at each floor are measured relative to a reference point R_1 located at the same position on each floor. If the closing error is worse than $\pm$ 0.5 mm, then the levelling process is repeated. Normal closing errors are within $\pm$ 0.2 mm.

8.3 FE analysis

Even though the floors are not exactly symmetrical (Fig. 8.2) due to the presence of different sizes of holes on each side, they are assumed to be symmetrical so that one-quarter of the slab can be considered in the analysis. The slabs are modelled with 9-noded generalised plate elements and the columns are modelled with 27-noded brick elements. Only the lower columns are included in the analysis until the slab above is cast. Subsequently, the top column is included when the slab above is struck. The columns are assumed to have points of contraflexure at mid-height. All the columns are modelled with brick elements neglecting the effects of cracking and reinforcement since it has been shown in section 6.9.2 that an analysis with the gross concrete section (without reinforcement) gives reasonable accuracy under service loads. The effect of creep in the column was also neglected since it has been observed by the author that slab deflections are relatively insensitive to column stiffness. A single-step analysis without the top column resulted in a maximum increase in deflection of 10% (at 3000 days) compared with a similar analysis with both top and bottom columns. It is believed that the effect of including creep in the column would have been similar.

8.3.1 Assumptions

The assumptions made in the modelling of deflections due to a time-varying load are given in section 6.2. Further assumptions regarding the analysis of Cardington slabs are:

1. The thickness of all the slabs is 250 mm as specified.

2. The reinforcement assumed in the analysis is equivalent to that specified, although some adjustments were made to accommodate the chosen FE mesh.

3. The values of f_{ct} and E_c used in the analysis are based on control tests. Creep coefficients and shrinkage strains were calculated using MC-90. The predicted creep coefficients agree well with test data (see Figs 8.3 to 8.5). The predicted shrinkage strains are less than measured values. For simplicity MC-90 shrinkage strains are also used in the analysis since they are relatively unimportant.

4. Simplified loadings were assumed for all the slabs.

8.3.2 Mesh-sensitivity

A mesh-sensitivity analysis was carried out to select a mesh with the minimum possible number of elements without significantly sacrificing accuracy. Three different meshes were considered in the analysis:

- Mesh 1: A very fine mesh with 651 elements of which 547 are plate elements and 104 brick elements.

- Mesh 2: A less fine mesh with 358 elements of which 262 are plate elements and 96 brick elements.

- Mesh 3: Same number (and arrangements) of plate elements as mesh 2, but with less brick elements. The total number of elements are 310 of which 262 are plate elements and 48 brick elements.

Four analyses were carried out with the three meshes. Elastic, instant deflections are calculated for 6 kN/m^2 uniformly distributed load and long-term deflections are

computed for 6 and 10 kN/m^2. Central point deflections for corner, external and internal panels are tabulated in Table 8.2.

Position	Deflection	Mesh 1	Mesh 2	Mesh 3
Corner	elastic, load 6 kN/m^2	5.68	5.64	5.59
	instantaneous, load 6 kN/m^2	6.31	6.18	6.15
	101 day, load 6 kN/m^2	12.63	12.45	12.40
	101 day, load 10 kN/m^2	26.99	26.72	26.60
Edge	elastic, load 6 kN/m^2	4.34	4.27	4.22
	instantaneous, load 6 kN/m^2	4.85	4.72	4.68
	101 day, load 6 kN/m^2	9.62	9.40	9.35
	101 day, load 10 kN/m^2	20.35	20.04	19.26
Interior	elastic, load 6 kN/m^2	2.49	2.43	2.39
	instantaneous, load 6 kN/m^2	2.77	3.01	2.96
	101 day, load 6 kN/m^2	5.58	5.51	5.47
	101 day, load 10 kN/m^2	11.29	11.19	12.30

Table 8.2 Mesh-sensitivity: Cardington slab

Even though mesh 2 has less than half the elements of mesh 1, the deflections are reasonably similar. A further reduction in brick elements in mesh 3 did not lead to any significant change in deflection. Deflections corresponding to mesh 3 are within 10% of those obtained with the very fine mesh 1. Since an analysis with mesh 1 is at least 4 times more time consuming than one based on mesh 3, for further analysis a mesh similar to mesh 3 (see Fig. 8.7) is adopted.

8.3.3 Simplified loading history

As shown in section 7.5.2, the contribution of creep due to construction load is less significant than the effect of cracking on final deflection. To simplify the problem of modelling the load history during construction, a simplified method was presented in section 7.5.3 where a spike load corresponding to peak construction load was applied instantly at the time of actual application. A similar simplified approach is adopted in the current analysis, where a spike load is applied to model possible further cracking due to construction load and the Rotilio unloading curve (see section 6.5.1) is used to model the residual deflection upon unloading. The level of cracking due the spike load is also stored. However, as the spike load is applied and unloaded instantaneously the simplified method does not consider the small amount creep due

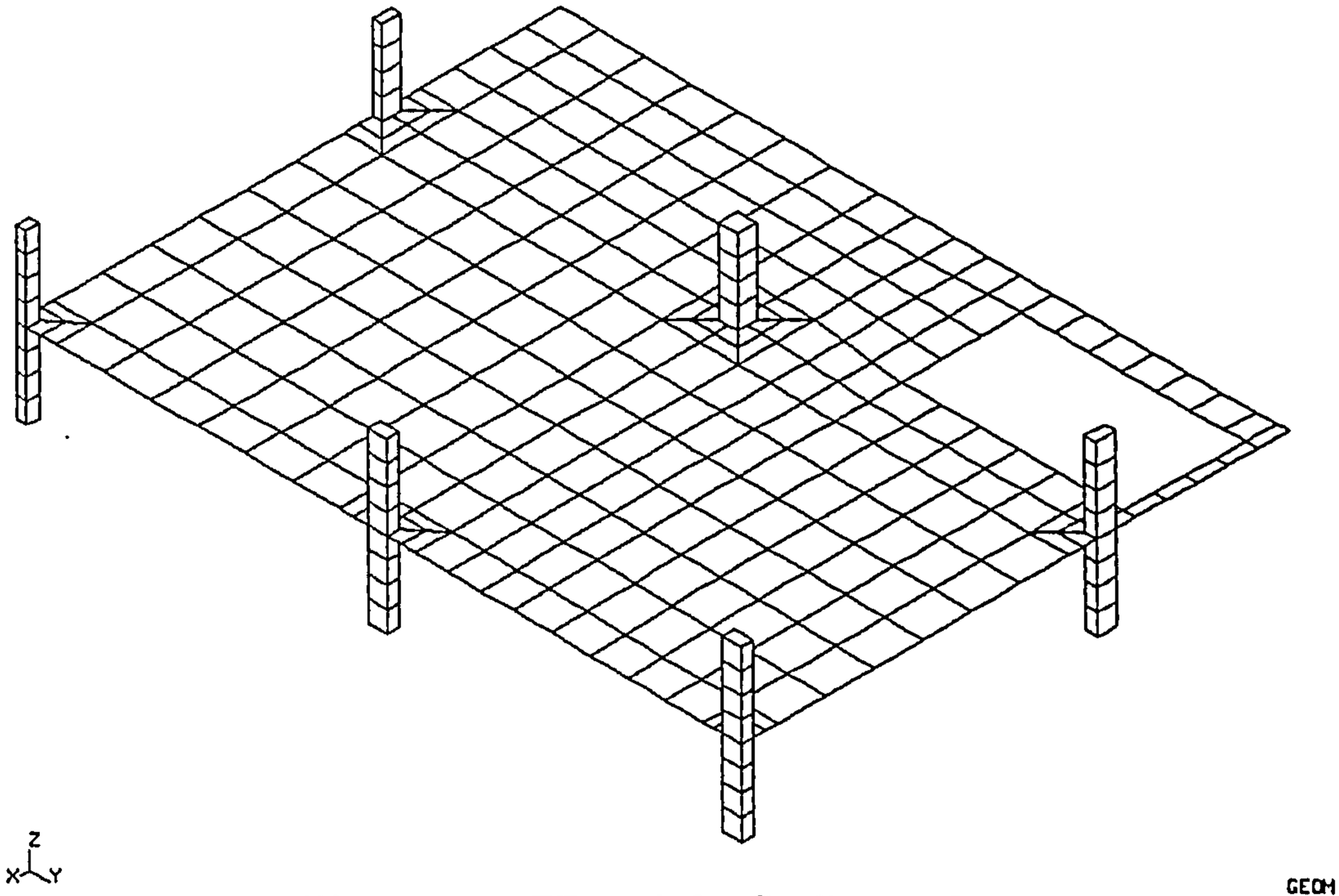


Figure 8.7 FE mesh for Cardington floors

to construction load. Figure 8.6 shows the simplified load history along with the actual idealised ones for slabs 3, 4 and 6. It should be noted here that the load histories shown in Fig. 8.6, are used only for the pattern load analyses (see section 8.7) and all other analyses of this chapter correspond to similar load histories with imposed load being applied at 300 days.

8.3.4 Material properties used

The material properties given in Table 8.3 are used in the FE analysis. At striking, measured values are used for E_c and f_{ct}. At other times, E_c and f_{ct} are estimated on the basis of 28-day strengths:

$$E_c = C_1 f_{cu}^{0.33} \tag{8.2}$$

$$f_{ct} = C_2 f_{cu}^{0.6} \tag{8.3}$$

where f_{cu} is the cube strength of concrete at concerned time. The coefficients C_1 and C_2 are calculated on the basis of 28-day strength:

$$C_1 = \frac{E_{cm}(28)}{f_{cu}^{0.33}(28)} \tag{8.4}$$

$$C_2 = \frac{f_{ct}(28)}{f_{cu}^{0.6}(28)} \tag{8.5}$$

where $E_{cm}(28)$, $f_{ct}(28)$ and $f_{cu}(28)$ are modulus of elasticity, tensile strength and cube strength respectively at 28-day. Creep coefficient and shrinkage strains are calculated using the MC-90 equations (on the basis of the actual 28-day concrete strength given in the first column of the table) since the predicted creep and total strains are similar to the measured strains. The relative humidity was assumed to be 70% (based on test data).

8.4 Modelling of deflection with time

Deflections have been calculated for floors 3, 4 and 6 for the load histories shown in Fig. 8.6. The results are presented in the following sections. Three different levels of cracking were used in the analysis to determine the sensitivity of deflection to cracking:

- The slabs were assumed to be uncracked.
- The measured or estimated tensile strengths (see eq. 8.3) given in Table 8.3 were used.
- The tensile strengths given in Table 8.3 were reduced by 33% in the analysis to correspond to the lower characteristic strength specified in MC-90.

Measured deflections corresponding to striking, and two other times before application of imposed loads are compared with the FE results.

The simplified single-step method described in section 7.5.4 was also used to calculate 3000-day deflections. Modified tensile strengths were calculated for striking, peak construction loading and permanent imposed load. The value corresponding to the imposed load using eq. 7.8 was found to be critical for all three slabs. The slabs

Slab	Time, days	E_c, GPa	f_{ct}, MPa	ϕ, (MC-90)	λ, (MC-90)	ϵ_{cs}, (MC-90) μs	β_2
Floor 3 $f_{cm}(28)$ =44.3 MPa	2, SW	27.0	2.7	0	0	0	1
	12, SW	27.0	2.7	0.61	0.72	26.7	1
	12, SWC	33.0	3.6	-	-	-	1
	12, SWCR	33.0	3.6	-	-	-	1
	300, SWCR	27.0	2.7	1.50	0.59	137.0	0.5
	300, SWI	33.0	3.6	-	-	-	1
	3000, SWI	33.0	3.6	2.00 (SW) 1.18 (IL)	0.57 (SW) 0.95 (IL)	300.7	0.5
Floor 4 $f_{cm}(28)$ =50.9 MPa	2, SW	29.3	2.5	0	0	0	1
	14, SW	29.3	2.5	0.60	0.69	26.7	1
	14, SWC	35.2	4.2	-	-	-	1
	14, SWCR	35.2	4.2	-	-	-	1
	300, SWCR	29.3	2.5	1.40	0.58	125.3	0.5
	300, SWI	35.2	4.2	-	-	-	1
	3000, SWI	35.2	4.2	1.87 (SW) 1.10 (IL)	0.55 (SW) 0.95 (IL)	275.3	0.5
Floor 6 $f_{cm}(28)$ =41.5 MPa	3, SW	23.3	2.0	0	0	0	1
	19, SW	23.3	2.0	0.73	0.77	34.9	1
	19, SWC	31.8	3.1	-	-	-	1
	19, SWCR	31.8	3.1	-	-	-	1
	300, SWCR	23.3	2.0	1.57	0.66	141.7	0.5
	300, SWI	31.8	3.1	-	-	-	1
	3000, SWI	31.8	3.1	2.09 (SW) 1.22 (IL)	0.63 (SW) 0.95 (IL)	311.6	0.5

SW= Self-weight, SWC= Self-weight+construction load, SWCR= Self-weight after construction load removed, SWI= Self-weight+Imposed load, IL=Imposed load

Table 8.3 Material properties used in FE analysis

were assumed to be loaded with an imposed load of 9 kN/m^2 at striking which was sustained for 3000 days. The concrete elasticity modulus was assumed to be that at striking and the FE mesh without any upper column was used in the analysis.

8.4.1 Deflection development: floor 3

The development of deflections of floor 3 with time for corner, external and internal panels are shown in Figs 8.8 to 8.10. The lowest curves correspond to the assumption that the slab is uncracked. The middle curves correspond to the mean value of tensile strength. The upper curves correspond to an estimated lower characteristic tensile strength (i.e. thirty percent lower than the mean). The analysis was carried out

with load imposed over the complete floor plate. Measured deflections corresponding to 3 days , 75 days and 269 days (no superimposed load) are also plotted. Measured deflections after the application of the imposed load are not plotted as the actual imposed load was only applied between grid-lines 2 and 4. For corner and external panels, deflections calculated using the mean tensile strength compare very well with measured deflections. For the internal panel, the comparison with results of test point 23 is good while test point 36 gives very high deflection. The peak construction load created further cracking which led to increased predicted deflections in all three panels when the construction load was removed.

The single-step method gives higher deflections in all the panels, since the deflections due to creep are overestimated as a result of the full load (9 kN/m^2) being applied at striking. Nevertheless, the prediction of deflection by the single-step method is reasonably good and requires much less computer time than the rigorous step analysis.

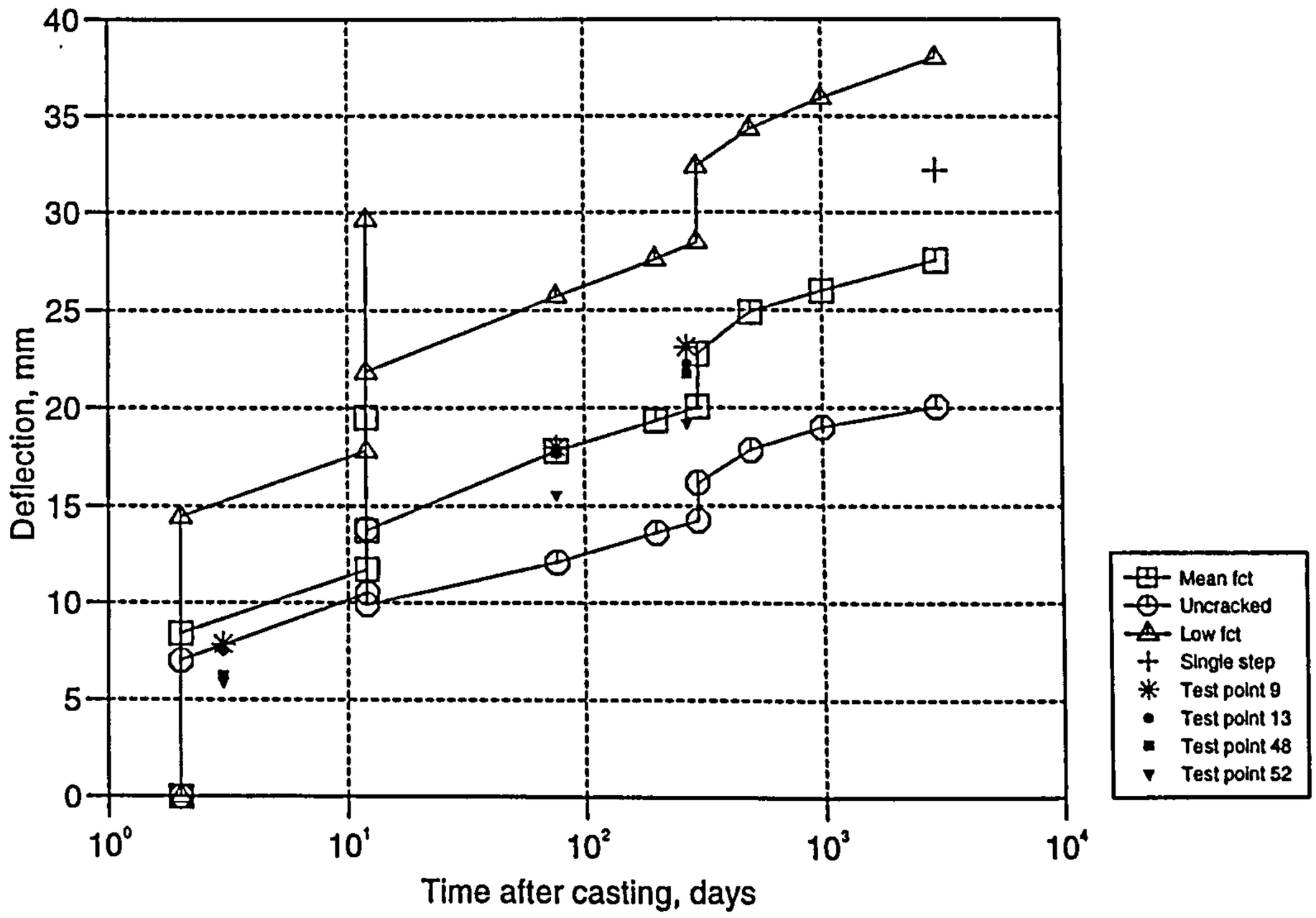


Figure 8.8 Deflection development with time: corner panel, floor 3

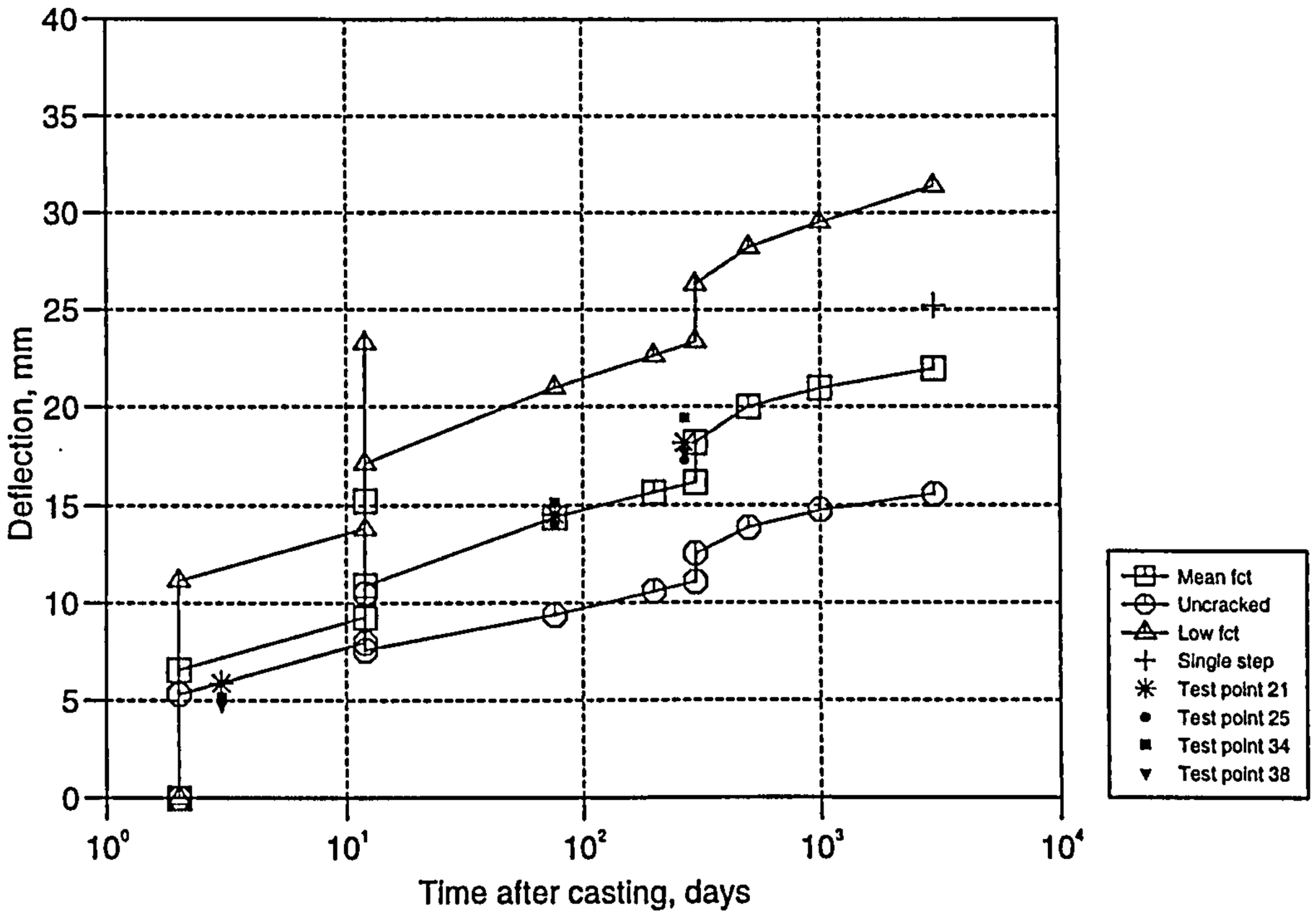


Figure 8.9 Deflection development with time: external panel, floor 3

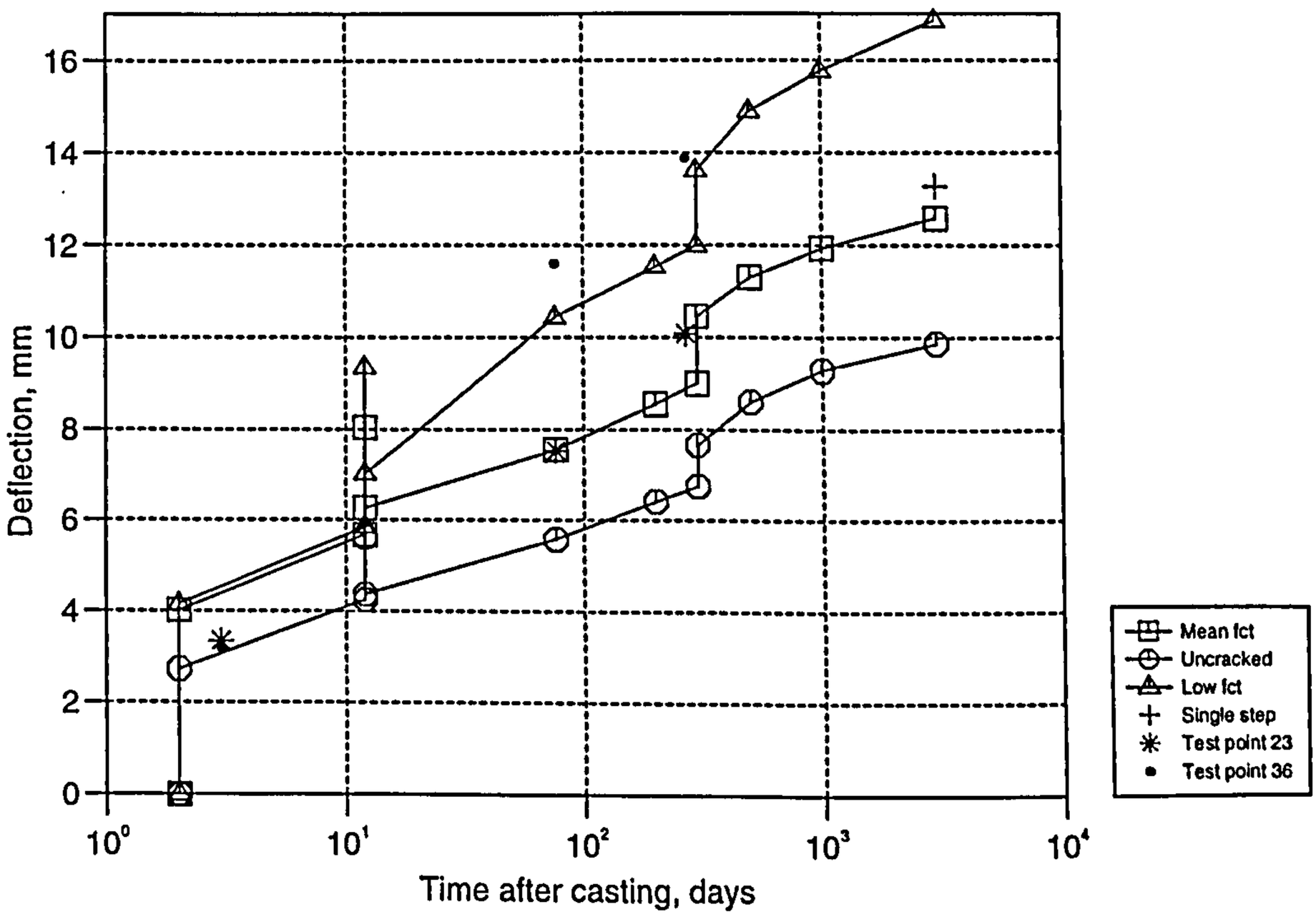


Figure 8.10 Deflection development with time: internal panel, floor 3

8.4.2 Deflection development: floor 4

The development of deflections of floor 4 with time for corner, external and internal panels are shown in Figs 8.11 to 8.13. The three curves correspond to the three different cracking levels. Measured deflections corresponding to 6 days (striking at 2 days), 62 days and 256 days are also plotted. For the corner panel, deflections calculated using the mean tensile strength compare very well with the measured deflections. For external and internal panels, the measured points lie between the uncracked curve and the mean tensile strength curve. For this floor, construction loading did not produce any further cracking. So, in theory, the deflections before and after the spike load should be same. However, deflections are slightly lower for the corner and external panels and slightly higher for the internal panel.

For all three panels, the single-step method gives deflections similar to those obtained with the more rigorous step analysis with mean tensile strength.

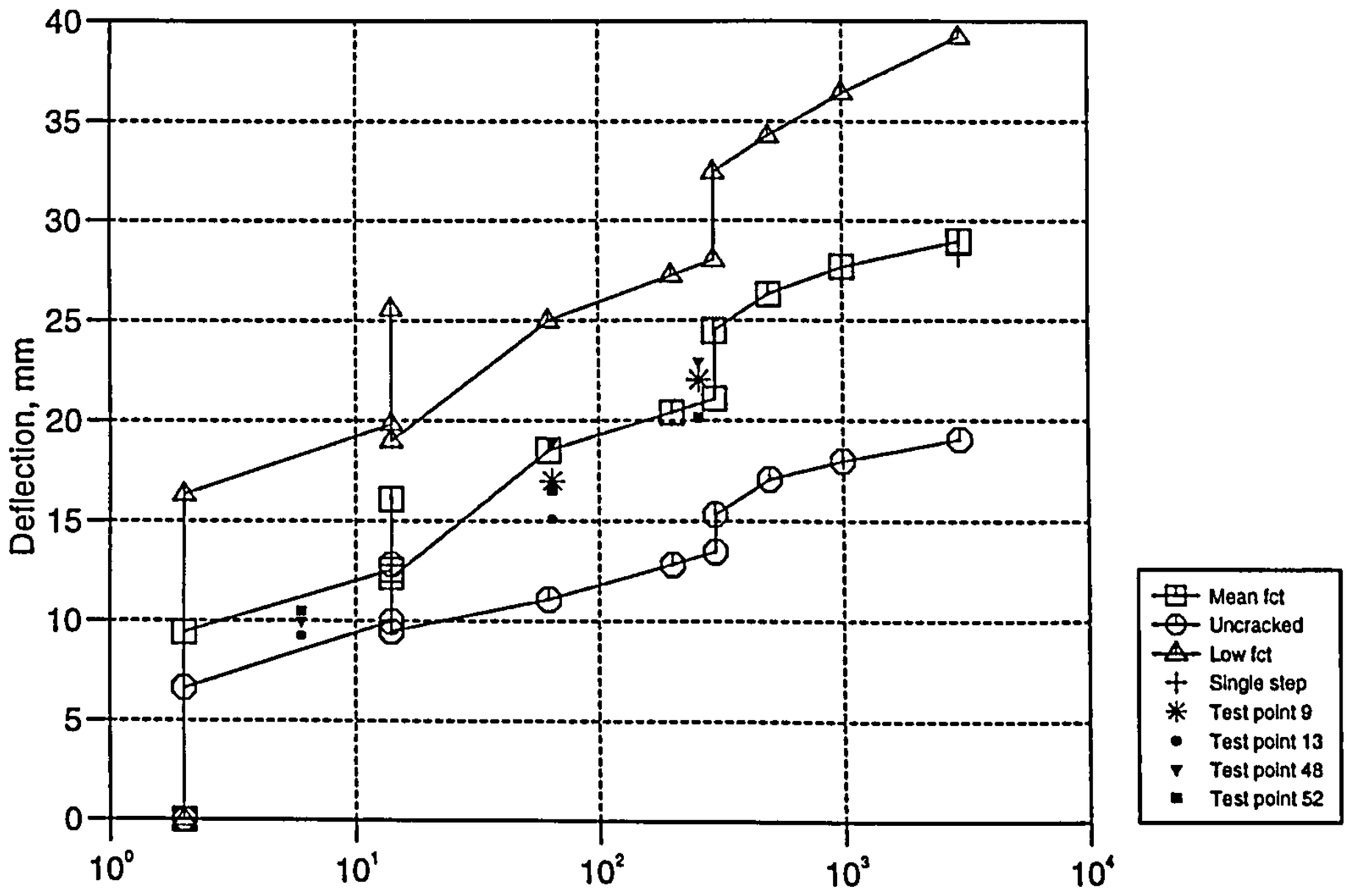


Figure 8.11 Deflection development with time: corner panel, floor 4

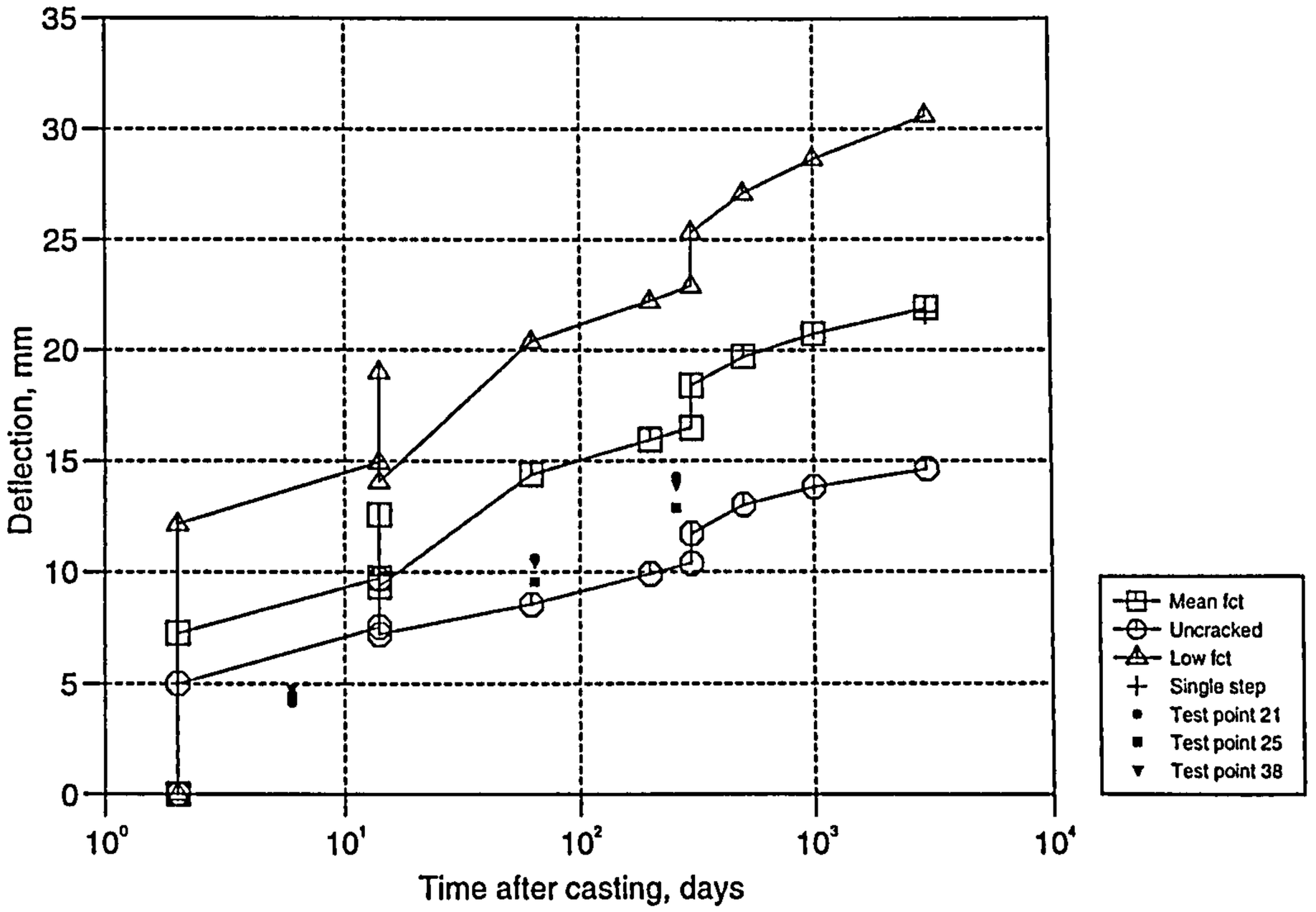


Figure 8.12 Deflection development with time: external panel, floor 4

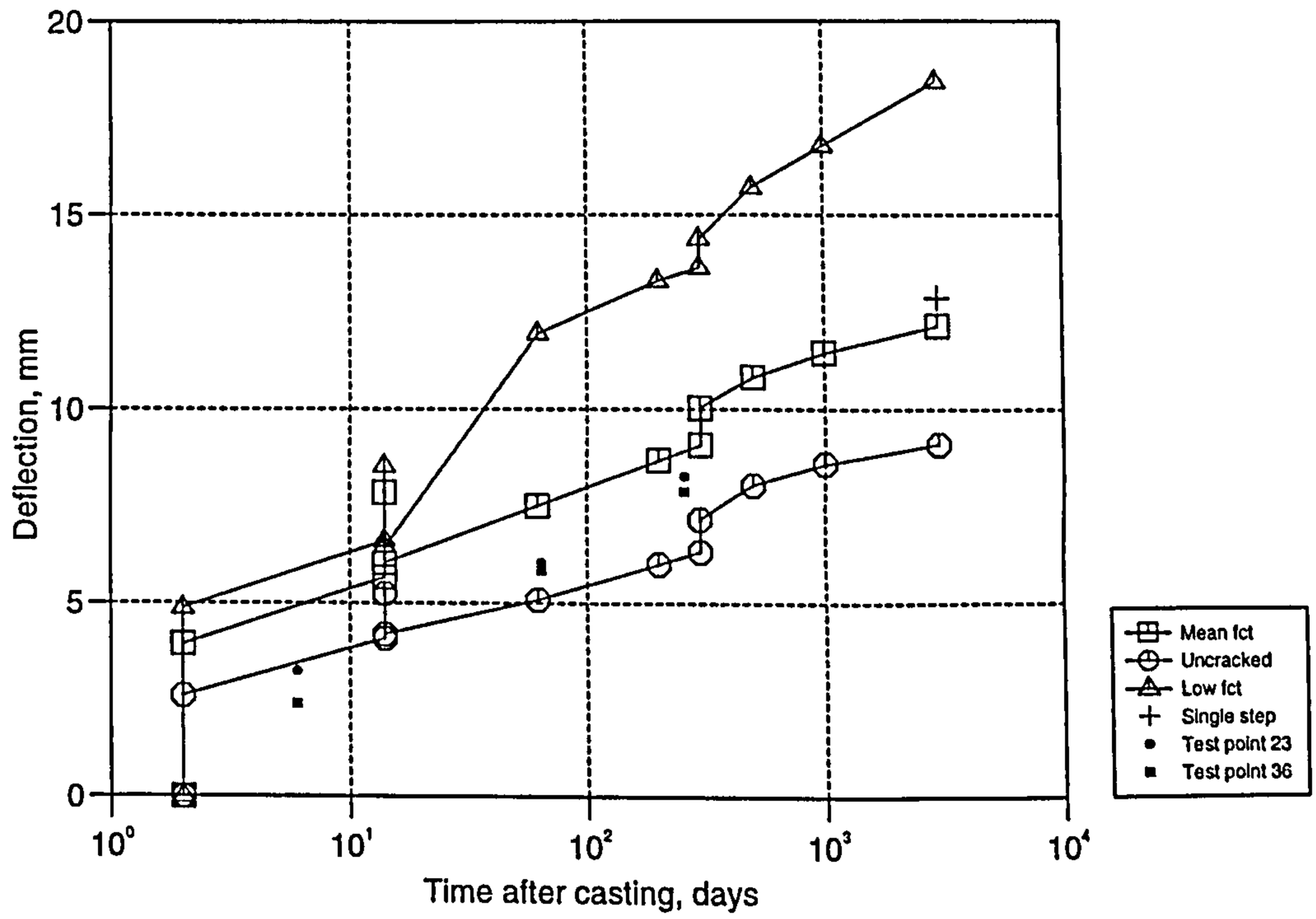


Figure 8.13 Deflection development with time: internal panel, floor 4

8.4.3 Deflection development: floor 6

The development of deflections with time of floor 6 for the corner, external and internal panels are shown in Figs 8.14 to 8.16. Again, the three curves correspond to three different cracking levels. Measured deflections corresponding to 3 days (striking at 3 days), 35 days and 229 days are also plotted. For all the panels, measured deflections at 3 days are less than those obtained with the mean tensile strength, in fact they are close to those calculated on the basis of an uncracked slab. At 35 and 229 days, the agreement between the measured deflection and the predicted deflection obtained with the mean tensile strength is very good for the corner and internal panels. For the external panel, the measured points lie between the curves corresponding to the uncracked slab and the mean tensile strength curve. For this floor, construction load did not produce any further cracking as in floor 4, and the pattern of deflections before and after spike load is similar to that of floor 4.

For all three panels, the single-step method gives higher deflection, as expected, in comparison with the more rigorous step analysis with 7 steps to model the full load history.

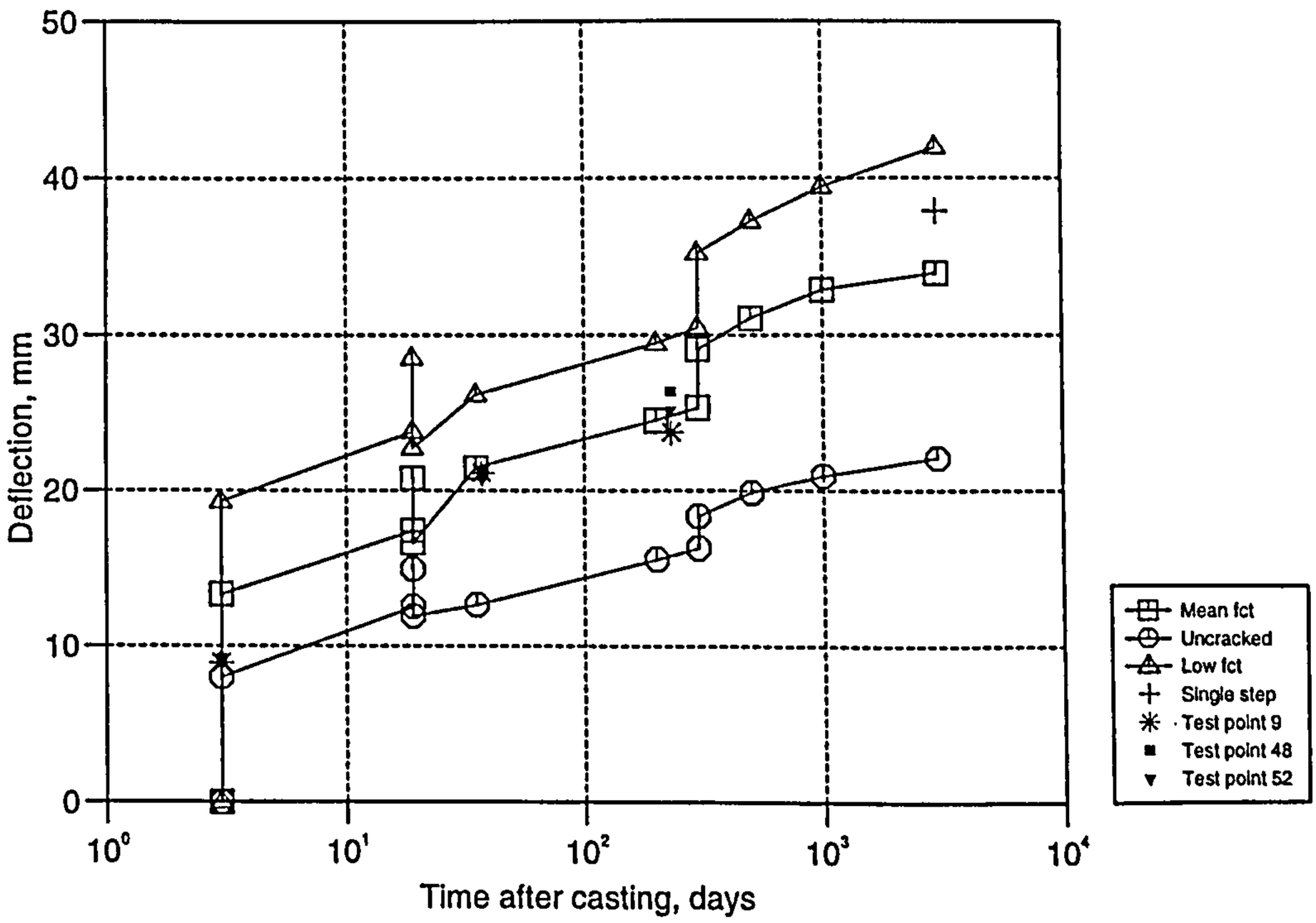


Figure 8.14 Deflection development with time: corner panel, floor 6

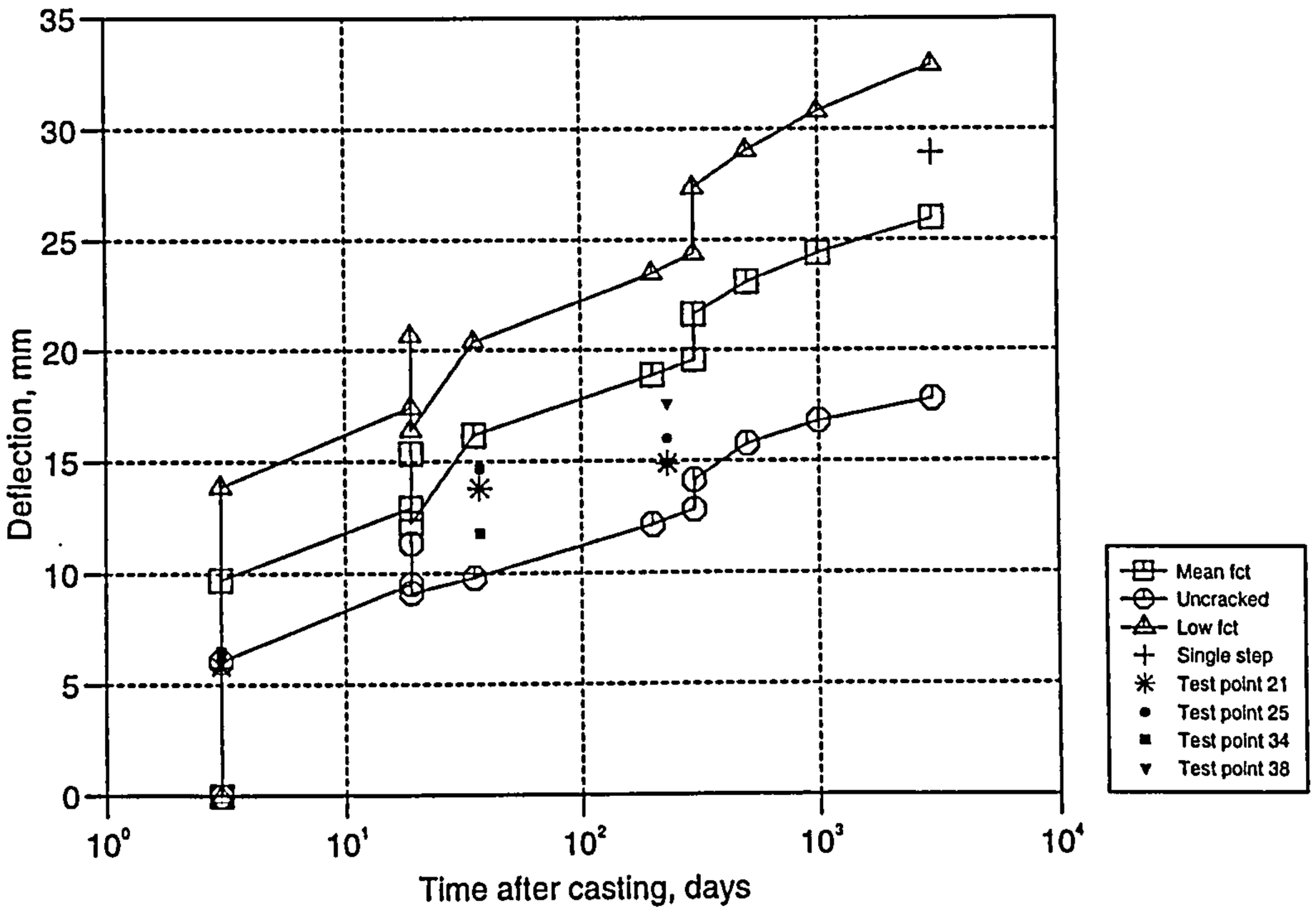


Figure 8.15 Deflection development with time: external panel, floor 6

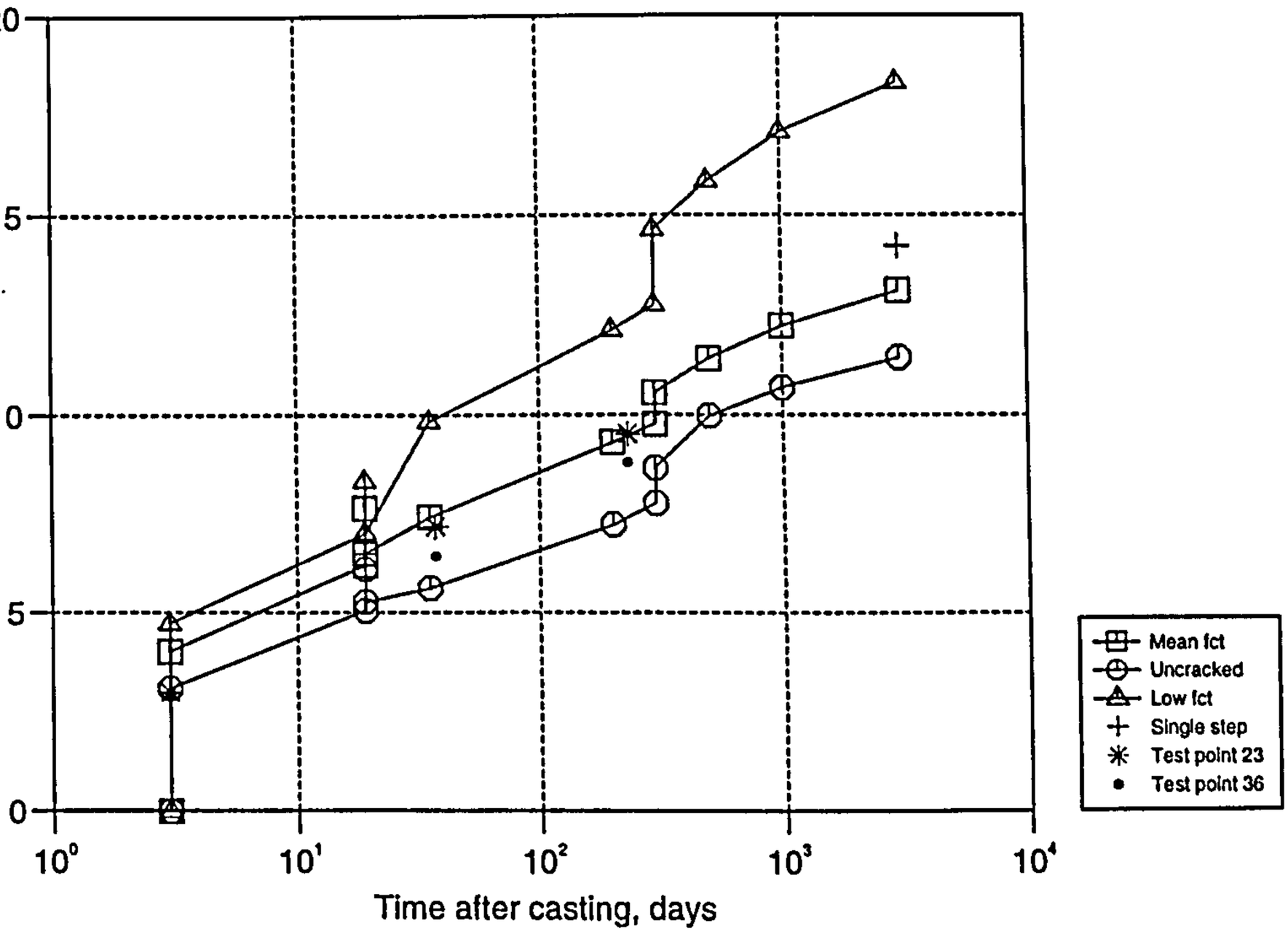


Figure 8.16 Deflection development with time: internal panel, floor 6

8.5 Contribution of creep and shrinkage

To identify the relative contributions of creep and shrinkage on long-term deflections, four cases have been considered in the analysis of floor 3:

- with creep and shrinkage contributions.
- with only shrinkage strains and ignoring creep.
- with only creep contributions and ignoring shrinkage.
- ignoring both creep and shrinkage (i.e. the change in deflection is only due to changes in load, cracking and loss of tension stiffening).

In all cases the mean tensile strength was used with all other material properties corresponding to Table 8.3.

The deflection with time curves for corner, external and internal panels are shown in Figs 8.17 to 8.19. The contribution of creep is much more significant than shrinkage. For the corner panel, deflections due to creep and shrinkage are 35.7 and 9.2% of the total deflection respectively. For external and internal panel the proportions are 35.8, 11.2 and 49.1, 8.1% respectively.

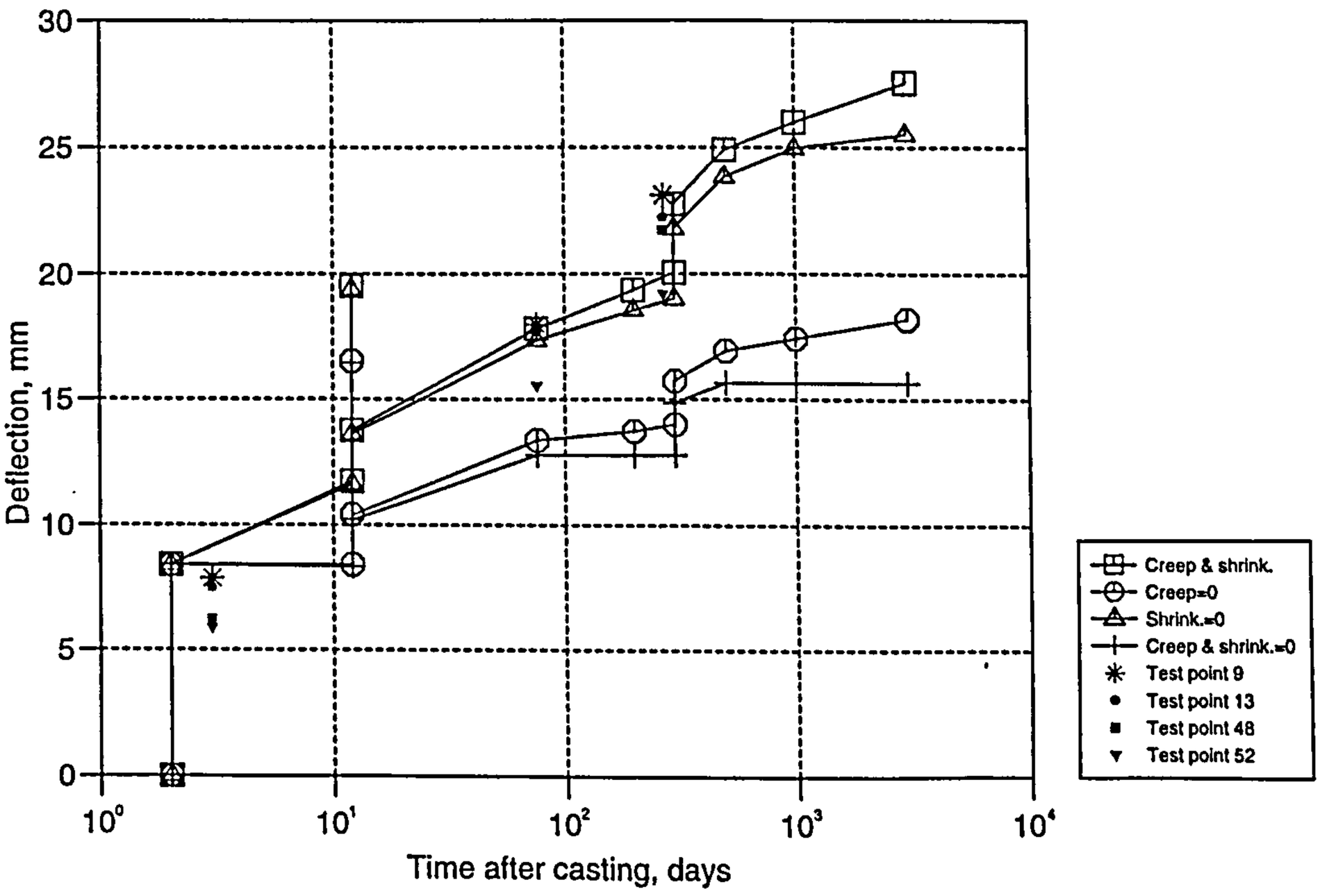


Figure 8.17 Contribution of creep and shrinkage: corner panel, floor 3

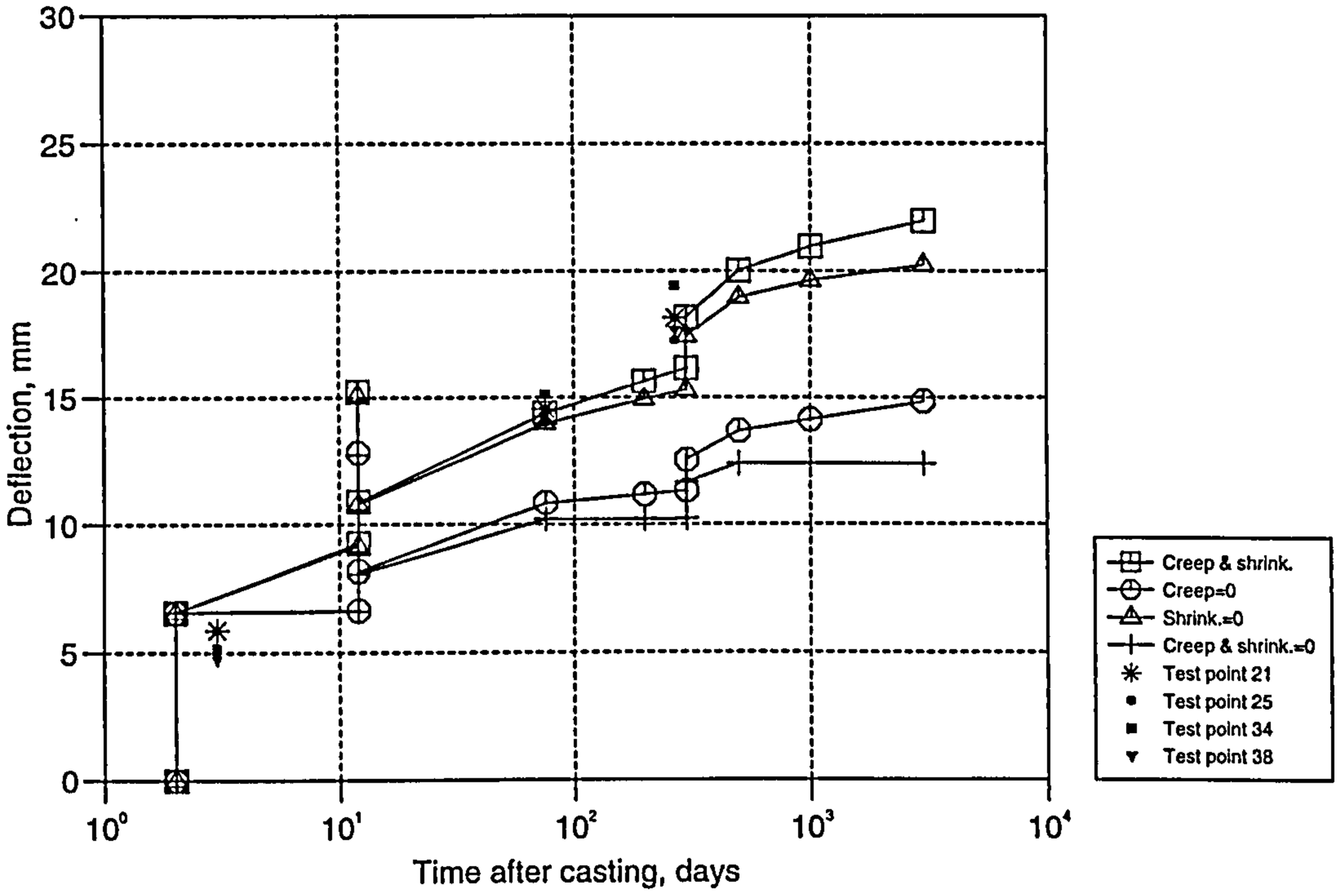


Figure 8.18 Contribution of creep and shrinkage: external panel, floor 3

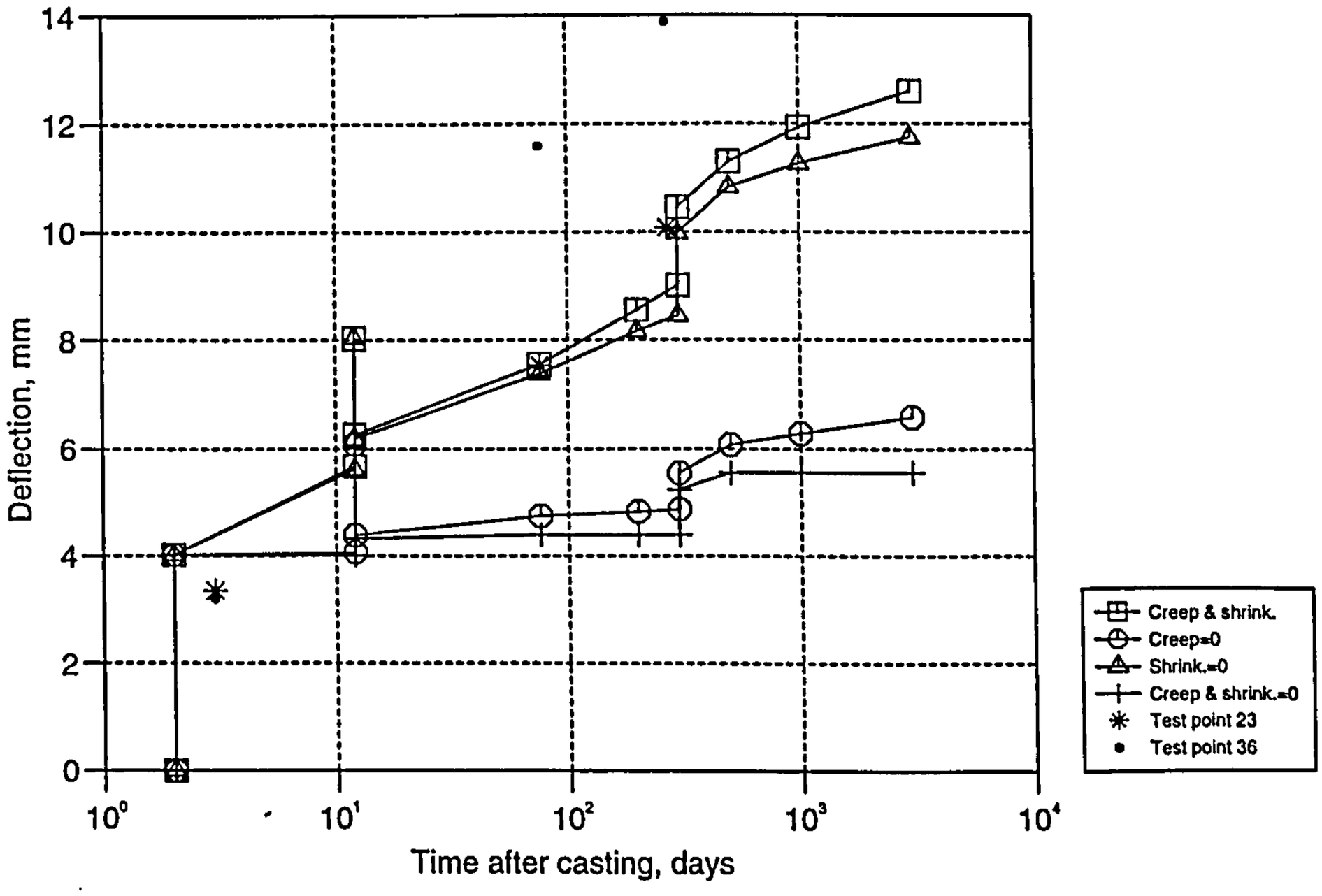


Figure 8.19 Contribution of creep and shrinkage: internal panel, floor 3

8.6 Contribution of reinforcement

The area of reinforcement provided and the reinforcement arrangements vary significantly between the floors due to different design and detailing methods adopted. The total weights of bending reinforcement calculated by Goodchild & Moss (1999) are 15.3, 14.5 and 25.5 tonnes for floor levels 3, 4 (if the full slab was designed by yield-line method) and 6 respectively. However, Figs 8.20 to 8.22, which compare measured deflections at the three floors show that floor 6 has greater deflection compared to floors 3 and 4. It shows that tensile strength, which determines the level of cracking, has a more significant influence on deflection than reinforcement.

To identify the relative contribution of reinforcement area and arrangement on deflection, the following cases have been studied:

- Floor 3 with reinforcement meshes corresponding to floor 3, 4 and 6.
- Floor 4 with reinforcement meshes corresponding to floor 4 and 3.
- Floor 6 with reinforcement meshes corresponding to floor 6 and 3.

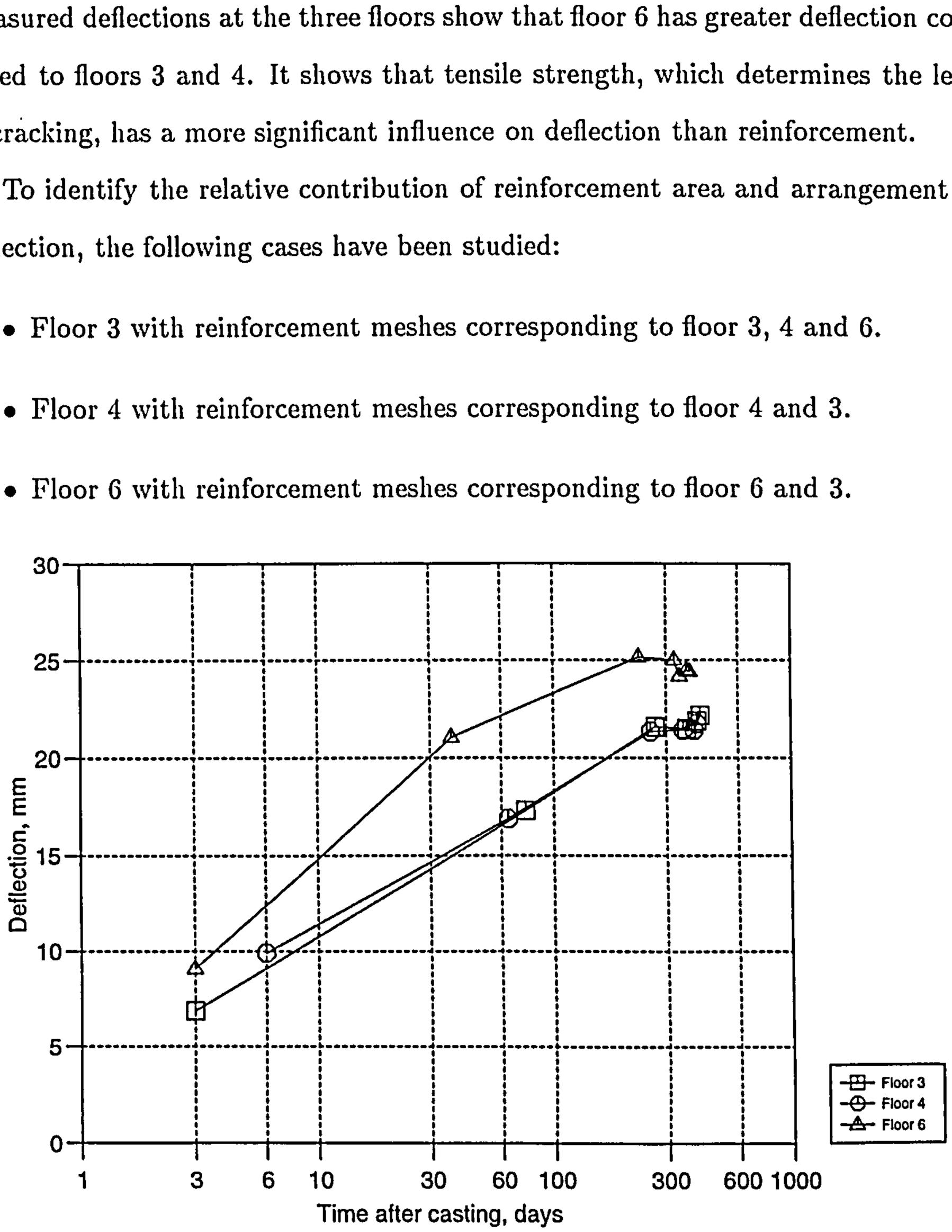


Figure 8.20 Comparison of measured deflections of different floors: corner panel

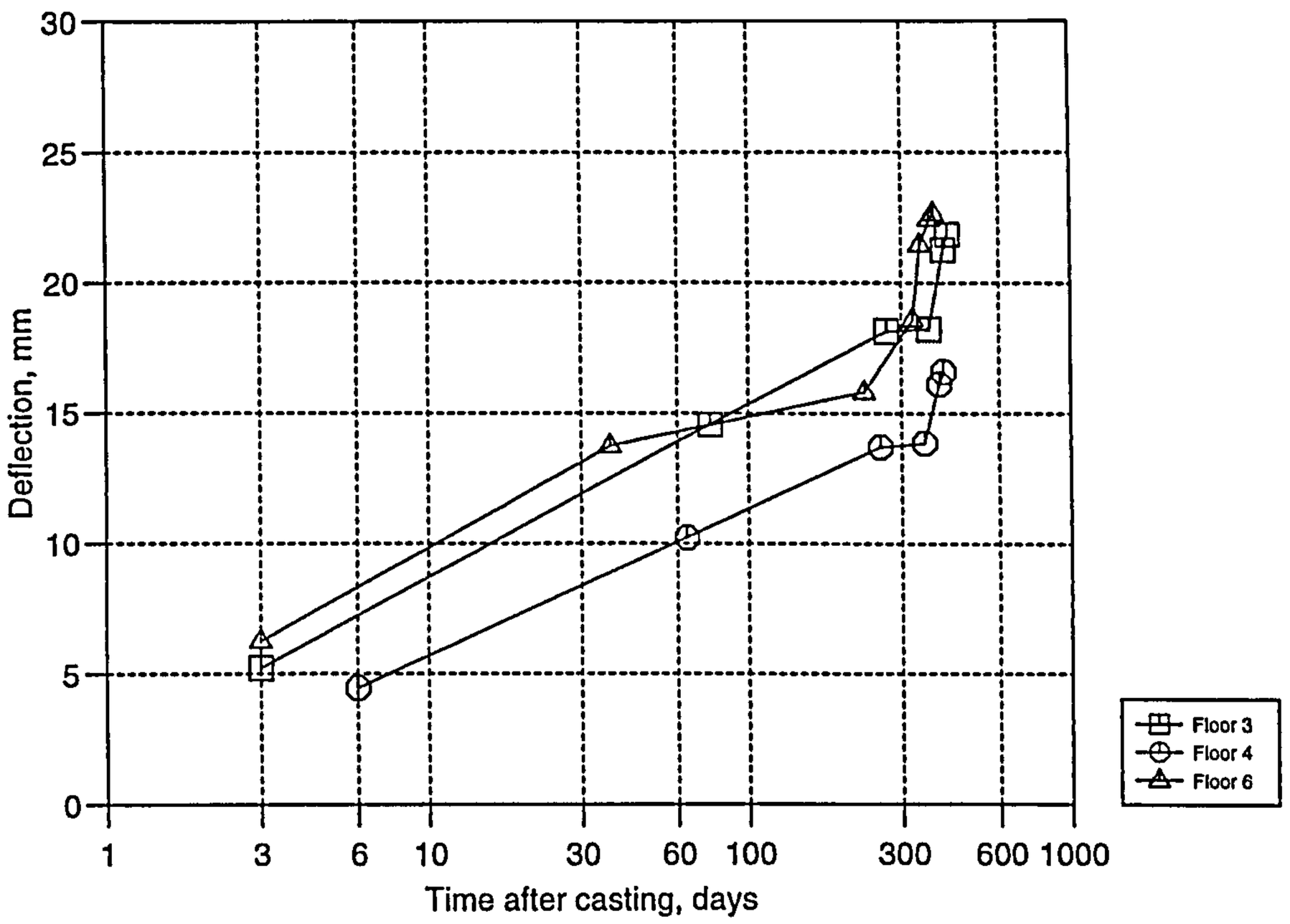


Figure 8.21 Comparison of measured deflections of different floors: external panel

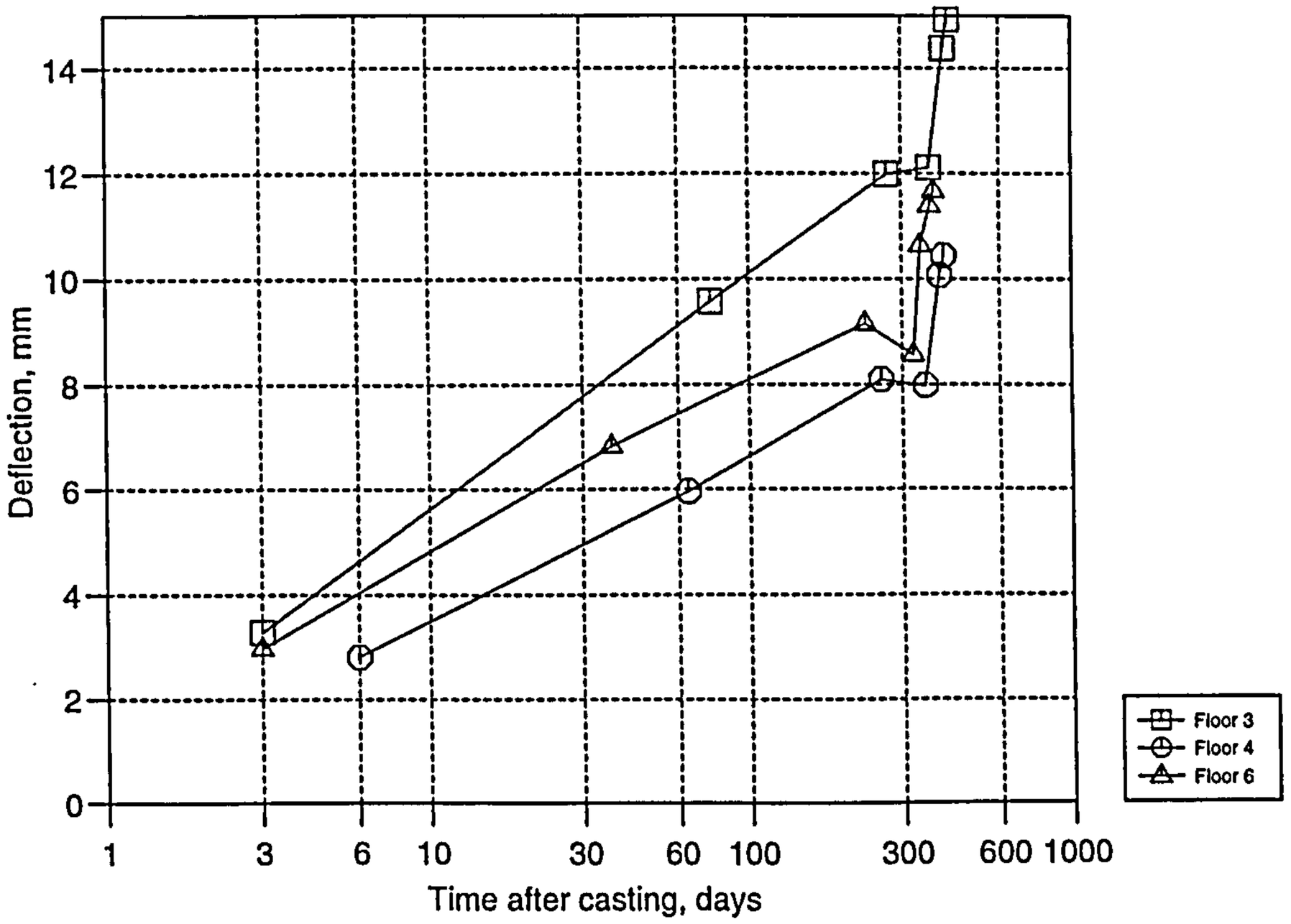


Figure 8.22 Comparison of measured deflections of different floors: internal panel

8.6.1 Reinforcement contribution: floor 3

Deflections of floor 3 for the corner, external and internal panels with three different reinforcement meshes are shown in Figs 8.23 to 8.25. The reinforcement mesh corresponding to floor 6 gives the smallest deflection while floor mesh 4, which was designed using yield-line analysis, gives the highest deflection. Using mesh 4 gives 10.6, 7.2, 11.8% higher deflections than those obtained with mesh 3 for corner, external and internal panels respectively at 3000 days. On the contrary, using mesh 6 resulted in reductions in the corresponding deflections by 5.3, 6.7, 9.2%. In terms of total bending reinforcement, floor 6 has the heaviest reinforcement while floors 4 and 3 have similar weights. The total reinforcement of floor 3 is slightly higher than that of floor 4, however, the former is found to be more effective in controlling deflection. Although the weight of floor 6 reinforcement is significantly higher, its effect on deflection reduction is not significant.

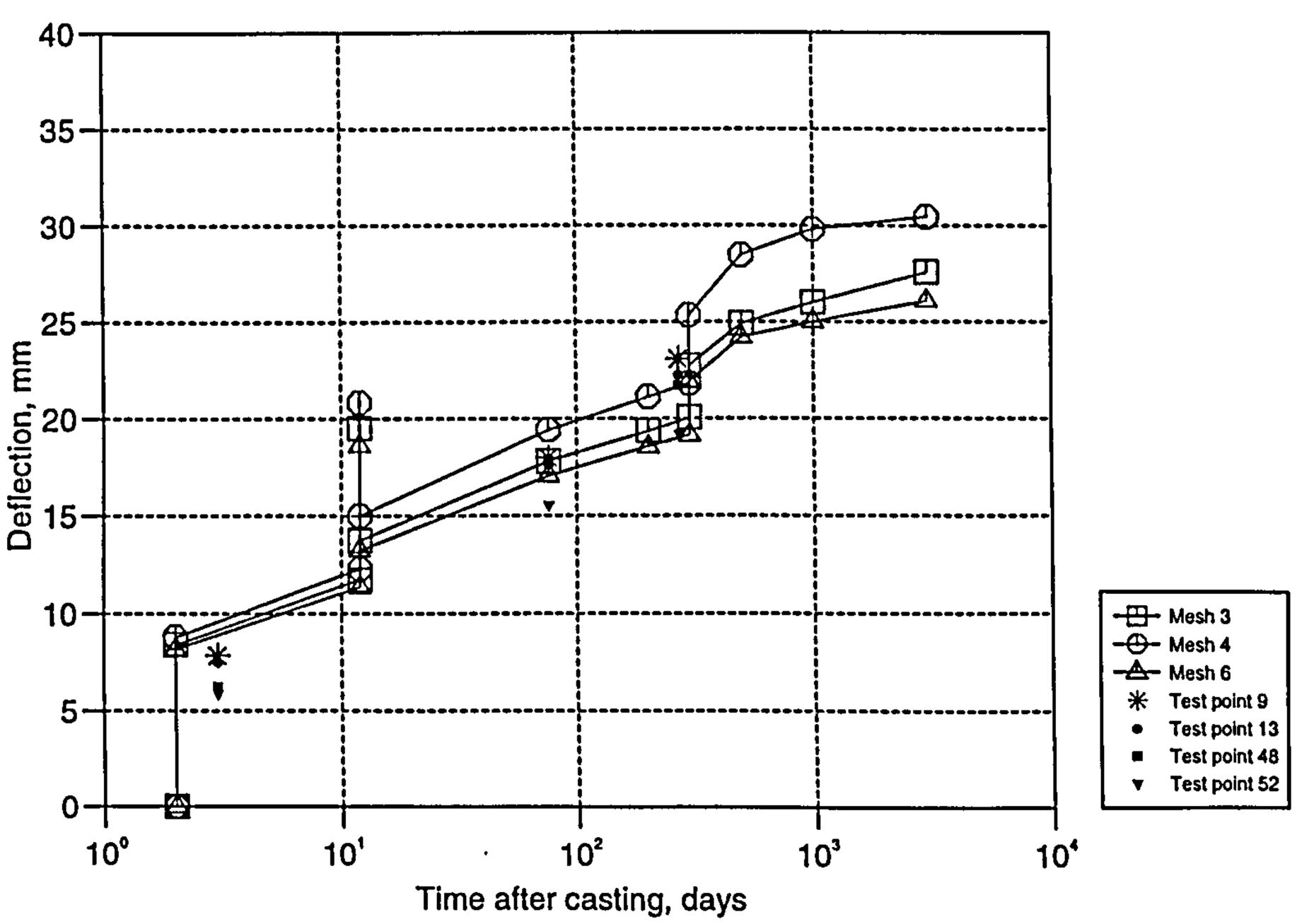


Figure 8.23 Contribution of reinforcement meshes: corner panel, floor 3

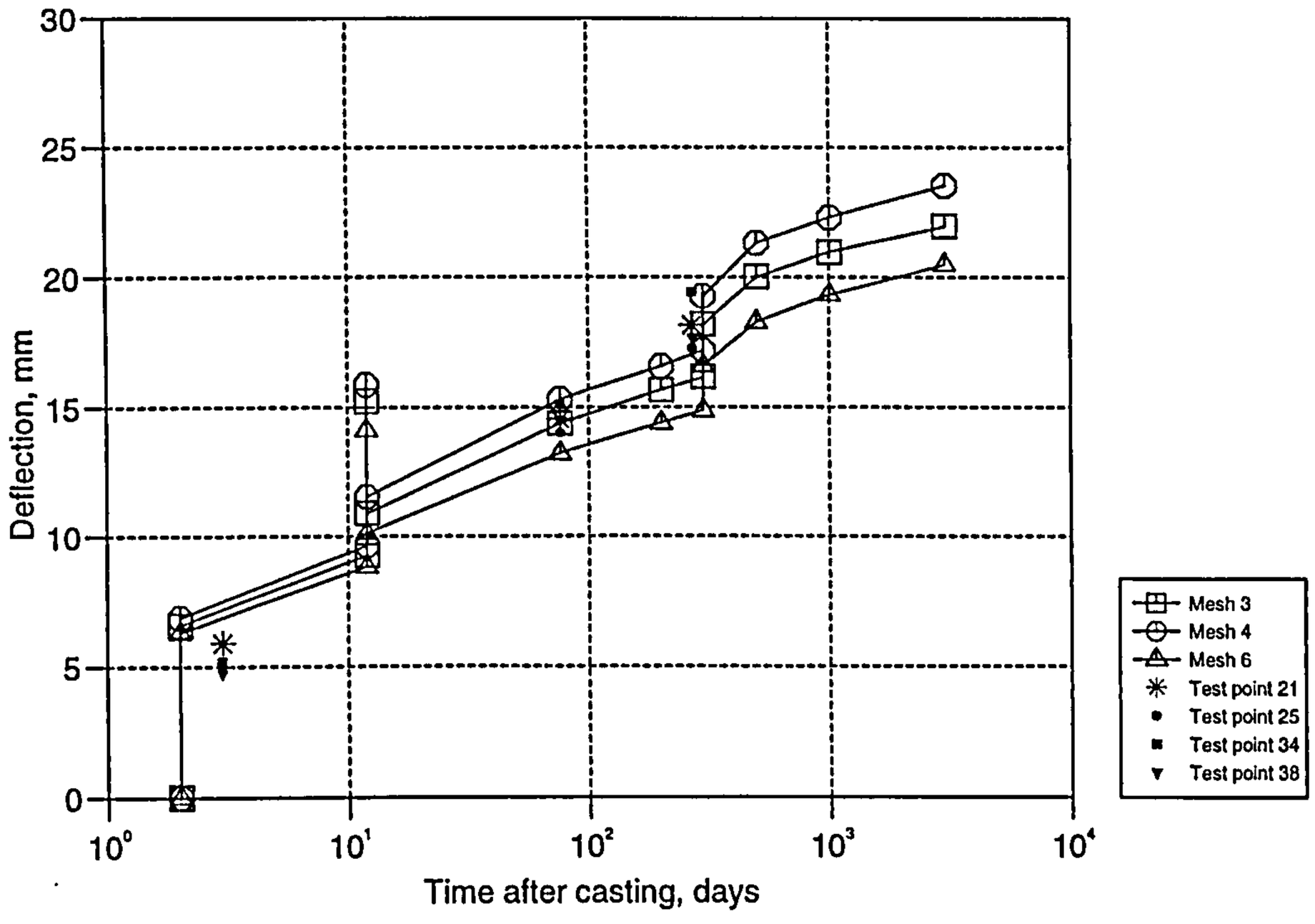


Figure 8.24 Contribution of reinforcement meshes: external panel, floor 3

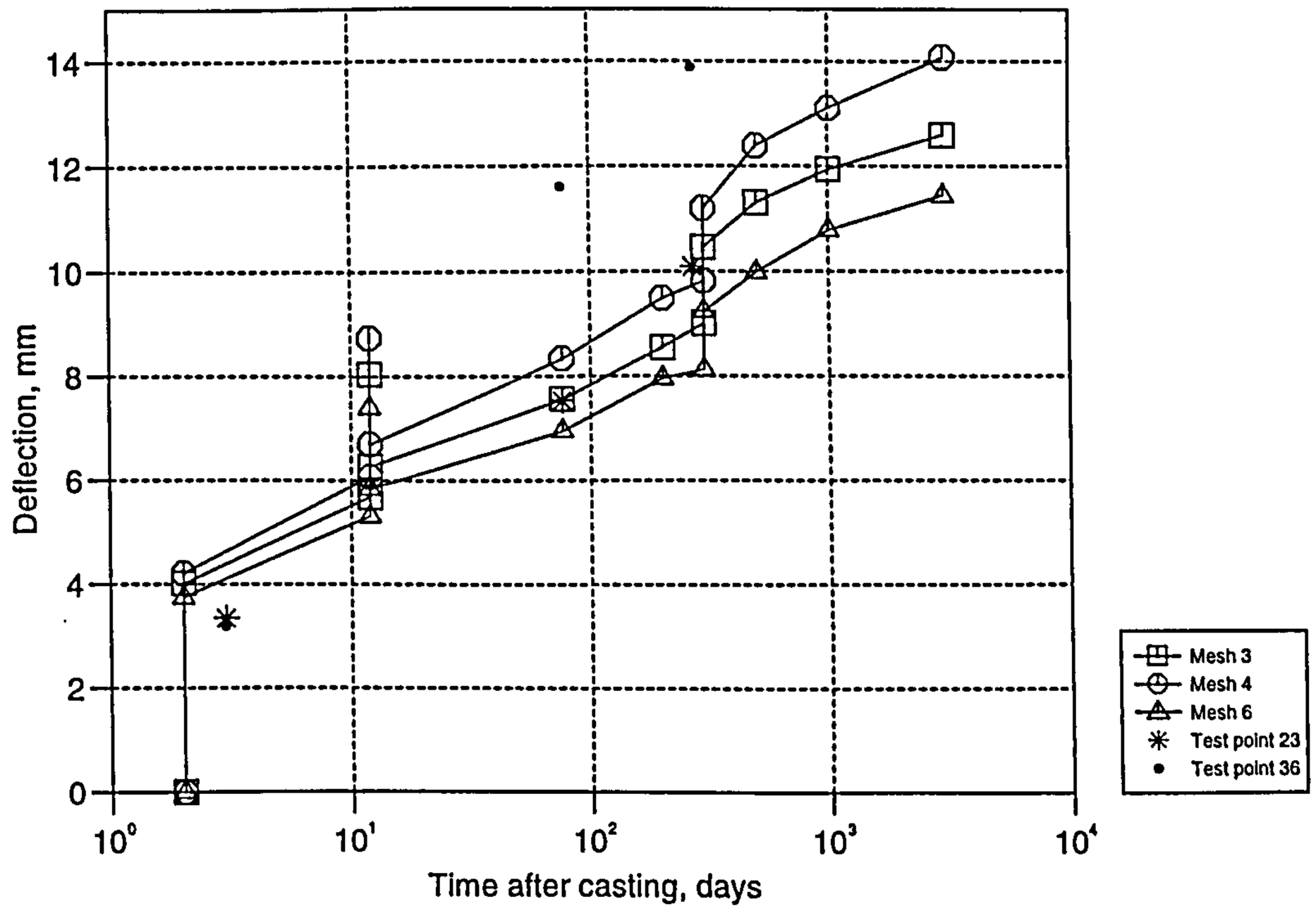


Figure 8.25 Contribution of reinforcement meshes: internal panel, floor 3

8.6.2 Reinforcement contribution: floor 4

Deflections of floor 4 for the corner, external and internal panels with two different reinforcement meshes are shown in Figs 8.26 to 8.28. The reinforcement mesh corresponding to floor 3 gives lower deflections than those obtained with floor mesh 4. 3000-day deflections are lowered by 10.4, 5.8 and 8.9% for corner, external and internal panels respectively.

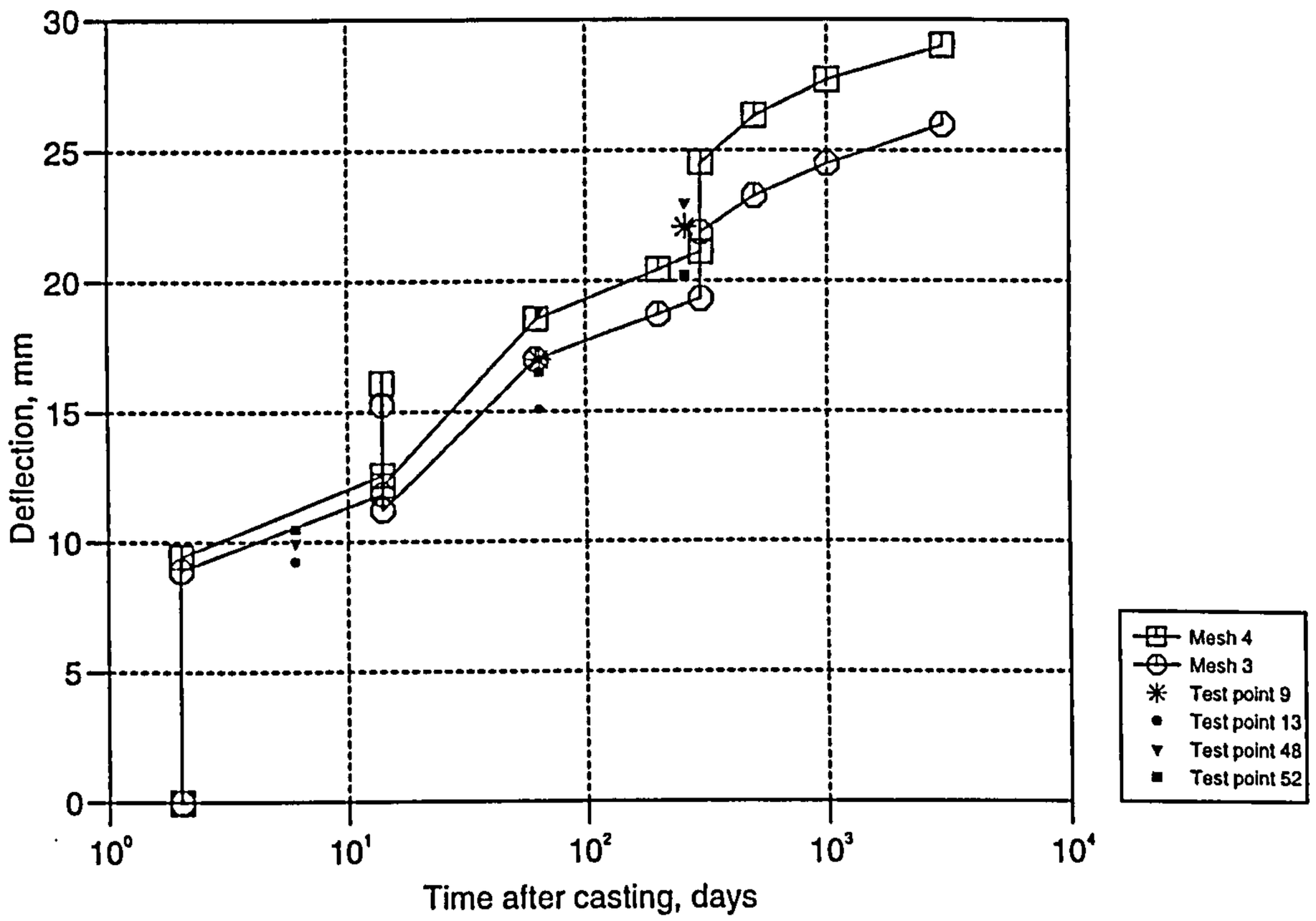


Figure 8.26 Contribution of reinforcement meshes: corner panel, floor 4

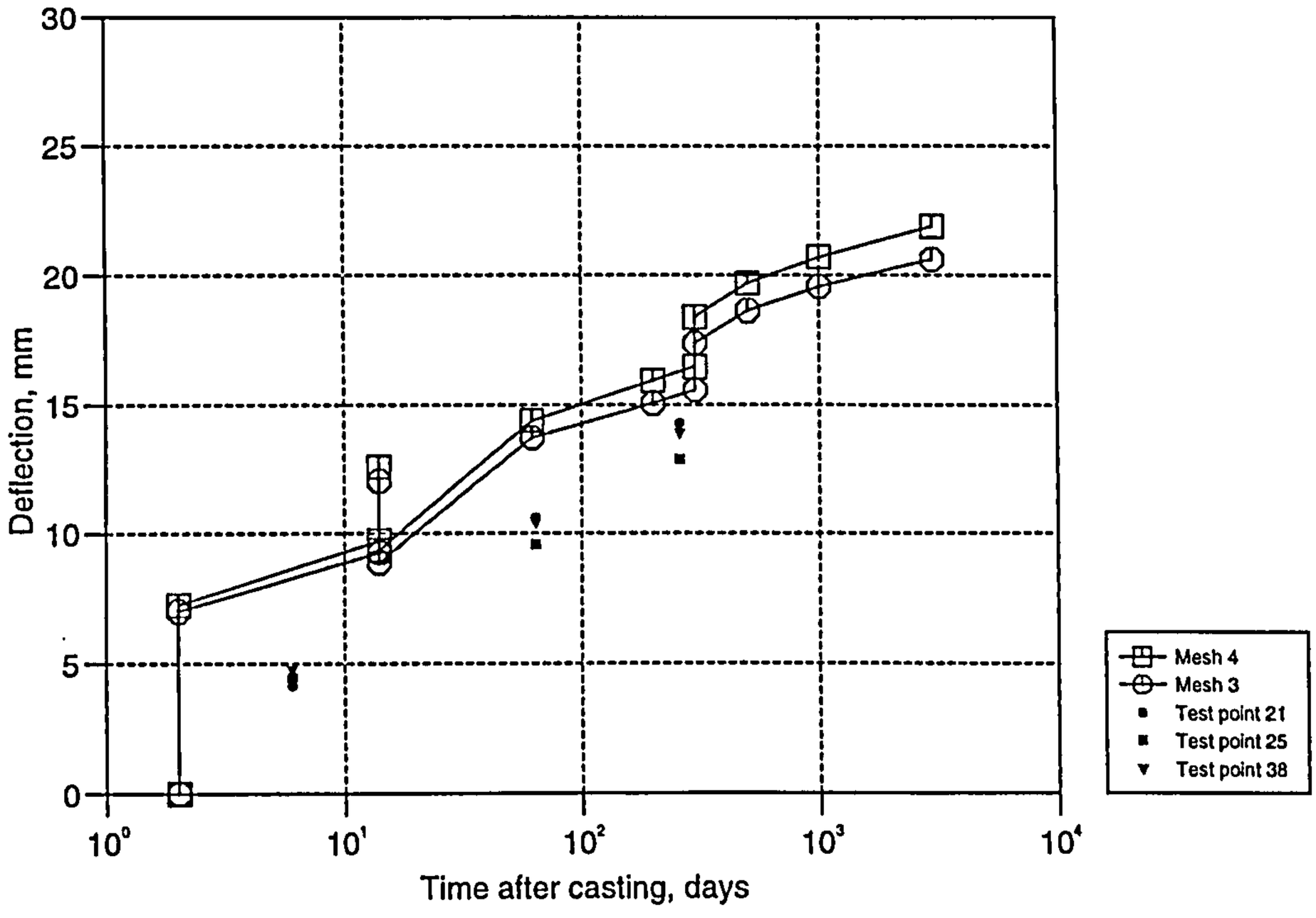


Figure 8.27 Contribution of reinforcement meshes: external panel, floor 4

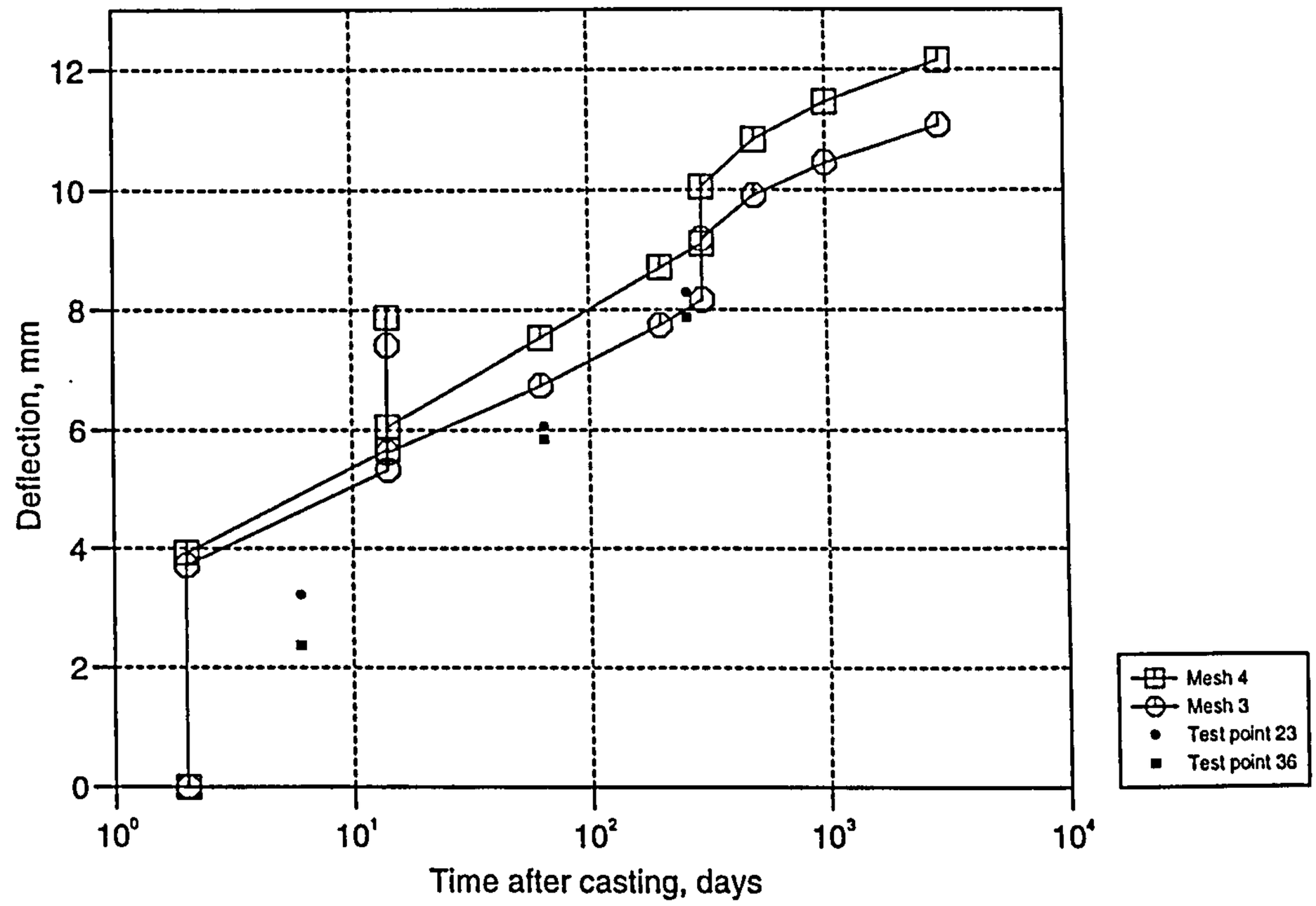


Figure 8.28 Contribution of reinforcement meshes: internal panel, floor 4

8.6.3 Reinforcement contribution: floor 6

Deflections of floor 6 for the corner, external and internal panels with two different reinforcement meshes are shown in Figs 8.29 to 8.31. Both meshes give similar deflections for the corner panel. For external and internal panels, mesh 3 gives 9.8 and 14.5% higher deflections than those obtained with mesh 6 at 3000 days. The total weight of reinforcement for floor 6 is significantly higher than that of floor 3, however, the effect of more steel on deflection is not appreciable.

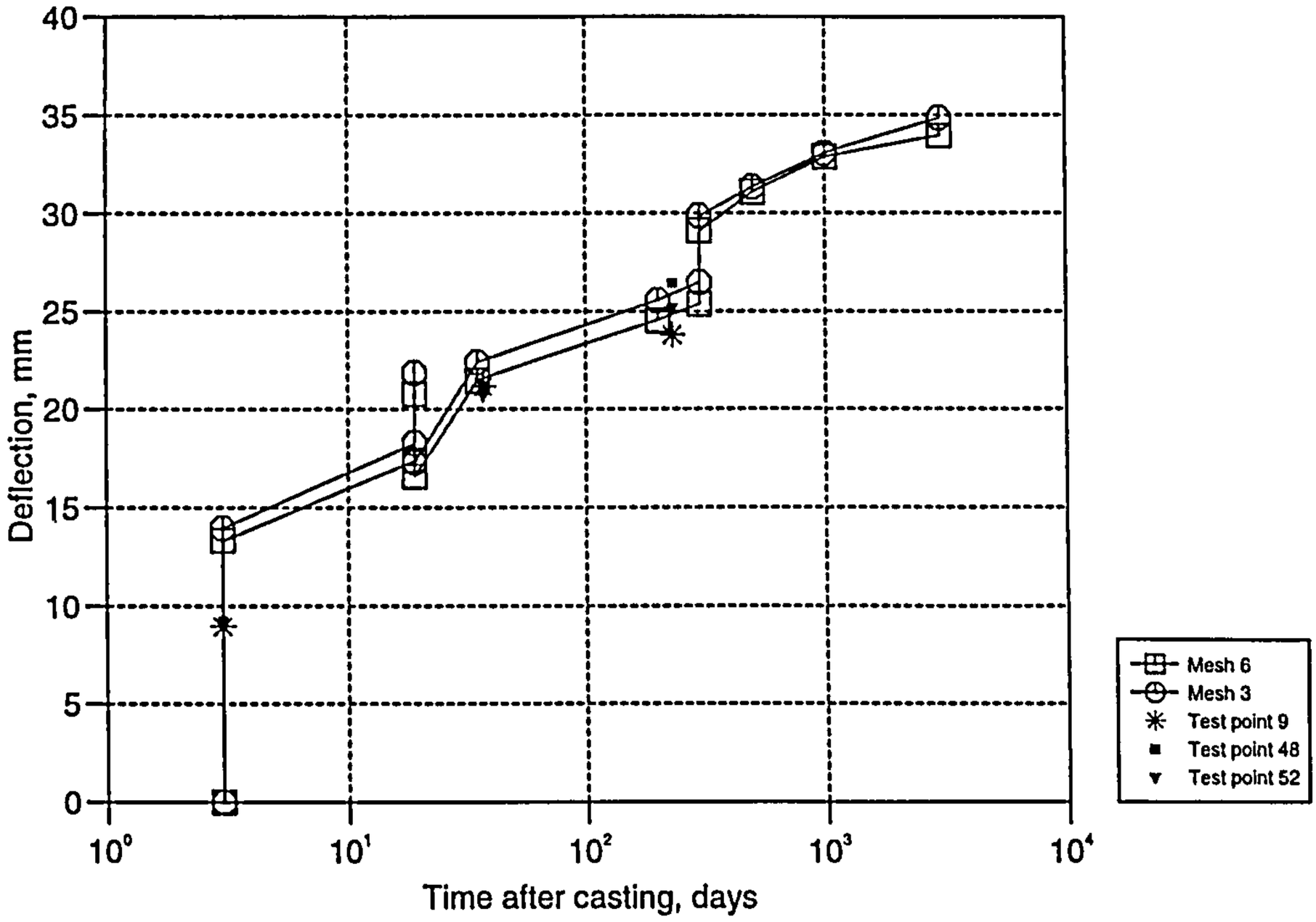


Figure 8.29 Contribution of reinforcement meshes: corner panel, floor 6

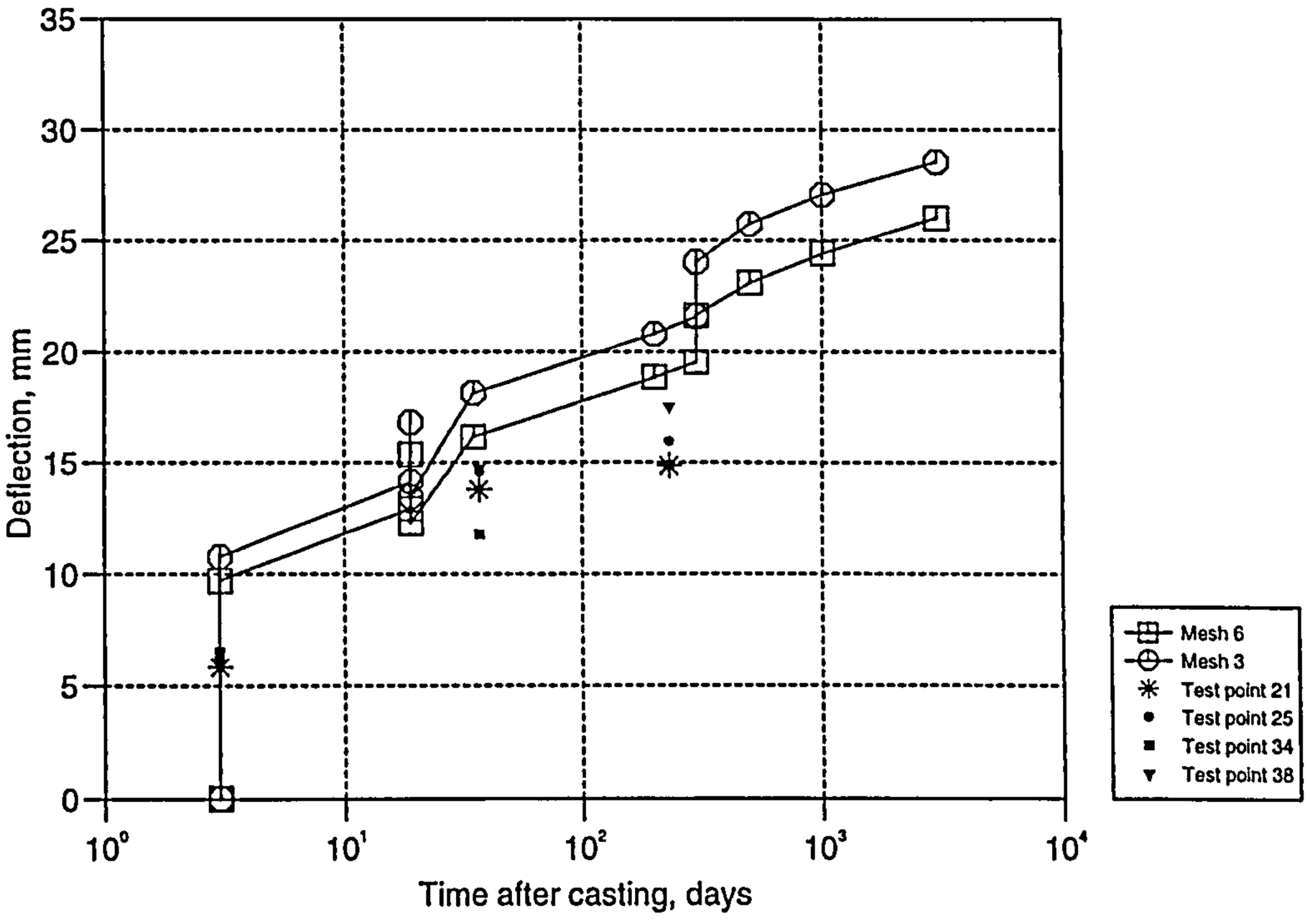


Figure 8.30 Contribution of reinforcement meshes: external panel, floor 6

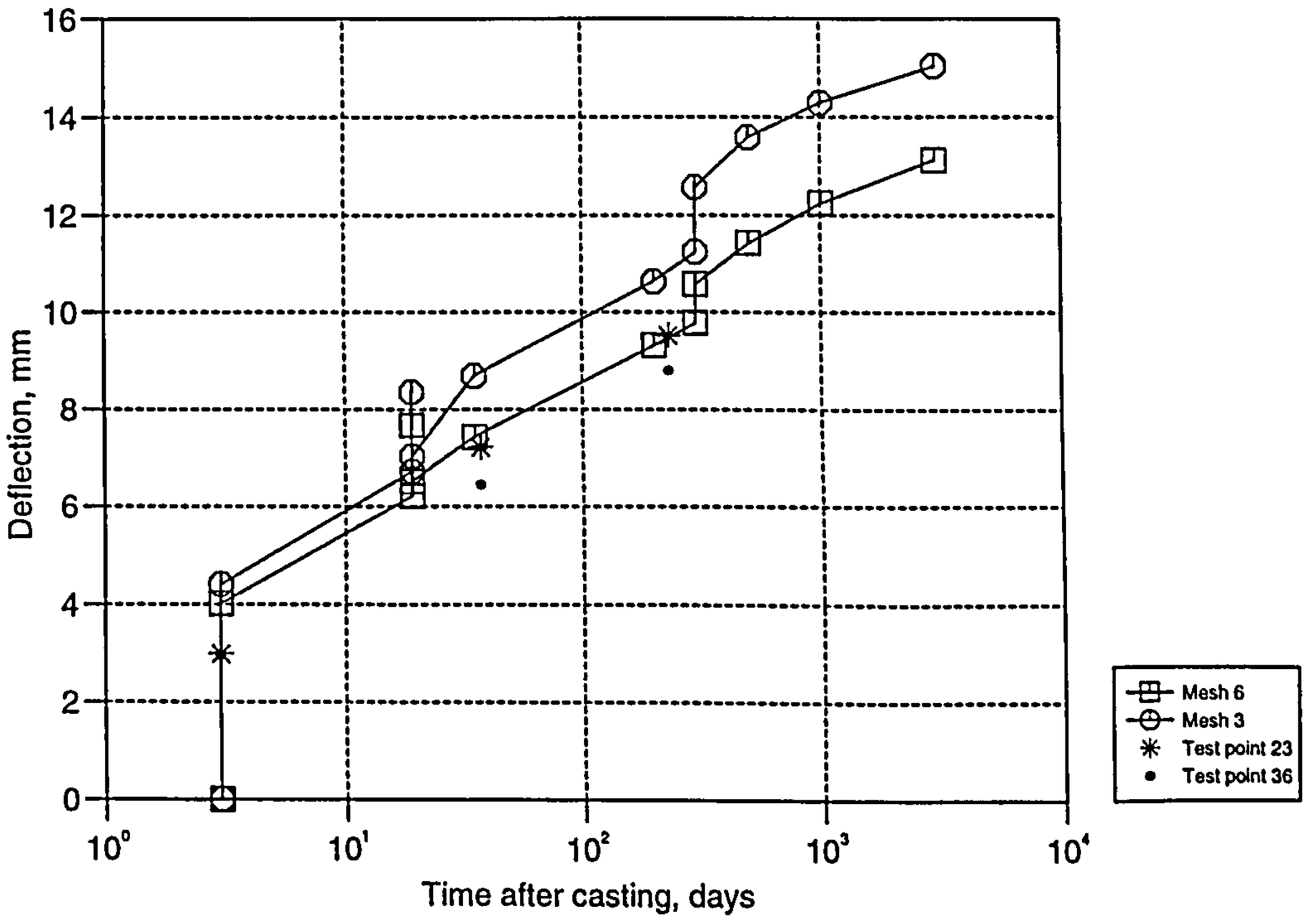


Figure 8.31 Contribution of reinforcement meshes: internal panel, floor 6

8.7 Pattern load

As part of the performance research project, the Cardington slabs are being loaded with a pattern imposed load of 3 kN/m^2. The panels are loaded only between grid-line 2 and 4 (see Fig. 8.2) so that the end bays to either side remain under self-weight. To model this loading, all the three slabs were analysed with corresponding simplified load history as before with the exception that imposed load was applied only on interior bays.

8.7.1 Deflections of floor 3

The development of deflections with time of floor 3 for the corner, external and internal panels are shown in Figs 8.32 to 8.34. FE results corresponding to both full imposed load on all panels and pattern-imposed load are plotted. It should be noted that the time of application of the pattern load has been changed to 382 days to represent the field loading, previously full imposed load was applied at 300 days. The deflection of the corner panel, as it was no longer loaded with the imposed load, follows almost the same curve as that under self-weight. The deflection of the external panel was slightly reduced under pattern load in comparison to full loading, whereas the deflection of internal panel was slightly increased.

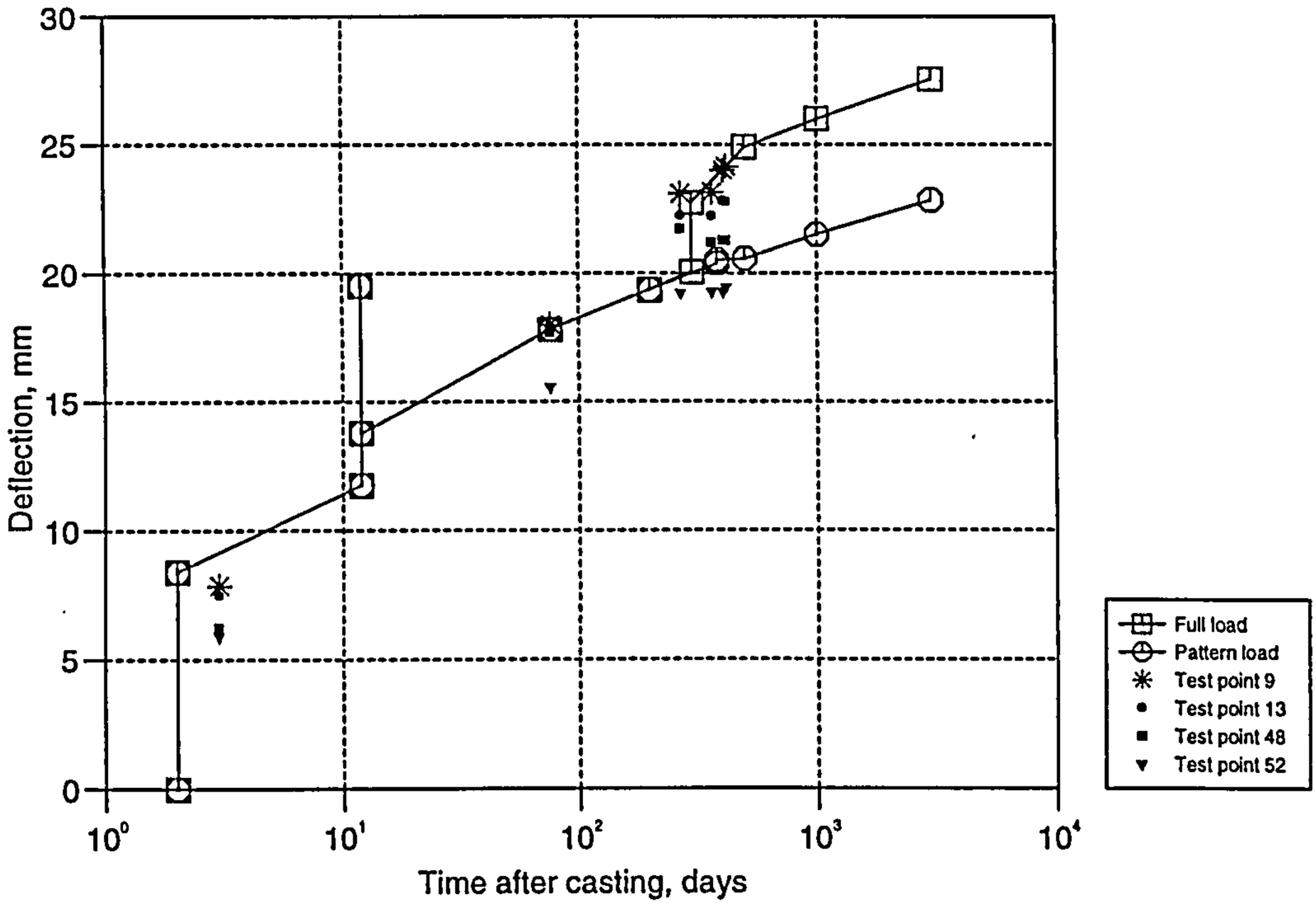


Figure 8.32 Pattern load: corner panel, floor 3

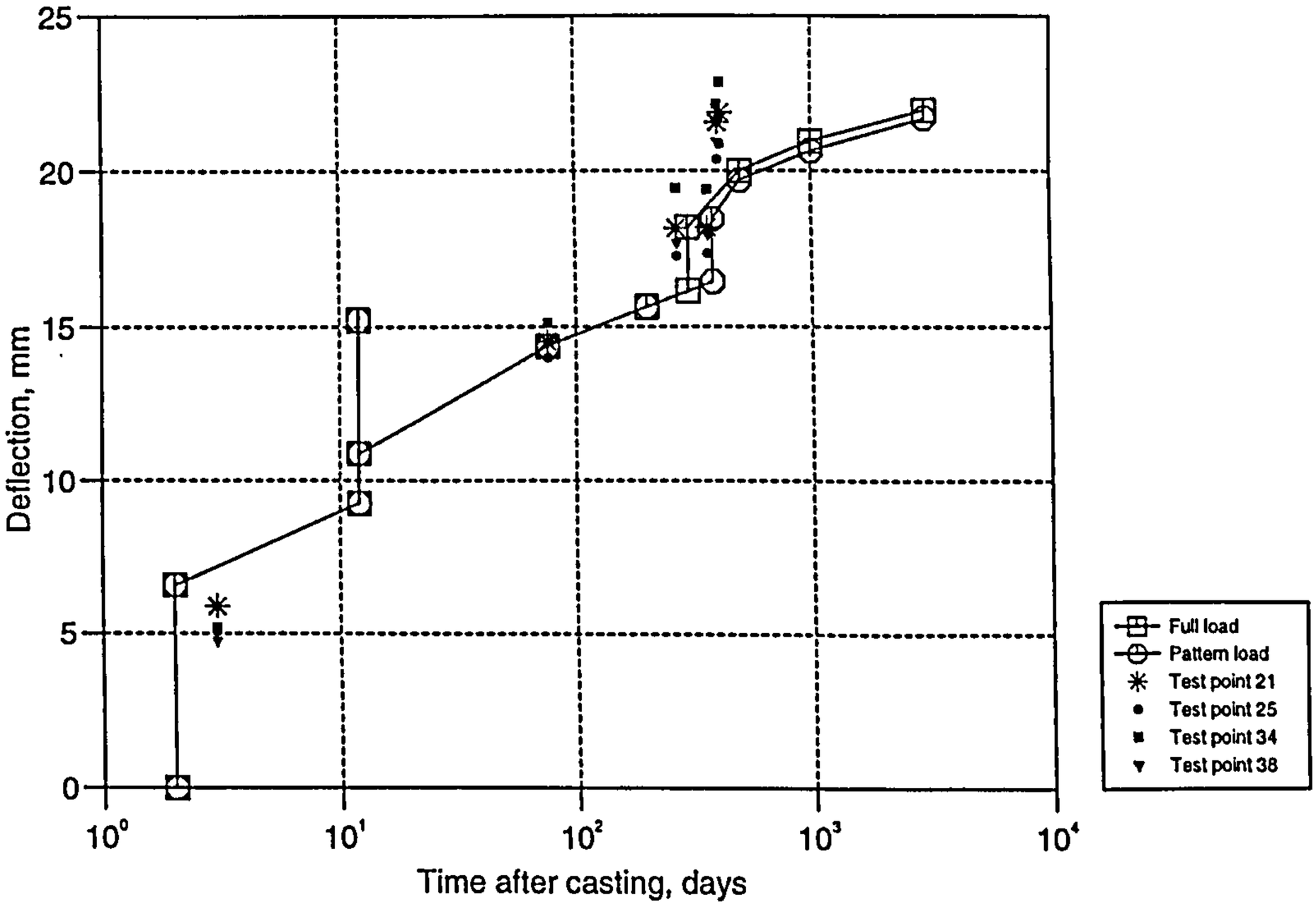


Figure 8.33 Pattern load: external panel, floor 3

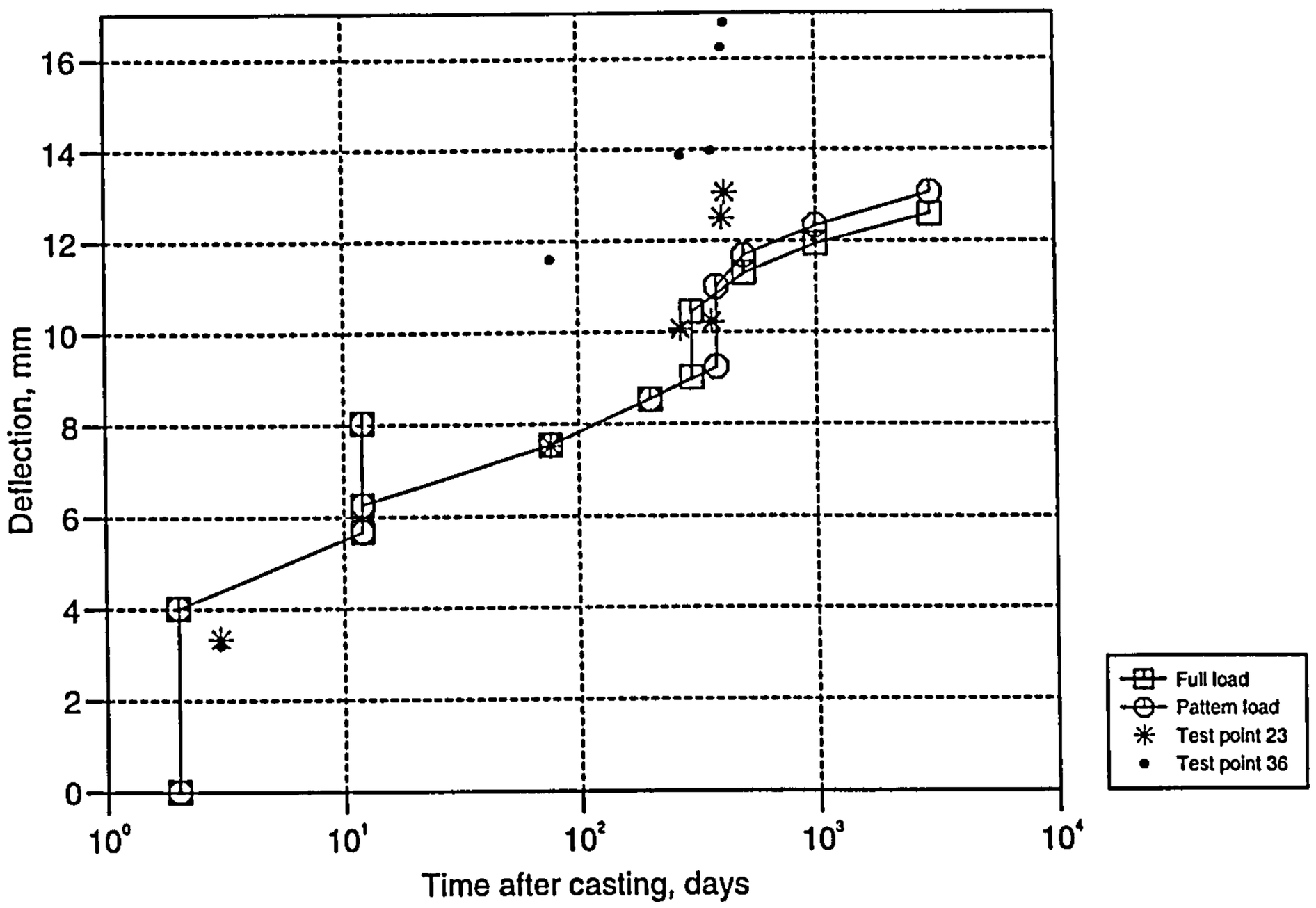


Figure 8.34 Pattern load: internal panel, floor 3

8.7.2 Deflections of floor 4

The development of deflections with time of floor 4 for the corner, external and internal panels are shown in Figs 8.35 to 8.37. FE results corresponding to both full imposed load on all panels and pattern-imposed load are plotted. The time of application of pattern load has been changed to 370 days to represent the field loading, previously full imposed load was applied at 300 days. Deflections under pattern-imposed load follow the same trend as those of floor 3.

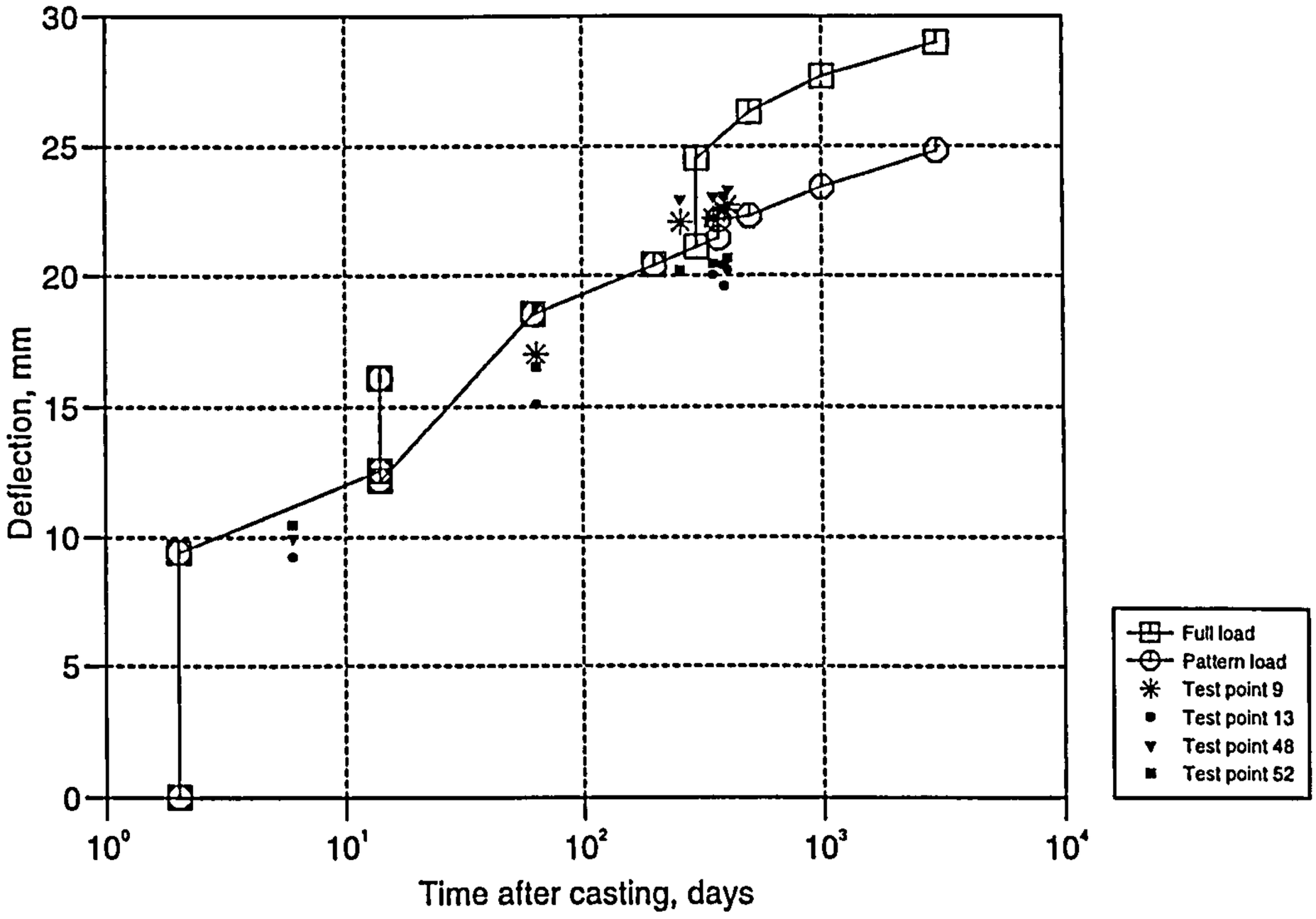


Figure 8.35 Pattern load: corner panel, floor 4

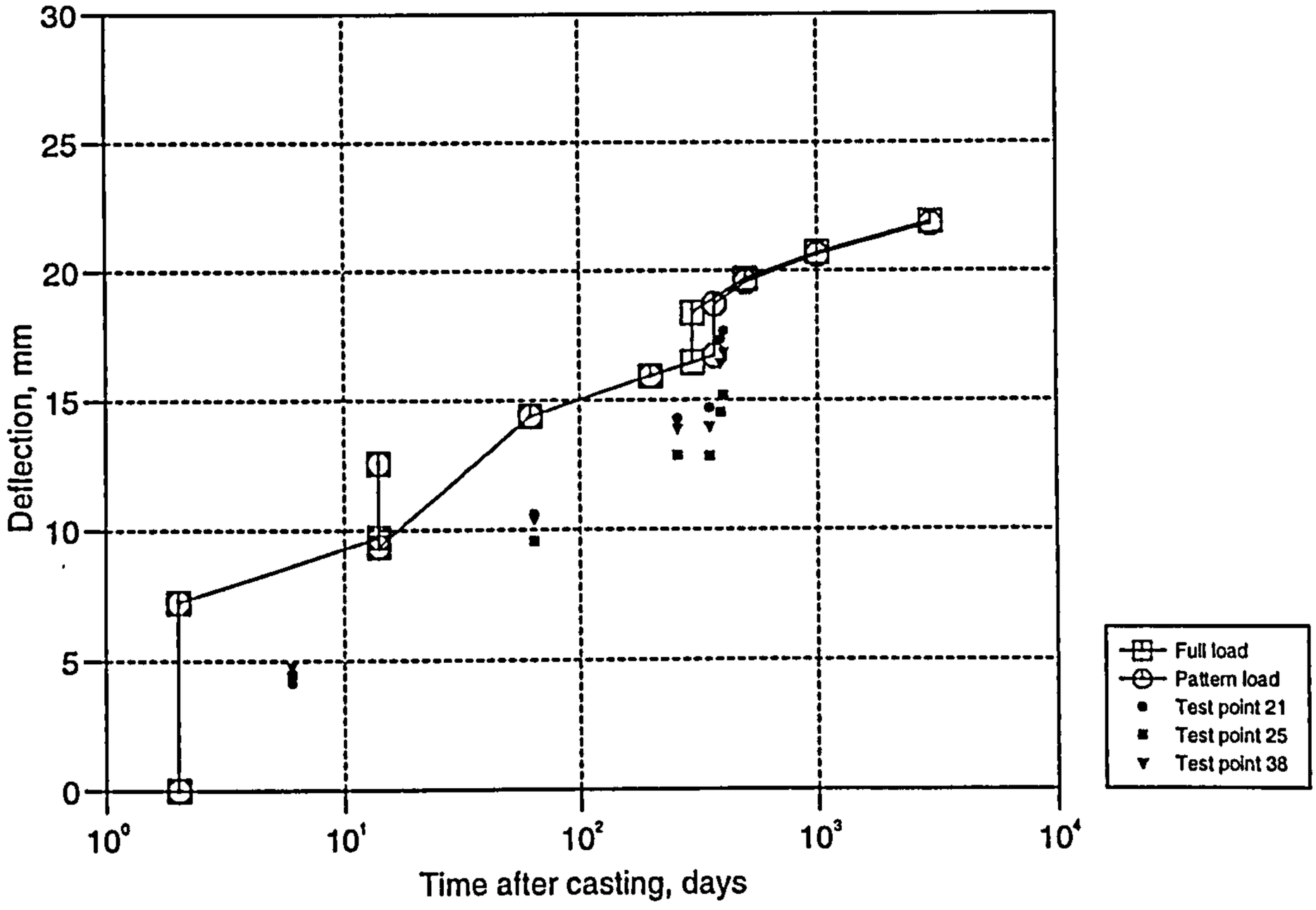


Figure 8.36 Pattern load: external panel, floor 4

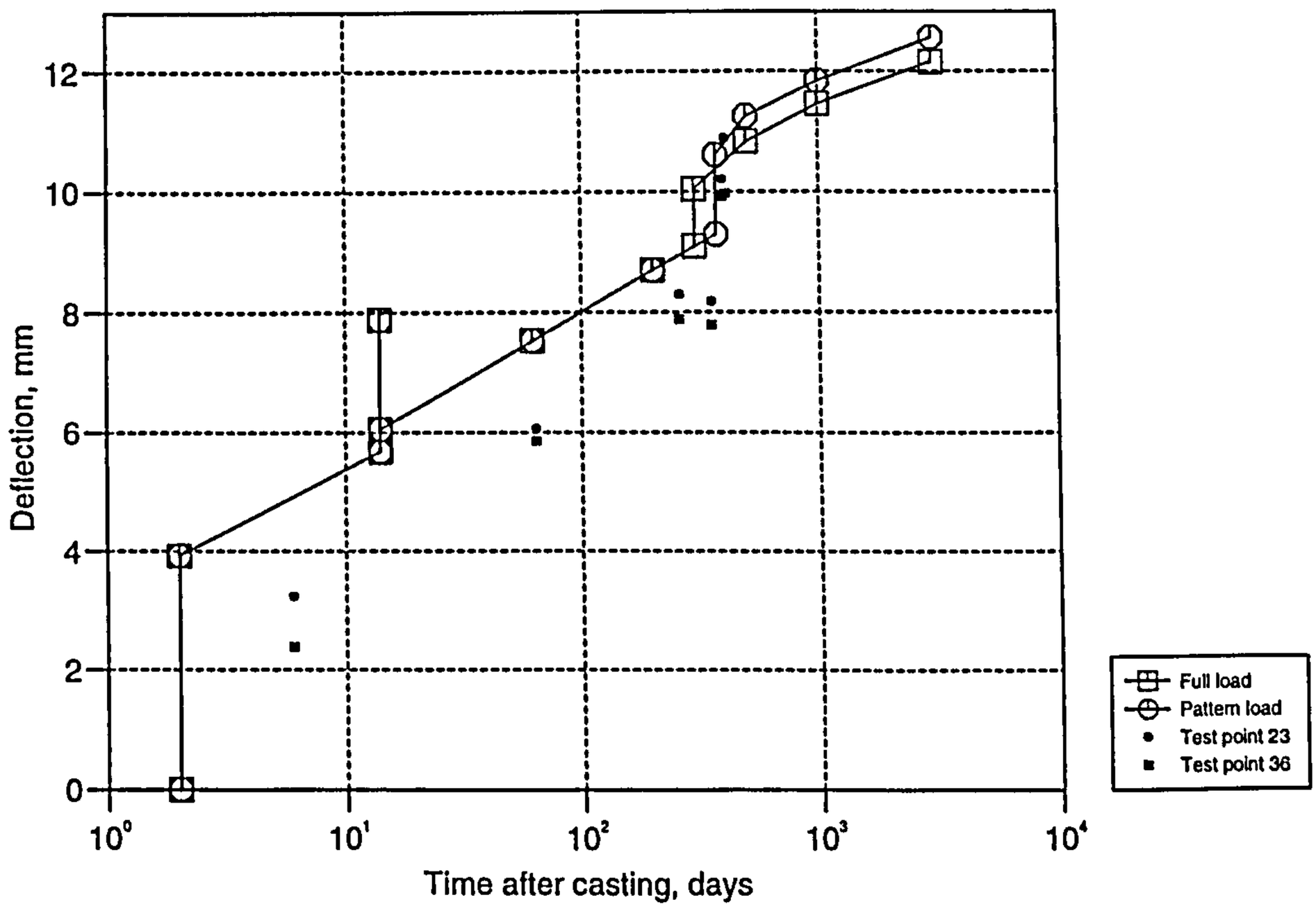


Figure 8.37 Pattern load: internal panel, floor 4

8.7.3 Deflections of floor 6

The development of deflections with time of floor 6 for the corner, external and internal panels are shown in Figs 8.38 to 8.40. FE results corresponding to both full imposed load on all panels and pattern-imposed load are plotted. The time of application of pattern load has been changed to 343 days to represent the field loading, previously full imposed load was applied at 300 days. Deflections under pattern-imposed load follow the same trend as those of floors 3 and 4.

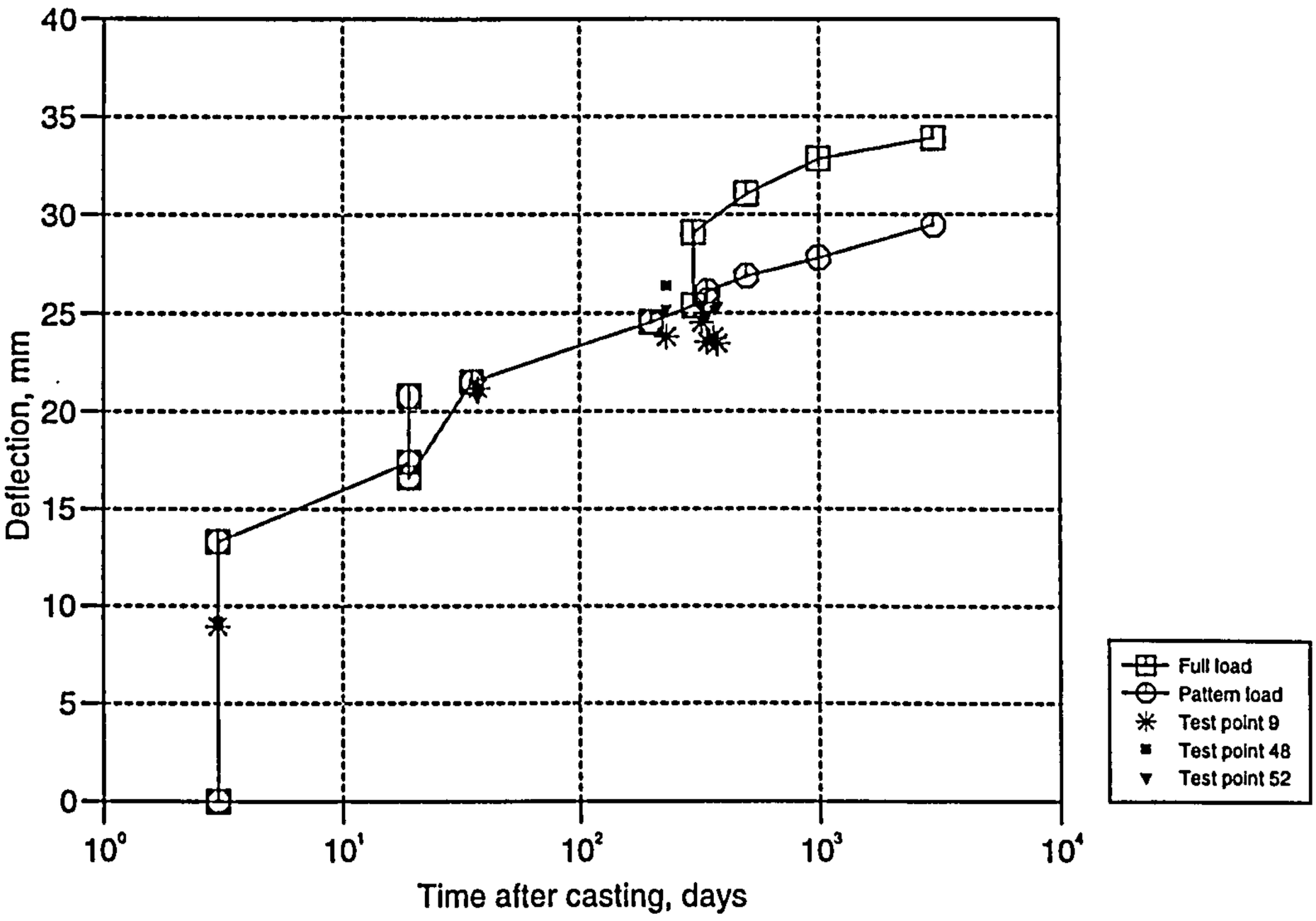


Figure 8.38 Pattern load: corner panel, floor 6

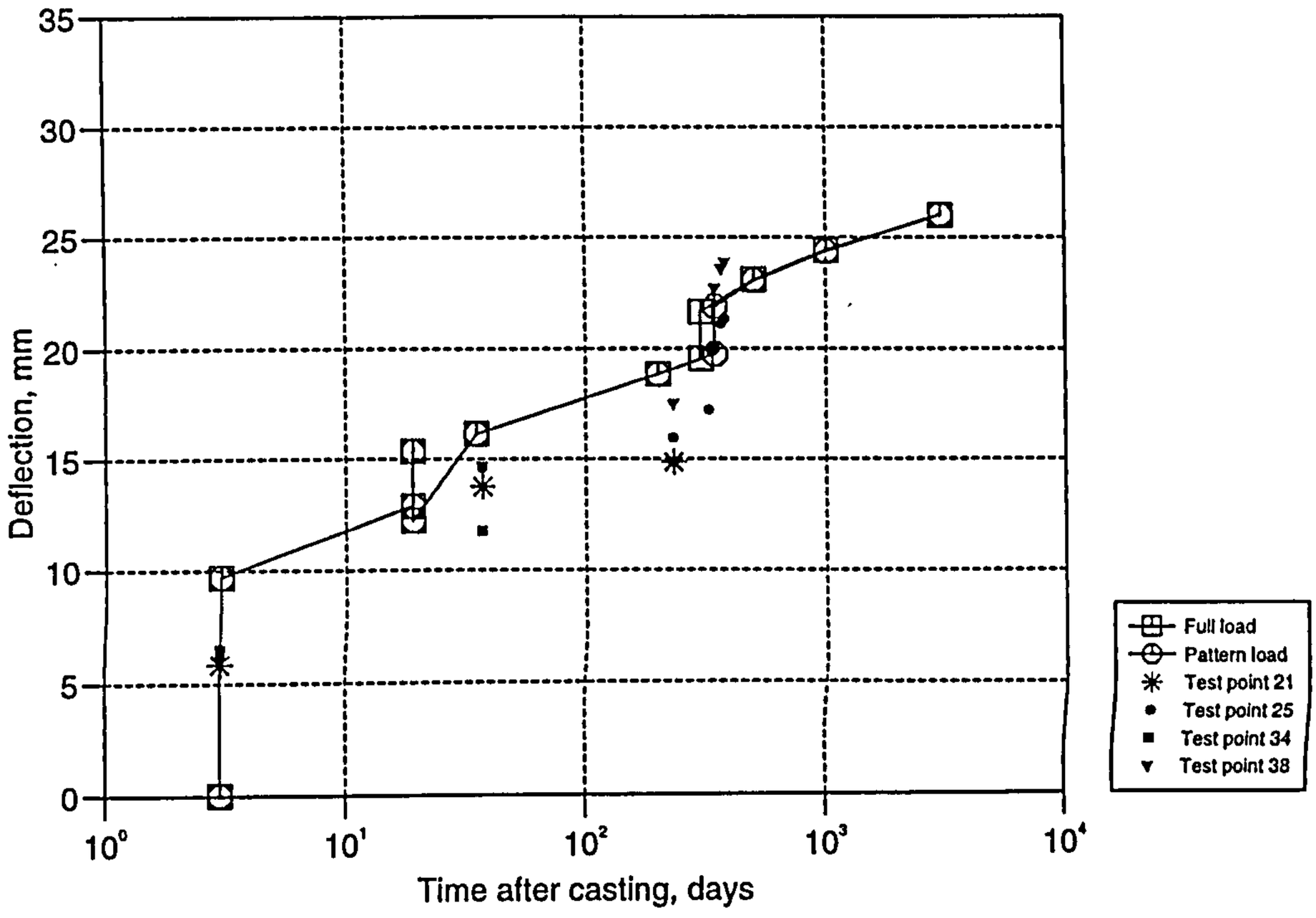


Figure 8.39 Pattern load: external panel, floor 6

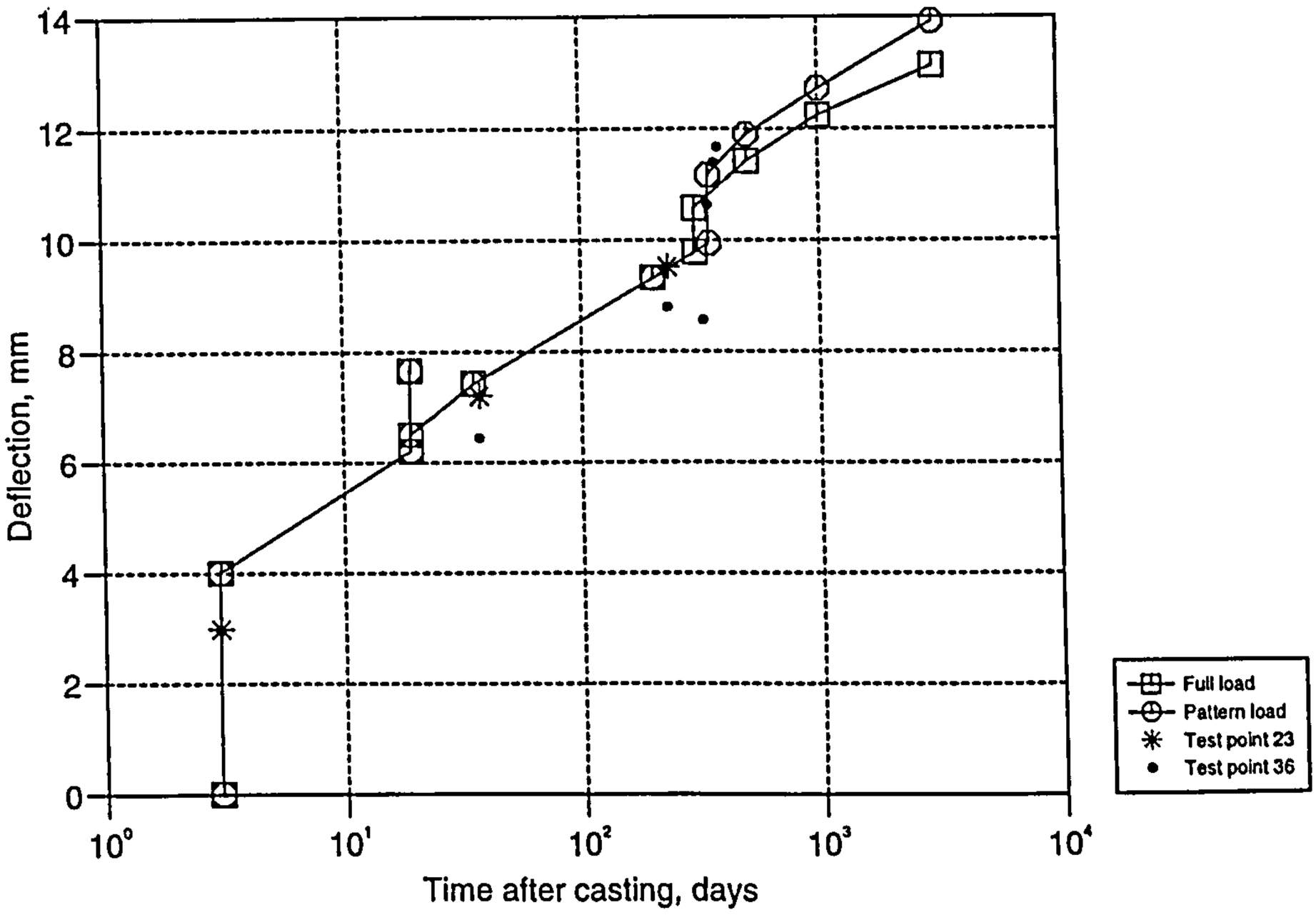


Figure 8.40 Pattern load: internal panel, floor 6

8.8 Conclusions

The method described in Chapter 6 has been found to realistically model the deflection history of the Cardington full-scale building floor. In most cases, measured deflections agree reasonably well with those predicted with mean tensile strength. Deflections were measured by precise levelling which ensured a reasonable level of accuracy. It should be pointed out that the level of cracking can drastically affect deflections, as shown in section 8.4. The level of cracking, in turn, depends on the tensile strength, which can vary appreciably for concretes designed for the same strength. There is also the possibility that other parameters which influence cracking moment, i.e. the actual thickness of the slab and the position of reinforcement may vary significantly in the field. Cracking can also be affected by the presence of in-plane restraint. Thus the cracking moment of a slab may be very different from that estimated in the design office. For the Cardington building, mean tensile strengths were calculated from splitting cylinder test or estimated from cube strength test results. In-plane restraint is believed to be very low for Cardington building since all the slabs were poured in one day and the steel bracing was positioned after the slabs were cast. It should also be noted that the steel flats used for bracing are considerably less effective than assumed in the design due to bowing resulting from initial lack of fit. The slab thickness and position of reinforcement were assumed to be in accordance with the design. Spot checks at different positions (edges and holes) at different floors showed that the slab thickness varies between 250 to 260 mm but in most cases is close to the specified 250 mm. In practice, significant variations from the specified thickness may occur in the field. Modelling deflections very accurately is virtually impossible due to the inherent variability in material and geometric properties, but predictions with mean creep and shrinkage properties by MC-90 equations seem reasonable if a realistic estimate of deflections is required. Further research is required to establish the tensile strength that should be used in analysis since it is related to restraint.

It should be pointed out that the total and incremental allowable deflections suggested by EC2 are 30 mm (span/250) and 15 mm (span/500) respectively for

these slabs. The latter is satisfied in all cases according to current calculations with mean tensile strength. However, the total deflection criteria is violated slightly for the corner panel of floor 6 and is close to 30 mm for floors 3 and 4. It seems that use of EC2 guidelines for permissible l/d ratios, (especially if additional tensile steel is provided to control deflection) may lead to total long-term deflections greater than span/250. If the Cardington slabs were constructed with a three-shore method as described in section 7.5.1, deflections would clearly be higher and at least the total deflection criteria would be violated at the corner and external panels.

The choice of β_2=0.5 to model loss of tension stiffening after the application of construction load seems reasonable. This reduces the cracking moment by about 30%. The present model does not include the effect of tensile stresses induced by restraint of shrinkage, which effectively reduces the cracking moment. However, the level of restraint is very small in case of Cardington slabs. In general, a value of β_2 smaller than 0.5 may be required to include the effect of stress induced by restraint of shrinkage in addition to loss of tension stiffening.

The single-step method for calculating long-term deflection with a minimum of computation has been found to be very efficient in modelling the Cardington deflections. This is particularly true because cracking under imposed load is critical for all three slabs. If construction load were to be critical, single-step method would give smaller deflections than the actual ones.

The effect of creep to long-term deflection is found to be more significant than that of shrinkage (see section 8.5).

The amount of reinforcement steel and its distribution has some effect on deflection, but the effect is not very significant. Analyses were carried out by interchanging reinforcement meshes between three floors, which are designed with different methods (equivalent frame and yield-line) and detailed with different arrangements. The results indicate that deflections are not influenced appreciably by the difference in three meshes.

Imposed loads applied in pattern or applied all over the slab do not make much difference for panels which are loaded in both cases. Panels which are not loaded with imposed load follow the curve under self-weight.

Chapter 9

Conclusions

9.1 Introduction

The principal objective of this thesis is to develop an FE-based numerical method to predict the long-term deflection of flat slabs under a time-varying load. Deflection modelling using non-linear FE analysis, for slabs under uniform load, has been the subject of much research over the last three decades. In recent years, the realistic estimate of slab deflections at the serviceability limit state has become more important due to the increasing use of high-strength materials. There is clearly a need to develop a method for predicting deflections that accounts for the full load history of a slab, including construction loads which often govern the level of cracking. To this end, the author has developed an FE-based numerical method which is capable of predicting slab deflections for a time-varying load history. Chapter 4 was concerned with the prediction of deflections of slabs under constant load. The method adopted in Chapter 4 was extended in Chapter 5 to model cracking, creep and shrinkage in columns. A method was developed in Chapter 6 for predicting deflections under a time-varying load which was used to predict the deflection of the Cardington floors in Chapter 8. In Chapter 7, an extensive parametric study was carried out to identify the influence of different geometrical, loading and material factors on slab deflections. Furthermore, two simplified methods were proposed for predicting long-term deflections due to a time-varying load.

The thesis is summarised in the following sections where emphasis is placed on the novel aspects of the author's work.

9.2 Summary of the work

9.2.1 Literature review

Chapter 2 described different code approaches for controlling or predicting slab deflections. The findings are as follows:

- Considerable uncertainties exist within the design community over the selection of flat slab thickness. Slab thicknesses are commonly based on compliance with permissible span-to-depth ratios proposed by codes of practice. These methods are relatively simple to apply but their accuracy is questionable as some key parameters which influence deflections (e.g. construction sequence, material properties) are not considered. Codes also provide simplified equations to calculate long-term deflections.

- Some codes [(ACI Committee 318, 1989), (British Standards Institution, 1997)] and authors [(Graham & Scanlon, 1986), (Sbarounis, 1984b), (Branson, 1977)] suggest multipliers, which vary considerably, to calculate long-term deflections from instantaneous deflections.

- Field measurements of deflection indicate a high level of variability, which is due to: 1) inherent variability in properties of concrete, 2) significant variations in actual slab thicknesses and the position of reinforcement, 3) the presence of in-plane restraint causing extra cracking which is not accounted for in design, and 4) different construction approaches which may lead to different levels of cracking.

There are several methods for calculating short- and long-term deflections which were described in Chapter 2. A survey was made of existing FE methods for predicting slab deflections in Chapter 3. The objective of the current work is to develop a simple but accurate method of modelling long-term deflection under service load. To this end, the effective-stiffness method has been found most suitable, since short-

and long-term moment-curvature relationships can be incorporated in existing FE programs. Secondly, as mentioned in section 3.4, for typical slab systems, accuracy of effective-stiffness formulations are comparable to those of the layered approaches (Polak *et al.*, 1996).

9.2.2 Modelling of cracking, creep and shrinkage

Several short-term crack models [i.e. the ACI 318-89 effective moment of inertia model (1989) which uses Branson's (1976) equation, the moment-curvature relationships of MC-90 (1993), and Gilbert (1983), (1988)] and the MC-90 long-term model have been incorporated into an existing FE package (see Chapter 4) to simulate cracking, creep and shrinkage in slabs. The program was used to predict the deflections of several short- and long-term slab experiments. Predictions were good in most cases for all the models.

The author has also developed a method for modelling the instantaneous and long-term behaviour of columns under biaxial bending and compression. The presence of the axial force makes the problem more complicated since the position of the neutral axis in the cracked state is dependent on the magnitude of the axial load and its position. The salient features of the method are:

- An iterative method based on a trial and error approach has been developed to find the neutral axis of a cracked section loaded with an axial force having two-directional eccentricity. Both the ACI and the MC-90 equations were used to find the mean curvature by interpolating between the uncracked and cracked states.

- The method was successfully used to model moment-curvature relationships obtained from the experiments on columns loaded with both one- and two-directional eccentricities.

- An FE method was proposed for an equivalent column section using brick and line elements. The equivalent-section method gives the same result as the curvature calculations.

- The FE method was successfully used to model two sets of short-term experiments with slabs supported on columns. Modelling of column cracking was found to have an insignificant effect on slab deflections, unless the column load was low or the moment was high.

9.2.3 Modelling of time-varying load history

Chapter 6 presented a novel method, based on the MC-90 moment-curvature relationship, for predicting deflections due to a non-uniform load history. The long-term total and incremental deflections depend on the full load history of the slab. Most importantly, construction loads can be very high, depending on the re-propping method used, and can cause severe cracking of slabs with relatively low early-age tensile strength. In such cases, long-term deflections will be very high compared to slabs where the construction load does not cause any significant extra cracking. With the use of the author's new method, it is possible to model deflection development for a full load history including striking of the slab, construction loading and unloading, creep recovery, and application of imposed load. The main assumption of the method is that superposition is valid. The main conclusions of Chapter 6 are:

- The proposed method was used to analyse the Taywood slab (Whittle, 1996) which was tested under a time-varying load history. Good deflection predictions were obtained for the slab. A value of β_2=0.5 was found to accurately model the cyclic application of test load.

- Similar predictions of deflections were obtained when 1) cracking, creep and shrinkage were modelled in the column and 2) the gross column section (i.e. without reinforcement) was used without modification for cracking, creep and shrinkage.

- The effect of allowing stress redistribution (due to cracking, creep and shrinkage) has been found to have a small but not significant effect on slab deflections and a negligible effect in columns. Therefore, for a quick estimate of slab deflections, it is reasonably accurate to use the author's method with elastic stresses (i.e. without any redistribution).

9.2.4 Parametric study

The results of an extensive parametric study were presented in Chapter 7. The main conclusions are summarised under the following headings:

Geometric properties

- Slab thickness has a very significant effect on instant and long-term deflections. The effect is most pronounced when cracking is reduced by increasing slab thickness.

- It is a common practice to provide more tensile steel in the span (i.e. bottom steel) than required for strength in order to reduce slab deflections. It was found that providing more bottom steel has little effect on deflections and the effect is least for thicker slabs. Deflections were also predicted to be relatively insensitive to the distribution of steel.

Material properties

- All the concrete properties (i.e. f_{ct}, E, ϕ, ϵ_{cs}) are related to the concrete compressive strength. Different levels of concrete strength were used in the analyses of the same slabs and the effect on deflection was found to be very significant.

- Concrete tensile strength, f_{ct}, determines the level of cracking and is, perhaps, the most important parameter in determining deflections. It is essential to estimate f_{ct} as accurately as possible. However, due to its inherent variability, it can vary appreciably around the mean which, in turn, leads to variations in deflection. It is important to include the variability of f_{ct} and other concrete properties in the analysis to minimise the risk of deflections exceeding tolerable limits.

- It has been found that all the material properties (i.e. f_{ct}, E, ϕ, ϵ_{cs}) affect deflection almost independently.

- Loss of tension stiffening, which is modelled by assigning a value of 0.5 to β_2 was found to increase long-term slab deflection greatly.

Construction parameters

- The magnitude and time of application of construction load are very important in determining the deflection of slabs. Excessive construction loads can lead to severe cracking of relatively young slabs and result in increased long-term deflections. It has been shown that different construction methods can lead to significantly different long-term deflections. It is important that the designer agrees a suitable construction method with the contractor to ensure that slab deflections are acceptable.

- The contribution of creep due to construction loading is usually small. Therefore, reasonable estimates of deflection are given if the construction load is modelled as a spike (see Fig. 7.35 in section 7.5.3) in the step analysis.

- In practice, a simple procedure is required to account for the effect of construction loading on deflection. Therefore, a single step analysis was also proposed in which the concrete tensile strength is modified to account for construction loading. This method gives similar prediction of deflection to the more rigorous incremental model. The main weakness of this method is that it does not model the residual deflection induced by loading and unloading.

Service-life parameters

- The magnitude of imposed load is very important in determining long-term deflections and needs to be estimated with reasonable accuracy. The time of application of the imposed load appears to have little effect on long-term deflections.

- Relative humidity influences long-term deflections significantly.

9.2.5 Modelling of Cardington slab

The method described in Chapter 6 has been found to be reasonably accurate in modelling the deflection history of the slabs of the Cardington full-scale building (see Chapter 8). The main findings of this chapter are:

- In most cases, measured deflections agree reasonably well with those obtained with the mean tensile strength, creep and shrinkage properties given by MC-90.

- Although the predictions were good, it should also be kept in mind that deflection is highly sensitive to the level of cracking, as shown in section 8.4. The level of cracking, in turn, depends on 1) the tensile strength, which can vary appreciably for concretes designed for the same strength, 2) the actual thickness of the slab and the position of reinforcement which may vary significantly in the field, and 3) the presence of in-plane restraint. Modelling deflections very accurately is virtually impossible due to the inherent variability in material and geometric properties.

- In all cases, the 10-years predicted (with mean material properties) incremental deflections due to imposed load (after construction of partitions) satisfy the EC2 limit of span/500, which minimises damage to finishes. However, the total deflection of the corner panel is close to or exceeds the EC2 limit of span/250 for all the floors analysed. The construction loads for the Cardington slabs were relatively small. If the three-shore method described in section 7.5.1 had been used, deflections would have clearly been higher and at least the total deflection criteria would have been violated for the corner and external panels. It seems that the EC2 span-to-depth guidelines may lead to total long-term deflections greater than span/250, particularly if slabs are made thinner with more tensile steel added to reduce deflections.

- The proposed single-step method which involves a minimum of computation has been found to be very efficient in modelling long-term deflections of the Cardington slabs.

- The amount of reinforcement steel and its distribution has some effect on deflection, but the effect is not significant. Analyses were carried out by interchanging reinforcement meshes between three floors, which were designed with different methods and detailed with different reinforcement arrangements. The predicted deflections were not significantly dependent on the reinforcement assumed.

9.3 Recommendations for future work

Chapter 8 presented the modelling of deflection development for the Cardington slabs. Comparison with field measurements obtained to date are good. Monitoring of deflections will continue for one more year and, if needed, the model will be adjusted. However, there is a clear need for more tests on full-scale slab elements with simple boundary conditions. It is recommended that further research should be carried out to study:

- The loss of tension stiffening with time.
- The effect of restraint of early age thermal strains and shrinkage on slab deflections.
- The effect of loading and unloading on slab deflections.
- Accurate prediction of deflection is virtually impossible due to the inherent variability in material and geometric properties. A variability-type analysis utilising the author's method to model time-varying load history is recommended for minimising the risk of the estimated deflection exceeding tolerable limits.
- The span-to-depth rules of EC2 should be modified to account for the effects of construction loads and variations in material properties. The provisions for reducing slab thicknesses by increasing the area of reinforcement should be reviewed.
- Extend the current work to predict crack widths in slabs.

- It was reported by Favre *et al.* (1990) that the tensile strength of concrete is less at the top than at the bottom face of the slabs due to segregation. The effect of this on deflection should be investigated further.

- Extend the current work to include slabs with beams.

- Extend the work to model yielding of reinforcement using the MC-90 moment-curvature relationship.

Appendix A

Effective steel

A detailed investigation has been carried out to check different equations to calculate effective steel in the principal directions for isotropic mesh and meshes of different level of orthotropy under biaxial and skew bending. Different initial condition e.g. A_{sn}=A_{st} and ϵ_n=ϵ_t have been considered. Equations similar to those proposed by Jofriet & McNeice (1971) have been derived (see section 4.4.1) to calculate the effective areas of steel in the principal directions for the general case of plate bending where the levers in the two directions are not equal. The area effective in normal direction is given by:

$$A_{sn} = A_{sx}\left[\cos^4\theta\frac{Z_x}{Z_n} + \mu\sin^4\theta\frac{Z_y}{Z_n} + \frac{1}{r_{nt}}(\frac{Z_x}{Z_n} + \mu\frac{Z_y}{Z_n})\cos^2\theta\sin^2\theta\right] \qquad \text{(A.1)}$$

And the effective steel in the transverse direction is :

$$A_{st} = A_{sn}r_{nt}\frac{M_tZ_n}{M_nZ_t} \qquad \text{(A.2)}$$

Johansen's plasticity criterion (Johansen, 1972) leads to the following equations:

$$A_{sn} = A_{sx}\left[\cos^2\theta + \mu\sin^2\theta\right] \qquad \text{(A.3)}$$

$$A_{st} = A_{sx}\left[\sin^2\theta + \mu\cos^2\theta\right] \qquad \text{(A.4)}$$

Also, it is suggested by Cope & Clark (1984) that it is conservative to use the following equations, which neglect the r_{nt} containing terms of eq. A.1 (with equal

lever arms), for both one and two directional cracks.

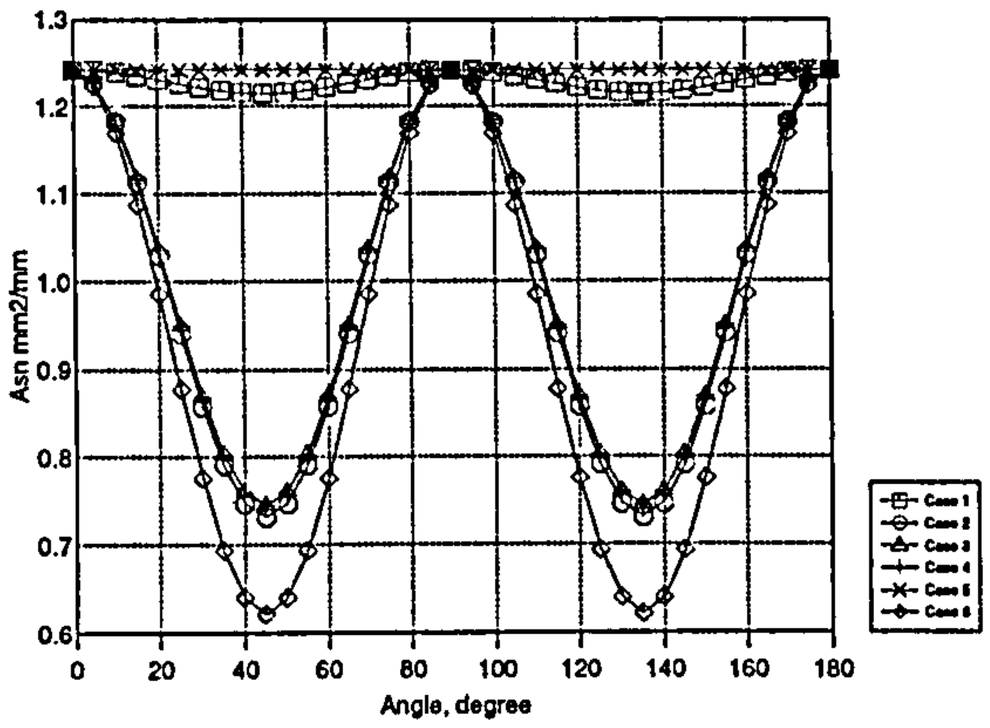
$$A_{sn} = A_{sx}\left[\cos^4\theta + \mu\sin^4\theta\right] \tag{A.5}$$

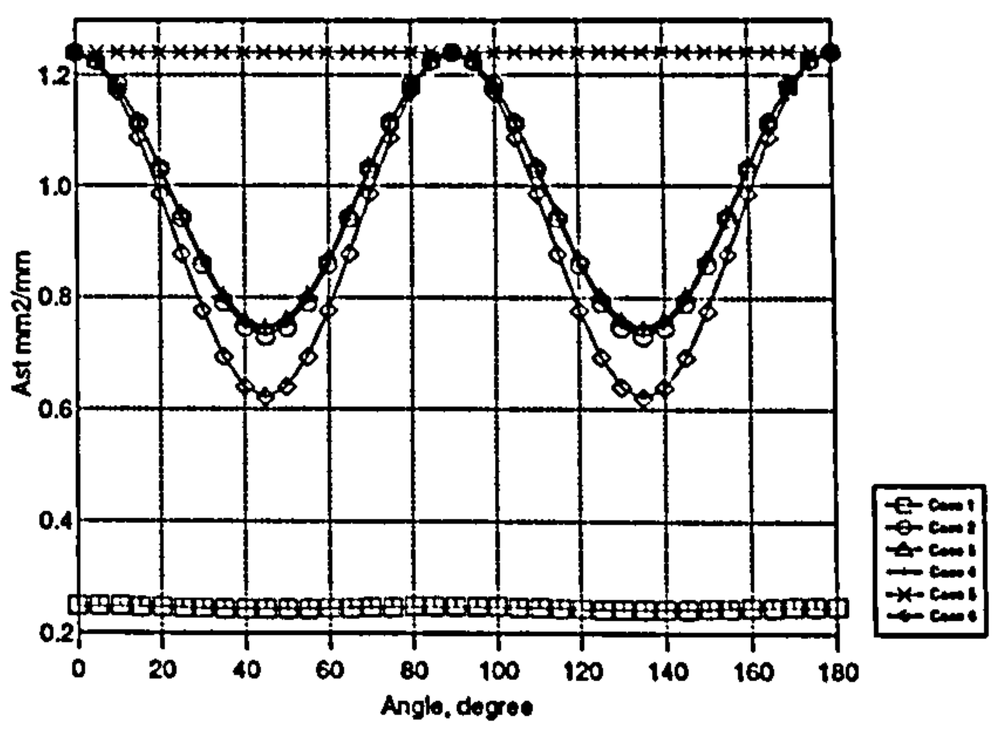
$$A_{st} = A_{sx}\left[\sin^4\theta + \mu\cos^4\theta\right] \tag{A.6}$$

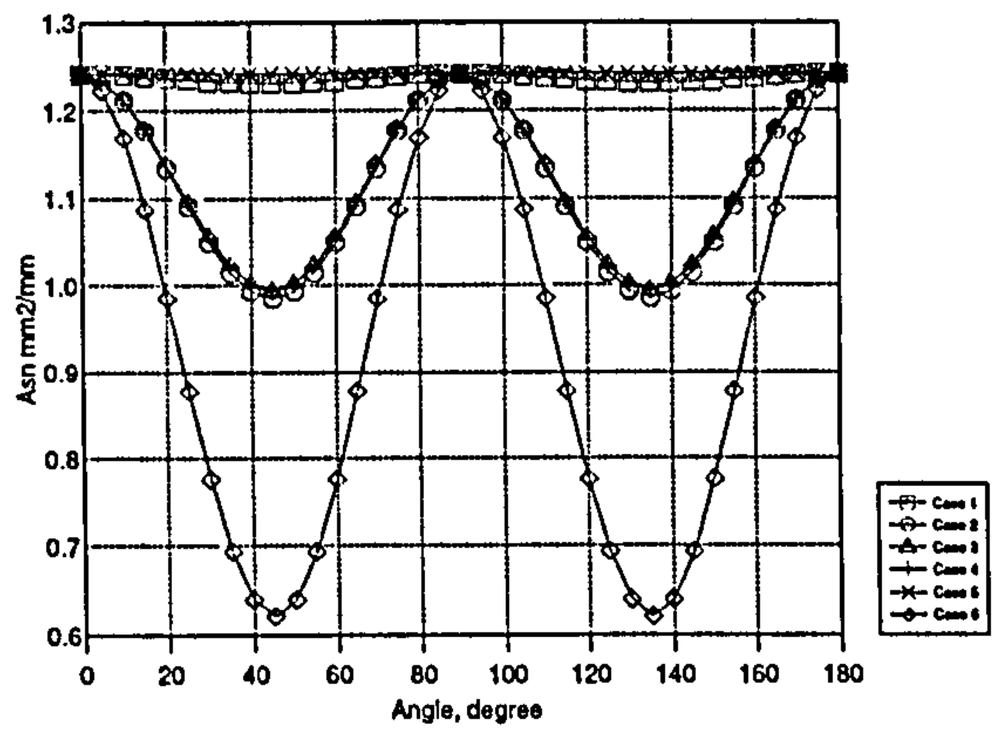
Six possible cases have been considered in the study:

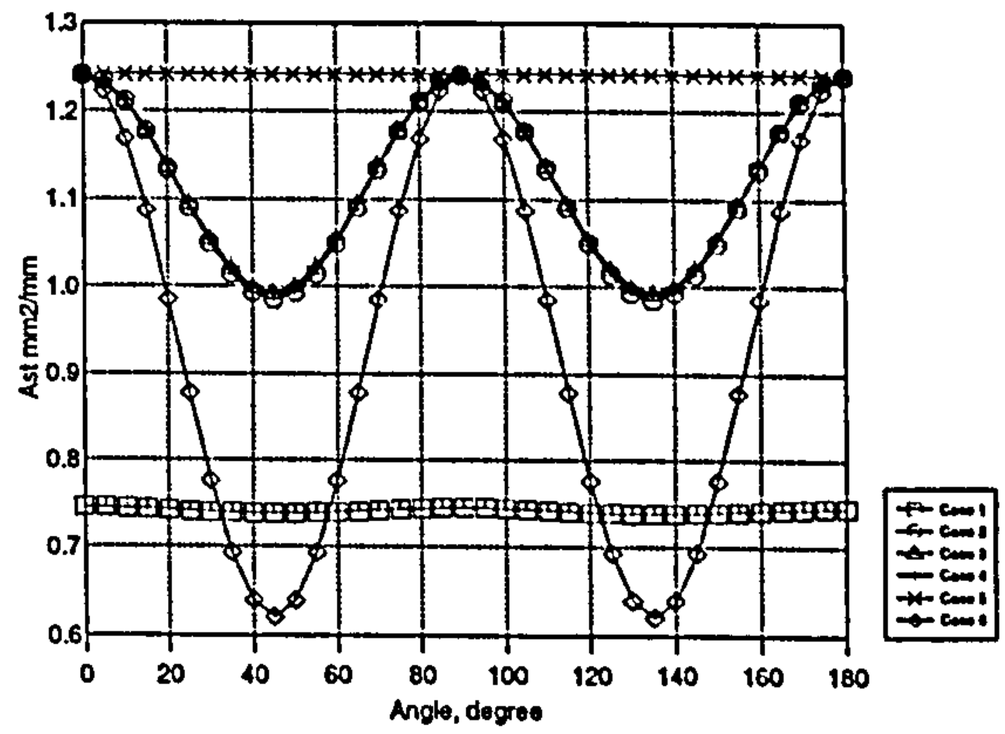
1. Equations A.1 and A.2 with initial condition $\epsilon_n=\epsilon_t$.
2. Equations A.1 and A.2 with initial condition $A_{sn}=A_{st}$.
3. Equations A.1 and A.2 with equal lever arms and initial condition $\epsilon_n=\epsilon_t$.
4. Equations A.1 and A.2 with equal lever arms and initial condition $A_{sn}=A_{st}$.
5. Equations A.3 and A.4.
6. Equations A.5 and A.6.

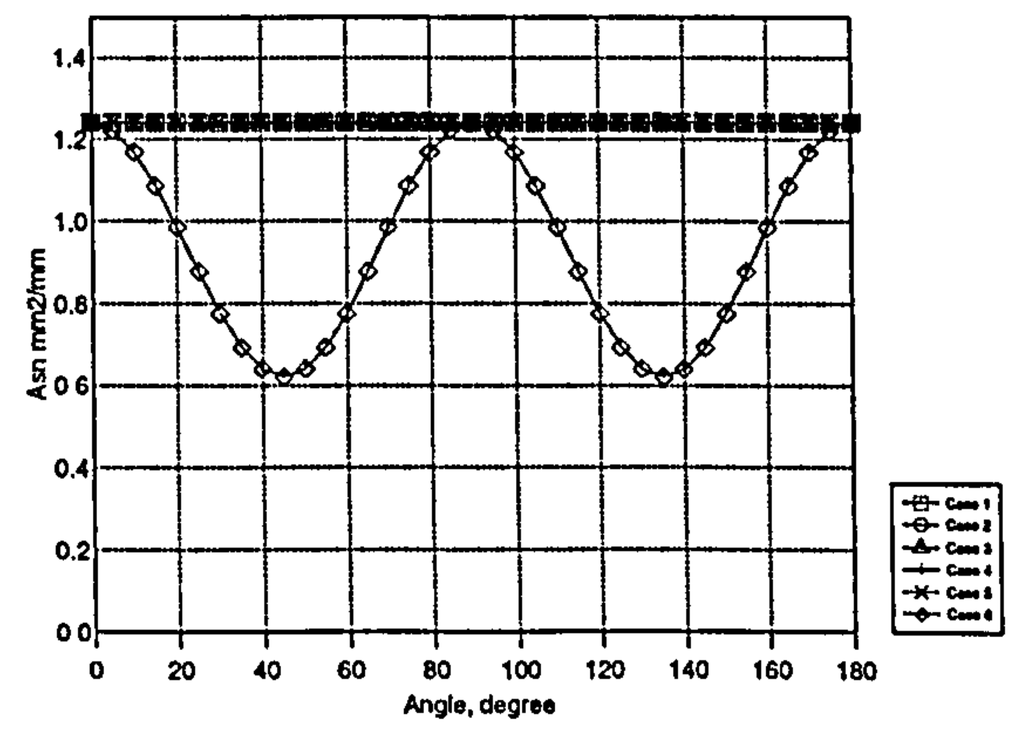
In cases 1 and 2, the lever arm Z is derived from section analysis. Effective steel calculated from cases 1 to 6 for isotropic and different orthotropic meshes under biaxial and skew bending are presented from Fig. (A.1) to (A.6) for different angles of principal directions. Case 1 always converges to a point where $\epsilon_n Z_n=\epsilon_t Z_t$. Cases 2, 3 and 4 lead to almost the same steel and always result in $A_{sn}=A_{st}$.











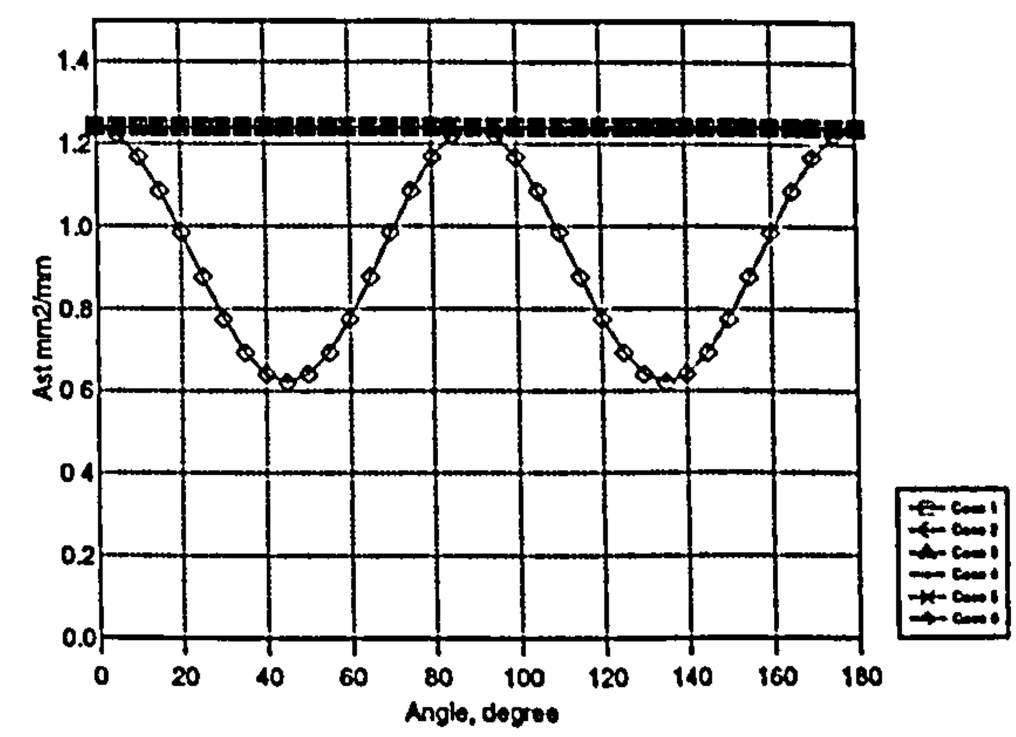
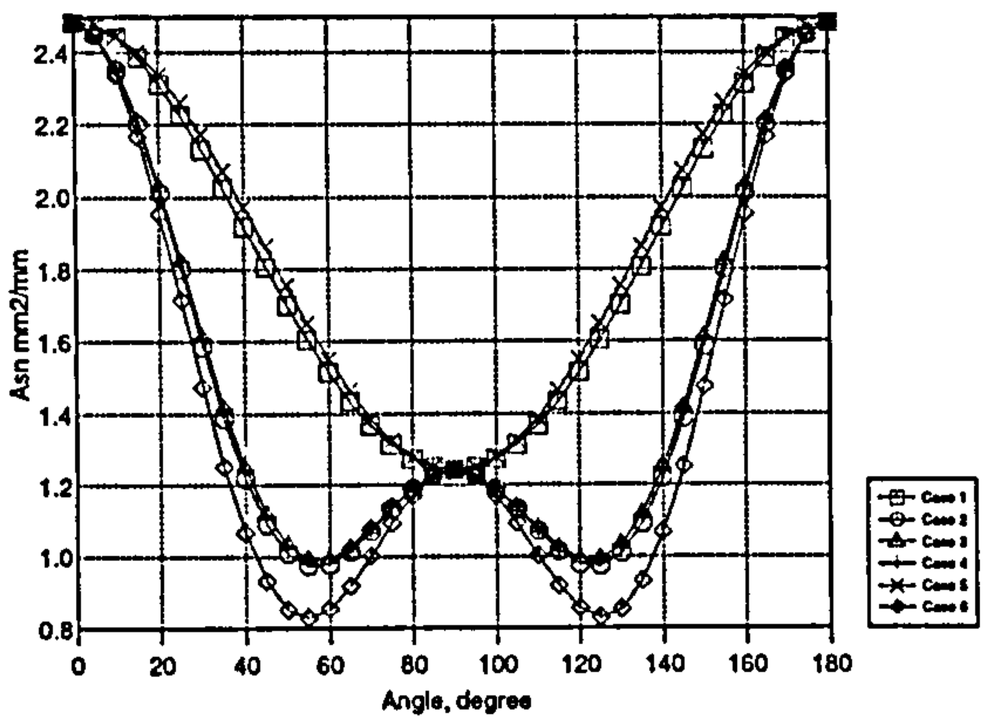
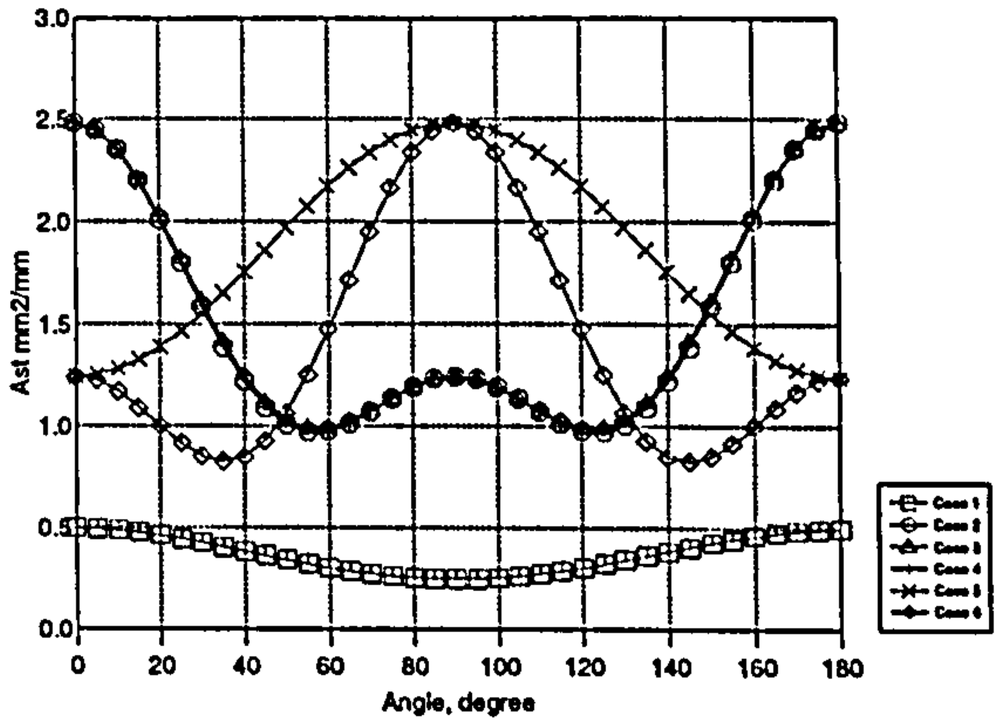
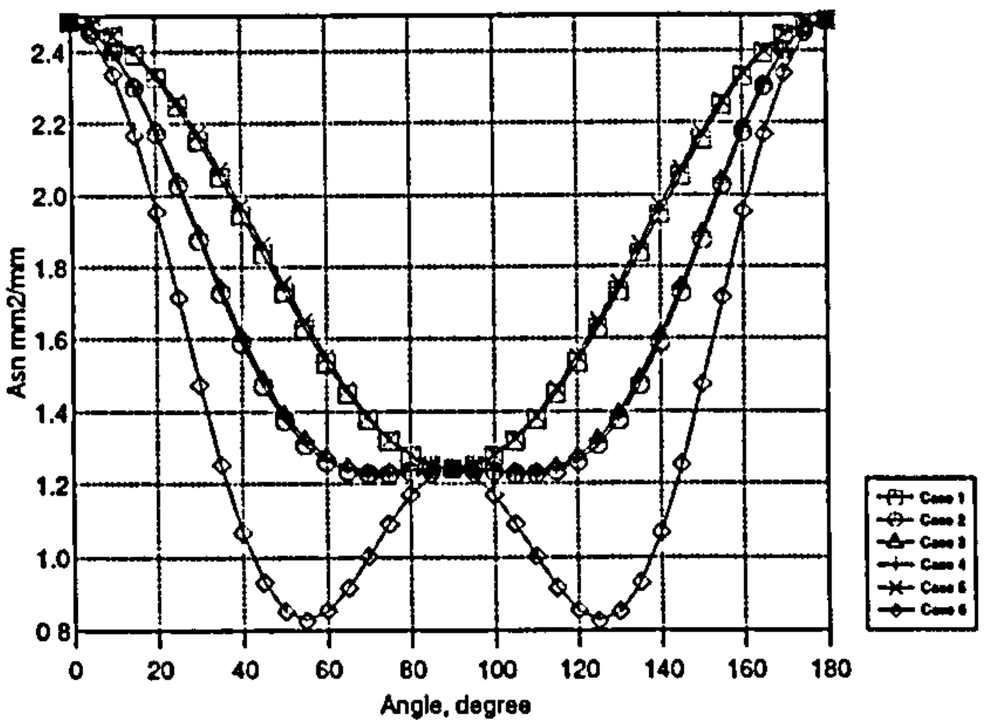
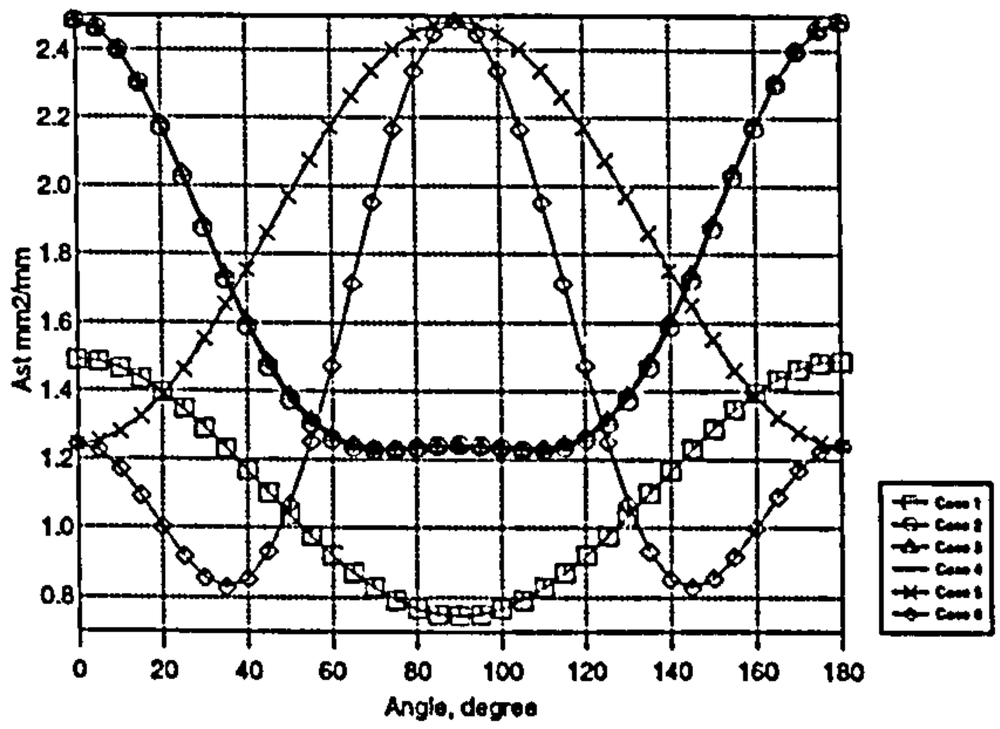


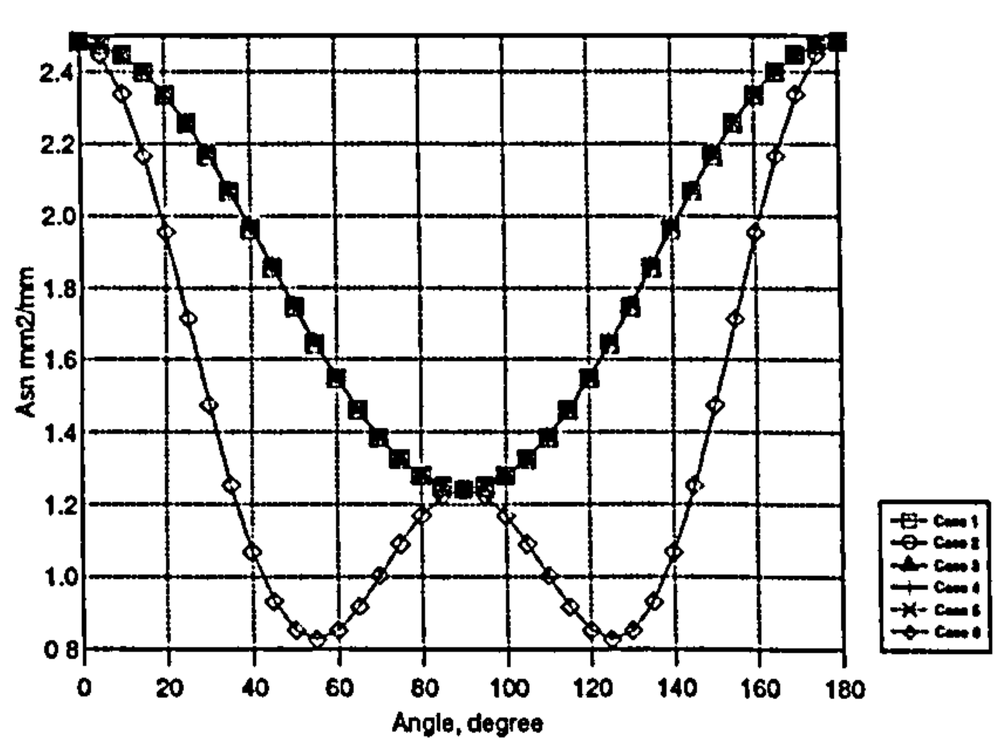
Figure A.1 Isotropic mesh: A_{sx}=0.6% and A_{sy}=0.6%











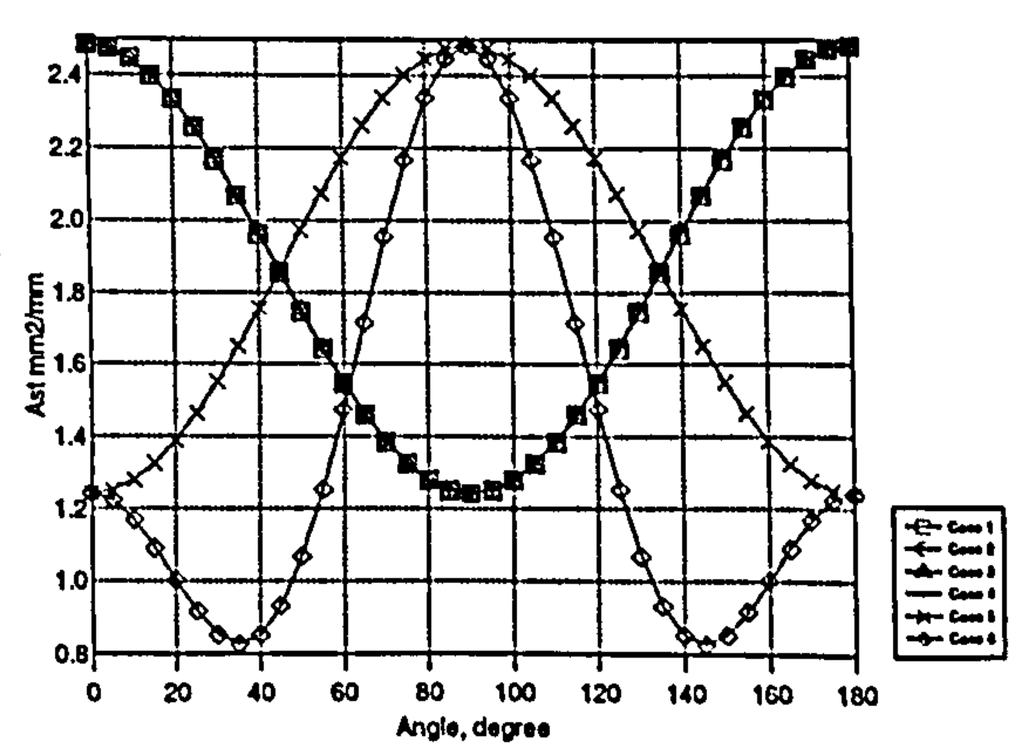
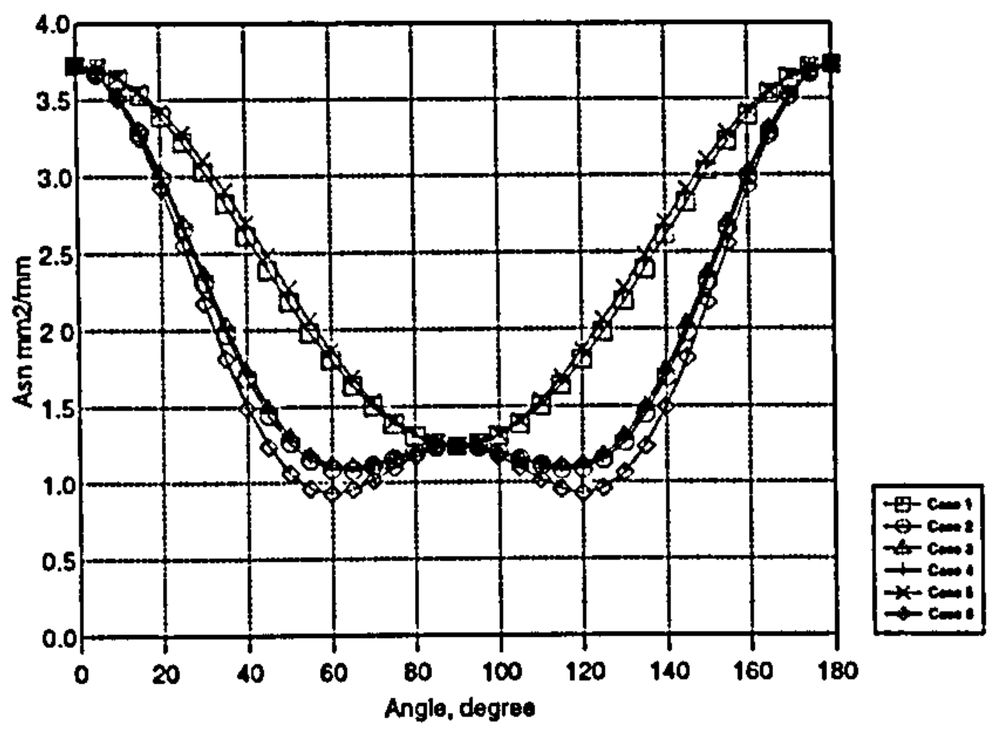
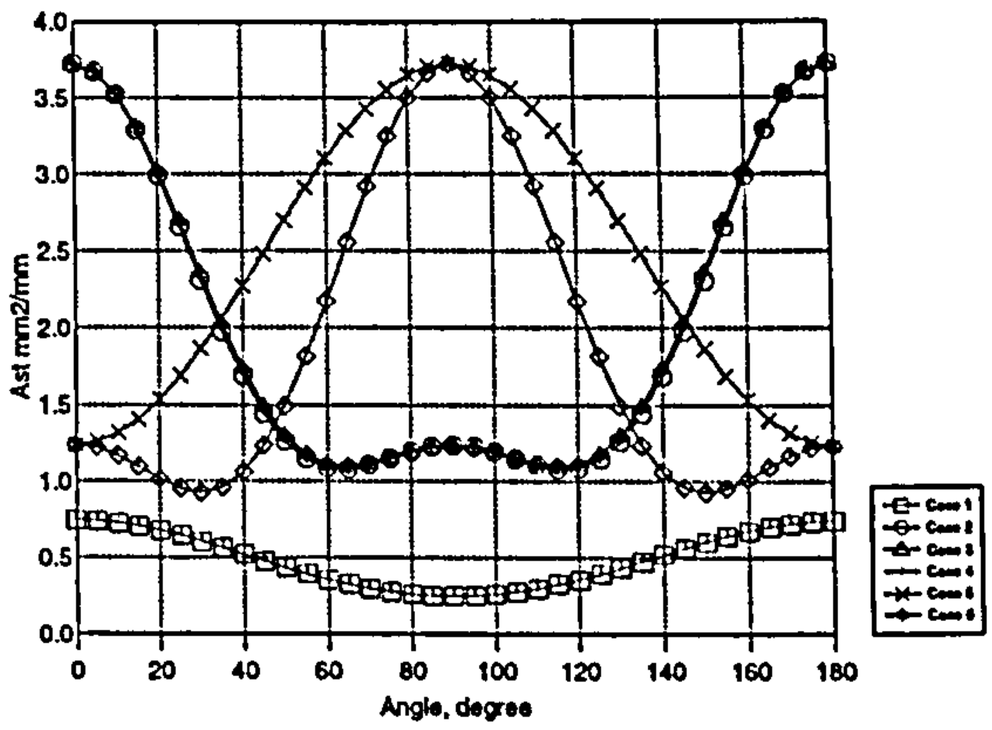
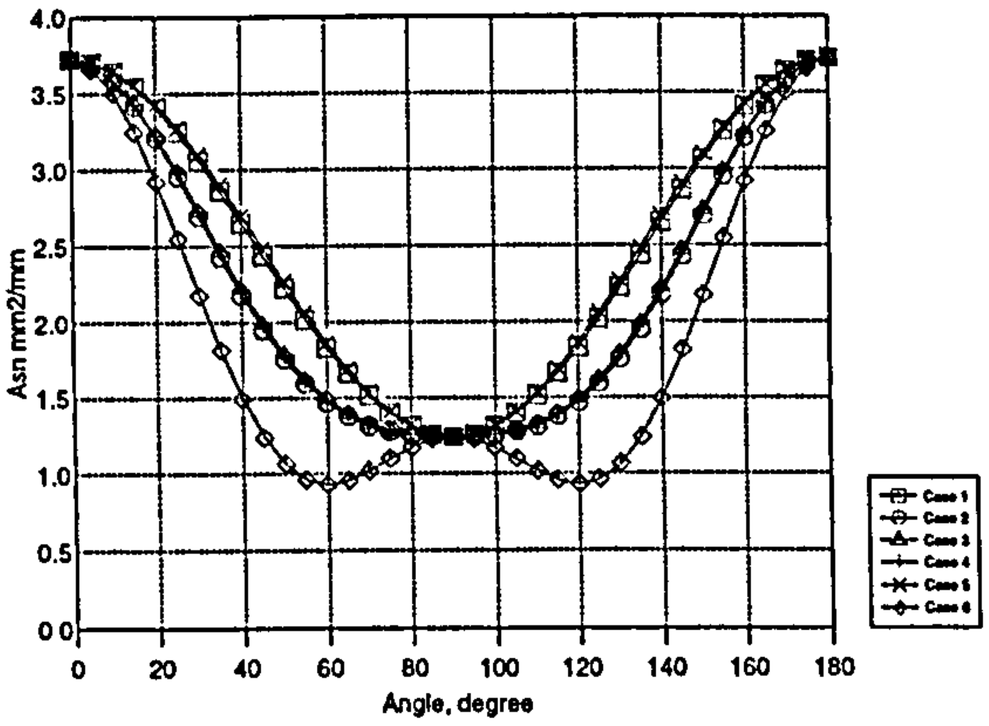
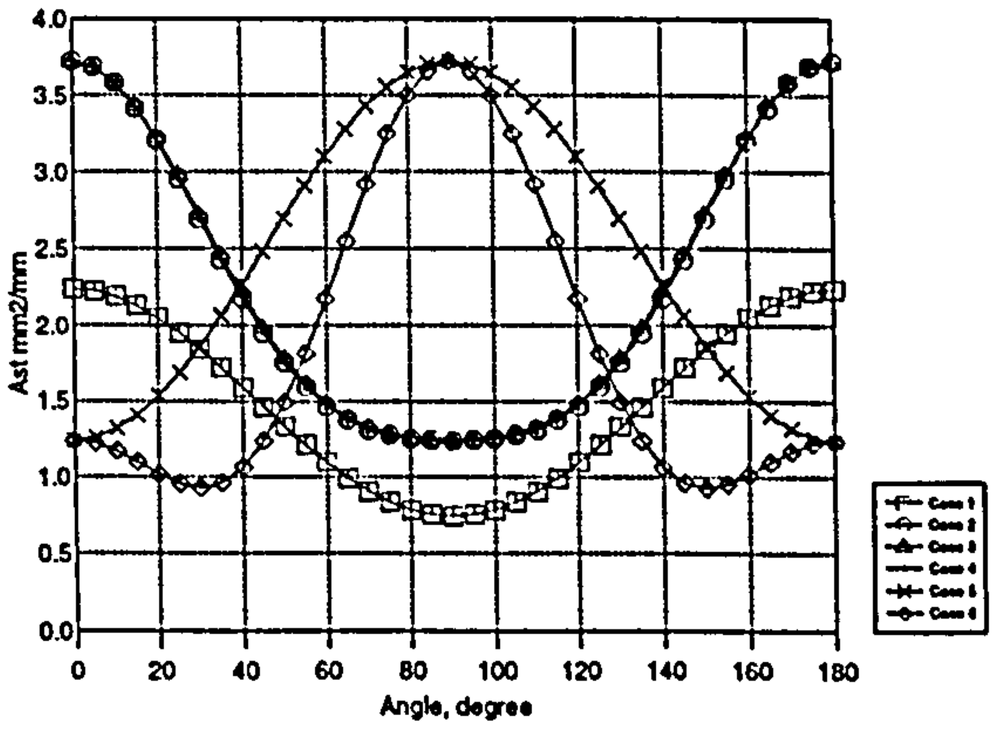


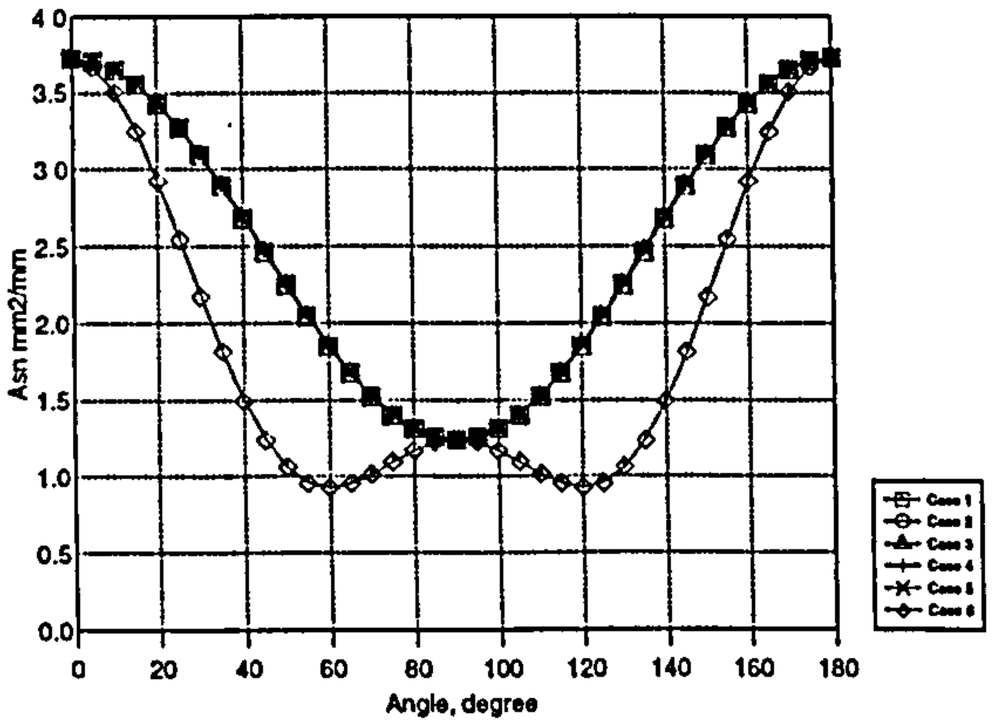
Figure A.2 Orthotropic mesh: A_{sx}=1.2% and A_{sy}=0.6%











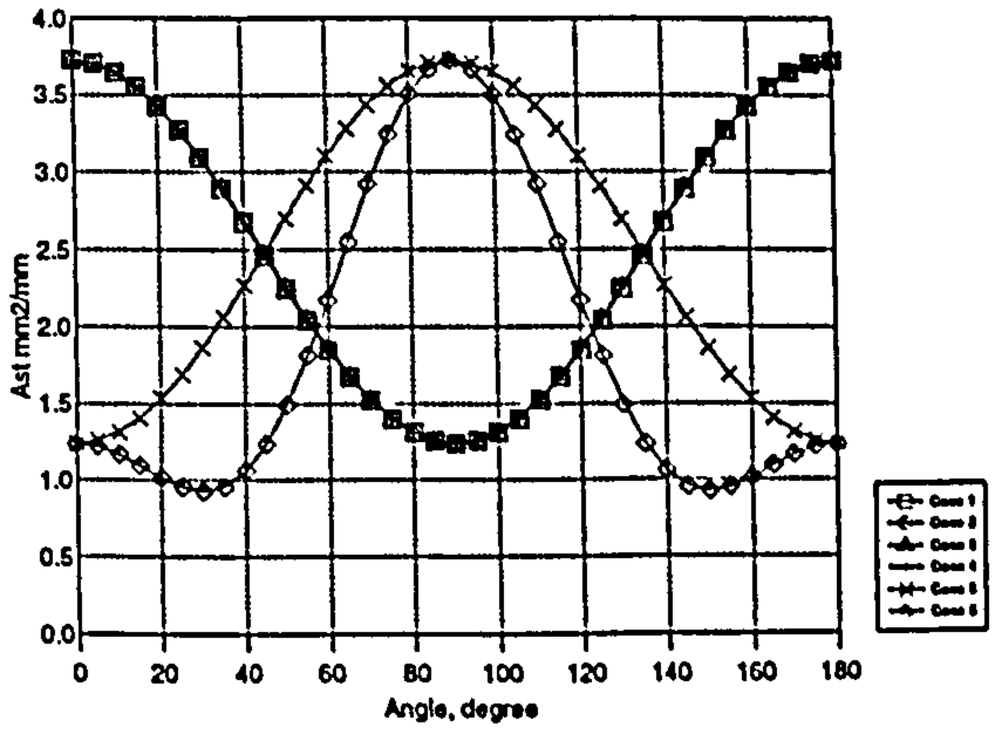
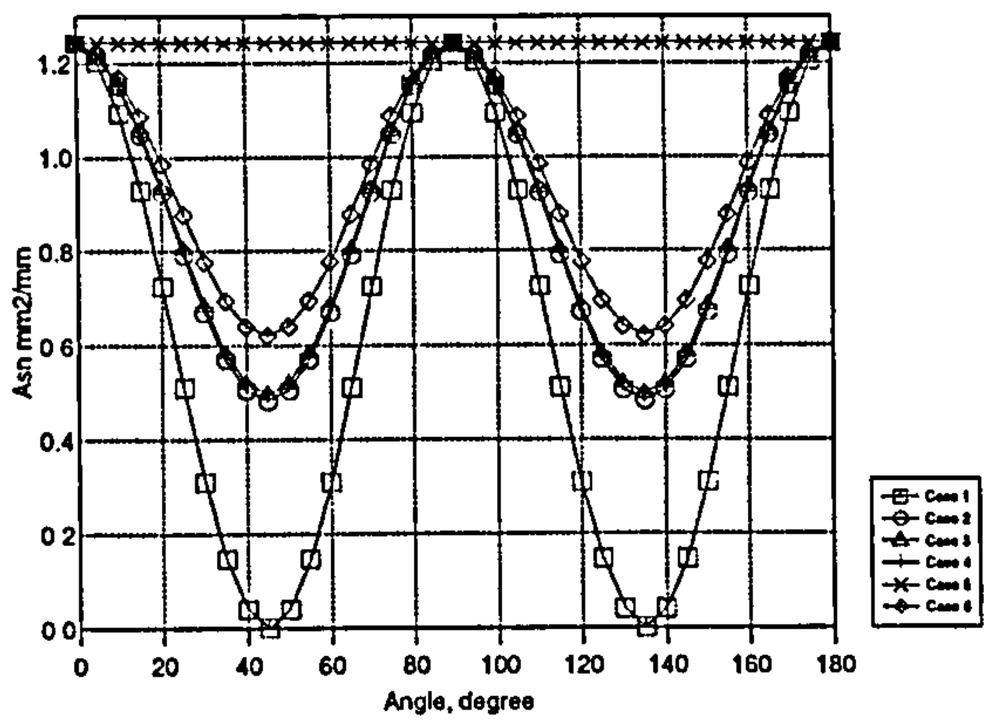
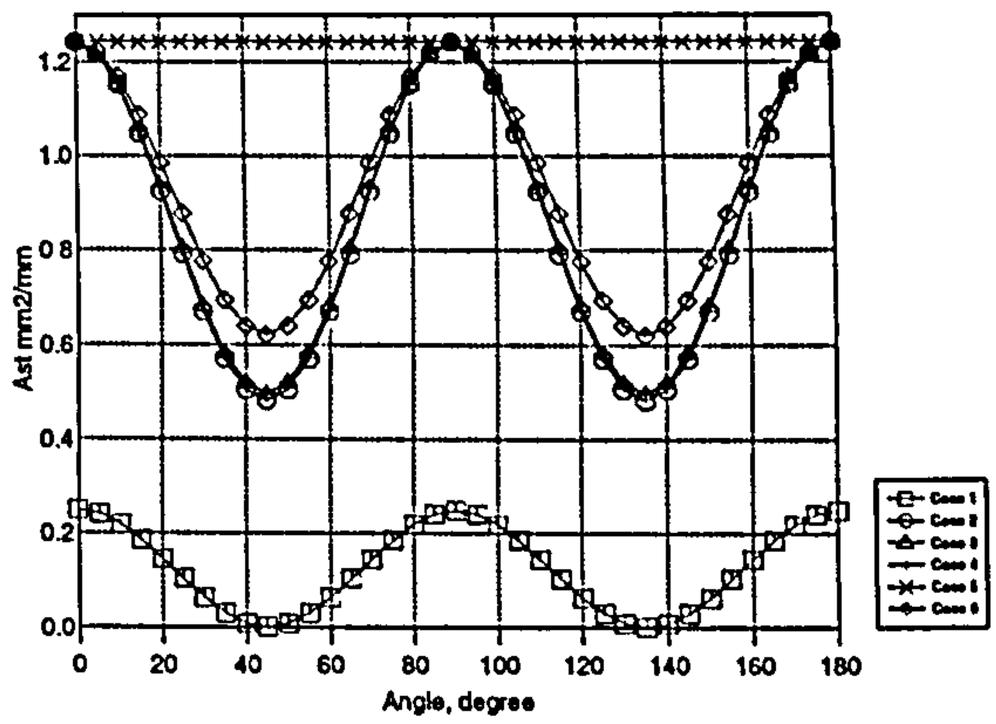
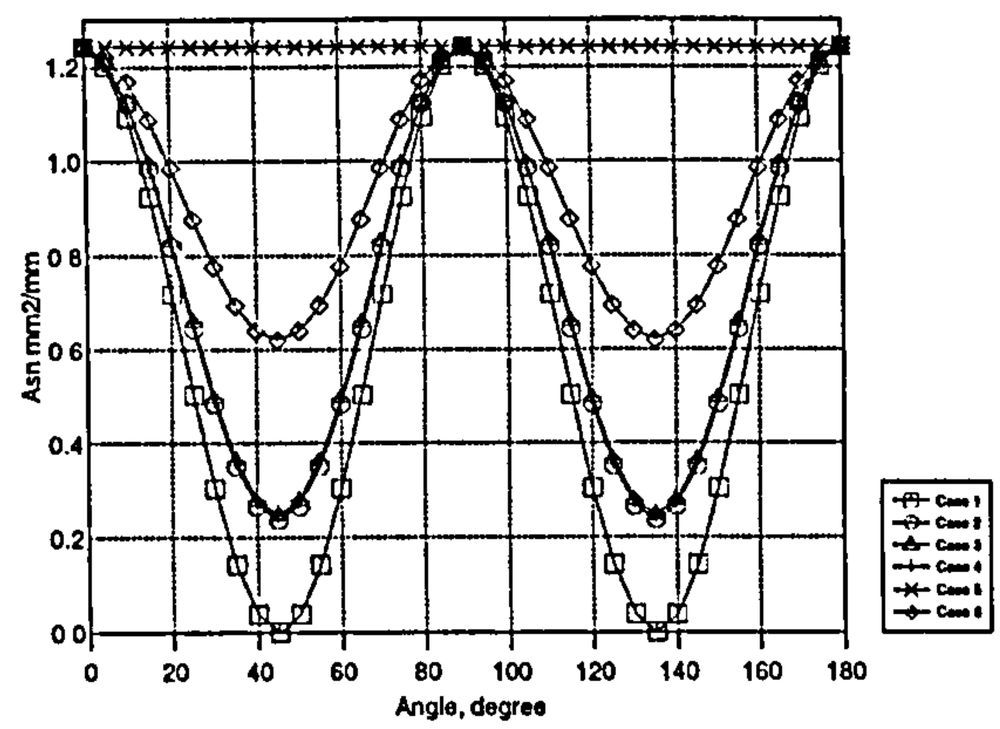
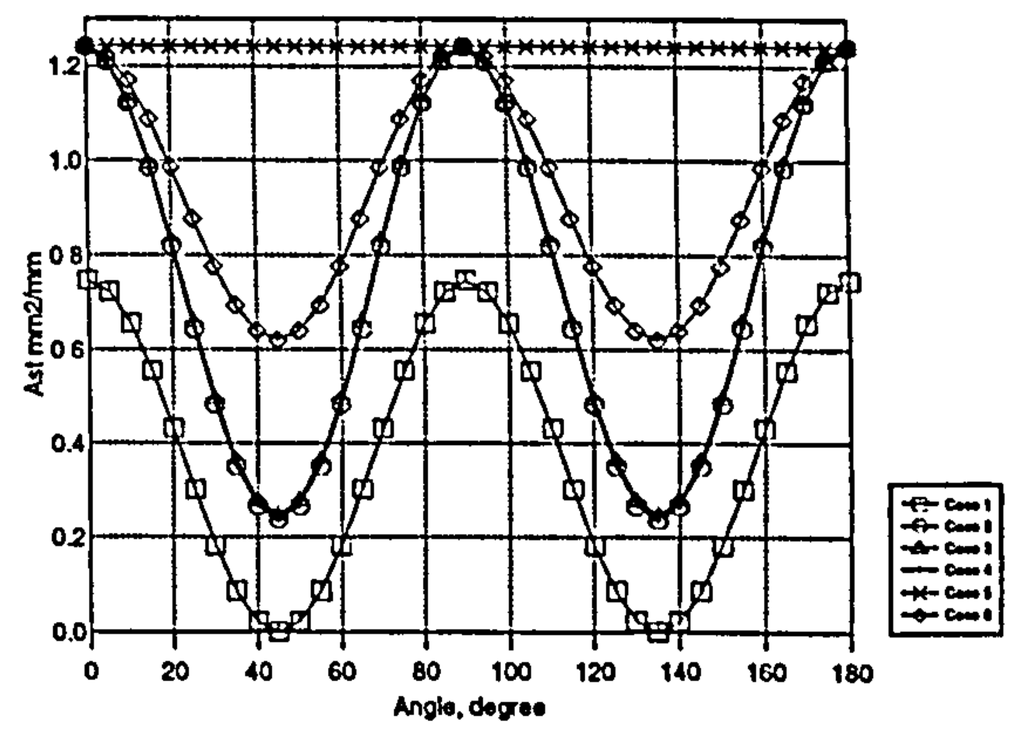


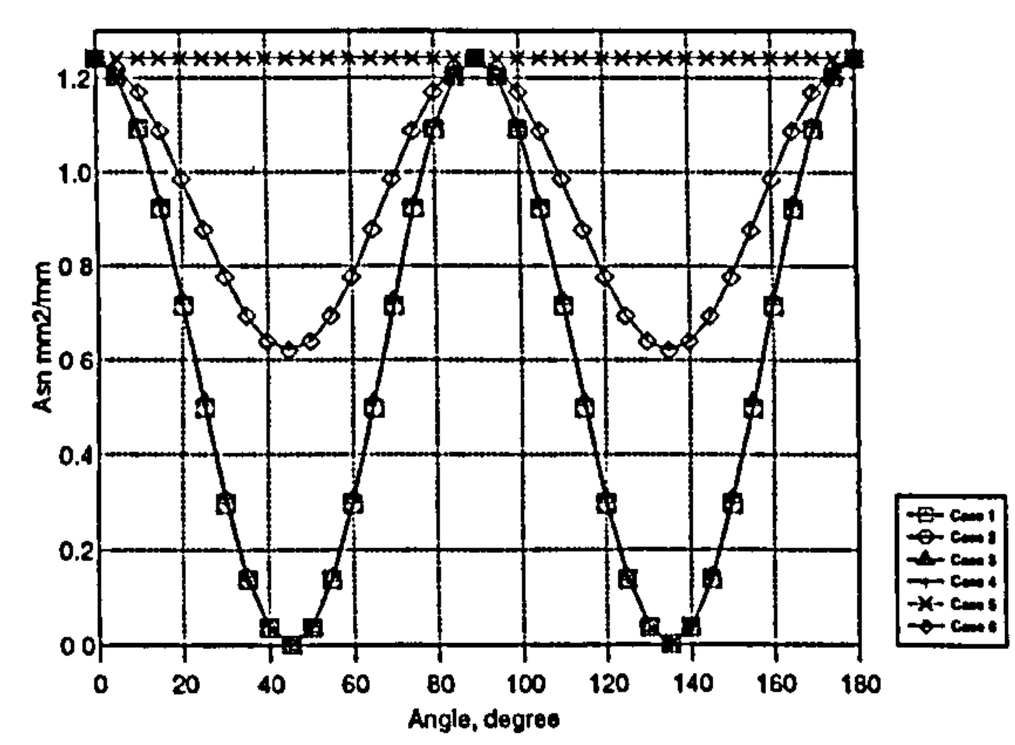
Figure A.3 Orthotropic mesh: A_{sx}=1.8% and A_{sy}=0.6%











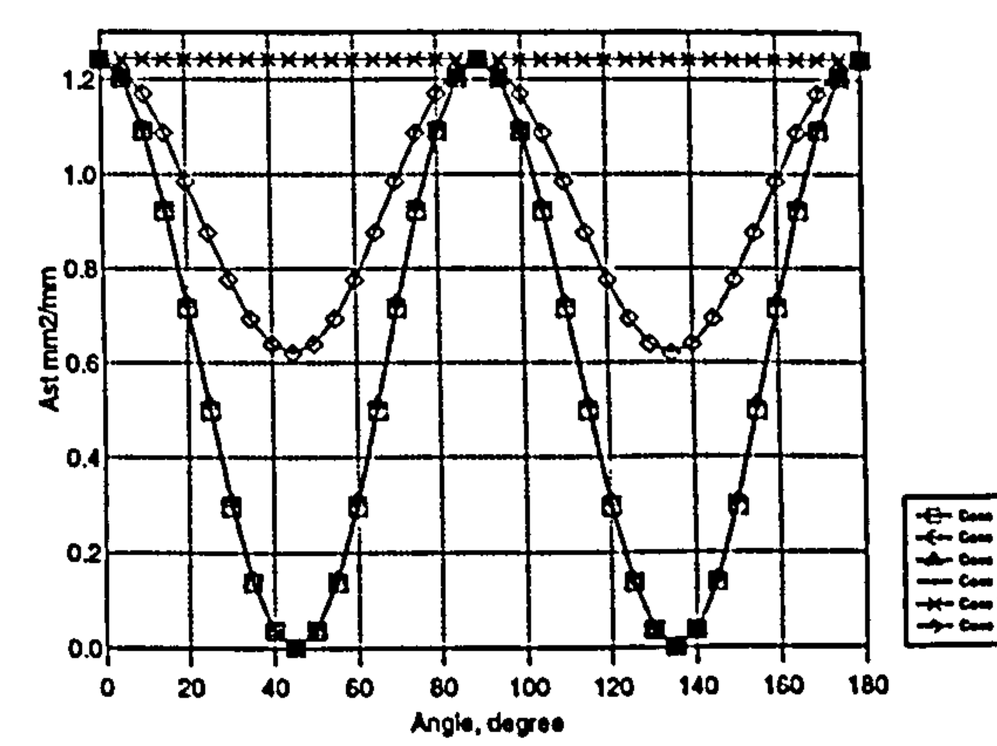
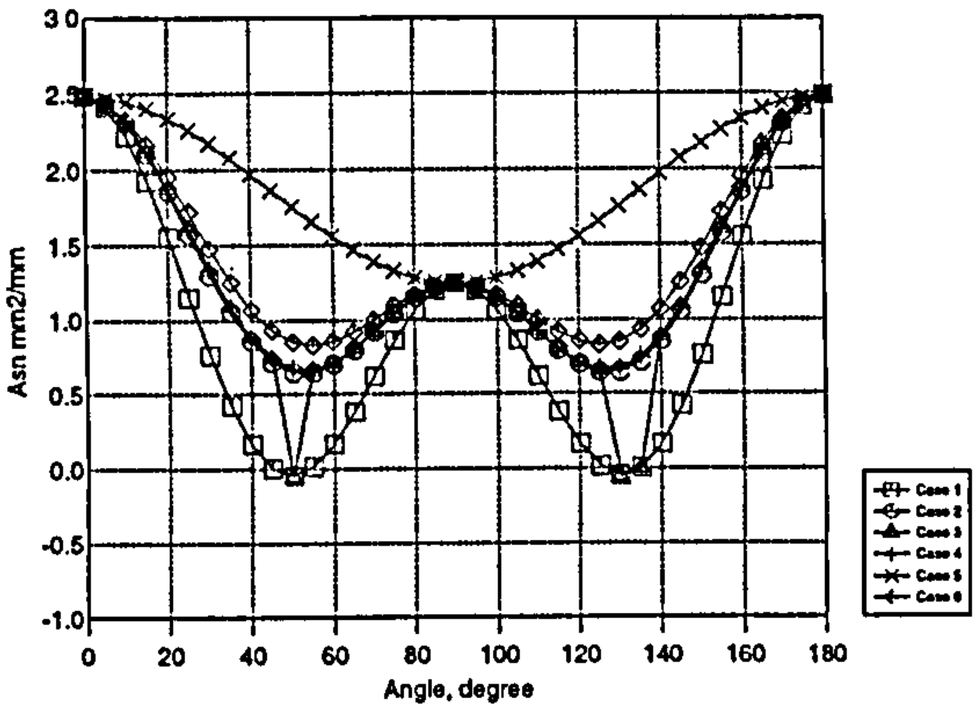
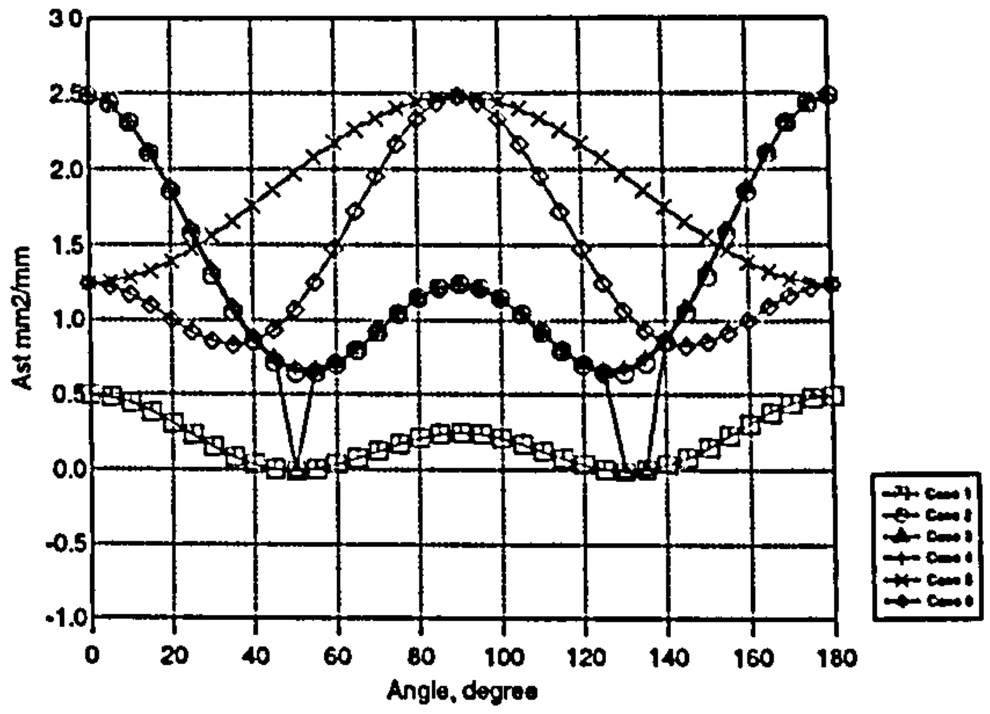
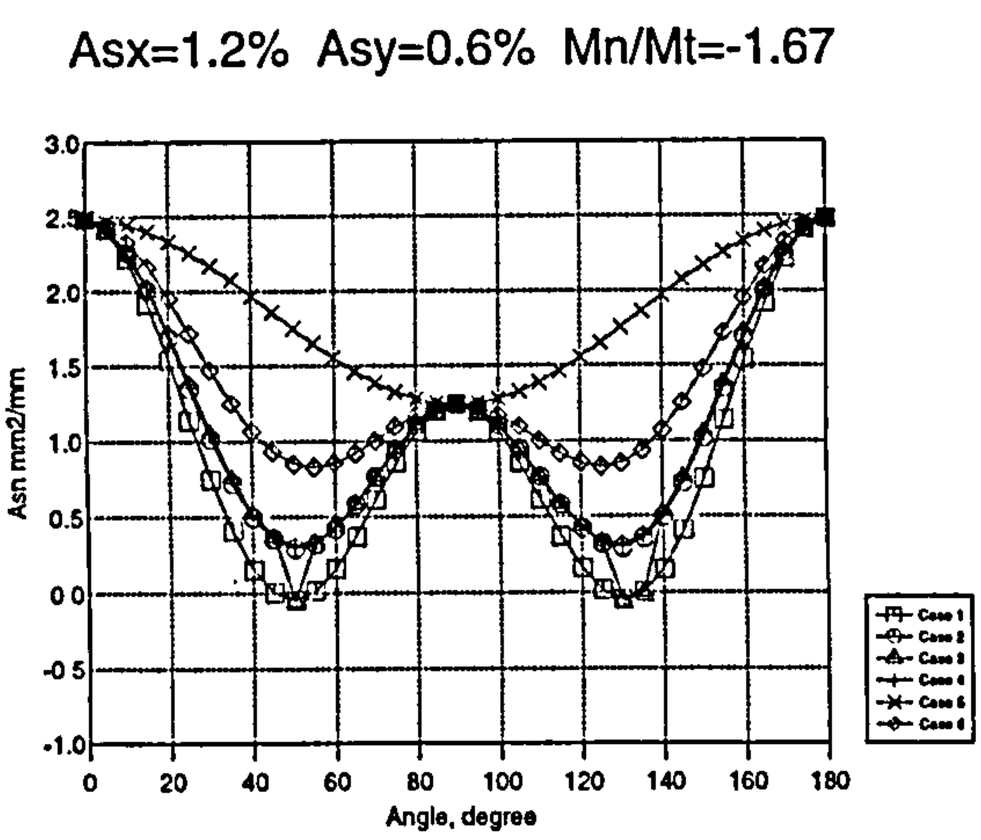
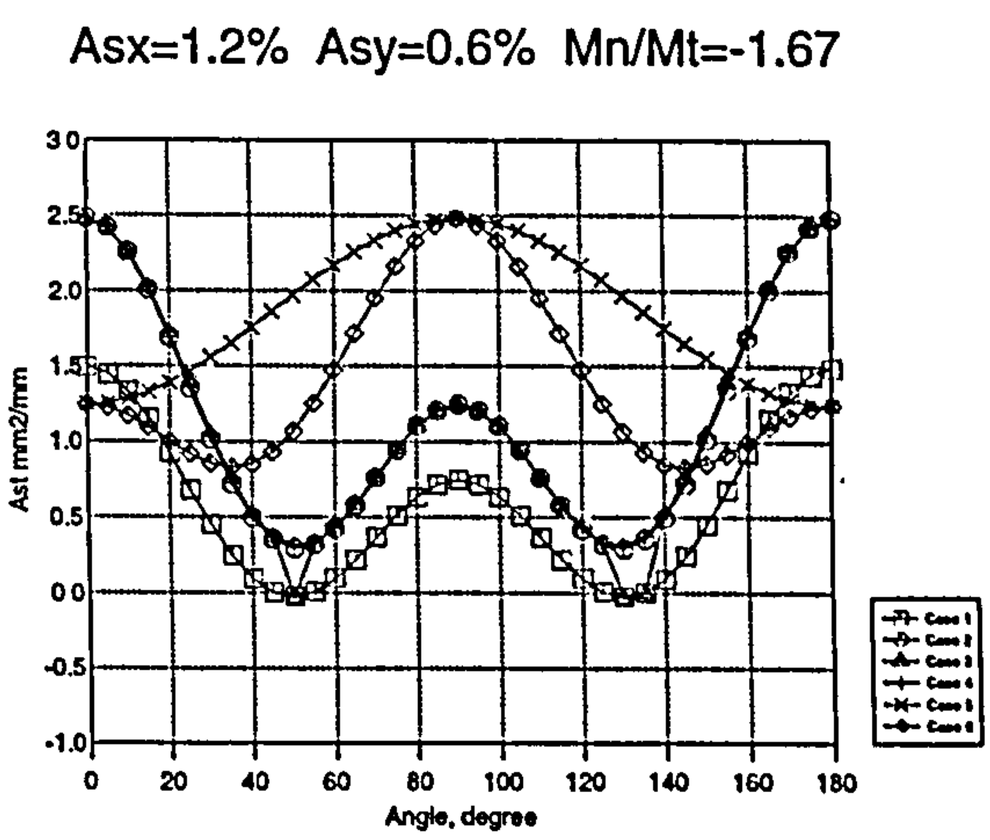


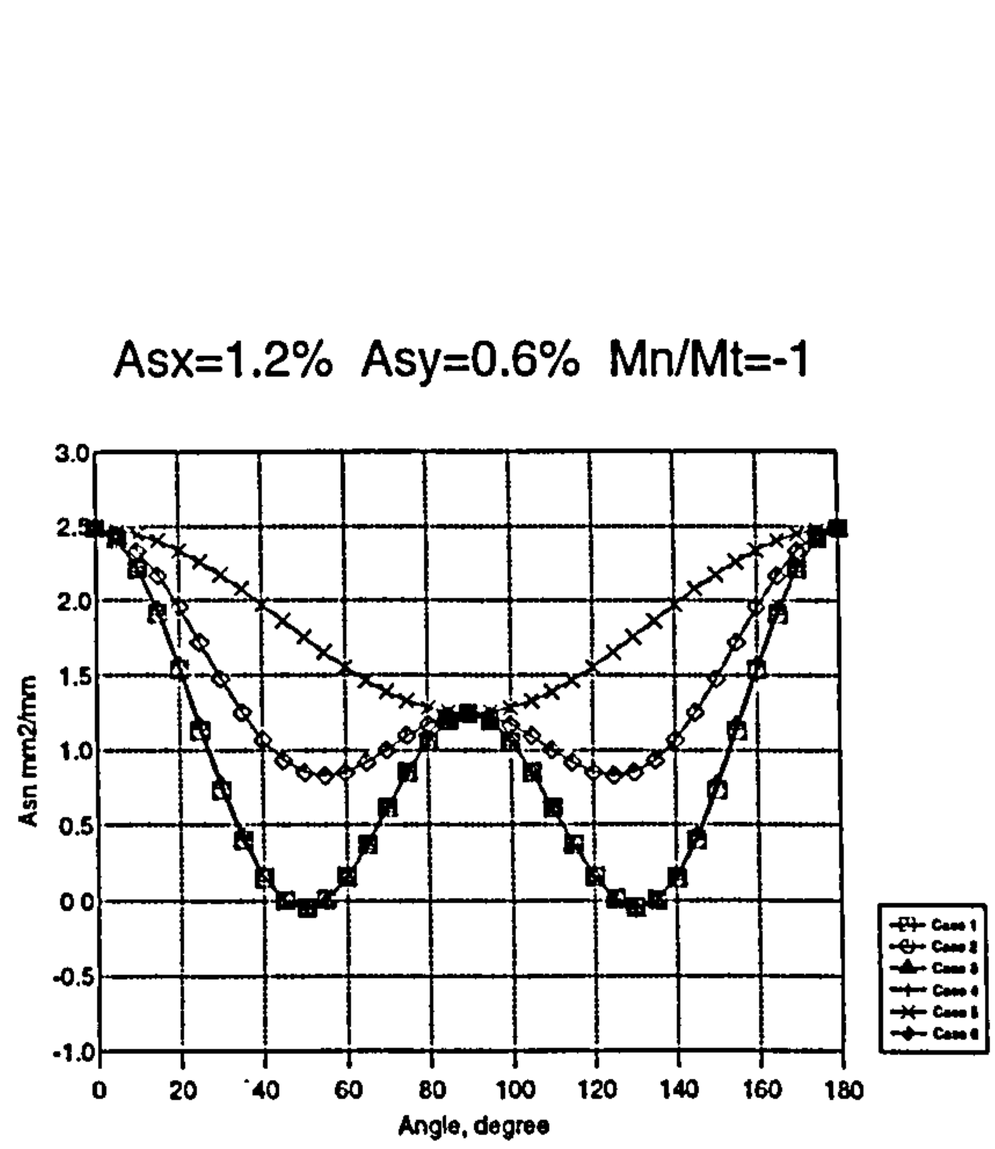
Figure A.4 Isotropic mesh: A_{sx}=0.6% and A_{sy}=0.6%











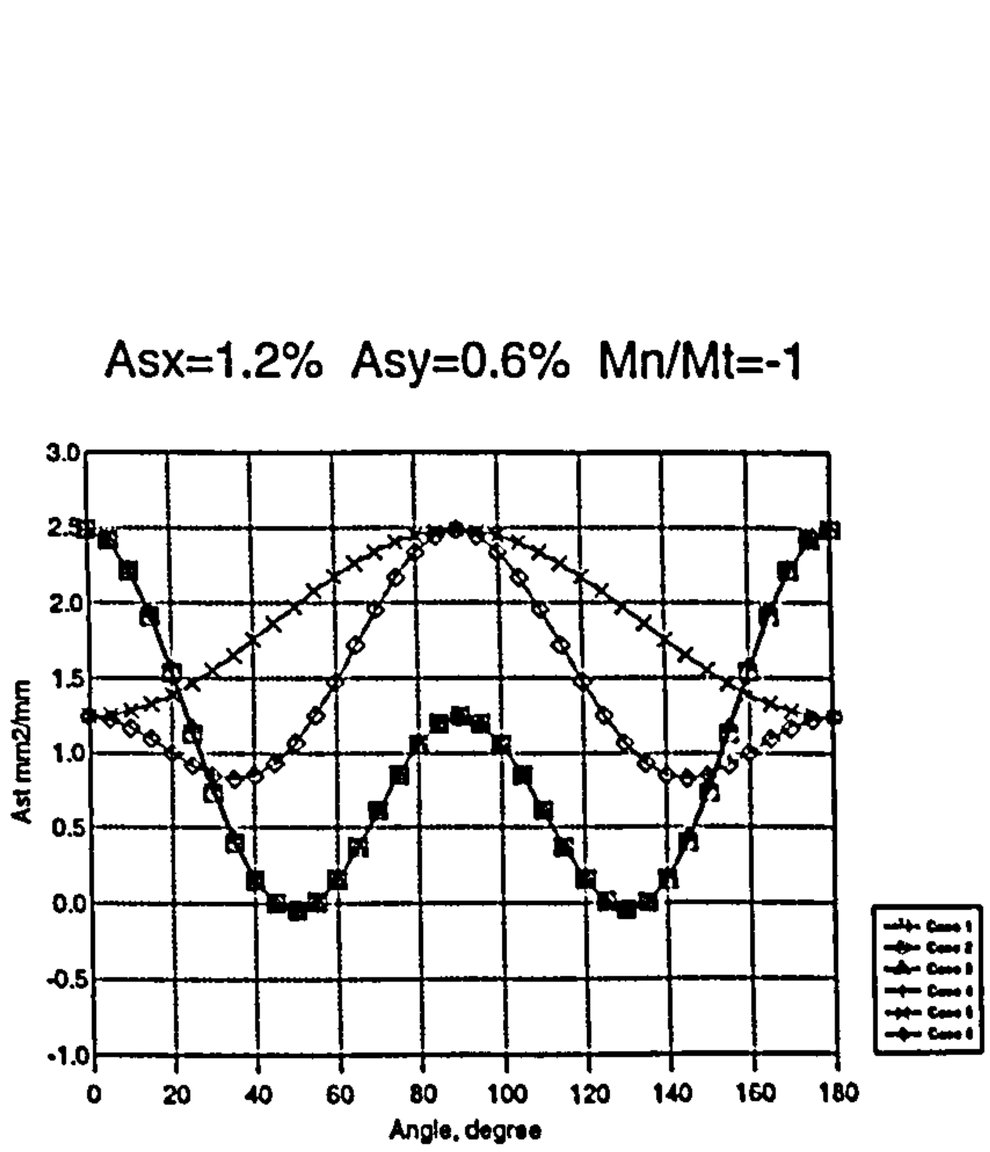
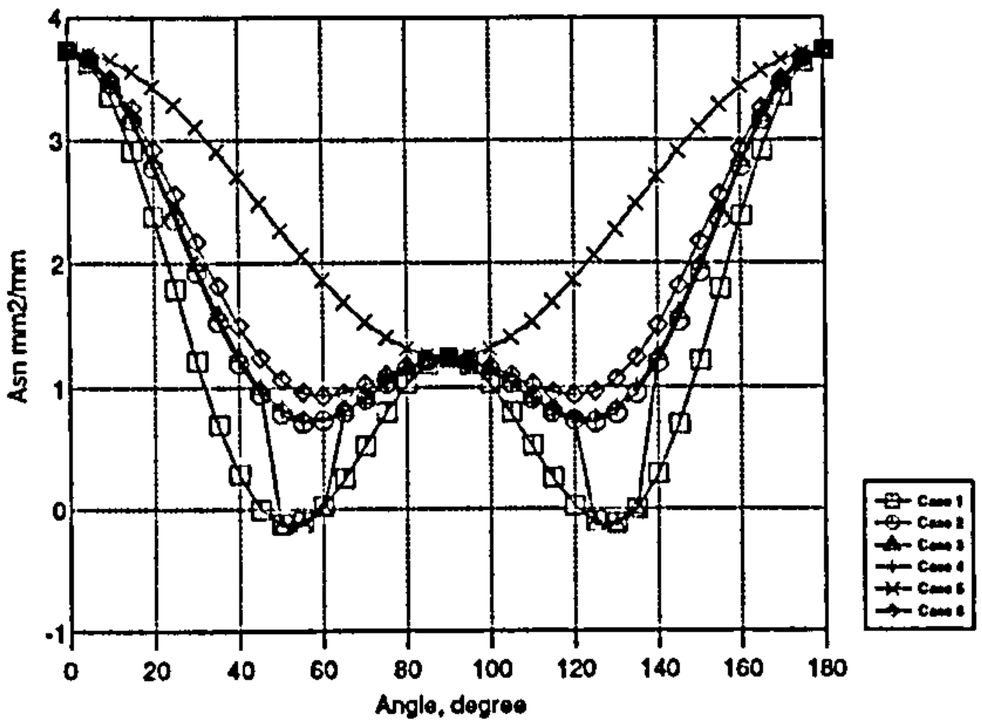
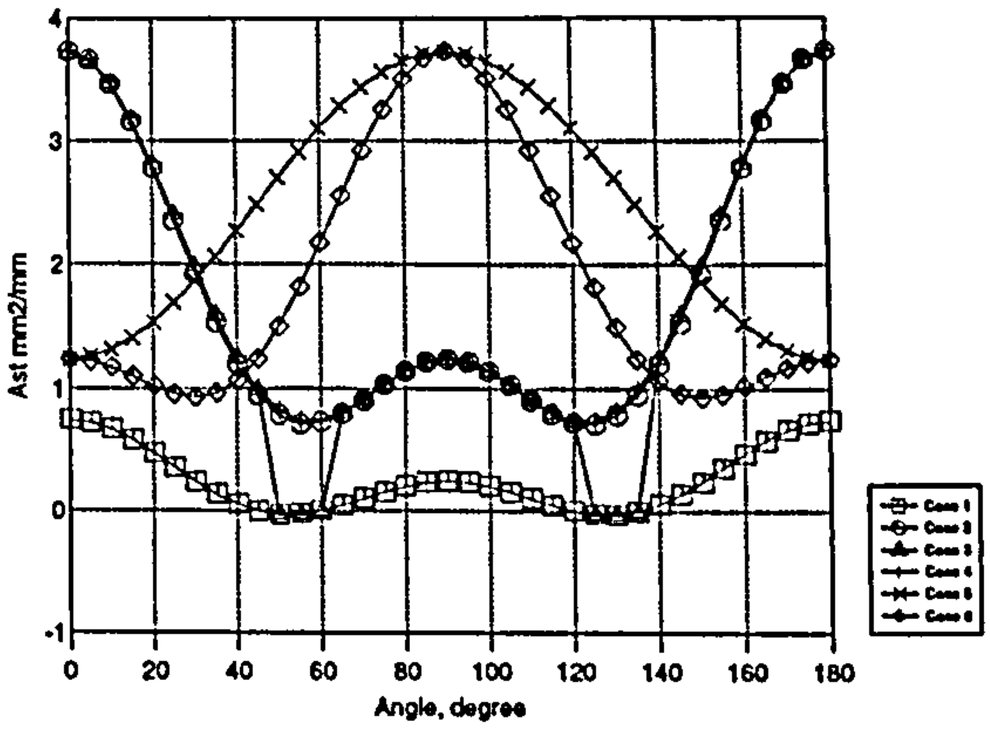
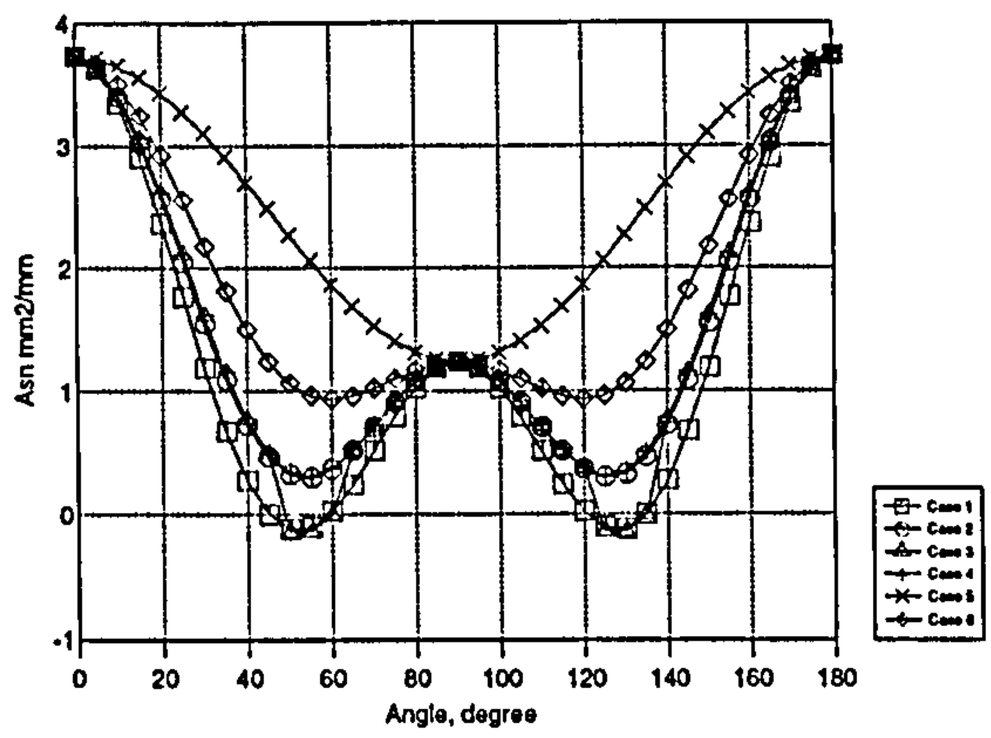
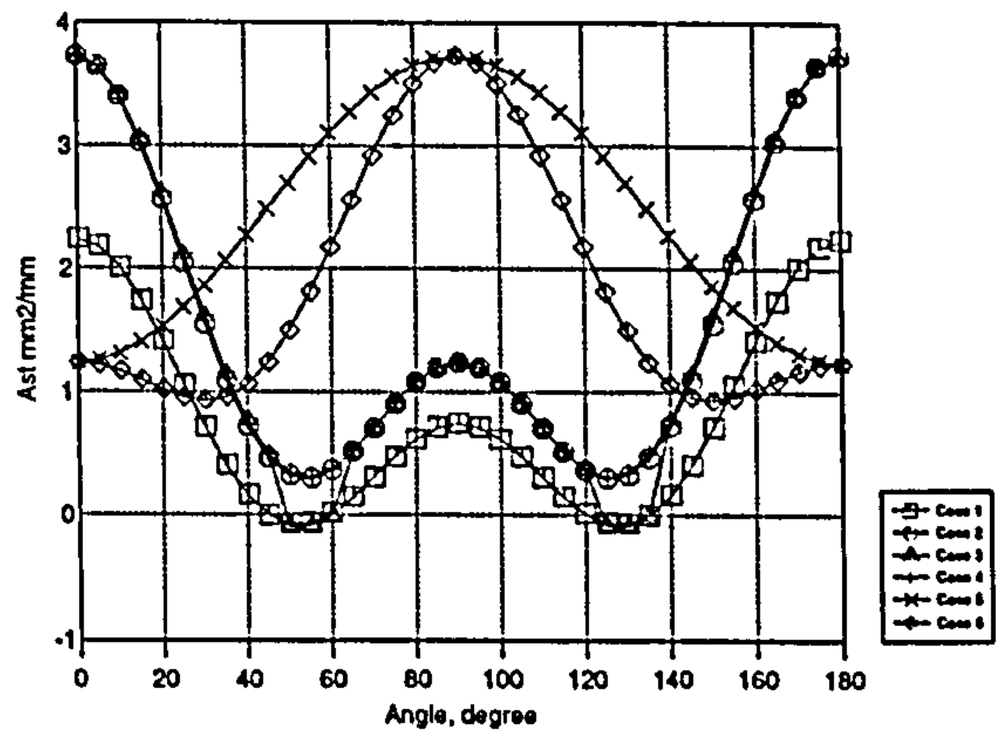


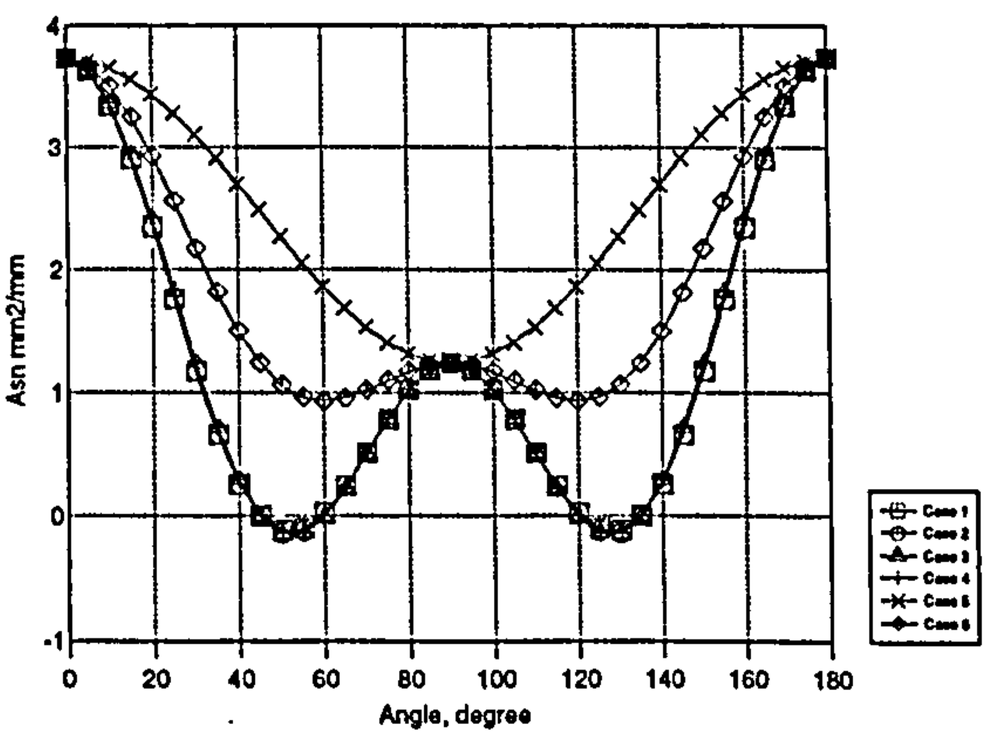
Figure A.5 Orthotropic mesh: A_{sx}=1.2% and A_{sy}=0.6%











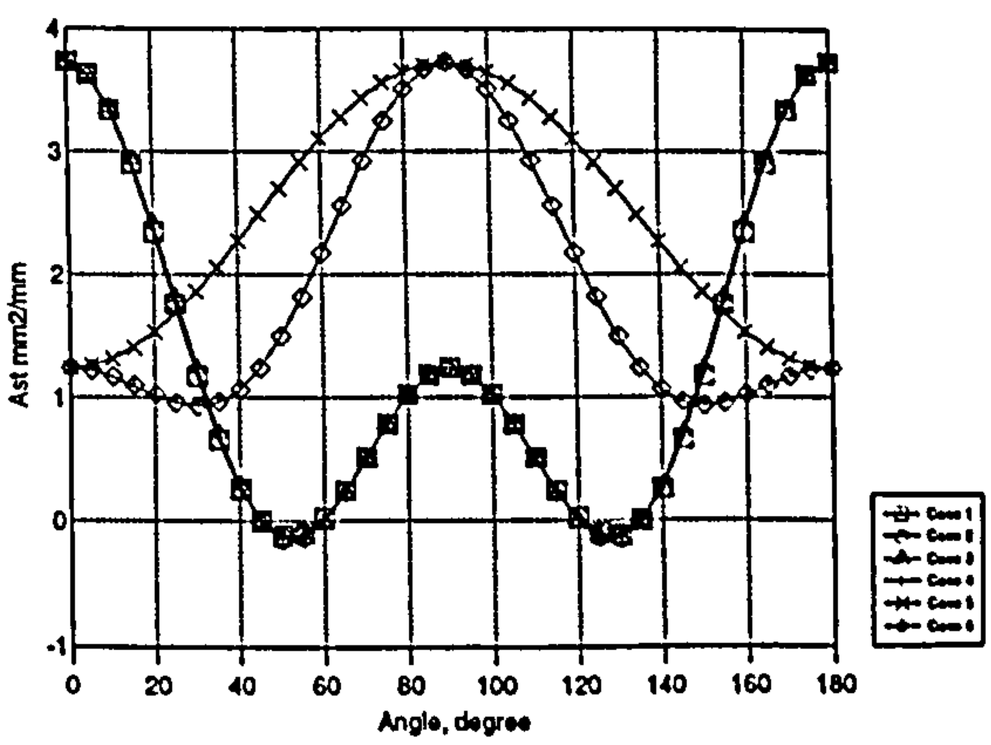


Figure A.6 Orthotropic mesh: A_{sx}=1.8% and A_{sy}=0.6%

Appendix B

MC-90 creep coefficient and shrinkage strain

B.1 Development of modulus of elasticity with time

The modulus of elasticity of concrete, $E_c(28)$ (MPa), at age 28 days, for normal weight concrete can be estimated from characteristic compressive strength, f_{ck} (for MPa):

$$E_c(28) = 21500 \left[\frac{f_{ck}(28) + 8}{10}\right]^{\frac{1}{3}} \tag{B.1}$$

The modulus of elasticity of concrete at the time of loading t_0 may be estimated by:

$$E_c(t_0) = \beta_E(t_0) E_c(28) \tag{B.2}$$

where,

$$\beta_E(t_0) = \sqrt{\exp\left[s(1 - \sqrt{\frac{28}{t_0}})\right]} \tag{B.3}$$

with s being a coefficient depending on type of cement; s is equal to 0.2, 0.25 and 0.38, respectively, for rapidly hardening high-strength cements, for normal and rapidly hardening cements, and for slowly hardening cements.

B.2 Creep coefficient

The equations given in this section are to be used when creep occurs under stress not exceeding 40 percent of the mean uniaxial compressive strength. Under sustained stress, the strain increases with time due to creep and the total strain- instantaneous plus creep at time t is:

$$\epsilon_c(t) = \frac{\sigma_c(t_0)}{E_c(t_0)}[1 + \phi(t, t_0)] \tag{B.4}$$

where the coefficient ϕ represent the ratio of creep to the instantaneous strain; its value increases with the decrease of age at loading t_0 and the increase of the length of the period $(t - t_0)$ during which the stress is sustained. The value also depends on quality of concrete, ambient temperature and humidity as well as the dimensions of the element considered.

The strain $\epsilon_c(t)$ is expressed in MC-90 by the equation:

$$\epsilon_c(t) = \frac{\sigma_c(t_0)}{E_c(t_0)}[1 + \frac{E_c(t_0)}{E_c(28)}\phi_{\text{CEB}}(t, t_0)] \tag{B.5}$$

Comparing eqs B.4 and B.5 indicates that

$$\phi(t, t_0) = \phi_{\text{CEB}}\frac{E_c(t_0)}{E_c(28)} \tag{B.6}$$

The value of $E_c(t_0)$ can be obtained from eq. B.2. The equation given by MC-90 for ϕ_{CEB} is adjusted below to give the creep coefficient $\phi(t, t_0)$ as defined above:

$$\phi(t, t_0) = \phi_0\beta_c(t - t_0)\frac{E_c(t_0)}{E_c(28)} \tag{B.7}$$

where β_c is a coefficient describing development of creep with time after loading; ϕ_0 is a notional creep coefficient given by:

$$\phi_0 = \phi_{\text{RH}}\beta(f_{cm})\beta(t_0) \tag{B.8}$$

$$\phi_{\text{RH}} = 1 + \frac{1 - (\text{RH}/100)}{0.46(h_0/100)^{1/3}} \tag{B.9}$$

$$\beta(f_{cm}) = \frac{5.3}{\sqrt{(f_{ck} + 8)/10}} \tag{B.10}$$

$$\beta(t_0) = \frac{1}{0.1 + t_0^{0.2}} \tag{B.11}$$

The symbol h_0 (mm) is the notional size of the member defined by:

$$h_0 = \frac{2A_c}{u} \tag{B.12}$$

where A_c and u are the area and perimeter in contact with the atmosphere of the cross-section of the considered member. Development of creep with time is expressed by:

$$\beta_c(t - t_0) = \left(\frac{t - t_0}{\beta_H + t - t_0}\right)^{0.3} \tag{B.13}$$

β_H (mm) is a function of the notional size h_0 (mm) and the relative humidity, RH (percent):

$$\beta_H = \frac{150h_0}{100}[1 + (0.012\text{RH})^{18}] + 250 \leq 1500\text{mm} \tag{B.14}$$

B.3 Shrinkage

Shrinkage starts at time t_s (days) when curing is stopped. On the other hand, concrete immersed in water at time t_s starts to swell. The shrinkage or swelling at any time t (days) may be estimated by:

$$\epsilon_{cs}(t, t_s) = \epsilon_{cs0}\beta_s(t - t_s) \tag{B.15}$$

where $\beta_s(t - t_s)$ is a function describing the development of shrinkage or swelling with time, given by:

$$\beta_s(t - t_s) = \left(\frac{t - t_s}{350(h_0/100)^2 + t - t_s}\right)^{0.5} \tag{B.16}$$

where h_0 (mm) is the notional size of the member defined by eq. B.12, ϵ_{cs0} is the notional shrinkage given by:

$$\epsilon_{cs0} = \epsilon_s(f_{cm})\beta_{RH} \tag{B.17}$$

where

$$\epsilon_s(f_{cm}) = 10^{-6}[160 + 10\beta_{sc}(9 - f_{cm}/10)] \tag{B.18}$$

with β_{sc} equalling 4, 5 or 8, respectively, for slowly hardening cements, for normal or rapidly hardening cements, and for rapidly hardening high-strength cements.

$$\beta_{\mathrm{RH}} = -1.55\left[1 - \left(\frac{\mathrm{RH}}{100}\right)^3\right] \quad \text{for } 40\% \leq \mathrm{RH} < 99\% \tag{B.19}$$

$$\beta_{\mathrm{RH}} = +0.25 \quad \text{for RH} \geq 99\% \text{ (immersed in water)} \tag{B.20}$$

Positive β_{RH} indicates swelling.

References

ABAQUS. 1994. *ABAQUS/Standard: Example problems manual, Volume II, Version 5.4.* Hibbit, Karlsson & Sorensen, Inc., USA.

ACI Committee 318. 1989. *Building code requirement for reinforced concrete.* American Concrete Institute, Michigan. (Revised 1992).

Agarwal, R. K. & Gardner, N. J. 1974. Form and shore requirements for multistory flat slab type buildings. *ACI Journal*, **71**(11), 559–569.

Ambrose, T. P., Huston, D. R., Fuhr, P. L., Devino, E. A. & Werner, M. P. 1994. Shoring systems for construction load monitoring. *Smart Materials and Structures*, **3**(1), 26–34.

Austin, J. A. 1998. Over design: Fact or fiction? *The Structural Engineer*, **76**(2), 17–21.

Base, G. D., Read, J. B., Beeby, A. W. & Taylor, H. P. J. 1966. An investigation of the crack control characteristics of various types of bar in reinforced concrete beams. *Research report no. 18*, December.

Beeby, A. W. 1998. *Early striking of formwork and forces in backprops: European Concrete Building Project, Cardington (Final report).* School of Civil Engineering, University of Leeds. December.

Branson, D. E. 1977. *Deformation of concrete structures.* McGraw-Hill Book Co., New York.

Branson, D. E. & Trost, H. 1982. Unified procedures for predicting the deflection and centroidal axis location of partially cracked nonprestressed and prestressed concrete members. *ACI Journal*, **79**(2), 119–130.

British Cement Association. 1993. *Concise Eurocode, for the design of concrete buildings* . BCA, London.

British Standards Institution. 1984. *Code of practice for dead and imposed loads.* BSI, London. BS 6399: Part 1.

British Standards Institution. 1985. *Structural use of concrete.* BSI, London. BS 8110: Part 1.

British Standards Institution. 1997. *Structural use of concrete.* BSI, London. BS 8110: Part 1.

Brøndum-Nielsen, T. 1980. Stress analysis of cracked arbitrary concrete section under service load. *ACI Journal*, **77**(6), 458–468.

Brøndum-Nielsen, T. 1984. Serviceability limit state analysis of concrete sections under biaxial bending. *ACI Journal*, **81**(5), 448–455.

Brøndum-Nielsen, T. 1986a. Serviceability limit state analysis of cracked, polygonal concrete sections under biaxial or symmetrical bending. *ACI Journal*, **83**(2), 209–218.

Brøndum-Nielsen, T. 1986b. Stress analysis for cracked reinforced concrete section under symmetrical bending in serviceability limit state. *ACI Journal*, **83**(3), 355–358.

Brøndum-Nielsen, T. 1986c. Serviceability limit state analysis of cracked, partially prestressed or reinforced concrete sections under symmetrical bending. *ACI Journal*, **83**(4), 547–552.

Brøndum-Nielsen, T. 1987. Concrete sections under biaxial bending. *Journal of Structural Engineering*, ASCE, **113**(10), 2137–2144.

Brøndum-Nielsen, T. 1997. Serviceability analysis of concrete sections under biaxial bending. *Journal of Structural Engineering,* ASCE, **123**(1), 117–119. technical note.

Cardenas, A. E. 1971. Discussions on finite element analysis of reinforced concrete slabs (original paper by Jofriet and McNeice, 1971). *Journal of the Structural Division,* ASCE, **97**(12), 2905–2907.

CEB. 1985. *CEB design manual on cracking and deformation.* Comité Euro-International du Béton (CEB), Lausanne.

CEB-FIP. 1993. *CEB-FIP Model Code 1990- design code.* Comité Euro-International du Béton (CEB), Lausanne.

Cope, R. J. & Clark, L. A. 1984. *Concrete slabs analysis and design.* Elsevier Applied Science Publishers, Amsterdam.

Crisfield, M. A. 1982. Variable step-lengths for nonlinear structural analysis. *Report no. 1049.*

EC2 editorial group. 1991. *Design of concrete structures, Part 1, General rules and rules for buildings, Revised final text* . EuroCode 2, October.

El-Sheikh, M. & Chen, W. 1988. Effects of fast construction rate on deflections of R. C. buildings. *Journal of Structural Engineering,* ASCE, **114**(10), 2225–2238.

Elstner, R.C. & Hognestad, E. 1956. Shearing strength of reinforced concrete slabs. *ACI Journal*, **53**(1), 29–58.

Favre, R., Charif, H. & Jaccoud, J. P. 1990. Improved serviceability of reinforced concrete slabs with the use of high-strength concrete. *Pages 89–108 of:* Hester, W. T. (ed), *High-strength concrete, second international symposium.* ACI, Michigan. SP-121.

Favre, R., Charif, H. & Jaccoud, J. P. 1992. Large reduction of deflections due to high performance concrete. *Pages 160–185 of:* Malier, Y. (ed), *High performance concrete: From material to structure.* E & FN Spon, London.

Fitzpatrick, A, Johnson, R., Mathys, J. & Taylor, A. 1992. *An assessment of the imposed loading needs for current commercial office buildings.* Stanhope.

Ganeswaran, R. & Rangan, B.V. 1996. Long-term deflections of high strength concrete beams and one-way slab. *Pages 243–266 of:* Nawy, E. G. (ed), *Recent developments in deflection evaluation of concrete.* ACI, Michigan. SP-161.

Gardner, N. J. 1990. Design and construction interdependence. *Concrete Internationsl: Design & Construction*, **12**(11), 32–38.

Gardner, N. J. & Fu, H. C. 1987. Effect of high construction loads on the long-term deflections of flat slabs. *ACI Structural Journal*, **84**(4), 349–360.

Ghali, A. 1989. Prediction of deflections of two-way floor systems. *ACI Structural Journal*, **86**(5), 551–562.

Ghali, A. 1993. Deflection of reinforced concrete members: A critical review. *ACI Structural Journal*, **90**(4), 364–373.

Ghali, A. & Favre, R. 1994. *Concrete structures: stresses and deformations.* 2 edn. E & F Spon, London.

Gilbert, R. I. 1983. Deflection calculation for reinforced concrete beams. *Civil Engg. Transaction*, **25**(2), 128–134.

Gilbert, R. I. 1988. *Time effects in concrete structures.* Elsevier Applied Science Publishers, Amsterdam.

Gilbert, R. J. & Warner, R. F. 1978. Tension stiffening in reinforced concrete slabs. *Journal of the Structural Division,* ASCE, **104**(12), 1885–1900.

Goodchild, C. & Moss, R. 1999. Reinforcing Cardington. *Concrete for the Construction Industry*, **33**(1), 11–14.

Graham, C. J. & Scanlon, A. 1986. Long-time multipliers for estimating two-way slab deflections. *ACI Journal*, **83**(6), 899–908.

Grundy, P. & Kabaila, A. 1963. Construction loads on slabs with shored formwork in multistorey buildings. *ACI Journal*, **60**(12), 1729–1738.

Hitchings, D. 1994. *Fe77 user manual.* Aeronautics Dept., Imperial College.

Hsu, C. T. & Mirza, M. S. 1973. Structural concrete-biaxial bending and compression. *Journal of the Structural Division,* ASCE, **99**(2), 285–290.

Jain, S. C. & Kennedy, J. B. 1974. Yield criterion for reinforced concrete slabs. *Journal of the Structural Division,* ASCE, **100**(3), 631–644.

Jofriet, J. C. & McNeice, G. M. 1971. Finite element analysis of reinforced concrete slabs. *Journal of the Structural Division,* ASCE, **97**(3), 785–806.

Johansen, K. W. 1972. *Yield-line formulae for slabs.* Cement and Concrete Association, London.

Jokinen, E. P. & Scanlon, A. 1987. Field measured two-way slab deflections. *Canadian Journal of Civil Engg*, **14**, 807–819.

Kotsovos, M. D. & Pavlović, M. N. 1999. *Ultimate limit state design of concrete structures: a new approach.* Thomas Telford, London.

Kripanarayan, K. M. & Branson, D. E. 1976. Short-time deflection of flat plates, flat slabs and two-way slabs. *ACI Journal*, **73**(December), 686–690.

Lenshow, R. & Sozen, M. A. 1966. *A yield criterion for reinforced concrete under biaxial moments and forces.* Univ. of Illinois, Urbana.

Liu, X. L., Chen, W. F. & Bowman, M. D. 1985. Construction load analysis for concrete structures. *Journal of Structural Engineering,* ASCE, **111**(5), 1019–1036.

Liu, X. L., Lee, H. M. & Chen, W. F. 1988. Analysis of construction loads on slabs and shores by personal computer. *Concrete Internationsl: Design & Construction*, **10**(6), 21–30.

Marosszeky, M. 1972. Construction loads imposed in multistory structures. *Civil Engg. Transaction*, **14**(1), 91–93.

McNeice, G. M. 1967. *Elastic-plastic analysis of flat plates by the finite element method.* Ph.D. thesis, University of London.

Parker, D. E. & Bullman, P. J. M. 1998. Edge-column connections in flat-slab construction. *The Structural Engineer*, **76**(13), 253–257.

Polak, M. A. 1996. Effective stiffness model for reinforced concrete slabs. *Journal of Structural Engineering,* ASCE, **122**(9), 1025–1030.

Polak, M. A. & Vecchio, F. J. 1993. Nonlinear analysis of reinforced concrete shells. *Journal of Structural Engineering,* ASCE, **119**(12), 3439–3462.

Polak, M. A., Scanlon, A. & Phillips, D. V. 1996. Deflection analysis of reinforced concrete members using finite element method. *Pages 75–96 of:* Nawy, E. G. (ed), *Recent developments in deflection evaluation of concrete.* ACI, Michigan. SP-161.

Reinforced Concrete Council. 1990. *Economic long-span floors.* BCA, London.

Reinforced Concrete Council. 1993. *Cost model study, a report on the comparative costs of concrete and steel framed office buildings.* BCA, London.

Rotilio, J. 1998. Moment-curvature relationship: Part I. *Pages I2–I14 of: Serviceability behaviour of RC and PC road bridges under cyclic actions.* XIIIth FIP Congress and Exhibition.

Sakai, K. & Kakuta, Y. 1980. Moment-curvature relationships of reinforced concrete members subjected to combined bending and axial force. *ACI Journal*, 77(3), 189–194.

Sbarounis, J. A. 1984a. Multistory flat plate buildings: construction load and immediate deflections. *Concrete Internationsl: Design & Construction*, 6(2), 70–77.

Sbarounis, J. A. 1984b. Multistory flat plate buildings: effect of construction loads on long-term deflections. *Concrete Internationsl: Design & Construction*, 6(4), 62–70.

Sbarounis, J. A. 1984c. Multistory flat plate buildings: measured and computed one-year deflections. *Concrete Internationsl: Design & Construction*, 6(8), 31–35.

Scanlon, A. & Murray, D. W. 1974. Time-dependent reinforced concrete slab deflections. *Journal of the Structural Division,* ASCE, **100**(9), 1911–1924.

Scanlon, A. & Murray, D. W. 1982. Practical calculation of two-way slab deflections. *Concrete Internationsl: Design & Construction*, 4(11), 43–50.

Shukla, S. N. & Mittal, M. K. 1976. Short-term deflection in two-way reinforced concrete slabs after cracking. *ACI Journal*, **73**(July), 416–419.

Solanki, H. 1996. Deflection and minimum thickness requirements in the CEB and ACI codes. *Pages 25–50 of:* Nawy, E. G. (ed), *Recent developments in deflection evaluation of concrete.* ACI, Michigan. SP-161.

Stivaros, P. C. & Halvorsen, G. T. 1992. Construction load analysis of slabs and shores using microcomputers. *Concrete Internationsl: Design & Construction*, 14(8), 27–32.

Tam, K. S. S. & Scanlon, A. 1986. Deflection of two-way slabs subjected to restraint volume change and transverse loads. *ACI Journal*, **83**(5), 737–744.

Thompson, D. P. & Scanlon, A. 1988. Minimum thickness requirements for control of two-way slab deflections. *ACI Journal*, **85**(1), 12–22.

Timoshenko, S. P. & Woinowsky-Krieger, S. 1959. *Theory of plates and shells.* 2 edn. McGraw-Hill Book Co., New York.

Vollum, R. L. 1998. *Interim report on creep and shrinkage tests for Cardington in-situ building.* CRIC, Imperial College. Report CRIC/98/10/01, June.

Vollum, R. L. & Hossain, T. R. 1998. Assessment of slab deflections in the in-situ concrete frame building. *In: 3rd Cardington Conference, Whole building research: the latest developments.* Building Research Establishment.

Vollum, R. L., Hossain, T. R. & Pavlović, M. N. 1998. Slab deflections in the cardington insitu concrete building: a comparison of theory and practice. *Pages 151–171 of: BCA Concrete Communication Conference.* British Concrete Association.

Wang, G. G. & Hsu, C. T. 1992. Complete biaxial load-deformation behaviour of RC columns. *Journal of Structural Engineering,* ASCE, **118**(9), 2590–2609.

Whittle, R. 1996. *Taywood high strength concrete slab.* personal communication.

Zaghlool, E. R. F., Rawdon de Paiva, H. A & Glockner, P. G. 1970. Tests of reinforced concrete flat plate floors. *Journal of the Structural Division,* ASCE, 96(3), 487–507.

BIBL
LONDON
UNIV.